U.S. DEPARTMENT OF ENERGY

PNNL-18303

Prepared for the U.S. Department of Energy
Under Contract DE-AC05-76RL01830

Sequestration of Sr-90 Subsurface Contamination in the Hanford 100-N Area by Surface Infiltration of a Ca-Citrate-Phosphate Solution

JE Szecsody
ML Rockhold
M Oostrom
RC Moore
CA Burns
MD Williams
L Zhong
JS Fruchter
JP McKinley
VR Vermeul
MT Covert
TW Wietsma
AT Breshears
BJ Garcia

March 2009

Pacific Northwest
NATIONAL LABORATORY

DISCLAIMER

PACIFIC NORTHWEST NATIONAL LABORATORY
operated by
BATTELLE
for the
UNITED STATES DEPARTMENT OF ENERGY
under Contract DE-AC05-76RL01830

Printed in the United States of America

Available to DOE and DOE contractors from the
Office of Scientific and Technical Information,
P.O. Box 62, Oak Ridge, TN 37831-0062;
ph: (865) 576-8401
fax: (865) 576-5728
email: reports@adonis.osti.gov

Available to the public from the National Technical Information Service,
U.S. Department of Commerce, 5285 Port Royal Rd., Springfield, VA 22161
ph: (800) 553-6847
fax: (703) 605-6900
email: orders@ntis.fedworld.gov
online ordering: http://www.ntis.gov/ordering.htm

This document was printed on recycled paper.
(9/2003)

PNNL-18303

Sequestration of Sr-90 Subsurface Contamination in the Hanford 100-N Area by Surface Infiltration of a Ca-Citrate-Phosphate Solution

JE Szecsody
ML Rockhold
M Oostrom
RC Moore
CA Burns
MD Williams
L Zhong
JS Fruchter
JP McKinley
VR Vermeul
MT Covert
TW Wietsma
AT Breshears
BJ Garcia

March 2009

Prepared for
the U.S. Department of Energy
under Contract DE-AC05-76RL01830

Pacific Northwest National Laboratory
Richland, Washington 99352

Summary

The objective of this project is to develop a method to emplace apatite precipitate in the 100-N Area vadose zone, resulting in sorption and ultimately incorporation of Sr-90 into the apatite structure. The Ca-citrate-phosphate (Ca-citrate-PO_4) solution can be infiltrated into unsaturated sediments to result in apatite precipitate to provide effective treatment of Sr-90 contamination. Microbial redistribution during solution infiltration and a high rate of citrate biodegradation for river water microbes (water used for solution infiltration) produces a relatively even spatial distribution of the citrate biodegradation rate and ultimately, apatite precipitate in the sediment. Manipulation of the Ca-citrate-PO_4 solution infiltration strategy can be used to induce apatite precipitation in the lower half of the vadose zone (where most of the Sr-90 is located) and within low-K layers (which may have higher Sr-90 concentrations):

- *infiltration rate*: more rapid Ca-citrate-PO_4 solution infiltration resulted in greater depth of apatite precipitate, but less lateral spreading
- *decrease in infiltration rate*: rapid then slow solution infiltration resulted in greater lateral spreading of the apatite precipitate at depth
- *sequential solution then water infiltration*: water infiltration after solution infiltration effectively moved the apatite mass to depth in homogeneous sediment systems
- *solution concentration*: infiltration of higher Ca-citrate-PO_4 solution concentrations resulted in a greater depth of apatite precipitate
- *infiltration cycles*: repeated infiltration of the Ca-citrate-PO_4 solution with time between cycles to allow for water drainage increased depth and greater lateral spread of apatite
- low-K zones had a higher apatite precipitate due to higher residual water content
- solution then water infiltration into a complex heterogeneous system with low-K and high-K discontinuous zones (8 ft high) showed high apatite precipitate in low-K and medium-grained sediment, but low treatment in high-K zones due to low water content

The most effective infiltration strategy to precipitate apatite at depth (and with sufficient lateral spread) was to infiltrate a high concentration solution (6 mM Ca, 15 mM citrate, 60 mM PO_4) at a rapid rate (near ponded conditions), followed by rapid, then slow water infiltration. Repeated infiltration events, with sufficient time between events to allow water drainage in the sediment profile can be used to build up the mass of apatite precipitate at greater depth. Low-K heterogeneities were effectively treated, as the higher residual water content maintained in these zones resulted in higher apatite precipitate concentration. High-K zones did not receive sufficient treatment by infiltration, although an alternative strategy of air/surfactant (foam) was demonstrated effective for targeting high-K zones. The flow rate manipulation used in this study to treat specific depths and heterogeneities is not as easy to implement at field scale due to the lack of characterization of heterogeneities and difficulty tracking the wetting front over a large subsurface area. However, the use of real-time surface and cross-borehole geophysics can be used to track the infiltrating Ca-citrate-PO_4 front so some adjustments can be made in the infiltration rate to precipitate apatite in desired zones. In addition, the reactive transport code used in this study with field-scale physical parameters for sediments can be used to evaluate infiltration strategies along with preliminary water infiltration tests at field scale.

Contents

Figures

Tables

1.0 Introduction

This project was initiated to develop an *infiltration* strategy for emplacement in the difficult-to-inject Hanford formation using the same apatite-forming solution (Ca-citrate-phosphate [Ca-citrate-PO_4]) technology proven to precipitate apatite by *injection* in Hanford formation sediment (Moore et al. 2004; Williams et al. 2008). This infiltration strategy will supplement the current treatability test plan (DOE-RL 2004, 2005) for well injection of the Ca-citrate-PO_4 solution and is needed to reach the *Hanford Federal Facility Agreement and Consent Order* (Tri-Party Agreement, Ecology et al. 1989) technology evaluation milestone (Milestone M-016014(b)) for evaluating technologies in the 100-N Area. Infiltration of the solution from the land surface is advantageous for several reasons: a) implementation can occur at a larger range of river stages compared with well injection; b) it will treat sediments in the entire vadose zone profile, so will immobilize Sr-90 in sediments that would not be reached through well injection; c) potentially is less expensive to implement relative to well injection; and d) sediments closer to the river can be treated due to limitations in well drilling too near the river bank. While the formation of apatite precipitation from the apatite-forming solution had been shown to occur, development of the technology was focused upon water-saturated (aerobic, anaerobic) processes, and experiments have not been conducted at low water saturation.

The combined effects of biogeochemical and coupled precipitate/flow processes was quantified so that an infiltration strategy that produces a relatively uniform spatial distribution of the apatite precipitate in Sr-90 laden zones can be achieved at the field scale. A sequence of experiments was used in this project that increase in complexity and scale to quantify individual and coupled processes of apatite precipitation during liquid infiltration and Sr-90 sequestration. Small-scale experiments investigated citrate biodegradation rates as a function of water content and microbial population (Task 1). Low water content 1-D infiltration experiments were also conducted at differing apatite-forming solution concentrations and infiltration rates (Task 2). High solution concentration injections add complexities to both the infiltration method and initial Sr-90 migration, as previously shown in water-saturated systems. Theoretically, precipitation of 1.3 mg of apatite per gram of sediment should remove all Sr and Sr-90 for 300 years (10 half-lives of Sr-90), assuming 11% Sr substitution for Ca (found in natural apatites). Whether the theoretical capacity can be achieved in the 100-N Area depends on the rate at which Sr-90 is incorporated into the apatite structure relative to the Sr-90 flux rate. Long-term apatite recrystallization rate experiments were conducted to address the rate at which Sr is incorporated into apatite (Task 3) to evaluate the mass of apatite needed in the vadose zone. Geochemical and microbial reactions quantified in these small-scale experiments were then incorporated into the Subsurface Transport Over Multiple Phases (STOMP) simulator to determine the relative importance of processes, design larger scale experiments, and develop both injection and infiltration strategies (Task 4). Finally, small- to large-scale 2-D infiltration experiments were conducted to evaluate placement of apatite precipitate in homogeneous and heterogeneous sediments (Task 5). The simulation tool was used to design some 2-D infiltration experiments as well as conduct post-experiment quantification of processes.

1.1 Sr-90 Contamination in Subsurface and River Biota

The Hanford Site is a U.S. Department of Energy (DOE) site located in southeastern Washington State near Richland, Washington. The Hanford 100 Area is located along the Columbia River and includes nine DOE nuclear reactors previously used for plutonium production, one of which is the 100-N Reactor (Figure 1.1). The operation of the 100-N Area nuclear reactor required the disposal of pass-through cooling water from the reactor's primary cooling loop, the spent fuel storage basins, and other reactor-related sources. Two crib and trench liquid waste disposal facilities (LWDFs) were constructed to receive these waste streams, and disposal consisted of percolation into the soil. The first LWDF (1301-N) was constructed in 1963, about 244 meters (800 feet) from the river (Figure 1.1, lower center). Liquid discharges to this facility contained radioactive fission and activation products, including cobalt-60, cesium-137, strontium-90, and tritium. Minor amounts of hazardous wastes such as sodium dichromate, phosphoric acid, lead, and cadmium were also part of the waste stream. When Sr-90 was detected at the shoreline, disposal at the first LWDF was terminated and a second crib and trench (1325-N LWDF) was constructed further inland in 1983. Discharges to 1325-N ceased in 1993. A more complete history of the groundwater contamination at the 100-N Area can be found in the *Hanford 100-N Area Remediation Options Evaluation Summary Report* (TAG 2001).

Figure 1.1. Hanford 100-N Reactor and disposal trench.

Sr-90 transport in subsurface sediments from disposal cribs has reached the Columbia River, as evidenced by Sr-90 in the river, and in the sediments in shallow water (groundwater discharges to the river, red squares, Figure 1.2). In addition, Sr-90 is detected in Asian clams found on the 100-N shoreline (circles, Figure 1.2). The highest sediment and clam Sr-90 concentration is at river tube #5. A proposed 300-ft wide treatment zone of apatite will extend between river tubes #1 to #8.

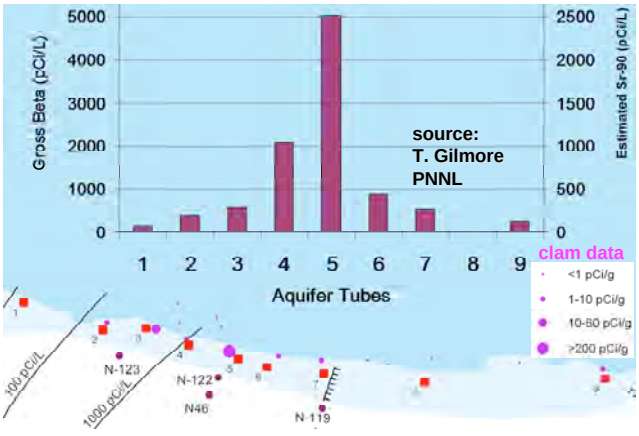

Figure 1.2. Sr-90 contamination in river sediments and clams.

The sediments (gravel with sand/silt) in the 100-N Area consist of a lower Ringold E unit and overlying Hanford formation (15- to 20-ft contact depth), which contain the unconfined aquifer. The Hanford formation is highly transmissive (Ksat 490 – 20,000 ft/day) compared to the underlying Ringold E (20 to 590 ft/day). The Ringold E unit is bounded by the underlying silty Ringold upper mud, ~200 ft thick, which

acts as an aquitard. Groundwater flows primarily in a north-northwesterly direction most of the year and discharges to the Columbia River. The groundwater gradient varies from 0.0005 to 0.003 ft/ft. Near the LWDF facilities, average groundwater velocities are estimated to be between 0.1 and 2 ft/day, with 1 ft/day average.

Sr-90 contamination in sediments reflects the hydrodynamics in the 100-N Area. Sr-90 has leached from trenches through the variable thickness vadose zone to groundwater and moved toward the Columbia River. Because the river stage changes daily (±5 ft) and seasonally (±8 ft for sustained periods), the saturated zone thickness changes and flow reversals do occur (i.e., movement of river water into the aquifer). The result on Sr-90 is a smearing of the plume vertically and horizontally. Given that the upper Hanford formation has generally 10 times greater groundwater flow than the underlying Ringold E Formation, most (but not all) of the Sr-90 contamination is found in the Hanford formation, with roughly a third of the mass in the lower Ringold E (Figure 1.3). The highest concentration is found 50 ft inland from the river edge (well N122), inland from river tube #5 (Figure 1.2), with lower Sr-90 concentrations in wells on both sides of this location. This vertical Sr-90 profile type is previously observed (Serne and LeGore 1996).

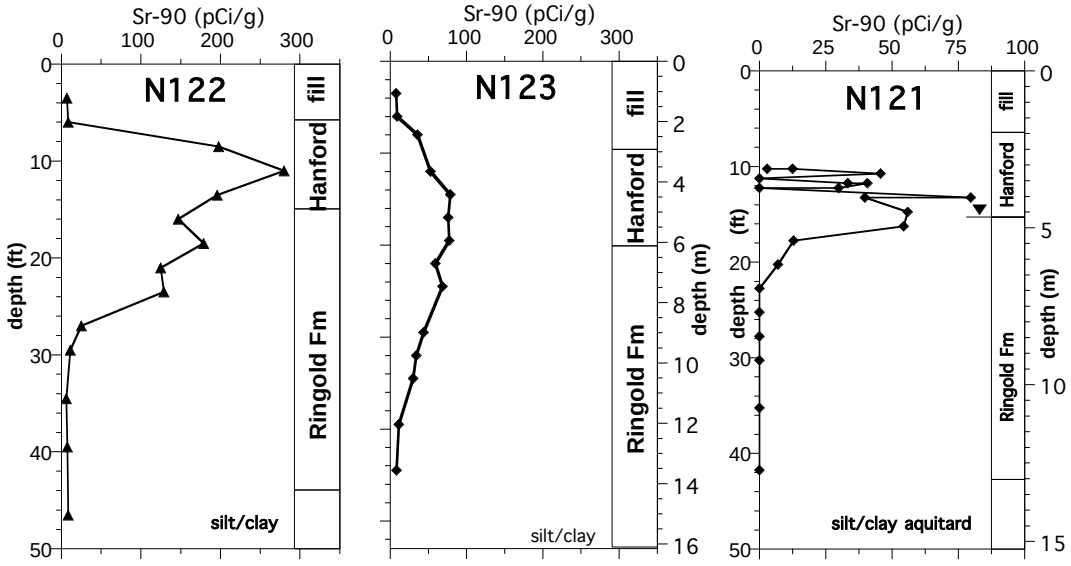

Figure 1.3. Sr-90 contamination in subsurface sediments.

Because of strong Sr-90 adsorption by ion exchange to sediments (K_d = 25 cm^3/g in groundwater, so a retardation factor (R_f) ~100; Moore et al. 2006; Routson et al. 1981; Steefel 2004), about 1% of the Sr-90 is in groundwater and 99% on sediments. As such, the pump-and-treat system operated since 1995 has only removed a small amount of Sr-90 from the aquifer, although it is effective for removal of mobile contaminants such as tritium. Because of the highly transmissive nature of sediments near the river, the pump-and-treat system removes Sr-90 from inland locations near the disposal trench. Given the high adsorption and short radioactive decay half-life of Sr-90 (29.1 years), only sediments near the river are at risk of entering the river (red/yellow highlighted area, Figure 1.1) before radioactive decay reduces Sr-90 activity to

negligible amounts. The pump-and-treat system has not influenced Sr-90 levels in wells near the river (red line, Figure 1.4, well N46 inland of river tube #5 and well N122, Figure 1.3).

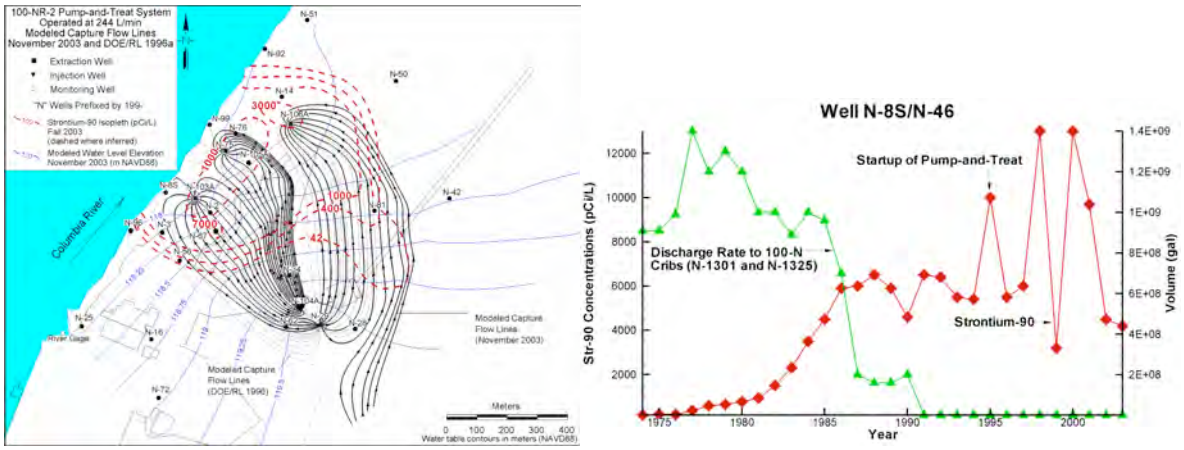

Figure 1.4. Simulation of pump and treat capture zone (a) and crib discharge (green) and Sr-90 levels in well N46 (b).

1.2 100-N Area Remediation History

The 100-N Area of the Hanford Site was placed on the National Priorities List (NPL) in 1989, the same year the Tri-Party Agreement (Ecology et al. 1989) signed by the DOE, U.S. Environmental Protection Agency (EPA), and the Washington State Department of Ecology (Ecology) established the procedural framework and schedule for the remedial response actions at Hanford. In 1995, a pump-and-treat system was installed as an interim measure to control the movement of Sr-90 to the Columbia River. As of June 2004, 1.6 Ci of Sr-90 were removed since beginning operations. Given that there are ~80 Ci of Sr-90 in the saturated sediments in the 100-N Area, at this removal rate, the time needed to meet the drinking water standard (8 pCi/L) is ~270 years. Although the pump-and-treat system may have met the objective of reducing the flow of groundwater to the river, it has not met the objective of reducing Sr-90 concentrations in aquifer pore fluid at the shoreline or in the stream bank storage zone. The pump-and-treat system was turned off in 2005, and alternate technologies of: a) apatite precipitation by Ca-citrate-PO_4 solution injection in near-river aquifer sediments, b) apatite precipitation by Ca-citrate-PO_4 solution infiltration (this project), and c) phytoremediation were investigated in laboratory experiments (infiltration) and laboratory/field experiments (injection, phytoremediation).

1.3 Sr-90 Immobilization with Apatite

Apatite [$Ca_{10}(PO_4)_6(OH)_2$] is a natural calcium phosphate mineral occurring primarily in the earth's crust as phosphate rock. It is also a primary component in the teeth and bones of animals. Apatite minerals sequester elements into their molecular structures via isomorphic substitution, whereby elements of similar physical and chemical characteristics replace calcium, phosphate, or hydroxide in the hexagonal crystal structure (Hughes et al. 1989; Spence and Shi 2005). Apatite has been used for remediation of other metals including U (Arey et al. 1999; Fuller et al. 2002,

2003; Jeanjean et al. 1995), lead (Bailliez et al. 2004; Mavropoulos et al. 2002; Ma et al. 1995), Pu (Moore et al. 2005), and Np (Moore et al. 2003). Because of the extensive substitution into the general apatite structure (Figure 1.5), over 350 apatite minerals have been identified (Moelo et al. 2000). Sr incorporation into apatite has also been previously studied (Smiciklas et al. 2005; Rendon-Angeles et al. 2000). Apatite minerals are very stable and practically insoluble in water (Tofe 1998; Wright 1990; Wright et al. 2004). The solubility product (K_{sp}) of hydroxyapatite is about 10^{-44}, while quartz crystal, which is considered the most stable mineral in the weathering environment, has a solubility product (K_{sp}) of 10^{-4} (Geochem Software 1994). Strontiapatite, $Sr_{10}(PO_4)_6(OH)_2$, which is formed by the complete substitution of Ca by Sr (or Sr-90), has a K_{sp} of about 10^{-51}, another 10^7 times less soluble than hydroxyapatite (Verbeek et al. 1977). The substitution of strontium for calcium in the crystal structure is thermodynamically favorable, and will proceed provided the two elements coexist. Sr substitution in natural apatites is as high as 11%, although dependent on available Sr (Belousova et al. 2002). Synthetic apatites have been made with up to 40% Sr substitution for Ca (Heslop et al. 2005). The mixed Sr-Ca-apatites have lower solubility than Ca-apatite or strontiapatite. The mechanism (solid-state ion exchange) of Sr substitution for Ca in the apatite structure has been previously studied at elevated temperature (Rendon-Angeles et al. 2000; Lindsay et al. 1989), but low temperature aqueous rates under Hanford groundwater conditions (i.e., Ca/Sr of 220/1) have not.

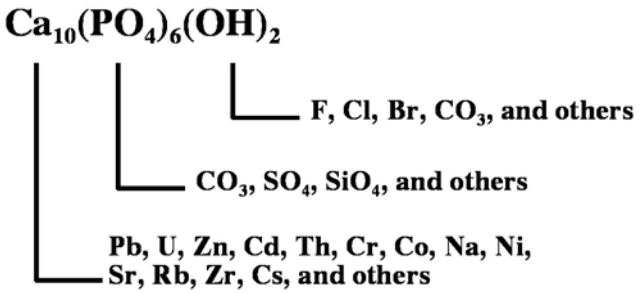

Figure 1.5. Cationic and anionic substitution in apatite.

1.4 Subsurface Apatite Placement by Solution Injection/Infiltration

The method of emplacing apatite in subsurface sediments at the 100-N Area is to inject or infiltration an aqueous solution containing a Ca-citrate complex and Na-phosphate (Moore et al. 2004, 2007). Phosphate adsorption is slow (hours) so rapid infiltration can result in deeper phosphate mass at depth. Citrate is needed to keep Ca in solution long enough (days) to inject into the subsurface; a solution containing Ca^{2+} and phosphate only will rapidly form mono- and di-calcium phosphate [$Ca(H_2PO_4)_2$, $CaHPO_4*2H_2O$], but not apatite (Andronescu et al. 2002; Elliot et al. 1973; Papargyris et al. 2002). Relatively slow biodegradation of the Ca-citrate complex (days) allows sufficient time for injection and transport of the reagents to the areas of the aquifer where treatment is required (Szecsody et al. 2007; Williams et al. 2008). As Ca-citrate is degraded (Van der Houwen and Valsami-Jones 2001; Misra 1998), the free Ca and phosphate combine to form amorphous apatite. The formation of amorphous apatite occurs within a week and crystalline apatite forms within a few weeks. Citrate biodegradation rates in Hanford 100-N sediments (water-saturated) at temperatures from 10°C to 21°C (aquifer temperature 15°C to 17°C) over the range of citrate concentrations to be used (10 mM to 100 mM) have been determined experimentally and simulated with a first-order model (Bailey and Ollis 1986; Bynhildsen and Rosswall 1997). In addition, the microbial biomass has been characterized with depth and position along the shoreline, and the relationship between biomass and the citrate biodegradation rate determined, as described in Section 4.0. Because Hanford

100-N Area injections typically use river water (~90% to 95%) with concentrated chemicals, microbes in the river water are also injected, which results in a somewhat more uniform citrate biodegradation rate in different aquifer zones.

Emplacement of apatite precipitate by a solution injection/infiltration has significant advantages over other apatite emplacement technologies for application at the Hanford 100-N Area. The major advantage is minimal disturbance of the subsurface (both vadose and saturated zone), as this technology only requires injection wells (for groundwater remediation) or a surface infiltration gallery (for vadose zone treatment), in contrast with excavation of the river bank for trench-and-fill emplacement of solid-phase apatite. Other apatite emplacement technologies were also considered for the 100-N Area (DOE-RL 2005), which included pneumatic injection of solid apatite and vertical hydrofracturing for apatite emplacement both as a permeable reactive barrier and grout curtain. Although each technology has advantages and disadvantages, the Ca-citrate-PO_4 injection technology was chosen as it appears to provide the most economic emplacement methodology to treat Sr-90 in the near-shore sediments. None of these apatite technologies remove the Sr-90 from the sediment until radioactive decay occurs, as the Sr-90 is incorporated into the apatite crystalline structure.

1.5 Need for Injection/Infiltration Strategy at River Shore

The current injection strategy is to inject the Ca-citrate-PO_4 solution separately into the Hanford formation and Ringold E Formation sediments (Williams et al. 2008). While there is a high degree of confidence that apatite precipitate will occur, the river hydrodynamics create a significant problem for the seasonal timing of the injection (Figure 1.6). Simulation of injections into the lower (less transmissive) Ringold E Formation at sustained low and high river stage show that the river stage does not move the Ca-citrate-PO_4 injection plume a significant distance before apatite is expected to precipitate, so lower river stage in late fall is best for injection into the Ringold E Formation to get some apatite movement toward the river, but the timing is not critical, as this formation is nearly always water-saturated.

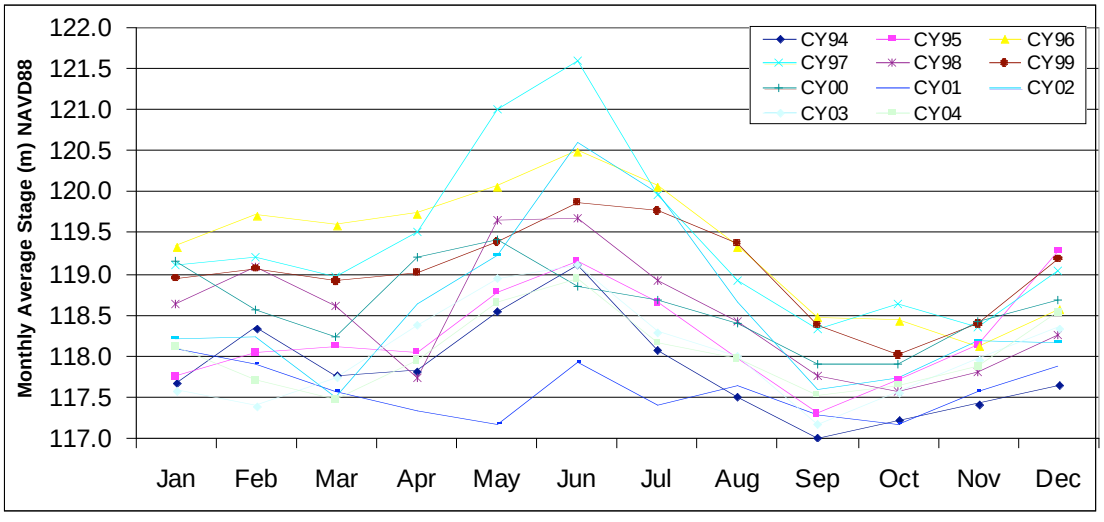

Figure 1.6. Columbia River stage 1994–2005 (Edrington 2005).

In contrast, apatite-forming solution injection into the upper Hanford formation needs to be done during high river stage so that the formation is water saturated (i.e., late spring, Figure 1.6). In addition, because movement of the solution toward the river is desired, the most desirable injection would be at a high river stage (saturating the formation) followed by a moderate river stage, to get slow flow toward the river. Injection during low river stage would result in rapid movement of the injection solution into the river (days) before precipitation would occur. Therefore, river hydrodynamics have a potentially significant influence on the effectiveness of the emplacement of the solution by injection. There are only short periods throughout the year where the river stage conditions are optimal for injection. The effectiveness of the low and high river stage injections at low concentration (~18 injections completed by July 2007) were described in a separate report (Williams et al. 2008). The effectiveness of high concentration injections in 2008 will be described in a separate report.

Infiltration of the Ca-citrate-PO_4 solution (this study) could be accomplished at a different river stage than injection, so an infiltration strategy extends the amount of time that apatite could be emplaced. Infiltration into the Hanford formation sediments would be optimal at periods of low river stage (leaving a greater thickness of unsaturated porous media), so could occur during summer/fall, or the second low stage of early spring. The formation of apatite during infiltration during these periods is less influenced by transmissivity in the formation and river stage, and more dependent on the rate of infiltration. Another potential benefit to infiltration is that cost of implementation may be much less than injection, as wells (a significant cost) do not need to be installed, although there is some cost associated with the infiltration method (i.e., trenches, drip emitters, etc.).

2.0 Background – Infiltration of a Ca-Citrate-PO_4 Solution to Form Apatite In Situ

2.1 Precipitation of Apatite in Subsurface Sediments

The method of emplacing apatite in vadose zone sediments at the 100-N Area is to infiltrate an aqueous solution containing a Ca-citrate complex and Na-phosphate (Szecsody et al. 2008). Citrate is needed to keep Ca in solution long enough (days) to inject into the subsurface; a solution containing Ca^{2+} and phosphate only will rapidly form mono- and di-calcium phosphate, but not apatite (Andronescu et al. 2002; Elliot et al. 1973; Papargyris et al. 2002). Relatively slow biodegradation of the Ca-citrate complex (days) allows sufficient time for injection and transport of the reagents to the areas of the aquifer where treatment is required. As Ca-citrate is degraded (Van der Houwen and Valsami-Jones 2001; Misra 1998), the free Ca and phosphate combine to form amorphous apatite. The formation of amorphous apatite occurs within a week and crystalline apatite forms within a few weeks. Citrate biodegradation rates in Hanford 100-N sediments (water-saturated) at temperatures from 10°C to 21°C (aquifer temperature 15°C to 17°C) over the range of citrate concentrations to be used (10 mM to 100 mM) have been determined experimentally and simulated with a first-order model (Bailey and Ollis 1986; Bynhildsen and Rosswall 1997). In addition, the microbial biomass has been characterized with depth and position along the shoreline, and the relationship between biomass and the citrate biodegradation rate determined, as described in Section 4.0.

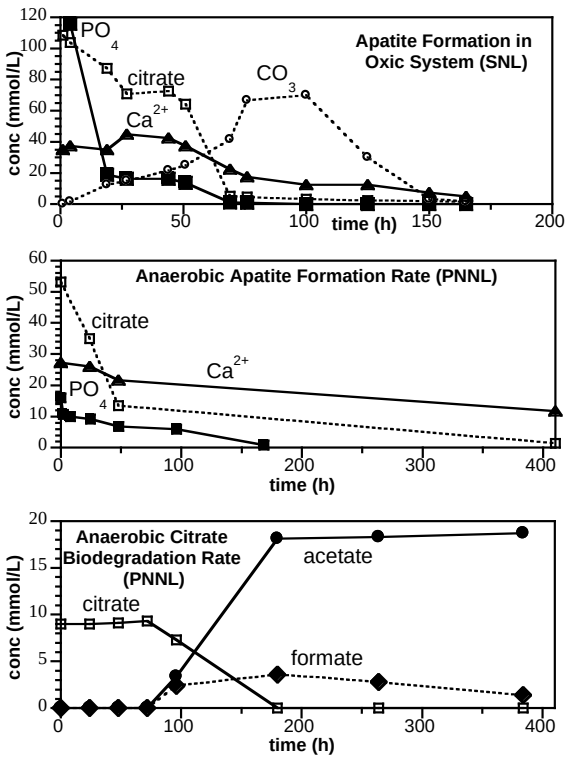

Figure 2.1. Apatite precipitation rate and citrate biodegradation: a) precipitation rate in aerobic system (reported as CO_3); b) precipitation rate in anaerobic system; and c) citrate biodegradation in anaerobic system.

Citrate is biodegraded in oxic sediment to carbon dioxide (Figure 2.1a) within a week. In anaerobic systems (demonstrated to occur during injections, once dissolved oxygen is consumed) occurs at somewhat slower rates (Figure 2.1b, c). For the infiltration studies in this project, aerobic citrate biodegradation is expected to occur. Issues that are investigated include the influence of low water saturation (i.e., does citrate biodegradation decrease at very low water content), can citrate biodegradation during infiltration be predicted as the sediment microbial biomass changes with depth, and does apatite still form in these highly oxic systems with great excess CO_2, or do carbonates form, utilizing Ca and Sr. The spatial variations in microbial population and citrate mineralization at the 100-N site was investigated as a function of depth and location

in sediments from monitoring and injection wells along the Columbia River shoreline at the 100-N remediation site. The microbial population in sediment samples from three wells decreased with increasing depth (Figure 2.2). Populations per gram of sediment, reported as cell equivalents or colony forming units (cfu), decreased by 5 orders of magnitude in these wells and were higher in the Hanford formation than in the deeper Ringold Formation.

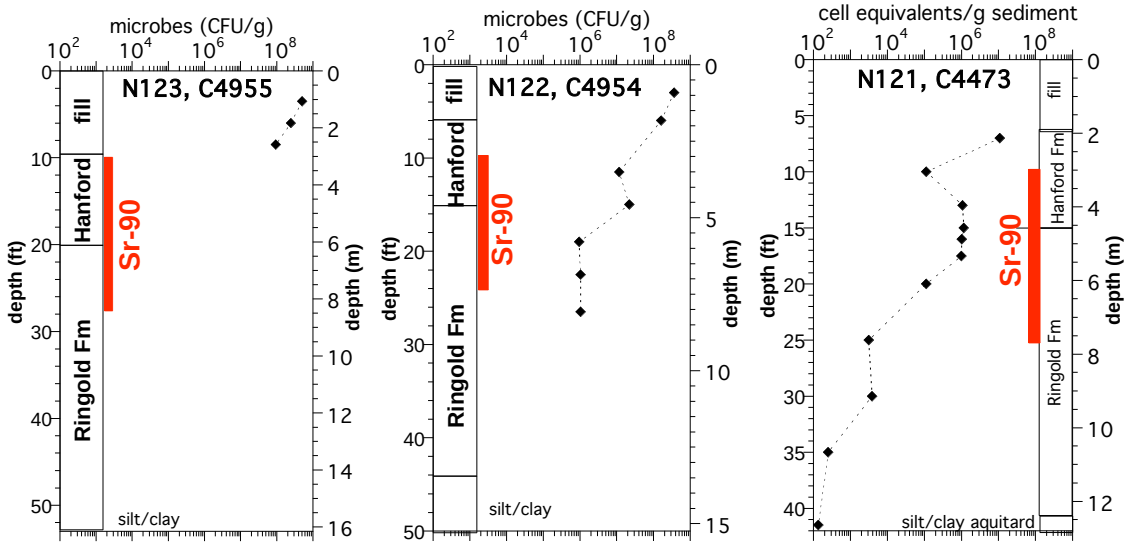

Figure 2.2. Microbial distribution with depth in 100-N wells.

2.2 Characterization of Apatite Precipitate

Previous studies have used multiple characterization techniques (Figure 1.6) to assess the crystal chemistry of the apatite formed by the microbial digestion of Ca-citrate in sediments (Moore et al. 2003, 2004). These techniques (and others) were used in this study to assess the apatite purity formed, the amount of organic carbon in the apatite (due to the presence of microbial biomass), inorganic carbon, and the mass of apatite in sediment (generally present at low concentrations). Previous studies used high-resolution transmission electron microscopy (HRTEM) and X-ray powder diffraction (XRD) to assess apatite crystallinity and to document the transformation from an amorphous calcium phosphate to nanocrystalline apatite. Energy dispersive (EDS) and Fourier transform infrared (FTIR) spectroscopy were used to analyze the chemical constituents. Blade-like apatite crystals in an amorphous matrix were ~0.1µm in size (Figure 2.3a, upper left). This was consistent with the observed broad overlapping peaks in the XRD pattern at 2 microns of ~32°, a typical characteristic of poorly crystallized apatite (Figure 2.3b, upper right; Waychunas 1989; Nancollas and Mohan 1970; Hughes and Rakovan 2002). The remaining peaks in the XRD correspond to components of the sediment. FTIR spectra are given for pure hydroxyapatite (top spectrum) produced by precipitation and heat treatment at 700°C and calcium phosphate precipitates in the Hanford 100-N sediment after one month (bottom spectrum). The lower resolution of the PO_4^- bands confirms the lower crystallinity of the sample, as observed by both HRTEM and XRD. The bands at 1455 cm^{-1} and

879 cm^{-1} indicate the presence of carbonate in the apatite structure. The TEM-EDS spectrum identifies calcium and phosphate as the major components with a stoichiometric apatite ratio of ~5:3.

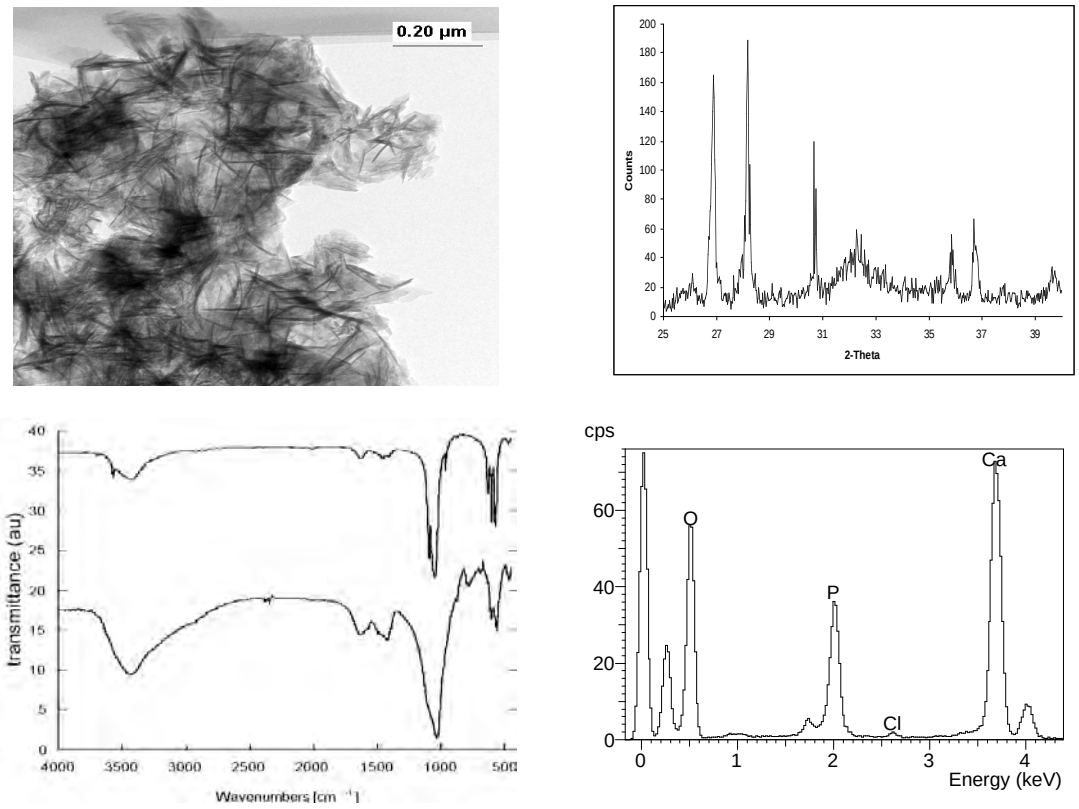

Figure 2.3. Characterization of nanocrystalline apatite formed in Hanford sediment by microbially mitigated Ca-citrate degradation in the presence of aqueous phosphorous: a) TEM, b) XRD, c) FTIR, and d) EDS.

2.3 Mass of Apatite Needed for Hanford 100-N Area

Two factors control the amount of apatite needed to sequester Sr-90 in the Hanford 100-N Area: Sr-90 uptake per amount of precipitate, and the rate of Sr-90 uptake must exceed the natural flux rate toward the river (Szecsody et al. 2007). First, from a mass balance (equilibrium) perspective, a specific amount of apatite is needed that will remove all Sr and Sr-90 from groundwater over the next 300 years (i.e., 10 half-lives of Sr-90 decay, half-life 29.1 years). This calculation is dependent on the crystal substitution of Sr for Ca in apatite. If 10% substitution is assumed (easily achieved in laboratory experiments), then 1.7 mg of apatite/g of sediment is sufficient to sequester Sr and Sr-90 from the estimated 3300 pore volumes of water that will flow through an apatite-laden zone. This calculation assumes an average groundwater flow rate of 0.3 m/day and a 10-m thick apatite-laden barrier. The 1.7-mg apatite/g of sediment does occupy some pore space in the aquifer, which has an average field porosity of 20%. Given a crystal lattice dimensions of 9.3 A by 6.89 A (i.e., assume a cylinder of dimensions 7.5E-21 cm^3/atom), the 1.7-mg apatite/g sediment would occupy 13.6% of the 20% pore space, so there should be some decrease in permeability.

The second factor that would control the amount of apatite needed to sequester Sr-90 is the rate of incorporation. This permeable reactive barrier concept of apatite solids in the aquifer works only if the flux rate of Sr and Sr-90 in the aquifer is slower than the removal rate of Sr and Sr-90 by apatite. If the groundwater flow rate is too high, even highly sorbing Sr and Sr-90 could advect through the apatite-laden zone more quickly than it is removed. The way to circumvent this issue is to have additional apatite in the groundwater system (upgradient) to essentially remove Sr-90 at an increased rate. Based on the experience in the 100-D Area where partially reduced sediment is slowly removing chromate (and nitrate), seasonal fluctuations in the river level lead to specific times of year when flow in the aquifer exceeds the chromate removal rate of the reduced sediment. Therefore, numerous experiments have been conducted in this study to clearly define the rate at which Sr and Sr-90 is incorporated into the crystal structure of apatite. Sr-90 migration in unsaturated sediments moves at a slower rate than in the aquifer. A worst-case scenario is when the vadose zone is entirely water saturated, which does occur during floods. Therefore, use of the 3.4-mg apatite/g sediment (i.e., value needed for water-saturated conditions) is a conservative estimate. In order to predict the average and transient advection of Sr-90 in the vadose zone sediments, simulations of the 100-N Area would need to be conducted that include river levels for decades.

Because Sr and Sr-90 interact with apatite by two processes (sorption by ion exchange and incorporation into apatite), the effect of addition of a small amount of apatite to sediment and the subsequent change in both sorption and incorporation can be calculated (Table 2.1). These calculations assume no Sr/Sr-90 is incorporated into apatite during the initial precipitation (experiments show 25% to 40% is incorporated). The possibility of Sr incorporation slowing at long time periods was investigated by measuring Sr with depth in apatite (Section 4.3.3.3).

Table 2.1. Apatite mass and change in Sr-90 mobilization.

System	Injected PO_4 (mM)	g apatite/ g sediment	Predicted[(a)] Sr-90 (pCi/L) w/sorption only	Predicted[(a)] Sr-90 (pCi/L) w/incorporation
Groundwater	0.0	0.0	1000	1000
Field inj. #1, #2	2.4	9.0E-05	999	165
Field inj. #3-10	10	3.8E-04	974	44
Max. infiltration	60	2.3E-03	825	7
300-year capacity	90	3.4E-03	767	4

(a) Assumptions: 1000 pCi/L initially in groundwater, K_d (Sr, sediment) = 25 cm^3/g, K_d (Sr, apatite) = 1370 cm^3/g, 10% Sr substitution for Ca in apatite.

What these calculations show is that even though the Sr sorption to apatite is very high (K_d = 1370 cm^3/g), because the mass of apatite is so small (as precipitate in pore space of sediment), the resulting sorption of Sr and Sr-90 onto apatite/sediment is small. The net effect is that right after apatite is placed in sediment (i.e., weeks), there will be little observed decreased in the Sr-90. Over the time scale of months, however, Sr and Sr-90 are slowly removed, and the amount of incorporation (10% crystal substitution of Sr for Ca in apatite is assumed in these

calculations) is fairly significant. Even the 2.4-mM of PO_4 injected in field injections #1 and #2 should eventually result in an 8-time decrease in the Sr-90 concentration (after 6 to 12 months). This small amount of apatite will be exhausted after a few years, so additional apatite is needed. A sequential low concentration injection followed by a 6- to 12-month wait period, then one or more high concentration injections are proposed for injection treatments. The purpose of these injections is to emplace sufficient apatite for 300 years of capacity, but minimize the initial desorption of Sr-90 in the injection zone. A similar method is proposed for the vadose zone to minimize Sr-90 downward migration, although the underlying water-saturated zone will already contain some apatite precipitate.

2.4 Sr and Sr-90 Incorporation Rate into Apatite

Because Sr^{2+} and Sr-90 behave essentially the same as Ca^{2+}, some Sr and Sr-90 is incorporated in apatite during the initial precipitation. Thermodynamically strontiapatite [$Sr_{10}(PO_4)_6(OH)_2$, $K_{sp} = 10^{-51}$] and mixed phases are favored relative to hydroxyapatite [$Ca_{10}(PO_4)_6(OH)_2$ $K_{sp} = 10^{-44}$]. However, the more rapid the apatite precipitation is, the Ca/Sr ratio in the crystalline structure will increasingly reflect the Ca/Sr ratio in the solution. Therefore, while it is relatively easy to make 40% Sr-substituted apatite from a solution containing 40% Sr, Hanford groundwater Ca/Sr ratio is 220:1, limiting the amount of Sr in the precipitate. Results in this report show that the amount of Sr substitution into apatite during the initial precipitation is far greater than 0.4% (1/220), and is generally in the 30% to 40% range, so reflects the influence of thermodynamics on the slow precipitation.

Once solid-phase apatite is precipitated, Sr and Sr-90 will additionally be incorporated into the apatite structure by solid-phase dissolution/recrystallization, as described below. The initial step in this process is Sr and Sr-90 sorption to the apatite surface. Results in this study show this sorption is quite strong ($K_d = 1370 \pm 439$ L/Kg) or 55 times stronger affinity than to sediment ($K_d = 24.8 \pm 0.4$ L/Kg). The rate of metal incorporation into the apatite crystal lattice can be relatively slow, on the order of days to years (LeGeros et al. 1979; Vukovic et al. 1998; Moore 2003, 2005). While there have been a number of studies of this Sr-substitution rate into apatite (Hill et al. 2004; Lazic and Vukovic 1991; Raicevic et al. 1996; Heslop et al. 2005; Koutsoukos and Nancollas 1981), geochemical conditions differ from the application in groundwater at the Hanford 100-N Area. However, in the presence of soluble phosphates, apatite acts as a seed crystal for the precipitation of metal phosphates (Vukovic et al. 1998). Homogeneous nucleation (precipitation directly from solution) will generally not occur except at very high metal concentrations, for example, greater than 10 parts per million (ppm). However, at low concentrations of the substituting cation (such as calcium) and in the presence of small amounts of phosphate and a seed crystal of apatite, heterogeneous nucleation occurs on the surface of the apatite seed crystal (Lower et al. 1998). The apatite itself serves as a small, but sufficient source of phosphate to solution, and thus perpetuates the precipitation reaction. Over time, the precipitated metals are sequestered into the apatite crystal matrix. The mechanism (solid-state ion exchange) of Sr substitution for Ca in the apatite structure has been previously studied at elevated temperature (Rendon-Angeles et al. 2000), but low temperature aqueous rates under Hanford groundwater conditions (i.e., Ca/Sr of 220/1) have not.

The amount of Sr-90 incorporation into solid-phase apatite has been characterized in previous studies by a variety of methods. The most reliable types of studies that prove the phenomena use pure apatite in a solution containing a specific Sr concentration, and the apatite solid phase is analyzed for percent Sr substitution by: a) dissolution and aqueous Sr or Sr-90 analysis, or b) electron microprobe with EDS or elemental detection of Sr. Analysis of the remaining Sr and Sr-90 aqueous concentration in a apatite/water system is insufficient to determine if Sr/Sr-90 has been incorporated into apatite. However, if the Sr/Sr-90 aqueous concentration, and ion exchangeable Sr concentrations are analyzed, then the remaining Sr/Sr-90 must be incorporated into the apatite structure.

Therefore, sequential extractions of selected chemical extraction were used to remove ion exchangeable Sr-90, organic-bound Sr-90, carbonate-bound Sr-90, and remaining (residual) Sr-90. Both Sr and Sr-90 were analyzed in extractions to determine if the Sr was retained differently from the Sr-90. It was expected that Sr was geologically incorporated into many different sediment minerals (Belousova et al. 2002), so should be more difficult to remove compared with Sr-90, which was recently added to the systems. The ion-exchangeable extraction consisted of the addition of 0.5 M KNO_3 to the sediment sample for 16 hours (Amrhein and Suarez 1990). The organic-bound extraction conducted after the ion-exchangeable extraction consisted of 0.5 M NaOH for 16 hours (Sposito et al. 1982). The carbonate-bound extraction conducted after the organic-bound extraction consisted of the addition of 0.05 M Na_3EDTA for 6 hours (Sposito et al. 1983a, 1983b; Steefel 2004). The residual extraction conducted after the carbonate-bound extraction consisted of the addition of 4 M HNO_3 at 80°C for 16 hours (Sposito et al. 1983a, 1983b). Apatite dissolution rates are highest at low pH (Chairat et al. 2004), so this extraction is expected to remove Sr-90 that is incorporated into the apatite.

2.5 Sr-90 Initial Mobilization and Sequential Injection Strategy

Because ~90% of the Sr and Sr-90 in the Hanford 100-N Area sediments is held by ion exchange, any solution that is injected into the aquifer (or infiltrating into the vadose zone) that has a higher ionic strength relative to groundwater (11.5 mM) and/or proportionally higher percentage of divalent cations will cause Sr and Sr-90 to desorb from sediments. At 100-N Area, pH (~7.8), Sr K_d value is ~15 L/Kg, or an approximate retardation factor of 125 (i.e., ~99% of the Sr and Sr-90 mass is sorbed). Injection of a low concentration of the Ca-citrate-PO_4 (4, 10, 2.4) solution results in a ~10 times increase in Sr and Sr-90 aqueous concentration. Injection of a much higher concentration Ca-citrate-PO_4 (40, 100, 24) solution results is >50 times increase in Sr and Sr-90 aqueous concentration. Injection of a Ca-citrate-PO_4 solution at the field scale will mobilize some Sr and Sr-90 in the injection zone (~3% of the sorbed Sr-90 mass for a low Ca-citrate-PO_4 concentration injection), and less Sr-90 for the zone that the spent solution migrates through. The injection/infiltration solution has been modified over time to be Ca-poor in order to minimize the initial Sr-90 mobilization and utilize some Ca^{2+} and Sr^{2+} held on sediments by ion exchange for the initial apatite precipitation (Szecsody et al. 2007, 2008). The final high concentration injection solution used (3.6 mM Ca, 9 mM citrate, 40 mM PO_4) contains <5% of the Ca^{2+} needed for apatite precipitation. Preliminary results of high concentration injections have shown ~10 times increase in Sr-90 aqueous concentration (maximum), which is considerably less than the >50 times increase in Sr-90 using a stoichiometric ration of Ca/PO_4 in laboratory experiments (Szecsody et al. 2007). As described in an earlier section, a total mass of

~1.7 mg apatite per gram of sediment is needed (assuming 10% Sr substitution for Ca in apatite) to sequester Sr-90 for 300 years (i.e., ~10 half-lives of the Sr-90 decay with a half-life of 29.1 years). This mass of apatite is equivalent to injections totaling 90 mM PO_4.

In order to emplace the total amount of phosphate needed to achieve sufficient Sr-90 sequestration capacity and minimize Sr-90 mobilization during the injections, a sequential injection/infiltration strategy was developed. Infiltration of a low concentration of the Ca-citrate-PO_4 (1, 2.5, 10, see Table 3.1) solution will cause a small increase in the Sr and Sr-90 during the weeks of emplacement (~5 times increase in aqueous concentration). Over the time scale of 6 to 12 months, most of the Sr-90 in the precipitate zone will be incorporated into the apatite structure. Note that this relatively low concentration infiltration has some capacity to incorporate Sr-90, but insufficient capacity to sequester Sr-90 that is upgradient of this apatite-laden zone that is slowly migrating toward the river over the next 300 years. After the time interval to sequester the local Sr-90 in the injection zone, then one or more higher concentration Ca-citrate-PO_4 (1, 25, 100, for example) can be infiltrated with minimal Sr-90 mobilization. These sequential experiments have been successfully conducted in the laboratory in water-saturated systems (Szecsody et al. 2007), and are reported in this study for infiltration systems.

3.0 Experimental and Modeling Methods

3.1 Task 1 – Apatite Formation at Low Water Saturation

This technology uses a Ca-citrate-PO_4 solution that does not precipitate until the citrate is biodegraded. The composition of this solution has changed over time, reflecting: a) increasing utilization of available Ca^{2+} from groundwater (and on ion-exchange sites) rather than injecting all the Ca^{2+} needed, and b) minimizing Sr and Sr-90 ion-exchange release from sediment upon injection. Initially, the solution composition did not reflect utilization of Ca^{2+} from groundwater or ion-exchange sites, so the infiltrating solution (Table 3.1) utilized a higher concentration of calcium chloride [$CaCl_2*2H_2O$] and trisodium citrate [$HOC(COONa)(CH_2COONa)_2*2H_2O$] compared to later injections. When combined, the solution at this low concentration is stable for days, depending on whether microbes are present in the makeup water (i.e., citrate biodegrades).

The citrate biodegradation rate can be assessed by measurements of aqueous citrate, calcium, and phosphate concentrations (reactants) or products carbon dioxide (oxic system) or organic acids acetate and formate (anaerobic system). Measurement of aqueous species at low water saturation is problematic, so citrate biodegradation rates were assessed by measurements of carbon dioxide formation using ^{14}C-labeled citrate. These gas-phase samplers cause minimal disturbance to experiments at differing water saturations. For these batch experiments, water saturations of 100%, 90%, 80%, 60%, 40%, and 20% were used. It should be noted that in preliminary infiltration simulations, water saturations of 60% or greater were generally observed in the apatite-forming solution infiltration area, so it is expected that higher water saturations are more applicable to field-scale infiltration. These citrate biodegradation rate experiments were assessed at 15ºC and 25ºC to be able to predict biodegradation rates that should be observed over the small temperature range expected in the field (14ºC to 17ºC, and possibly as high as 21ºC in late summer for near-shore sediments). In these batch experiments, 0.25-mL tubes containing 1 M NaOH were used as carbon dioxide traps. These traps were periodically sampled and refilled over time (to 1000 hours) to measure the rate of carbon dioxide production from the citrate biodegradation. The carbon dioxide was measured by liquid scintillation counting.

Citrate biodegradation experiments were additionally conducted with sediments of known microbial biomass (Figure 2.2), so that biodegradation rates can be quantified at different biomass concentration. Because previous studies have shown that the biomineralization rate of citrate is more uniform that expected based on only the in situ microbial biomass, additional experiments were conducted to assess the influence of microbial transport of in situ and injected biomass, and assess the relative contribution of in situ and injected microbes. This involved a set of five 30-ft long 1-D columns in which the Ca-citrate-PO_4 solution was injected to reach only to 20 ft in the column, then the column was taken apart to collect samples for phosphate analysis and biomass analysis (by acrodyne orange direct counts [AODC], phospholipids fatty acid [PLFA], and polymerase chain reaction [PCR]/DNA). Microbes can be detached from sediment and transported in response to shear forces (i.e., the velocity of injection shearing microbes off the surface) and in response to the higher ionic strength of the injecting solution. Both of these processes (shear and high ionic-strength solutions) are used to detach microbes for sediment samples. The baseline microbial transport experiment was a Ca-citrate-PO_4 (40 mM PO_4) solution injection (Table 3.1, proportions of field injection #3) over 24 hours, with live in situ microbes and unfiltered river water used for the solution (i.e., live injected microbial population).

The influence of shear to advect microbes was addressed by the comparison of this baseline experiment to a second injection experiment in which the same solution was injected over a 2-hour period (i.e., 10 times the injection rate). The influence of ionic strength to advect in situ and injected microbes was addressed by comparison of the baseline experiment to a third injection experiment with a low concentration Ca-citrate-PO_4 (4 mM PO_4). The relative influence of in situ and injected microbes on biodegrading the citrate and precipitating apatite were addressed by comparison of biomass and apatite distribution in the baseline experiment to a fourth experiment in which the injected water was 0.2 μm filtered (i.e., no injected microbes; live in situ microbes), and comparison to a fifth experiment in which the same solution (with unfiltered river water) was injected into sediment that was autoclaved to kill all the in situ microbes.

Table 3.1. Composition of Ca-citrate-PO_4 solutions utilized for field injections.

Name (conc in mmol/L)	Composition[(a)]	pH	Max. Solubility[(b)]	Ionic str. (mM)	Field Use
Ca-citrate-PO_4 (4, 10, 2.4)	**Solution 1**: 4.0 mM calcium chloride 10 mM trisodium citrate **Solution 2**: 2.0 mM disodium phosphate 0.4 mM sodium phosphate 1.0 mM ammonium nitrate	7.5 ± 0.1	 56 mM 140 mM 480 mM 200 mM	99.5	Field injection #1
Ca-citrate-PO_4 (2, 5, 2.4)	**Solution 1**: 2.0 mM calcium chloride 5.0 mM trisodium citrate **Solution 2**: 2.4 mM diammonium phosphate 1.0 mM sodium bromide	8.0 ± 0.1	 40 mM 100 mM 480 mM 200 mM	60.7	Field injection #2
Ca-citrate-PO_4 (1, 2.5, 10)	**Solution 1**: 1.0 mM calcium chloride 2.5 mM trisodium citrate **Solution 2**: 8.1 mM disodium phosphate 1.4 mM sodium phosphate 0.5 mM diammonium phosphate 1.0 mM sodium bromide	7.8± 0.1	 48 mM 120 mM 526 mM 91 mM 32 mM 65 mM	84.5	Low concentration injections in 2007
Ca-citrate-PO_4 (3.6, 9, 40)	**Solution 1**: 3.6 mM calcium chloride 9.0 mM trisodium citrate **Solution 2**: 32.4 mM disodium phosphate 5.6 mM sodium phosphate 2.0 mM diammonium phosphate 1.0 mM sodium bromide	7.8± 0.1	 48 mM 120 mM 526 mM 91 mM 32 mM 65 mM	293	High concentration injections in 2008
100-N groundwater	1.3 mM Ca, 0.2 mM K, 0.54 mM Mg, 1.1 mM Na, 0.60 mM Cl, 0.69 mM SO_4, 2.72 mM HCO_3	7.7-8.3		11.5	

(a) Concentrations listed are for the final mix of solutions 1 + 2.
(b) Tested solubility in complete solution.

The process of apatite precipitation using Ca-citrate-PO_4 solutions involves contacting the solution with sediment so that: a) microbes in the sediment biodegrade the citrate by a fermentation process, and b) the slow release of Ca from the citrate complex results in slow precipitation of apatite. Citric acid is utilized by many organic systems as part of the TCA (Krebs) photosynthetic process (Figure 3.1), where the citrate (a C6 organic acid) is converted to C6, C5, and C4 organic acids producing CO_2 and H^+, then cycled from oxaloacetic acid (C4) to citric acid (Bailey and Ollis 1986). Citrate can also be further degraded to acetic acid (C2), formaldehyde, formic acid (C1) and CO_2. For the purpose of this study, citrate is used to complex Ca, so only the decrease in citrate concentration (by biodegradation) is of significance, as the lower molecular weight organic acids only form weak complexes with Ca. Citrate ferments to form acetate and formate as has been observed in unamended sediments from the Hanford Site and in these same sediments amended with a known citrate-fermenting microorganism (see Section 4.0). A lag time of about 3 days prior to fermentation was observed in the unamended sediments likely due to low initial populations of microorganisms. While acetate and formate are the primary fermentation products, the amended sediments showed small amounts of lactate and propionate produced in addition to the acetate and formate. In these experiments, citrate fermentation followed the reaction stoichiometry shown in Eq. (3.1).

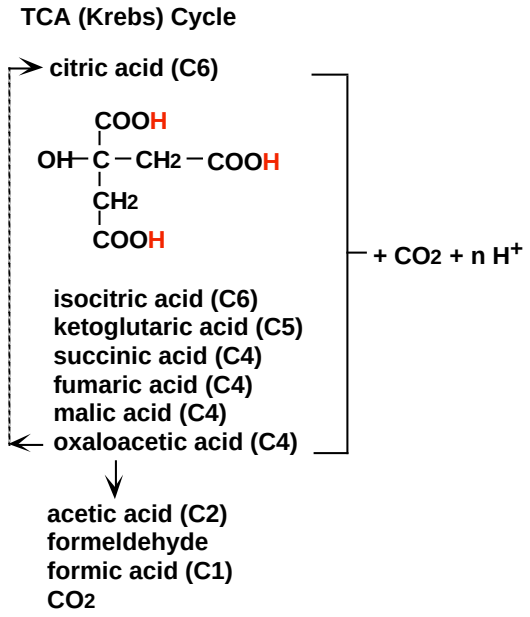

Figure 3.1. Biodegradation pathway for citrate.

$$C_6H_8O_7 + H_2O + OH^- \rightarrow 2C_2H_4O_2 + CH_2O_2 + HCO_3^- \qquad (3.1)$$

Biomass in the pre-test unamended sediment sample was 1.51×10^5 cells/g-soil and an average of 2.25×10^8 cells/g-soil after the 16-day incubation period. Using a generic cell formula of $C_5H_7O_2N$, the molecular weight of cells is 113 mg/mmole. These anaerobic citrate biodegradation experiments show that 73% of the carbon from citrate can be accounted for in formate and acetate, and it is likely that the other 25% is carbon dioxide, as shown in Eq. (3.1).

Initial Ca-citrate-PO_4 experiments were conducted in batch systems, and various aqueous species concentrations were measured (i.e., citrate, degradation products, PO_4, Ca, etc.). This type of data is predominantly used to determine the rate of citrate biodegradation, which is approximately equal to the rate of apatite precipitate formation (although apatite precipitate is not measured in this type of experiment). These experiments typically consisted of 10 to 100 mL of water mixed with 1 to 60 g of 100-N sediment, and the reaction pathway followed for 1 to 2 weeks by periodic sampling of the aqueous solution (Moore et al. 2007).

Solution stability experiments involved mixing high concentrations of solutions (Table 3.1), and quantifying the composition of the precipitate. In most cases, Ca-citrate precipitated out of solution (as measured by FTIR), as the solution was slightly over saturated. Laboratory solutions

made up with deionized water and aseptically filtered with a 0.1-μm filter to remove most microbes remained stable the longest. However, other solution stability experiments were conducted with groundwater and river water, as these occur during field-scale injections. The Hanford 100-N groundwater contains ~10^5 cfu/mL and the river water contains ~10^7 cfu/mL, so Ca-citrate-PO_4 solutions in most cases degraded within 24 to 48 hours, with measured loss of citrate and PO_4 (due to precipitation). For this reason (i.e., citrate degradation if the solution contains microbes), the concentrated chemicals are mixed with river water and injected into the well within minutes (i.e., continuously over the 8- to 60-hour injection periods).

Additional Ca-citrate-PO_4 batch experiments were conducted to measure the composition of the apatite precipitation. In the batch experiments described above where the solution is fully mixed with the sediment, the amount of precipitation is relatively small and difficult to measure both the quantity of precipitate and its composition. For example, a 2.4-mM PO_4 solution will result in 0.05 mg of apatite per gram of sediment (i.e., 0.005%), which is too small for XRD (0.5% or possibly as low as 0.1%). One approach used was to precipitate apatite from higher concentration solutions. A solution containing 28 mM PO_4 (maximum solubility of the Ca-citrate-PO_4 solution) would result in 0.56 mg apatite per gram of sediment (0.056%), assuming 100% of the aqueous PO_4 precipitates. Because only the microbes from the sediment are needed (if Ca from ion-exchange sites are not being utilized), an approach used to additionally concentrate the amount of apatite produced was to use a small amount of sediment (2 to 5 g) in a woven Teflon bag in 5 L of a high concentration apatite solution. This isolates the sediment from the precipitate, which can be dried and characterized. Due to the extremely low soil to solution ratio in these experiments, the citrate biodegradation rate was considerably slower (weeks).

3.2 Task 2 – 1-D Infiltration of Ca-Citrate-PO_4 Solutions

In this task, a series of 1-D unsaturated column experiments were conducted to assess rates at which apatite precipitation occurs with depth at varying Ca-citrate-PO_4 concentration. We hypothesize that uniform apatite precipitate distribution can be achieved at high solution concentration and high infiltration rates, but the kinetics of phosphate adsorption and microbial growth at low infiltration rates will limit the depth of apatite precipitate.

In the water-saturated zone during injection, high concentration (100 mM citrate) apatite solutions are 3% to 4% more dense than groundwater, so density effects (plume sinking) may be significant. In the unsaturated zone, density effects should be less significant due to the mitigating effects of capillarity. These studies move up in scale to idealized 1-D representation of field infiltration (beyond the batch studies in Task 1).

In this task, 1-D infiltration experiments were conducted at differing apatite solution concentrations ranging from 1 to 60 mM PO_4. These 1-D unsaturated column studies were conducted in conjunction with 1-D simulations conducted in Task 4 to design experiments and assess results. Column transport experiments were conducted at a fixed infiltration rate (steady flow), with measurement of Ca, PO_4, and citrate aqueous concentrations and the moisture content. The influence of heterogeneities were not investigated in 1-D columns, but were investigated in 2-D infiltration systems (Task 4) where a high-K zone and a low-K zone were included.

3.3 Apatite and Ca-PO_4 Solid-phase Characterization

Apatite characterization methods used included: a) XRD, b) electron microprobe analysis with EDS detector (purity of apatite formed), c) electron microprobe analysis with elemental detector (for Sr substitution in apatite), d) apatite dissolution in 0.5 M or 4 M nitric acid and aqueous PO_4 analysis (i.e., aqueous PO_4 extraction), e) surface area measurement by Brunauer-Emmett-Teller (BET) isotherm, f) inorganic carbon analysis (to determine if carbonate is present in the apatite), g) organic carbon analysis (to determine if microbial biomass is incorporated into the apatite), and h) fluorimetry for specific substituted apatites.

Aqueous PO_4 extraction experiments consisted of mixing 0.5 to 5.0 g of sediment (with or without precipitated apatite) with 5 mL of 0.5 M or 4 M HNO_3 and PO_4 analysis of samples taken at time intervals ranging from minutes to days. It was determined that the 100-N sediment (without added apatite precipitate) contains ~2.3 mg PO_4/g of sediment. Electron microprobe analysis does show some P in quartz-associated mineral grains, so these may be primary mineral phases. It was also noted that phosphoric acid was used in the 100-N trenches, so there may be some PO_4 associated with the waste. A 2.4-mM PO_4 solution would result in 0.05 mg apatite/g sediment or 0.028 mg PO_4/g of sediment. Because this represents only 1.2% of the PO_4 initially in the sediment, it is unlikely that it can be accurately measured. A 15-mM PO_4 solution would result in 0.315 mg apatite/g or 0.18 mg PO_4 g (7.8% of the PO_4 initially in the sediment). Finally, a total of 90 mM PO_4 solution would result in 1.65 mg apatite/g of sediment or 0.94 mg PO_4/g sediment (41% of the PO_4 initially in the sediment). This higher concentration can possibly be identified by this aqueous PO_4 extraction. Experiments conducted with the pure precipitated apatite showed that it dissolved in the 0.5 M HNO_3 by 10 minutes, whereas the PO_4 from the sediment took 1 to 4 hours to dissolve. Therefore, utilizing low acid concentrations and short extraction time increases the apatite precipitation identification.

Thin sections of sediment and sediment/apatite mixtures were prepared for the electron microprobe by mixing specific concentrations of apatite with sediment, then encasing the dried composite in epoxy and making a 10-micron-thick section. Microprobe analysis could identify extremely small concentrations of apatite. Typically a 2-mm by 2-mm section of the thin section was scanned with a 15-µm beam, 15-µm scan step, 120 x 120 grid (14,400 points) with 1000 milliseconds scan per point, for a total scan time of 30 hours per sample. With that relatively long scan time at each point, P could be detected at a concentration of 10 ppm within the 15-µm beam using elemental detectors. In addition to scanning for P, Mg and Ca were also measured.

A second method for measuring phosphate was acid extraction (0.5M NO3 for 15 minutes, described in Section 4.1.6) then aqueous PO_4 measurement (Hach 8178, Figure 3.2). This method was used because of the interference of citrate with the Hach 8114 method. This Hach 8178 method (also called Orthophosphate or Amino Acid Method) uses a different set of reagents and has to react for 10 minutes (instead of 3 minutes for Hach 8114). The range of this Hach 8178 is slightly smaller (0 to 30 mg/L) than the previous method, but the presence of citrate at the concentrations of interest do not interfere with the phosphate analysis.

At the PO_4 infiltration concentration of interest (2.4 mM to 40 mM, with citrate concentration of 2.5 mM), the presence of anything less than 20 mM citrate does not interfere with the analyzed

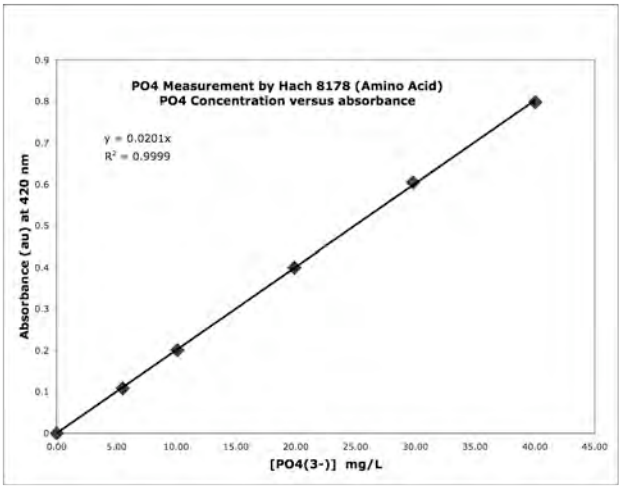

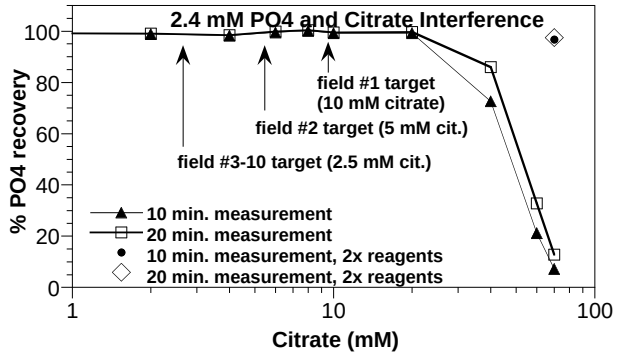

Figure 3.2. Hach 8178 PO_4 analysis (amino acid) of ultraviolet absorbance at 530 nm: a) without citrate present and b) with citrate present showing significant interference.

PO_4 concentration (Figure 3.2), so the method is suitable for the 5-mM citrate concentration of injection #2 and 10-mM citrate concentration of injection #1. At much greater citrate concentrations, the presence of citrate results in less apparent measurement of PO_4, possibly due to the amino acids complexing with citrate. If additional (2 times) amino acid reagents are added to a solution of 2.4 mM PO_4 and 80 mM citrate, then the PO_4 measurement is accurate.

3.4 Task 3 – Apatite Sr Capacity and Uptake Rate

In this Task, the uptake of Sr-90 into apatite will be characterized to determine: a) total mass of apatite precipitate needed to sequester Sr-90 for ~300 years (sufficient time for radioactive decay given the Sr-90 half-life of 29.1 years), and b) rate of Sr-90 uptake into the apatite structure. It is hypothesized that only a small amount of apatite is needed to sequester Sr-90 for 300 years, but that the rate at which apatite recrystallizes and incorporates Sr/Sr-90 will define the amount of apatite mass needed to be emplaced by infiltration. The capacity of apatite to uptake Sr/Sr-90 was determined experimentally. As described in the background section, some natural apatites have up to 11% substitution of Sr for Ca. Given 10% substitution, a total of 1.7 mg of apatite per gram of sediment is needed to sequester Sr and Sr-90 for 300 years. Given that the initial apatite precipitate is somewhat amorphous, and relatively pure Ca-apatite [$Ca_{10}(PO_4)_6(OH)_2$], the substitution approaching 10% Sr [$SrCa_9(PO_4)_6(OH)_2$] is thermodynamically favored given the higher solubility product of strontiapatite of 10^{-51} being 7 orders of magnitude less soluble than apatite (10^{-44}). The maximum amount of Sr substitution into Ca-apatite was verified experimentally with a long-term batch study with solid-phase apatite (only, no sediment) and a solution containing the proportions of cations found in Hanford 100-N groundwater (i.e., Ca/Sr ratio of 220/1) to demonstrate that Sr substitution under these conditions occurs.

The rate of Sr substitution into Ca-apatite was experimentally determined through a series of long-term batch studies at different temperatures (22ºC, 42ºC, 62ºC, and 82ºC) to be able to project the rate of Sr substitution that will occur under field conditions at 15ºC and determine the activation energy of the process. Low activation energies (<10 kJ/mol) would indicate the process is rate limited by diffusion, which could be increased by increasing the surface area (i.e.,

change the precipitation process to precipitate smaller crystals). Activation energies >15 kJ/mol would be indicative of a chemically controlled process. In these experiments, solid-phase apatite and mixtures of sediment and apatite will be used, with solid-phase sampling at period time intervals to 1 year with sequential extractions to determine the amount of Sr-90 substitution into the apatite.

Technical basis for apatite mass and 300-year longevity to sequester Sr-90:

1. 300 years of capacity is purely a function of the Sr-90 half-life (29.1 years), so 10+ half-lives would decay 99.90% of the Sr-90. Whether Sr-90 is held in the apatite or is inland from the Columbia River and does not reach the river, only 10% will remain after 100 years and <0.1% after 300 years.

2. Basis for number of pore volumes of water passing through the barrier for 300 years: pv/15-m thick barrier x 0.3 m/day (average groundwater flow) x 365.25 day/year x 300 years = 2191 pv.

   or roughly 2200 pore volumes of water traveling at 0.3 m/day (1 ft/day) average groundwater flow rate will pass through a 15-m (45-ft) thick barrier in 300 years.

3. Sr advection through the barrier in 300 years/2200 pore volumes: 0.2 mg Sr/L (average groundwater flow) or 2.0E-04 mg Sr/cm^3 x 2200 pore volumes = 0.44 mg Sr/cm^3 liquid.

4. Amount of apatite needed to sequester this amount of Sr: 0.44 mg Sr/cm^3 x 1/[44 g Sr/ 1004 g apatite (11% substitution of Sr for Ca)] = 10.01 mg apatite/cm^3 liquid.

5. Given the sediment field porosity (0.20 cm^3/cm^3) and dry bulk density (1.78 g/cm^3), the amount of apatite per gram of sediment is: 10.01 mg apatite/cm^3 liquid x 0.2 cm^3 liquid/cm^3 total x cm^3 total/1.78 g sediment = 1.12 mg apatite/g sediment.

6. Phosphate solution (mol/L) required to achieve 1.2 mg apatite/g sediment deposition mass: 10.01 mg apatite/cm^3 liquid x 1000 cm^3/L x g/1000 mg x mol apatite/1004 g apatite x 6 mol PO_4/mol apatite = 0.059 mol PO_4/L.

7. Volume considerations of apatite in the pore space: unit cell of apatite: a = 9.3A x c = 6.89 A.

   Assume cylinder (a/2)2*3.14*c = 7.488 x 10-21 cm^3/atom or 4509.6 cm^3/mol of apatite 1.7 mg apatite/g sed * mol/502 g * 1/1000 * 4509.6 cm^3/mol = 0.0153 cm^3/g sed. Give the dry bulk density and porosity: 1.78 $g/cm^3/0.2$ = 8.9 g/cm^3 pore space. Pore space occupied by apatite: 0.0153 cm^3 ap/g sed x 8.9 g sed/cm^3 pore space = 0.136
   …or 1.7 mg apatite/g sediment occupies 14% of the pore space (small, but likely some decrease in permeability).

8. The above pore volume calculation (b) is appropriate for groundwater flow (not vadose zone flow). Given the average annual precipitation at Hanford of 16 cm/year, the recharge rate (i.e., downward flux rate) is estimated at 0.1% to 2% (less with plant cover, more with coarse

surface sediment and no plants) based on multiple different techniques and studies at Hanford. Therefore, downward migration of Sr-90 in the vadose zone is very slow. However, the Sr-90 contamination zone that is being remediated is near the Columbia River, and this zone may be at low water saturation or be seasonally part of the unconfined aquifer. As such, the worst case for vadose zone treatment is that Sr-90 is migrating in groundwater (i.e., the vadose zone is water-saturated 100% of the time), so we are designing the same amount of precipitation in the vadose zone as in the saturated zone.

3.5 Major Cation/Anion and Radiochemical Analysis

Liquid scintillation counting was used for Sr-90, Sr-85, Ca-45, Na-22, and C-14 analysis. Inductively coupled plasma (ICP) was used for measurement of cations and ion chromatography for selected anions (citrate, phosphate, carbonate). In addition, a colormetric method was used for phosphate analysis for selected samples. For most radionuclides, counting was relatively straightforward, with a 0.1-mL to 1.0-mL sample mixed with scintillation fluid, and counting dependent on the activity of the sample (typically 10 minutes to 180 minutes per sample). Scintillation counting was performed using a Packard 2550 liquid scintillation counter with newly upgraded counting software. Quench for each sample was compared to a quench curve for each isotope. Typical background was 18 to 22 counts per minute/mL, and a typical experiment had 10,000 to 20,000 counts per minute/mL of the radionuclide added. Field sediments with field-contaminated Sr-90 contained lower counts.

Counting the activity of Sr-90 was slightly more complicated because Sr-90 (29.1-year half-life) decays to Y-90; Y-90 (64.1-hour half-life) decays far more rapidly to Zr-90. The result is that there is far more (4054 times) decay activity measured from the Y-90 decay than Sr-90 decay. Quantifying the Sr-90 concentration requires waiting (~30 days or ~10 half-lives of the Y-90 64.1 hours) after which time half of the activity measured is from Sr-90 and half from Y-90 decay. Simulations of Sr-90 and Y-90 radioactive decay with different starting proportions were conducted to examine the secular equilibrium wait time.

At secular equilibrium where half of the activity is from Sr-90 and half from Y-90, 99.97% of the mass is Sr-90 and 0.0252% is Y-90. Solutions (with no solids) should be at secular equilibrium, so can be counted immediately. In contrast, an experiment containing a Sr-90 solution and a solid phase (sediment, apatite) may not be at secular equilibrium initially due to preferential sorption of Y over Sr (which should take minutes to hours). However, after 30 days wait, aqueous samples taken from an experiment should also be at secular equilibrium. However, a solid-phase extraction (i.e., dissolving apatite with acid to extract the Sr-90) will likely not be at secular equilibrium. For all cases that contained >0.025% Y-90 initially, total activity decreases over time (~30 days; Figure 3.3). For one case containing no Y-90 initially (and cases containing <0.025% Y-90), total activity increases over time. Therefore, counting before 30 days, then at 30 days (with counts increasing or decreasing) is indicative of the solid-phase extraction conducted preferentially removing more or less Y-90 relative to Sr-90. Secular equilibrium is reached within 30 days for most cases (percent Y-90 from 0% to 10%, equilibrium is 0.0252%, Figure 3.3 a-d) likely to occur. A longer (1.5 to 2 months) period of time to reach secular equilibrium is needed for extreme cases containing >10% Y-90 (Figure 3.3 e-h).

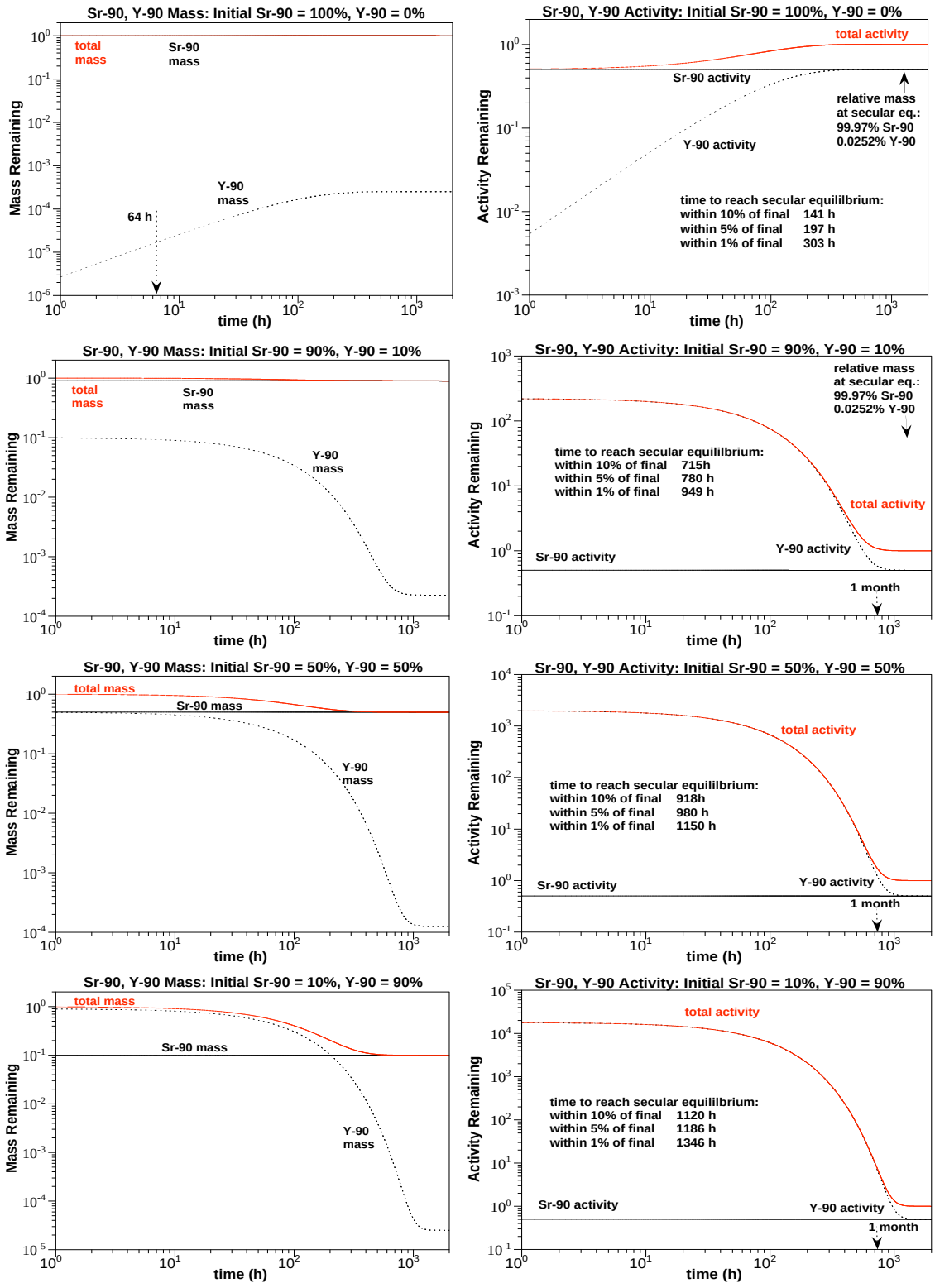

Figure 3.3. Sr-90 and Y-90 mass and activity for different initial Sr-90 and Y-90 activity: a) and b) 0% Y-90, c) and d) 10% Y-90, e) and f) 50% Y-90, and g) and h) 90% Y-90.

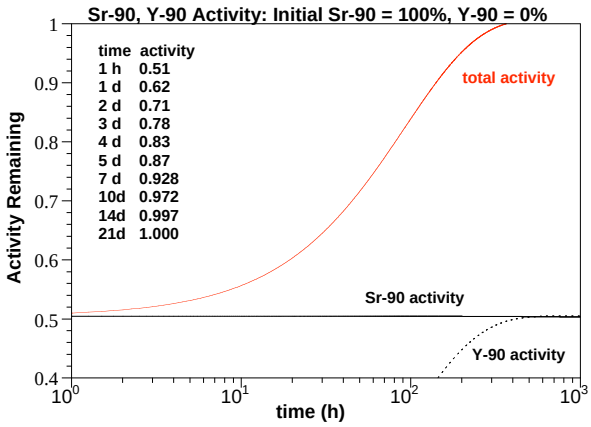

Figure 3.4. Sr-90 and Y-90 total activity with no initial Y-90 (linear activity scale).

Aqueous samples separated from sediment/water experiments in this study generally increased in activity over the 30 days, indicating Y-90 was preferentially sorbed to the sediments. Radiochemical analysis of extraction experiments in this study have typically found counts increasing over 30 to 40 days, which implies the sample was extracted deficient in Y-90 (<0.024%). However, for the most extreme case of 0% Y-90 initially, secular equilibrium is reached within 14 days (Figure 3.3b and Figure 3.4). Additional count increases observed for 30 to 40 days is suggestive of an experimental artifact. This issue is currently being investigated.

3.6 Task 4 – Simulation of Apatite-Forming Solution Infiltration

In this Task, the reactions controlling apatite-forming solution injection, citrate biodegradation, apatite precipitation, Sr/Ca/Na/Mg ion exchange, and Sr-90 slow incorporation into apatite structure were incorporated into the STOMP numerical model. Model parameters were calibrated using data from batch studies (Task 1 and 3) and 1-D infiltration column studies (Task 2). The model was used to assist in the design of 2-D experiments that determined the accuracy of the conceptual approach for emplacement of an apatite barrier by infiltration. Finally, the model was used to design the field-scale infiltration strategy. The reactions account for the observed increase in aqueous Sr-90 in groundwater during the first few hours of Ca-citrate-PO_4 injection (generally due to cation exchange reactions), subsequent citrate biodegradation, apatite formation, and Sr removal by precipitation with apatite. The reactions included: a) Sr, Ca, Mg, Na, K, NH_4 ion exchange; b) metal-OH, -CO_3, -PO_4, and -citrate aqueous speciation; c) citrate biodegradation; and d) solids apatite, $CaCO_3$, and $SrCO_3$, which was 42 reactions with 51 species. Selected simulations are included in this report.

A new reactive transport module, ECKECHEM, has recently been written for the STOMP simulator (White and Oostrom 2004). This module solves coupled equilibrium, component, and kinetic equations for chemical reactions. However, this module does not currently account for multicomponent ion-exchange processes. Ion exchange was incorporated into STOMP, as ion-exchange reactions will have a significant influence on the injection scheme. Ion-exchange reactions are important in this remediation strategy because: a) apatite precipitation depends on the stoichiometry of Ca and PO_4 available in the pore fluid, and b) Sr-90 desorption occurs as a result of the injection of a higher ionic strength. The apparent Sr-90 K_d decreases from 35 cm^3/g in groundwater to 2.5 with a high ionic-strength solution. To lessen the Sr-90 release into solution caused by high ionic-strength addition (i.e., the salt effect), infiltrations can be staged, with an initial injection of lower solution concentrations, which would also provide for more rapid citrate biodegradation (and ultimately better control of the apatite placement). With a 40-mM citrate injection, the Sr K_d = 13 cm^3/g, which results in a 2-time increase in Sr-90 groundwater concentration.

Designing the field-scale injection strategy (Task 4.3) was accomplished with a combination of experimental data (batch, 1-D, and 2-D) and simulations. While experimental data shows the combined effects of reactions in a specific flow field, these experimental systems are smaller in scale and typically do not incorporate natural heterogeneities found at the field scale. Simulations can be used to test the influence of a wide range of different infiltration parameters that could not all be tested experimentally. In addition, the influence of heterogeneities (randomly generated hydraulic conductivity field, for example) can be simulated to determine how significant heterogeneities are on infiltration. An idealized set of Sr-90 reactions were used in preliminary infiltration experiments to demonstrate the influence of: a) proper reactions, and b) physical and geochemical heterogeneities (Section 4.5.6). These simulations show that the level of geochemical reaction complexity and heterogeneity complexity change the timing and concentration of Sr-90 leaching from the system.

A smaller set of reactions was used in a reactive transport code (RAFT) to simulate the influence of long-term presence of apatite in sediment on the Sr-90 mobility (i.e., months to hundreds of years). Because the citrate reactions described above are relatively short term (i.e., hours to months), they were not included in these simulations. Simulations with this model approximate the long-term migration of Sr (and Sr-90) through the apatite-laden zone (i.e., as a permeable reactive barrier), with Sr ion exchange onto sediment, Sr ion exchange onto apatite, and Sr incorporation into apatite. A smaller set of cations was used for these simulations that included calcium, strontium, and sodium.

3.7 Task 5 – 2-D Infiltration of Ca-Citrate-PO_4 Solution

In this Task, the infiltration strategy for achieving a relatively uniform apatite precipitate was experimentally tested during 2-D infiltration at a 1.5-m scale. It was hypothesized that the residence time is the key factor that determines how uniform the apatite precipitate distribution that can be achieved from a Ca-citrate/phosphate infiltration. Therefore, control of the location of the Ca-citrate-PO_4 mass through change in the infiltration rate, solution concentration, and surface application method can be used to control the depth of apatite precipitate.

Initial 2-D infiltration experiments were conducted in homogenous sediment (Szecsody et al. 2008). In general, batch and 1-D infiltration experiments provided a basis for predicting solution infiltration and apatite precipitation distribution behavior in homogeneous systems, but do not incorporate lateral spreading, which slows the wetting front. The influence of the solution density (at high concentration) is pronounced during injection in a well, but should have little effect during infiltration, as the infiltration timing is largely controlled by capillary suction in the sediment. In addition, we expect there to be little effect of the amount of apatite precipitation on the flow field. In theory, the calculated maximum amount of apatite precipitate (1.7 mg/g of sediment) to achieve 300 years of capacity would occupy 15% of the pore space. This reduction in hydraulic conductivity where precipitate forms initially would, in theory, alter the flow field for subsequent fluid to regions of higher permeability. The net effect should be a more lateral spread of the infiltration profile with the hypothesized reduction in permeability directly beneath the infiltration location. However, we expect that this effect will be insignificant, especially compared with the influence of field-scale heterogeneities.

Because low-K and high-K heterogeneities were expected to influence the distribution of apatite precipitate that will occur, modification of the injection strategy (injection rate, variable solution concentration) was addressed with 2-D infiltration experiments into systems containing low-K and high-K heterogeneities. It was additionally hypothesized that Sr-90 would be present at a higher concentration in low-K layers in the 100-N Area vadose zone due to somewhat greater adsorption, lower advective flow (when the groundwater level is high), and higher residual water content. For the purpose of forming a precipitate barrier for Sr-90 sequestration, both unsaturated and water-saturated flow scenarios need to be considered in the Hanford formation. If the Hanford formation were to always be a vadose zone, then infiltration of the Ca-citrate-PO_4 solution into the heterogeneous porous media would, in general, result in greater apatite precipitate mass in finer grained porous media. Precipitation events driving Sr-90 held in the soil profile deeper would move more readily in this finer grained porous media, so the Sr-90 would be sequestered.

Experiments in this task will be conducted in a variety of 2-D system ranges to efficiently develop an infiltration strategy. A number of initial infiltration experiments were conducted in three non-instrumented systems: a) 38.3 cm wide by 55.8 cm high by 1.1 cm thick, b) 69.3 cm wide by 55.8 cm high by 1.1 cm thick, and c) 115.2 cm wide by 55.8 cm high by 1.1 cm thick. Generally, the solution was applied in a corner of the surface of the 2-D system so that vertical and lateral spread of the infiltrating plume. Because infiltration rates varied from 0.2 mL/hour to 150 mL/hour, the Ca-citrate-PO_4 solution made using river water would not be stable for more than a day due to the microbial population in the river water degrading the citrate. A multi-channel Kloehn syringe pump was used to mix river water, concentrated Ca-citrate, and concentrated Na-PO_4 (Table 2.1), then apply this solution at a fixed rate to the 2-D sediment system. A 50-µL to 1.25-mL syringe was used in the Kloehn syringe pump so that the hold time of the mixed solution was 2 to 12 minutes. Three larger infiltration systems were used for experiments containing heterogeneities: a) 140 cm wide by 40 cm high by 5.0 cm thick, b) 55.8 cm wide by 115.2 cm wide by 1.1 cm thick, and c) 122 cm wide by 244 cm high by 1.1 cm thick. Initial conditions for experiments varied from uniform water content (3% to 9% g water/g sediment) to initial water saturation drained to a water table near the bottom of the system. The general location of the waterfront was visually tracked from the increase in water content, although this was qualitative at best. At the end of each experiment, the 2-D systems were taken apart and 25 to 120 sediment samples were taken for measurement of water content, aqueous PO_4, and PO_4 precipitate.

A few 2-D infiltration experiments were conducted in a highly instrumented 2-D system in the Environmental Molecular Sciences Laboratory (EMSL) Subsurface Transport Laboratory. The 2-D system was 60 cm wide by 40 cm high by 5.0 cm thick. Both homogeneous and heterogeneous (low-K inclusion) experiments were conducted, and the water content was scanned using a dual-source gamma system. The water table in these systems was not static, but there was groundwater movement. The Ca, citrate, and phosphate concentrations was measured by collecting aqueous samples through small lysimeters during the experiment and by sediment samples taken at the end of the experiments.

4.0 Results

The objective of this project is to develop a method to emplace apatite precipitate in the 100-N vadose zone (Szecsody et al. 2008; Thompson et al. 2009), which results in sorption and ultimately incorporation of Sr-90 into the apatite structure. Sr-90 sequestration with this technology occurs by the following steps: 1) injection of Ca-PO_4-citrate solution (with a Ca-citrate solution complex, Moore et al. 2004, 2007), 2) in situ biodegradation of citrate resulting in apatite [$Ca_6(PO_4)_{10}(OH)_2$] precipitation (amorphous, then crystalline), 3) adsorption of Sr-90 to the apatite surface, 4) apatite recrystallization with Sr-90 substitution for Ca (permanent), and 5) radioactive decay of Sr-90 to Y-90 to non-radioactive Zr-90. Although this is a complicated process, field-scale evidence indicates the process is effective in the 100-N saturated zone. The Ca-citrate-PO_4 solution has been injected into the 100-N saturated zone at low (10 mM PO_4) and high (40 mM PO_4) concentration through a series of 16 wells (10 screened in the Hanford and Ringold formations and 6 screened only in the Ringold Formation). Phosphate extractions of sediments taken in March 2008 clearly showed evidence of the phosphate injections, with PO_4 (in mg PO_4/g sediment) averaging 0.102 ± 0.133 mg/g over the entire depth (7 to 26 ft), or 0.150 mg/g in the Hanford formation and 0.041 mg/g in the Ringold Formation. Barrier injection operations completed by the spring of 2008 using the low concentration formulation (10 mM PO_4) were designed to emplace 0.136 mg PO_4/g sediment, or 0.34 mg apatite/g of sediment. Therefore, PO_4 extraction data from post-treatment core samples indicates that, at a radial distance of ~15 feet from adjacent injection wells, the Hanford formation received an average treatment of 110% and the Ringold Formation received an average treatment of 30% of the targeted apatite content. The fraction Sr-90 that was ion exchangeable (of total Sr-90 in the sediment) in the treatment zone (i.e., field treatment with 10 mM PO_4) averaged 61.2 ± 22.4%. Untreated sediments from the 13-ft depth of N-122 showed 86.7% ion exchangeable Sr-90 (2005 results), so the current results indicate about 25% of the Sr-90 mass (i.e., 86.7% ion exchangeable pretreatment minus 61.2% ion exchangeable post low concentration treatment) in the 100-N sediment may have been incorporated into apatite and is not migrating in groundwater.

Prior to initiation of this project, precipitation of apatite from Ca-PO_4-citrate solution at low water saturation had not been tested. Concerns that include the rate at which citrate might biodegrade at low water saturation, the influence of the large decrease in microbial biomass with depth would have on predicting the citrate biodegradation rate, the formation of Ca-carbonates and not apatite (with the excess CO_2 generated from citrate biodegradation) are addressed in Task 1 results. The ability to control infiltration sufficiently to emplace apatite at a desired depth is addressed in 1-D infiltration in homogeneous sediment systems (Task 2 results) and in 2-D infiltration studies in homogeneous and heterogeneous sediments (Task 5 results). The long-term performance of the apatite precipitate depends on the continued incorporation of Sr-90 into the apatite structure for 300 years (i.e., ~10 half-lives of Sr-90 decay). A realistic amount of Sr substitution for Ca in the apatite structure (i.e., mass balance) that can be expected in Hanford groundwater (with 220 times more Ca to Sr) and the rate at which Sr is incorporated into apatite are quantified in Task 3 studies. Finally, a simulation tool of the biogeochemical processes during solution infiltration is developed (Task 4 results) in order to be able to predict processes in during field-scale infiltration.

4.1 Task 1 – Apatite Formation at Low Water Saturation

4.1.1 Citrate Biodegradation at Variable Water Saturation

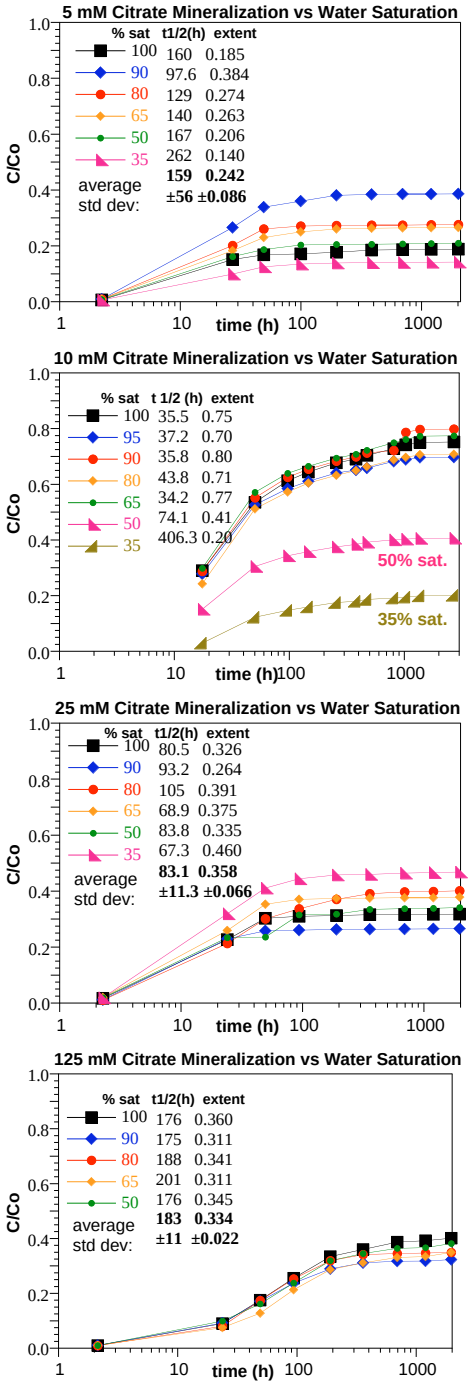

Figure 4.1. Citrate mineralization (CO_2 shown) at different water saturations with: a) 5 mM, b) 10 mM, c) 25 mM, and d) 125 mM citrate in Ca-citrate-PO_4 solutions.

Citric acid is utilized by many organic systems as part of the TCA (Krebs) photosynthetic process, where the citrate (a C6 organic acid, Figure 3.1) is converted to C6, C5, and C4 organic acids producing CO_2 and H+, then cycled from oxaloacetic acid (C4) to citric acid (Bailey and Ollis 1986). Citrate can also be further degraded to acetic acid (C2), formaldehyde, formic acid (C1), and CO_2. For the purpose of this study, citrate is used to complex Ca, so only the decrease in citrate concentration (by biodegradation) is of significance, as the lower molecular weight organic acids only form weak complexes with Ca.

Because the observed anaerobic citrate degradation produces (acetate and formate) could possibly interfere or hinder the formation of apatite, the extent of citrate mineralization in 100-N sediments was investigated over a range of conditions, including initial citrate concentrations, percent of sediment water saturation, sediment depth, and biomass. All experiments were performed under initially aerobic conditions.

Mineralization of ^{14}C-labeled citrate was examined over a range of initial citrate concentrations (5, 10, 25, and 125 mM) and percent water saturation of the composite 100-N sediment (35% to 100%) at 20°C to 22ºC (Figure 4.1). These Ca-citrate-PO_4 solutions contained the exact proportions of constituents to form citrate (i.e., Table 3.1, solutions similar to field injection #1).

In general, low concentration solutions (5 mM and 10 mM citrate) showed a decrease in the citrate mineralization rate at lower water content, whereas the highest concentration (125 mM citrate) showed no difference in the mineralization rate and extent with a difference in water content (Figure 4.2a). Preparation of the sediment included slow evaporation of water to reach a water content of 25%, then the slight addition of water (with the Ca-citrate-PO_4 solution) was conducted to achieve the desired concentration and water content. The 5, 25, and 125 mM citrate

experiments were done on the same batch of sediment (initial microbial biomass 2 x 10^7 cells/g) and the experiment at 10 mM citrate was conducted with a higher initial microbial biomass (3 x 10^8 cells/g), which accounts for the differing results. The mineralization extent was generally lower at low water content (<20%, Figure 4.2b), and mineralization did not vary a significant amount with a wide range of water content and citrate concentration. The single most significant factor that changed the citrate mineralization rate and extent was the initial microbial biomass concentration; 10 times higher biomass resulted in ~4 times more rapid mineralization rate and 2 times greater mineralization extent. Although these batch results are indicative of the significance of microbial biomass, additional processes of microbial transport/redistribution and infiltration of river water microbes increase the complexity of the citrate biodegradation rate, as described in Sections 4.1.2 and 4.2.3.

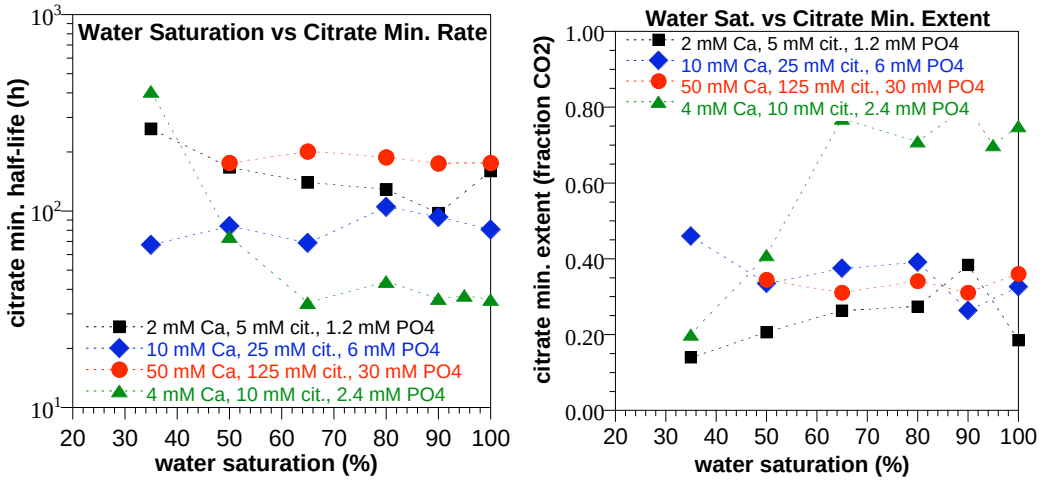

Figure 4.2. Correlation of water saturation and citrate mineralization half-life (a) and extent (b).

4.1.2 Citrate Biodegradation and Microbial Biomass

The spatial variations in microbial population and citrate mineralization at the 100-N site was investigated as a function of depth and location in sediments from monitoring and injection wells along the Columbia River shoreline at the 100-N remediation site (Figure 2.2) in a previous Fluor-funded 100-N study. The microbial population in sediment samples from three wells decreased with increasing depth (Figure 2.2). Populations per gram of sediment, reported as cell equivalents or colony forming units (cfu), decreased by 5 orders of magnitude with depth in these wells and were higher in the Hanford formation than in the deeper Ringold Formation.

Citrate mineralization was measured in suspensions of sediments taken from different depth intervals from these wells. Experiments were conducted with a Ca-citrate-PO_4 solution (2 mM, 5 mM, 2.4 mM) (Figure 4.3). The citrate mineralization rate showed a modest correlation (R = 0.52) with the microbial density (cfu/ml) measured in the sediment suspensions used in these experiments (Figure 4.4a), with generally slower rates (to 733 hours half-life) at very low populations and the highest rates (46 hours half-life) with higher microbial populations. The correlation of the mineralization half-life versus biomass (Figure 4.4a) shows that while biomass in sediments changed 5 orders of magnitude, the mineralization half-life only changed about 1 order of magnitude.

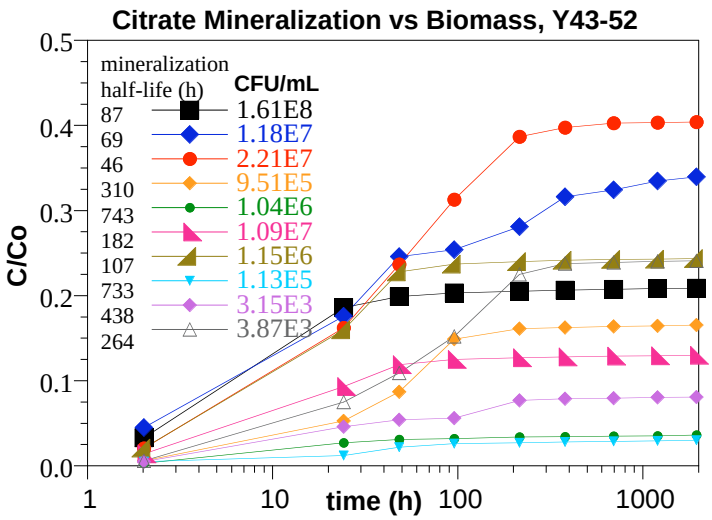

Figure 4.3. Citrate mineralization and biomass.

The extent of mineralization varied from 3% to 80% with an average of 23% with essentially no correlation of microbial biomass to mineralization extent (Figure 4.4b). The likely cause of the relative uniformity of the citrate biodegradation rate in sediments that varied 5 orders of magnitude in biomass is due to the activity of the microbes injected from the river water, and the redistribution of in situ and injected microbes during infiltration. In field injection experiments, 5% concentrated Ca-citrate-PO_4 chemicals (by volume) are injected with 95% river water (by volume). River water biomass measured in March 2006 was 2.2 x 10^6 cfu/mL (equivalent to 7.1 x 10^5 cfu/g), generally lower than the 10^6 to x 10^8 cfu/g measured in shallow sediment. As described in Section 4.2.3, river water microbes appear biodegrade citrate much more rapidly than in situ microbes, so the measurement of the microbial biomass (in situ versus river water) is insufficient to predict citrate biodegradation activity.

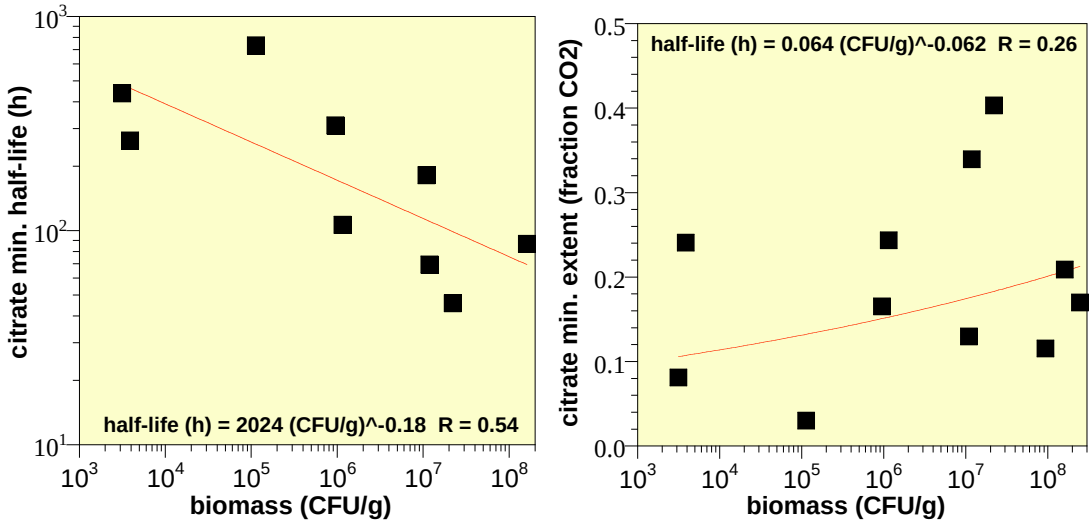

Figure 4.4. Sediment biomass relationship to citrate mineralization rate (a) and mineralization extent (b).

4.1.3 Citrate Biodegradation with Differing Ca-Citrate-PO_4 Concentration

Results of experiments from a separate Fluor-funded 100-N study quantifying the citrate degradation/mineralization rates as a function of Ca-citrate-PO_4 concentration and temperature were modeled in this study to quantify the activation energy and change in biodegradation rate with citrate concentration. Two different modeling approaches were considered to quantify

citrate biodegradation, a pseudo first-order model (Figure 4.4) and Monod model. A first-order model is an empirical approach that describes citrate removal with a single reaction rate coefficient. A Monod model is also an empirical approach that describes citrate removal externally to microbial organisms with a similar mathematical form of enzyme degradation (Michaelis-Menton kinetics, Bailey and Ollis 1986). Monod kinetics is utilized when the observed data clearly shows a considerable slowing of reaction rate at low concentration that cannot be accounted for using the simpler first-order kinetic model. Citrate biodegradation described by Monod kinetics:

$$\frac{d\,citrate}{dt} = -\frac{mu1}{y1} \cdot m \cdot \left[\frac{d}{kd1 + d}\right] \cdot \left[\frac{a1}{a1 + ka1}\right]$$

where mu1 is the degradation rate per microbe, m the biomass, y the yield, d is the concentration of electron donor (citrate), a is the concentration of the electron acceptor (oxygen in an oxic environment, citrate in a reducing environment), and kd and ka are half-saturation constants for the electron donor and acceptor. In general, biodegradation occurs at a specific rate, but at lower and lower concentrations, less of the enzyme systems in the microbe are able to utilize that substrate, so the overall rate decreases. The half-saturation constants are the concentration at which the rate is half the maximum concentration. If the half saturation constants are very small, the expression is reduced to a zero order model (rate is independent of concentration). A first order model:

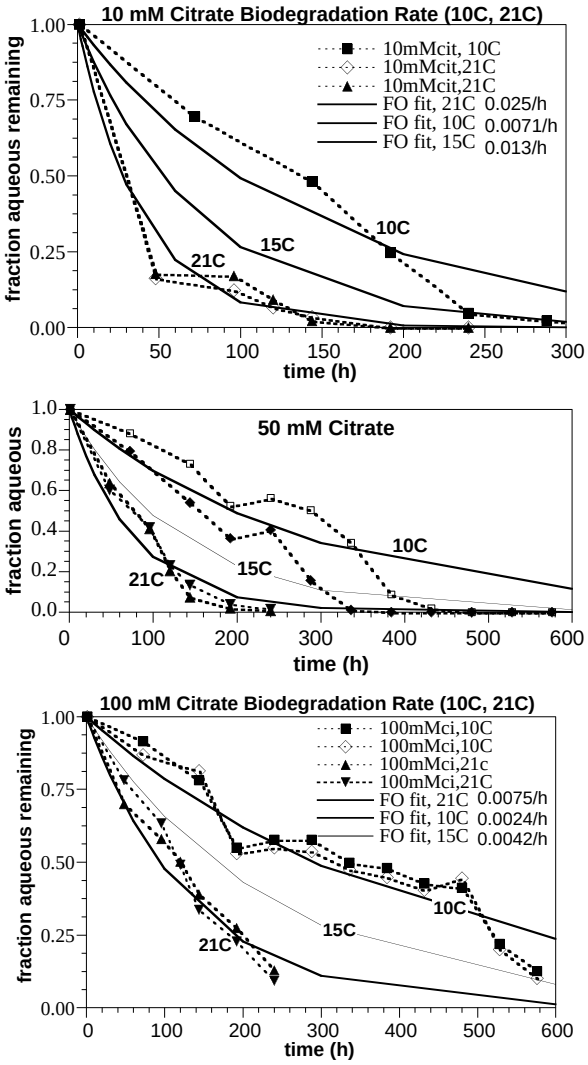

Figure 4.5. Citrate biodegradation by Hanford 100-N sediments verses temperature at: a) 10 mM citrate, b) 50 mM citrate, and c) 100 mM citrate concentration.

$$d\ citrate/dt = -k\ (citrate)$$

describes an empirical approach where there is some control of the overall rate by the citrate concentration.

Citrate biodegradation experiments show a slower rate at colder temperature and at higher citrate concentration (Figure 4.5, Table 4.1). At 10 mM citrate concentration, citrate was not detectable by 200 (21°C) to 300 hours (10°C, Figure 4.5a). At 50 mM citrate concentration, citrate was nondetect by 250 (21°C) to 450 hours (10°C, Figure 4.5b). At 100 mM citrate concentration, a

Table 4.1. Citrate degradation rates at different temperature and concentration, using a pseudo first order model.

Citrate (mM)	Rate (1/hour) 10°C	Rate (1/hour) 15°C	Rate (1/hour) 21°C
10	0.0071	0.013	0.025
50	0.0074	0.0036	0.013
100	0.0024	0.0042	0.0075

small amount of citrate remained at 300 (21°C) to 600 hours (10°C, Figure 4.5c). Duplicate experiments showed similar results. So over the concentration range evaluated, there was no decrease in citrate biodegradation rate at lower concentration (in fact the rate increased slightly), so the Monod kinetic approach was not used.

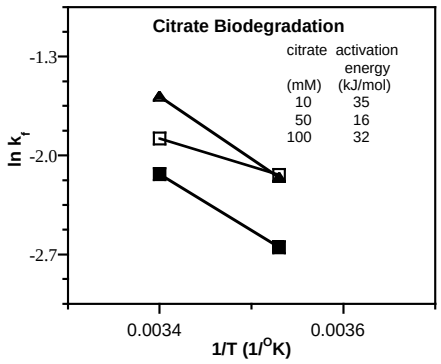

Figure 4.6. Arrhenius plot of citrate biodegradation.

A first-order model (lines, Figure 4.5) showed good fits, and indicated that in some cases, citrate biodegradation may be somewhat more rapid at lower concentration than a first-order approximation. For example, the 100 mM citrate data at 10°C (Figure 4.5) showed a good first-order fit to 500 hours, but then citrate degraded more rapidly. This effect is observed for all citrate concentrations at 10°C, but not at 21°C. A Monod kinetic model would describe the data equally as well with small half-saturation constants, but would describe the data more poorly with higher concentration half-saturation constants, which would slow citrate biodegradation at low concentration, the opposite effect of that observed. Therefore, a pseudo first-order model was used to quantify the rate data (Table 4.1).

Rates determined from these experiments show that the citrate biodegradation rate increases with temperature (2.7 times from 10°C to 25°C) and decreases with increasing citrate concentration (3.0 times from 10 mM to 100 mM). The 100-N low-concentration injections at 10 mM citrate and 15°C have an estimated half-life of 50 hours, whereas high concentration injections (40 mM citrate) have an estimated half-life of 170 hours.

The citrate biodegradation rate was 3.0 (10°C data) to 3.3 times slower (21°C data) as the citrate concentration increased from 10 mM to 100 mM. The citrate biodegradation rate averaged 3.3 times slower as the temperature decreased from 21°C to 10°C. The activation energy estimated from the reaction rate change with temperature is 35 kJ/mol (10 mM citrate), 16 kJ/mol (50 mM citrate), and 32 kJ/mol (100 mM citrate). These activation energies indicate the rate is controlled by the biochemical reaction and not diffusion, which is expected (Figure 4.6).

4.1.4 Sediment Spatial Variability of Citrate Biodegradation

The spatial variation citrate biodegradation/mineralization at the 100-N site was investigated as a function of depth and location in sediments from monitoring and injection wells along the Columbia River shoreline at the 100-N remediation site on a separate Fluor-funded project and is presented here in order to provide an estimate of the spatial distribution and variability of microbial activity for future infiltration of Ca-citrate-PO_4 solutions (Figure 4.7, 4.8). A composite of the

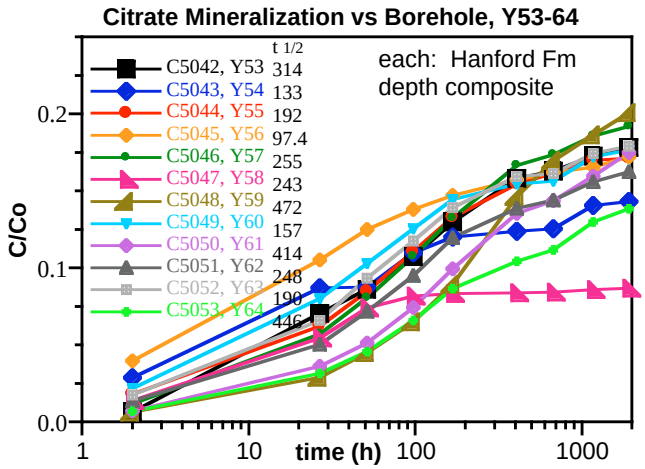

Figure 4.7. Citrate mineralization versus borehole (composite).

Hanford formation for each of 10 Hanford/Ringold wells (i.e., 8 to 15 ft depth) indicates relatively little variation and no observable trends along the 300-ft long section of the 100-N Area. These experiments were then spiked with ^{14}C-labeled citrate (4 mM), 2 mM Ca, and 2.4 mM PO_4 (i.e., solution used in field injection #2). A trend would be of a section of increased microbial activity (for example) could indicate that some sediment may have contained another carbon source that caused an increase in biomass (e.g., diesel spill), which could degrade citrate faster. The citrate mineralization half-life averaged 263 ± 125 hours for the 12 boreholes (range 133 to 472 hours, Figure 4.7). The citrate mineralization extent (at 1920 hours) averaged 0.165 ± 0.030%.

Depth-discrete samples were taken in some of the boreholes in the 100-N Area, so citrate mineralization studies were conducted in five different boreholes at differing depths (Figure 4.8). Given that the water table is generally (i.e., most of the year) at ~20 ft depth, shallower samples are typically not water-saturated. For brief periods in the spring, the water table can rise a few feet. For these experiments, water-saturated conditions were used in all samples. Microbial biomass decreased with depth (Figure 2.2), so these mineralization studies were expected to show a decrease in mineralization rate and extent with depth.

Results of the citrate mineralization studies in five boreholes with depth (Figure 4.8) show an imperfect inverse correlation of mineralization rate with depth.

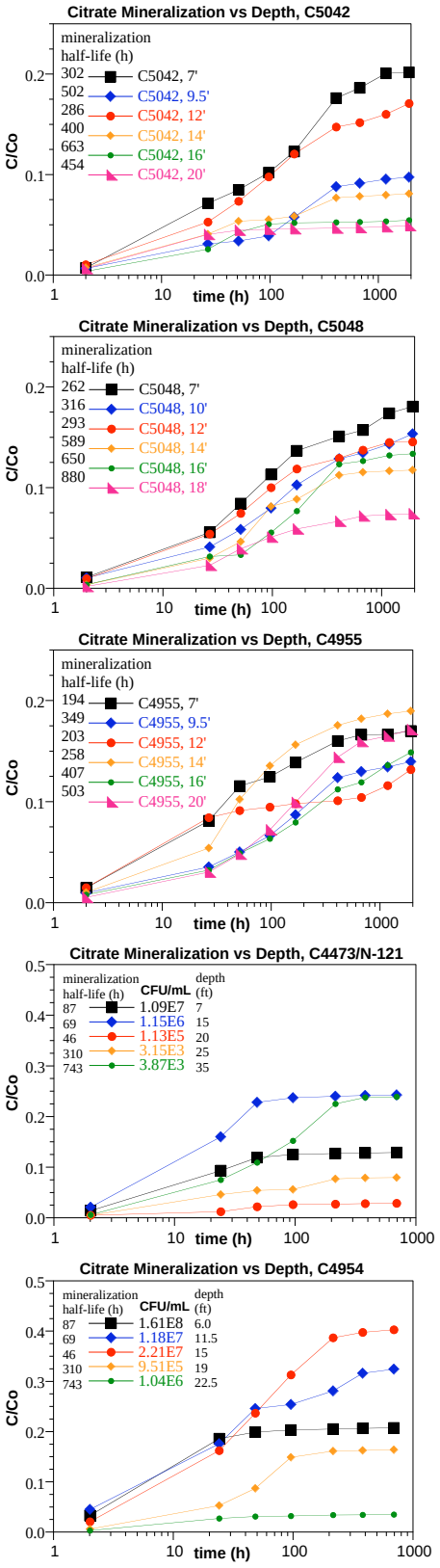

Figure 4.8. Citrate mineralization versus depth in five different boreholes in the 100-N Area.

Because the true independent variable is microbial biomass, deeper samples in different boreholes may have different biomass. For example, the 20-ft depth for C5042, 18-ft depth for C5048, and 20-ft depth for C4473 had relatively slow mineralization rates and extent, but in contrast, the 20-ft depth for C4955 had the highest mineralization rate in that borehole.

Plotting the depth versus mineralization half-life and mineralization extent in each borehole (Figure 4.9) shows the general trend of decreasing rate (increasing mineralization half-life) with depth, but there is no correlation of mineralization extent. Significantly lower microbial populations at greater depths results in only slightly slower citrate degradation rate in these tests. The stronger correlation shown in larger scale transport studies (Section 4.2.3) are not apparent in these batch studies as microbial transport processes are not included. The injection of river microbes and the transport of some portion of the injected and in situ population with the advance of the wetting front results in a redistribution of microbes with depth compared to preinfiltration conditions (Figure 2.2).

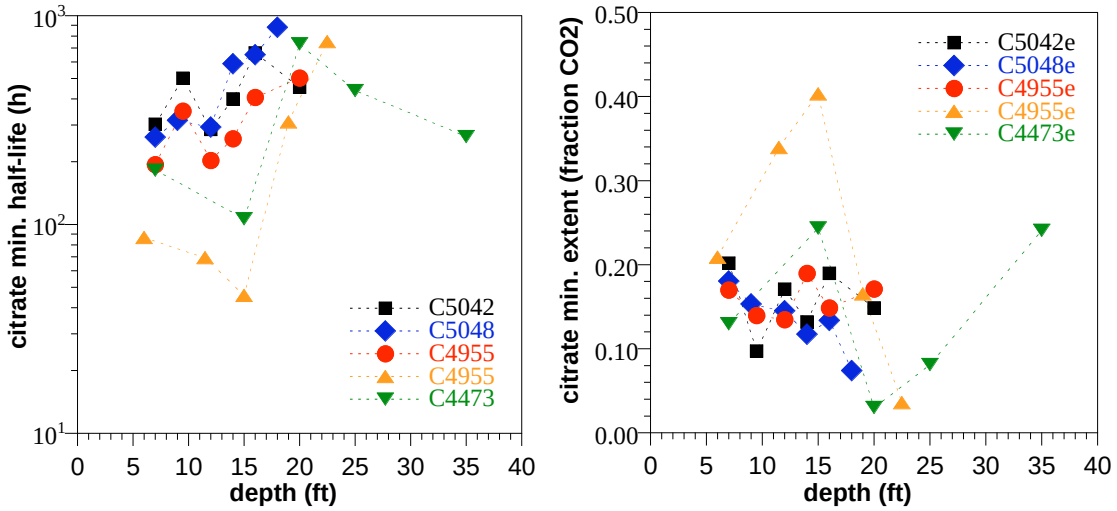

Figure 4.9. Citrate mineralization and depth in five boreholes showing a) mineralization half-life and b) trend of mineralization extent

In summary, citrate is mineralized under low water saturation conditions in 100N vadose zone sediments. The degradation/mineralization rate increases with increasing microbial biomass, lower citrate concentration, and increasing temperature. The mineralization extent (10% to 60%) correlates with mineralization rate. Although the mineralization rate should directly correlate with microbial biomass, experiments varying the biomass five orders of magnitude resulted in only an order of magnitude change in mineralization rate. The reason for this apparent lack of correlation is the relative contribution of in situ microbes and injected microbes (in the river water used in the Ca-citrate-PO_4 solution) to biodegrading citrate (described in Section 4.2.3). River water microbes, although present at much lower concentration than in situ microbes, degraded citrate much more rapidly, so the observed citrate biodegradation rate was controlled by both in situ and injected microbes for shallow sediment (high in situ microbial biomass), but mainly by injected microbes for deeper (>10 ft depth) sediments (lower in situ microbial biomass. The result is that injection or infiltration of the Ca-citrate-PO_4 solution will result in

much less variation in rate/extent of citrate biodegradation, so there is a greater ability to predict the rate and extent than expected from monitoring of just the in situ microbial biomass.

4.1.5 Phosphate Adsorption to 100-N Sediments

The location of apatite precipitate that results from Ca-citrate-PO_4 solution infiltration is dependent on citrate degrading, so that Ca and PO_4 (at pH 7.3 to 8.3) can precipitate as apatite. The citrate biodegradation half-life of 50 hours (5 mM citrate) to 200 hours (50 mM citrate) indicates the Ca-citrate-PO_4 solution can infiltrate for a few days with little degradation. Phosphate adsorption also controls the transport of a component of the Ca-citrate-PO_4 solution. At equilibrium and at 2 to 40 mM PO_4 concentrations used in field injections, adsorption results in a retardation factor of 1.6 to 2.4 for phosphate. Adsorption isotherms were conducted in a separate Fluor-funded study with 100-N sediments at 1- and 24-hour contact time to characterize whether sorption was occurring or there was some precipitation. If Ca-PO_4 precipitation was a significant component of the PO_4 mass loss from solution, the isotherm line would be closer to vertical and not exhibit a 1:1 slope at low concentration indicative of sorption. Adsorption isotherms for 1- (field R_f = 2.7) and 24-hour contact time (field R_f = 9.8), pH 8, 50 mM PO_4 and r_{sw} (Figure 4.10) implies that the PO_4 removal from solution is due primarily to sorption. If it was precipitation, there would be no regular partitioning with change in concentration (pure precipitation would show as a vertical line, where there would be a finite amount in aqueous solution (no matter how much PO_4 is added). Each isotherm was fit to a Langmuir equation with identical sorption maxima (M= 1500 mg sites/Kg sediment). The linear region of the isotherms at both 1 and 24 hours (low concentration) and same adsorption maxima (high concentration) appear to be indicative of adsorption in the short time scale.

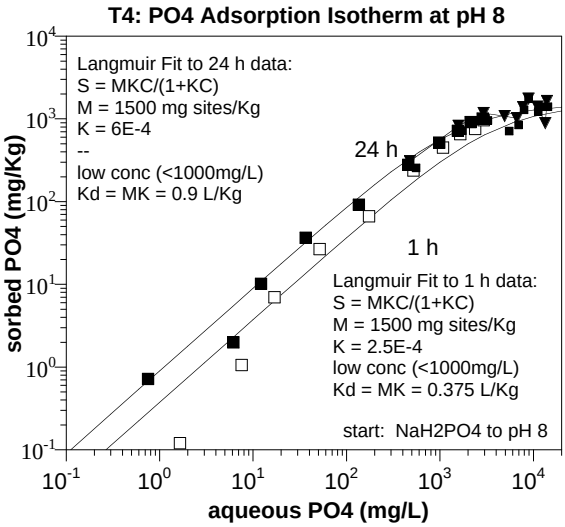

Figure 4.10. Adsorption isotherm for Na-PO_4 at 1 and 24 hours.

Phosphate removal from solution by adsorption is difficult to separate from precipitation, as shown in batch studies measuring PO_4 in solution over hundreds of hours (Figure 4.11). Phosphate adsorption appears to reach equilibrium within hours (plateau in some data at 1 to 20 h), but the effects of adsorption and precipitation produce an increasing lag during injection/infiltration due to the kinetics of (primarily) precipitation. The injection of Na-PO_4 into 100-N sediment columns

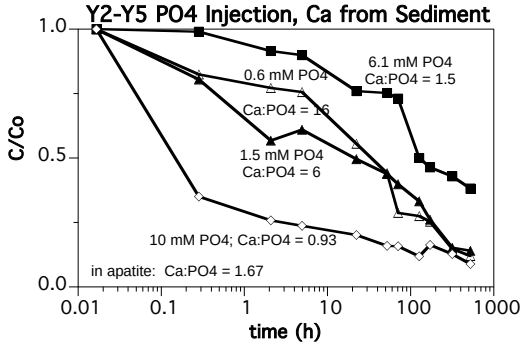

Figure 4.11. Time scale of PO_4 removal rate from solution at differing different Ca/PO_4 ratios.

(Szecsody et al. 2007) results in a time-dependent PO_4 sorption and time-dependent PO_4 precipitation. The apparent sorption results in retardation factors ranging from 1.0 to 2.4 (average PO_4 Rf = 2.0 ± 1.1). This is an apparent K_d = 0.433 ± 0.248 cm^3/g (apparent as it may include sorption and precipitation mass removal from solution).

4.1.6 Apatite Precipitate Measurement by Acid Extraction

One method used to measure the small concentrations of apatite precipitate in sediment was aqueous measurement of phosphate after apatitedissolution in acidic solution. Acid dissolution of the sediment/apatite mixture will result in PO_4 from both sediment minerals and the added apatite. Because the added apatite are relatively small (sub micron) crystals, a weak acid for a limited amount of time was used to dissolve all the added apatite but dissolve less of the sediment mineral phase PO_4. Initial experiments with 0.5 M and 5.0 M HNO_3 (Szecsody et al. 2007) showed that even by 15 minutes, aqueous PO_4 had reached equilibrium. For the acid dissolution of the pure apatite (no sediment), the amount recovered was equal to the predicted amount for both the 0.5 M and 5 M HNO_3, so the lower acid concentration was sufficient. Ultimately both the 0.5 M and 0.1 M HNO_3 treatments for 15 minutes could be used to dissolve the added apatite (Figure 4.12), where the slopes were the same (i.e., because of the same amount of addition). The intercepts (i.e., baseline PO_4 from sediment minerals dissolving) differed with the weaker acid dissolving less of the apatite minerals, as expected, so produced a lower baseline. The background (baseline) phosphate extracted from the sediment (with no added apatite) was 0.45 mg/g. The slope of 0.86 means the method recovered ~86% of the apatite added. Subsequent results in this study subtract out the baseline phosphate concentration so that the observed phosphate concentration is the result of the Ca-citrate-PO_4 added.

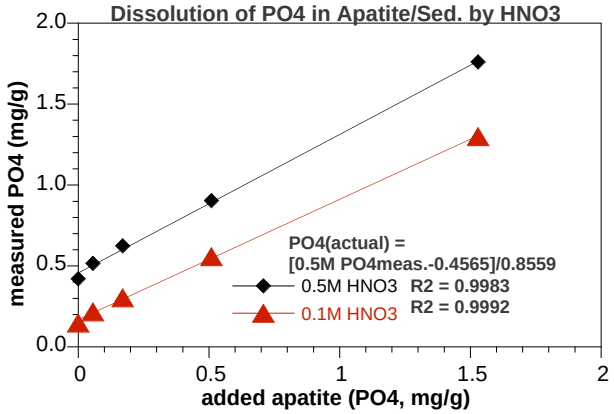

Figure 4.12. Aqueous phosphate measurement after acid dissolution of apatite/sediment mixtures with a) 0.5 M HCl and b) 0.1 M HCl.

In addition to the acid extraction to dissolve apatite (and other PO_4 precipitates), water and a high ionic-strength solution (1 M KNO_3) was used to desorb PO_4 in order to evaluate the mass of PO_4 present in solution or adsorbed on the sediment surface or present as precipitate. The amount of PO_4 present in solution (water extracted) was essentially equivalent to the PO_4 present adsorbed on the sediment, indicative of very little adsorbed PO_4 (Figure 4.13a). These values were <2% of the total PO_4 present on the surface as precipitate (Figure 4.13b). These results are consistent with previous results (Figure 4.11), which indicate phosphate eventually precipitates as one or more phases on the sediment surface.

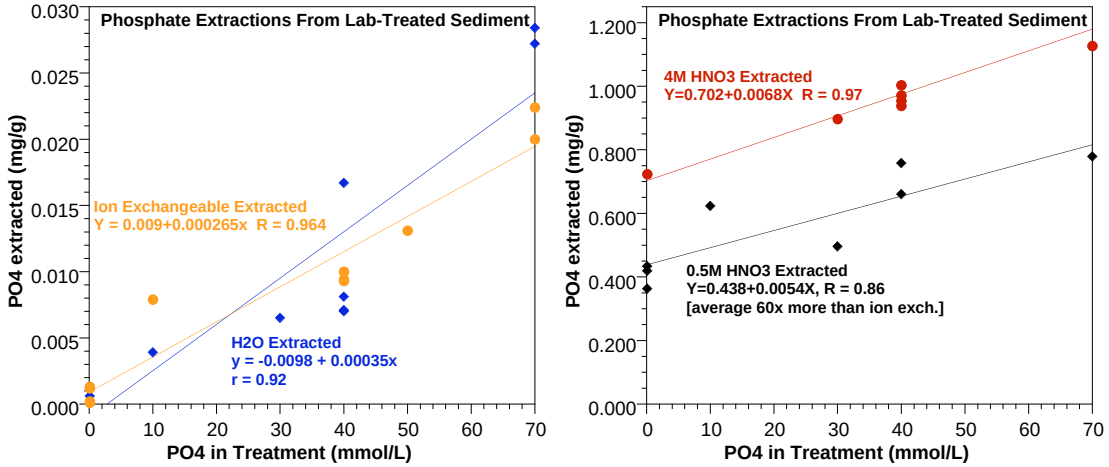

Figure 4.13. Phosphate extracted from Ca-citrate-PO_4-treated 100-N sediment using: a) water and ion exchangeable (1 M KNO_3) treatments, and b) 0.5 M HNO_3 and 4 M HNO_3 treatment.

4.1.7 Apatite Precipitate Measurement by Electron Microprobe Analysis

The use of XRD to identify the small concentrations of apatite in sediment has not been used due to the very low concentrations. XRD is typically limited to 0.5% or above for proper identification. XRD has been used to identify that a pure phase precipitate has the crystal structure of apatite (i.e., Figure 2.1). The scanning electron microprobe (SEM) has successfully been used to identify low concentrations of apatite in sediment. The process involves taking a small sediment sample (0.5 g), encasing it in epoxy, then creating a thin section of the sediment sample, which shows both surface precipitates and crystal structure of the sediment minerals. A total of 7 thin sections were made with a range of apatite concentrations in the sediment (Table 4.2).

Table 4.2. Apatite-laden sediments.

Name	Sed.(g)	Apatite (mg)
Y25	2.0	0.0 (none, background)
Y26	2.0	0.033 mg
Y27	2.0	0.10 mg (2.4 mM PO_4)
Y28	2.0	0.33 mg
Y29	2.0	0.63 mg (17 mM PO_4)
Y30	2.0	1.0 mg
Y31	2.0	3.3 mg (90 mM PO_4)

The SEM can identify elements at an extremely small point (~10 micron beam width, adjustable), so to identify small amounts of apatite in sediment grains, an automated scanning routine was used. Using a beam width of 15 microns and scan time of 100 milliseconds per point, a 60 x 60 grid was scanned on each sample (i.e., 3600 points, 900 microns x 900 microns), which took ~12 hours. The SEM used had multiple high-resolution element detectors, which were set on the elements Ca, P, Si, and Fe. The silica is used to correct for the sediment area (to exclude the area on the slide composed of epoxy). One example (Figure 4.14) of the electron backscatter (brighter color for more dense material; epoxy is black) shows that sediment grains compose about 60% of the surface area of the slide. The Ca image (Figure 4.14, warmer color indicates higher concentration) shows many minerals that contain calcium, whereas the P image (Figure 4.14c) shows very few mineral phases containing P. Note that some mineral phases to contain P, so the combination of P plus Ca (Figure 4.14d, in yellow) is consistent with the presence of precipitated apatite.

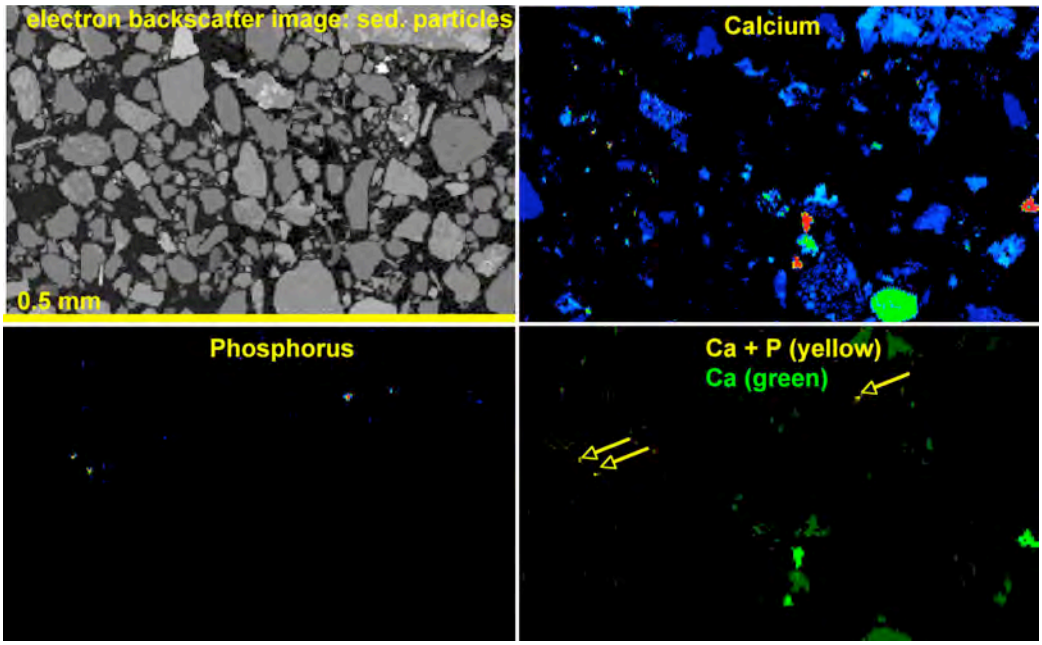

Figure 4.14. Scanning electron microprobe image of a sediment thin section containing 0.033 mg apatite/g sediment. Images are: a) electron backscatter illustrating sediment grains (grey) in the black epoxy background, b) calcium density, c) P density, and d) addition of Ca + P.

Images of the phosphorous density of four separate samples (Figure 4.15) show an increasing number of spots of phosphorus, which is likely the added apatite, with some spots being phosphate in mineral grains. Multiple spots were then revisited and scanned for a longer period of time to identify whether the spot was a sediment mineral containing P or the added apatite. For example, the large white spot in the upper left corner of the Figure 4.15a sediment image is a sediment mineral that contains P. Apatite fluorescence (Figure 4.16) was also considered.

To illustrate the identification process, a single small P spot from one image (Figure 4.17a) was focused on at high magnification (Figure 4.17b). This electron backscatter image shows that this crystal is highly likely added apatite, as sediment grains are generally far larger and this small crystal is located on the surface of a mineral grain. An EDS detector scan of this grain (Figure 4.17c) with peaks clearly shows that the crystal structure is apatite (pure apatite phase EDS scan in Figure 2.1d, for comparison).

While the use of the electron microprobe shows that very small concentrations of apatite can be quantitatively identified, the cost of the analysis is significant, as is the time to processes the samples. As such, acid extraction of phosphate was generally used in experiments as a rapid and reliable method of identifying small concentrations of apatite is needed for the field-scale application.

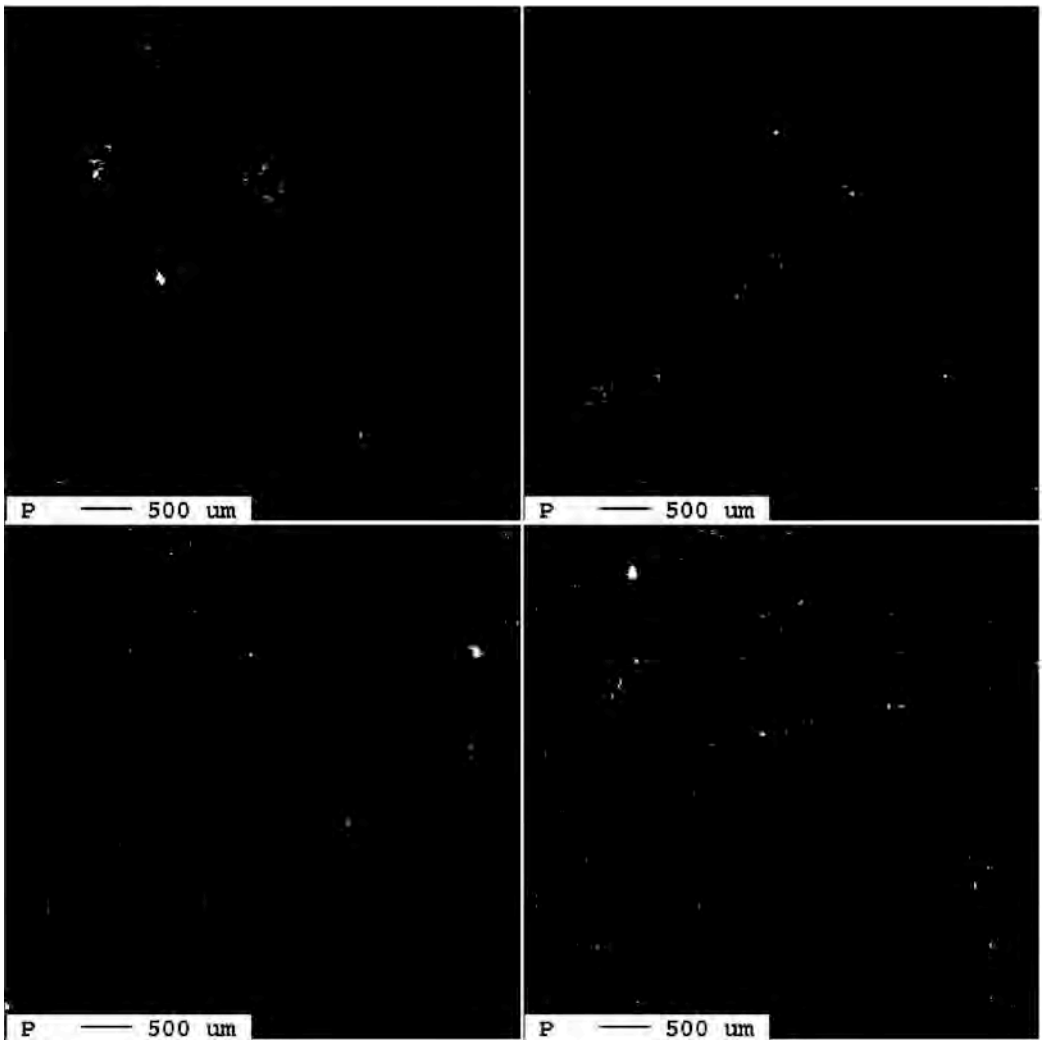

Figure 4.15. Scanning electron microprobe images of sediment samples with differing amounts of added apatite in sediment: a) 0.033 mg/g, b) 0.10 mg/g, c) 0.33 mg/g, and d) 3.3 mg/g. Phosphorous elemental scan shown (white = P location).

4.1.8 Apatite Precipitate Measurement in Sediment by Fluorescence and FTIR

A third method of measuring added apatite in sediment investigated was the use of fluorescence scans. While pure hydroxyapatite does not fluoresce, apatites with F or carbonate substitution do fluoresce. Apatite precipitated in groundwater (Figure 4.16, black line) does fluoresce, and the sediment sample (no apatite added, green line) does not. This method is still in development, and how low a concentration of substituted apatite cannot be measured as yet.

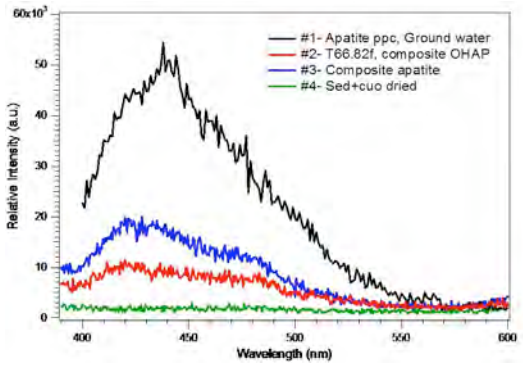

Figure 4.16. Fluorescence scans of precipitated apatite (black, blue, red) and sediment with no apatite (green) showing low levels of background fluorescence from the sediment.

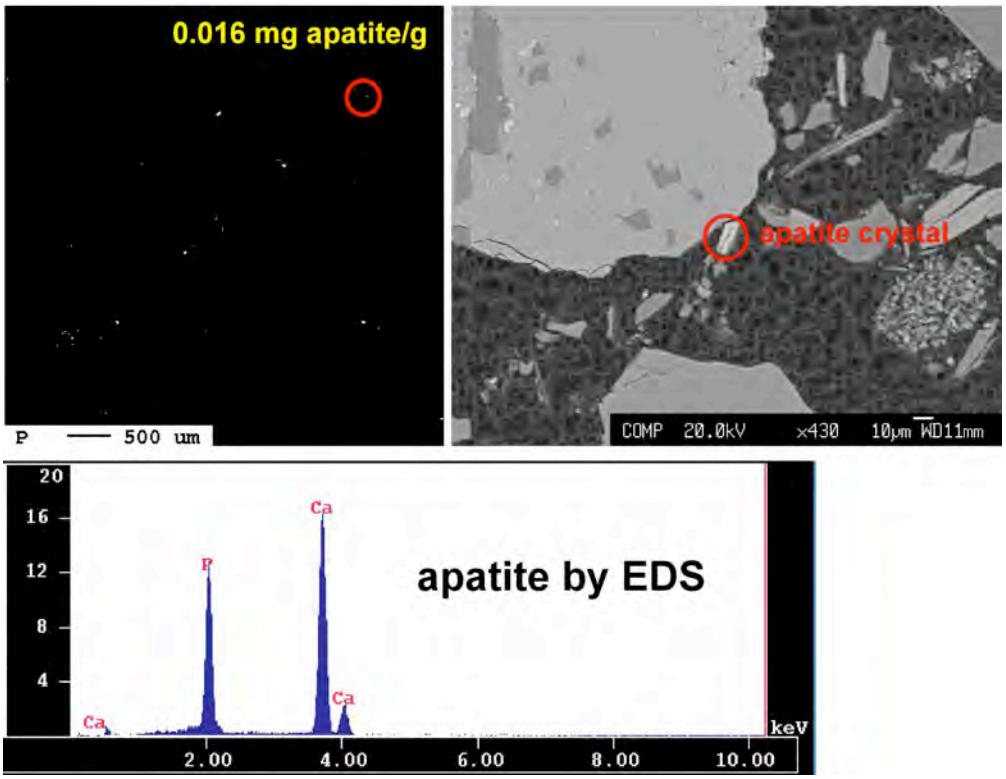

Figure 4.17. Mineral phase identification of a location with high phosphorous concentration (a). Electron backscatter of the location is indicative of a surface precipitate (b), with identification of this mineral as apatite (c) by comparison to a standard.

A surface area measurement of the Ca-citrate-PO_4 precipitated apatite (61.5 m^2/g) was somewhat greater than the Sigma apatite (52 m^2/g). The inorganic carbon content of the precipitated apatite was measured at 0.02%, so in spite of high carbonate concentrations in groundwater, there appears to be little carbonate substitution into the apatite under the conditions (i.e., pH ~7.8, field injections ranged from 7.5 to 8.0). In the laboratory precipitate at very high microbial biomass concentrations (10^9 cfu/mL), there was some incorporation of organic carbon into the apatite (i.e., 0.78% organic carbon). It is expected that field injections will not have as high a biomass concentration (certainly for the injections so far the citrate concentration was far less than used in the laboratory experiments).

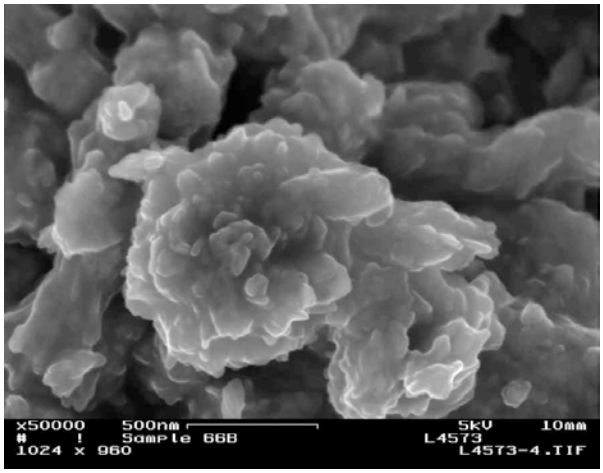

Figure 4.18. SEM image of citrate precipitated apatite used in Sr incorporation studies at 82°C.

The stable Sr suspensions aged for 0.86 and 1.36 months at each temperature have been characterized by SEM/EDS. The SEM image of the citrate precipitated apatite used in the stable Sr incorporation series and aged for 1.36 months at 82°C (Figure 4.18) showed discrete aggregated crystalline clusters ranging

from 75 to 600 nm in diameter and significant porosity. The presence of Sr associated with the citrate precipitated apatite was examined by EDS in samples aged for 0.86 and 1.36 months at 22°C and 82°C. EDS spectrum obtained at 62 distinct sites on apatite particles in these 4 samples confirmed the presence of Sr at all sites. A typical EDS spectrum for apatite aged at 82°C for 0.86 month shows a clearly resolved Sr peak (Figure 4.19). As noted above, ion exchangeable Sr had been removed by an overnight wash with 0.5 M KNO_3, so the Sr detected by EDS was either a discrete Sr phase on the apatite surface or incorporated into the apatite structure. Although qualitative, the EDS estimation of Sr incorporation into the citrate precipitated apatite was consistent with ICP-mass spectrometer (MS) measurements of Sr incorporation in these same samples (see Section 4.3.3).

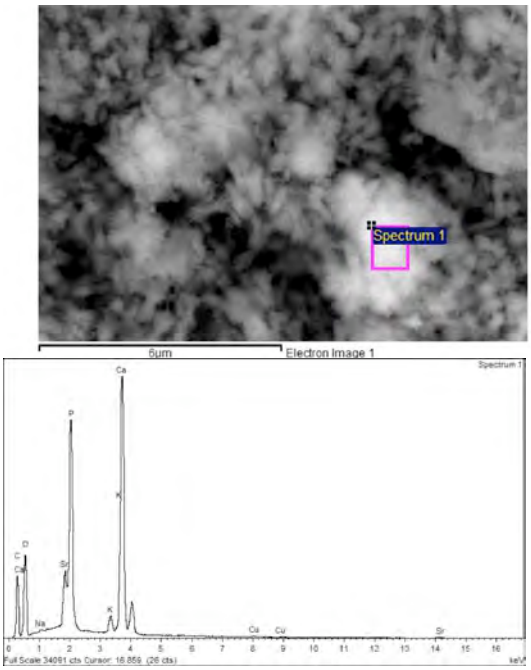

Figure 4.19. Image of apatite grain (a) showing square region for which EDS spectrum was obtained (b) for apatite aged at 82°C for 0.86 month.

Fast XRD scans have been carried out on the citrate precipitated and Sigma apatites and confirmed the presence crystalline apatite as the major phase in these starting materials. Fast XRD scans on selected samples of the Sr substituted apatites yield the same result (Figure 4.19). Currently, slower more precise XRD scans are being performed in order to detect trace phases within the major phase and any changes in crystallinity due to Sr substitution.

Control FTIR spectra have been run on both the Sigma and citrate apatite starting materials. FTIR scans of the 82°C citrate precipitated apatite aged for 5.99 months demonstrated that no secondary phases, e.g., $SrPO_4$ or SrOH precipitate, have formed within the apatite structure, as shown in Figure 4.20 in which peaks for the Ca-apatite (Sigma standard) and Sr-substituted apatite are similar, but do not show characteristic peaks of the $Sr(OH)_2$ or $Sr(PO_4)$. Although the presence of Sr has been confirmed by ICP-MS and EDS which strongly suggests that Sr has been incorporated, the FTIR analysis has not detected a difference between the Sr incorporated apatite samples and the control samples. Additional FTIR analysis of samples aged for longer periods with a higher percentage of Sr incorporation are attempting to observe this difference and thus definitively confirm that the Sr is replacing the Ca within the apatite structure.

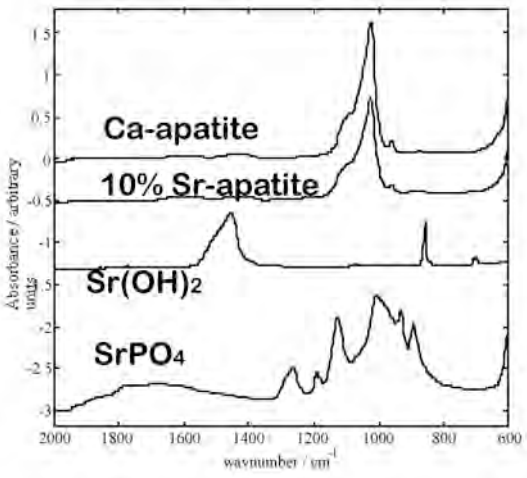

Figure 4.20. FTIR spectra of apatite, Sr-substituted apatite, and $Sr(OH)_2$, $SrPO_4$ standards.

4.2 Task 2 – 1-D Infiltration of Ca-Citrate-PO_4 to Precipitate Apatite

4.2.1 Small Scale 1-D Infiltration and Optimizing Apatite Precipitate Depth

Small (50 cm length) 1-D infiltration experiments were conducted to quantify the influence of the infiltration rate and solution concentration on the depth of apatite precipitate. Although 1-D infiltration is not representative of lateral spreading and heterogeneity influence on the field infiltration rate, these studies were conducted to understand the precipitate distribution under conditions constrained to linear advection and longitudinal dispersion.

Steady-state infiltration simulations (Figure 4.21) show the development of specific water contents that are somewhat greater at higher infiltration rates. Because citrate biodegradation is considerably slower at low (<50%) water content (Section 4.1.1), higher infiltration rates were used. Experiments were conducted using 1.5-cm internal diameter clear polyvinyl chloride (PVC) columns that were packed with a mixture of 100-N sediment (<4 mm) and sand (picture in Appendix A, Section A.3). The sand was added to the <4-mm sediment to replace the gravel fraction removed in order to maintain the same phosphate K_d as field sediment (phosphate adsorption in Section 4.1.5). In three experiments, the infiltration rate was 0.4, 1.0, and 4.0 cm/hour (Figures 4.22 and 4.23). The initial water saturation was 65.8% and a 10 mM PO_4 solution (Ca-citrate-PO_4, Table 3.1) was used. The rapid infiltration was 12 hours, and the slowest infiltration took 100 hours. Vertical profiles of the PO_4 distribution (Figure 4.23) showed a rough correlation between a faster infiltration rate and accumulation of greater phosphate at depth. The slowest infiltration rate resulted in most of the precipitate in the shallowest 15 cm, whereas the most rapid infiltration rate had phosphate distributed throughout the entire profile. Based on the integrated precipitate mass recovered and PO_4 injected, all three experiments had nearly the same percentage of phosphate recovered as precipitate (75% to 78%).

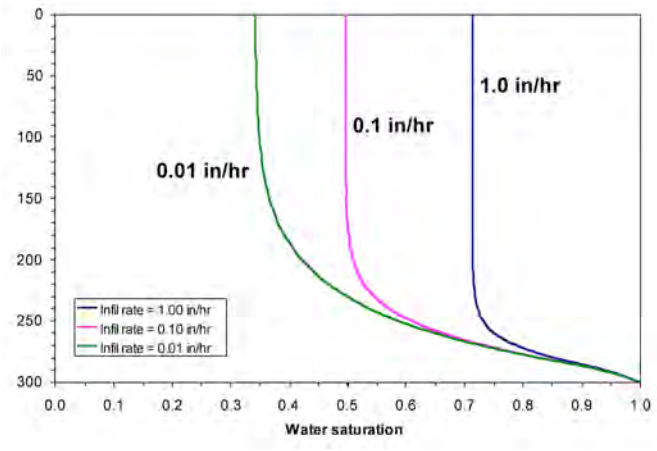

Figure 4.21. Steady-state infiltration simulations at different infiltration rates.

Phosphate was eluded out the bottom of these columns (Figure 4.22), which accounted for the balance of the phosphate mass injected.

One additional small-scale 1-D infiltration column experiment was conducted at an infiltration rate of 1.0 cm/hour, but using a 20 mM PO_4 solution (see Appendix A). There was little difference in the precipitate profile between 10 mM (Figure 4.22b) and 20 mM PO_4 infiltrations.

Further small 1-D experiments were not conducted, as 2-D infiltration studies would more realistically simulate the infiltration front (with both vertical and lateral spreading) that would occur in the field. Some large (12-ft high) 1-D infiltration experiments were conducted (next section) to be at field scale.

4.2.2 Large-Scale 1-D Infiltration

After the majority of 2-D experiments funded in this EM-22 study, a Fluor-funded task was initiated to test the infiltration rate developed in the 0.5- to 1.2-m studies to a scale nearly that of the field. For that purpose, two 3.6-m (12-ft) high infiltration column experiments were conducted, as described in this section, and a 2.4-m (8-ft) high by 1.2-m (4-ft) wide 2-D infiltration experiment was conducted. Columns were 2.6 cm in diameter by 3.6 m (12 ft) high clear PVC. The initial water content was 6.2%, with a standing water table for the bottom 2 cm (Figure 4.24a).

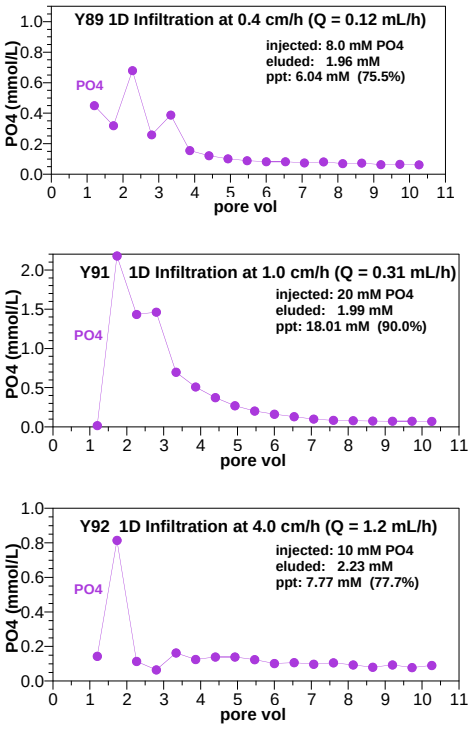

Figure 4.22. PO_4 breakthrough for 1-D infiltration experiments.

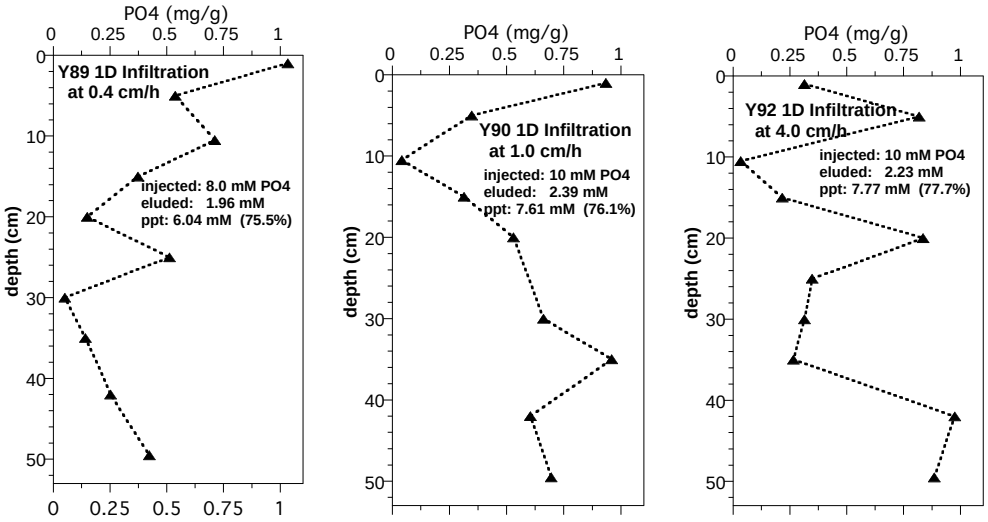

Figure 4.23. 1-D infiltration of Ca-citrate-PO_4 solution (10 mM PO_4).

The infiltration strategy developed in 2-D infiltration studies was a rapid infiltration of a more concentrated Ca-citrate-PO_4 solution minimizes phosphate adsorption and citrate biodegradation, thus leading to the transport of greater PO_4 to depth. However, just rapid solution infiltration does not provide sufficient time for lateral spreading of the infiltrating plume (in a 2-D or 3-D system). To further drive PO_4 mass to depth and provide some time for lateral spreading, the

infiltration strategy was further modified to infiltrate water (without Ca-citrate-PO_4) at a slow rate after the Ca-citrate-PO_4 infiltration. In the first 2-D infiltration experiment, the volume of water infiltrated after the Ca-citrate-PO_4 solution was roughly the same. While this strategy provided PO_4 transport to depth (see Section 4.5.1) at a 0.5- to 1.2-m scale, apatite precipitate was generally evenly distributed in the 12-ft high column (Figure 4.24b) with a slight additional mass at a 6-ft depth. The picture (Figure 4.24a) shows the infiltration front reaching a 6-ft depth by 32 minutes. Modification of the infiltration strategy to inject four times more water compared to the PO_4 injected resulted in driving the apatite precipitate to depth (Figure 4.24c). In this case, the majority of the precipitate (>78%) was at the 6- to 12-ft depth, which is desirable because Sr-90 is found in the lower half of the vadose zone (Figure 1.3, 8- to 15-ft depth).

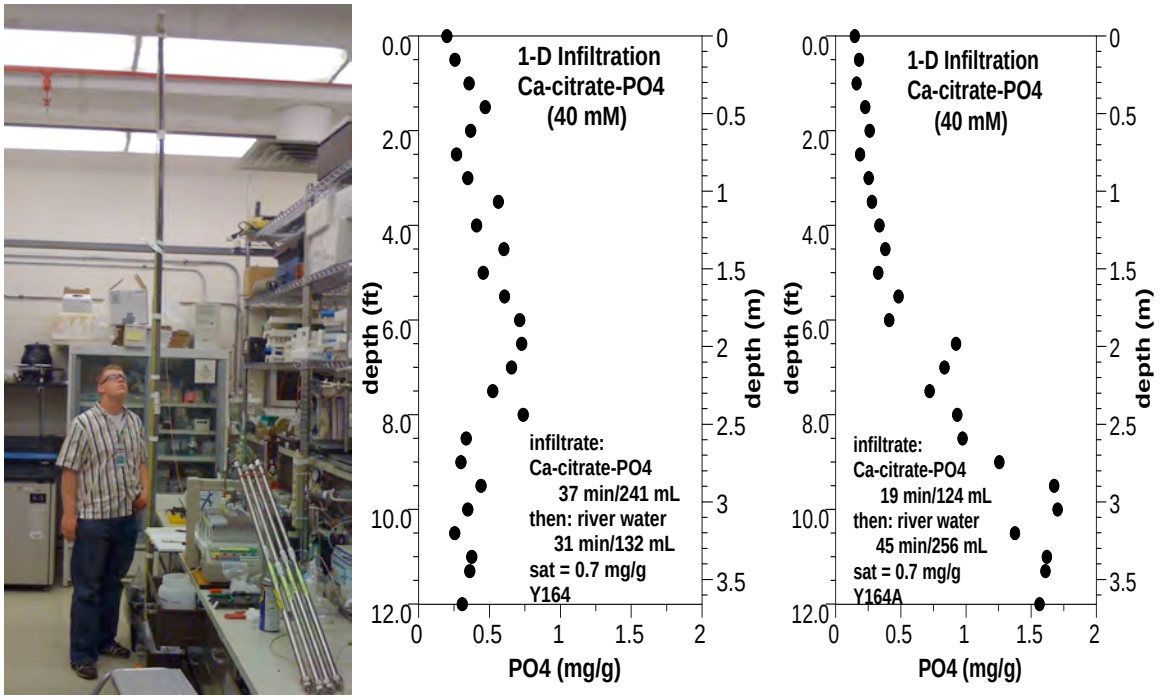

Figure 4.24. 1-D infiltration of Ca-citrate-PO_4 (40 mM PO_4) at a rapid rate followed by water.

4.2.3 Microbial Transport/Redistribution and Influence on Apatite Formation

An additional large laboratory-scale study funded by Fluor was the investigation of the role of microbial transport during Ca-citrate-PO_4 injections and future infiltration studies in the field. Batch citrate biodegradation studies showed that when in situ microbial biomass was varied 5 orders of magnitude, the citrate biodegradation rate only varied an order of magnitude (Figures 4.3 and 4.4). Measurements of the river water biomass indicated low values compared with in situ biomass, so the contribution of river water microbes to biodegrade the citrate was initially not considered important. An additional process (microbial detachment and transport in sediment) by the shear forces induced during injection and/or the high ionic strength of the injecting/infiltrating solution will lead to the redistribution of microbes to during injections, and potentially the relatively uniform citrate biodegradation rate. These processes were considered of greater importance for infiltration studies, as the microbial biomass is very high for shallow sediment (10^8 cells/g, Figure 2.2), and decreases 4 orders of magnitude by a 15-ft depth.

In this section, experiments were conducted to address:

- how far do in situ microbes move in response to the water flow rate (i.e., shear)
- how far do in situ microbes move in response to the ionic strength of the solution
- what is the relative contribution of in situ and injected microbes for degrading citrate.

Five 9.1-m (30-ft) long by 1.5-cm diameter columns were used for this study in which the solution was injected to reach only to 20 ft. The columns were packed with a composite 100-N Hanford formation sediment (<4 mm) mixed with sand. The average groundwater biomass is 1.5×10^5 cells/mL (equivalent to 4.8×10^5 cells/g) and pre-experiment sediment biomass was 7.8×10^8 cells/g (i.e., K_d (microbes) = 5173, R_f(microbes) = 16133). The average river water biomass is 2.2×10^6 cells/mL (equivalent to 7.1×10^5 cells/g; Table 4.3), so river water biomass is 1100 times less than in situ microbial biomass. The base case injection was a 40-mM Ca-citrate-PO_4 solution injected to a 20-ft distance in 24 hours (interstitial velocity of 20 cm/hour) using unfiltered river water and live in situ microbes.

Table 4.3. Microbial biomass and phosphate mass results in 30-ft 1-D column injection experiments.

#		v (cm/h)	live insitu bugs	live injected bugs	injected PO4 (mg)	recovered PO4* (mg)	recovered PO4* frac. of inj.	biomass conc. (cells/g)	total** (cells)	cells, ratio to preinj.
Y177	base case, 40 mM Ca-cit-PO4 inj, 24 h	20.20	yes	yes	1588	1225	0.771	3.40E+09	6.70E+12	4.4
Y178	40 mM Ca-cit-PO4 inj, 2 h (fast injection)	307.2	yes	yes	1718	1185	0.690	6.40E+09	1.25E+13	8.9
Y179	10 mM Ca-citr-PO4 inj, 23.6 h	28.17	yes	yes	464	354	0.763	3.96E+09	8.32E+12	5.47
Y180	40 mM Ca-cit-PO4 inj, 24.8 h	26.30	yes	no	1823	919	0.504	1.00E+10	2.24E+13	14.0
Y181	40 mM Ca-cit-PO4 inj, 26.5 h	26.88	no	yes	1998	1200	0.601	6.10E+09	1.34E+13	8.4
	river water							7.06E+05		
	groundwater							4.81E+04		
	pre-experiment sediment							7.76E+08	1.52E+12	

*20 points along column analyzed for PO4 (mg/g), intergrated area under curve
**14 points along column analyzed for biomass, average of 9 counts each by AODC

Data collected in these experiments included phosphate and microbial biomass at 20-30 locations along the column length after the experiment is completed. The electrical conductivity of the injecting solution was measured by flow-through electrodes located at a 10-ft and 20-ft location in the column (data in Appendix A, Section A.3). Phosphate was measured by acid extraction (Section 4.1.6). Microbial biomass was measured by AODC, which is a DNA stain technique. Sediment samples were additionally taken for biomass measurement by PLFA and PCR/DNA.

Phosphate distributions with length (Figure 4.25) provided an indirect indication of microbial activity. The 40-mM Ca-citrate-PO_4 injection with live in situ and live injected microbes (Table 4.3, experiments Y177, Y178, and Y179) resulted in 70% to 77% of the injected phosphate recovered as precipitate. The precipitate was located in the first 20 ft of the column length (Figure 4.25a, c, and e). Autoclaving the sediment before packing the column (i.e., killing the in situ microbial population, experiment Y181) resulted in no measurable change in the phosphate distribution with length (Figure 4.25i), although only 60.1% of the phosphate injected was recovered as precipitate. Conversely, filtering the river water (0.1-µm filter) to remove river water microbes resulted in substantially less PO_4 precipitate (Figure 4.25g) with 50.4% of the injected phosphate recovered as precipitate (i.e., precipitation decreased to 68% relative to live

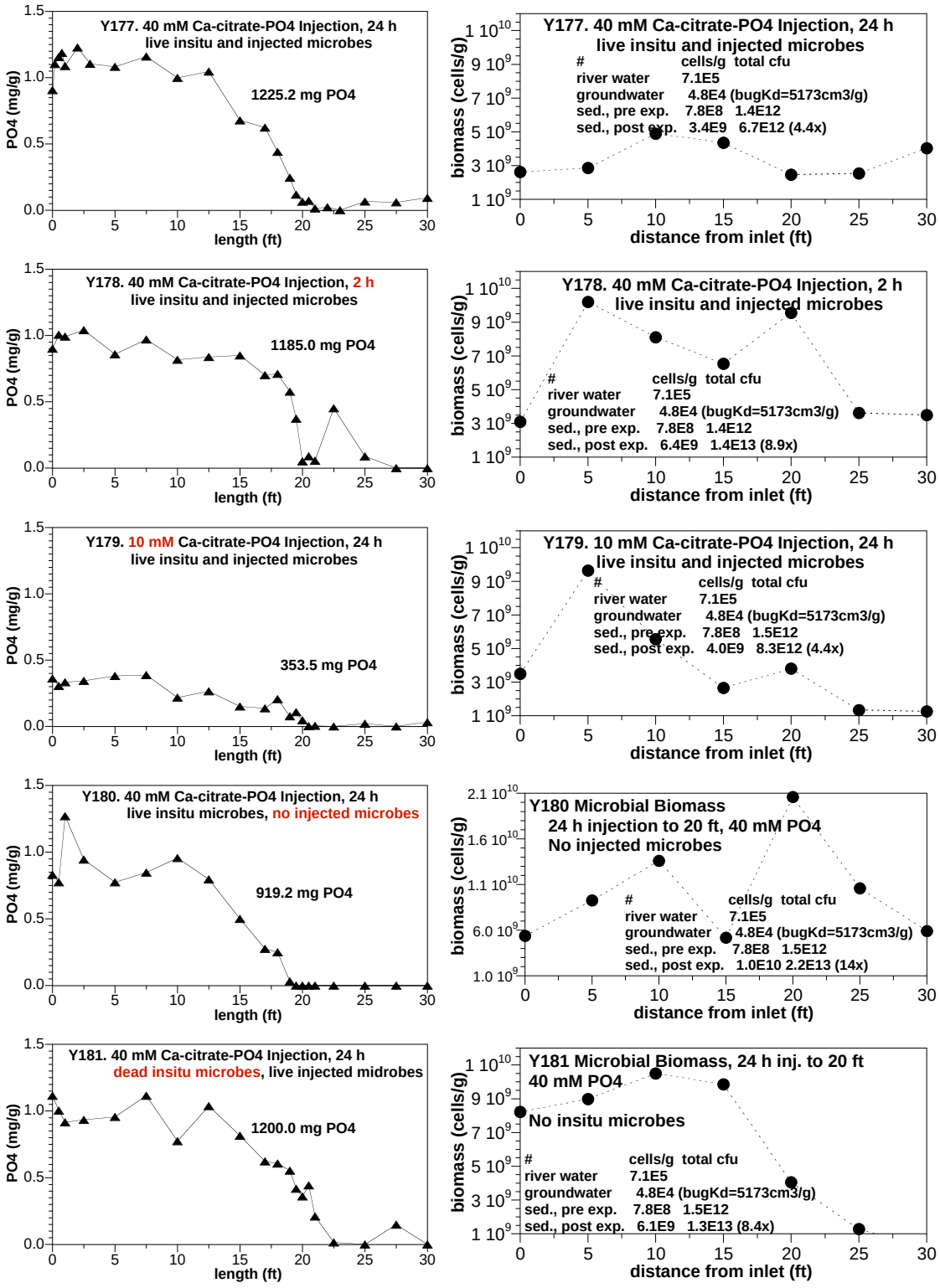

Figure 4.25. Phosphate and microbial biomass distributions in 30-ft 1-D columns.

injected microbes). Therefore, although the river water microbes are 1100 times less, they are contributed to a greater extent to the citrate biodegradation.

The microbial biomass data (by AODC) did show some differences between experiments, but these differences were not necessarily correlated to citrate reactivity. As 1100 times less river water microbes could degrade a significant amount of citrate, these measurements of total biomass are not necessarily correlated with the apparent subset of the population that biodegrades citrate. A separate study separating different types of microbes and which biodegrade citrate may (in progress) provide some answers.

The comparison of Ca-citrate-PO_4 injection over 24 hours (20.2 cm/hour) to a 2-hour injection (307 cm/hour; Table 4.3, experiments Y177, Y178) showed no difference in the precipitate spatial distribution or mass amount. There was ~2 times greater total biomass for the fast injection relative to the slow injection (Table 4.3), although the spatial distribution of microbes was located within the first 20 ft of the 30-ft column (Figure 4.26a). Therefore, over the range of velocity tested, there was no influence on injection velocity and the resulting apatite precipitate mass and distribution, so field injections/infiltrations at differing velocities should not have to account for changes in microbial activity due to the change in injection velocity.

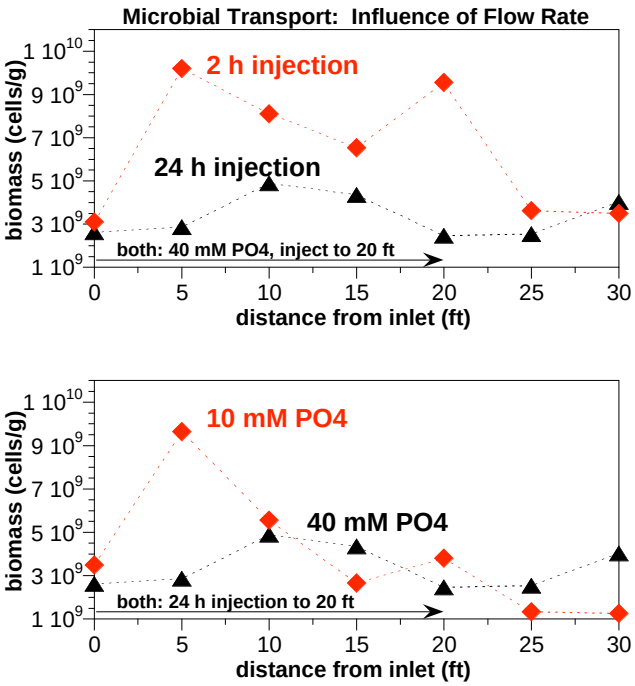

Figure 4.26. Microbial redistribution in 30-ft columns from change in injection velocity (a) and solution ionic strength (b).

A change in the solution concentration injected from 40 mM PO_4 to 10 mM PO_4 did change the mass of measured precipitate by 4 times (Table 4.3, Figure 4.25a and e), as expected. There was very little difference in the microbial biomass distribution with length (Figure 4.26b), which indicated that over the small range of ionic strength tested, there was no change in microbial detachment and redistribution.

Therefore, over a field-relevant range of injection velocity (2 or 24 hours to reach a 20-ft distance) and solution concentration (10 mM PO_4 and 40 mM PO_4), there was no measurable change in the apatite distribution. The most significant finding, however, was that river water microbes present at 1100 times lower concentration than in situ microbes had roughly twice the impact on the citrate biodegradation rate. These experiments were conducted with a very high in situ microbial biomass (7.8 x 10^8 cells/g), which is present only in shallow sediment (Figure 2.2). These results would be generally applicable for infiltration experiments, which would occur in these shallow sediments. The 100-N injections occur at >15 ft depth, where the in situ microbial biomass is present at 10^2 to 10^6 cells/g. At these concentrations relative to the much more active

river water biomass, the injected river water microbial population would dominate nearly all the citrate biodegradation. To date, the temporal distribution of the river water biota has not been measured. The population in the open river water decreases as the temperature decreases, but the population near the water/sediment interface remains active throughout the year (Amoret Bunn, personal communication), so some consideration of the temporal distribution of the river water microbes may be necessary for future injections in order to be able to predict the citrate biodegradation rate and ultimately the location of the apatite precipitate.

4.2.4 Air/Surfactant Injection of Ca-Citrate-PO_4

The use of a surfactant (sodium laurel sulfate) was investigated as an alternate means (to solution infiltration) to emplace the Ca-citrate-PO_4 solution into vadose zone sediments. The generalized scenario for surfactant (foam) injection of Ca-citrate-PO_4 solution at field scale is to inject the foam into groundwater injection wells at low water table (i.e., a small screened section in the Hanford formation is unsaturated) so that the foam advects out and up from near the water table. The advantage of this injection scenario is any mobilized Sr-90 (from the solution injection) will be advected away from the saturated zone, which will minimize risk. As the surfactant tends to travel in high-K formations, this technology could be used to augment solution infiltration, which tends to deposit less PO_4 in high-K formations.

Figure 4.27. 25-ft long column containing Hanford formation sediment used in surfactant injection.

The surfactant/solution injection into these 25-ft long 1-D columns (Figure 4.27) was composed of a 1% sodium laurel sulfate (surfactant) solution that was advected with air pressure through a stainless steel frit to make a consistent bubble size. For this injection, 1% of the air volume was liquid containing 30 mM PO_4 (in Ca-citrate-PO_4 solution). In the first experiment, the inlet pressure was limited to 60 psi, and while the foam was initially at <10 psi, as water was deposited in the sediment, the pressure increased. Ultimately, the pressure limitation slowed the foam injection, which was initially at 250 mL/hour (average 113 mL/hour over the 79 hours). The total duration of the foam injection was 79 hours. At the end of the experiment, the sediment was carefully removed from the column and analyzed for water content and phosphate concentration. Although the volume of air was relatively high (113 mL/hour), the volume of liquid injected with the air was small (1%), so the solution injection rate was 1.13 mL/hour and, as a consequence, the total mass of PO_4 injected was small. At these slow solution injection rates, there is greater PO_4 adsorption and greater citrate biodegradation (described in Section 4.5), so it was expected that the phosphate would not be transported a great distance. Results (Figure 4.28a) showed that the foam and some water was advected to 5.4 m (18 ft), and appeared to be relatively uniform. The phosphate, however, was only advected a

meter or less (Figure 4.28b). The mass of PO_4 extracted from the sediment (229 mg PO_4) was 90% of the PO_4 injected (255 mg PO_4), so recovery was good.

A second 1-D column experiment was conducted using coarser sediment (>0.5-mm and <4-mm sieved Hanford formation sediment) and a higher injection pressure (110 psi). Results were about the same, with the foam reaching 6.5 m (21 ft) by 40 hours (Figure 4.29a), but PO_4 reaching a meter or less (Figure 4.29b). Phosphate recovery was also about the same (93% or 192 mg PO_4 recovered). These experiments were very useful for developing an understanding of the foam injection and sediment water content changes that occur throughout the experiment. Initially the sediment is at very low water content (6%), and foam (which is primarily air) easily infiltrates the column. Prior to injection of foam into the column, air injection into the column at 400 mL/hour (gas) resulted in <1 psi pressure drop over the 25-ft column length, so there is little resistance to air movement in this coarse sand sediment. However, infiltration of the surfactant (as foam) results in some resistance due to the resistance of forcing millimeter-sized bubbles through small pores. In addition, over time water advected in with the surfactant is deposited in sediment pores as bubbles break and reform. As the water content increases, the air permeability decreases and so the foam injection pressure increases. The 60-110 psi pressure used in these 25-ft long 1-D columns is not very representative of what is expected occur in the field, where radial flow from an injection well would cause less restriction of flow. In Section 4.5.7, results of two surfactant injections into large 2-D laboratory systems are described, and there was significantly less pressure.

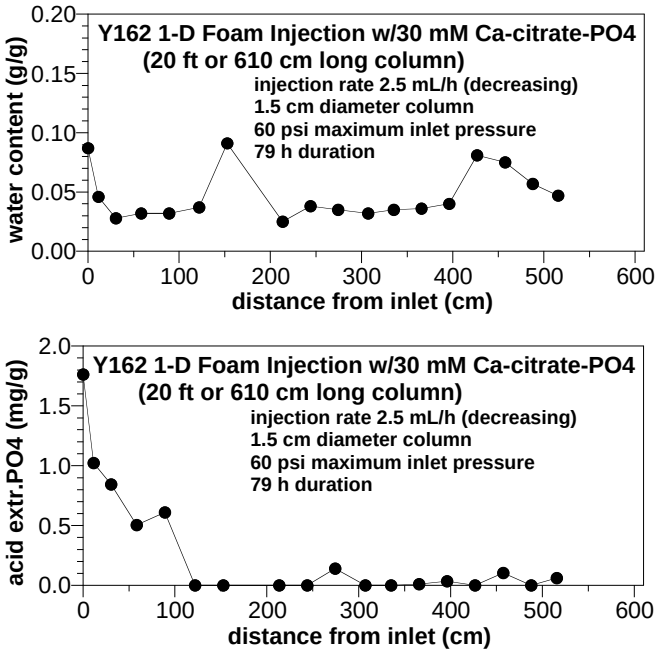

Figure 4.28. 25-ft long column of surfactant/Ca-citrate-PO_4 injection at 60 psi.

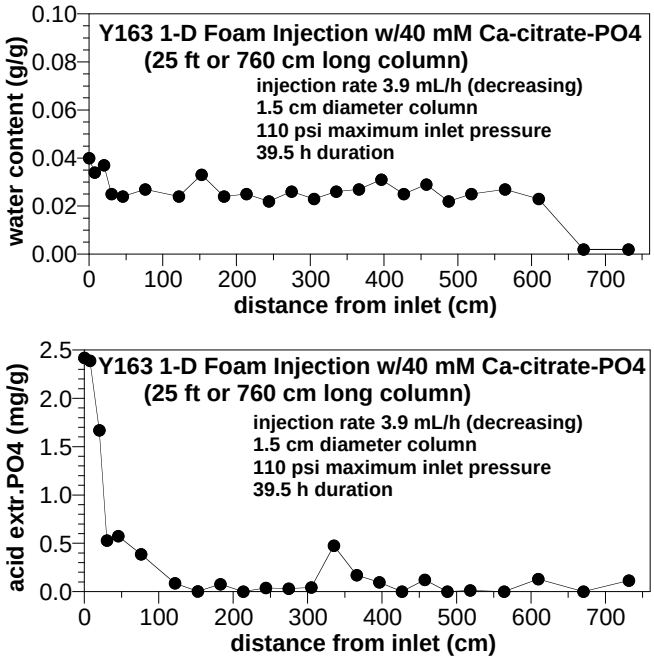

Figure 4.29. 25-ft long column of surfactant/Ca-citrate-PO_4 injection at 110 psi.

4.3 Task 3 – Sr Incorporation into Apatite: Mass and Rate

4.3.1 Sr Ion Exchange on Sediment

Batch experiments were conducted to measure the Sr-90 sorption rate in untreated and Ca-citrate-PO_4 solution-treated 100-N sediments and Sr-90 sorption at differing concentration (Figure 4.30). In some experiments, Sr-85 is used (easier to count, but short half-life, so not useful for long-term experiments), and in other experiments, Sr-90 was used (30-day wait period before it can be accurately counted, see Section 3.5). The starting sediment in both cases was a composite from the 10- to 42-ft depth at well N-121. The treated sediment contained ~0.5 g of apatite after being contacted with a Ca-citrate-PO_4 mixture (25, 50, 17.5 μM) for 3 days. This one treated sediment is referred to below as the apatite-laden sediment. To achieve a soil/water ratio near that in saturated porous media in both the untreated and apatite-laden sediments, 70 ml of Hanford groundwater containing 0.2 mg Sr/L was added to 116 g sediment. Each of these experiments was initiated by the addition of Sr-90 to achieve 45,000 pCi/L or an equivalent mass of Sr-85. The ionic strength in the treated sediment was ~0.1 M, diluted from the original Ca, PO_4, citrate treatment mixture, while that of the untreated sediment was that of the groundwater (0.011 M). At specified time intervals, 0.5 mL of water was removed, filtered with a 0.45-micron PTFE filter (13-mm diameter), and placed in a scintillation vial with scintillation fluid for counting. These samples were counted after 30 days after Sr-90/Y-90 secular equilibrium was achieved and the Sr-90 activity was half of the total activity.

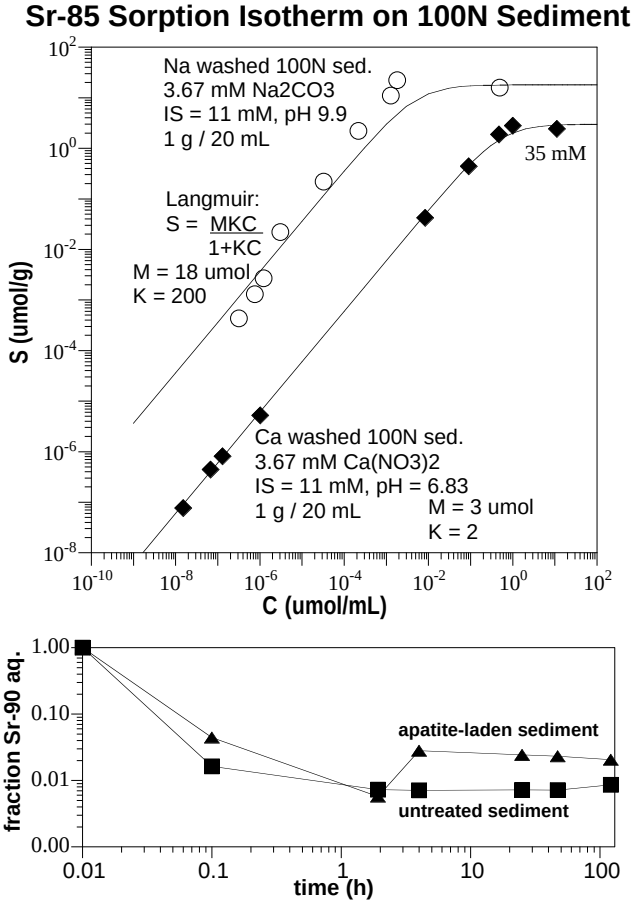

Figure 4.30. Sr-85/90 sorption: a) in groundwater, b) in mono- or divalent-saturated sediment, and c) time scale for Sr-90 sorption by untreated and apatite-laden 100-N composite sediment.

Sr-90 added to aqueous suspensions of untreated and treated 100-N sediments was rapidly sorbed (Figure 4.30b). The untreated sediment reached sorption equilibrium (squares) within 2 hours, giving a Sr K_d value of 24.7 cm^3/g. For the apatite-laden sediment that contained precipitated apatite, there was initial rapid uptake of Sr-90 (<1 hour) that was likely sorption. In this case, the solution Sr-90 continued to decrease even after 120 hours, likely due to some uptake by the apatite. Thus, we can conclude that for both the untreated and apatite treated sediment sorption is quite rapid.

The mechanism for Sr retention by sediment is ion exchange, as demonstrated in isotherm (and other) experiments. The 24-hour Sr-90 sorption in groundwater also showed a Sr K_d value of 24.7 cm^3/g in Ca-saturated sediment (black diamonds, Figure 4.30a), Sr-85 sorption over a wide range of concentration showed Langmuir behavior, indicating retention by primarily one type of site. If the slope at low Sr concentration was not equal to 1, this can indicate more than one type of surface site. Because the system is Ca-saturated (ionic strength 11 mM), both Ca and Sr compete for the same sites. In a Na-saturated sediment, 24-hour Sr sorption isotherm (open circles, Figure 4.30a) showed similar Langmuir behavior, but with ~600 times greater retention of Sr due to it more easily displacing Na from ion-exchange sites. In typical groundwater, the molar ratio of Ca/Sr is 220 to 400 times, so this 600 times greater retention simply reflects the divalent Sr displacing the monovalent Na on surface sites.

Small 1-D column experiments were conducted to measure the amount of Sr-90 mobilized by injection of a Ca-citrate-PO_4 solution relative to Hanford groundwater (results from 100-N injection project). Previous batch studies show that Sr (and Sr-90) K_d = 25 cm^3/g in Hanford groundwater (<4 mm size fraction of 100-N composite sediment). For a baseline of Sr behavior in sediments, two 1-D columns in which Sr-85 was added to the sediment and allowed to equilibrate for several days, injection of Hanford groundwater resulted in a K_d of 11.8 and 9.1 cm^3/g (i.e., Rf = 61 and 47.6, respectively, Figure 4.31), or slightly lower than shown in the previous batch studies.

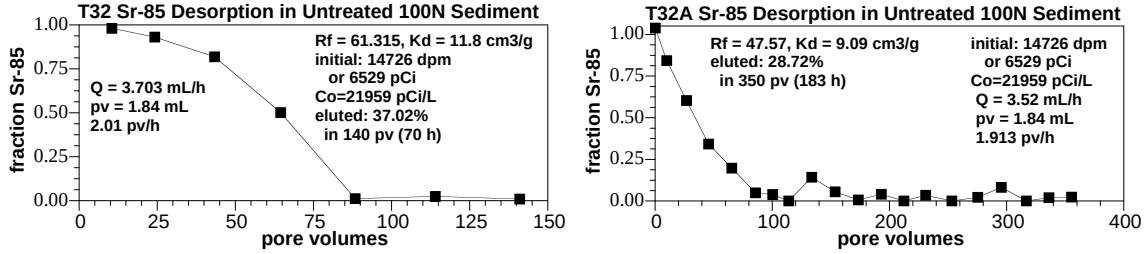

Figure 4.31. Sr-85 desorption in a 1-D column with Hanford groundwater injection.

In these experiments, a total of 140 and 350 pore volumes of Hanford groundwater were flushed through the columns. Over that amount of flushing, 37% and 29% of the Sr-85 was eluded. These results are applicable to the field, as the "flushing" with groundwater is simply exchanging the Sr-85/Sr on the sediment surface sites with Sr in groundwater. In general, the system is at equilibrium at all times, as there is no change in the mixture of cations (Ca, Na, K, Sr) and anions (CO_3, Cl, SO_4), and we assume the sediment was initially in equilibrium with groundwater.

Sr sorption to apatite-laden sediment was less than the untreated sediment, primarily due to the higher initial ionic strength of the apatite-laden sediment. For the apatite-laden sediment, the apparent K_d at 120 hours was 7.6 cm^3/g, which was smaller than the untreated sediment due to the higher solution ionic strength (described in detail in the following section). This was not unexpected because Sr-90 retention in Hanford 100-N sediments was primarily due to ion exchange (Serne and LeGore 1996). In a study of the influence of major ions on Sr retention by Hanford sediments, Routson et al. (1981) reported a Sr K_d of 49 cm^3/g (0.001 M $NaNO_3$) and K_d

of 16 cm^3/g (0.1 M $NaNO_3$), so there was a 3-time decrease in the K_d value by increasing the ionic strength with Na^+ (which was the predominant cation in the treated sediment after dilution with Hanford groundwater). In general, Sr^{2+} retention by ion exchange is controlled to a large extent by divalent cation (primarily Ca^{2+} and Mg^{2+}) concentration, as shown by a similar change in Ca^{2+} ionic strength (0.001 to 0.1), which resulted in a 38-time decrease in the Sr K_d value from 25 cm^3/g (in groundwater) to 2.0 cm^3/g (Ca-citrate-PO_4 at 40 mM, 100 mM, and 24 mM). Evidence to support our contention that sorption is predominately ion exchange is provided solid-phase extraction of these sediments in Section 4.3.3.

4.3.2 Sr Ion Exchange on Apatite

The sorption of Sr by citrate-precipitated crystalline apatite was investigated in batch experiments to determine 1) the rate of removal of Sr naturally occurring in 100-N groundwater, and 2) how this Sr was initially bound to the apatite within the first 4 days of contact. Both of these objectives are important in determining the effectiveness of and modeling of Sr remediation strategies. The 100-N groundwater used contained 0.225 mg/L of Sr (2.3 µM) to which a Sr-85 tracer was added. The loss of Sr-85 from solution was measured in a series of 10-ml apatite groundwater suspensions at pH 7 and room temperature. The solid to solution ratio (r_{sw}) in these individual suspensions varied from 0.27 to 30 g/L (100 times). This covers the range of estimated apatite mass required for the Sr barrier described in Section 2.3 (Table 2.1). After addition of the groundwater containing Sr and Sr-85, the individual suspensions were repetitively sampled for 100 hours.

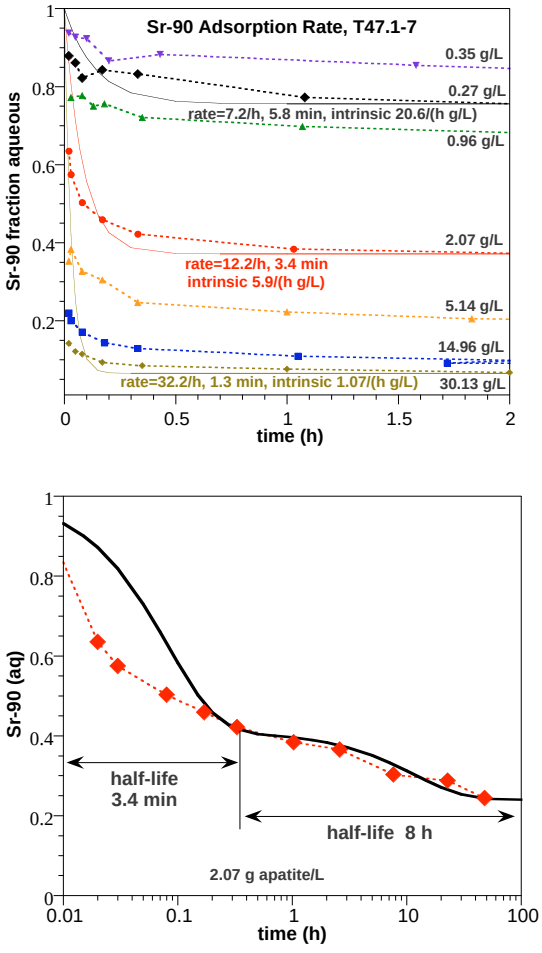

Figure 4.32. Initial rates of Sr sorption by apatite.

In all suspensions, two distinct rate steps were obvious for the sorption process. The initial sorption of Sr was quite rapid occurring with sorption half-lives ranging from 1.3 to 5.8 minutes for the high to low solid/solution ratio, respectively (Figures 4.32 and 4.33). First-order fits of the data are shown by solid lines and yielded rates of 32.2, 12.2, and 7.2 $hours^{-1}$ and intrinsic incorporation rate of 1.1, 5.9, and 20.6 (hours g L^{-1}) for the 30, 2.1, and 0.27 g/L suspensions, respectively. Following the initial rapid sorption step, sorption continued out to 100 hours (Figure 4.32b) at which point experiments were terminated. First-order fits for the times >2 hours (solid curves) provided rates of 0.085, 0.085, and 0.045 $hour^{-1}$ for the same three suspensions. The initial rapid removal of Sr from solution is most likely due to reaction of Sr with

easily accessible exchange sites on the apatite surface, with the slower step resulting from intra-particle diffusion to less accessible sites.

The fraction of Sr removed from solution is clearly dependent on the r_{sw} of the suspension with ~33% and 95.5% of the Sr sorbed for the 0.27- and 30.1-g/L apatite suspensions. The K_ds calculated from this data after 100 hours of contact show a near linear inverse dependence on the solid/solution ratio (Figure 4.34), and an average K_d = 1370 ± 429 cm^3/g. This shows that the adsorption affinity of Sr for the apatite surface is 55times stronger than the sediment (i.e., Sr K_d(apatite) = 1370 K_d(sed.) = 25). It is likely that the trend observed reflects a lack of sorption equilibrium for the higher apatite concentrations (i.e., diffusion into pores is taking longer), or reflects a small change in pH.

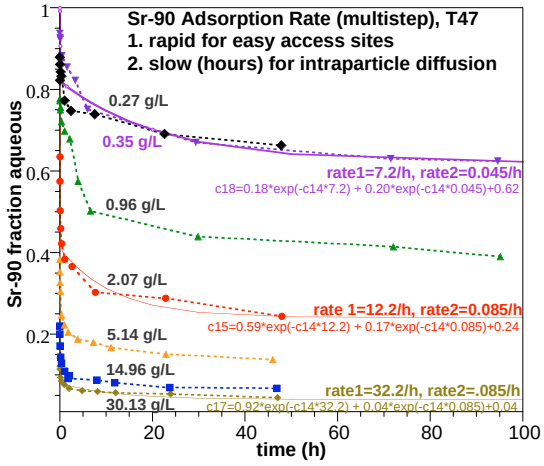

Figure 4.33. Long-term rates of Sr sorption by apatite.

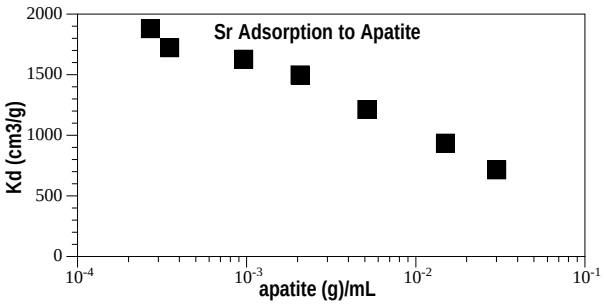

Figure 4.34. Sr sorption K_d by apatite verses mass of apatite.

Using the observed density and pore volume of 100-N sediments, the apatite soil to water ratios used in these experiments can be converted into g apatite/g sediment. That is, 30.1 and 0.27 g/L are equivalent to 3.1 x 10^{-3} and 2.7 x 10^{-5} g apatite/g sediment, respectively. This covers the range of apatite mass/g sediment targeted for field injections # 1 through #10 and 300-year capacity barrier for Sr removal described in Table 2.1. Based on the assumptions made in Table 2.1, this range of r_{sw} covers the quantity of apatite anticipated in field injections #1 through #10, with the maximum r_{sw} equivalent to that required for the 300-year capacity barrier. The small variation in K_d with changes in r_{sw}, or g apatite/g sediment, suggests that the inevitable spatial variations in the precipitation of apatite in the field will not significantly affect the sorption of Sr by apatite. As a result, the K_d values and the rates of sorption derived from these experiments should provide a reasonable basis for field simulations.

A parallel experiment to those shown in Figure 4.34 was conducted using a suspension containing 0.37 g apatite/L to determine if Sr-90 removed from solution in these experiments was bound to the apatite surface by ion exchange and whether after 100 hours, Sr-90 incorporation into the apatite structure (recrystallization) could be detected. After a 100-hour contact time, the suspension was centrifuged and following decanting of the supernatant, the wet apatite pellet was extracted with 0.5 M KNO_3 for 100 hours. A correction was made for the aqueous Sr-90 remaining in the pore water of the wet apatite pellet. The fraction sorbed was consistent with the 0.35 g/L suspension shown in Figure 4.34 and all of the sorbed fraction was recovered by the KNO_3 extraction, within the 4% error of the extraction and correction for solution Sr-90 in

the wet apatite. This indicates first, that Sr is bound to the apatite surface by ion exchange and second, that after 100 hours incorporation of Sr into the apatite structure at room temperature was not detectable, or if incorporation did occur, it was less than 4%.

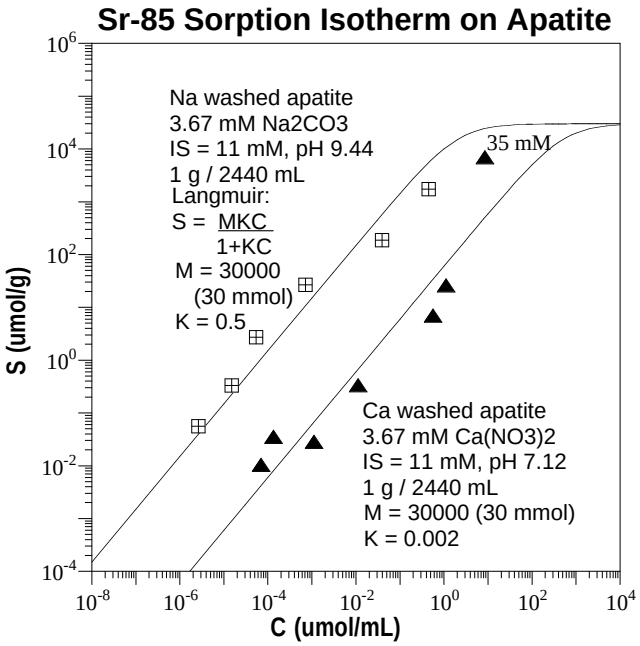

Figure 4.35. Sr ion exchange on apatite in Na- and Ca-saturated systems at differing Sr concentration.

The Sr sorption on apatite (24 hours) as a function of Sr concentration was also investigated. The pH (pzc) of the apatite is ~7.6, so Sr sorption at lower pH (pH 7.12 was investigated, Figure 4.35) should have much lower sorption (i.e., sites neutral to slightly positively charged) than Sr sorption at higher pH (pH 9.44 shown in Figure 4.35). Sr sorption at different concentration was fairly linear, reflecting a single type of sorption site, as expected. The adsorption maxima, unfortunately, was not well characterized, and is 30 mmol/g or higher. Comparison of Sr sorption on pure apatite at pH 7.1 (Figure 4.35, triangles) to sediment at pH 7.1 (Figure 4.30a) indicates the Sr affinity for the apatite surface is 100 times greater than for the sediment (i.e., M x K = K_d, for low concentrations not near the maxima). This is similar to the 55 times from different experiments. The relative adsorption maxima values on apatite (30 mmol/g) and sediment (18 μmol/g) show at 1660 times greater number of sites for the apatite. Relative sorption was also calculated for expected field apatite concentrations. For field injections #3 to #18, it is expected that there would be 0.00038 g of apatite per gram of sediment, assuming 100% of the phosphate injected forms apatite precipitate. At this low concentration, Sr adsorption mass balance is 99.2% sorbed, with 97.23% sorbed on sediment and 2.0% sorbed on apatite, excluding Sr incorporated into the apatite crystal structure. At the final maximum apatite concentration of 0.0038 g apatite per gram of sediment (Table 2.1, 300-year design capacity), 99.34% of the Sr-90 is adsorbed, but with 82.4% sorbed on sediment and 16.9% sorbed on apatite.

Sorption of Sr-90 on sediment and apatite performs several functions. First, sorption simply decreases the Sr-90 flux toward the river, whether or not apatite is present. As described earlier (Table 2.1), the influence of adding apatite will not be apparent in the short time frame as the fraction of Sr-90 in solution changes very little. Sorption on the apatite, however, is also necessary for incorporation into the apatite structure. If there were absolutely no Sr-90 sorption on apatite, there would likely be no Sr incorporation into the structure. It was hypothesized that the incorporation rate is dependent on the amount of Sr sorption on apatite. However, simulation of these ion exchange and Sr incorporation processes shows that the Sr incorporation rate does not change with less Sr sorption to apatite. The reason appears to be that the ion exchange is 5 to

6 orders of magnitude more rapid compared to incorporation, therefore, as long as there is some Sr sorption on apatite, the incorporation reaction will proceed.

4.3.3 Sr Incorporation into Apatite

4.3.3.1 Influence of Ca/Sr Ratio

The sorption and subsequent incorporation of aqueous Sr by apatite is known to depend on solution composition and, in particular, on the mole ratio of aqueous Ca to Sr (Ca_{aq}/Sr_{aq}) (Raicevic et al. 1996; Heslop et al. 2005). For this reason the influence of aqueous Ca and solution composition on the uptake of Sr by citrate precipitated apatite has been investigated. A series of batch experiments have been conducted using either distilled water or groundwater suspensions of apatite, which differed in their Ca_{aq}/Sr_{aq} mole ratios, ionic strength, and solution composition. Adjustments to ionic strength and aqueous Ca concentrations in both distilled and groundwater suspensions were made with Na and Ca perchlorate (Figure 4.36). In the groundwater suspensions, the starting ionic strength and Ca_{aq}/Sr_{aq} mole ratio were 16.75 and 1.36 mM, respectively, with the largest contribution to ionic strength coming from Ca ions. All suspensions contained 0.378 g/L apatite to which stable Sr (as $SrCl_2$) and a Sr-90 tracer were added to obtain an initial Sr_{aq} concentration of 0.35 mM. Suspensions were adjusted to an initial pH of 8.4 and were maintained at 82°C during the 9.5-month sampling period. Loss of Sr from solution was determined by Sr-90 measurements. Although the aqueous $Ca_{(aq)}/Sr_{(aq)}$ mole ratios were varied

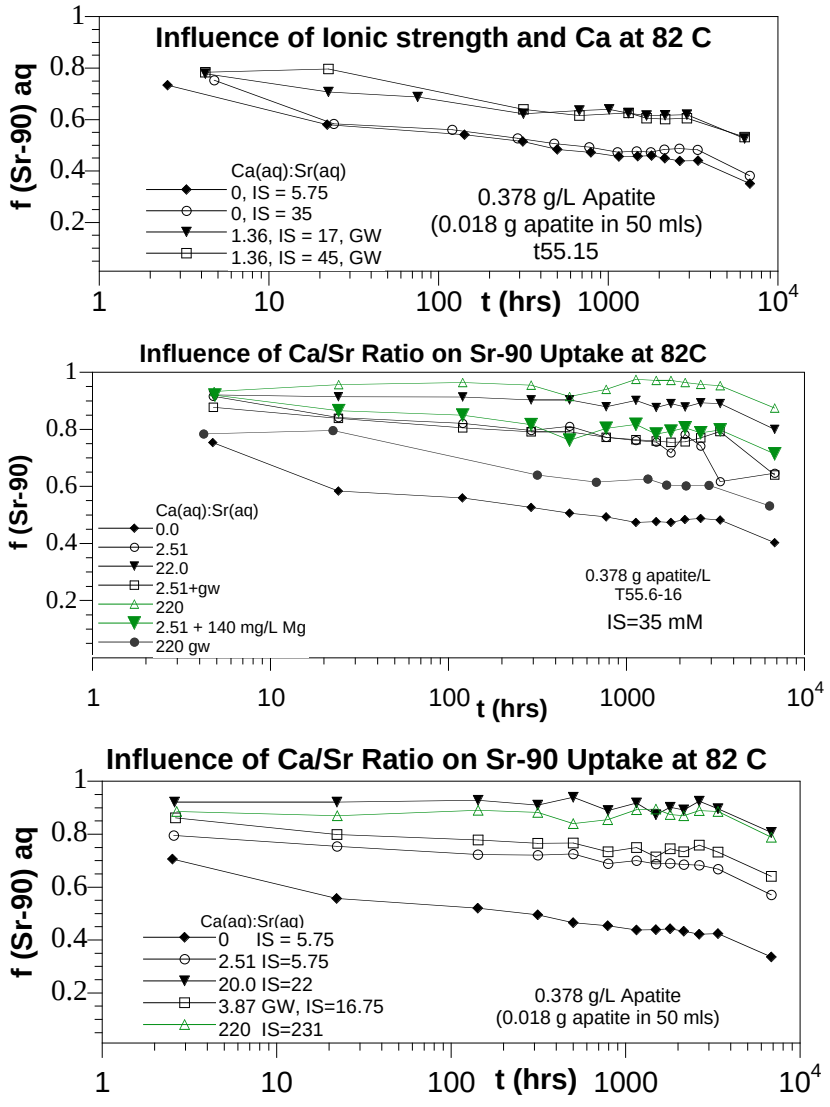

Figure 4.36. Influence of Ca, groundwater, and ionic strength at 82°C on Sr uptake by apatite.

from 0 to 220, the mole ratio of Ca in the apatite lattice to the Sr in solution ($Ca_{(s)}/Sr_{(aq)}$) was identical in all suspensions ($Ca_{(s)}/Sr_{(aq)} = 10$).

The initial rapid Sr uptake by apatite, due to sorption, was followed by the much slower uptake out to 7000 hours, due to Sr incorporation by apatite (Figure 4.36). The extent of Sr uptake was greatest for $NaClO_4$ suspensions containing no aqueous Ca ($Ca_{aq}/Sr_{aq} = 0$) for which Sr removal reached 57% after 1000 hours in both the 5.75 and 35 mM ionic-strength suspensions (Figure 4.36a). Thus, Na ions and the contribution of Na ions to ionic strength had negligible affect on Sr uptake. In groundwater suspensions with $Ca_{aq}/Sr_{aq} = 1.36$ and ionic strengths of 16.75 and 45 mM, the uptake of Sr was identical, but uptake had dropped to 37% after 1000 hours (Figure 4.36a). The difference in ionic strength between these two suspensions, due to $NaCl_2$ addition, made no difference in uptake, consistent with uptake in the Ca-free suspensions. The decrease in Sr uptake was due to the presence of di-valent Ca ions and their competitive influence on Sr ion exchange by apatite. This is further demonstrated in distilled water suspensions as the Ca_{aq}/Sr_{aq} ratio was increased to 2.5 (ionic strength = 5.75 mM) and 20 (ionic strength = 22 mM) and uptake dropped to 30% and 10%, respectively, after 1000 hours (Figure 4.36b). As the Ca_{aq}/Sr_{aq} ratio was further increased to 220 (ionic strength = 231), no further decrease in Sr uptake was observed relative to that at a ratio of 20.

From Sr uptake after 9.5 months (Table 4.4), we can conclude that: 1) the mono-valent background electrolyte $NaClO_4$ has no effect on Sr uptake by apatite and thus Na salts are the preferred choice for injection chemicals; 2) groundwater concentrations of divalent Ca reduces Sr uptake from 62 to 35; 3) at a Ca_{aq}/Sr_{aq} ratio of 220, typical of field injection solutions, Sr uptake by apatite had reached 17%; and 4) Sr uptake from solution by apatite, although slow, has not ceased to occur after 9.5 months. In addition, if all of the Sr removed from solution in these experiments were incorporated into the apatite structure by Sr substitution for a structural Ca, the percentage of the total Ca sites occupied by Sr would be small (1% to 7%) for conditions examined here (Table 4.5). For the $Ca_{(s)}/Sr_{(aq)}$ mole ratio (=10) used here, there should be ample capacity for additional Sr incorporation for contact times in excess of the 9.5 mouths.

Table 4.4. Sr uptake by citrate precipitated apatite in Figure 4.36 after 9.5 months versus aqueous Ca to Sr mole ratio.

Ca_{aq}/Sr_{aq} Mole ratio	**0** (Na)	**1.36(**GW)	**3.87(**Ca+GW)	**20**(Ca)	**220**(Ca)
Ionic strength	5.75	16.75	16.75	22	231
% Sr_{aq} uptake	62.4	35.1	31.9	16.3	17.1
% of Ca_s sites occupied by Sr	7.0	4.4	3.1	1.7	1.0

Symbols in parentheses indicates major electrolyte cation; GW indicates groundwater. Percent Ca_s sites in apatite occupied by Sr is based on measured Ca:P mole ratio = 1.27.

The rates of Sr/Sr-90 sorption and the subsequent incorporation into the citrate precipitated apatite structure were determined as a function of temperature (22°C, 42°C, 62°C, and 82° C) in aqueous suspensions of apatite. These batch experiments were performed using apatite suspensions made up in 50 ml of two different solutions (Table 4.5). The first suspension was made up in distilled water and contained 2.62 mM $NaClO_4$ as a background electrolyte, no Ca ions, and 1.04 mM stable Sr added as $SrCl_2$ (Figure 4.37). The second suspension was made up in 100-N groundwater containing 19 mg/L Ca ions and 0.11 mg/L (1.2 µM) Sr (Figure 4.38). Sr-90 was added to each suspension. The total Sr_{aq} in the $NaClO_4$ suspension was a factor of 867 times greater than the Sr_{aq} present in the groundwater suspensions. This accounts for the difference in the Ca_s/Sr_{aq} ratio between the $NaClO_4$ and groundwater suspensions. Sr-90 loss from solution was measured periodically over the 9.6-month course of the experiments.

For both suspensions and at all temperatures examined the initial fast sorption/ion-exchange phase (0 to 50 hours) was followed by a slower gradual uptake (50 to 1300 hours) and has continued out to 9.6 months (Figures 4.37 and 4.38). The extent of uptake increased ~10% with increasing temperature in both solutions (Table 4.5). The percentage of Sr uptake from the groundwater suspension (lower Sr_{aq} concentration with Ca ions) was 14% to 22% greater than from the $NaClO_4$ suspension with no apparent temperature dependence (Table 4.6). The reason for greater percentage uptake from the groundwater suspension, despite the presence of Ca ions, was the much higher concentration of Sr_{aq} (867 times) in the $NaClO_4$ suspension and thus the much higher occupancy of the Ca sites by Sr (Table 4.6). This estimation of Sr occupancy of apatite Ca sites assumes (as above) that all of the Sr_{aq} removed from solution after 9.6 months was substituted

Table 4.5. Conditions of Sr sorption-incorporation versus temperature experiments; units in mM.

	$NaClO_4$	Groundwater
Ionic strength	5.75	11
Sr_{aq}	1.04	0.0012
Ca_{aq}	0	0.48
Apatite (g/L)	0.38	0.34
Ca_{aq} : Sr_{aq}	0	392
Ca_s : Sr_{aq}	3.60	2938
Initial pH	8.0	7.6

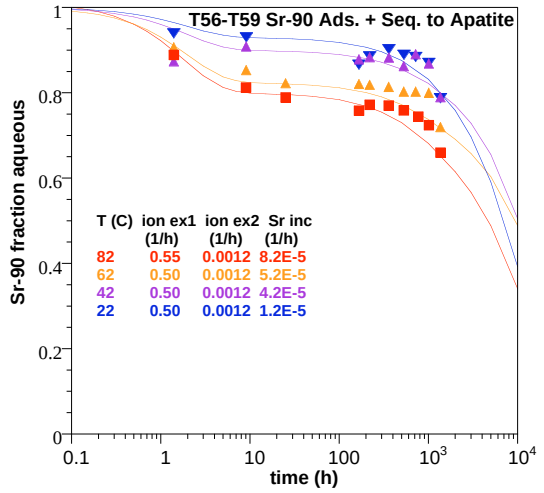

Figure 4.37. Sr-90 uptake by hydroxyapatite at 22°C to 82°C in deionized water with model fit of sorption and incorporation rate.

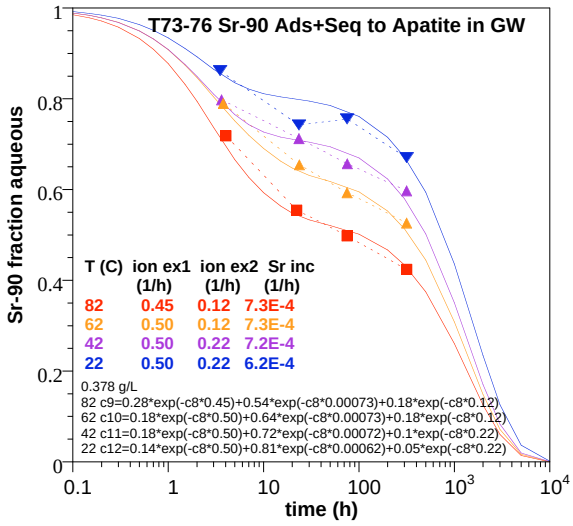

Figure 4.38. Sr-90 uptake by hydroxyapatite at 22°C to 82°C in groundwater with model fit of sorption and incorporation rate.

into the apatite by replacing a structural Ca. This estimated percent of Ca sites occupied by Sr was typically 580 times higher in the $NaClO_4$ suspension than in the groundwater suspension. This suggests that Sr incorporation at a low Ca site occupancy (low Sr loading of apatite) may be more 'effective' than at a much higher occupancy (or Sr loading) because of differences in Ca site accessibility to the sorbed Sr. This would lead to a saturation effect as aqueous and thus sorbed Sr increased. It should be noted that the assumption made in calculating the percent of Ca sites occupied by Sr (i.e., that all the sorbed Sr is incorporated into apatite) is consistent with the interpretation of data from the solid-phase HNO_3 digestion and ICP-MS analysis of apatite suspensions after 6 months of contact with Sr (see below).

Table 4.6. Sr uptake mass fraction and rate by apatite versus temperature after 9.6 and 8.6 months; GW indicates 100-N groundwater. Percent Ca_s sites in apatite occupied by Sr is based on measured Ca:P mole ratio = 1.27.

Suspensions		**22°C**	**42°C**	**62°C**	**82°C**
Apatite only in $NaClO_4$ (Sr=1 mM, 9.6 mo.)	% uptake	41.6	47.4	47.3	50.4
	% Ca sites occupied by Sr	13.5	15.3	15.3	16.3
[exp. T56, Figure 4-37]	Sr ion exch. rate (1/hour)	1.2E-03	1.2E-03	1.2E-03	1.2E-03
	Sr uptake rate (1/hour)	8.2E-05	5.2E-05	4.2E-05	1.2E-05
Apatite only in groundwater (Sr=2.3 µM, 8.6 mo.)	% uptake	61.4	61.2	69.4	72.3
	% Ca sites occupied by Sr	0.023	0.024	0.026	0.028
[exp. T73, Figure 4-38]	Sr ion exch. rate (1/hour)	0.12	0.12	0.22	0.22
	Sr uptake rate (1/hour)	6.2E-04	7.2E-04	7.3E-04	7.3E-04
apatite + sediment in groundwater (Sr= 2.3 µM, 8.6 mo.)	% uptake	63.5	69.7	66.4	72.6
	% Ca sites occupied by Sr	0.030	0.026	0.028	0.031
[exp. T69, Figure 4-36]	Sr ion exch. rate (1/hour)	0.45	0.45	0.45	0.50
	Sr uptake rate (1/hour)	6.5E-05	6.5E-05	3.5E-05	2.9E-05

A first-order model was used to derive sorption (two steps) and incorporation rate constants from uptake data from Figures 4.37 and 4.38. The fits to the data are shown by solid curves at each temperature in those figures along with the derived rate constants. Incorporation rate constants in the groundwater suspensions at the low Sr concentration were 8 times and 60 times greater than those in the $NaClO_4$ suspension at 22°C and 82°C, respectively. This further suggests a difference in the effectiveness or energetics of the Sr incorporation reaction as a function of Sr loading of available Ca sites.

The calculated activation energy of the rate of Sr-90 incorporation into apatite is 11.3 kJ/mol (Figure 4.39), using data of Sr-90 uptake from groundwater (Figure 4.37). This relatively low activation energy suggests the rate-controlling step is diffusion of Sr-90 into the apatite structure (i.e., activation energies <10 kJ/mol). Large activation energies (30 to 50 kJ/mol) suggest chemical control. The rate of diffusion can be altered with a different apatite precipitate particle size, where smaller precipitations with greater surface area will have a more rapid uptake. The

amount and location of Sr in the surface apatite has been characterized by several different methods, as described in the following section. Additional electron microprobe work is in progress in order to characterize the mass of Sr with depth within the apatite precipitate in order to determine if Sr is diffusing throughout the apatite volume, or is limited to near surface substitution, as described in the following section.

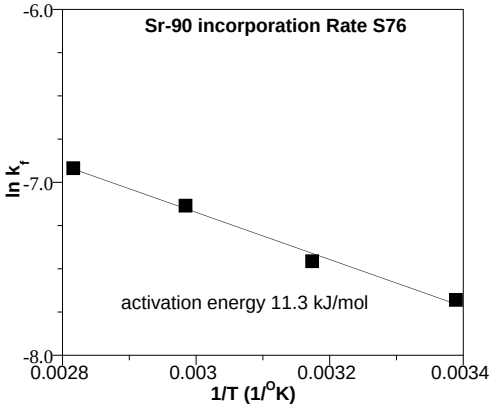

Figure 4.39. Change in Sr-90 incorporate with temperature and calculated activation energy.

4.3.3.2 Solid-phase Characterization for Sr Incorporation in Apatite

In this series of experiments, Sr incorporation into apatite was examined by ICP-MS analysis of the HNO_3 digested apatite phase after liquid-solid phase separation and removal of exchangeable and carbonate Sr phases from the apatite by sequential KNO_3 and EDTA extractions. Experimental conditions differed from those described in the preceding paragraphs of this section in that 1) no $NaClO_4$ was used to maintain the ionic strength, 2) no aqueous Ca was added to suspensions, and 3) both the apatite mass and aqueous Sr concentrations were increased (Table 4.7). In addition, two parallel experimental series were conducted, one using stable Sr plus a Sr-90 tracer and the second using only stable Sr. The stable Sr series was conducted to facilitate SEM, XRD, and FTIR analyses of non-radioactive apatite. In each experimental series, aqueous suspensions of both a commercial (Sigma) and citrate precipitated apatite (no sediment) were made up in distilled water to which $SrCl_2$ was added to obtain the same ratio of solid-phase Ca to aqueous Sr ratio (i.e., Ca_s/Sr_{aq} = 3.33 in both series). All suspensions were adjusted to an initial pH of 8 and maintained at 22°C and 82°C until individual suspensions in each series were sacrificed for analysis. The pH of all remaining suspensions were monitored periodically and returned to their original pH of 8 with NaOH. The differences in experimental conditions between the Sr-90 and stable Sr series are summarized in Table 4.7.

Table 4.7. Conditions of Sr sorption-incorporation experiments at 22°C and 82°C.

	Sr-90 Series	Stable Sr Series
Ionic strength (mM)	6.67	14.9
Apatite mass (g)	0.15	0.2
$SrCl_2$ (mM)	2.21	5.0
Volume (ml)	203	120
Measurements	Aqueous Sr-90, solid phase incorporated Sr90	Aqueous-ICP, SEM, XRD, FTIR, incorporated-ICP

For the Sr-90 series, five suspensions from each of the 22°C and 82°C experiments were sacrificed at regular intervals. Suspensions were characterized by analyzing for aqueous Sr-90 and performing the sequential 0.5 M KNO_3, 0.5 M ethylenediaminetetracetic acid (EDTA), and 4 M HNO_3 extractions on the recovered apatite. After aging for 4.9 months, the majority of the starting Sr remained in the aqueous phase, however, 11% and 14% of the starting Sr had been incorporated (HNO_3 extraction) into the apatite structure at 22°C and 82°C, respectively

Table 4.8. Percent distribution of Sr in apatite suspension for Sr-90 series (a) and mole percent of apatite Ca sited occupied by incorporated Sr (b) (aged 4.9 months).

	22°C	82°C
(a) % of total Sr in each phase		
Aqueous	86.8	82.9
Exchangeable (0.5 M KNO_3)	1.19	0.86
Carbonate (0.05 M EDTA)	0.85	1.9
Incorporated (4 M HNO_3)	11.1	14.3
(b) % of apatite Ca sites occupied by Sr	3.14	3.73

(Table 4.8). A small increase in incorporation occurred at the higher temperature. Only a small percentage of the Sr associated with the apatite remained in the exchangeable phase after 4.9 months. The mole percent of apatite Ca sites occupied by incorporated Sr after 4.9 months increased slightly with temperature. Suspensions sacrificed at 7 and 11 months at each temperature are currently being characterized.

For the stable Sr series, 15 apatite suspensions have been sacrificed to date, after aging between 0.86 and 6.15 months. Following centrifugation, the aqueous phase was saved for future Sr and Ca analysis. The apatite pellet was washed with 0.5 M KNO_3 overnight to remove ion exchangeable Sr and then washed several times in deionized water prior to solid-phase analysis. A portion of the apatite was digested in HNO_3 and analyzed for Sr and Ca by ICP-MS with the remainder of the apatite used for SEM, XRD, and FTIR characterization. No EDTA extraction carried out on these samples because the Sr carbonate phase was typically 1% or less of the total Sr in suspensions after 5 months (Table 4.9). The ICP-MS analysis of the HNO_3 digested citrate precipitated apatite showed that Sr incorporation was 16% and 33% of the total Sr in the system after 0.86 months at 22°C and 82°C, respectively (Table 4.9). This factor of two difference persisted during the course of these experiments. Comparison of the percent of incorporation that occurred at 0.86 months with that occurring between 2.68 and 3.89 months indicates that the rate of incorporation was decreasing. The Sr incorporation in these stable Sr suspensions at 22°C and 82°C was a factor of 1.9 and 2.7 greater, respectively (Table 4.9), than that found in the Sr-90 series (Table 4.8). The calculation of the percent of total Ca sites occupied by the observed incorporation of Sr in these HNO_3 extraction experiments after 6 months differed by a factor of two for suspensions at 22°C and 82°C (Table 4.9). This is not consistent with the calculated percent of Ca sites occupied by Sr for uptake experiments (Table 4.6) where the difference between 22°C and 82°C was typically 10%. The reason for these discrepancies is currently being investigated. Incorporation in the commercial Sigma apatite was approximately half of that achieved with the citrate-precipitated apatite. This was most likely due to differences in their morphology,

Table 4.9. Percent of total aqueous Sr incorporation into citrate precipitated and Sigma apatites for stable Sr series.

	Aged(m)	% Aqueous Sr Uptake	% Ca Sites Occupied by Sr
apatite			
22°C	0.86	16.3	4.90
	1.36	19.3	5.79
	2.68	21.9	6.59
	3.89	25.1	7.54
	4.93	21.1	6.33
	5.99	20.0	6.00
82°C	0.86	33.3	10.0
	1.36	33.3	10.0
	2.68	37.3	11.2
	3.89	42.4	12.7
	6.15	38.3	11.5
Sigma			
22°C	5.99	10.6	3.18
82°C	2.68	17.1	5.10
	5.99	19.0	5.69

although their BET surface areas are similar (Sigma, 61 m^2/g; citrate-precipitated, 55 m^2/g).

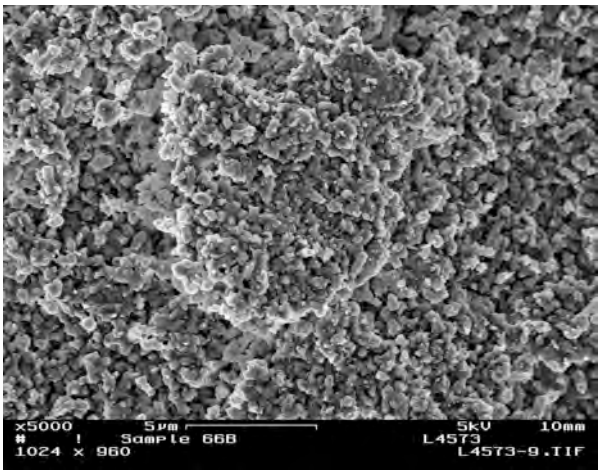

Figure 4.40. SEM image of citrate precipitated apatite used in Sr incorporation studies at 82°C.

The stable Sr suspensions aged for 0.86 and 1.36 months at each temperature have been characterized by SEM/EDS. The SEM image of the citrate precipitated apatite used in the stable Sr incorporation series and aged for 1.36 months at 82°C (Figure 4.40) showed discrete aggregated crystalline clusters ranging from 75 to 600 nm in diameter and significant porosity. The presence of Sr associated with the citrate precipitated apatite was examined by EDS in samples aged for 0.86 and 1.36 months at 22°C and 82°C. EDS spectrum obtained at 62 distinct sites on apatite particles in these 4 samples confirmed the presence of Sr at all sites. A typical EDS spectrum for apatite aged at 82°C for 0.86 month shows a clearly resolved Sr peak (Figure 4.41). As noted above, ion exchangeable Sr had been removed by an overnight wash with 0.5 M KNO_3, so the Sr detected by EDS was either a discrete Sr phase on the apatite surface or incorporated into the apatite structure. Although qualitative, the EDS estimation of Sr incorporation into the citrate-precipitated apatite was consistent with ICP-MS measurements of Sr incorporation in these same samples (Table 4.9).

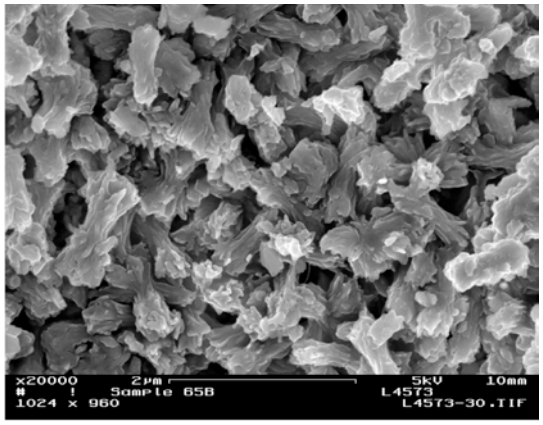

Figure 4.41. Image of apatite grain (a) for which EDS spectrum was obtained (b).

Fast XRD scans have been carried out on the citrate precipitated and Sigma apatites and confirmed the presence of crystalline apatite as the major phase in these starting materials (Figure 4.41). Fast XRD scans on selected samples of the Sr substituted apatites yield the same result. Currently, slower more precise XRD scans are being performed in order to detect trace phases within the major phase and any changes in crystallinity due to Sr substitution. This confirmed Sr incorporation within the apatite structure (next section). Magnification change on the apatite (5,000 times in Figure 4.40, 20,000 times in Figure 4.41a, and 100,000 times in Figure 4.42) show the rod-like structure of agglomerated apatite crystals that are 1 to 5 microns in size (Figure 4.41a), which are composed of 20- to 30-nm diameter apatite rods (Figure 4.42).

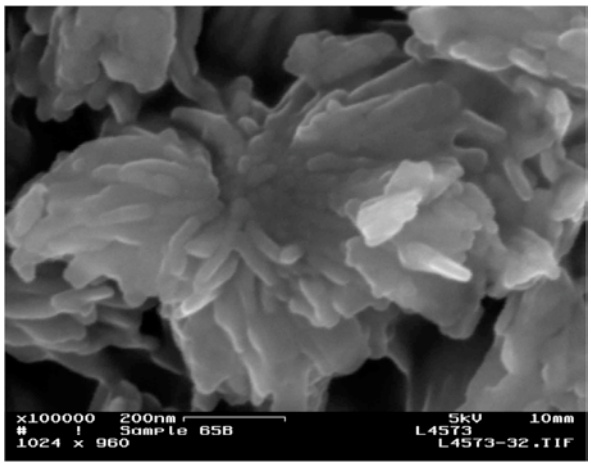

Figure 4.42. SEM image close-up (100,000 times) showing 20 to 30 nm apatite crystals.

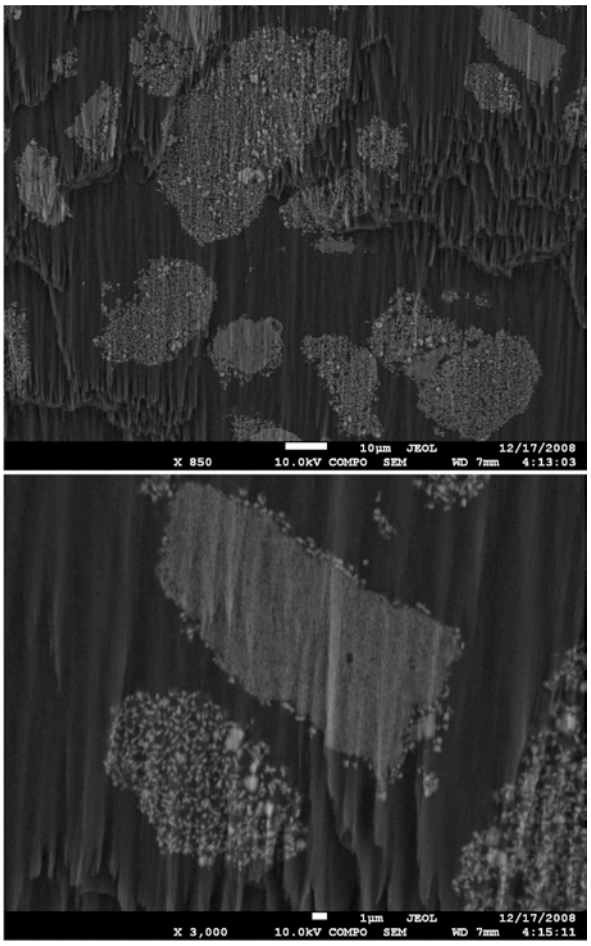

Figure 4.43. Electron backscatter picture of apatite particles (10 µm and 1 µm bars noted for scale).

Control FTIR spectra have been run on both the Sigma and citrate apatite starting materials. FTIR scans of the 82°C citrate precipitated apatite aged for 6.0 months demonstrated that no secondary phases (e.g., $SrPO_4$ or SrOH precipitate) have formed within the apatite structure, as shown in Figure 4.20 in which peaks for the Ca-apatite (Sigma standard) and Sr-substituted apatite are similar, but do not show characteristic peaks of the $Sr(OH)_2$ or $Sr(PO_4)$. Although the presence of Sr has been confirmed by ICP-MS and EDS, which strongly suggests that Sr has been incorporated, the FTIR analysis has not detected a difference between the Sr incorporated apatite samples and the control samples. Additional FTIR analysis of samples aged for longer periods with a higher percentage of Sr incorporation are attempting to observe this difference and thus definitively confirm that the Sr is replacing the Ca within the apatite structure.

4.3.3.3 Sr-Substituted Apatite: Depth Profile

As shown in the previous section, the slow substitution of Sr for Ca in the apatite structure can be as high as 13% (mol/mol) after 5 months (Table 4.9) and is expected to continue. Experiments conducted over a range of temperature (22°C to 82°C) were used to determine the activation energy (11.3 kJ/mol, Figure 4.39), which indicates likely rate control by diffusion. Higher activation energy (>15 kJ/mol) would be indicative of a chemical reaction rate control. At field scale, the emplaced apatite is expected to continue substitution of Sr for Ca for hundreds of years. It is possible that this high Sr substitution at short (<1 year) time scales would decrease if the morphology of the apatite precipitate varied with depth or diffusion was not controlling the substitution rate.

The electron microprobe was used to confirm that the Sr substitution in apatite (Figures 4.43-4.46) was diffusion controlled by measuring the Sr substitution with depth in single apatite

crystals. For this analysis, a Sr-substituted apatite from an experiment running for 1.3 years was used.

The dried apatite particles were encased in epoxy, then an edge cut and the electron beam was used to cut an edge for 12 hours. The resulting face (Figure 4.43) has a "curtain effect" from the plasma beam, but cleanly cuts the particles. These electron backscatter images show greater light intensity for higher molecular weight, so the black background is epoxy and grey particles are apatite (confirmed by EDS detection). Many of the particles show considerable color variation (i.e., vary from white to black), which appears to indicate these particles are actually conglomerates of very small apatite precipitate particles (<0.1 μm) making up the 10 to 50 μm-sized particles. Fewer of the particles have a single color, which indicates these are a single apatite crystal. In Figure 4.43b, the two morphologies are more clearly shown (3000 times magnification) with an upper single crystal and lower conglomerate particle. It should be noted that the single apatite crystal has some small apatite particles on its surface. Elemental detectors were used to focus on a 1.0 ± 0.5 μm spot (with depth of scan 1.0 μm) for measurement of Ca, Sr, and P (shown in Figure 4.41b).

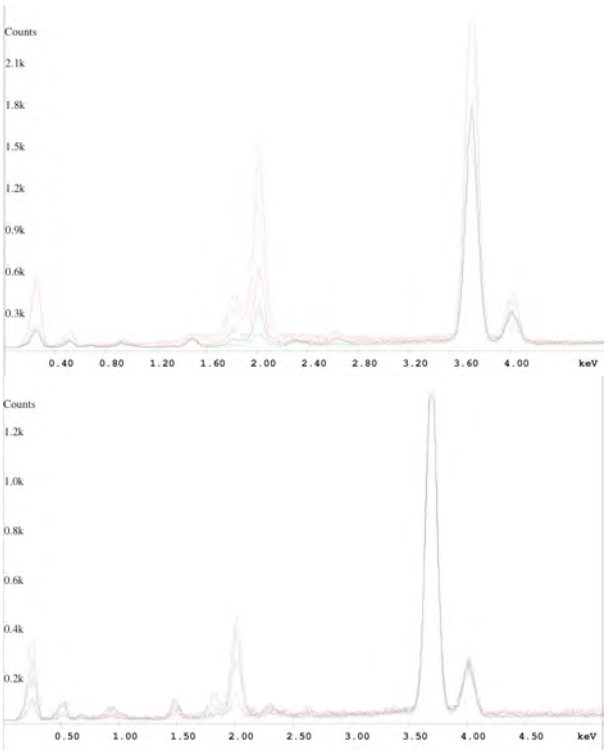

Figure 4.44. EDS scans of six points in two different particles.

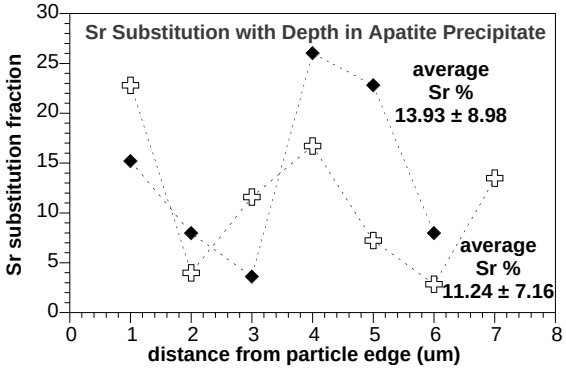

Figure 4.45. Sr substitution with depth in apatite precipitate with conglomerate morphology.

Two conglomerate particles were chosen to measure the Sr substitution with six points at different depth within a single particle. The EDS scans are superimposed for each of the six scans of the two particles (Figure 4.44). A separate sample from this batch experiment was treated to remove ion exchangeable Sr on the surface, then dissolved in acid and the liquid was measured for Ca and Sr by ICP to determine the average percentage Sr substitution. This averaged 16.1% after the 1.3 years. The Sr substitution for Ca in two different conglomerate particles did not have a trend with depth from the edge of the particle (Figure 4.45), indicating substitution was occurring throughout the presumed open structure.

Additional EDS scans of single apatite crystals were conducted to measure the variability in Sr uptake relative to the conglomerate type of particles. A low magnification (370 times,

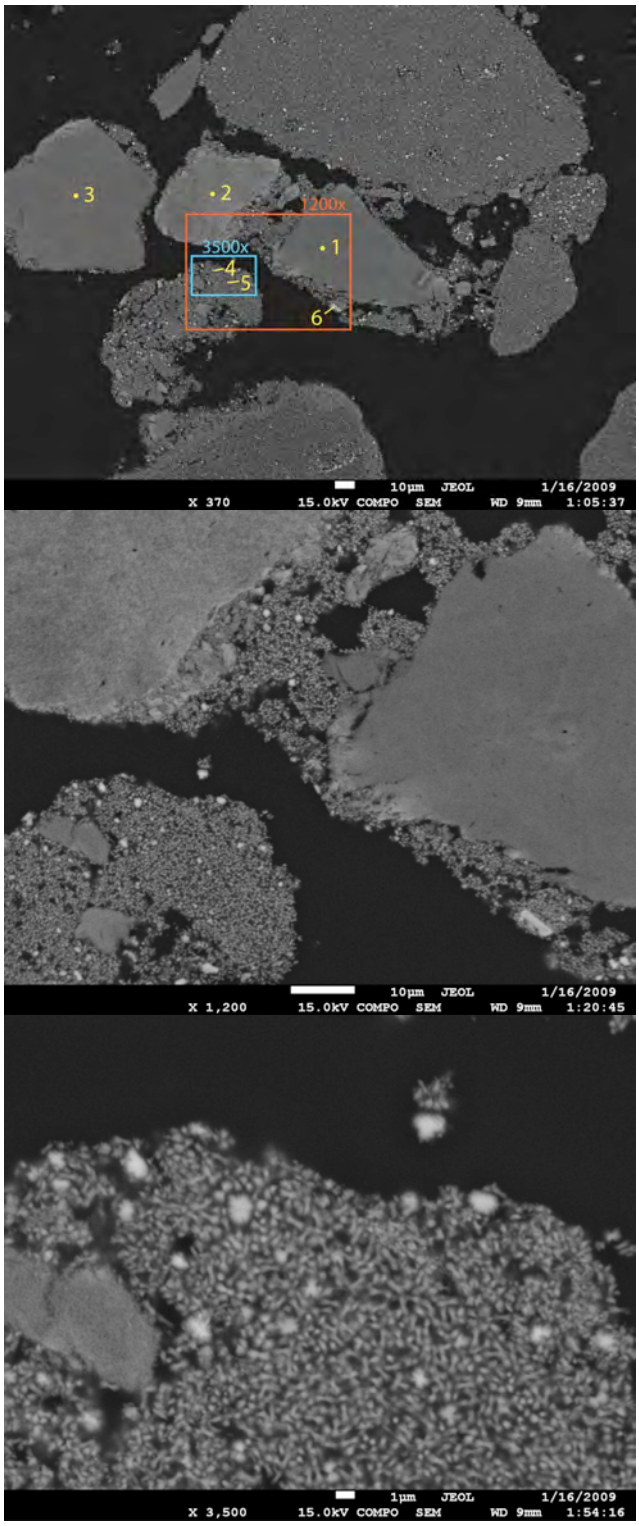

Figure 4.46. Sr substitution with depth in apatite precipitate with conglomerate morphology.

Figure 4.46a) electron backscatter image shows the location of the six EDS scans. The percent Sr substitution for Ca in these solid apatite particles averaged 9.15 ± 1.02% (7.96, 7.91, 9.90, 9.81, 9.06, and 10.28 for points 1 to 6), which was less than the average for conglomerate particles (Figure 4.45), although within statistical variability. The variablity of the Sr substitution between the six crystalline particles was, however, considerably less (standard deviation was 11.1% of the mean) and was also considerably less than the variability for the conglomerate particles (standard deviation was 65% of the mean).

Higher magnification of the apatite crystals (Figure 4.46b, c) show striking differences in electron backscatter (lighter color is higher molecular weight) between the conglomerate particles and the crystalline particles. The conglomerate particles appear to be composed of apatite crystals 0.1 to 1.0 micron in length, with a minor proportion (15%) larger crystals.

4.4 Task 4 – Simulation of Ca-Citrate-PO_4 Infiltration and Reactions

4.4.1 Simulation of Ion Exchange and Sr Incorporation into Apatite

To quantify the influence of a) the presence of sediment and b) aging of the Sr-90 on sediment, solid-phase extractions were conducted on these sediments. As previously described in Section 4.3.3, in untreated sediment (i.e., no apatite added), at the sediment/water ratio of one batch experiment, 5.6% of the Sr-90 was aqueous (Figure 4.47a, open triangles). In addition, the ion exchangeable fraction was 85%,

giving the total "mobile" (= aqueous + ion exchangeable) fraction of 90%, which remained constant over time, since there was no apatite addition. In contrast, the addition of the Ca-citrate-PO_4 solution (4, 10, 2.4 mM) caused several changes in Sr-90 proportions over time, as shown in Figure 4.47. Between 100 and 300 hours, the aqueous + ion exchangeable Sr-90 (mobile) fraction decreased from 90% to 43%, which is consistent with previous experiments reported (Sections 4.3.1, 4.3.2), in which a fraction of the Sr-90 (not all) is incorporated into apatite as it precipitates in hundreds of hours. The sequential extractions of the solid phase (carbonate and residual together = solid-associated) show that the remaining Sr-90 fraction (41%) cannot be mobilized with a high ionic-strength solution because it is incorporated into apatite. By 11,000 hours (15 months) 99.4% of the Sr-90 was associated with apatite in the experiment using field contaminated Sr-90 (containing 80 pCi/g Sr-90, no additional Sr-90 was added, Figure 4.47). The experiment in which Sr-90 was added showed essentially no difference in behavior throughout most of the experiment (to 4000 hours), but the last data point indicated less Sr-90 incorporation in apatite. Therefore, there appears to be no effect of aging (i.e., decades of Sr-90 contact time with sediment) on the use of this process to incorporate Sr-90 into apatite. These results are consistent with a previous study (Serne and LeGore 1996), in which ion-exchange experiments showed Sr-90 was readily desorbed after decades of contact with sediment. Because these experiments contained the spent Ca-citrate-PO_4 solution (i.e., high ionic strength relative to groundwater) for the entire experiment, additional long-term experiments were conducted to characterize the uptake rate and mass under conditions more likely to be encountered in the field, namely a groundwater aqueous phase.

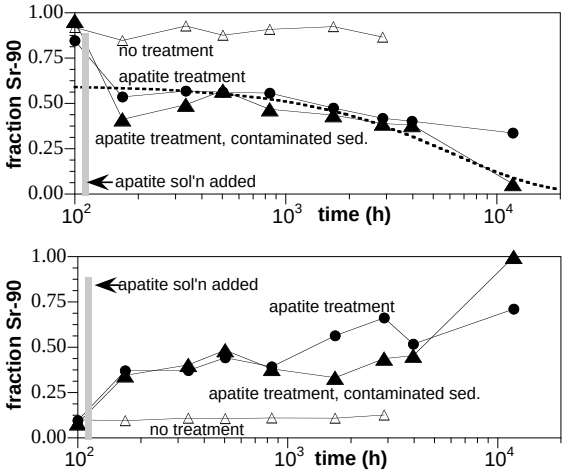

Figure 4.47. Sr-90 extractions of treated sediments originally containing Sr-90 or with Sr-90 added: a) aqueous + ion exchangeable (i.e., mobile) and b) solid phase associated (i.e., incorporated). Data from 100-N injection project.

Additional experiments were conducted as a function of temperature in this project to determine the Sr uptake rate from groundwater suspensions of 100-N sediment containing citrate precipitated apatite, as described in Section 4.3.3. The objective was to compare uptake in these suspensions with suspensions containing only apatite. For that reason, experimental conditions were identical to those used in the groundwater suspensions containing only apatite (Table 4.9), except here 1 g of sediment was added. Individual suspensions were adjusted to an initial pH = 7.6 and maintained at 22°C, 42°C, 62°C, and 82°C for 8.6 months, during which time they were periodically samples to determine Sr-90 loss from solution.

At all temperatures, the initial uptake of Sr due to sorption was very rapid as previously observed for suspensions containing only 100-N sediment or apatite. This Sr ion exchange was simulated as a two-step sorption process, with a rapid uptake <1 hour (assumed to be ion exchange) and a somewhat slower uptake to 100 hours (also ion exchange, but rate limited by diffusion to ion-exchange sites (Figure 4.48).

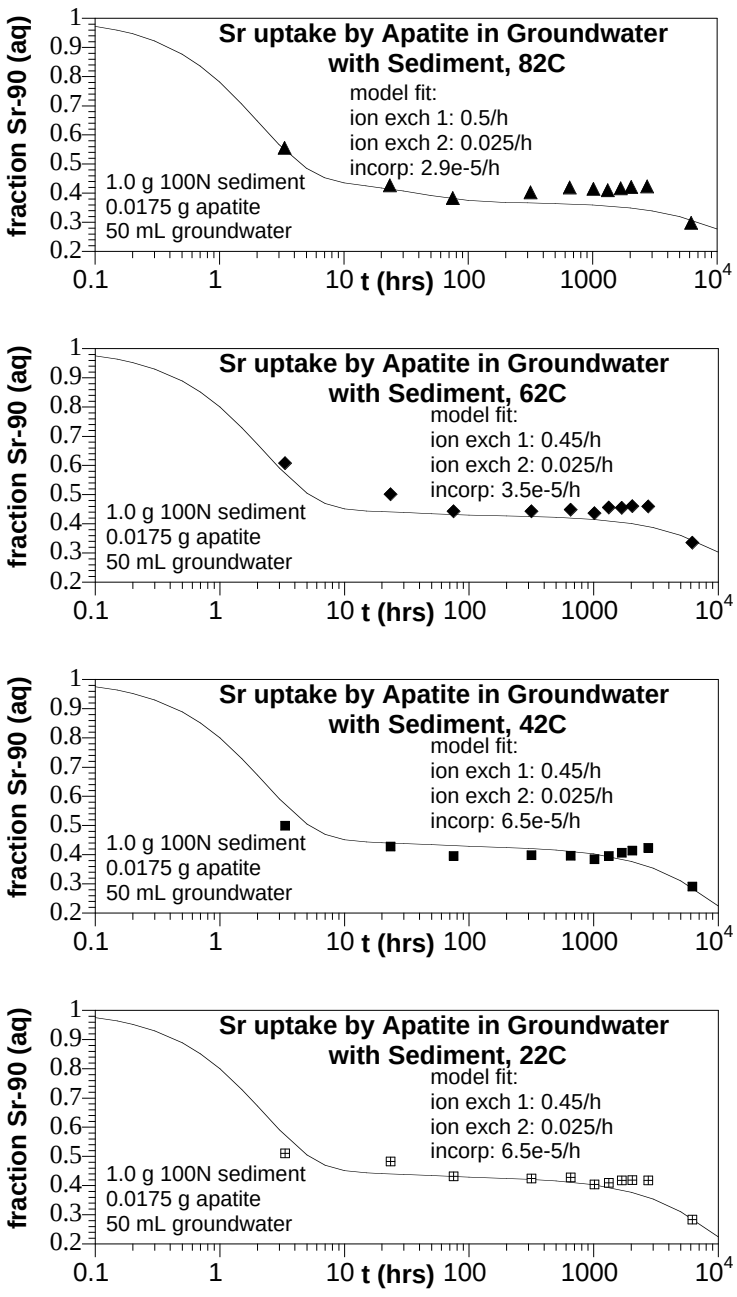

Figure 4.48. Sr uptake from groundwater suspension of 0.34 g/L apatite and 20 g/L sediment at 22°C to 82°C. Model fit of a two-step adsorption reaction and uptake from solution.

After ion-exchange equilibrium was reached (100 hours), there was a period of much slower uptake out to 6200 hours (8.6 months, Figure 4.48). After 8.6 months, 63.5% of the Sr had been removed from solution at 22°C compared to 72.6% at 82°C (Table 4.9). This extent of uptake and the difference in uptake with temperature were virtually identical to that observed in suspensions containing only apatite performed under identical conditions (compare results in Table 4.9). It is clearly evident that the sediment was playing a negligible role in the uptake of Sr. Thus, we can conclude that apatite was responsible for the continued uptake after the initial rapid sorption of Sr and that this continuation in uptake was most likely due to Sr substitution for structural Ca.

An additional simulation effort was conducted using the Sr-90 uptake data in the system with groundwater and sediment at 82°C (i.e., Figure 4.48a, experiment T69). The purpose of this simulation was to accurately simulate ion exchange and incorporation processes from laboratory data, and project the time scales of the same processes at the field scale with a much higher sediment/water ratio. A series of five reactions were used for this modeling effort: a) Ca-Na-Sr ion exchange on the sediment surface (2 reactions), b) Ca-Na-Sr ion exchange on the apatite surface (2 reactions), and c) Sr incorporation from Sr sorbed to apatite (1 reaction). The partial differential equations describing the time rate of change of eight species were initially numerically integrated within Mathcad, but later incorporated into a reactive transport code (RAFT) for future reactive transport simulations (see Appendix A, Section A.6). The simulation fit (lines, Figure 4.49) has initial conditions of 100% of the Sr in solution and Na-Ca ion-exchange equilibrium between aqueous solution, sediment ion-exchange sites, and apatite ion-exchange

sites. The simulation fit to data between 0.1 and 30 hours, ion-exchange reactions shows Sr (aqueous) decreasing to 0.45 (red), with an increase in ion exchange on the sediment (purple) and on apatite (blue). The Sr ion-exchange rate onto sediment was set slightly faster than onto apatite, so there is initially somewhat more Sr on the sediment (1 to 3 hours), which decreases by 30 hours as equilibrium is reached. Sr incorporation from Sr sorbed on the apatite occurs in thousands of hours, which is generally simulated. One interesting aspect of the simulation is that the incorporation data (red triangles) show an 11% drop in aqueous Sr, the actual incorporation is 32% (i.e., 1000 to 7000 hours), as Sr mass is also removed from ion-exchange sites on the sediment (5% decrease, purple) and sorbed on apatite (11% decrease, blue).

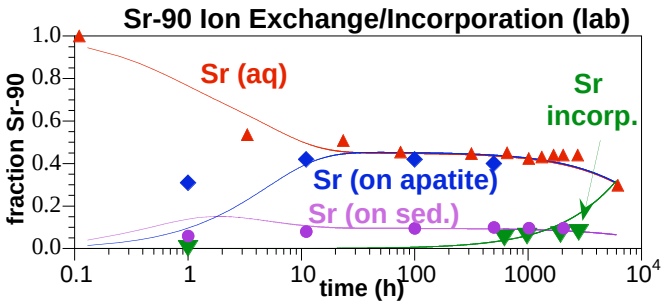

Figure 4.49. Sr uptake from groundwater suspension of 0.34 g/L apatite and 20 g/L sediment at 82°C. Model fit consists of Ca-Na-Sr ion exchange on sediment, Ca-Na-Sr ion exchange on apatite, and Sr incorporation within the apatite structure.

One fundamental question driving many experiments was whether the incorporation rate differs if the amount of Sr sorption on the apatite is different. At very high sediment/water ratios in the field, there is a significant amount of sorption to sediment, so there is proportionally less sorption to apatite. In addition, experiments described in Section 4.3.3 start with a simple system of aqueous Sr (no Ca or groundwater) and apatite only, and build in complexity with the addition of increasing amounts of Ca (which competes for ion-exchange sites on the apatite surface), and sediment (which sorbs both Ca and Sr). The mass fraction of Sr-90 sorbed in different apatite/ sediment/water systems (laboratory and field) can be illustrated to describe Sr-90 sorbed mass differences between laboratory and field systems (Table 4.10). First, comparison of Sr/apatite and Sr/sediment laboratory systems (lines 1 to 4, Table 4.10) show the 55 times stronger Sr affinity for apatite results in a higher fraction sorbed.

Table 4.10. Sr-90 fraction sorbed in different sediment/apatite/water systems.

							ion exchange equilibrium			
system	#	Kd, apa. (cm3/g)	Kd, sed. (cm3/g)	apatite mass (g)	sediment mass (g)	volume (mL)	fraction aqueous	fraction sorbed on apatite	fraction sorbed on sediment	fraction sorbed total
laboratory systems										
Sr/apatite only	1	1350		0.0038		50	0.9069	0.0931	0	0.0931
	2	1350		0.0038		1.0	0.1631	0.8369	0	0.8369
Sr/sediment only	3		25		0.0038	50	0.9981	0	0.0019	0.0019
	4		25		0.0038	1.0	0.9132	0	0.0868	0.0868
Sr/apatite/sed.	5	1350	25	0.0038	0.0038	50	0.9054	0.0929	0.0017	0.0946
	6	1350	25	0.0038	0.0038	1.0	0.1606	0.8241	0.0153	0.8394
	7	1350	25	0.0038	1.0	50	0.6240	0.0640	0.3120	0.3760
	8	1350	25	0	1.0	50	0.6667	0.0000	0.3333	0.3333
field systems										
Sr/sediment only	9	1350	25	0	1.0	0.2	0.0079	0.0000	0.9921	0.9921
Sr/sed./apatite	10	1350	25	0.00038	1.0	0.2	0.0078	0.0200	0.9723	0.9922
Sr/sed./apatite	11	1350	25	0.0038	1.0	0.2	0.0066	0.1691	0.8243	0.9934

More specifically, for the system with 1.0 mL of water and 0.0038 g apatite (line 2), 84% of the Sr-90 is sorbed on the apatite. In contrast, for the system with 1.0 mL of water and 0.0038 g of sediment (line 4), only 9% of the Sr-90 is sorbed. When the system contains both sediment and apatite (line 6, 0.0038 g apatite, 0.0038 g sediment), sorption on apatite drops slightly (82%), but sorption on the sediment drops significantly (1.5%).

While laboratory systems can contain significant quantities of apatite and only a little sediment, the field system has a very high sediment/water ratio. Assuming 20% porosity, 1.0 g of sediment is in contact with 0.2 mL of water, so Sr is 99.2% sorbed (line 9), leaving 0.8% in solution. If 3.8E-04 g of apatite per gram of sediment is added (i.e., Table 2.1, amount injected in field injections #3 to #18), Sr-90 total sorption is essentially the same (line 10, last column), but 2% of the sorbed mass is now on apatite. If the final design mass fraction of apatite is added (3.8E-03 g apatite/g sediment, line 11), the total Sr-90 sorption fraction increases very slightly, but now 17% of the Sr-90 mass is sorbed on apatite.

To test whether Sr-90 incorporation into apatite is dependent on the mass fraction of Sr-90 sorbed onto the apatite, reaction parameters derived from a laboratory experiment (Figure 4.49), which includes Ca-Na-Sr ion exchange on apatite and sediment, and Sr incorporation into apatite, was used in a simulation of the same system with the only changing being the increased sediment/water ratio of the field (20% porosity assumed). Comparison of the laboratory simulation (Figure 4.49) to field simulation (Figure 4.50) shows the obvious much greater proportion of Sr mass sorbed on the sediment in the field system (1 to 1000 hours), as compared to the laboratory system. The proportion of Sr mass sorbed on apatite, therefore decreased from 45% (laboratory system) to 17% (field simulation, Figure 4.50). However, this decrease in Sr mass sorbed to apatite did not change the Sr incorporation rate (green line in Figures 4.48 and 4.49), which has a half-life of 15 months in both cases. The reason for this lack of change is the relative time scales of ion-exchange reactions versus the incorporation reaction being 5 to 6 orders of magnitude different. Any small amount of Sr sorbed on apatite is slowly incorporated and additional Sr mass sorbs onto the apatite. Ion-exchange equilibrium is quickly reached, so has no influence on slowing down the incorporation reaction. In contrast, if the ion exchange and incorporation reaction rates were only an order of magnitude different, then there the ion-exchange reaction would slow the apparent incorporation rate.

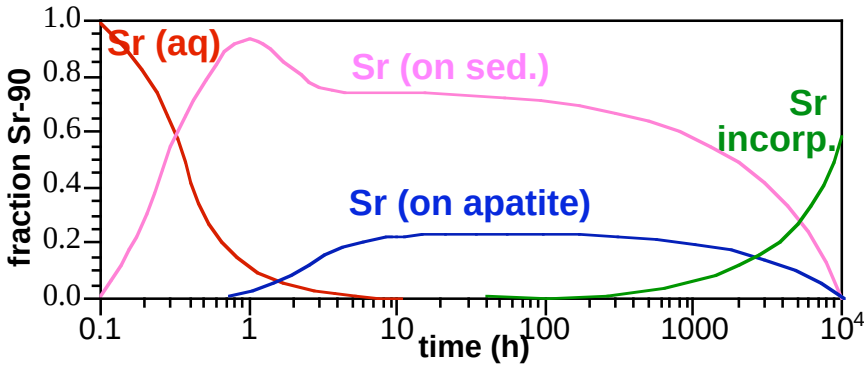

Figure 4.50. Simulation of Sr-90 mass changes under field conditions of 20% porosity and 0.0038 g apatite/g sediment. Simulation includes Ca-Na-Sr ion exchange on sediment, Ca-Na-Sr ion exchange on apatite, and Sr incorporation into apatite.

4.4.2 Geochemical Speciation with Biodegradation and Precipitation

Geochemical equilibrium simulations of Ca-citrate-PO_4 solution mixed with groundwater were used to identify reactions major species changes that occur during citrate biodegradation. These reactions were used in the equilibrium/kinetic reactive transport simulations in the following sections. Placement of $CaCl_2$ and Na_3citrate in deionized water (Appendix A, Section A.6) results in 60% Ca-citrate complex and 40% free citrate (pH 7-8), so 2.5 times greater citrate relative to injected Ca is needed to maintain the Ca-citrate complex (and prevent apatite precipitation). Placement of 4 mM Ca and 10 mM citrate in Hanford 100-N groundwater (Appendix A, Section A.6, simulation 2) at pH 7.9 results in a slight difference in citrate speciation (51% Ca-citrate, 35.4% free citrate, 8.2% Na-citrate, and 5.3% Mg-citrate) relative to the solution in deionized water. Addition of 4 mM Ca, 10 mM citrate, and 2.4 mM PO_4 (with 50 mM Na, field injection formula #1, Table 3.1) in a geochemical equilibrium model results in the rapid precipitation of Ca-PO_4, so most of the Ca is no longer in solution. In reality, the Ca-citrate-PO_4 solution is stable for 24 to 36 hours before precipitation occurs (in the absence of citrate biodegradation).

Simulation of half of the 10 mM citrate being degraded to 2.5 mM acetate and 2.5 mM formate in Hanford groundwater (Appendix A, Section A.6, simulation 4) results in the Ca-citrate complex being maintained; 80% of citrate is the Ca-citrate complex, 8.4% as free citrate, and 8.2% as Mg-citrate. Finally, simulation of all of the 10 mM citrate being degraded to 5 mM acetate and 5 mM formate in Hanford groundwater (Appendix A, Section A.6, simulation 5) obviously has no Ca-citrate complex. There are minor concentrations of Ca-formate and Ca-acetate, which account for <6% of the injected Ca mass. Therefore, the presence of citrate in Hanford groundwater will support the Ca-citrate complex, and biodegradation of citrate will then result in available Ca^{2+}, as the citrate degradation products formate and acetate form weak Ca-complexes.

4.4.3 1-D Infiltration Simulation

A reactive transport model (STOMP) capable of 3-D unsaturated and saturated zone transport was modified with the series of reactions to account for metal-CO_3, -OH, -citrate and PO_4 aqueous speciation, cation exchange (Sr, Ca, Mg, Na, K, NH_4), citrate biodegradation, and solids precipitation/dissolution (apatite, $CaCO_3$, $SrCO_3$). This was ~42 reactions with 51 species (listed in Appendix A, Section A.7). Simulation of 1-D injection of ammonium phosphate into a 1-m long column (experiment Y17, Figure 4.51; data from Fluor 100-N injection project) with this highly complex model fit the experimental data well. This data set was initially chosen as it represents injection of phosphate without Ca-citrate (simpler system to model). Calcium and strontium peaks (~3 times) by solution injection due to ion exchange, while appear large, actually account for an insignificant amount of Ca and Sr mass desorbing from the sediment ion-exchange sites. Integration of the Sr mass desorbing (Figure 4.51b) relative to the mass on ion-exchange sites (Figure 4.51d) shows that 3.1% of the Sr was removed by the injection process. The dip in Na sorbed to sediment (X-Na) resulted from the NH_4 replacing about 30% of the Na (NH_4 has a stronger affinity for the surface compared with Na).

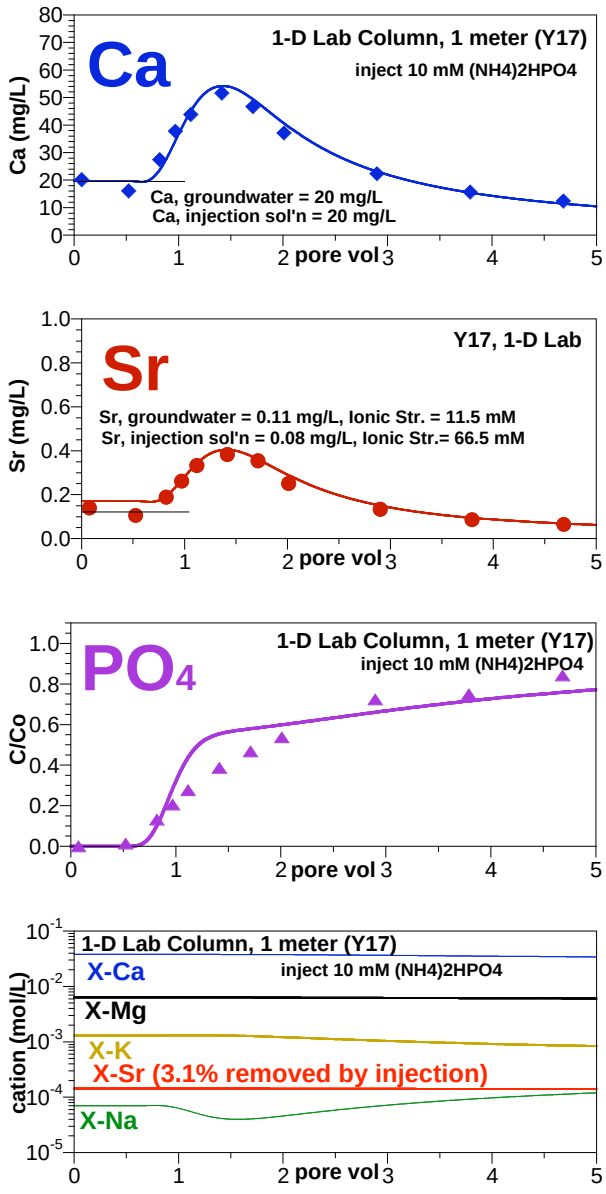

Figure 4.51. 1-D reactive transport simulation of a 1-meter sediment column injection of a PO_4 solution (experiment Y17 from 100-N Injection Project).

Simulation of the injection of a Ca-citrate-PO_4 solution (1, 2.5, 10 mM) over a 31-day period (Figure 4.52, experiment Y88, data from Fluor 100-N injection project) also shows general agreement between the data and simulation of the multiple break-through species. In this experiment, the Ca-citrate-PO_4 solution was injected at a rapid rate to achieve a 6.9-hour residence time for a total of 24 hours or 3.5 pore volumes (similar to a field injection), followed by a 30-day slow flow rate injection of groundwater with a 453-hour residence time. This solution is similar in major component concentrations to field injections #3 to #18 (Table 3.1), but differs in the fact that this laboratory experiment used 20 mM NH_4^+, whereas the field injection used 17.6 mM Na^+ and 1.0 mM NH_4^+, to limit both N for microbes and also limit Ca^{2+} and Sr^{2+} ion exchange.

The experimental data shows Ca^{2+} (third panel, Figure 4.52) and Sr^{2+} (first panel) concentration during initial solution break-through at 5 to 10 hours peaking at ~6 times the equilibrium groundwater concentration. Phosphate break through lags (green line, second panel), but apatite precipitation starts to occur in the 10- to 100-hour time frame, then decreases in extent. The final change that occurs in the system is at 800 hours, when the large Na^+ pulse is eluded out of the system due to the slow groundwater injection, and Sr^{2+} and Ca^{2+} decrease, largely (in this case) due to ion exchange onto the sediment (not precipitation).

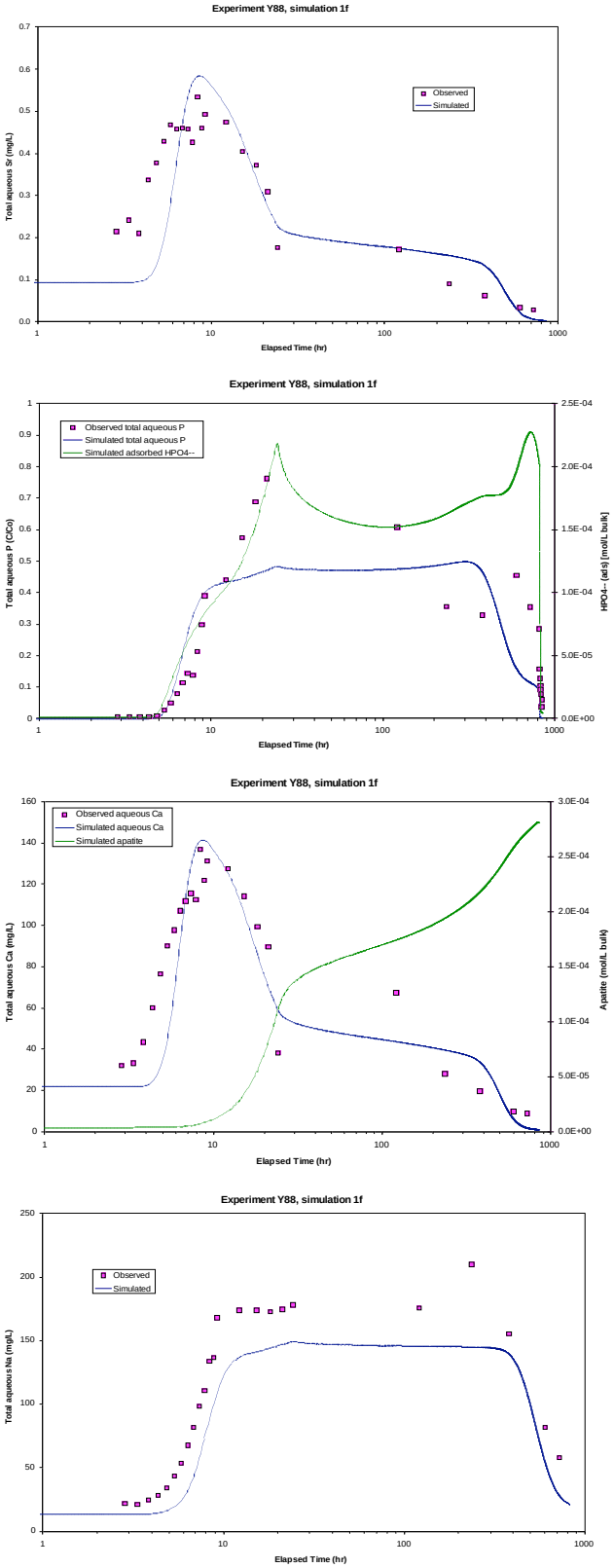

Figure 4.52. Simulation of 1-D injection of a Ca-citrate-PO_4 solution (experiment Y88, similar to field injections #3 to #18).

Some numerical issues were encountered with STOMP when solving the coupled equilibrium-component-kinetic equations associated with the Ca-phosphate-citrate reaction network, which includes ion-exchange, biodegradation, cell growth, and precipitation-dissolution reactions. One problem appears to be associated with the logK values and the different species used for the apatite reactions in different thermodynamic databases. The kinetic equations solved by STOMP for mineral precipitation-dissolution reactions are based on transition-state theory (TST) and can be expressed as

$$R_k = A_m k\left[1-\left(\frac{Q}{K_{eq}}\right)\right]; k = k_{ref}\left[\frac{-E_a}{R}\left(\frac{1}{T}-\frac{1}{T_{ref}}\right)\right] \tag{4.1}$$

where R_k is the mineral precipitation or dissolution rate, A_m is the mineral specific surface area (m^3/kg aqueous), k is the intrinsic rate constant (mol/m^2 s), Q is the reaction quotient (dimensionless), and K_{eq} is the equilibrium constant for the reaction. The parameter k_{ref} is the rate constant determined at reference temperature T_{ref} (C), E_a is the activation energy (J/mol), and R is the gas constant.

The apatite precipitation-dissolution reaction given in the Geochemist's Workbench, V5.0 database, thermo_minteq.dat, is

$$\text{Hydroxyapatite} = 5Ca^{++} + 3PO4^{---} + H2O - H^{+} \quad \log K = -44.33 \tag{4.2}$$

with logK independent of temperature. The reaction quotient for Eq. (4.2) is

$$Q = \frac{[Ca^{++}]^5[PO4^{---}]^3}{[H^+]} \tag{4.3}$$

The apatite precipitation-dissolution reaction given in the CRUNCH database, datacom.dbs, is

$$\text{Hydroxyapatite} = 5Ca^{++} + 3HPO4^{--} + H2O - 4H^{+} \quad \log K = \text{variable} \tag{4.4}$$

with logK dependent on temperature. The reaction quotient for Eq. (4.4) is

$$Q = \frac{[Ca^{++}]^5[HPO4^{--}]^3}{[H^+]^4} \tag{4.5}$$

The temperature-dependence of the hydroxyapatite logK shows a decrease with increasing temperature.

Table 4.11 shows calculated values of Q/K_{eq} (see Eq. 4.1) based on typical groundwater concentrations for the aqueous species in Eq. (4.2) and Eq. (4.4). As shown in Table 4.11, the Q/K_{eq} ratios are dramatically different, depending not only on which K_{eq} value is used, but also on

which form of the apatite precipitation reaction is used (Eq. 4.2 or Eq. 4.4). The reaction rates are not determined solely by Q/K_{eq}, since they are modulated by the values of k and A_m in Eq. (4.1). However, the reaction rates predicted by these different values of Q/K_{eq} for different reaction equations and $\log K_{eq}$ values will be dramatically different.

The faster rates predicted by Eq. (4.4) are due primarily to the magnitude of the denominator in Eq. (4.5), but also to the higher concentrations of HPO_4^{--} relative to PO_4^{---} used in Eq. (4.3). The small value of $[H^+]$ = 2.8E-08 mol/L, raised to the fourth power, yields 6.14E-31. When the numerator in Eq. (4.5) is divided by this small number, a very large number (2.49E+49) results that can cause numerical difficulties.

Table 4.11. Calculated values of Q/K_{eq} for apatite precipitation-dissolution reactions (Eq. 4.3 and Eq. 4.5) based on typical aqueous solution concentrations and logK values from different thermodynamic databases.

		Reaction Quotient Eq. (4.3)		Reaction Quotient Eq. (4.5)	
Species	Conc. (mol/L)	Q/K_{eq} $\log K_{eq}$ = -44.33	Q/K_{eq} $\log K_{eq}$ = -3.0746 for 25°C	Q/K_{eq} $\log K_{eq}$ = -44.33	Q/K_{eq} $\log K_{eq}$ = -3.0746 for 25°C
Ca^{++}	4.00E-04	1.15E+12	6.39E-30	2.94E+49	1.63E+08
PO_4^{---}	2.45E-08				
HPO_4^{--}	2.02E-03				
H^+	2.80E-08				

Using Eq. (4.5) with logK = -44.33 generally resulted in convergence failure for STOMP. Using Eq. (4.3) with $\log K_{eq}$ values for apatite based on the CRUNCH database resulted in more stable simulations. However, even when using the $\log K_{eq}$ values for apatite from the CRUNCH database, STOMP had some convergence difficulties when higher concentrations of reagents were used. The convergence problems do not appear to be due solely to the TST rate equations, but the TST rate equation for apatite seemed to be the most problematic. Some improvement could be obtained by increasing the number of allowed iterations, which is currently hard-wired in STOMP. A limited number of attempts were also made to reformulate the reaction network to yield a more stable set of equations, but these met with limited success. Therefore, some additional effort may be required to generate a more stable reaction network for this particular problem and/or to modify the ECKEChem solution algorithms to improve their robustness.

Significantly more effort is required to set up simulations for reactive transport modeling using the coupled equilibrium-component-kinetic equations in STOMP than in some other more simplistic modeling approaches. This extra effort has to do with determining initial and boundary conditions for both aqueous and solid or sorbed species whose concentrations are not typically measured but that are in equilibrium with waters of different chemical composition.

4.4.4 2-D Infiltration Simulation

For the purpose of this study, 2-D infiltration of Ca-citrate-PO_4 and river water into homogeneous and simplified heterogeneous Hanford sediments was simulated to quantify reaction rates occurring in experiments and develop the ability to simulate the same reactions in larger scale field systems.

A 2-D unsaturated sediment system containing a single low-K zone was chosen for simulations to match the dimensions of 2-D infiltration experiments conducted in the EMSL laboratories (Appendix A, Section A.8; Figures 4.53 to 4.56). These simulations were conducted to achieve a steady-state water-saturation profile before the solution was infiltrated at a specified rate. At infiltration rates of 0.4 and 1.6 cm/hour, the steady-state water-saturation profile (Figure 4.53) shows greater water saturation in the low-K lens (as expected), and within the low-K lens, the greatest water saturation at the bottom of the low-K lens due to the need to build up the suction (to nearly water-saturated conditions) so that water would infiltrate the underlying high-K media. Corresponding apatite profiles (Figure 4.54) show that most of the apatite mass is formed near the infiltration point. This is caused by the adsorption of PO_4 and relatively rapid citrate biodegradation rate relative to the time scale of infiltration (which was relatively slow). This conclusion was based on 2-D infiltration experiments conducted over a wide range of infiltration rates (see Section 4.5.1).

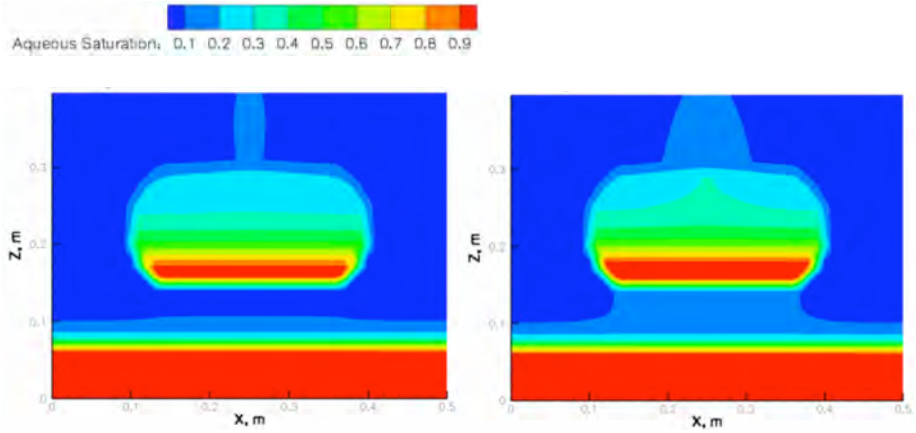

Figure 4.53. Simulation of Ca-citrate-PO_4 infiltration into a 2-D system containing a low-K zone showing steady-state water saturation for infiltration at a) 0.4 cm/hour and b) 1.6 cm/hour.

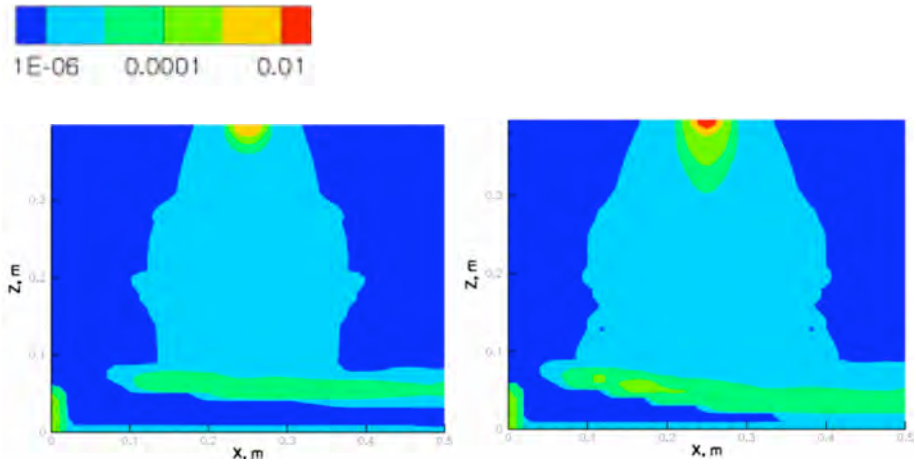

Figure 4.54. Simulation of Ca-citrate-PO_4 infiltration into a 2-D system containing a low-K zone showing final apatite concentration for infiltration at a) 0.4 cm/hour and b) 1.6 cm/hour.

2-D unsaturated simulations of Ca-citrate-PO_4 infiltration into a system containing a single high-K lens were also conducted at the same infiltration rates of 0.4 and 1.6 cm/hour. The water-saturation profile (steady-state) that develops shows very low water saturation in the high-K zone, and water driven by gravity and suction infiltrating around the zone (Figure 4.55). A more rapid solution infiltration rate (Figure 4.55b) resulted in a slightly greater water saturation above the high-K zone.

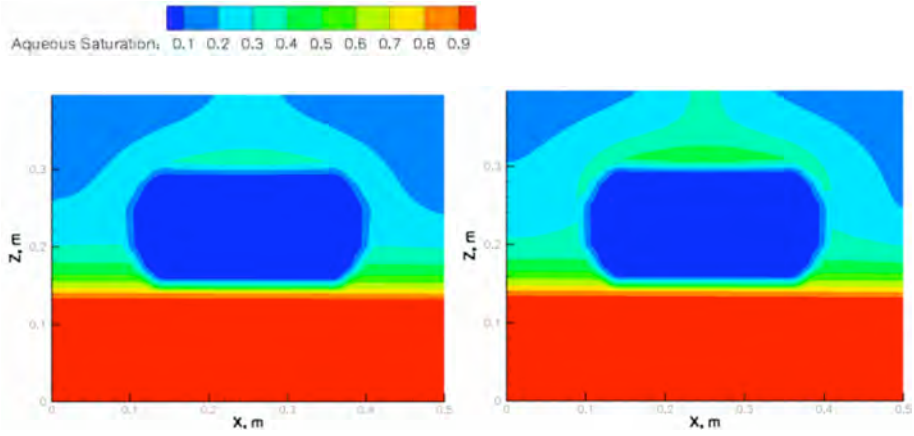

Figure 4.55. Simulation of Ca-citrate-PO_4 infiltration into a 2-D system containing a high-K zone showing steady-state water saturation for infiltration at a) 0.4 cm/hour and b) 1.6 cm/hour.

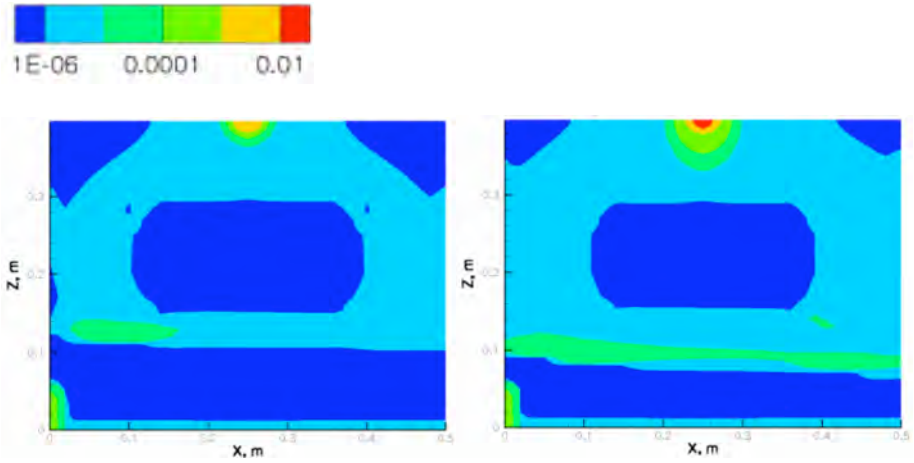

Figure 4.56. Simulation of Ca-citrate-PO_4 infiltration into a 2-D system containing a high-K zone showing final apatite concentration for infiltration at a) 0.4 cm/hour and b) 1.6 cm/hour.

The apatite distribution that results from Ca-citrate-PO_4 solution slow infiltration into this system with a high-K zone (Figure 4.56) is predictable from the water content distribution. Most of the apatite is near the infiltration location due to relatively low water advection rate relative to the PO_4 adsorption rate and citrate biodegradation rate. However, low concentration of apatite is found surrounding the high-K zone.

Numerous 2-D infiltration experiments were conducted to refine the relationship between apatite precipitate location and solution infiltration rate, concentration, and other variables. A general conclusion that can be reached from these simulations is the apatite distribution will, to some extent, follow the water-saturation distribution. Therefore, high-K zones that maintain a low water saturation will have a correspondingly low apatite precipitate mass.

A series of 2-D field-scale simulations were conducted to assess infiltration rates needed to result in apatite precipitate throughout the sediment profile. These simulations represent a cross section of the 100-N Area sediment profile to the Columbia River (constant head boundary at the left). The simulations show a trench (dug through the road fill, which has a relatively low infiltration rate, Figures 4.57-4.59). The reaction set used for these simulations was significantly reduced relative to the 51 reactions shown above. These reactions include first-order citrate biodegradation (with a half-life of 50 hours), apatite precipitation (which occurs rapidly after Ca-citrate dissociation due to citrate biodegradation), PO_4 adsorption (K_d approach), and Ca adsorption (K_d approach, not ion-exchange approach). Due to the simplification of the cation exchange not being included, the corresponding movement of Ca (critical for the formation of apatite) is somewhat unrealistic, although these simulations do provide a rough estimate of the balance of physical and biogeochemical process time scales in order to precipitate apatite in desired locations. Two simulations were conducted at a low infiltration rate (0.1 cm/hour) and at a high infiltration rate (1.0 cm/hour). In each, the Ca-citrate solution infiltrated (Figure 4.57) into the sediment profile, with a lag of phosphate (Figure 4.57b) due to phosphate adsorption. The corresponding apatite precipitate formed in locations of calcium and phosphate (Figure 4.57d). Free Ca (from Ca-citrate) only forms after citrate is biodegraded. Even though infiltration of this high ionic-strength solution (relative to groundwater) causes desorption of some of the Ca^{2+} on ion-exchange sites (Figures 4.51 and 4.52), significant available Ca^{2+} remains available (about 70%-90% is still on ion-exchange sites) for the formation of apatite. The Ca profile (Figure 4.57c) represents only aqueous Ca^{2+} initially in the system, as the reactions included do not include the Ca-Mg-K-Na ion exchange needed to correctly approximate Ca mass in the system.

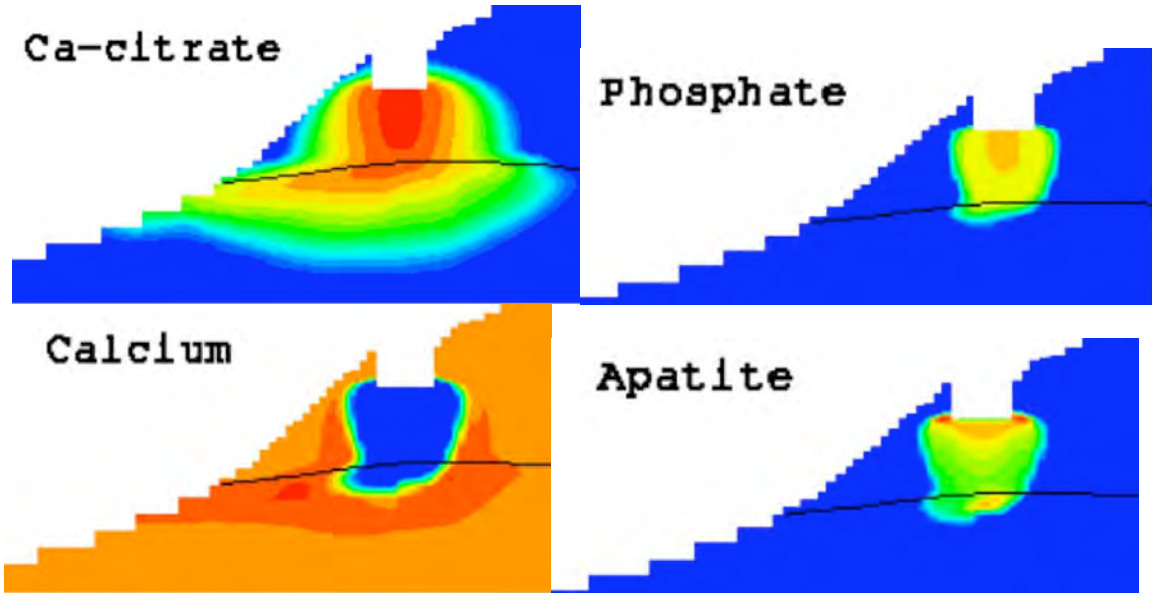

Figure 4.57. Field simulation of Ca-citrate-PO_4 infiltration at 1.0 cm/hour infiltration rate.

At an infiltration rate of 0.1 cm/hour, Ca-citrate-PO_4 solution continuous infiltration for 16 days (Figure 4.59) appears to result in a relatively uniform spatial distribution of apatite with depth and laterally. In this case, ~30% of the solution is leaching out into the river. In reality,

Ca-citrate-PO_4 solution infiltration (see Section 4.5) results in considerably greater lag in PO_4 than shown here due to both kinetic sorption of PO_4 (minutes to hours) and precipitation of Ca-PO_4 phases (hours to hundreds of hours). Infiltration rates this slow typically resulted in apatite precipitate forming only near the infiltration source (shown in Figures 4.54 and 4.56).

At a more rapid infiltration rate (1.0 cm/hour), the Ca-citrate-PO_4 solution appears to infiltrate so rapidly that most of it is washed out into the river (Figure 4.58; ~90% of the solution does not form apatite). This situation has not been observed in experiments. Rapid solution infiltration as

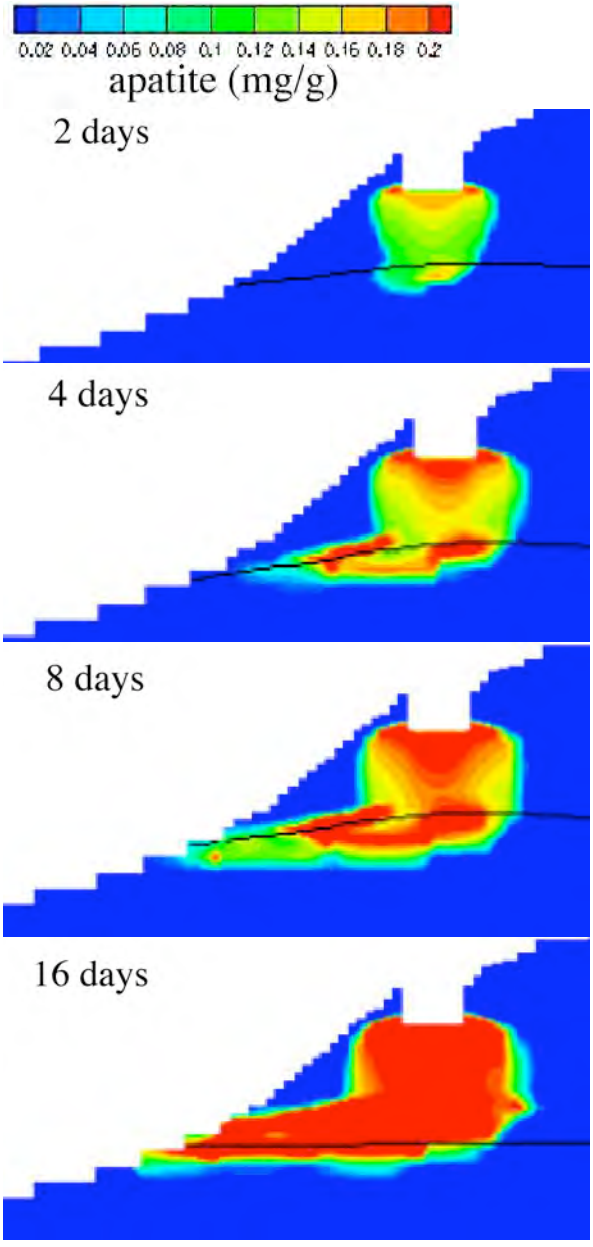

Figure 4.58. Simulation of Ca-citrate-PO_4 infiltration into a 2-D field system at 1.0 cm/hour infiltration rate.

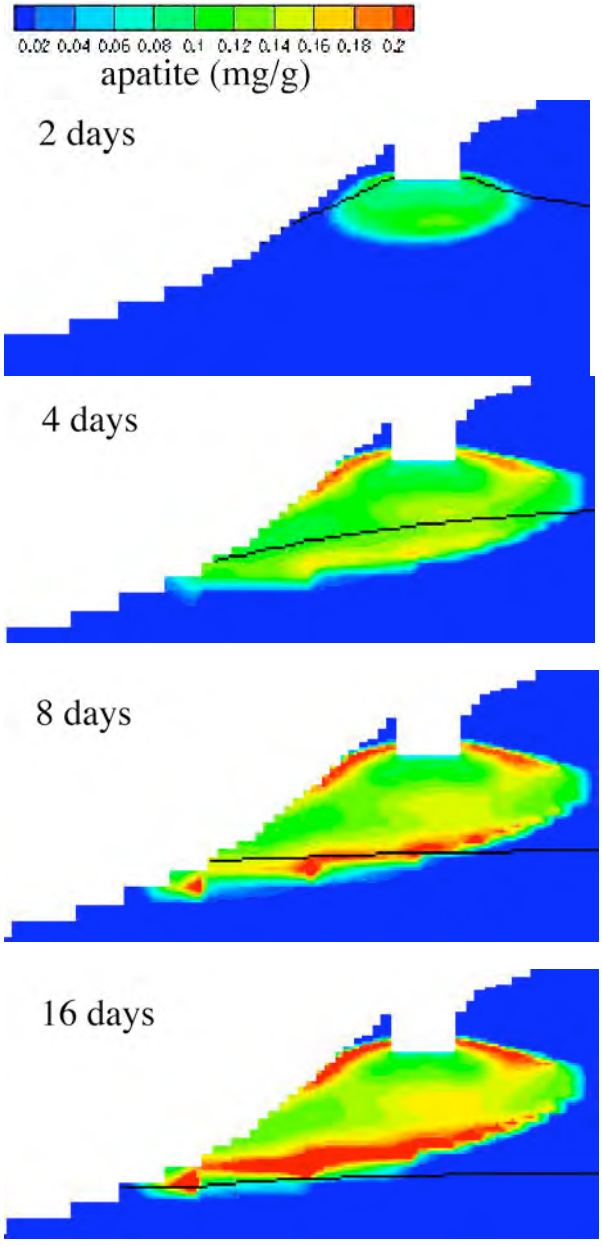

Figure 4.59. Simulation of Ca-citrate-PO_4 infiltration into a 2-D field system at 0.1 cm/hour infiltration rate.

possible (i.e., ponded surface conditions) in 12-ft high 1-D columns still resulted in lag of phosphate and the ultimate formation of apatite at various depths (Figure 4.24). In water-saturated systems, the Ca-citrate-PO_4 solution could be even more rapidly injected into sediment. Injecting a Ca-citrate-PO_4 solution into a 30-ft long 1-D column over 2 or 24 hours both show some evidence of lag associated with adsorption of phosphate (Figure 4.25). Infiltration experiments (following section) have generally shown that nearly all solution infiltrated into sediment results in the formation of apatite precipitate. Infiltrating the solution too slow results in apatite near the sediment surface, whereas more rapid infiltration results in a more uniform apatite distribution with depth, although still in the upper half of the 0.5- to 2.4-m (vertical) sediment profile. Infiltration of water following Ca-citrate-PO_4 solution infiltration did result in precipitation of apatite to greater depths.

4.5 Task 5 – 2-D Infiltration of Ca-Citrate-PO_4 to Precipitate Apatite

Infiltration experiments were conducted in 2-D systems to quantify the influence of infiltrate rate, variation in infiltration rate, solution concentration, sequential solution/water infiltration rate, and heterogeneities on the resulting apatite spatial distribution. The intended purpose of this technology is to precipitate apatite in the Hanford 100-N Area in locations of Sr-90 that cannot be accessed by Ca-citrate-PO_4 solution injection. For the 300-ft long zone of highest Sr-90 concentration in the 100-N Area, a series of 16 wells are installed (location in Figure 4.60), and Sr-90 profiles for selected depths in these 16 wells have been characterized (Figure 4.61). These profiles do show that 40% to 70% of the Sr-90 is above the highly variable water table (~15 ft depth). Some of this variably saturated zone can be accessed through injections at high river level. However, since Sr-90 concentrations are the highest directly beneath the road fill (7- to 10-ft depth) in many wells, Ca-citrate-PO_4 solution placement is more effective through infiltration. Some locations also show low concentrations of Sr-90 in the fill (Table 4.12), although it should be noted that generally sediment samples were not taken in the fill. This could be caused by the water saturation during the operational period at 100-N Area, when discharge to the trenches was occurring, which was significantly higher than current conditions.

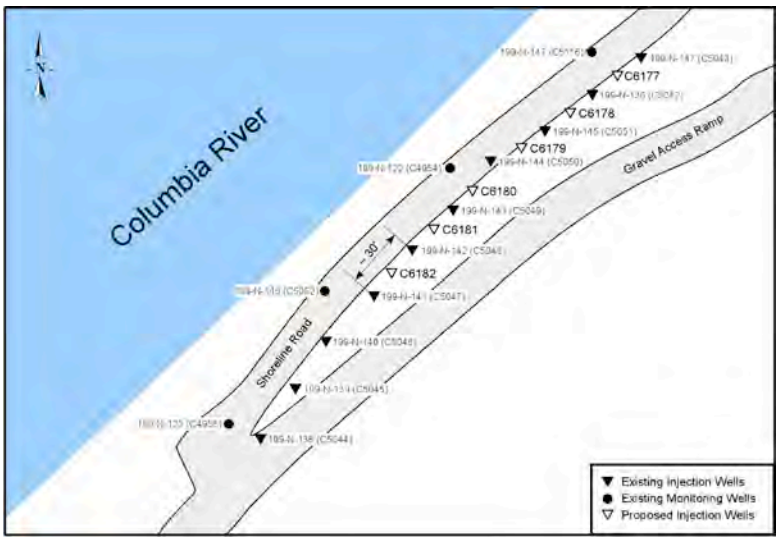

Figure 4.60. Location of 100-N Area injection wells.

More recent total Sr-90 data shows greater detail of the Sr-90 vertical profiles (Figure 4.61 bottom graphs). In four of these boreholes (C6182, C6180, C6179, C6178), two Sr-90 peaks with depth are observed which correspond to a peak in the Hanford and Ringold formations. The

two peaks may be caused by the combination of the water table and differences in groundwater flow between the two formations. During the winter, the river level drops sufficiently desaturating the Hanford formation so the only groundwater movement is in the underlying Ringold Formation. This may lead to greater lateral movement of Sr-90 in the Ringold Formation. Sr-90 contamination in the Ringold Formation is in the shallow (<25 ft) portion, with values decreasing considerably (in several wells to zero) at greater depth.

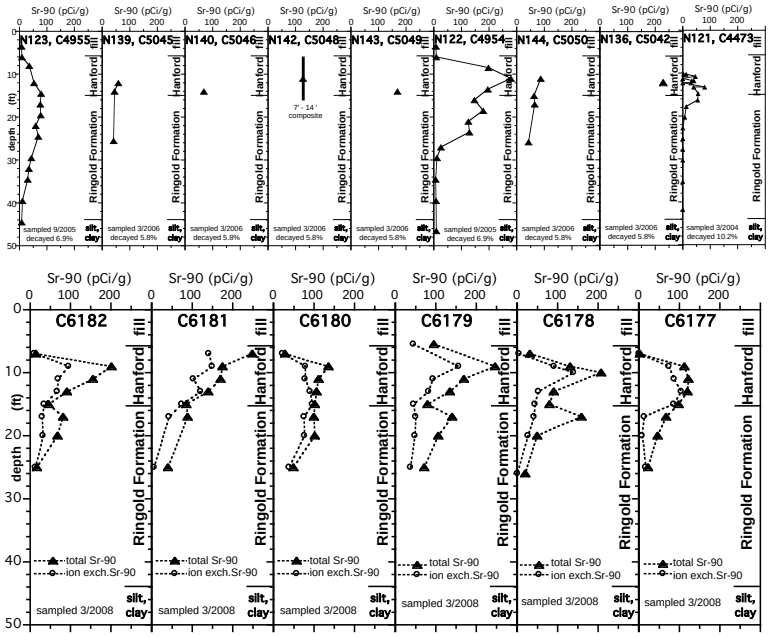

Figure 4.61. Total Sr-90 in sediment (pCi/g) for sediment cores taken in 2004 to 2006 (a) and in 2008 (b).

Laboratory 2-D infiltration experiments (in addition to 1-D infiltration experiments, Section 4.2) were conducted to understand both the downward and lateral migration of water, solution components, and the resulting apatite distribution. As such, infiltration was typically accomplished at a side edge of the 2-D system. 2-D infiltration systems (Table 4.13) ranged in size from 56 cm (high) by 38 cm (wide) by 1.1 cm wide to 244 cm (high) by 122 cm (wide) by 1.1 cm wide, which is about half the vertical distance of the 100-N vadose zone (15 ft or 4.6 m).

Table 4.12. Total Sr-90 in sediments (pCi/g) in different formations.

well	fill, 7' Sr-90 (pCi/g)	Hanford Fm Sr-90 range (pCi/g)	Ringold Fm Sr-90 range (pCi/g)	maximum Sr-90 (pCi/g)	depth (ft)
N-123	9.1	35.9 - 78.7	59.3 - 75.9	78.7	14.5
N-139	--	44.6 - 58.4	41.0	58.4	12
N-140	--	67.8	--	67.8	12
C6182	14.4	46.0 - 201.3	67.6 - 81.7	201.3	9
N-142	--	127.3	--	127.3	7-14*
C6181	--	85.2 - 248.6	39.6 - 88.5	248.6	7
N-143	--	169.0	--	169.0	14
C6180	29.6	88.6 - 135.4	46.9 - 101.6	135.4	9
N-122	8.7	196 - 280	6.0 - 179	280.0	11
N-144	--	63.0 - 87.1	42.3 - 65.0	87.1	12
C6179	95.0	79.1 - 246.7	71.2 - 140.4	246.7	9
C6178	31.4	79.6 - 207.8	19.5 - 159.2	207.8	10
N-136	--	229.0	--	229.0	12
C6177	1.85	97.7 - 122.1	22.1 - 66.9	122.1	11
N-121	--	0 - 79.7	0 - 55.9	79.7	13.25
mean:	23.7±26.0	104.9±68.1	55.4±47.7	*composite	
# points	11	55	44		

Table 4.13. Apatite mass balance in 1-D and 2-D experimental systems.

#	experiment type	system dimensions X, vertical (cm)	Y (cm)*	Z (cm)	volume (cm3)	porous media** (sed./sand mix)	heterogeneities	solution concentration Ca (mM)	citrate (mM)	PO4 (mM)	sequential solution, river water	infiltrate rate (mL/h)	duration (h)	volume infiltrated (mL)	PO4 infiltrated (mg)	PO4*** measured (mg)	PO4 recovered (fraction)
Y89	1-D infiltration	50.0	1.55R	1.55R	94.3	57.4%/42.5%		1.0	2.5	10.0		0.12	96	11.5	8.0	6.04	0.755^
Y90	1-D infiltration	50.0	1.55R	1.55R	94.3	57.4%/42.5%		1.0	2.5	10.0		0.31	47	14.6	10.0	7.61	0.761^
Y91	1-D infiltration	50.0	1.55R	1.55R	94.3	57.4%/42.5%		2.0	5.0	20.0		0.31	47	14.6	20.0	18.01	0.900^
Y92	1-D infiltration	50.0	1.55R	1.55R	94.3	57.4%/42.5%	(2) low-K	1.0	2.5	10.0		1.2	12.5	15.0	10.0	7.77	0.777^
Y124	2-D infiltration	130.0	40.0	5.0	26000.0	57.4%/42.5%		water only				40	1.61	64.4	--	--	--
Y125	2-D infiltration	55.8	38.3	1.1	2350.9	57.4%/42.5%		1.0	2.5	10.0		8.33	17.1	142.4	135.5	60.1	0.444
Y126	2-D infiltration	55.8	69.3	1.1	4253.6	57.4%/42.5%		1.0	2.5	10.0		3.32	44.2	146.7	139.6	126.9	0.909
Y127	2-D infiltration	55.8	69.3	1.1	4253.6	57.4%/42.5%		3.0	7.5	30.0		3.32	44.2	146.7	418.7	443.8	1.060
Y128	2-D infiltration	55.8	38.3	1.1	2350.9	57.4%/42.5%		0.74	1.85	7.4		0.913	113	103.2	72.6	60.2	0.829
Y129	2-D infiltration	55.8	69.3	1.1	4253.6	57.4%/42.5%		3.0	7.5	30.0		0.706	281	198.4	566.0	570.9	1.009
Y130	2-D infiltration	55.8	69.3	1.1	4253.6	57.4%/42.5%		6.0	15	60.0		0.706	281	198.4	1132.0	1202.5	1.062
Y131	2-D infiltration	55.8	38.3	1.1	2350.9	58.8%/41.1%		3.0	7.5	30.0		0.28	430	120.4	343.5	89.99	0.262
Y132	2-D infiltration	55.8	69.3	1.1	4253.6	58.8%/41.1%		3.0	7.5	30.0		141.5	1.17	165.6	472.3	456.75	0.967
Y133	2-D infiltration	55.8	69.3	1.1	4253.6	58.8%/41.1%		3.0	7.5	30.0	1 sequence	141.5	1.17	165.6	472.3	441.6	0.935
Y134	2-D infiltration	55.8	69.3	1.1	4253.6	58.8%/41.1%		6.0	15	60.0	1 sequence	5.0	40	200.0	1141.2	849.5	0.744
Y135	2-D infiltration	55.8	69.3	1.1	4253.6	58.8%/41.1%		6.0	15	60.0	1 sequence	5.0	40	200.0	1141.2	153.3	0.134
Y136	2-D infiltration	115.2	55.8	1.1	7071.0	58.8%/41.1%	(2) low-K, (1) high-K	6.0	15	60.0	1 sequence	141.5	10.7	168.6	962.0	593	0.616
Y137	2-D infiltration	55.8	38.3	1.1	2350.9	58.8%/41.1%	(1) low-K	3.0	7.5	30.0	1 sequence	141.5	2.8	106.0	302.4	340.3	1.125
Y149	2-D foam injection	55.8	115.2	1.1	7071.0	66.0%/34.0%	(2) low-K	3.0	7.5	30.0		0.60	22	13.2	37.7	31.3	0.831
Y158	2-D foam injection	130.0	40.0	5.0	26000.0	66.0%/34.0%	(2) low-K, (1) high-K	4.0	10	40.0		1.88	25	47.0	178.8	160.6	0.898
Y162	1-D foam injection	762.0	1.55R	1.55R	1437.8	66.0%/34.0%		3.0	7.5	30.0		1.13	79	89.3	254.7	229.4	0.901
Y163	1-D foam injection	762.0	1.55R	1.55R	1437.8	66.0%/34.0%		4.0	10	40.0		1.13	48	54.2	206.3	191.6	0.929
Y164	1-D infiltration	366.0	2.6R	2.6R	1943.2	58.8%/41.1%		4.0	10	40.0		391	0.62	242.4	922.2	934.7	1.014
Y64a	1-D infiltration	366.0	2.6R	2.6R	1943.2	58.8%/41.1%		4.0	10	40.0		391	0.32	125.1	476.0	452.1	0.950
Y168	1-D saturated injection	100.0	2.5R	2.5R	490.9	40.0%/60.0%		4.6	11.6	51.5		14.0	11.26	157.6	772.1	770.5	0.998^
Y172	2-D infiltration	55.8	38.3	1.1	2350.9	58.8%/41.1%		4.0	10	40.0	1 sequence	141.5	0.92	130.2	495.2	505.8	1.021
Y173	2-D infiltration	55.8	69.3	1.1	4253.6	58.8%/41.1%		4.0	10	40.0	2 sequences	141.5	1.88	266.0	1011.9	939.1	0.928
Y174	2-D infiltration	55.8	69.3	1.1	4253.6	58.8%/41.1%		4.0	10	40.0	3 sequences	141.5	2.63	372.1	1415.6	1250	0.883
Y175	2-D infiltration	55.8	115.2	1.1	7071.0	58.8%/41.1%		4.0	10	40.0	4 sequences	141.5	3.55	502.3	1900.7	1542.5	0.812
Y176	2-D infiltration	55.8	115.2	1.1	7071.0	58.8%/41.1%	(1) low-K	4.0	10	40.0	4 sequences	141.5	3.55	502.3	1910.8	1523.4	0.797
Y177	1-D saturated injection	914.4	1.57R	1.57R	1770.2	58.8%/41.1%		4.0	10	40.0		17.68	23.65	418.0	1588.4	1225.1	0.771
Y178	1-D saturated injection	914.4	1.57R	1.57R	1770.2	58.8%/41.1%		4.0	10	40.0		176.7	2.233	394.7	1501.4	1185.4	0.790
Y179	1-D saturated injection	914.4	1.57R	1.57R	1770.2	58.8%/41.1%		1.0	2.5	10.0		20.64	23.58	488.7	464.3	354	0.762
Y180	1-D saturated injection	914.4	1.57R	1.57R	1770.2	58.8%/41.1%	no injected microbes	4.0	10	40.0		20.72	24.8	513.6	1951.8	919.2	0.471
Y181	1-D saturated injection	914.4	1.57R	1.57R	1770.2	58.8%/41.1%	no in situ microbes	4.0	10	40.0		14.22	24.0	341.3	1298.7	1200.1	0.924
Y190	2-D infiltration	243.8	121.9	1.1	32691.1	58.8%/41.1%	(23) low-K, (5) high-K	6.0	15	60.0		1260	1.25	1575.0	8987.0	0	0.000

*R = round column

**100N composite sediment sieved < 4 mm and percentage > 4 mm replaced with 20/30 accusand

*** based on acid extraction and PO4 analysis of sediment samples in system after experiment

^ PO4 recovered includes sediment and effluent samples

4.5.1 Infiltration Rate and Apatite Precipitate Location

The spatial distribution of apatite that results from Ca-citrate-PO_4 solution infiltration, biodegradation (from in situ and injected microbial populations), is influenced by the vertical and lateral movement of water in the unsaturated sediments as well as reactions (phosphate adsorption, citrate biodegradation, ion exchange of Ca-Mg-K-Na, and apatite precipitation). At very slow infiltration rates, capillary forces dominate water movement at low water content (Figure 4.62a), which results in a relatively uniform (but low) moisture profile with depth and laterally (Figure 4.62b), which is under transient conditions (not a steady-state profile). This is, however, not a viable method to "hold" the Ca-citrate-PO_4 solution in the unsaturated sediments because of the rates of phosphate adsorption (hours) and citrate biodegradation (tens to hundreds of hours) were much faster than the infiltration rate (430 hours to reach 50 cm depth). Essentially all of the phosphate infiltrated formed apatite precipitate within a few centimeters of the point of infiltration (Figure 4.62c).

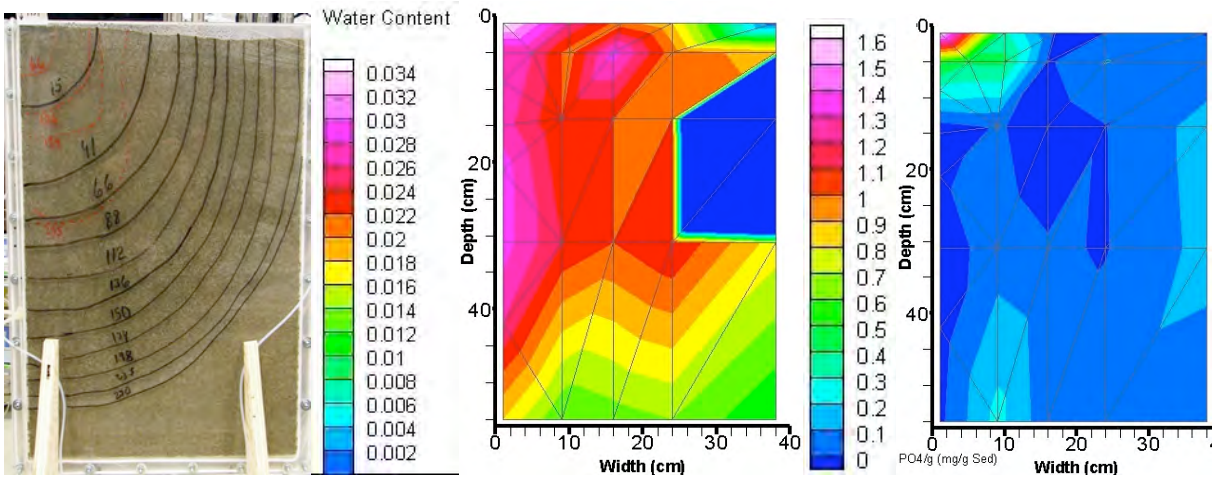

Figure 4.62. Slow (0.28 mL/hour) infiltration of a Ca-citrate-PO_4 solution showing final results at 430 hours: a) picture, b) water content, and c) apatite distribution.

In contrast, rapid infiltration of a solution can be controlled by gravity and capillary forces (vertically), which results in the rapid transport (and drainage) of the solution in a short period of time with little lateral spreading (Figure 4.63a, b). The resulting apatite distribution (Figure 4.63c) is relatively uniform with depth directly beneath the infiltration point, but does not exhibit much lateral distribution. Of the 472 mg of PO_4 infiltrated (Table 4.13), 97% could be accounted for in the precipitate (Figure 4.63c).

Varying the infiltration rate (0.28, 0.71, 3.3, 5.0, 8.3, and 142 mL/hour; Figure 4.64, all data in Table 4.13, Appendix A.8) showed that intermediate infiltration rates had greater apatite lateral distribution (i.e., with sufficient time for the solution to move laterally by capillary forces), but did not precipitate to as great a depth as the most rapid infiltration rates. In fact, a generalized shape of the apatite precipitate (i.e., depth of precipitate/width of precipitate) was a function of the infiltration rate (Figure 4.65a), which just reflects the shape distribution of the water profile at the different infiltration rates (i.e., more lateral movement at low infiltration rates). Greater

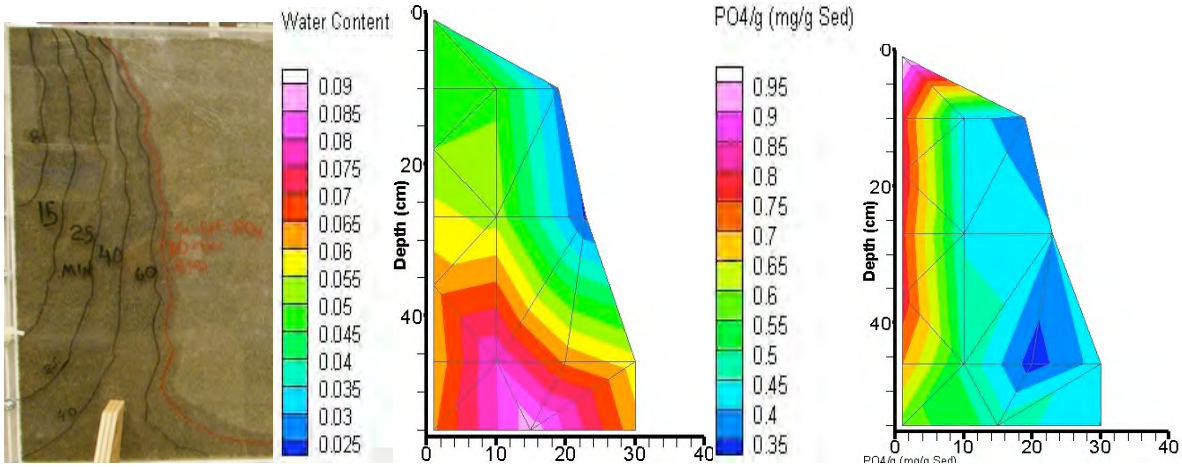

Figure 4.63. Rapid (141 mL/hour) infiltration of a Ca-citrate-PO_4 solution showing final results at 24 hours: a) picture, b) water content, and c) apatite distribution.

subsurface area contained apatite precipitate (Figure 4.65b) for intermediate infiltration rates. Therefore, in order to form apatite precipitate at depth (from a surface infiltration), a variable infiltration rate is needed with initial rapid infiltration (to move the solution to depth with minimal precipitation) then a slower infiltration rate of water without the Ca-citrate-PO_4 solution to result in lateral movement of the solution at depth (described in the following section). The fraction PO_4 recovered (Figure 4.65c) was somewhat greater at lower infiltration rates, and probably reflects the number of sampling points and recovery error. The very slowest infiltration rate (0.28 mL/hour, Figure 4.62) showed poor apparent recovery due to the inability to accurately sample the apatite mass concentrated in a small area.

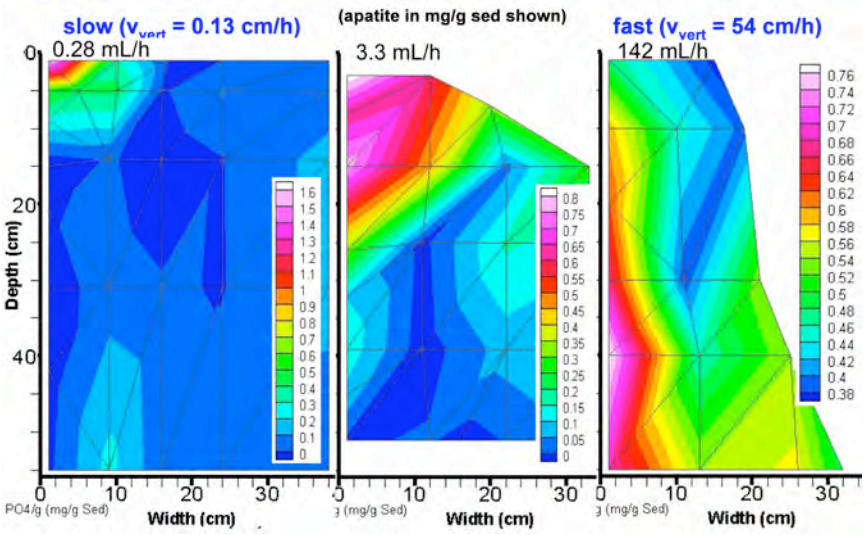

Figure 4.64. Influence of increasing infiltration rate on vertical and lateral apatite distribution.

4.5.2 Influence of Microbes on Apatite Precipitate Location

Previous water-saturated 1-D experiments (Section 4.2.3) showed that both in situ and injected (in the river water) microbial populations contribute to citrate biodegradation. Microbes are generally attached to sediment, but both advection (shear forces due to water injection) and the

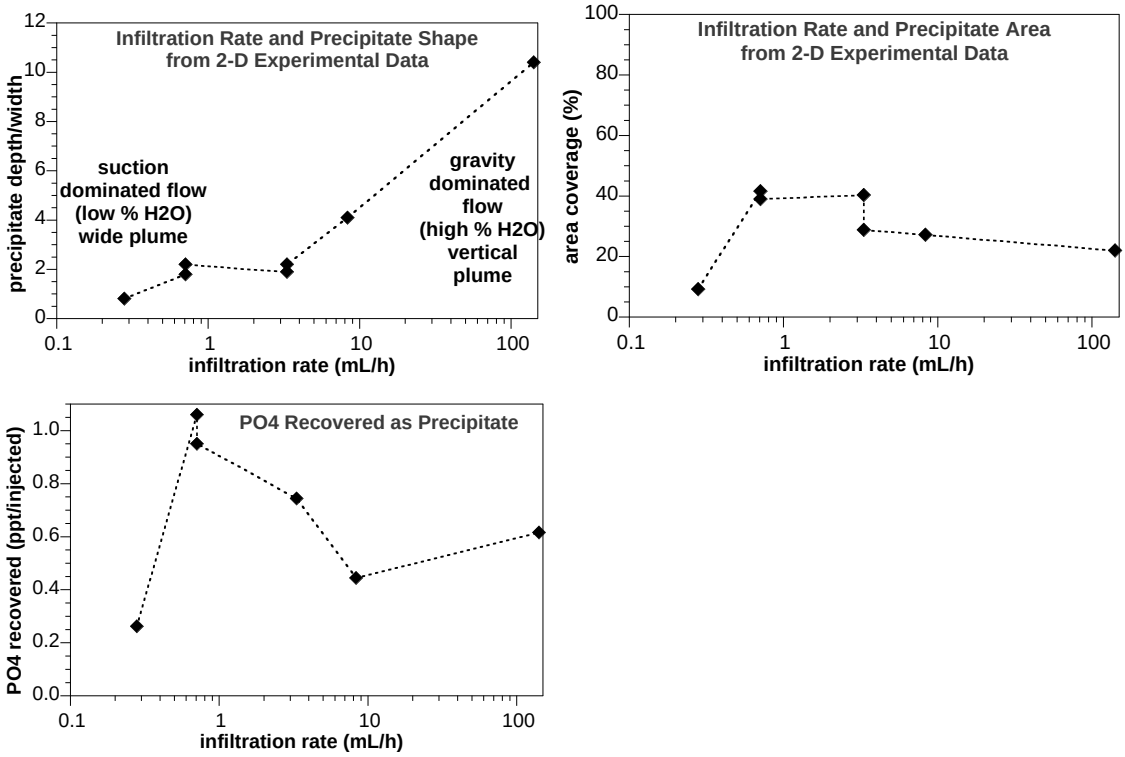

Figure 4.65. Influence of increasing infiltration rate on the apatite shape (a), area coverage (b), and PO_4 recovered as apatite precipitate (c).

ionic strength of the injecting solution can cause microbial detachment and movement. Two parallel infiltration experiments were conducted using a 60-mM Ca-citrate-PO_4 solution infiltrating at a moderate rate (5 mL/hour for 40 hours). To evaluate the importance of biodegradation of citrate, a bactericide was added to the infiltrating solution. The final water content profiles were similar (Appendix A, Section A.8, experiments Y134, Y135) with higher water content at the bottom of the sediment profile. The apatite precipitate distribution was significantly less for the system with the bactericide (Figure 4.66b). In fact, only 13.4% of the injected PO_4 was recovered as precipitate for the system with the bactericide (Table 4.13) compared with 74.4% for the system with no bactericide.

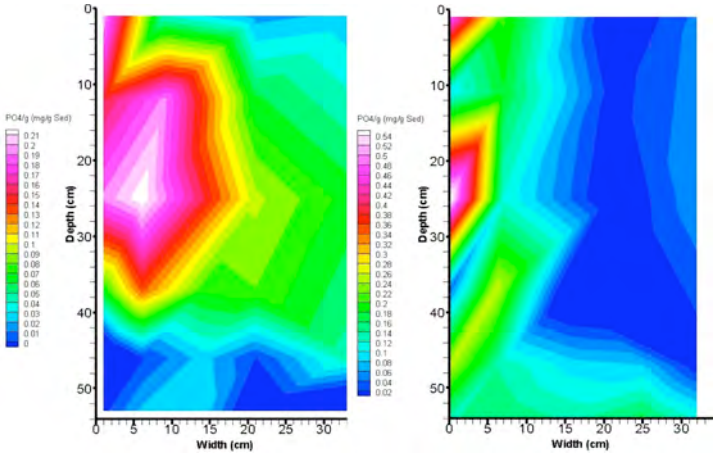

Figure 4.66. Infiltration of a 60-mM Ca-citrate-PO_4 solution at 5.0 mL/hour: a) no bactericide and b) with bactericide.

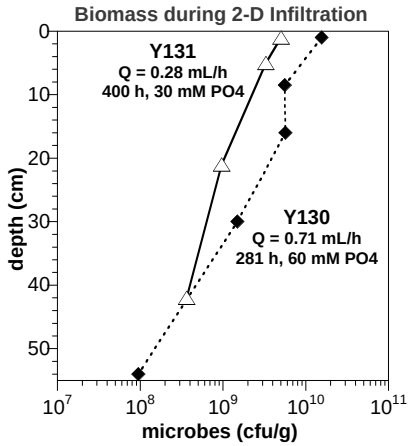

Figure 4.67. Microbial depth profile after Ca-citrate-PO_4 infiltration.

Measurement of the microbial population after Ca-citrate-PO_4 infiltration does show an increase in microbial population at shallower depth (Figure 4.67). Initially the systems had a uniform microbial population with depth (since the sediment was mixed before packing). In the system with a very low infiltration rate (Y131, 0.28-mL/hour infiltration rate), the microbial population decreases an order of magnitude form 4.0E+09 cells/g at the sediment surface to 6.0E+08 cells/g at a 40-cm depth. The infiltrating Ca-citrate-PO_4 solution did reach approximately to a 40-cm depth (Figure 4.62, moisture profile), and previous water-saturated injection experiments (Figure 4.52) show very little retardation of the citrate, but phosphate is retarded (Rf =1.6 to 2.4, time-dependent). The resulting apatite precipitate, however, was significantly retarded (Figure 4.62c), which only reached a few centimeters of depth. Therefore, citrate may be biodegraded over a wider range of depth than the phosphate is available to form apatite with the Ca^{2+} released from the Ca-citrate complex.

At a faster infiltration rate (Figure 4.67, Y130, 0.71 mL/hour), the microbial population shows a 2-order of magnitude decrease from the surface to a 50-cm depth. In this case, the apatite precipitate was spread out from the surface to a 30-cm depth (Appendix A, Section A.8). In both cases, measurement of the microbial population did provide a rough indication that there was some microbial activity, but was not useful in predicting the location of the apatite precipitate. This AODC measurement of the overall microbial population may not reflect the subset of microbes that are degrading citrate. A similar conclusion was reached in Section 4.2.3, where a much smaller overall microbial population in the river water appeared to be degrading citrate at a much faster rate (i.e., so bulk microbial population was not useful in predicting the resulting citrate biodegradation rate and the subsequent mass/location of apatite precipitate).

4.5.3 Ca-Citrate-PO_4 Solution Concentration and Apatite Precipitate Location

Infiltration of a higher Ca-citrate-PO_4 concentration solution influences PO_4 adsorption (see Section 4.1.5) and results in a lower citrate biodegradation rate (see Section 4.1.3) and increase microbial detachment and mobility (see Section 4.2.3). All of these processes generally result in the Ca-citrate-PO_4 solution infiltration to a greater depth before apatite precipitates. 2-D infiltration experiments varying the solution concentration (keeping the infiltration rate constant) did show an increase in the apatite precipitate depth with increasing concentration (Figure 4.68). In addition, there was greater lateral spread of the precipitate, likely by the same processes; decreased PO_4 adsorption and slower citrate biodegradation rate allowed more time for the solution to move vertically and laterally before citrate was degraded and apatite precipitated.

4.5.4 Sequential Ca-Citrate-PO_4 Solution and Water Infiltration

Infiltration of water (no Ca-citrate-PO_4) after Ca-citrate-PO_4 solution can drive PO_4 to a greater depth (Figure 4.69). Because phosphate sorption is time-dependent (minutes to hours,

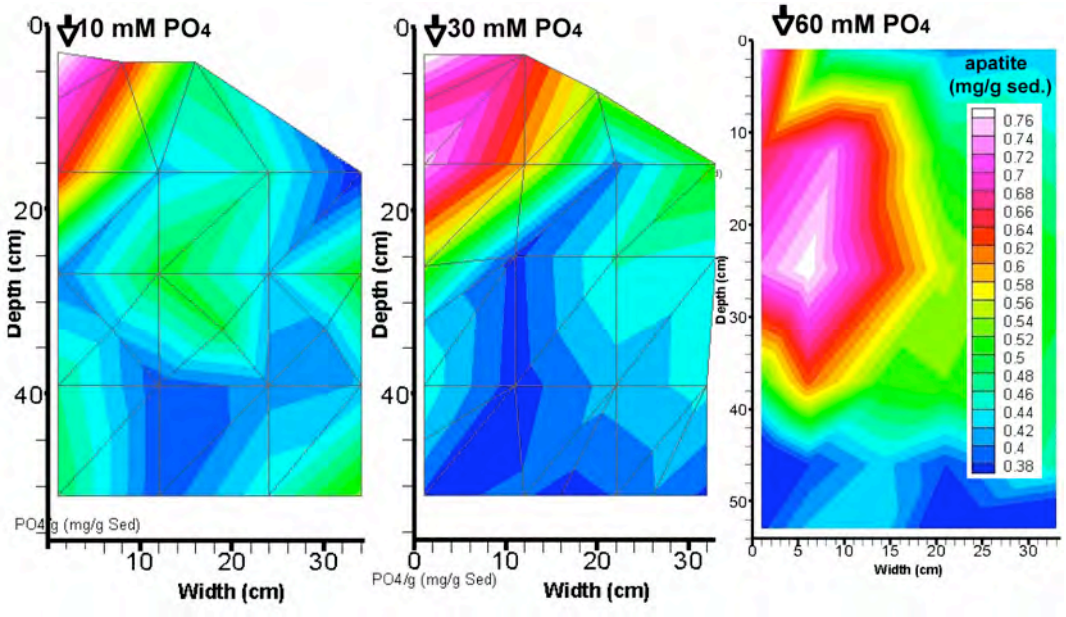

Figure 4.68. Ca-citrate-PO_4 solution infiltration at 10 mM (a), 30 mM (b), and 60 mM (c) PO_4 concentration.

Section 4.1.5), the more rapidly the solution or water advects through the sediment, less PO_4 adsorption occurs. Ultimately, the infiltration strategy is: a) rapid Ca-citrate-PO_4 infiltration, b) rapid water infiltration, and c) slow water infiltration. The slow infiltration allows for lateral migration (shown in Figure 4.62). This strategy is shown in Section 4.5.6. The relative volume of water infiltrating after the Ca-citrate-PO_4 solution in the 2-D system (Figure 4.69) is 1:1, although a larger scale 1-D column (12 ft high, described in Section 4.2.2) and 2-D systems (Section 4.5.7), a ratio of 2:1 to 4:1 was used in order to advect the PO_4 to depth.

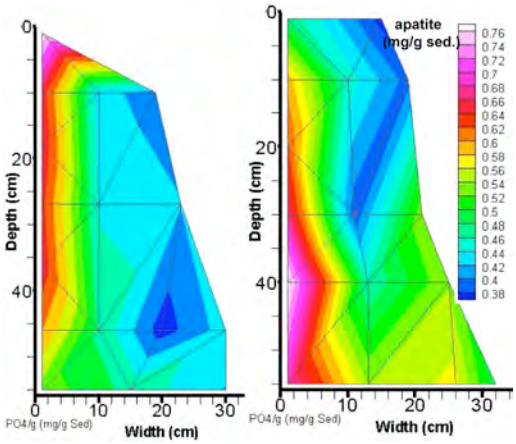

Figure 4.69. Solution infiltration (a), and sequential solution, then water infiltration (b), all at 141 mL/hour.

4.5.5 Sequential Infiltration Cycling to Build Up Precipitate Mass

The ultimate mass of apatite needed in the vadose zone is controlled by: a) equilibrium calculation to adsorb and incorporate all Sr and Sr-90 for 300 years (~10 half-lives of Sr-90 decay), and b) kinetic calculation of Sr incorporation rate compared to the Sr transport rate through the sediment (described in detail in Section 2.3). Although natural water infiltration and downward infiltration at Hanford is extremely slow (infiltration rate of 0.1 to 1 cm/year, given average annual precipitation of 16 cm/year) at the 100-N Area, the partially saturated zone (i.e., surface to 15 ft depth) can be partially water saturated in the spring due to high river levels, and

can even become fully water saturated during floods. Therefore, a conservative estimate of the mass of apatite needed in the vadose zone is 3.4 mg/g (Table 2.1), which is equal to the mass needed in the water-saturated zone.

Infiltration of a 60-mM PO_4 solution (Table 4.13) at a large scale (8-ft high 2-D system; described in Section 4.5.7) has resulted in large areas of 0.5 to 0.75 mg/g PO_4 (5 to 7.5 mg/g apatite) and small zones of 1.0 mg/g PO_4 (10 mg/g apatite). Although low-K zones received high treatment (due to higher residual water content retaining solution mass in the zone long enough for precipitate to form), high-K zones received minimal treatment (0 to 0.2 mg/g PO_4). Therefore, repeated solution infiltration events will likely be needed to build up precipitate mass. The most efficient means to infiltrate the solution to result in significant mass being held up in the vadose zone (i.e., depend on transient conditions to precipitate apatite) is to allow sufficient time between infiltration events to allow water to drain. Repeated infiltration cycling was tested in small (60 cm deep) 2-D systems that were allowed to drain for a week before an additional solution was infiltrated. Homogeneous and heterogeneous sediment systems were used.

It was hypothesized that sequential infiltrations will result in a buildup of apatite precipitate at depth, as shallower PO_4 adsorption sites are both occupied and occluded with precipitate. For one to four sequential infiltrations, there was a small buildup in the observed water content at depth (Figure 4.70). The 56 cm deep (vertical) by 35 cm to 52 cm wide (only 35 cm shown) by 1.1 cm thick flow systems used allowed for drainage at the bottom of the box.

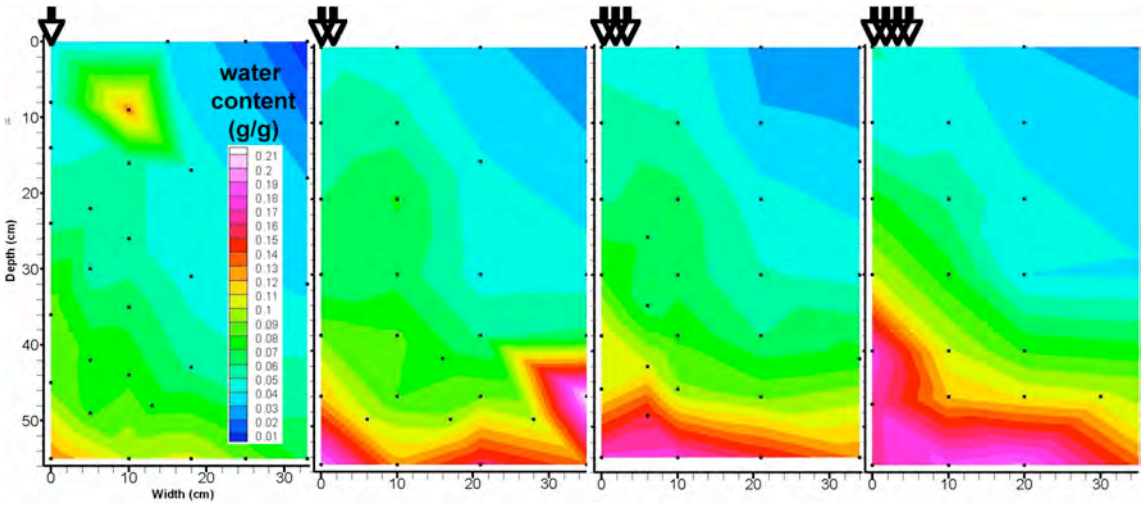

Figure 4.70. Water content for sequential infiltration with 1 week between doses.

The resulting apatite distribution for sequential infiltrations (Figure 4.71) did show an increase in precipitate mass at depth for each subsequent infiltration. In addition, there was additional apatite precipitate laterally from the infiltration point. This did not appear to result from an increased width of moisture (Figure 4.70).

For a system containing a single low-K heterogeneity, it is expected that the low-K zone will retain a higher residual water content over time, which will likely result in a greater apatite

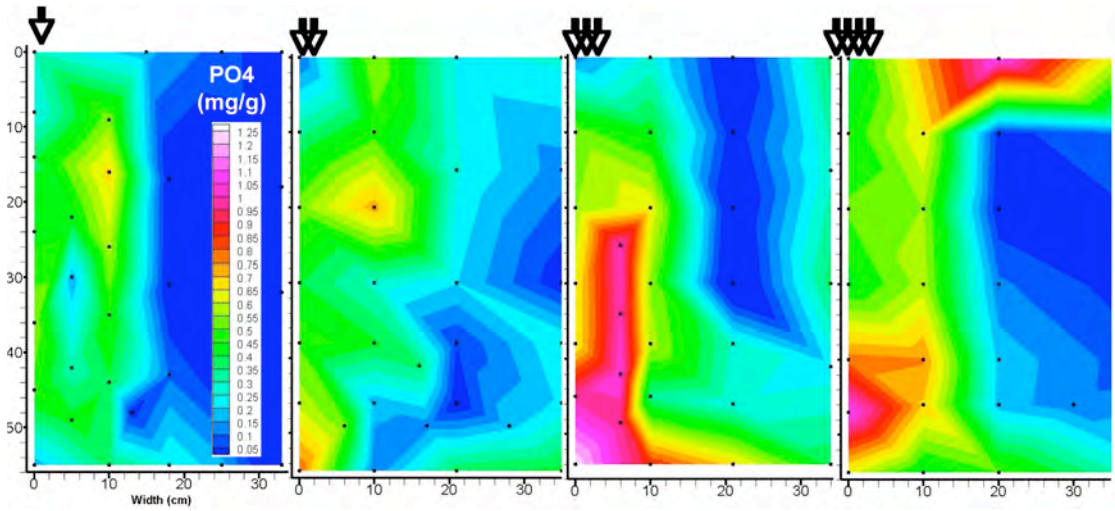

Figure 4.71. Apatite precipitate for sequential infiltration with 1 week between doses.

precipitate concentration. For these systems, a high, then low infiltration rate of 40 mM Ca-citrate-PO_4 solution, then river water was used, as described in the following section. Comparing a single dose to four doses (each with a 1-week lag between doses), the water content profile looks similar, with residual water at depth (Figure 4.72) that is similar to homogeneous systems (Figure 4.70), but with residual water maintained within the low-K zone. There was no smoothing used to plot points; the color contouring is a simple linear contour between points. As such, there are artifacts of the contouring such as apparent "wedges" of color that do not exist in reality.

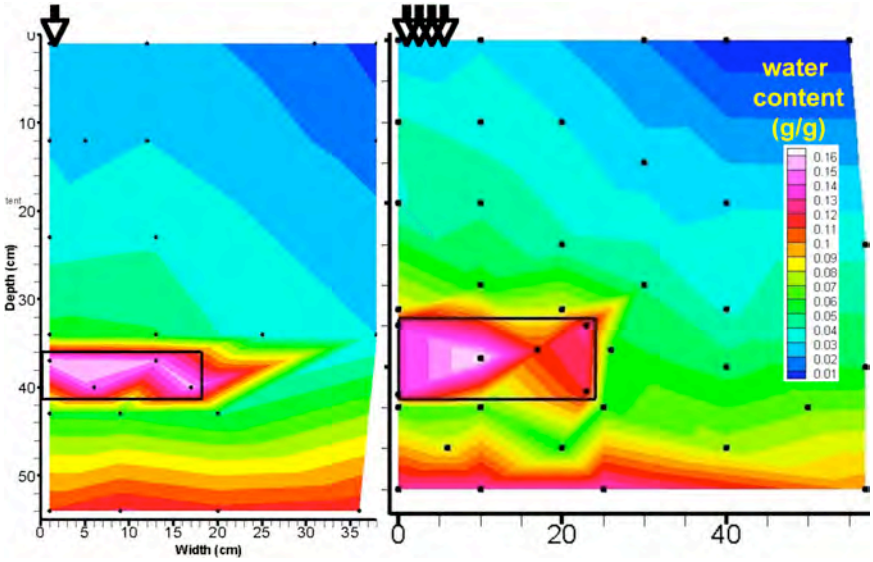

Figure 4.72. Water content for sequential infiltration with 1 week between doses (low-K zone).

Because of the high residual water content retained in the low-K zone in combination with the high rate of Ca-citrate-PO_4 solution infiltration followed by slow rate of water infiltration, the resulting apatite distribution for one dose is generally within the low-K zone and slightly above/around the low-K zone (Figure 4.73a). With four doses, close to four times as much apatite has precipitated (Table 4.13, experiment Y137 and Y176) that is located within the low-K zone and above/below the low-K zone (Figure 4.73b). The intended purpose of this infiltration

strategy was to emplace apatite in the lower half of the vadose zone and within low-K zones (as low-K zones likely have higher Sr-90 concentrations). The strategy appears to have succeeded in these relatively small 2-D systems for low-K zones (primarily due to the higher water retention in low-K zones). In Section 4.5.7, a large (8 ft high by 4 ft wide) system containing 23 low-K and 5 high-K zones was used. As shown in that section, the infiltration strategy is relatively successful for medium and low-K zones, but high-K zones exhibiting very low residual water content resulted in low apatite precipitate.

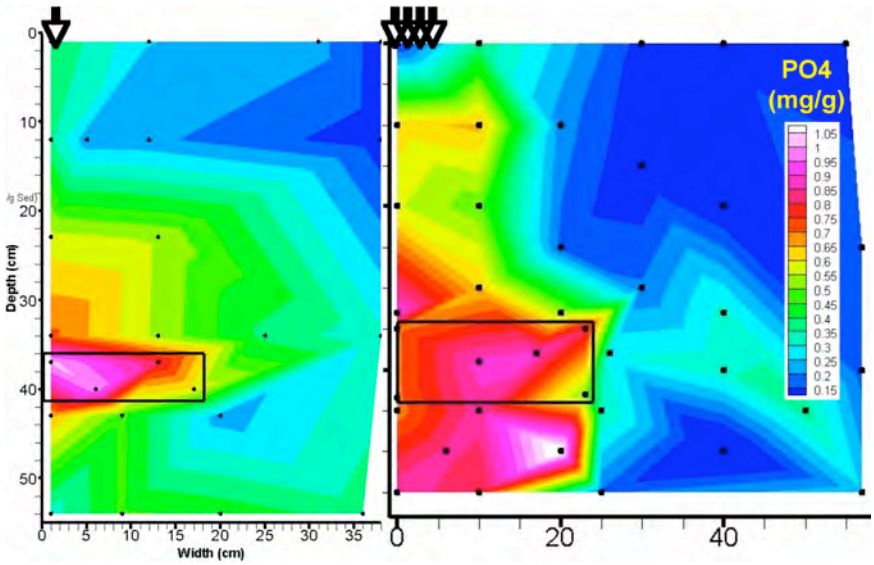

Figure 4.73. Apatite for sequential infiltration with 1 week between doses (low-K zone).

4.5.6 Infiltration Strategy for Targeting Low-K and High-K Zones

A 2-D visualization experiment was conducted to demonstrate the process of varying the infiltration rate of a solution to achieve solution coverage in desired areas (Figure 4.74). Constant infiltration rate into a heterogeneous system containing a low-permeability lens is shown in the left panels. Infiltration at a constant rate results in some lateral spreading and incomplete coverage in the low-permeability layer (Figure 4.74c). Infiltration below the low-permeability zone is also incomplete. In contrast, by varying the infiltration rate (Figure 4.74, right panels), the low-permeability unit was fully saturated with the infiltrating solution and nearly all the area under the low-permeability unit was also saturated. To achieve this spatial solution coverage, the rate of infiltration of the solution was slowed during the time period when the solution was infiltrating within the low-permeability unit (Figure 4.74b and d) as capillary forces controlled lateral solution movement. Once the solution had nearly saturated the low-permeability lens with some solution, the infiltration rate was increased to exceed the infiltration rate of the low-permeability unit, thereby forcing lateral transport of water at high saturation across the top of the low-permeability unit and down the sides (Figure 4.74f). This resulted in multiple locations that were infiltrating into the sediment under the low-permeability lens (Figure 4.74h).

Additional 2-D experiments were conducted in the EMSL subsurface transport laboratory in systems with a single low-K zone (Figure 4.75a). The water content at selected times during the experiment was measured with a gamma system (Figure 4.75b, shown scanning a 1-D system). Steady-state water, then solution infiltration was conducted and water contents compared to pre-experiment simulations (Figure 4.76), which showed good agreement. Post-experiment

simulations were also conducted with a reactive transport code in order to determine infiltration rates that should be used to result in apatite precipitate in desired locations (Section 4.4.4).

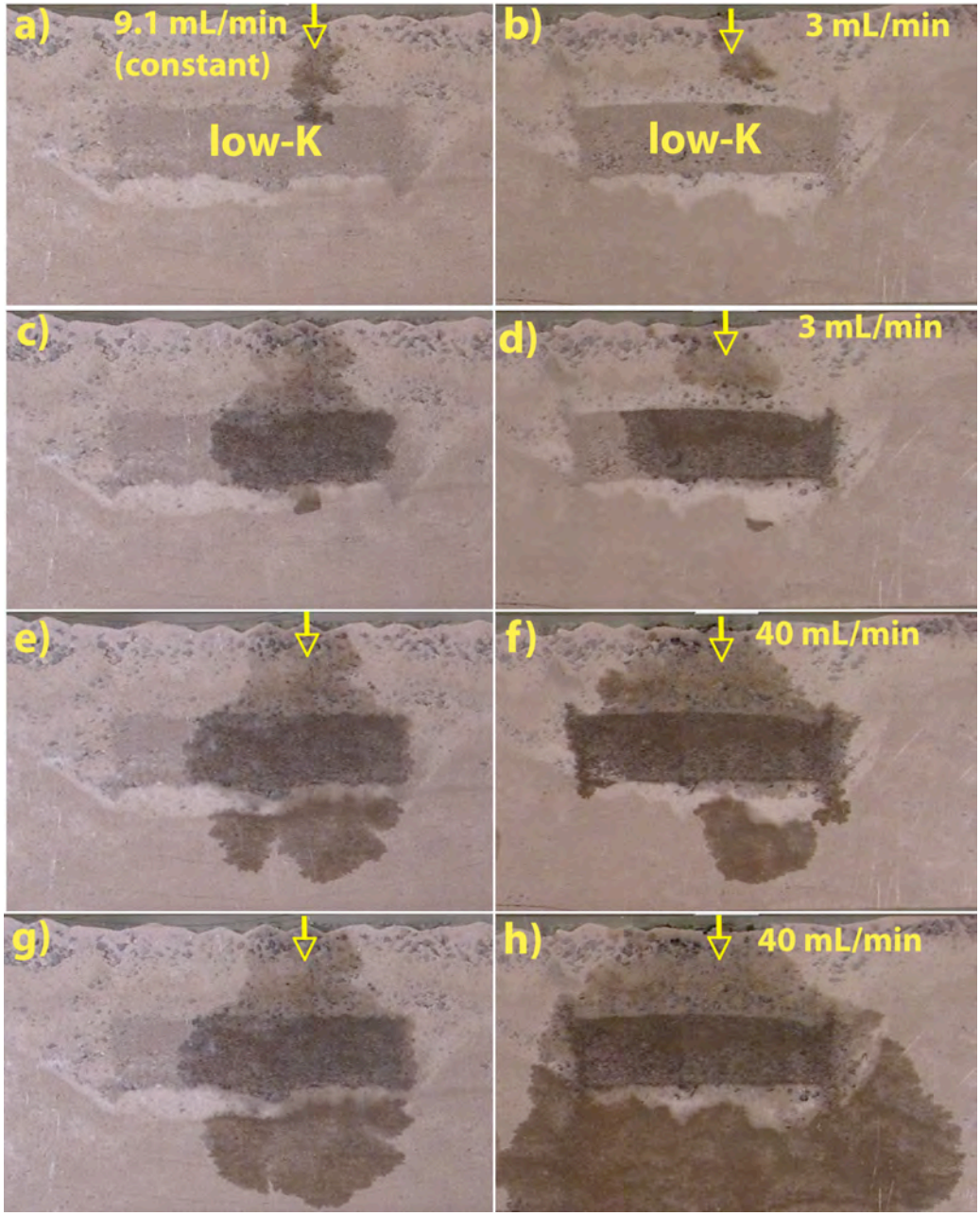

Figure 4.74. 2-D unsaturated infiltration into a low-K zone at constant infiltration rate (left panels) and at varying infiltration rate (right panels).

The Sr-90 distribution with depth in the 100-N Area peaks in unsaturated sediments directly beneath the road fill (Figure 4.61, Table 4.12), so in terms of the entire vadose zone, is located in the lower half of the vadose zone. Field implementation of the infiltration strategy developed in this project may result in either surface infiltration of the solution in the road fill or in a trench

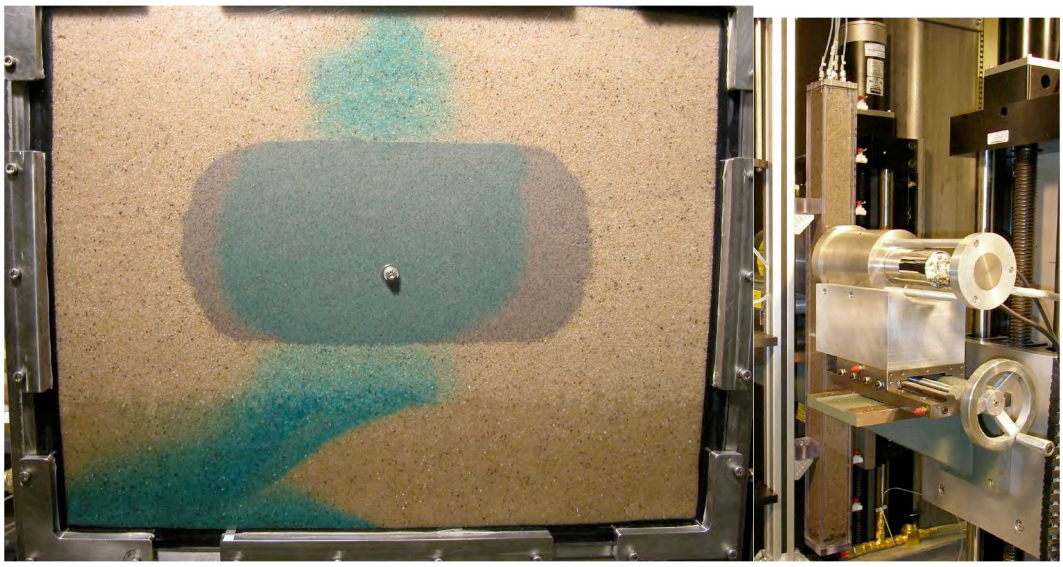

Figure 4.75. Dye injection into 2-D system with low-K zone and underlying water table (a). Water in the saturated zone is moving right to left. Gamma system for water content (b).

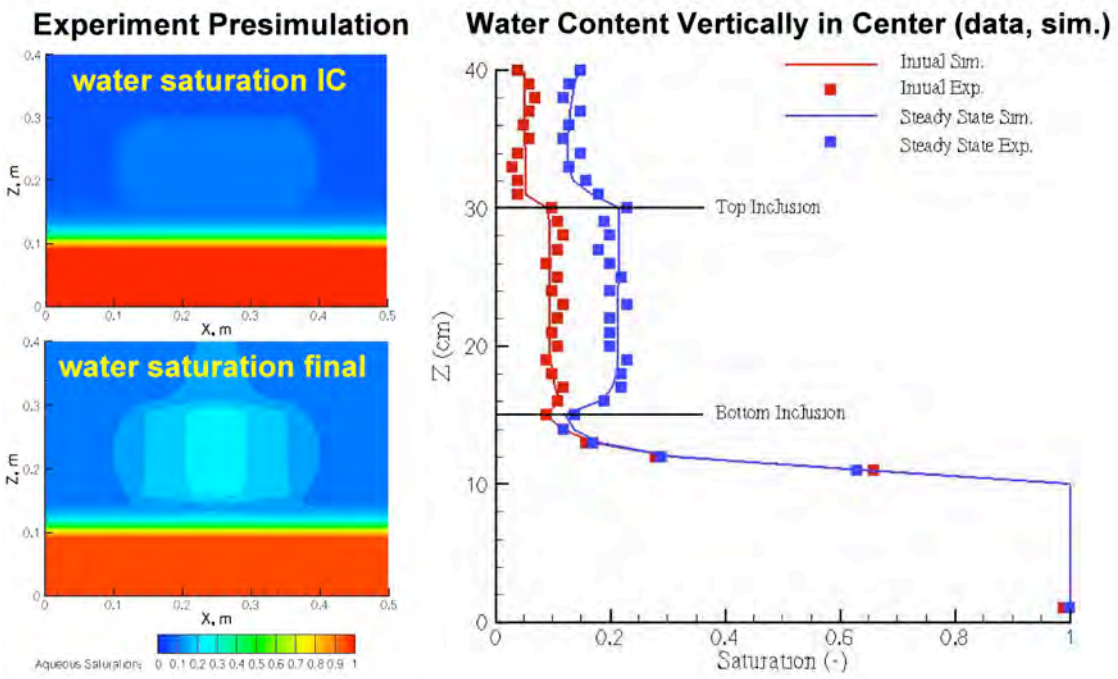

Figure 4.76. Apatite for sequential infiltration with 1 week between doses (low-K zone).

dug part way through the road fill. The objective of the experiments in this section is to develop an infiltration strategy to result in apatite precipitate in the lower half of the vadose zone as well as within low-K zones. In the field, low-K zones likely contain higher Sr-90 concentrations due to lower advective movement of water and somewhat higher adsorption of Sr-90.

A 2-D experiment was conducted in which 40 mM Ca-citrate-PO_4 solution was infiltrated at a rapid rate (141 mL/min) into a system containing a single low-K zone (Figure 4.77a) for 1 hour, then river water (contains microbes) was infiltrated at a slow rate (1.0 mL/min) for 42 hours to flush the PO_4 to depth and also allow for lateral movement within the low-K zone (strategy shown in Figure 4.74). The resulting water content at the end of the experiment showed residual water in the bottom of the system (56 cm depth, Figure 4.77b) as well as with the low-K zone. The apatite distribution showed a high concentration within nearly all the low-K zone (Figure 4.77c), and a moderate apatite concentration in the center half of the box (i.e., from 15 to 50 cm depth) with significant lateral spreading (i.e., to 30 cm in width). The high apatite concentration in the low-K zone is mainly caused by the high residual water content retaining chemical mass in that zone long enough for precipitate to form.

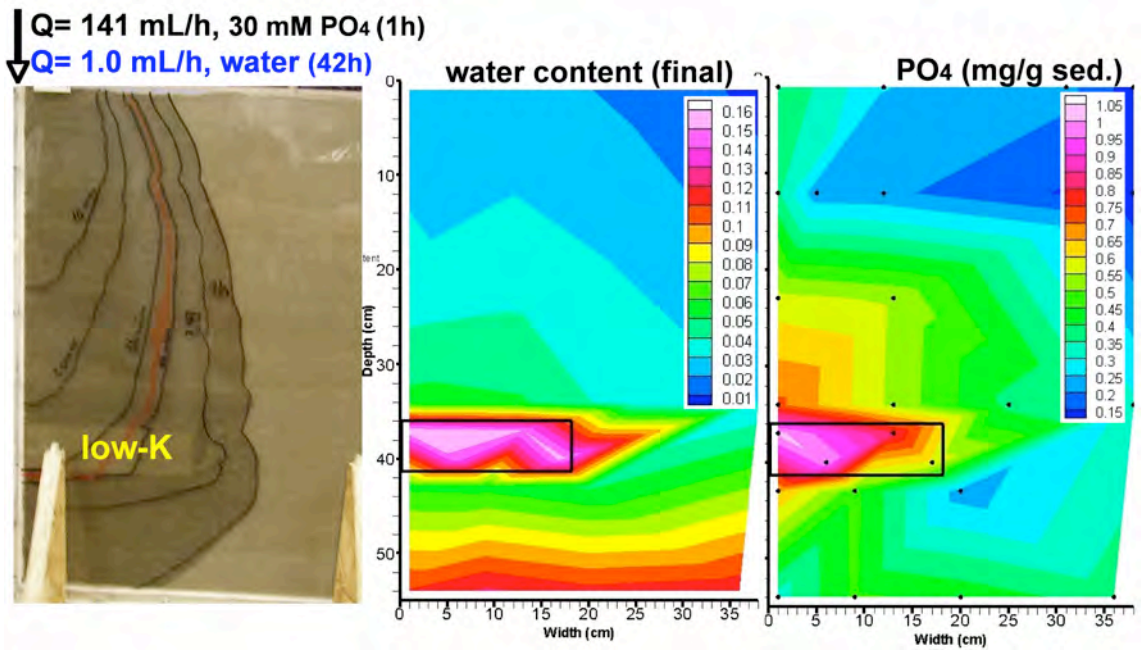

Figure 4.77. Sequential Ca-citrate-PO_4 infiltration followed by slow river water infiltration.

The low apatite concentration near the surface (to 15 cm depth) is due to the flushing of water after the Ca-citrate-PO_4 solution (also shown in Figure 4.69). The large lateral distribution of apatite is caused by the time for slow water infiltration, allowing the solution to travel laterally. This lateral spreading of water above the low-K zone is increased by near water-saturated conditions in the low-K zone (i.e., additional water could not enter the low-K zone, so moved laterally by capillary forces). Additional infiltration sequences into a system with a low-K zone does result in additional apatite formation within the low-K zone, as well as above and below the low-K zone (Figure 4.73).

In a system with idealized low-K and high-K zones (Figure 4.78), the same observation is reached in the low-K zones, with higher water retention leads to higher apatite precipitate concentration. It should be noted that only a few sampling points were taken in this relatively large system (1.2 m high by 0.56 m wide). The high-K zone (larger zone, located at 70 to 80 cm depth) had a slightly

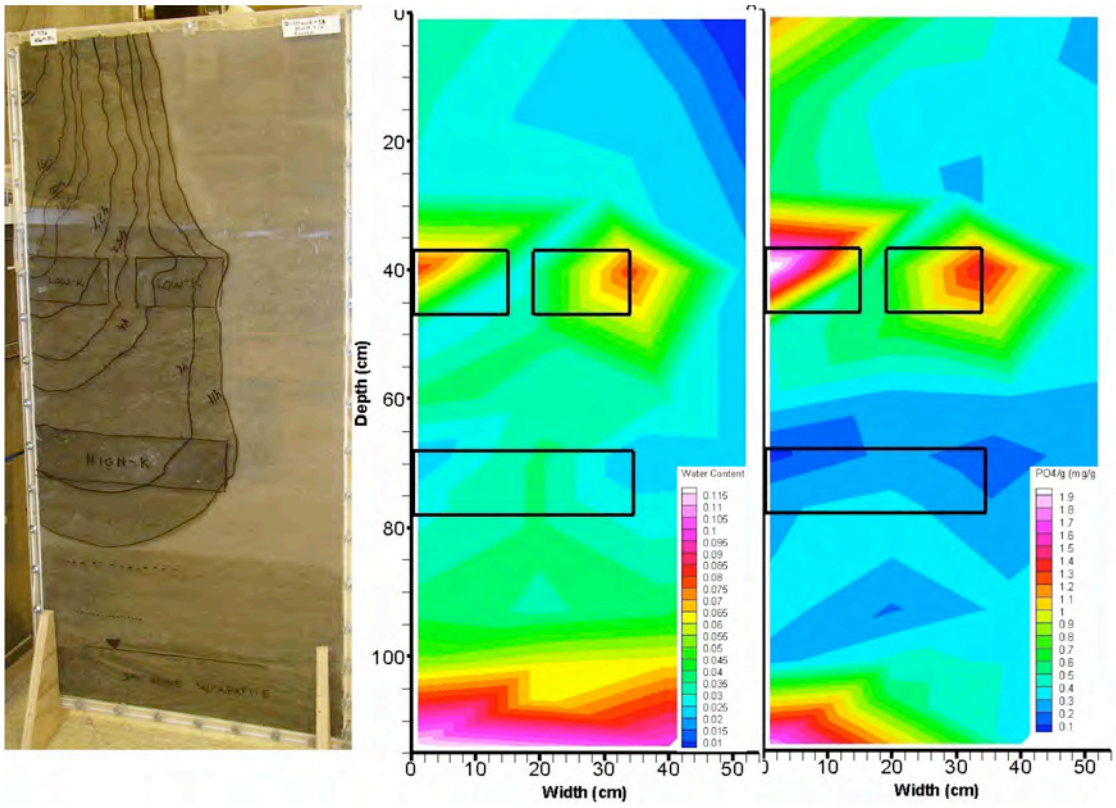

Figure 4.78. Large 2-D system (1.2 m or 4 ft high) with two low-K (40 cm depth) and one high-K zones (70 cm depth): a) infiltration at 11 hours, b) water content at 25 hours, and c) apatite at 25 hours.

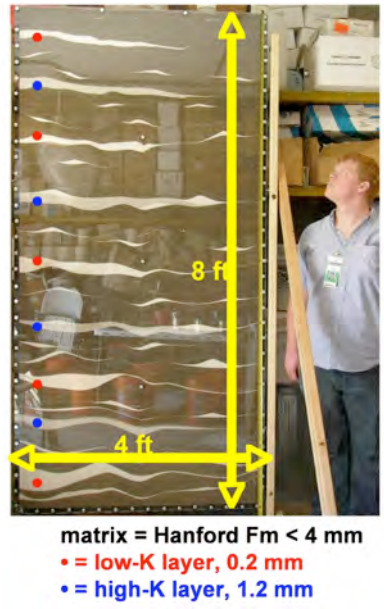

Figure 4.79. Large 2-D system containing 23 low-K zones (white) and 5 high-K zones.

lower water content at the end of the experiment due to more rapid drainage out of this zone. The result was lower apatite concentration within the high-K zone, although there are only a few data points (3) within the high-K zone. In the following section, a large-scale (8 ft high by 4 ft wide) 2-D system was used with a number of low-K and high zones and much greater sampling density to quantify the apatite distribution.

4.5.7 Large-Scale Infiltration in Heterogeneous Sediment

The final 2-D infiltration experiment was conducted in a system that was roughly half that of field scale (8 ft high; 15 ft maximum vadose zone in the 100-N Area). This system contained random low-K and high-K zones that were thin layers (Figure 4.79), which tend to occur from the fluvial deposited sediments. The objectives of this experiment were: a) test the infiltration strategy determined in smaller scale experiments to

deliver apatite mass into the middle to lower half of the system, and b) determine the extent of downward decrease in apatite concentration in high-K zones and low-K zones.

A 60-mM (PO_4) Ca-citrate-PO_4 solution was infiltrated at a 1260-mL/hour rate for 75 minutes (1575 mL), then river water was infiltrated at the same rate for 2 hours (2373 mL), then the system equilibrated as the water drained for 4 days (Figure 4.80). The solution migrated vertically with little lateral spread (at this rapid an infiltration rate, which was gravity dominated) in the medium-K sediment.

Figure 4.80. Sequential 60 mM Ca-citrate-PO_4 then water infiltration in large 2-D system.

The solution and water migrated laterally twice the distance in low-K zones due to capillary forces. The sediment profile was observed to qualitatively drain by 23 hours by the condensation on the plastic sides (white color where the wet sediment was) in the upper three-fourths of the system, with high water content in the lower quarter of the system.

In the high-K layers, fingering was clearly observed (Figure 4.81, white layer upper one-third), so the solution was infiltrating through high-K zones in discontinuous pathways with little initial water content, leaving low residual water content. This would likely result in lower apatite concentration in high-K zones.

Although the infiltration strategy of Ca-citrate-PO_4 solution followed by water infiltration is effective for flushing the reactant mass downward in homogeneous or simple heterogeneous systems (i.e., Figures 4.71, 4.73, 4.77), there is a loss in efficiency for this strategy for highly heterogeneous systems such as this one. Early times (0 to 75 minutes, Figure 4.80) moved the Ca-citrate-PO_4 solution to a 6-ft depth, and laterally in the medium grained sediment to a 2-ft width and in low-K zones to a 3.5-ft width. The subsequent water infiltration would push much of the Ca-citrate-PO_4 solution downward in the medium grained sediment, but Ca-citrate-PO_4 solution wicked into low-K zones laterally would actually be pushed out further, as shown by 23 hours (Figure 4.80). It should also be noted that lateral movement of water in even very thin low-K zones (Figure 4.81, 0.5-mm thick in picture center) results in additional water saturation in the medium-grained sediment near the low-K zone.

Figure 4.81. Close-up of the large 2-D system showing migration in low-K and high-K zones.

After the experiment, 140 sediment samples were collected for measurement of water content and apatite concentration. Results are presented in a 2-D color contour plot, as well as points separated into low-K, medium-K, and high-K zone plots. For these "balloon" plots, both the increasing size and warmer color reflect higher values of either water content or apatite precipitate. The final water content (Figure 4.82 and 4.84a) contour plot shows obvious signs of the low-K and high-K layer structure, with layers of low and moderate water content. The lower 20 cm of the flow system has a higher residual water content from drainage. The separate "balloon" plots (Figure 4.82b-d) more clearly illustrate the water content in the differing porous media. The medium-grained sediment (med-K, Figure 4.82c) shows a relatively low water content (average 0.06 g/g), so efficiently drained over the 4 days. The high-K porous media never had a high water content, so the final water content was low (average 0.02 g/g). Nearly all the residual water was retained in the low-K media (average 0.26 g/g), and was relatively uniform throughout the profile vertically and laterally from under the infiltration location (left top of the system).

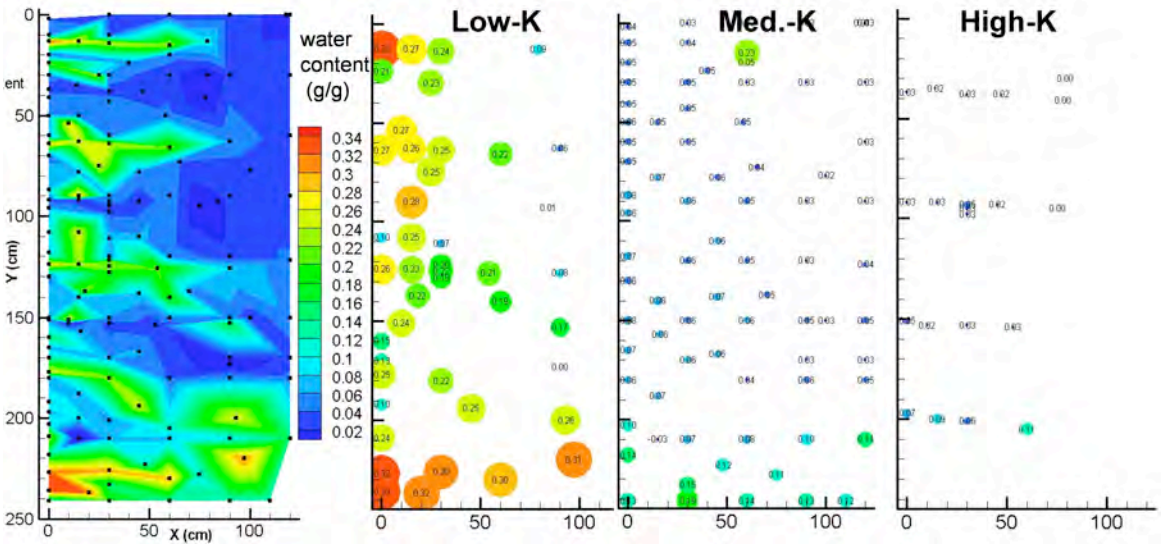

Figure 4.82. Final water content for large 2-D infiltration system with low-K and high-K zones.

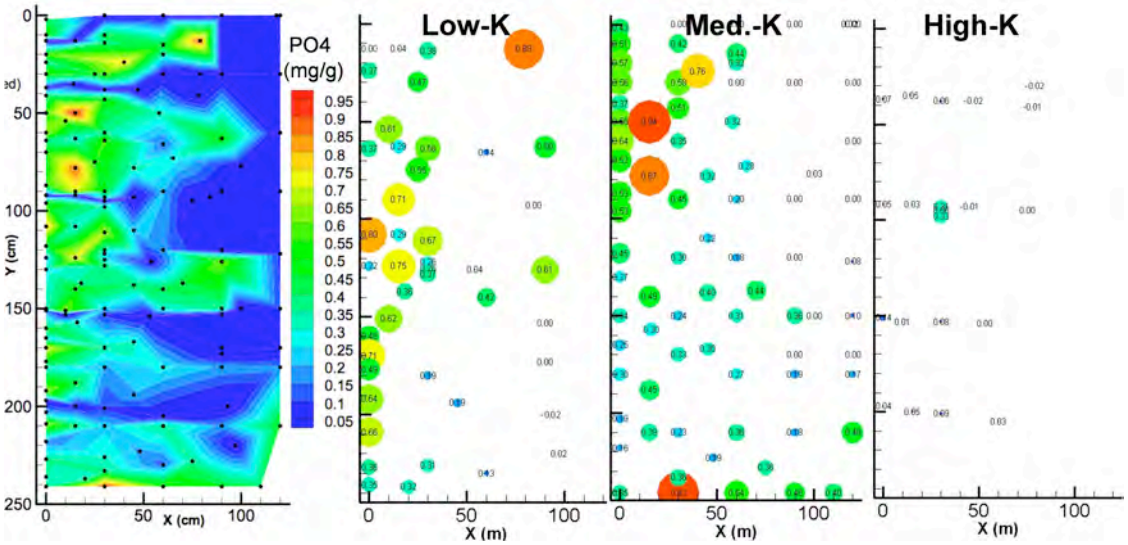

Figure 4.83. Apatite precipitate for large 2-D infiltration system with low-K and high-K zones.

The final apatite precipitate distribution did correspond to the higher residual water content in the low-K media (Figure 4.83b), but also contained significant precipitate within the medium-grained sediment (Figure 4.83c). Vertically, apatite mass in the low-K porous media was low in the upper quarter of the system and was relatively uniform throughout the vertical profile. As hypothesized, zones at large distances laterally in low-K zones retained a high apatite content. In the medium-grained sediment, apatite was concentrated in the upper half of the flow system, although low to moderate apatite concentration was distributed in the lower half of the flow system. Subsequent infiltration events would likely result in more apatite in the lower half of the flow system, as previously shown (Figures 4.71 and 4.73). As predicted, apatite was nearly absent from high-K layers due to very low water content maintained in these zones throughout the experiment and observed fingering (Figure 4.81). Overall, this large-scale experiment demonstrated that Ca-citrate-PO_4 infiltration followed by water infiltration can be used to distribute apatite precipitate in most formations in highly heterogeneous sediment (medium-grained and small-grained layers/discontinuous zones) with the exception of high-K zones. An alternate strategy to emplace apatite mass in high-K zones is described in the following section.

The final water content with depth directly beneath the infiltration source (left top of system) clearly shows a relatively uniform water content for the medium-grained sediment throughout the 8-ft profile, with higher water content for the bottom 20 cm (Figure 4.84a). The apatite distribution was relatively uniform in the upper half of the system for the medium grained sediment (~0.6 mg/g PO_4) and about half that concentration in the lower half of the system (~0.3 mg/g PO_4, Figure 4.84b). The low-K porous media reflected more variability throughout the profile, but was generally lower in the upper half of the system (0 to 0.6 mg/g PO_4) and higher in the lower half of the system (0.2 to 0.8 mg/g PO_4).

4.5.8 Air/Surfactant Injection of Ca-Citrate-PO_4

Water infiltration was successfully used to deliver the Ca-citrate-PO_4 solution in homogeneous and heterogeneous sediment that contained low-K zones. Apatite precipitate location could be

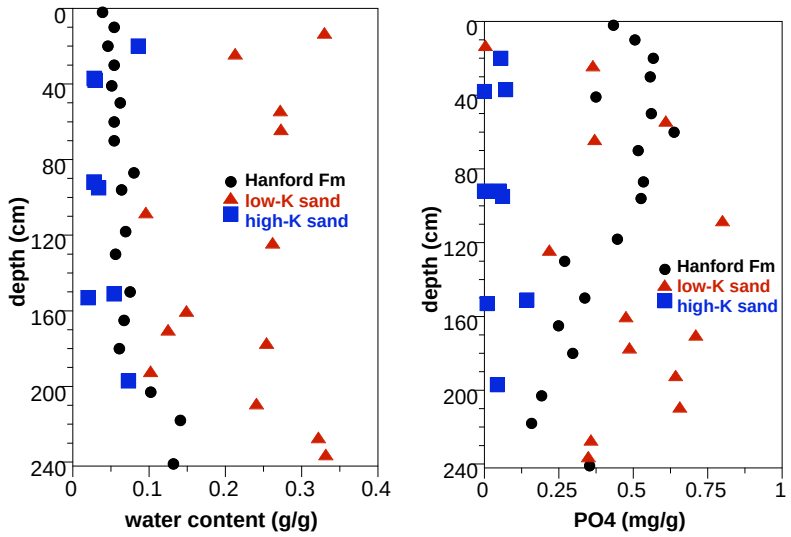

Figure 4.84. Final water content and PO_4 vertically beneath the infiltration stream for large 2-D infiltration system.

controlled by the residence time of the solution in a specific zone maintained for sufficient time (tens of hours) to precipitate apatite. This can be accomplished by manipulation of physical parameters (infiltration rate, sequence of solution and water, multiple infiltration events) and chemical parameters (solution concentration, solution chemistry). As shown in the previous section, high-K zones were not successfully treated generally due to low water content through out the experiment. In this section, experiments are described in which foam (surfactant, air with 1% water; Zhong et al. 2009a, 2009b) injection is used to deliver the Ca-citrate-PO_4 solution to the porous media. As this solution is being primarily advected through air-filled pores, there is more rapid foam transport in high-K zones (initially). Over time, as the foam breaks down, the liquid is deposited in the porous media, increasing the water content (and foam injection pressure). In homogeneous sediment, this "rind" of higher water content deposits at the limit of foam breakdown, and slowly increases in size over time. In heterogeneous systems (low-K and high-K zones), a more dynamic water deposition pattern occurs, with high-K zones maintaining low water content (i.e., foam advection in these zones maintaining the high air content) and higher residual water content in low-K zones, which have lower air permeability, especially with some water content.

Two 2-D foam injection experiments were conducted, and one is presented in this section (the second is in Appendix A, Section A.9). Additional work is needed to optimize conditions for delivery of liquid reactants (shown here) or solid-phase reactants. These experiments only demonstrate that liquid reactants can be delivered to heterogeneous porous media with a relatively uniform apatite distribution in high-K and medium-K porous media (less PO_4 deposition in low-K media), so is an attractive strategy to augment solution infiltration of Ca-cirate-PO_4 to result in treatment in low-K, medium-K, and high-K zones. One possible field-scale application strategy would be to inject foam into 100-N Area wells at low water content, which could result in lateral advection of the Ca-citrate-PO_4 laden foam in high-K zones and a slow vertical rise of the foam in vadose zone sediments.

The physical setup of the foam injection experiment (Figure 4.85) was central injection, and air withdrawal at the left and right sides of the 2-D experimental system, reflecting the generalized field injection scenario described above. This system was 140 cm long, 40 cm high, and 5 cm thick. A single high-K zone was placed in the left half of the flow system, and two low-K zones

placed in the right half of the flow system. In this experiment, the foam was injected at a rate of 60 mL/min and contained 1% surfactant and 1% water with 30 mM Ca-cirate-PO_4.

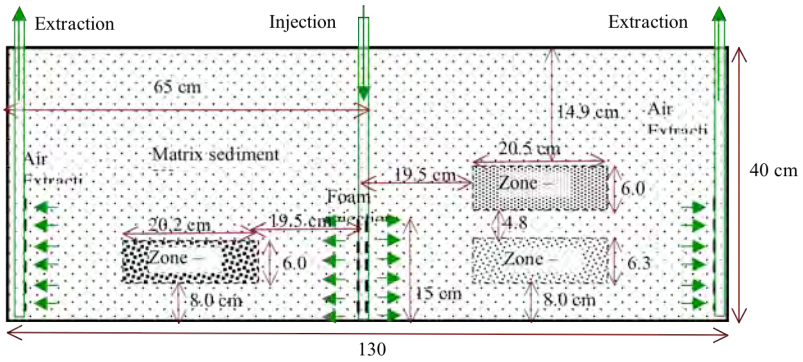

Figure 4.85. 2-D system used for foam injection of Ca-citrate-PO_4.

Foam could clearly be seen moving in the porous media (close-up video), and over time a water content "halo" could be observed to increase in size (Figure 4.86) over the 48-hour experiment. There did appear to be higher residual water content on the high-K size (left) of the system.

Over the course of the foam injection experiment (24 hours), aqueous samples were collected at both the high-K end (left side) and low-K end (right side) using in line collection bottles on the vacuum system. The vacuum was balanced to 30 mL/min at both ends. A total of 2.7 L of 30 mM Ca-citrate-PO_4 solution was injected into the system and a total of 1.17 L of liquid was collected from the high-K (left) side and 0.22 L of liquid from the low-K (right) side.

The final water content of the system (Figure 4.87a) did reflect observations, which high water content was above the high-K zone (left side), and also high water content in the low-K zones. It should be noted that this air advection technology appeared to not emplace water in low-K zones by advection, but rather the foam (with 1% water) advection in the medium-grained porous media between the low-K zones resulted in lateral deposition of water in the low-K zones.

The apatite precipitate distribution did not, as predicted, reflect the water content profile. Precipitate

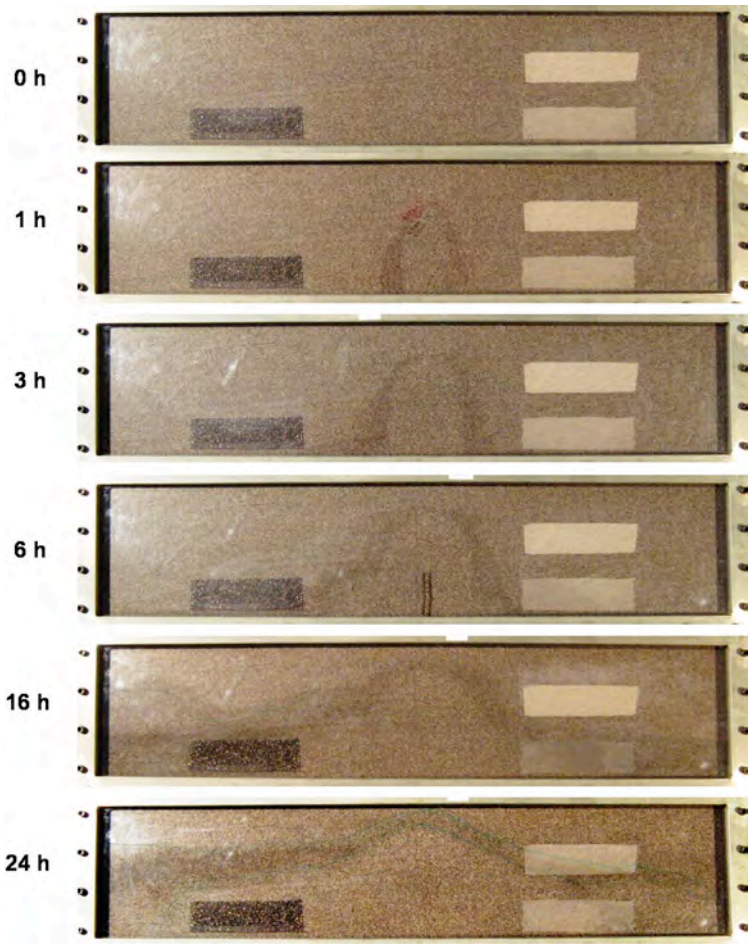

Figure 4.86. Development of the residual water content halo over time for foam injection in a 2-D system.

was relatively uniformly deposited at a very high concentration at the injection point (6 mg/g PO_4), and at a moderate concentration in the zone adjacent to the high-K zone, and within the high-K zone (Figure 4.87b). There was low to no apatite precipitate in the low-K zones, although there was apatite in the medium-grained sediment around low-K zones. This deposition pattern reflects air advection and the water deposition migration "halo" (Figure 4.86). The reason for the very high apatite concentration at the injection location is the relatively long time scale for foam injection actually moves only a small amount of Ca-citrate-PO_4 mass into the porous media, so biodegradation was apparently taking place near the injection location (similar conclusion for very low infiltration rates in Section 4.5.1). The measured microbial biomass at the injection location was 1.1E+09 cells/g, versus 3.2E+08 cells/g on the high-K (left) edge of the system and 4.7E+07 cells/g on the low-K (right) edge of the system. In general, foam injection showed promising results and warranted additional investigation. Additional processes need to be understood such as the influence of the 1% Na associated with the surfactant on Sr mobility during the foam injection, and additional testing of the buildup of pressure during injection. Although pressure buildup did not occur in this relatively short (i.e., 70 cm flow path length from the center to each end) system, pressure buildup was significant in two 25-ft long 1-D columns in which foam was injected (Section 4.2.4).

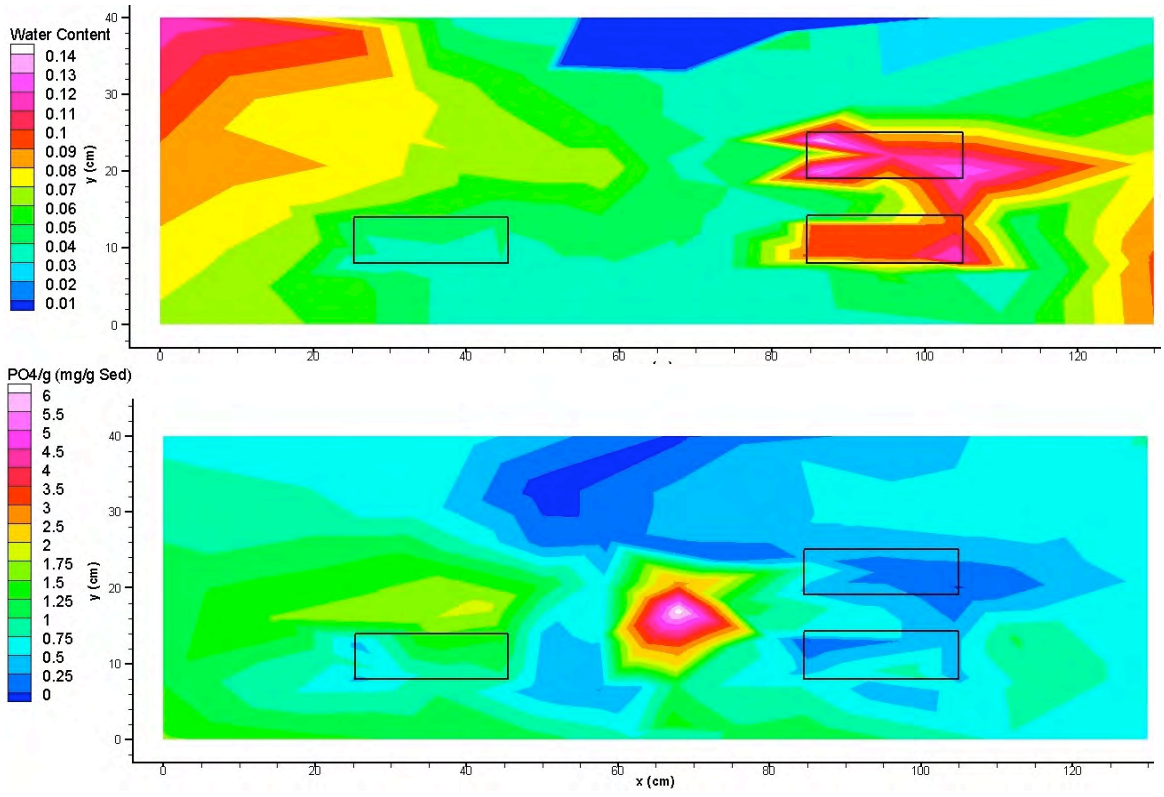

Figure 4.87. Final water content (a) and apatite (b) for foam injection in a 2-D system.

5.0 Summary

The objective of this project is to develop a method to emplace apatite precipitate in the 100-N Area vadose zone, which results in sorption and ultimately incorporation of Sr-90 into the apatite structure. Sr-90 sequestration with this technology occurs by the following steps: 1) injection of Ca-PO_4-citrate solution (with a Ca-citrate solution complex, Moore et al. 2004), 2) in situ biodegradation of citrate resulting in apatite [$Ca_{10}(PO_4)_6(OH)_2$] precipitation (amorphous, then crystalline), 3) adsorption of Sr-90 to the apatite surface, 4) apatite recrystallization with Sr-90 substitution for Ca (permanent), and 5) radioactive decay of Sr-90 to Y-90 to stable Zr-90. Although this is a complicated process, field-scale evidence indicates the process is effective in the Hanford 100-N saturated zone (Williams et al. 2008). Prior to initiation of this project, precipitation of apatite from Ca-citrate-PO_4 solution at low water saturation had not been tested. Concerns included: a) the rate at which citrate might biodegrade at low water saturation, b) the influence of the large decrease in microbial biomass with depth, c) the formation of Ca-carbonates and not apatite (with the excess CO_2 generated from citrate biodegradation), d) the ability to control infiltration sufficiently in homogeneous sediment to emplace apatite at a desired depth, e) the influence of vertical and lateral infiltration and heterogeneities on apatite precipitate location, and f) long-term performance of the apatite precipitate at low water saturation.

5.1 Citrate Biodegradation at Low Water Saturation

Within a few days of Ca-citrate-PO_4 solution contact with sediment, biodegradation of the citrate occurs in both oxic and anoxic environments in water-saturated sediments and apatite quickly precipitates (Szecsody et al. 2007). In the absence of citrate biodegradation (i.e., by using a bactericide in the sediment), apatite essentially does not precipitate (Figure 4.67). Citrate mineralization experiments in this study were conducted at water saturations from 35% to 100% over a range of citrate concentrations from 5 mM to 125 mM. There was a decrease in the citrate mineralization rate at very low water saturation (up to an order of magnitude, Figure 5.1), but the citrate mineralization rate from 50% to 100% water saturation was constant. In addition, the citrate mineralization extent was relatively invariant with water saturation.

Microbial biomass in unsaturated sediments does decrease orders of magnitude with depth in Hanford 100-N sediments. Within or slightly below the road fill, biomass is as high

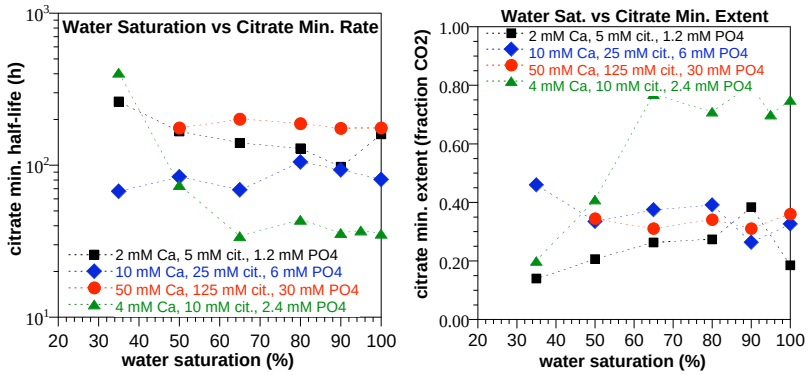

Figure 5.1. Correlation of water saturation and citrate mineralization half-life (a) and extent (b).

as 4 x 10^8 cells/g, and by the 15 ft depth (approximate lower limit for proposed infiltration studies), biomass has decreased to 6 x 10^5 cells/g (Figure 2.2). Biomass decreases further with depth in water-saturated sediments to 10^2 cells/g by a 40-ft depth. Citrate mineralization studies in sediments with different initial biomass did show a general correlation of higher initial biomass with a more rapid mineralization rate, but while biomass in sediments changed 5 orders of magnitude, the mineralization half-life only changed about 1 order of magnitude (Figure 4.4). This conclusion appears inconsistent with results of others (Francis et al. 1996), but further investigation into the role of in situ and infiltrating microbial populations (from the river water used) revealed the reason for the apparent difference.

Measurements of the river water biomass (2.2 x 10^6 cells/mL equivalent to 7.1 x 10^5 cells/g) indicated low values compared with in situ biomass (10^5 to 5 x 10^8 cells/g), so the contribution of river water microbes to biodegrade the citrate was initially not considered important. However, both in situ and injected microbial populations are redistributed in sediments during solution infiltration, so the measured citrate biodegradation rate may be somewhat averaged as the solution infiltrates vertically. Experiments measuring the influence of water velocity on microbial movement (i.e., shear forces detaching some portion of the population) and the ionic strength of the infiltrating solution (Figure 4.25) indicated both processes are redistributing microbes in subsurface sediments. The most significant finding was the comparison of apatite formation experiments in systems with either a killed in situ or injected microbial population. Results indicated that river water microbes present at 1100 times lower concentration than in situ microbes (7.8 x 10^8 cells/g) had roughly twice the impact on the citrate biodegradation rate. The implications are significant for both infiltration and injection of Ca-citrate-PO_4 into 100-N sediments. Proposed infiltration of the solution in 100-N sediments would likely be influenced by both in situ and injected microbial populations. The 100-N injections occur at >15 ft depth, where the in situ microbial biomass is present at 10^2 to 10^6 cells/g. At these concentrations relative to the much more active river water biomass, the injected river water microbial population would dominate nearly all the citrate biodegradation.

5.2 Apatite Precipitate Formation and Characterization

Different experimental techniques were used to identify the small amount of apatite precipitate that results from Ca-citrate-PO_4 infiltration into sediments. The final 300-year design capacity should have 3.4 mg apatite/g of sediment. Techniques used and being developed on this project include: a) XRD, b) SEM with EDS and elemental detectors (Figure 5.2), c) acid dissolution of the sediment and phosphate measurement (i.e., aqueous PO_4 extraction, Szecsody et al. 2008), and d) fluorescence of substituted apatites. Results of these techniques are described below. Additional characterization techniques were used on the apatite precipitate to determine specific properties that included: a) BET surface area (62.5 m^2/g), b) FTIR scan to determine apatite crystallinity and change in crystallinity upon Sr substitution, and c) organic and inorganic carbon analysis. The inorganic carbon content (0.02%) was low, indicating little carbonate coprecipitation with the apatite.

While the use of the electron microprobe shows that very small concentrations of apatite can be quantitatively identified, the cost of the process is significant, as is the time to process the samples. An example (Figure 5.2) shows 0.016 mg apatite/g of sediment with an EDS detector

clearly identifying apatite precipitate outside mineral grains. One method involves the aqueous measurement of phosphate, after the apatite was dissolved in acidic solution, which does not have the low detection limits of the electron microprobe (Figure 4.12). Infiltration of 2.4 mM PO_4 solution results in a calculated 0.1 mg apatite/g of sediment are likely not detectable, but 10 mM PO_4 (calculated 0.4 mg apatite/g sediment) are likely detectable. A third method of measuring added apatite in sediment investigated was the use of fluorescence scans. While pure hydroxyapatite does not fluoresce, apatites with F or carbonate substitution do fluoresce. Apatite precipitated in groundwater (Figure 4.17, black line) does fluoresce, and the sediment sample (no apatite added, green line) does not. This method is still in development, and a detection limit has not yet been determined.

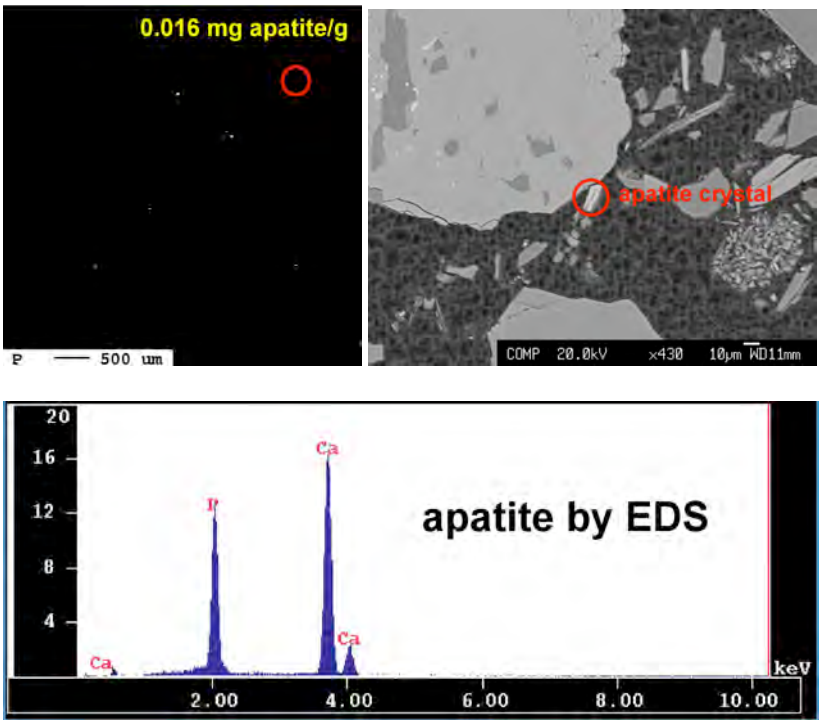

Figure 5.2. Scanning electron microbe images of a single apatite crystal.

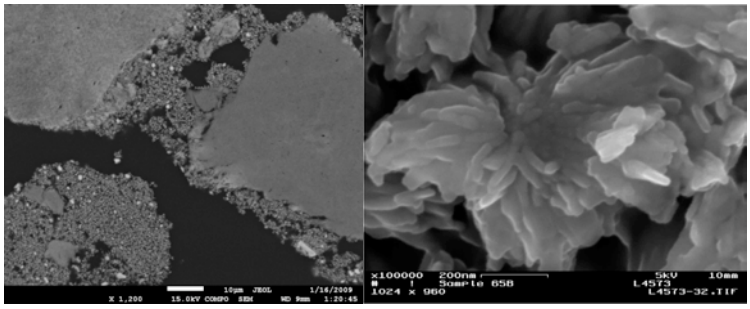

Figure 5.3. Electron backscatter image of apatite conglomerate and microcrystalline particles (a) and close-up of 20- to 30-nm apatite rods.

Electron microbe analysis of apatite formed in sediment in contact with the Ca-citrate-PO_4 solution reveled that two distinct morphologies result (Figure 5.3a). Most apatite precipitates are actually conglomerates of very small rod-shaped apatite precipitate particles (20 to 30 nm, Figure 5.3b) making up the 10 to 50 µm-sized particles. Fewer of the particles appear with a single color, which indicates microcrystalline structure.

5.3 Sr-90 Incorporation Mass and Rate Into Apatite

The ultimate mass of apatite needed in the vadose zone is controlled by: a) equilibrium calculation to adsorb and incorporate all Sr and Sr-90 for 300 years (~10 half-lives of Sr-90 decay with a half-life of 29.1 years), and b) kinetic calculation of Sr incorporation rate compared

to the Sr transport rate through the sediment (described in detail in Section 2.3). Although natural water infiltration and downward infiltration at Hanford is extremely slow (infiltration rate of 0.1 to 1 cm/year, given average annual precipitation of 16 cm/year), at the 100-N Area, the partially saturated zone (i.e., surface to 15 ft depth) can be partially water saturated in the spring due to high river levels, and can even become fully water saturated during floods. Therefore, a conservative estimate of the mass of apatite needed in the vadose zone is 3.4 mg/g (Table 2.1), which is equal to the mass needed in the water-saturated zone. From a mass balance perspective, a specific amount of apatite is needed to remove all Sr and Sr-90 from groundwater over the next 300 years (i.e., 10 half-lives of Sr-90 decay, half-life 29.1 years). This calculation is dependent on the crystal substitution of Sr for Ca in apatite. If 10% substitution is assumed, then 1.7 mg of apatite (per gram of sediment) is sufficient to sequester Sr and Sr-90 from the estimated 3300 pore volumes of water that will flow through a water-saturated apatite-laden zone. Various experiments in this study have measured Sr substitution (for Ca in apatite) values of 16.3% after 1.3 years at 22°C.

The second factor that controls the amount of apatite needed to sequester Sr-90 is the rate of Sr-90 incorporation into apatite. This permeable reactive barrier concept of apatite solids in the aquifer works if the flux rate of Sr and Sr-90 is slower than the removal rate of Sr and Sr-90 by apatite. If the groundwater flow rate is too high, even highly sorbed Sr and Sr-90 could advect through the apatite-laden zone more quickly than it is removed. The way to circumvent this issue is to have additional apatite in the subsurface system to remove Sr-90 at the increased flux rate. Based on the experience in the 100-D Area where partially reduced sediment is slowly removing chromate (and nitrate), seasonal fluctuations in the river level lead to specific times of year when flow in the aquifer exceeded the chromate removal rate of the reduced sediment. Therefore, numerous experiments have been conducted in this study to clearly define the rate at which Sr and Sr-90 is incorporated into the crystal structure of apatite.

Infiltration of a 60-mM PO_4 solution (Table 4.13) at a large scale (8-ft high 2-D system; described in Section 4.5.6) has resulted in large areas of 0.5 to 0.75 mg/g PO_4 (5 to 7.5 mg/g apatite) and small zones of 1.0 mg/g PO_4 (10 mg/g apatite). Although low-K zones received high treatment (due to higher residual water content retaining solution mass in the zone long enough for precipitate to form), high-K zones received minimal treatment (0 to 0.2 mg/g PO_4). Therefore, repeated solution infiltration events will likely be needed to build up precipitate mass. The most efficient means to infiltrate the solution to result in significant mass being held up in the vadose zone (i.e., depend on transient conditions to precipitate apatite) is to allow sufficient time between infiltration events to allow water to drain (Figures 4.71 through 4.75).

Control FTIR spectra have been run on both the Sigma and citrate apatite starting materials. FTIR scans of the 82°C citrate precipitated apatite aged for 6 months demonstrated that no secondary phases (e.g., $SrPO_4$ or $Sr(OH)_2$ precipitate) have formed within the apatite structure, as shown in Figure 5.4, in which peaks for the Ca-apatite (Sigma standard) and Sr-substituted apatite are similar, but do not show characteristic peaks of the $Sr(OH)_2$ or $Sr(PO_4)$. The presence of Sr in the apatite structure (adsorbed Sr removed) has been confirmed by ICP-MS and EDS.

Electron microbe analysis of Sr substitution into apatite precipitated from a Ca-citrate-PO_4 solution after 1.3 years of Sr-apatite contact revealed an average of 12.6 ± 7.5 mol/mol (moles Sr

per mole of Ca in the apatite structure) for the conglomerate particles (Figure 5.5). There was no Sr decrease with depth in the particle (Figure 5.5), which would occur of Sr were adsorbing then substituting on the outer edge of the particle then there was slow diffusion into the particle. Additional EDS scans of Sr substitution for the microcrystalline apatite particles (Figure 5.3) revealed 9.2 ± 1.1 mol/mol, so somewhat less substitution in these crystalline versus the looser structure of the conglomerate particles (and considerably less variability).

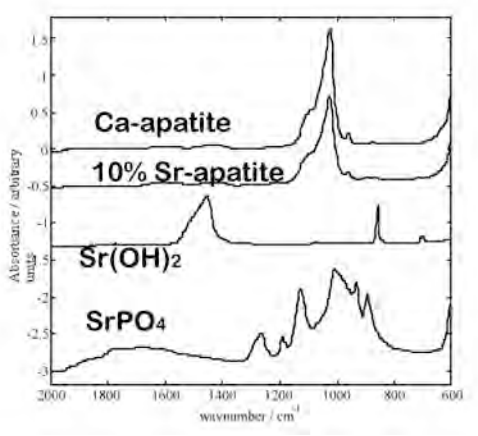

Figure 5.4. FTIR scans of apatite, Sr-substituted apatite, and other Sr phases (standards).

Laboratory experiments describing the Sr incorporation rate into apatite over months to over a year were used to calculate the Sr uptake rate into apatite. This was accomplished using a reaction simulation of the Ca-Na-Sr ion exchange onto the sediment surface, Ca-Na-Sr ion exchange onto apatite, and Sr incorporation from sorbed Sr on apatite (Figure 5.6a). Because field systems of packed porous media had higher sediment/water ratios, additional simulations were conducted to determine if the higher fraction of Sr on the sediment surface (and not on the apatite surface) would decrease the Sr incorporation rate into apatite. The proportion of Sr mass sorbed on apatite, therefore decreased from 45% (laboratory system) to 17% (field simulation, Figure 5.6b). However, this decrease in Sr mass sorbed to apatite did not change the Sr incorporation rate (green line in Figure 5.6a and b), which has a half-life of 15 months in both cases. The reason for this lack of change is the relative time scales of ion-exchange reactions versus the incorporation reaction being 5 to 6 orders of magnitude different. Any small amount of Sr sorbed on apatite is slowly incorporated and additional Sr mass sorbs onto the apatite. Ion-exchange equilibrium is quickly reached, so has no influence on slowing down the incorporation reaction. In contrast, if the ion exchange and incorporation reaction rates were only an order of magnitude different, then there the ion-exchange reaction would slow the apparent incorporation rate.

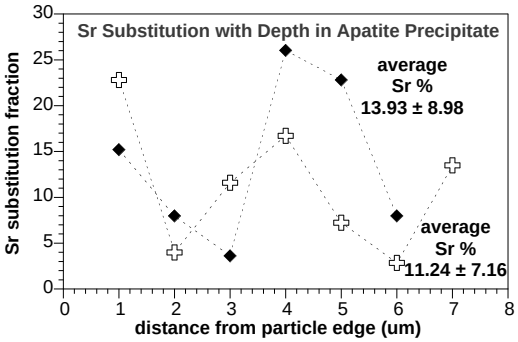

Figure 5.5. Sr substitution with depth in apatite precipitate with conglomerate morphology.

To be able to assess whether Sr-90 incorporation rates into apatite can be an effective field-scale reactive barrier in the Hanford 100-N Area, the natural Sr groundwater flux rate toward the river needs to be compared to calculated Sr uptake rates based on experimental results. For these calculations, the total Sr in each was considered. Sr incorporation rates were calculated for both initial uptake during apatite precipitation (more rapid uptake rate), and for solid-phase incorporation (Szecsody et al. 2007). Two different amounts of apatite were considered in the sediment that included the 0.38 mg apatite/g sediment produced from field injections #3 to #18, and the 3.4 mg apatite/g sediment final design (Table 2.1), which is based on 10% Sr substitution for Ca

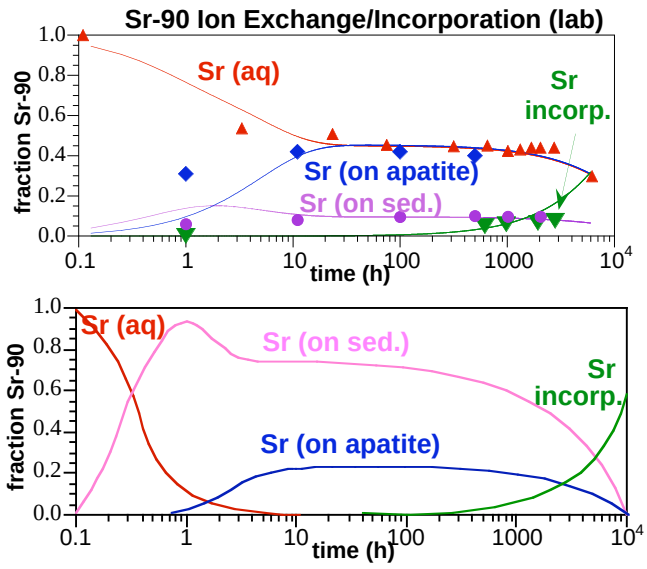

Figure 5.6. Sr uptake from groundwater suspension of 0.34 g/L apatite and 20 g/L sediment (a, data and simulation), and field conditions with 20% porosity and 3.8 mg apatite/g sediment (b).

in apatite. The Sr uptake (incorporation) rate was calculated in mmol Sr per day per cm^2 cross sectional area of sediment within a 30-ft wide barrier. These calculated uptake rates were initially fairly rapid during the initial apatite precipitation phase, then decreased about 2 orders of magnitude during solid-phase incorporation. For the field scenario of low concentration injections (i.e., 10 mM PO_4 injected in wells, or 0.34 mg apatite/g sediment), the Sr uptake rate was 8.8 x 10^{-6} mmol Sr/day/cm^2, or 6.5 times the average Sr groundwater flux rate in groundwater (1.36 x 10^{-6} mmol Sr/day/cm^2). Therefore, on a rate basis, all of the Sr (and Sr-90) would be consumed by the apatite in the barrier. It should be noted that zones of higher groundwater flux (10 to 100 times) would exceed the barrier uptake rate for this low apatite loading (0.38 mg apatite/g sediment). This low apatite loading would also not be able to incorporate Sr and Sr-90 for 300 years, so additional apatite is needed to increase the loading to 3.4 mg apatite/g sediment. At this high loading, the Sr uptake rate during initial precipitation is 3600 times more rapid than the average Sr groundwater flux rate, and the Sr uptake rate during solid-phase incorporation is 57 times more rapid than the average Sr groundwater flux rate, so the barrier will effectively remove all Sr except in extreme high groundwater flow conditions.

5.4 Solution Infiltration and Apatite Spatial Distribution

Recent Sr-90 depth profile data from the Hanford 100-N Area (Table 4.12) show that 40% to 70% of the Sr-90 is in the above the highly variable water table (~15 ft depth, Williams et al. 2008). Some of this variably saturated zone can be accessed through injections at high river level. However, since Sr-90 concentrations are the highest directly beneath the road fill (7 to 10 ft depth) in many wells, Ca-citrate-PO_4 solution placement is more effective through infiltration. Some locations also show low concentrations of Sr-90 in the fill (Table 4.12), although it should be noted that generally sediment samples were not taken in the fill. This could be caused by the water saturation during the operational period at 100-N Area, when discharge to the trenches was occurring, which was significantly higher than current conditions.

Based on the Sr-90 depth distribution, infiltration experiments in this study were focused on delivery of apatite into the lower half of the unsaturated sediment (i.e., transport the solution through most of the road fill to the underlying Hanford formation at 7 to 15 ft depth). In addition, it is hypothesized that there is a greater mass of Sr-90 in low-K zones due to lower advective flow in the field and slightly greater adsorption in the finer grained sediments. Heterogeneous systems were, therefore, mainly focused on apatite precipitate in low-K zones,

although final 2-D systems contained multiple low-K and high-K zones. 2-D infiltration systems were generally used in order to characterize the apatite distribution both with depth and laterally from the infiltration point. 2-D systems ranged in size from 56 cm (high) to 244 cm high (8 ft). Some 1-D column studies were also conducted that ranged in height to 3.6 m (12 ft). The spatial distribution of apatite that results form Ca-citrate-PO_4 solution infiltration, biodegradation (from in situ and injected microbial populations), is influenced by the vertical and lateral movement of water in the unsaturated sediments as well as reactions (phosphate adsorption, citrate biodegradation, ion exchange of Ca-Mg-K-Na, and apatite precipitation). An infiltration strategy was developed by manipulation of physical infiltration parameters (infiltration rate, variable rate of infiltration, sequential solution/water infiltration, multiple infiltration events) and chemical parameters (solution concentration, solution chemistry)(Szecsody et al. 2008; Thompson et al. 2009). Infiltration experiments were conducted in homogeneous sediment, then simple heterogeneous systems (single low-K zones), then complex heterogeneous systems (multiple low-K and high-K zones). The general findings were:

- *infiltration rate*: more rapid Ca-citrate-PO_4 solution infiltration resulted in greater depth of apatite precipitate, but less lateral spreading
- *decrease in infiltration rate*: rapid then slow solution infiltration resulted in greater lateral spreading of the apatite precipitate at depth
- *sequential solution then water infiltration*: water infiltration after solution infiltration effectively moved the apatite mass to depth in homogeneous sediment systems
- *solution concentration*: infiltration of higher Ca-citrate-PO_4 solution concentrations resulted in a greater depth of apatite precipitate due to less PO_4 adsorption and slower citrate biodegradation
- *infiltration cycles*: repeated infiltration of the Ca-citrate-PO_4 solution with time between cycles to allow for water drainage resulted in an increased depth and greater lateral spread of apatite precipitate mass (homogeneous and simple heterogeneous systems)
- systems with simple low-K zones had a higher apatite precipitate concentration in the low-K zone due to higher residual water content
- infiltration rate manipulation can be used to infiltration solution into specific subsurface areas (i.e., above or beneath low-K zones)
- solution then water infiltration into a complex heterogeneous system with low-K and high-K discontinuous layers (large scale, 8 ft high) showed high apatite precipitate in low-K zones and medium-grained sediment, but very low treatment in high-K zones due to low initial and residual water content
- an alternate method to emplace apatite mass in unsaturated sediments (air/surfactant injection) appears to target high-K zones and resulted in moderate apatite precipitate adjacent and within high-K zones.

At very slow infiltration rates, capillary forces dominate water movement at low water content, which results in a relatively uniform (but low) moisture profile with depth and laterally (Figure 5.7a), which is under transient conditions (not a steady-state profile). This is, however, not a viable method to "hold" the Ca-citrate-PO_4 solution in the unsaturated sediments because of the rates of phosphate adsorption (hours) and citrate biodegradation (tens to hundreds of

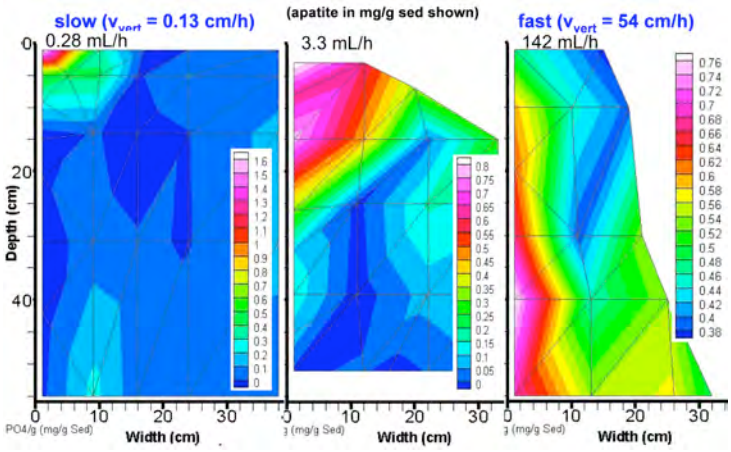

Figure 5.7. Influence of increasing infiltration rate on vertical and lateral apatite distribution.

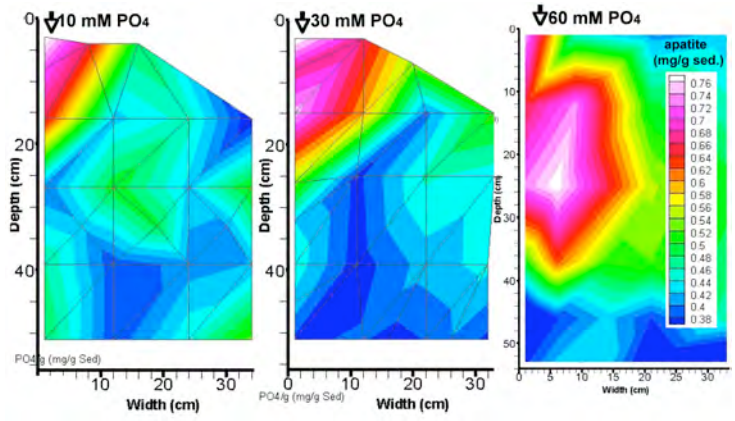

Figure 5.8. Apatite precipitate with infiltration at 10 mM (a), 30 mM (b), and 60 mM (c) PO_4 concentration.

hours) were much faster than the infiltration rate (430 hours to reach 50 cm depth). Essentially all of the phosphate formed apatite precipitate within a few centimeters of the point of infiltration (Figure 5.7a). In contrast, rapid infiltration of a solution can be controlled by gravity and capillary forces (vertically), which results in the rapid transport (and drainage) of the solution in a short period of time with little lateral spreading. The resulting apatite distribution (Figure 5.7c) is relatively uniform with depth directly beneath the infiltration point, but does not exhibit much lateral distribution.

Infiltration of a higher concentration Ca-citrate-PO_4 solution influences PO_4 adsorption (see Section 4.1.5), results in a lower citrate biodegradation rate (see Section 4.1.3), and increases microbial detachment and mobility (see Section 4.2.3). All of these processes generally result in the Ca-citrate-PO_4 solution infiltration to a greater depth before apatite precipitates. 2-D infiltration experiments varying the solution concentration (keeping the infiltration rate constant) demonstrated an increase in the apatite precipitate depth with increasing concentration (Figure 5.8). In addition, there was greater lateral spread of the precipitate, likely by the same processes; decreased PO_4 adsorption and slower citrate biodegradation rate allowed more time for the solution to move vertically and laterally before citrate was degraded and apatite precipitated.

Repeated infiltration cycles of the solution followed by a week of no infiltration to allow for reactions to form apatite (and the solution to drain) resulted in an increase in precipitate mass at depth for each subsequent infiltration (Figure 5.9). In addition, there was additional apatite precipitate laterally from the infiltration point. This did not appear to result from an increased width of moisture (Figure 4.70).

Solution infiltration into systems with simple heterogeneities (i.e., single low-K lens) was most effectively treated by the infiltration strategy of rapid solution infiltration (to transport the solution to depth with minimal PO_4 sorption and citrate biodegradation) followed by slow water

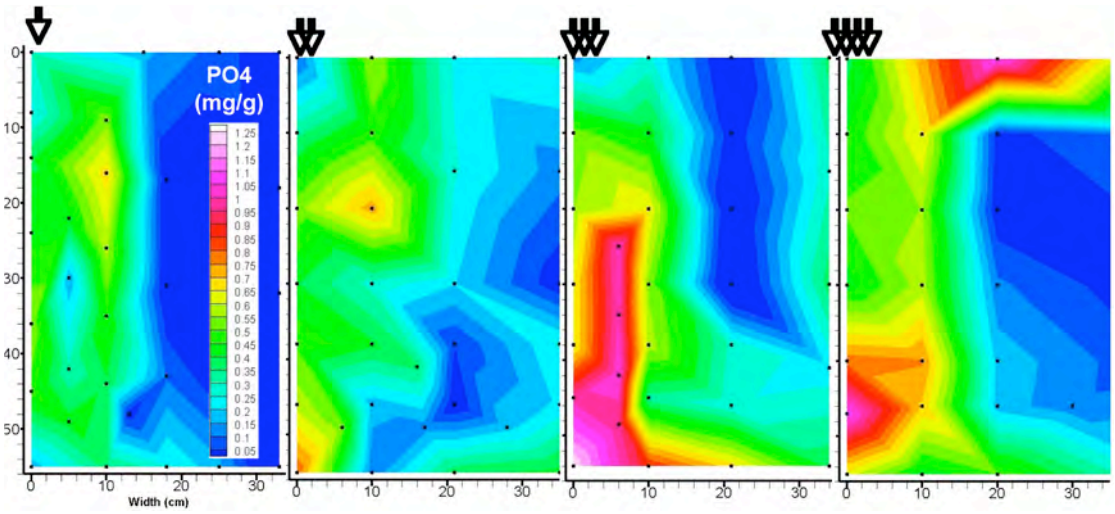

Figure 5.9. Apatite precipitate for sequential infiltration with 1 week between doses.

infiltration (to move additional reactants to depth and allow time for lateral spread of the solution at depth). A single infiltration event using this infiltration scenario resulted in the highest concentration of apatite within the low-K zone (due to retention of high water content), and moderate apatite precipitate concentration in most of the sediment profile except the top quarter (Figure 5.10a). Repeated infiltration cycles did build up precipitate mass within the low-K zone, as well as above and below the low-K zone (Figure 5.10b).

Infiltration into a large 2-D system (8 ft high by 4 ft wide) that was half that of field scale containing many discontinuous low-K and high-K zones (Figure 5.11) was focused on the effectiveness of treatment with depth in the different layers. At the initial rapid infiltration rate of the solution for 1.2 hours, then water for 2.0 hours, the solution migrated vertically within hours (Figure 5.11a), and drained by 23 hours (Figure 5.11b). Significant lateral movement is observed in low-K zones (white) and fingering in high-K zones (Figure 5.11c).

The final water content with depth directly beneath the infiltration source (left top of system) clearly shows a relatively uniform low water content for the medium-grained sediment throughout the 8-ft profile (caused by drainage), with higher water content for the bottom 20 cm (Figure 5.12a;

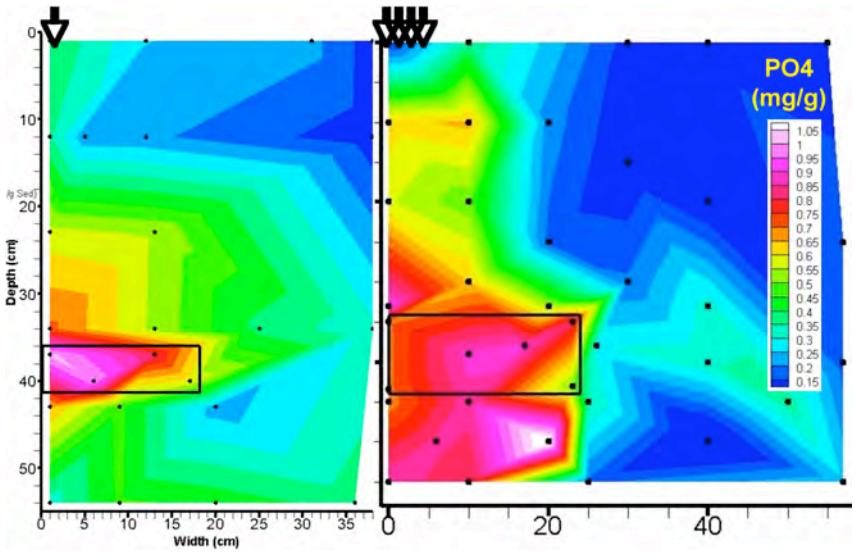

Figure 5.10. Apatite for sequential infiltration with 1 week between doses (low-K zone).

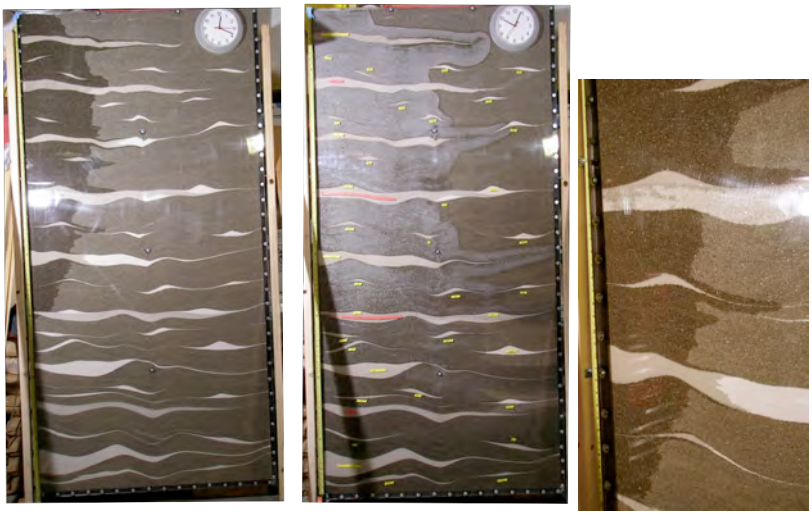

Figure 5.11. Solution infiltration in large 2-D system (8 ft high x 4 ft wide) at a) 1 hour, b) 23 hours, and c) close-up at 3 hours.

full 2-D water content profile in Figure 4.81). For the area the solution infiltrated into, the apatite distribution was relatively uniform in the upper half of the system for the medium grained sediment (~0.6 mg/g PO_4) and about half that concentration in the lower half of the system (~0.3 mg/g PO_4, Figure 5.12b; full 2-D apatite concentration in Figure 4.82). Although the solution drained to low water content by 23 hours, there was sufficient time the solution stayed in the medium-grained sediment to form apatite precipitate. The low-K porous media reflected more variability throughout the profile, but was generally lower in the upper half of the system (0 to 0.6 mg/g PO_4) and higher in the lower half of the system (0.2 to 0.8 mg/g PO_4). The high-K layers received ineffective treatment, due to very low water content at all times.

An alternate method to deliver Ca-citrate-PO_4 solution to unsaturated sediments consisted of air injection with a surfactant (foam) and 1% water content (containing the Ca-citrate-PO_4 solution). As this solution is being primarily advected through air-filled pores, there is more rapid foam transport in high-K zones (initially). Over time, as the foam breaks down, the liquid is deposited in the porous media, increasing the water content (and foam injection pressure). In homogeneous sediment, this "rind" of higher water content deposits at the limit of foam breakdown, and slowly increases in size over time. In heterogeneous systems (low-K and high-K zones), a more dynamic water deposition pattern occurs, with high-K zones maintaining low water content (i.e., foam advection in these zones maintaining the high air content) and higher residual water content in low-K zones, which have lower air permeability, especially with some water content.

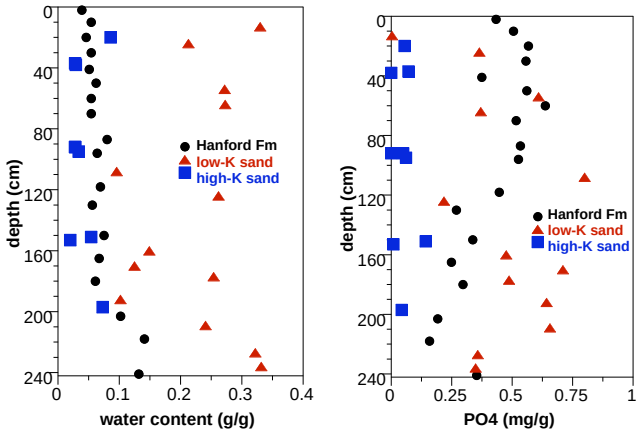

Figure 5.12. Final water content and PO_4 vertically beneath the infiltration stream for large 2-D infiltration system.

In contrast to Ca-citrate-PO_4 solution infiltration, the apatite precipitate distribution for these foam-injected solution did not, reflect the water content profile. Precipitate was relatively uniformly deposited at a very high concentration at the injection point (6 mg/g PO_4), and at a moderate concentration in the zone adjacent to the

high-K zone and within the high-K zone (Figure 4.86). There was low to no apatite precipitate in the low-K zones, although there was apatite in the medium-grained sediment around low-K zones. This deposition pattern reflects air advection and the water deposition migration "halo" (Figure 4.85). The reason for the very high apatite concentration at the injection location is the relatively long time scale for foam injection actually moves only a small amount of Ca-citrate-PO_4 mass into the porous media, so biodegradation was apparently taking place near the injection location. In general, foam injection showed promising results and warrants further investigation. Additional processes need to be understood such as the influence of the 1% Na associated with the surfactant on Sr mobility during the foam injection, and additional testing of the buildup of pressure during injection.

In summary, the Ca-citrate-PO_4 solution can be infiltrated into unsaturated sediments to result in apatite precipitate to provide effective treatment of Sr-90 contamination. After 1.3 years of contact, 9 to 16% Sr-90 had substituted for Ca in apatite. Sr-90 substitution in apatite did not decrease with depth due to the 20-30 nm apatite crystals conglomerated forming a porous 10 to 50 micron conglomerate precipitate. Microbial redistribution during solution infiltration and a high rate of citrate biodegradation for river water microbes (water used for solution infiltration) results in a relatively even spatial distribution of the citrate biodegradation rate and ultimately apatite precipitate. Manipulation of the Ca-citrate-PO_4 solution infiltration strategy can be used to result in apatite precipitate in the lower half of the vadose zone (where most of the Sr-90 is located) and within low-K layers (which are hypothesized to have higher Sr-90 concentrations). The most effective infiltration strategy to precipitate apatite at depth was to infiltrate a high concentration solution (6 mM Ca, 15 mM citrate, 60 mM PO_4) at a rapid rate (near ponded conditions), followed by rapid, then slow water infiltration (Szecsody et al. 2008). Repeated infiltration events, with sufficient time between events to allow water drainage in the sediment profile can be used to buildup the mass of apatite precipitate at greater depth. Low-K heterogeneities were effectively treated, as the higher residual water content maintained in these zones resulted in higher apatite precipitate concentration. High-K zones did not receive sufficient treatment by infiltration, although an alternative strategy of air/surfactant (foam) was demonstrated effective for targeting high-K zones. The flow rate manipulation used in this study to treat specific depths and heterogeneities are not as easy to implement at field scale due to the lack of characterization of heterogeneities and ability to monitor the wetting front during infiltration. However, the use of real-time surface and cross-borehole geophysics can be used to track the infiltrating Ca-citrate-PO_4 front so adjustments can be made in the infiltration rate to precipitate apatite in desired zones. In addition, the reactive transport code used in this study with field-scale physical parameters for sediments can be used to evaluate infiltration rates along with preliminary water infiltration tests at field scale.

6.0 References

Andronescu E, E Stefan, E Dinu, and C Ghitulica. 2002. "Hydroxyapatite Synthesis." *Key Engineering Materials* 206-213:1595-1598.

Arey JS, JC Seaman, and PM Bertsch. 1999. "Immobilization of Uranium in Contaminated Sediments by Hydroxyapatite Addition." *Environmental Science & Technology* 33:337-342.

Amrhein C and DL Suarez. 1990. "Procedure for Determining Sodium-Calcium Selectivity in Calcareous and Gypsiferous Soils." *Soil Science Society of America Journal* 54:999-1007.

Bailey JE and DF Ollis. 1986. *Biochemical Engineering Fundamentals.* McGraw-Hill Publishing Co., New York.

Bailliez S, A Nzihou, E Beche, and G Flamant. 2004. "Removal of Lead by Hydroxyapatite Sorbent." *Process Safety and Environmental Protection* 82:175-180.

Belousova EA, WL Griffin, SY O'Reilly, and NI Fisher. 2002. "Apatite as an Indicator Mineral for Mineral Exploration: Trace-Element Compositions and Their Relationship to Host Rock Type." *Journal of Geochemical Exploration* 76:45-69.

Bynhildsen L and T Rosswall. 1997. "Effects of Metals on the Microbial Mineralization of Organic Acids." *Water, Air, and Soil Pollution* 94(1-2):45-57.

Chairat C, EH Oelkers, S Kohler, N Harouiya, and JE Lartique. 2004. "An Experimental Study of the Dissolution Rates of Apatite and Britholite as a Function of Solution Composition and pH from 1-12." In *Water-Rock Interaction*, W S II (ed.), p. 671-674. Taylor & Francis Group, London.

DOE-RL. 2004. *Calendar Year 2003 Annual Summary Report for the 100-HR-3, 100-KR-4, and 100-NR-2 Operable Unit (OU) Pump & Treat Operations.* DOE/RL-2004-21, U.S. Department of Energy, Richland Operations Office, Richland, Washington.

DOE-RL. 2005. *Aquatic and Riparian Receptor Impact Information for the 100-NR-2 Groundwater Operable Unit*. Accessed February 9, 2009, at http://www.washingtonclosure.com/projects/endstate/risk_library.html#narea.

Ecology – Washington State Department of Ecology, U.S. Environmental Protection Agency, and U.S. Department of Energy. 1989. Hanford Federal Facility Agreement and Consent Order (The Tri-Party Agreement). Document No. 89-10, as amended through February 12, 2008, Olympia, Washington. Accessed February 9, 2009, at http://www.hanford.gov/?page=91&parent=0.

Edrington RS. 2005. Unpublished Columbia River stage data. Fluor Hanford, Inc., Richland, Washington.

Elliot JC, PE Mackie, and RA Young. 1973. "Monoclinic Hydroxyapatite." *Science*, 180:1055-1057.

Francis AJ, GA Joshi Tope, and CJ Dodge. 1996. "Biodegradation of Nickel-Citrate and Modulation of Nickel Toxicity by Iron." *Environmental Science & Technology* 30:562-568.

Fuller CC, JR Bargar, and JA Davis. 2003. "Molecular-Scale Characterization of Uranium Sorption by Bone Apatite Materials for a Permeable Reactive Barrier Demonstration." *Environmental Science & Technology* 37:4642-4649.

Fuller CC, JR Bargar, JA Davis, and MJ Piana. 2002. "Mechanisms of Uranium Interactions with Hydroxyapatite: Implications for Groundwater Remediation." *Environmental Science & Technology* 36:158-165.

Geochem Software, Inc. 1994. *Mac MINTEQ-A2: Aqueous Geochemistry for the Macintosh.* Published by Geochem Software, Inc., Reston, Virginia.

Heslop DD, Y Bi, AA Baig, M Otsuka, and WI Higuchi. 2005. "A Comparative Study of the Metastable Equilibrium Solubility Behavior of High-Crystallinity and Low-Crystallinity Carbonated Apatites Using pH and Solution Strontium as Independent Variables." *Journal of Colloid and Interface Science* 289:14-25.

Hill RG, A Stamboulis, RV Law, A Clifford, MR Towler, and C Crowley. 2004. The Influence of Strontium Substitution in Fluorapatite Glasses and Glass-Ceramics. *Journal of Non-Crystalline Solids* 336:223-229.

Hughes JM, M Cameron, and KD Crowley. 1989. "Structural Variations in Natural F, OH and Cl Apatites." *Amer Mineral* 74:870-876.

Hughes JM and J Rakovan. 2002. "The Crystal Structure of Apatite, $Ca_5(PO_4)_3(F,OH,Cl)$." In *Phosphates: Geochemical, Geobiological and Materials Importance*, Reviews in Mineralogy and Geochemistry, Vol. 48, Mineralogical Society of America, Washington, D.C., p. 1-12.

Jeanjean J, JC Rouchaud, L Tran, and M Fedoroff. 1995. "Sorption of Uranium and Other Heavy Metals on Hydroxyapatite." *J. Radioanal. Nucl. Chem. Letters* 201:529-539.

Koutsoukos PG and GH Nancollas. 1981. "Influence of Strontium Ion on the Crystallization of Hydroxylapatite from Aqueous-Solution." *Journal of Physical Chemistry* 85:2403-2408.

Lazic S and Z Vukovic. 1991. "Ion-Exchange of Strontium on Synthetic Hydroxyapatite." *Journal of Radioanalytical and Nuclear Chemistry-Articles* 149:161-168.

LeGeros RZ, G Quirolgico, and JP LeGeros. 1979. "Incorporation of Strontium in Apatite - Effect of pH." *Journal of Dental Research* 58:169-169.

Lindsay WL, PLG Vlek, and SH Chien. 1989. "Phosphate Minerals." *Minerals in Soil Environments*, 2 ed., Soil Science Society of America, Madison, Wisconsin, p. 1089-1131.

Lower SK, PA Maurice, SJ Traina, and EH Carlson. 1998. "Aqueous Pb Sorption by Hydroxylapatite: Application of Atomic Force Microscopy to Dissolution, Nucleation, and Growth Studies." *American Mineralogist* 83:147-158.

Ma QY, SJ Traina, and TJ Logan. 1995. "In Situ Lead Immobilization by Apatite." *Environmental Science and Technology* 27:1803-1810.

Mavropoulos E, AM Rossi, AM Costa, CAC Perez, JC Moreira, and M Saldanha. 2002. "Studies on the Mechanisms of Lead Immobilization by Hydroxyapatite." *Environmental Science & Technology* 36:1625-1629.

Misra DN. 1998. "Interaction of Some Alkali Metal Citrates with Hydroxyapatite - Ion-Exchange Adsorption and Role of Charge Balance." *Colloids and Surfaces a-Physicochemical and Engineering Aspects* 141:173-179.

Moelo Y, B Lasnier, P Palvadeau, P Leone, and F Fontan. 2000. "Lulzacite, Sr2Fe2+(Fe2+,Mg)(2)Al-4(PO4)(4)(OH)(10), a New Strontium Phosphate (Saint-Aubin-des-Chateaux, Loire-Atlantique, France)." *Comptes Rendus De L Academie Des Sciences Serie Ii Fascicule a-Sciences De La Terre Et Des Planetes* 330:317-324.

Moore R, J Szecsody, M Truex, K Kelean, R Bontchev, and C Ainsworth. 2007. "Formation of Nanosize Apatite Crystals in Sediments for Contaminant and Stabilization of Contaminants." *Environmental Applications of Nanomaterials, Synthesis, Sorbents, and Sensors*, (eds) G Fryxell and G Cao, Imperial College Press, p. 89-109.

Moore RC, J Szecsody, MJ Truex, K Helean, R Bontchev, and C Ainsworth. 2006. "Formation of Nanosize Apatite Crystals in Sediments for Containment and Stabilization of Contaminants." *Environmental Applications of Nanomaterials*, CRC Press, in press.

Moore RC, M Gasser, N Awwad, KC Holt, FM Salas, A Hasan, MA Hasan, H Zhao, and CA Sanchez. 2005. "Sorption of Plutonium(VI) by Hydroxyapatite." *Journal of Radioanalytical and Nuclear Chemistry* 263:97-101.

Moore RC, C Sanchez, K Holt, P Zhang, H Xu, and GR Choppin. 2004. "Formation of Hydroxyapatite in Soils Using Calcium Citrate and Sodium Phosphate for Control of Strontium Migration." *Radiochimica Acta* 92(9-11/2004):719-723.

Moore RC, K Holt, HT Zhao, A Hasan, N Awwad, M Gasser, and C Sanchez. 2003. "Sorption of Np(V) by Synthetic Hydroxyapatite." *Radiochimica Acta* 91:721-727.

Nancollas GH and MS Mohan. 1970. "The Growth of Hydroxyapatite Crystals." *Archives of Oral Biology* 15(8):731-745.

Papargyris AD, AT Botis, and SA Papargyri. 2002. "Synthetic Routs for Hydroxyapatite Powder Production." *Key Engineering Materials* 206-213:83-86.

Raicevic S, Z Vukovic, TL Lizunova, and VF Komarov. 1996. "The Uptake of Strontium by Calcium Phosphate Phase Formed at an Elevated pH." *Journal of Radioanalytical and Nuclear Chemistry-Articles* 204:363-370.

Rendon-Angeles JC, K Yanagisawa, N Ishizawa, and S Oishi. 2000. "Effect of Metal Ions of Chlorapatites on the Topotaxial Replacement by Hydroxyapatite under Hydrothermal Conditions." *Journal of Solid State Chemistry* 154:569-578.

Routson RC, G Barney, R Smith, C Delegard, and L Jensen. 1981. *Fission Product Sorption Parameters for Hanford 200 Area Sediment Types*. RHO-ST-35, Rockwell Hanford Operations, Richland, Washington.

Serne RJ and VL LeGore. 1996. *Strontium-90 Adsorption-Desorption Properties and Sediment Characterization at the 100-N Area*. Pacific Northwest Laboratory, Richland, Washington.

Smiciklas I, A Onjia, and S Raicevic. 2005. "Experimental Design Approach in the Synthesis of Hydroxyapatite by Neutralization Method." *Separation and Purification Technology* 44:97-102.

Spence RD and C Shi. 2005. *Stabilization and Solidification of Hazardous, Radioactive, and Mixed Wastes*. CRC Press, Boca Raton, Florida.

Sposito G, LJ Lund, and AC Chang. 1982. "Trace-Metal Chemistry in Arid-Zone Field Soils Amended with Sewage-Sludge. 1. Fractionation of Ni, Cu, Zn, Cd, and Pb in Solid-Phases." *Soil Science Society of America Journal* 46:260-264.

Sposito G, KM Holtzclaw, C Jouany, and L Charlet. 1983a. "Cation Selectivity in Sodium - Calcium, Sodium - Magnesium, and Calcium - Magnesium Exchange on Wyoming Bentonite at 298-K." *Soil Science Society of America Journal* 47:917-921.

Sposito G, CS Levesque, JP Leclaire, and AC Chang. 1983b. "Trace-Metal Chemistry in Arid-Zone Field Soils Amended with Sewage-Sludge. 3. Effect of Time on the Extraction of Trace-Metals." *Soil Science Society of America Journal* 47:898-902.

Steefel CI. 2004. "Evaluation of the Field-Scale Cation Exchange Capacity of Hanford Sediments." In *Water-Rock Interaction*, W. S. II (ed.), p. 999-1002, Taylor & Francis Group, London.

Szecsody J, J Fruchter, C Burns, M Rockhold, M Oostrom, M Williams, V Vermeul, and R Moore. 2008. "Sr-90 Immobilization by Infiltration of a Ca-Citrate-PO4 Solution into the Hanford 100N Area Vadose Zone." *Waste Management 2008 Conference*, Phoenix, Arizona.

Szecsody JE, CA Burns, RC Moore, JS Fruchter, VR Vermeul, MD Williams, DC Girvin, JP McKinley, MJ Truex, and JL Phillips. 2007. *Hanford 100-N Area Apatite Emplacement: Laboratory Results of Ca-Citrate-PO4 Solution Injection and Sr-90 Immobilization in 100-N Sediments*. PNNL-16891, Pacific Northwest National Laboratory, Richland, Washington.

Technical Advisory Group (TAG). 2001. *Hanford 100-N Area Remediation Options Evaluation Summary Report*. November 2001.

Thompson KM, RJ Fabre, J Szecsody, V Vermeul, R Fellows, M Williams, J Fruchter. 2009. "An Innovative Approach for Constructing an In Situ Barrier for Strontium-90 at the Hanford Site, Washington. *Waste Management 2009*, Phoenix, Arizona.

Tofe AJ. 1998. "Chemical Decontamination Using Natural or Artificial Bone." US Patent 5,711,015.

Van der Houwen JAM and AE Valsami-Jones. 2001. "The Application of Calcium Phosphate Precipitation Chemistry to Phosphorus Recovery: The Influence of Organic Ligands." *Environmental Technology* 22:1325-1335.

Verbeek RMH, M Hauben, HP Thun, and F Verbeek. 1977. "Solubility and Solution Behavior of Strontium hydroxyapatite." *Z. Phys. Chem*. (Wiesbaden) 108(2):203-215.

Vukovic Z, S Lazic, I Tutunovic, and S Raicevic. 1998. "On the Mechanism of Strontium Incorporation into Calcium Phosphates." *J. Serbian Chem. Soc.* 63.5:387-393.

Waychunas G. 1989. "Luminescence, X-ray Emission and New Spectroscopies." *Rev Mineral*. 18:638-698.

White MD and M Oostrom. 2004. *Subsurface Transport Over Multiple Phases (STOMP): User's Guide.* Version 3.1. PNNL-14478, Pacific Northwest National Laboratory, Richland, Washington.

Williams M, B Fritz, D Mendoza, M Rockhold, P Thorne, Y Xie, B Bjornstad, R Mackley, D Newcomer, J Szecsody, and V Vermeul. 2008. *Interim Report: 100-NR-2 Apatite Treatability Test: Low-Concentration Calcium-Citrate-Phosphate Solution Injection for In Situ Strontium-90 Immobilization*. PNNL-17429, Pacific Northwest National Laboratory, Richland, Washington.

Wright J. 1990. "Conodont Apatite: Structure and Geochemistry." *Biomineralization: Patterns, Processes and Evolutionary Trends.* J Carter (ed.), Van Nostrand Reinhold, New York.

Wright J, KR Rice, B Murphy, and J Conca. 2004. "PIMS Using Apatite II™: How It Works To Remediate Soil and Water." *Sustainable Range Management*, RE Hinchee and B Alleman (eds.), Battelle Press, Columbus, Ohio. www.batelle.org/bookstore, ISBN 1-57477-144-2, B4-05.

Zhong L, N Qafoku, J Szecsody, and Z Zhang. 2009. "Foam Delivery of Calcium Polysulfide to the Vadose Zone for Cr(VI) Immobilization: A Laboratory Evaluation." *Vadose Zone Journal*, in press.

Zhong L, J Szecsody, N Qafoku, E Dresel, and Z Zhang. 2009. "Foam Delivery of Remedial Amendments for Enhanced Vadose Zone Metal and Radionuclide Remediation." *Waste Management 2009*, Phoenix, Arizona.

Appendix

Appendix

Contents

A.1 Task 1 – Apatite Formation: Citrate Mineralization

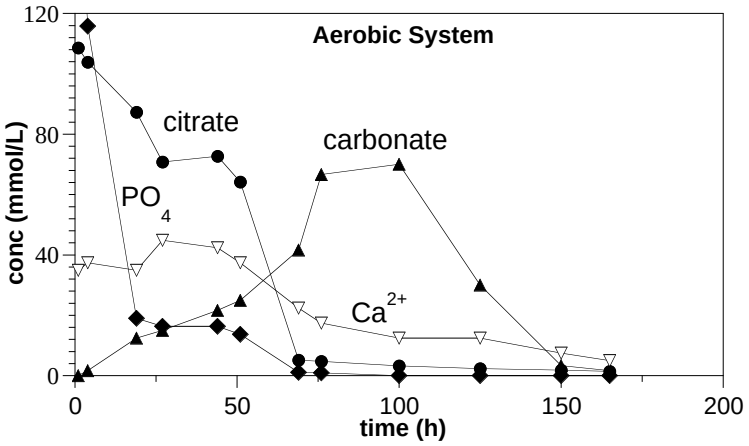

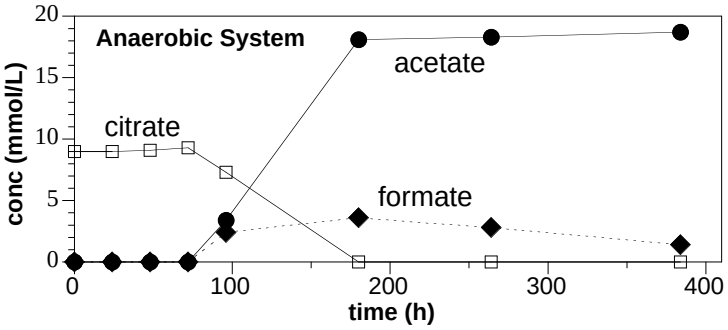

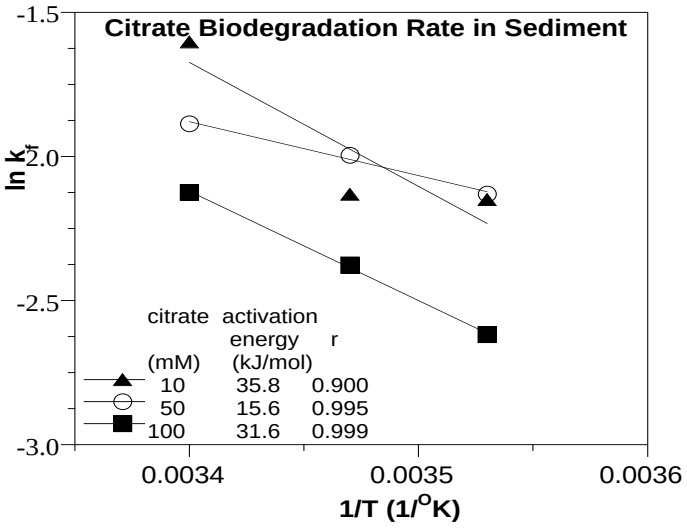

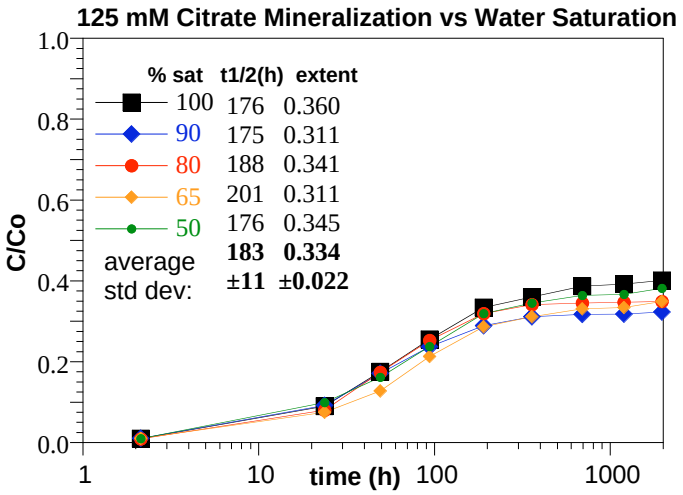
125 mM Citrate Mineralization vs Water Saturation
% sat t1/2(h) extent
100 176 0.360
90 175 0.311
80 188 0.341
65 201 0.311
50 176 0.345
average 183 0.334
std dev: ±11 ±0.022
C/Co
time (h)

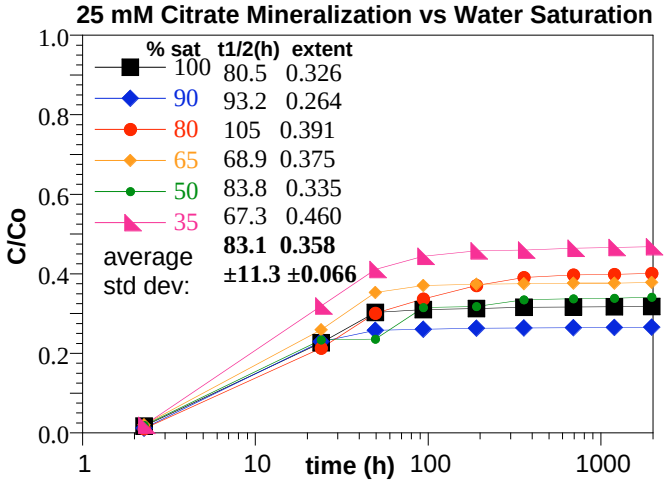
25 mM Citrate Mineralization vs Water Saturation
% sat t1/2(h) extent
100 80.5 0.326
90 93.2 0.264
80 105 0.391
65 68.9 0.375
50 83.8 0.335
35 67.3 0.460
average 83.1 0.358
std dev: ±11.3 ±0.066
C/Co
time (h)

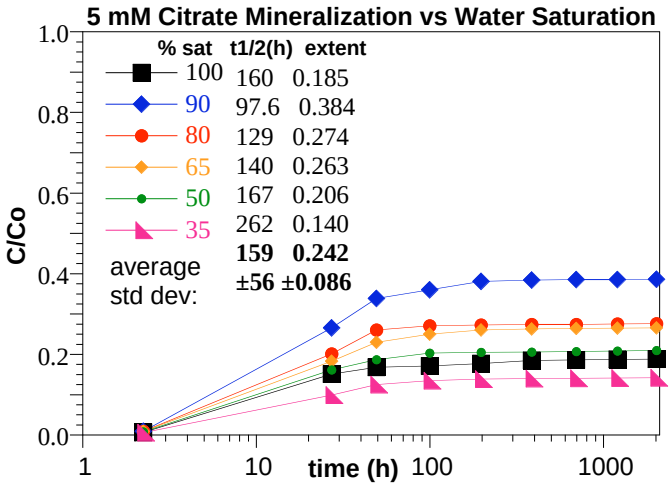
5 mM Citrate Mineralization vs Water Saturation
% sat t1/2(h) extent
100 160 0.185
90 97.6 0.384
80 129 0.274
65 140 0.263
50 167 0.206
35 262 0.140
average 159 0.242
std dev: ±56 ±0.086
C/Co
time (h)

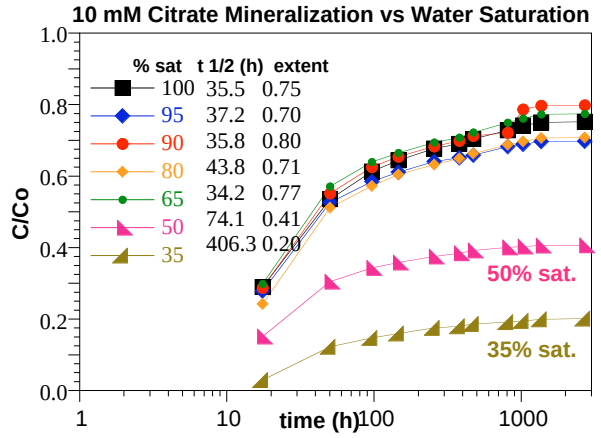
10 mM Citrate Mineralization vs Water Saturation
% sat t 1/2 (h) extent
100 35.5 0.75
95 37.2 0.70
90 35.8 0.80
80 43.8 0.71
65 34.2 0.77
50 74.1 0.41
35 406.3 0.20
50% sat.
35% sat.
C/Co
time (h)

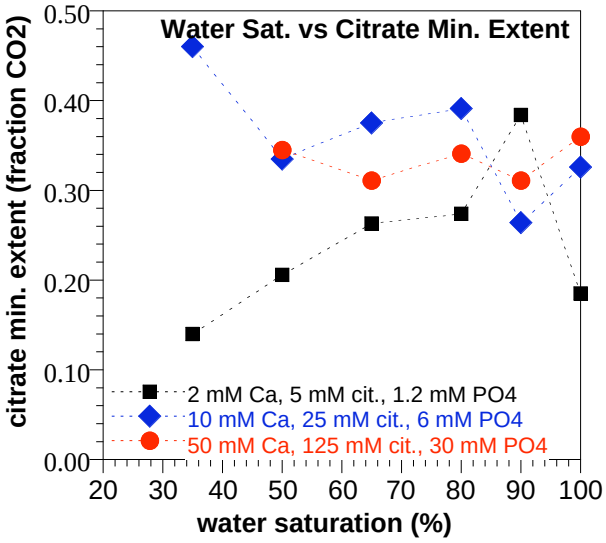
Water Sat. vs Citrate Min. Extent
citrate min. extent (fraction CO2)
2 mM Ca, 5 mM cit., 1.2 mM PO4
10 mM Ca, 25 mM cit., 6 mM PO4
50 mM Ca, 125 mM cit., 30 mM PO4
water saturation (%)

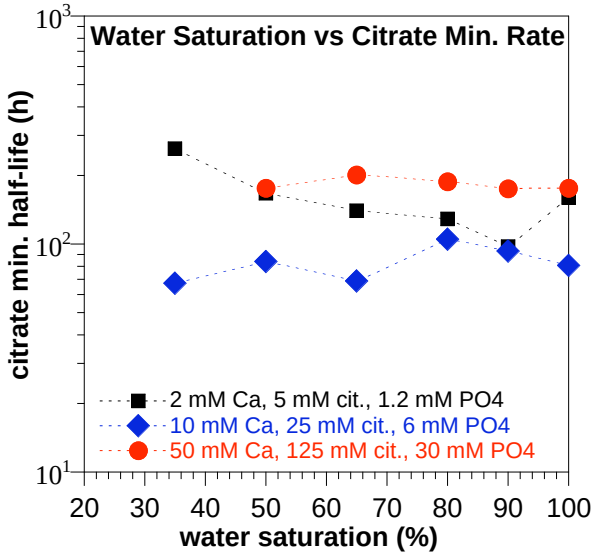
Water Saturation vs Citrate Min. Rate
citrate min. half-life (h)
2 mM Ca, 5 mM cit., 1.2 mM PO4
10 mM Ca, 25 mM cit., 6 mM PO4
50 mM Ca, 125 mM cit., 30 mM PO4
water saturation (%)

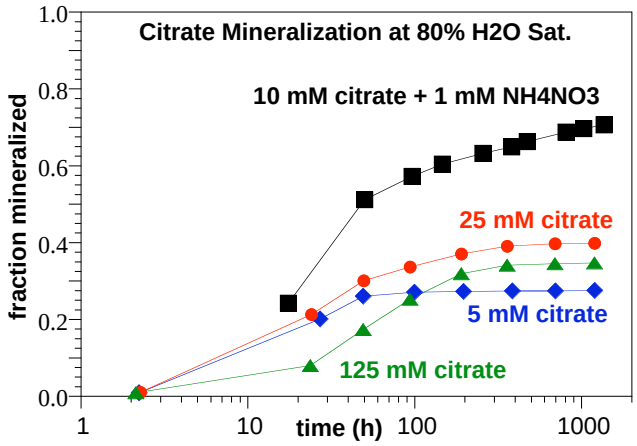
Citrate Mineralization at 80% H2O Sat.
10 mM citrate + 1 mM NH4NO3
25 mM citrate
5 mM citrate
125 mM citrate
fraction mineralized
time (h)
1.0
0.8
0.6
0.4
0.2
0.0
1
10
100
1000

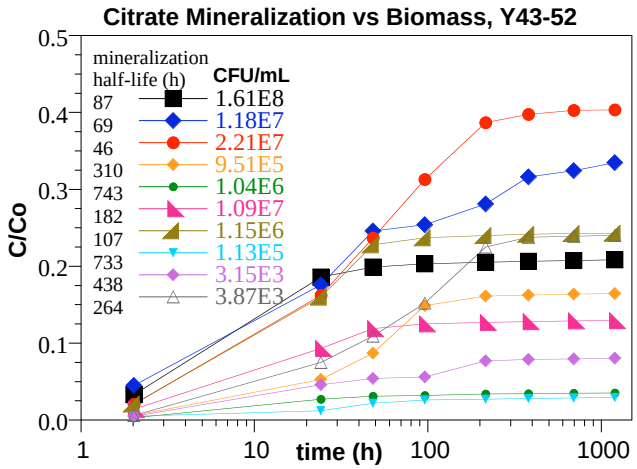
Citrate Mineralization vs Biomass, Y43-52
mineralization half-life (h)
CFU/mL
87 1.61E8
69 1.18E7
46 2.21E7
310 9.51E5
743 1.04E6
182 1.09E7
107 1.15E6
733 1.13E5
438 3.15E3
264 3.87E3
C/Co
time (h)
0.5
0.4
0.3
0.2
0.1
0.0
1
10
100
1000

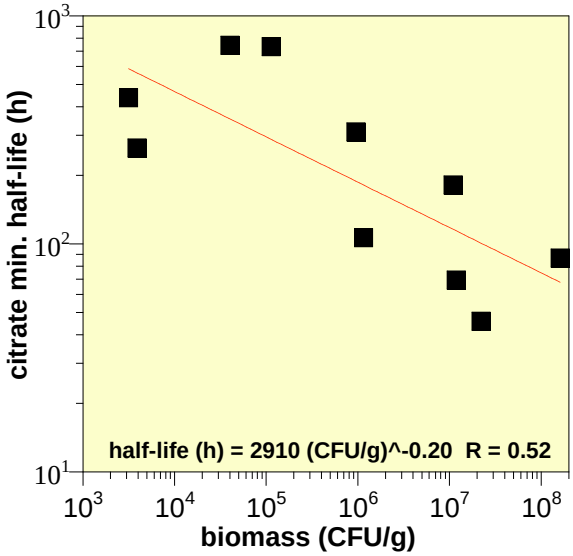
half-life (h) = 2910 (CFU/g)^-0.20 R = 0.52
citrate min. half-life (h)
biomass (CFU/g)
10^3
10^2
10^1
10^3
10^4
10^5
10^6
10^7
10^8

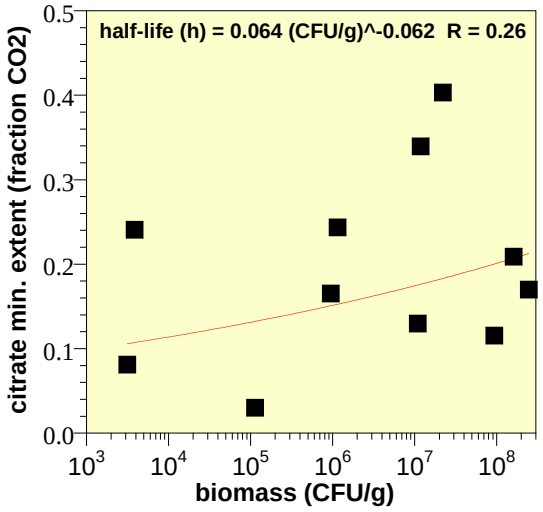
half-life (h) = 0.064 (CFU/g)^-0.062 R = 0.26
citrate min. extent (fraction CO2)
biomass (CFU/g)

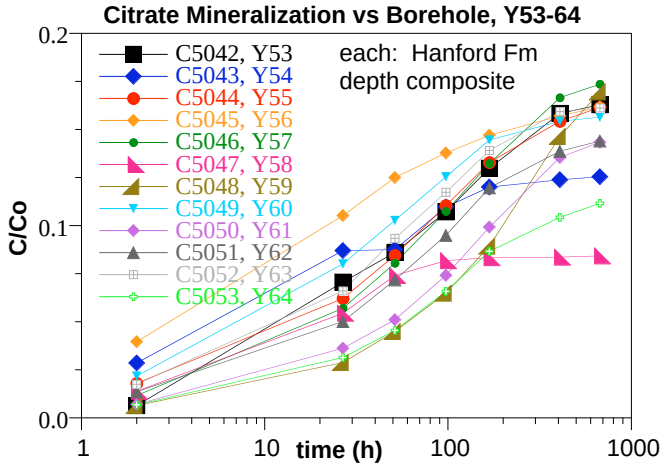
Citrate Mineralization vs Borehole, Y53-64
each: Hanford Fm
depth composite
C5042, Y53
C5043, Y54
C5044, Y55
C5045, Y56
C5046, Y57
C5047, Y58
C5048, Y59
C5049, Y60
C5050, Y61
C5051, Y62
C5052, Y63
C5053, Y64
C/Co
time (h)

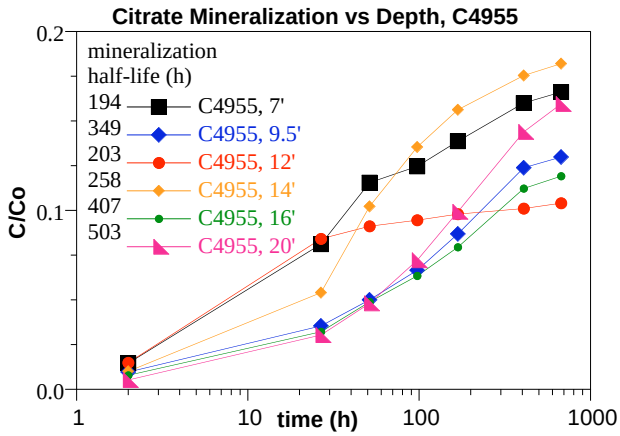
Citrate Mineralization vs Depth, C4955
mineralization
half-life (h)
194 C4955, 7'
349 C4955, 9.5'
203 C4955, 12'
258 C4955, 14'
407 C4955, 16'
503 C4955, 20'
C/Co
time (h)

A.2 Task 1 – Apatite/PO_4 Measurement in Sediment

Method 1. Acid extraction and aqueous measurement of PO_4.

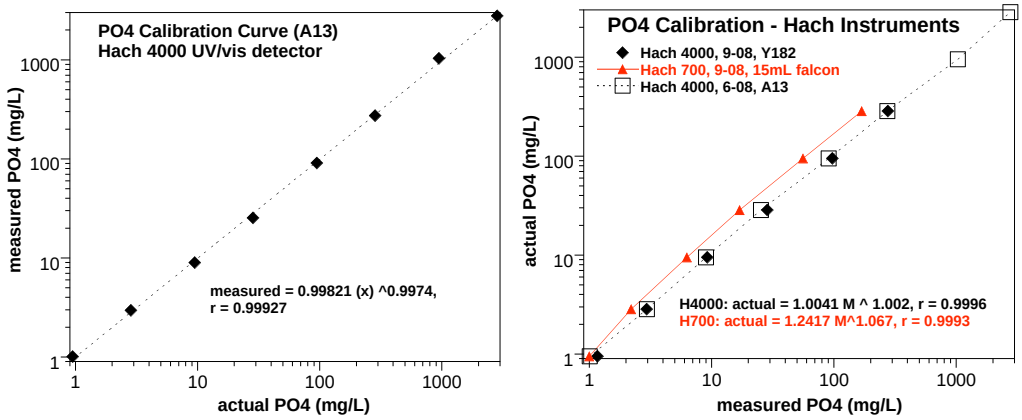

Y106. Test method – addition of apatite and PO_4 measurement.

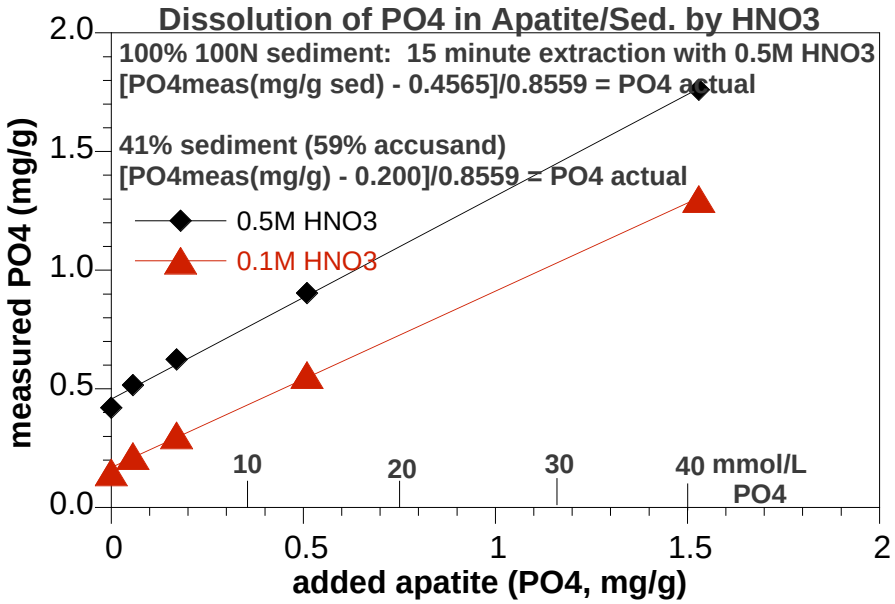

Y150. Apatite extraction of laboratory-treated sediments.

0.5M HNO_3 extraction times 15 minutes

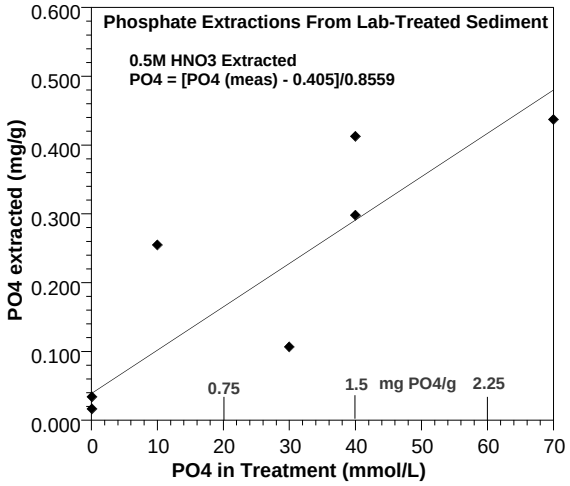

Water and 1M KNO_3 extraction times 1 hour

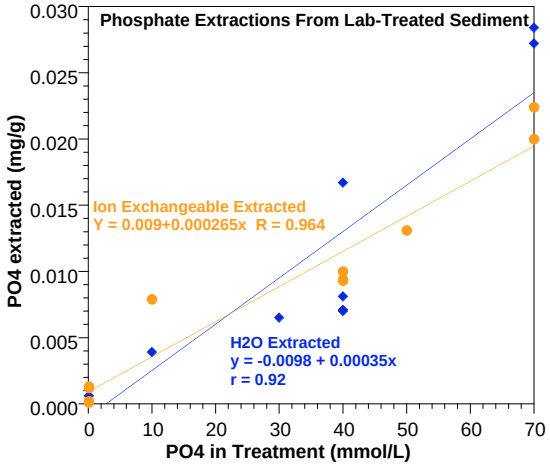

0.5M HNO_3 and 4M HNO_3 extraction times 15 minutes

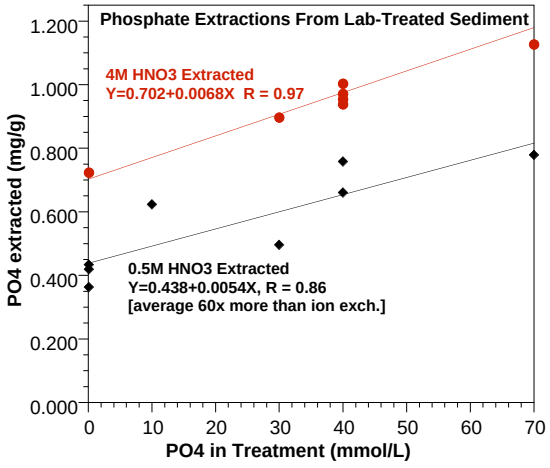

Method 2. Fluorescence of F-substituted apatite in sediment.

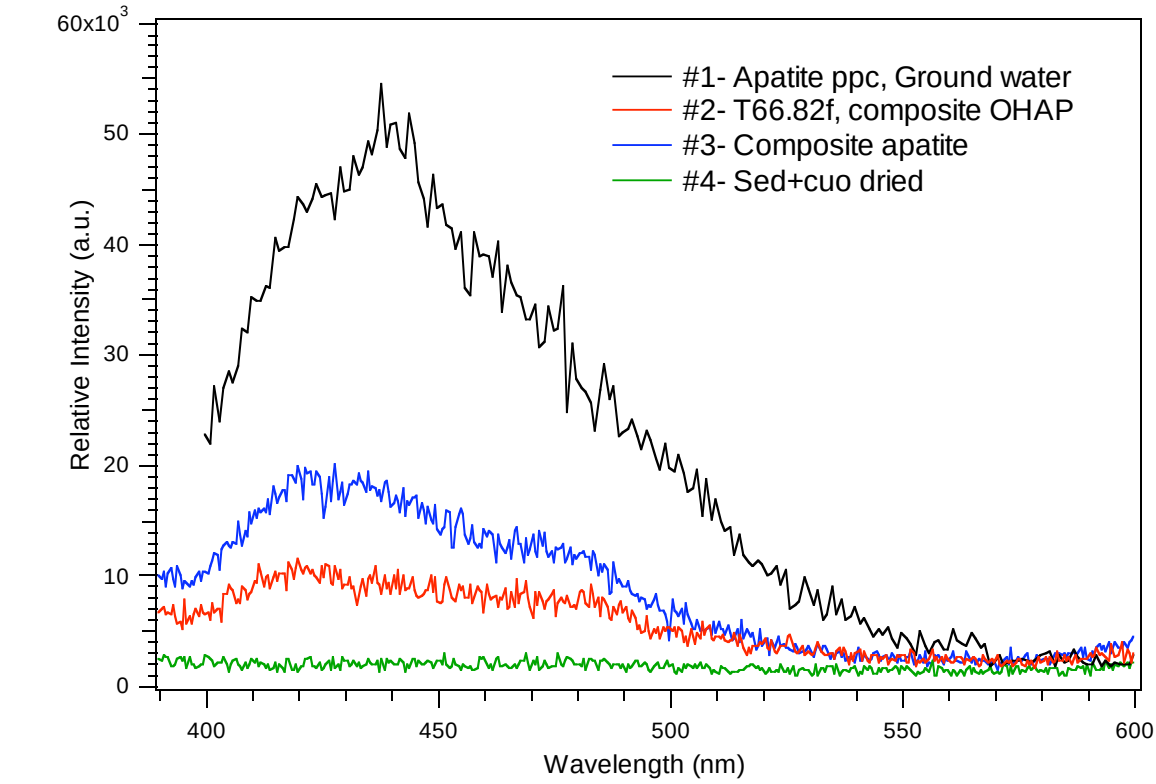

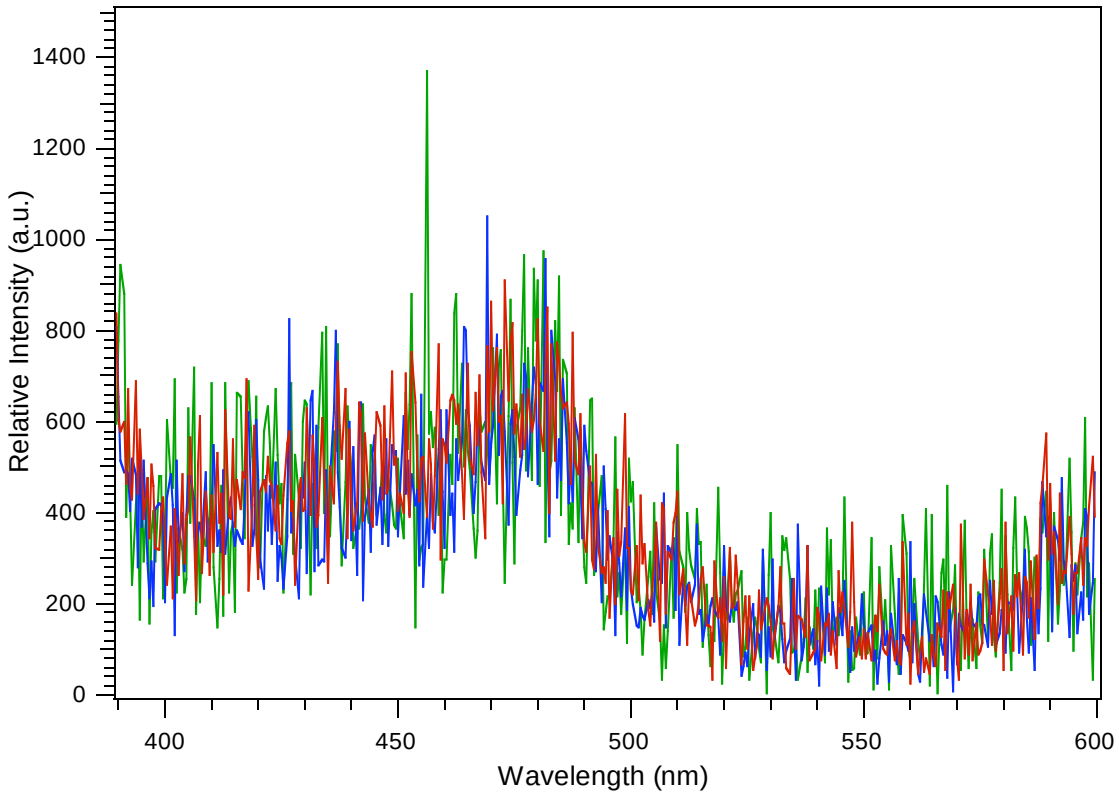

Method 3. FTIR

Line 1 = apatite; line 2 = 10% Sr-apatite; line 3 = $Sr(OH)_2$; line 4 $Sr\text{-}PO_4$

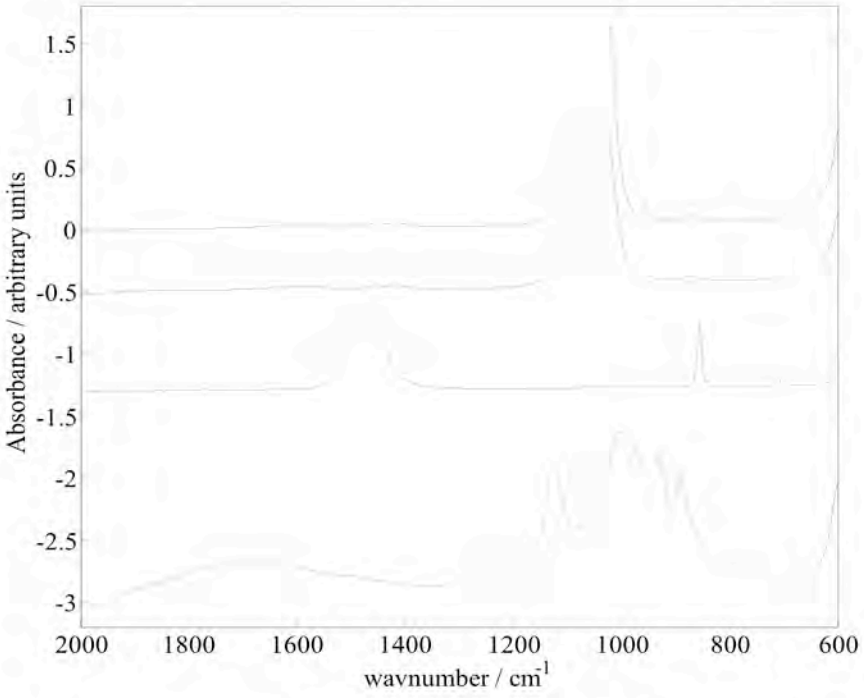

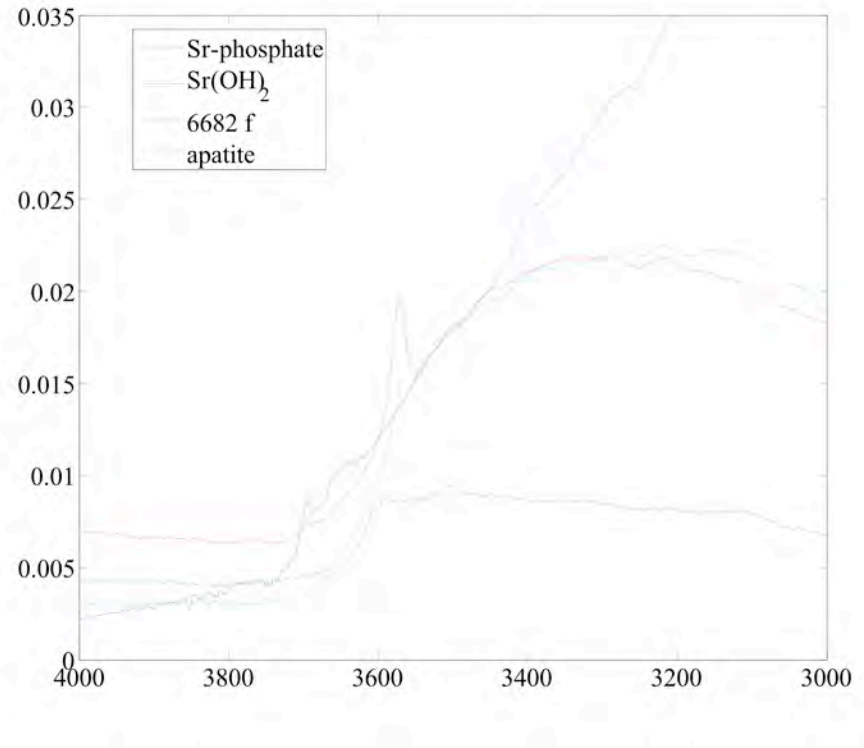

PO_4 Sorption to Sediment.

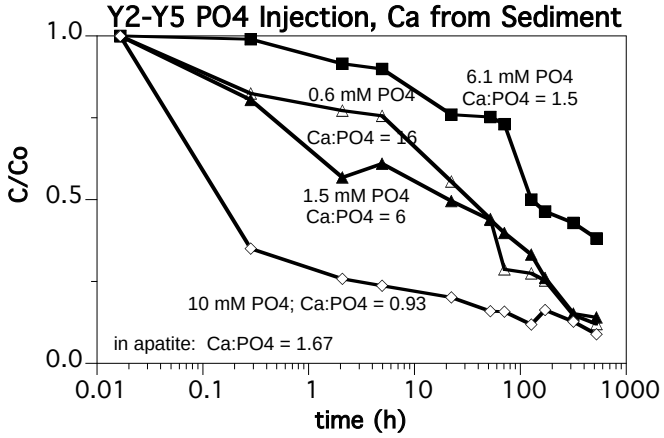

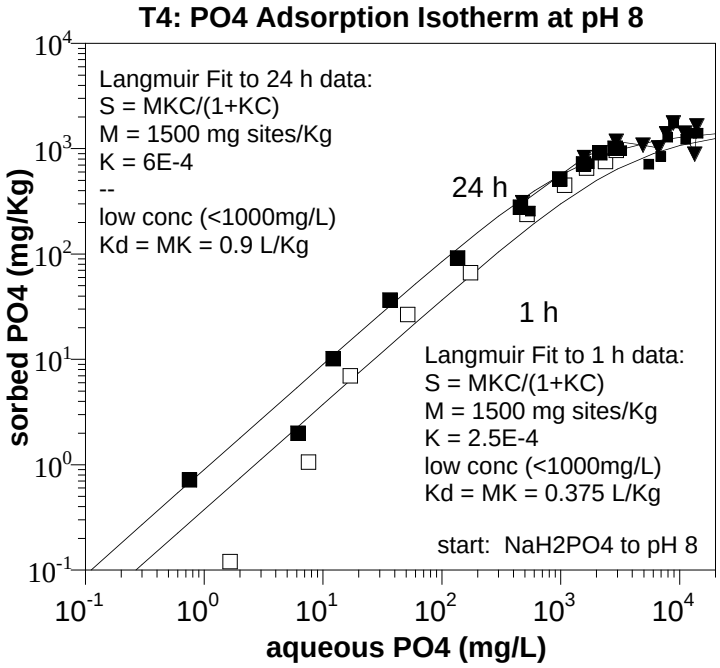

A.3 Task 2 – PO_4 Infiltration into 1-D Sediment Columns

Y89. Ca-citrate-PO_4 (10 mM) infiltration into 1-D column, 0.002 mL/minute, 50 cm length.

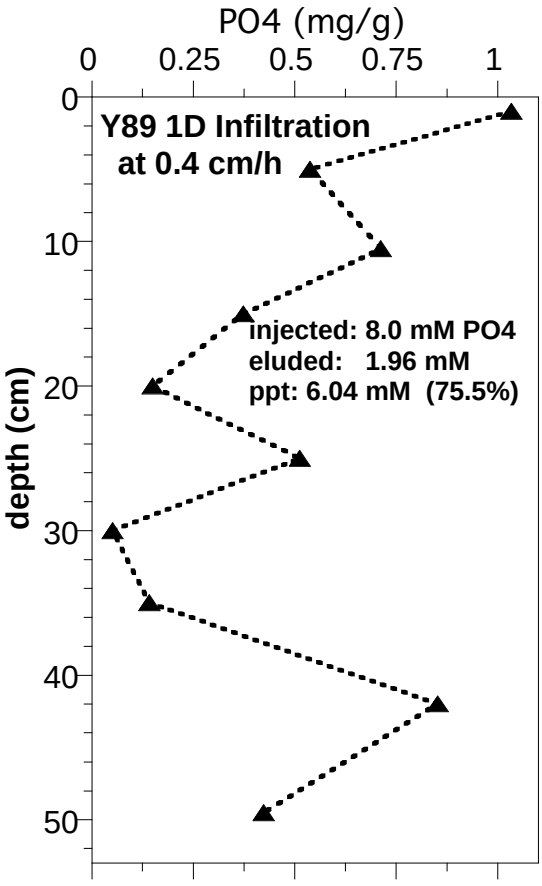

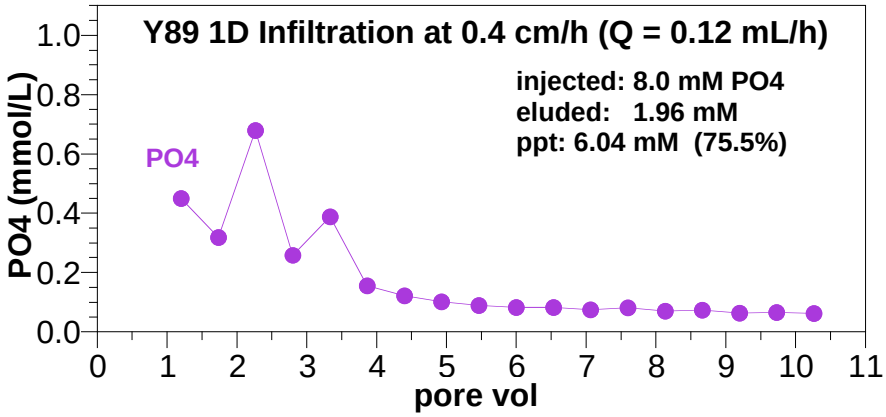

Y90. Ca-citrate-PO_4 (10 mM) infiltration into 1-D column, 0.005 mL/minute, 50 cm length.

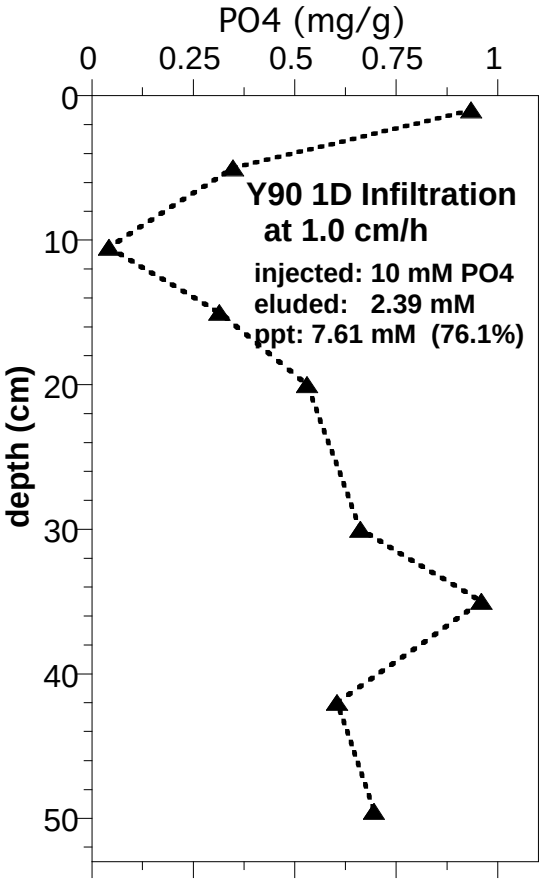

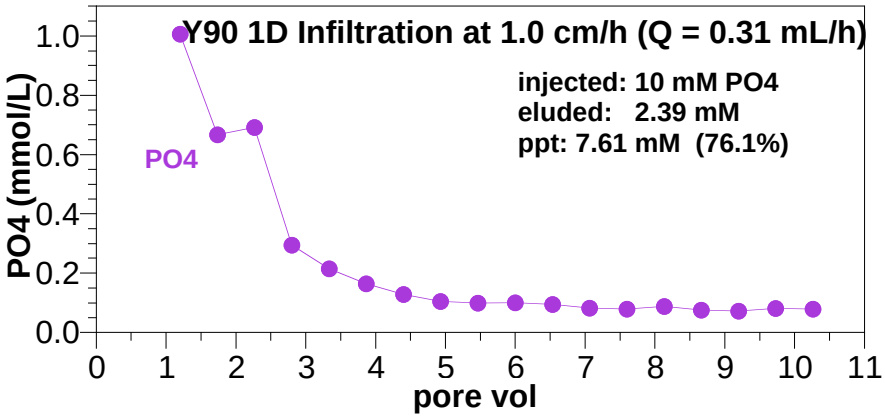

Y91. Ca-citrate-PO_4 (20 mM) infiltration into 1-D column, 0.005 mL/minute, 50 cm length.

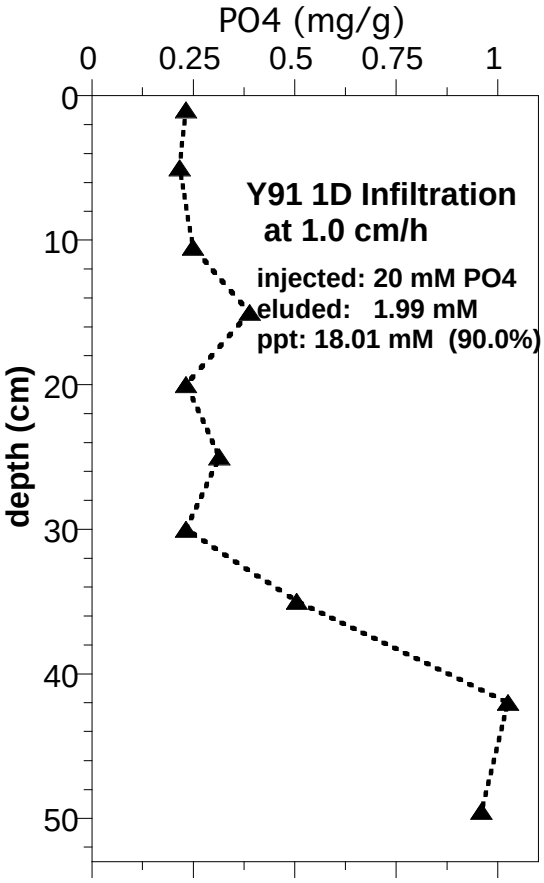

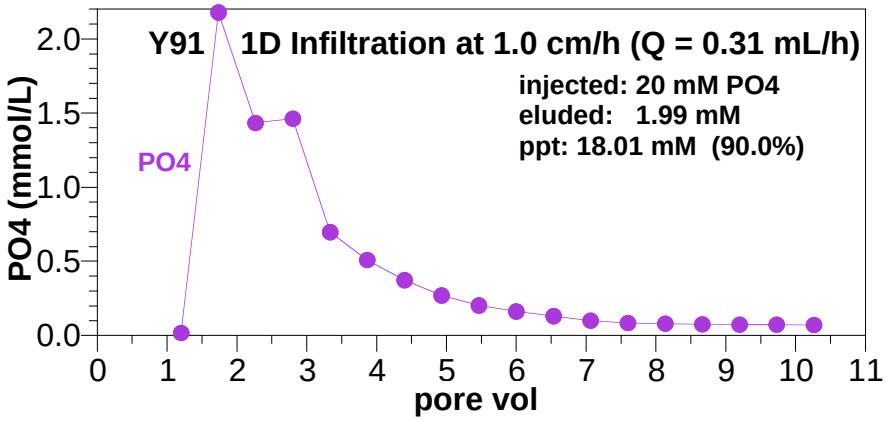

Y92. Ca-citrate-PO_4 (10 mM) infiltration into 1-D column, 0.02 mL/minute, 50 cm length.

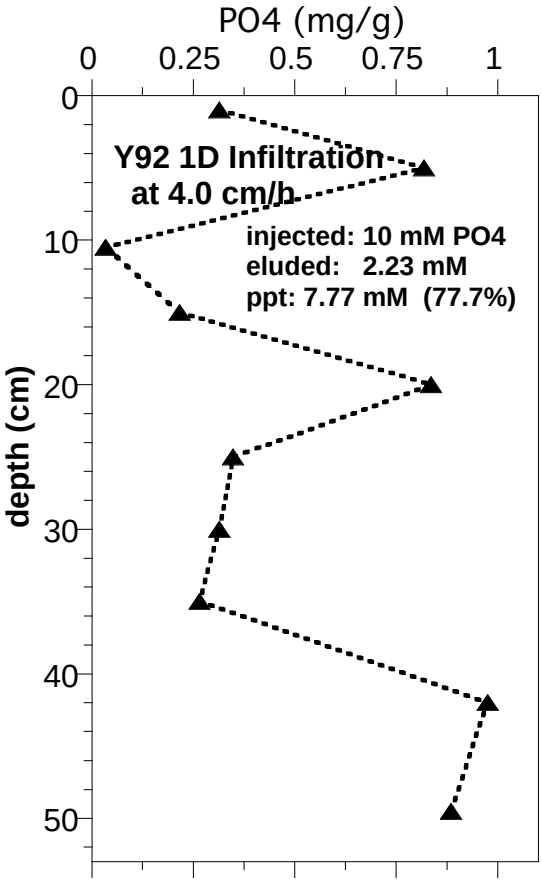

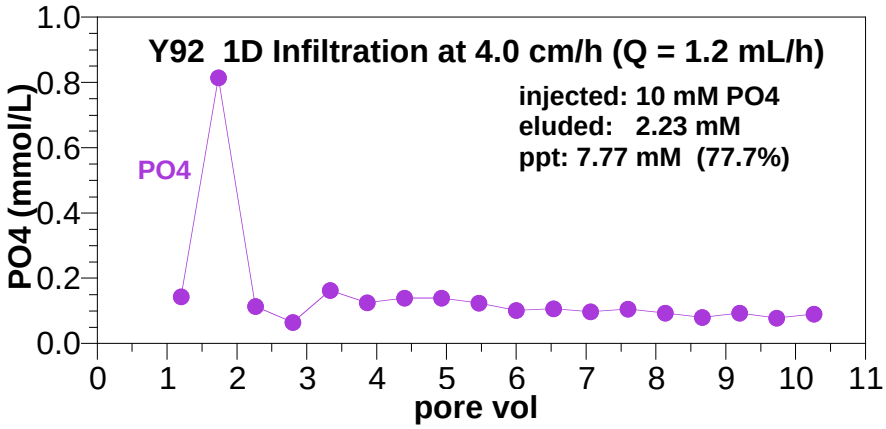

Y89-92.

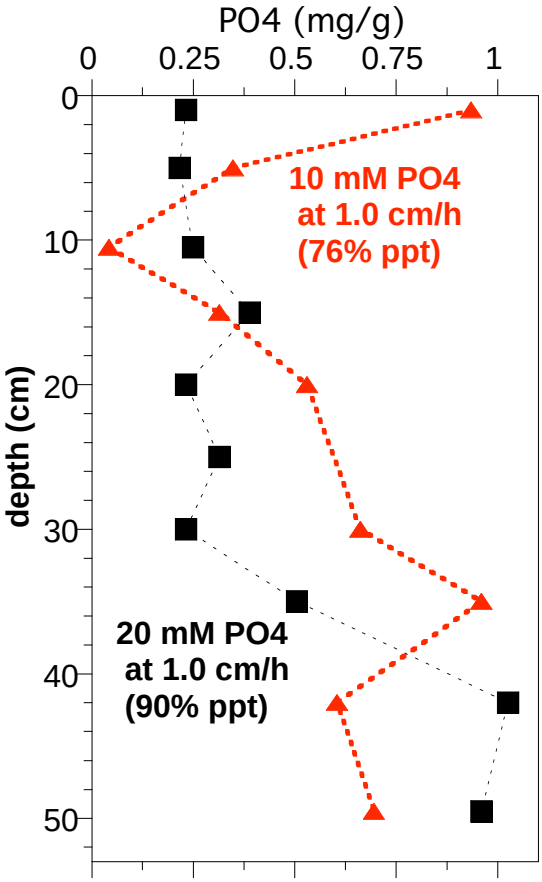
PO4 (mg/g)
0
0.25
0.5
0.75
1
depth (cm)
0
10
20
30
40
50
10 mM PO4
at 1.0 cm/h
(76% ppt)
20 mM PO4
at 1.0 cm/h
(90% ppt)

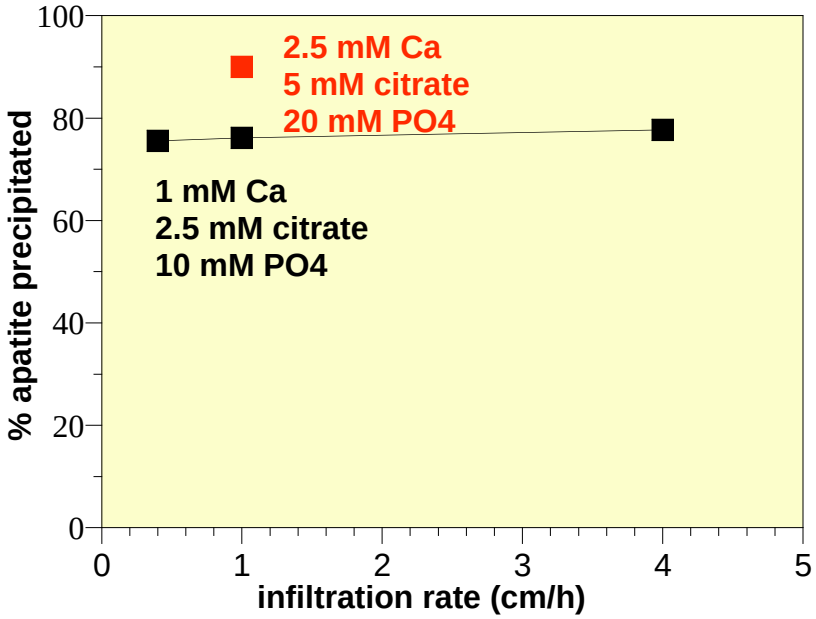
% apatite precipitated
100
80
60
40
20
0
0
1
2
3
4
5
infiltration rate (cm/h)
2.5 mM Ca
5 mM citrate
20 mM PO4
1 mM Ca
2.5 mM citrate
10 mM PO4

Y89-92.


HITACHI
791
792
RTL
236
Y90
PLASTIC FITTINGS
PLASTIC FITTINGS
BACKUP
PLASTIC TUBE CLIPS
EXTRA FITTINGS

Y164. Ca-citrate-PO_4 (40 mM) infiltration into 1-D column, 12-ft high, 6.5 mL/minute (37 minutes), then river water infiltration at 4.2 mL/minute (31 minutes).

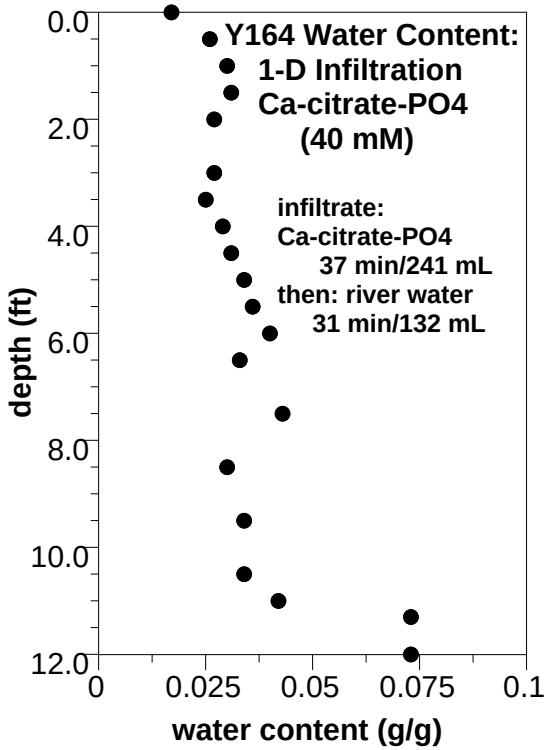

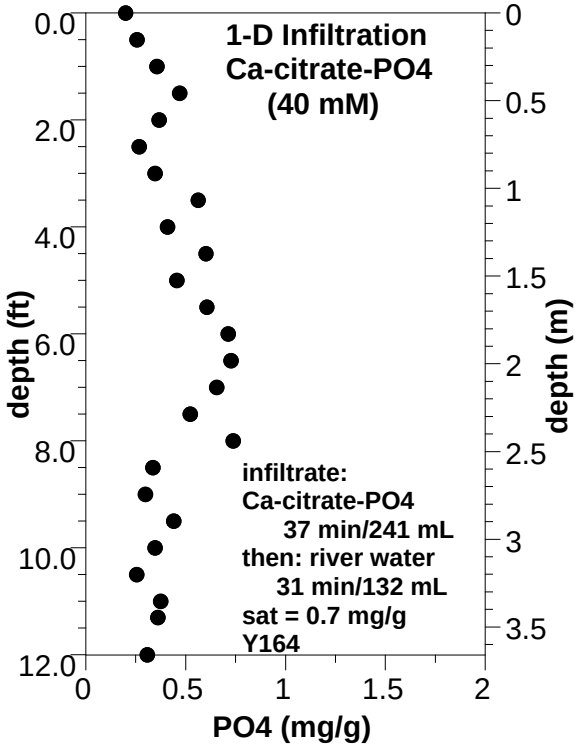

Y164A. Ca-citrate-PO_4 (40 mM) infiltration into 1-D column, 12-ft high, 6.5 mL/minute (19 minutes), then 4.2 mL/minute (47 minutes).

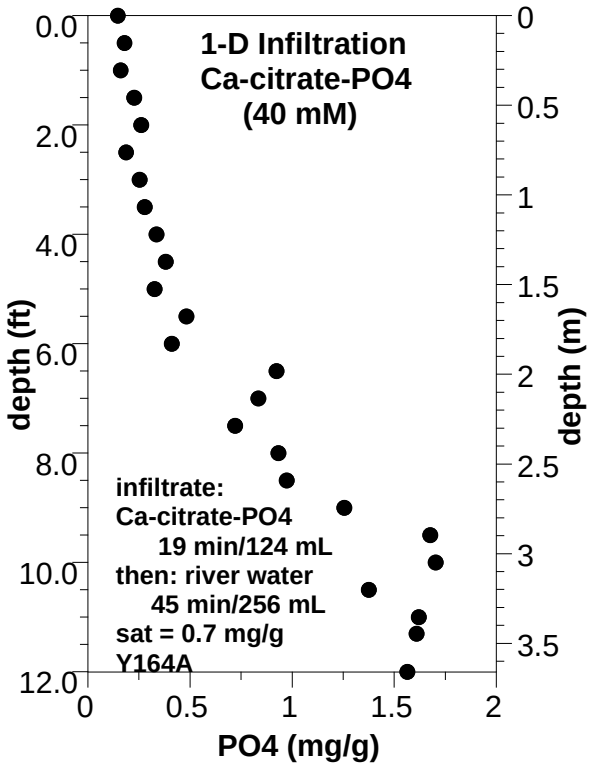

Y177. Ca-citrate-PO_4 (40 mM) infiltration into 1-D column, 30 ft long, 0.29 mL/hour x 24 hours. Live in situ and live injected microbial populations.

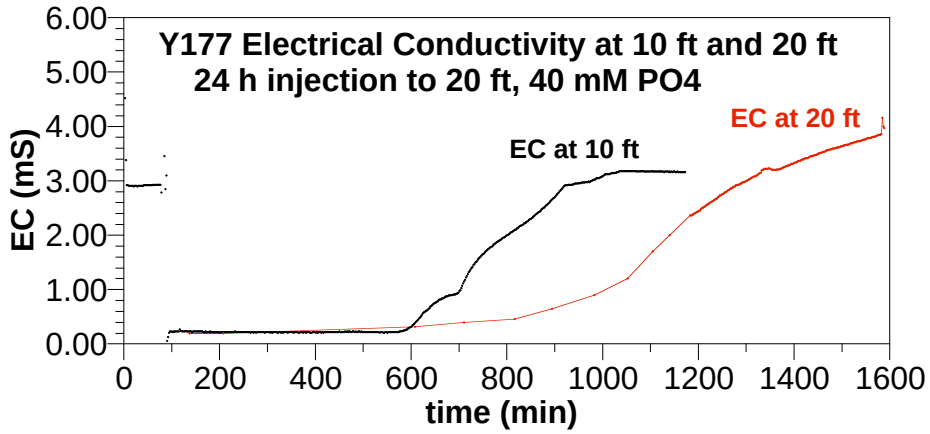

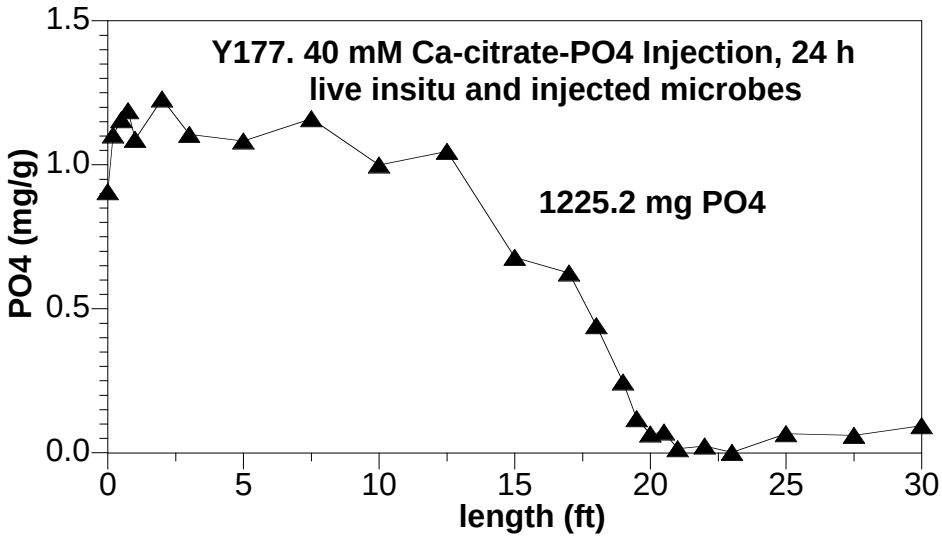

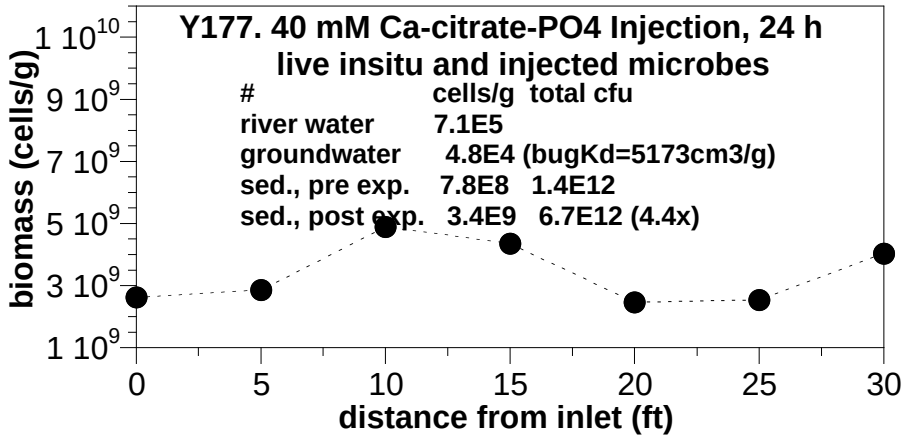

Y178. Ca-citrate-PO_4 (40 mM) infiltration into 1-D column, 30 ft long, 2.9 mL/hour x 24 hours. Live in situ and live injected microbial populations.

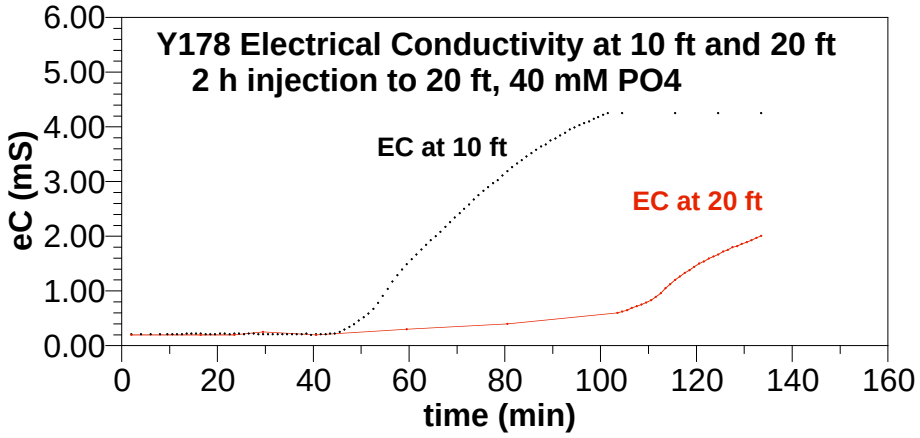

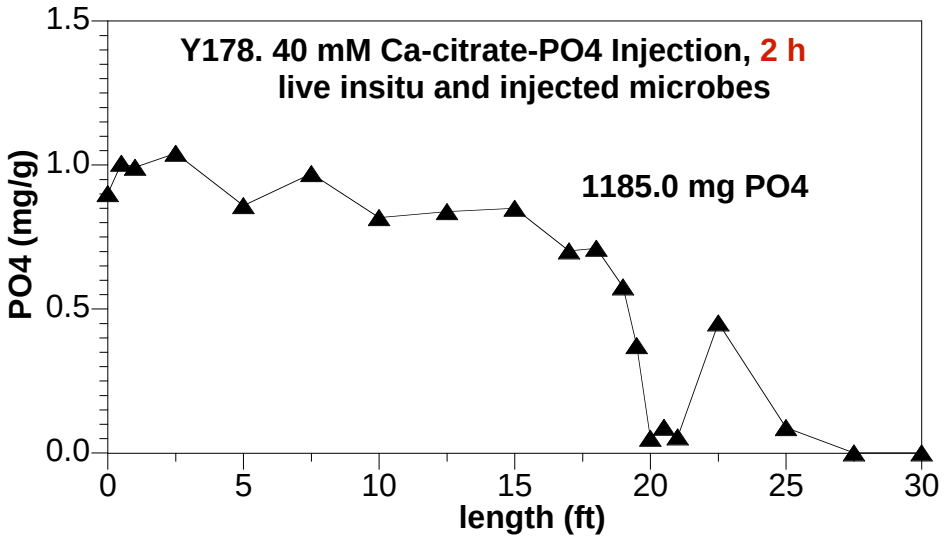

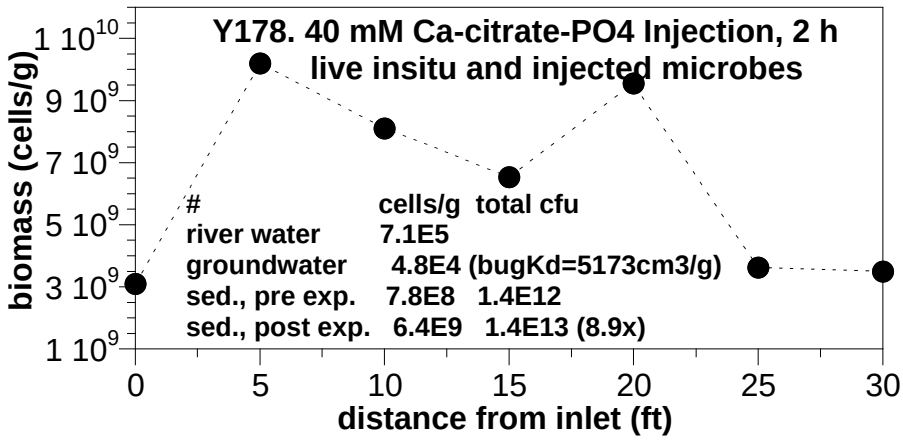

Y179. Ca-citrate-PO_4 (10 mM) infiltration into 1-D column, 30 ft long, 0.34 mL/hour x 24 hours. Live in situ and live injected microbial populations.

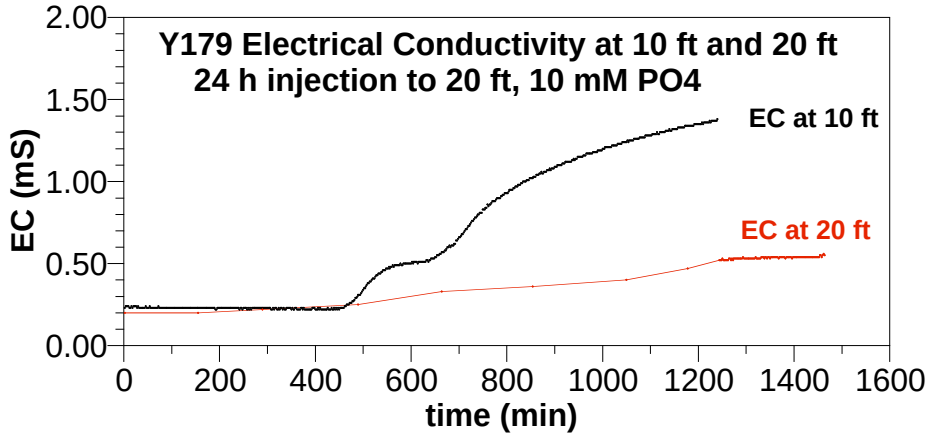

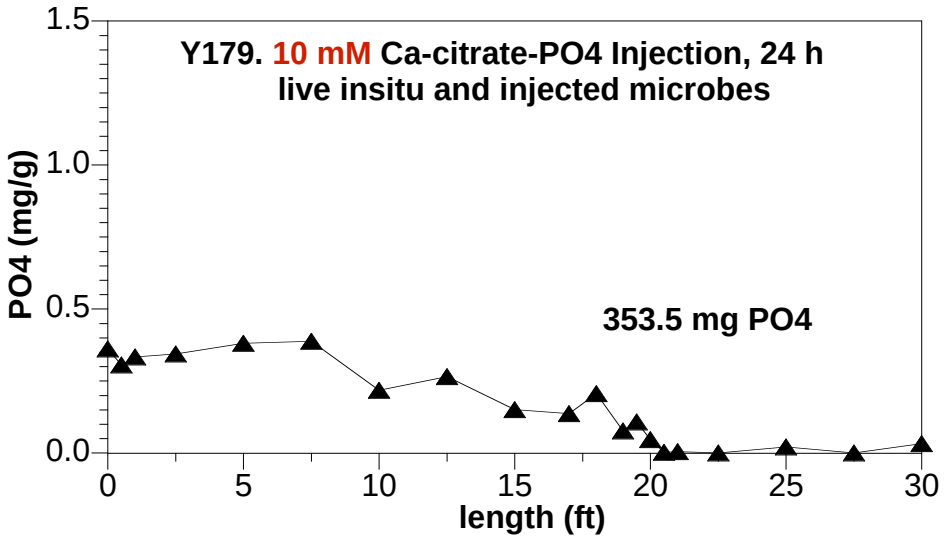

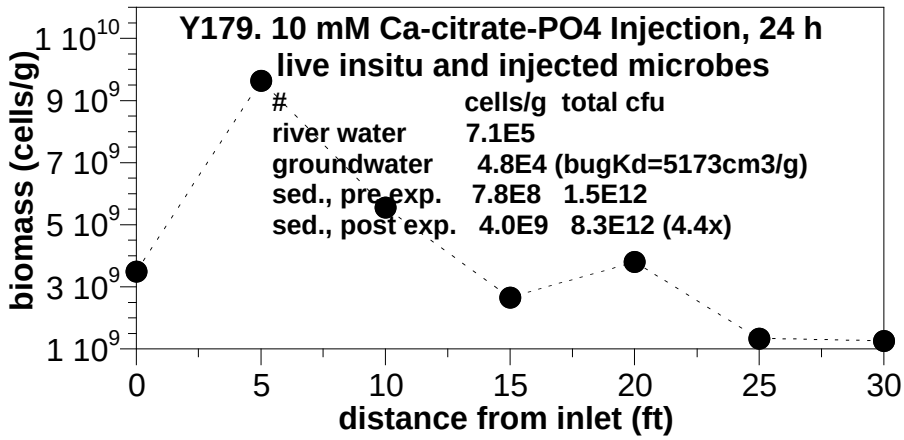

Y180. Ca-citrate-PO_4 (40 mM) infiltration into 1-D column, 30 ft long, 0.29 mL/hour x 24 hours. Live in situ microbial population, no injected microbes (filtered river water).

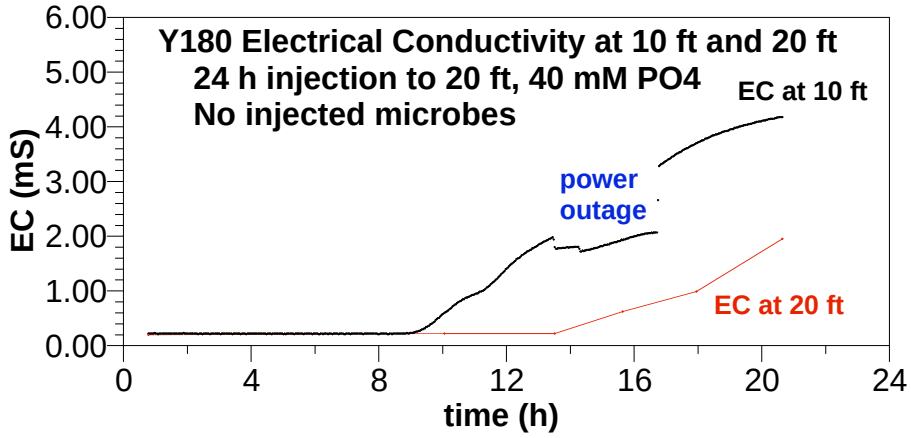

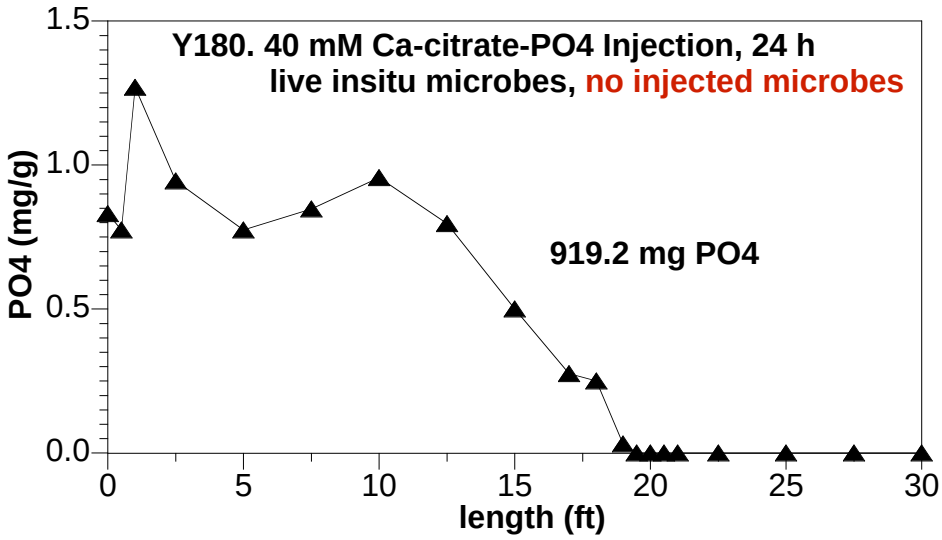

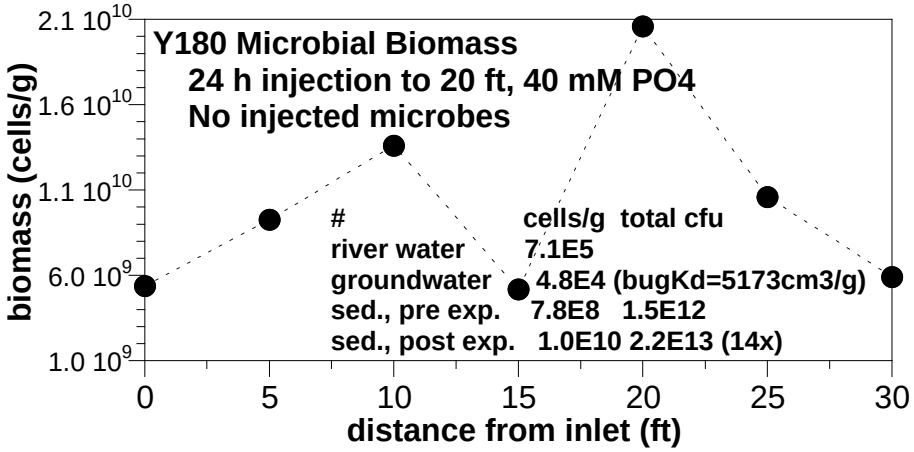

Y181. Ca-citrate-PO_4 (40 mM) infiltration into 1-D column, 30 ft long, 0.29 mL/hour x 24 hours. Live injected microbial population, killed in situ microbial population.

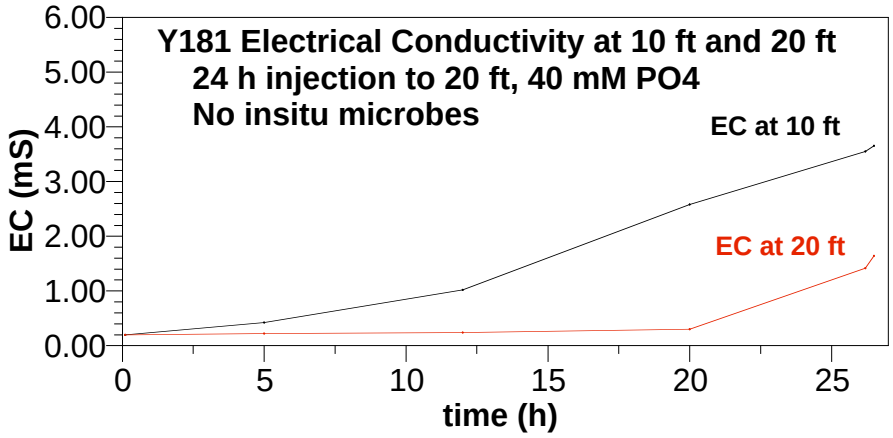

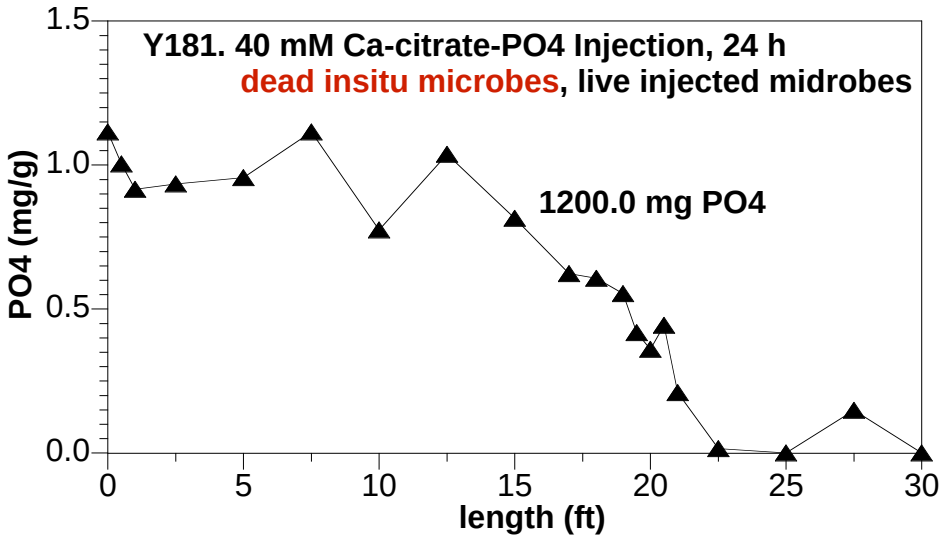

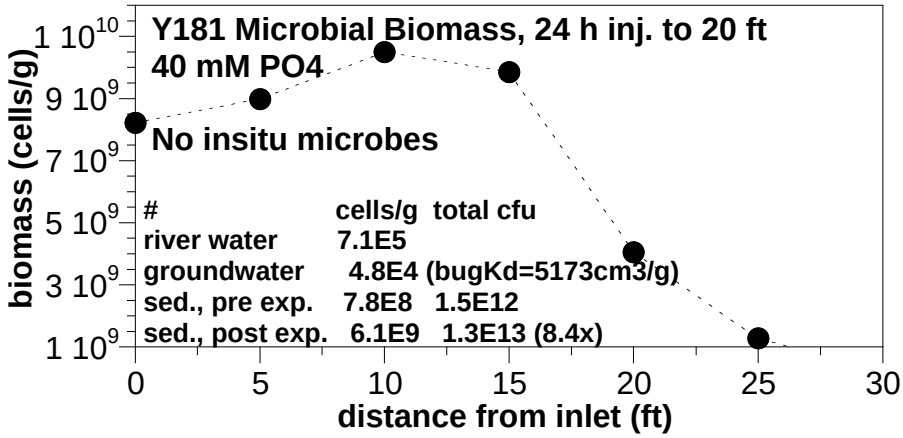

Y162. Foam (surfactant) injection at 2.5 mL/hour (N2) with 1% 30 mM Ca-citrate-PO_4 into 20-ft long 1-D column, 60 psi maximum. Sediment <4 mm 100-N composite.

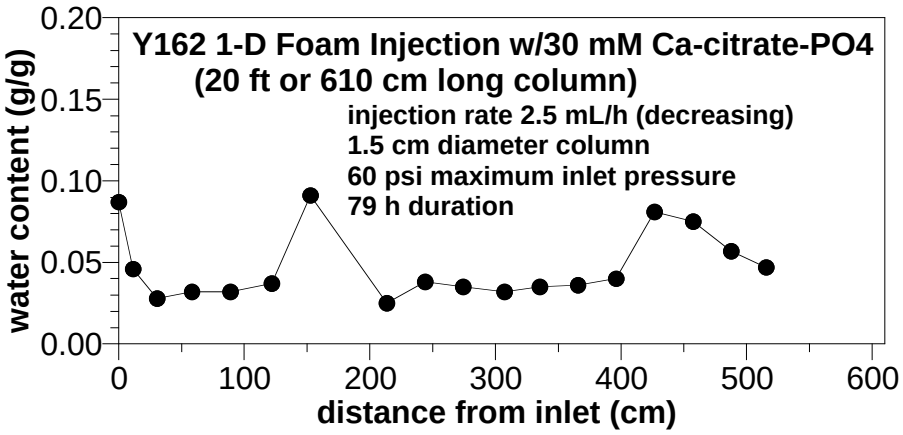

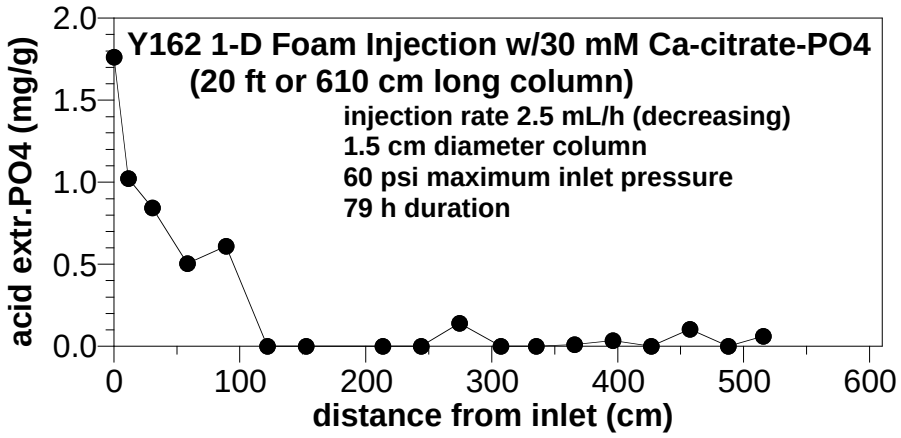

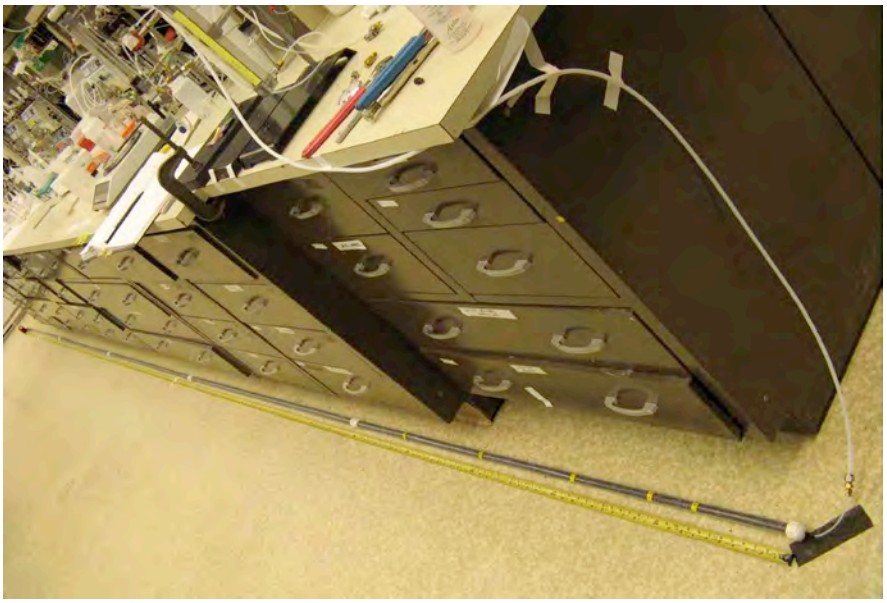

Y163. Foam (surfactant) injection at 3.9 mL/hour (N2) with 1% 40 mM Ca-citrate-PO_4 into 25-ft long 1-D column, 110 psi maximum. Sediment <10 mm and >0.5 mm 100-N.

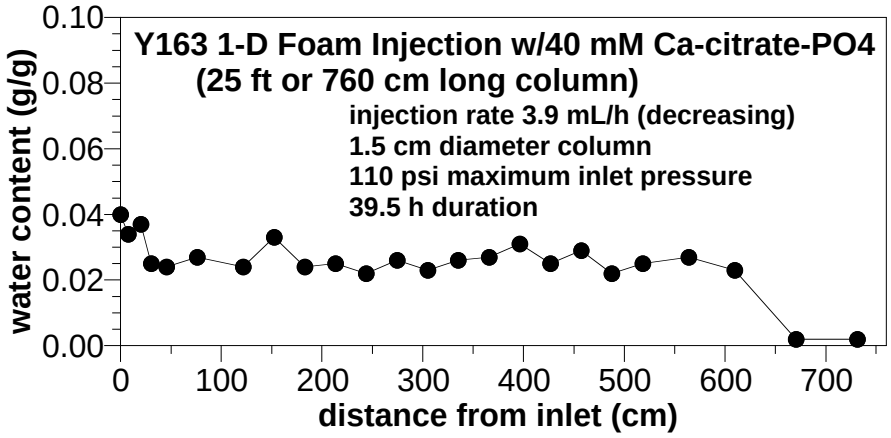

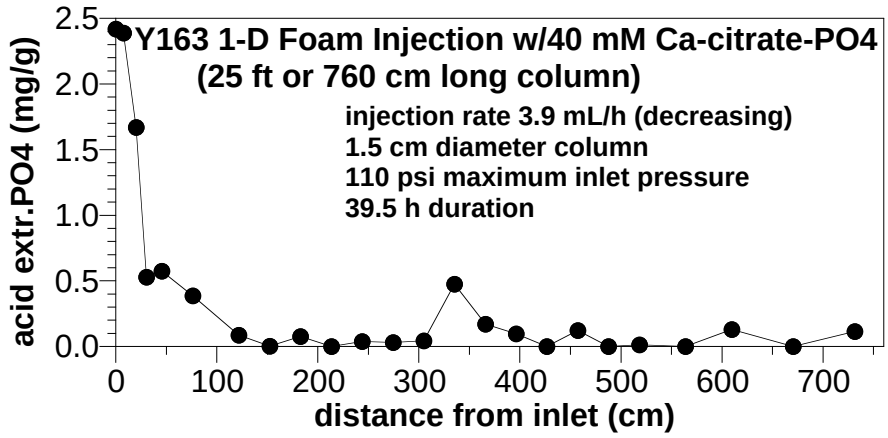

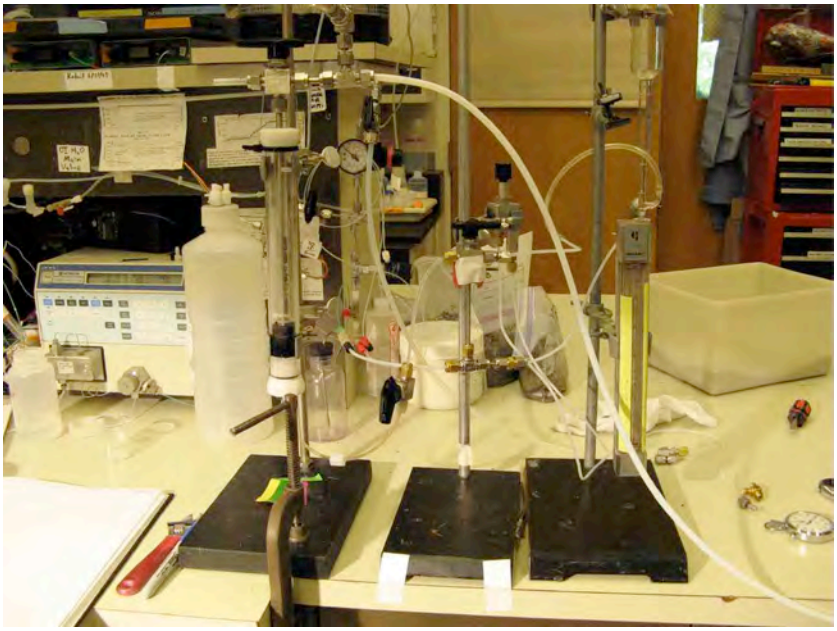

Y162,Y163 support experiments.

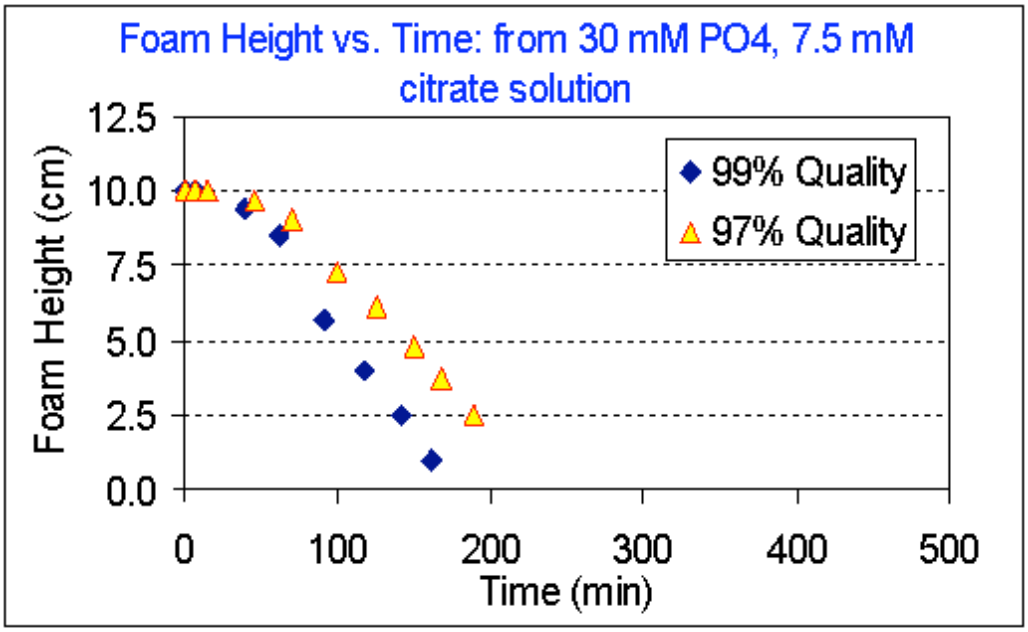

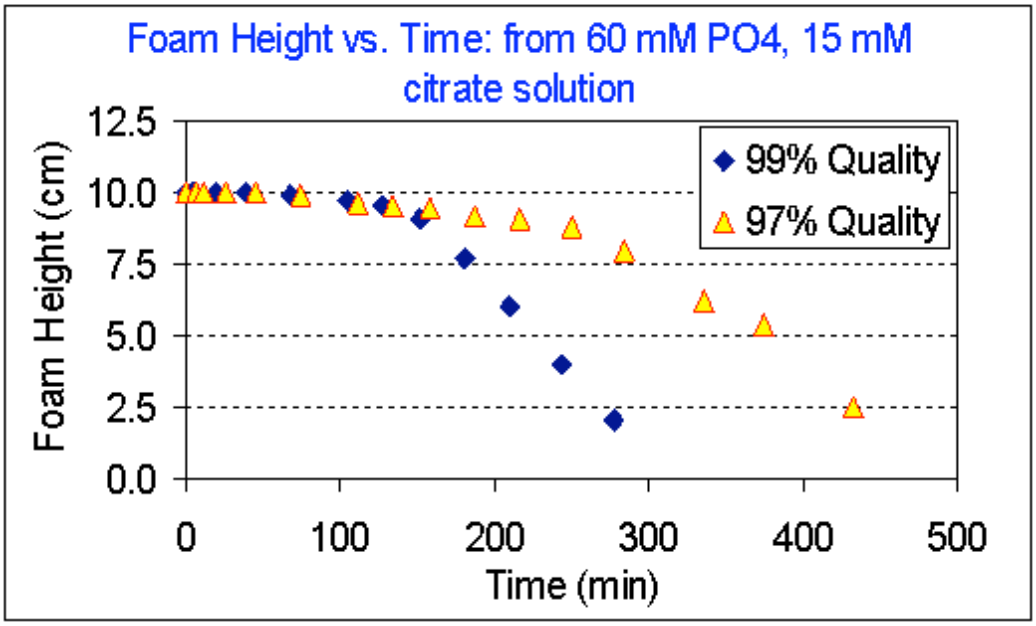

EMSL 1-D system.

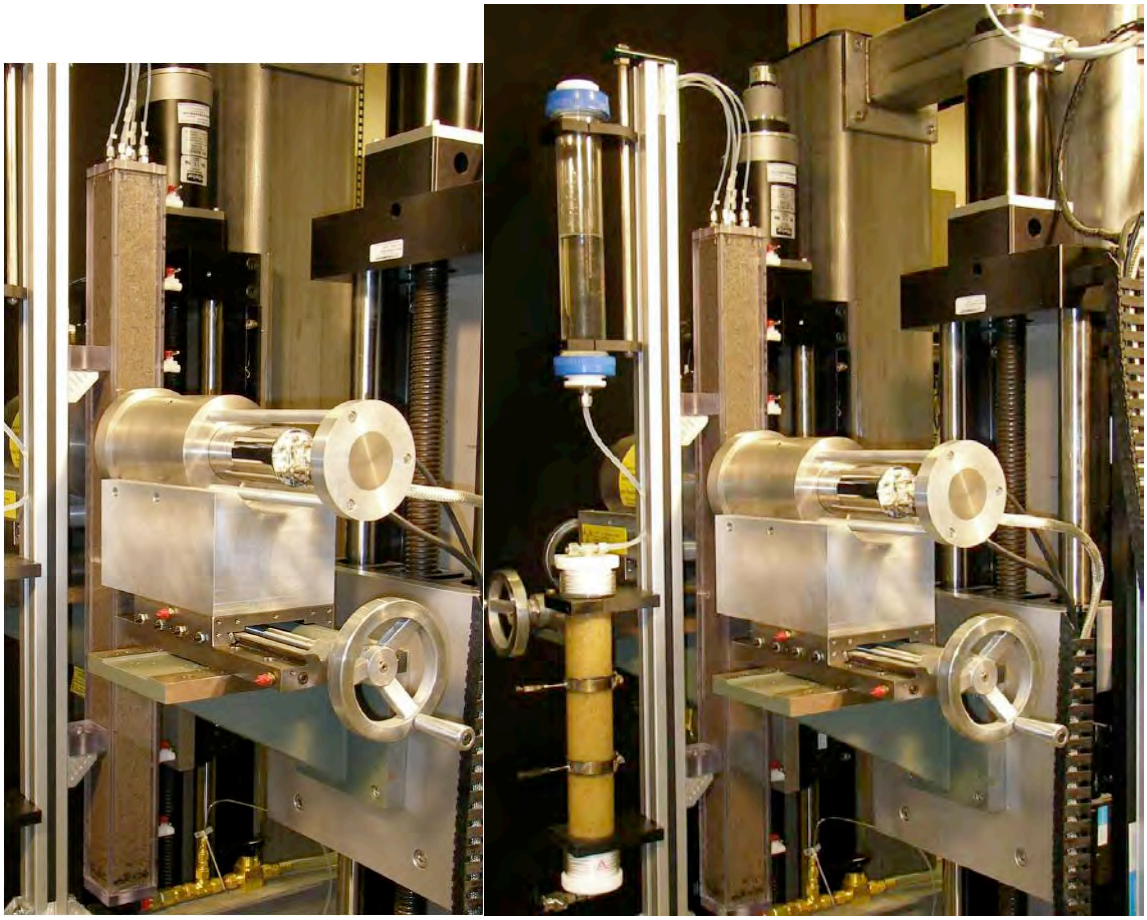

EMSL 1-D system.

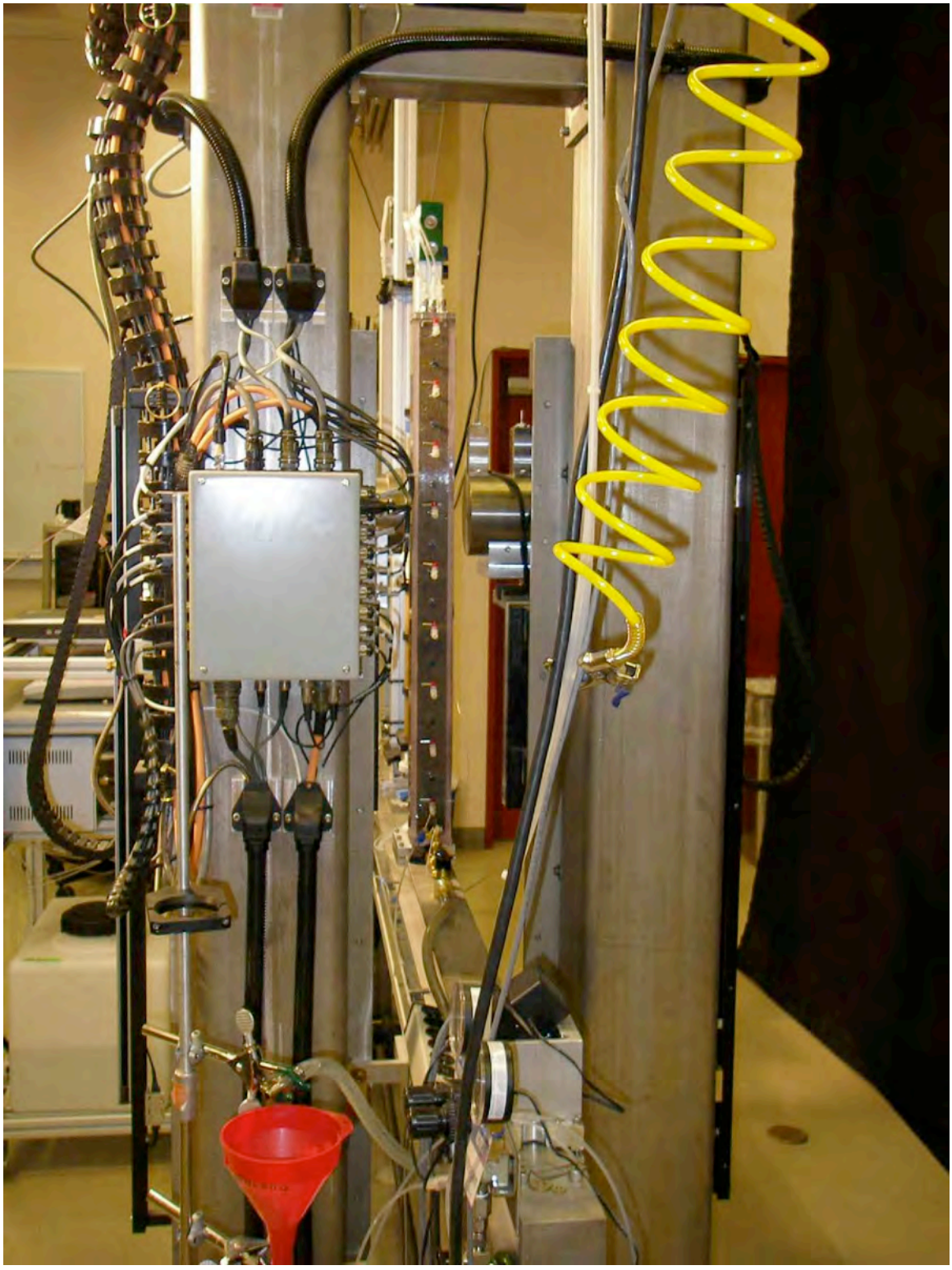

A.4 Task 3 – Sr-90 Ion Exchange on Sediment and Apatite

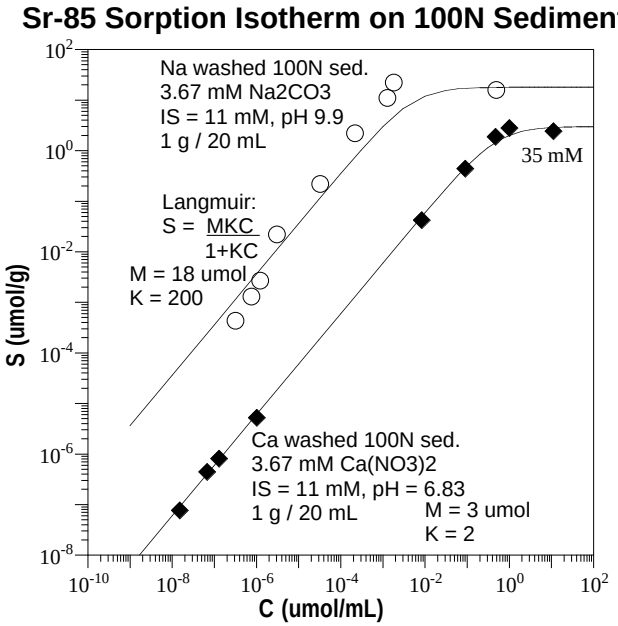

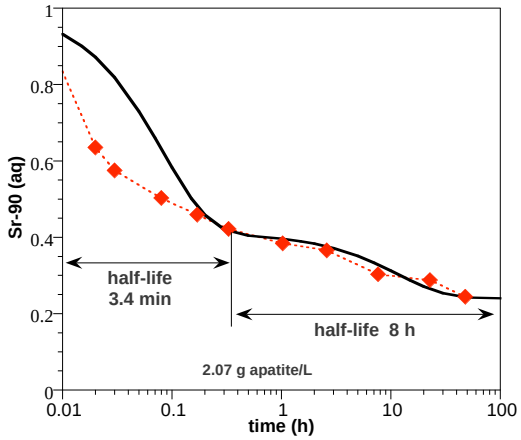
Sr-90 (aq)
time (h)
half-life
3.4 min
half-life 8 h
2.07 g apatite/L

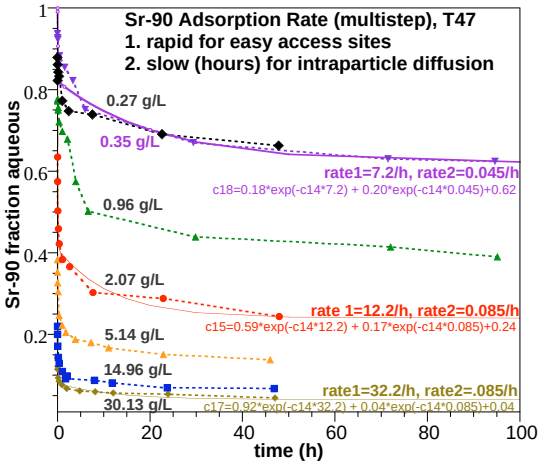
Sr-90 Adsorption Rate (multistep), T47
1. rapid for easy access sites
2. slow (hours) for intraparticle diffusion
Sr-90 fraction aqueous
time (h)
0.27 g/L
0.35 g/L
rate1=7.2/h, rate2=0.045/h
c18=0.18*exp(-c14*7.2) + 0.20*exp(-c14*0.045)+0.62
0.96 g/L
2.07 g/L
rate 1=12.2/h, rate2=0.085/h
c15=0.59*exp(-c14*12.2) + 0.17*exp(-c14*0.085)+0.24
5.14 g/L
14.96 g/L
rate1=32.2/h, rate2=.085/h
30.13 g/L
c17=0.92*exp(-c14*32.2) + 0.04*exp(-c14*0.085)+0.04

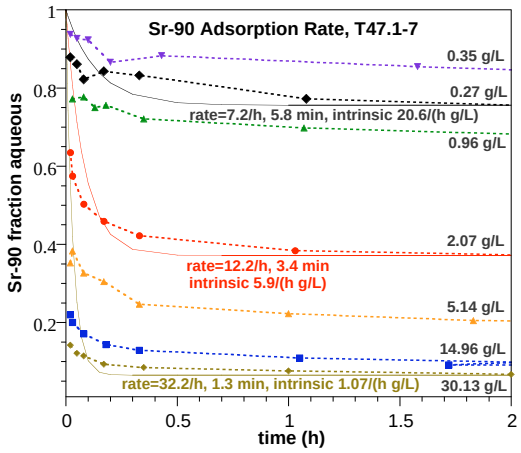
Sr-90 Adsorption Rate, T47.1-7
Sr-90 fraction aqueous
time (h)
0.35 g/L
0.27 g/L
rate=7.2/h, 5.8 min, intrinsic 20.6/(h g/L)
0.96 g/L
2.07 g/L
rate=12.2/h, 3.4 min
intrinsic 5.9/(h g/L)
5.14 g/L
14.96 g/L
rate=32.2/h, 1.3 min, intrinsic 1.07/(h g/L)
30.13 g/L

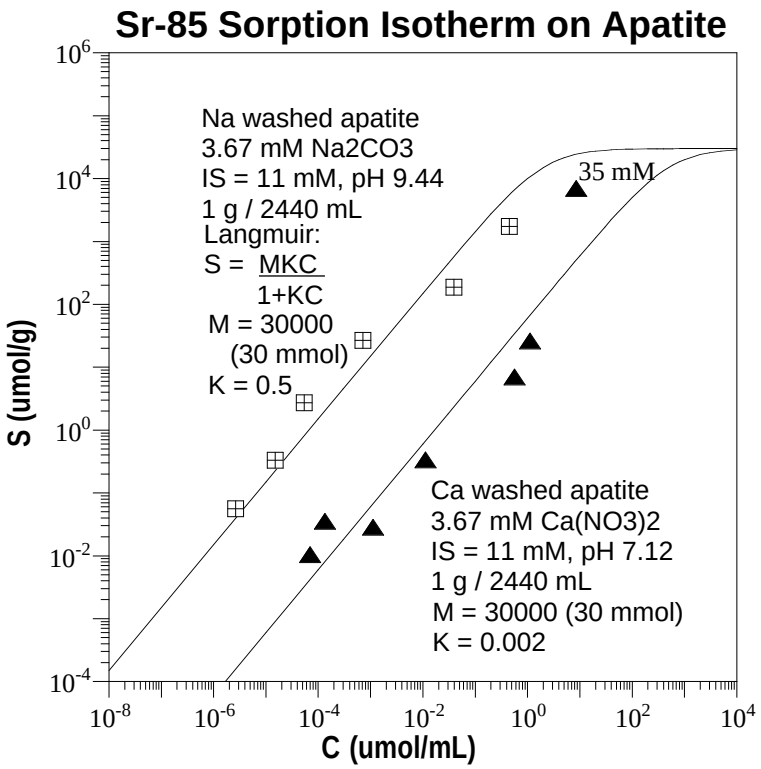
Sr-85 Sorption Isotherm on Apatite
Na washed apatite
3.67 mM Na2CO3
IS = 11 mM, pH 9.44
1 g / 2440 mL
Langmuir:
S = MKC / 1+KC
M = 30000
(30 mmol)
K = 0.5
35 mM
Ca washed apatite
3.67 mM Ca(NO3)2
IS = 11 mM, pH 7.12
1 g / 2440 mL
M = 30000 (30 mmol)
K = 0.002
S (umol/g)
C (umol/mL)

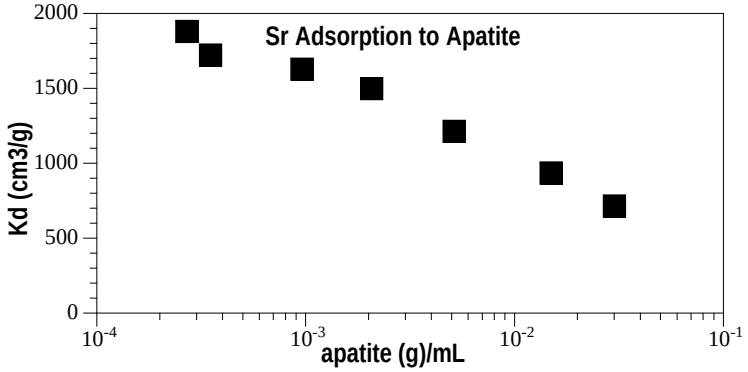
Sr Adsorption to Apatite
Kd (cm3/g)
apatite (g)/mL

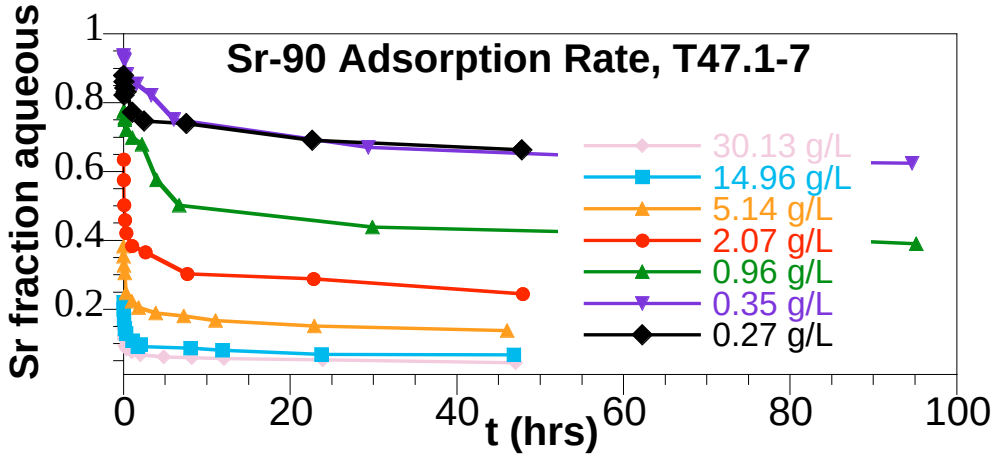
Sr-90 Adsorption Rate, T47.1-7
Sr fraction aqueous
t (hrs)
30.13 g/L
14.96 g/L
5.14 g/L
2.07 g/L
0.96 g/L
0.35 g/L
0.27 g/L

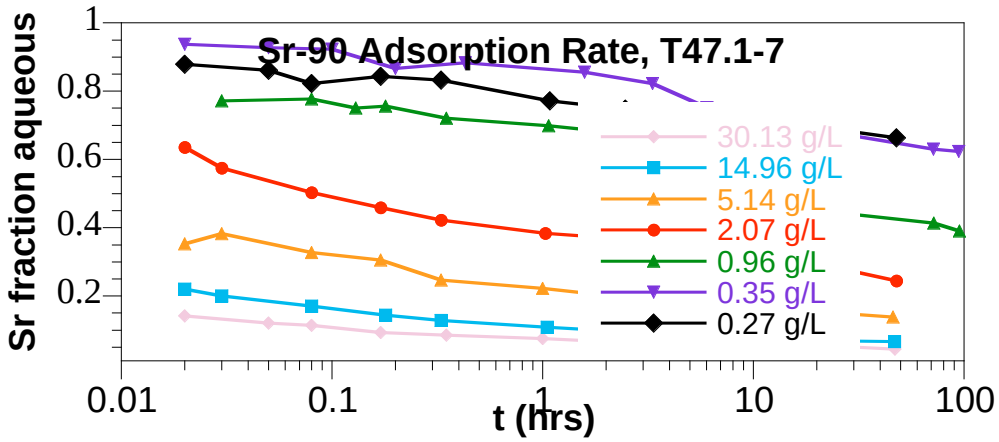
Sr-90 Adsorption Rate, T47.1-7
Sr fraction aqueous
t (hrs)
30.13 g/L
14.96 g/L
5.14 g/L
2.07 g/L
0.96 g/L
0.35 g/L
0.27 g/L

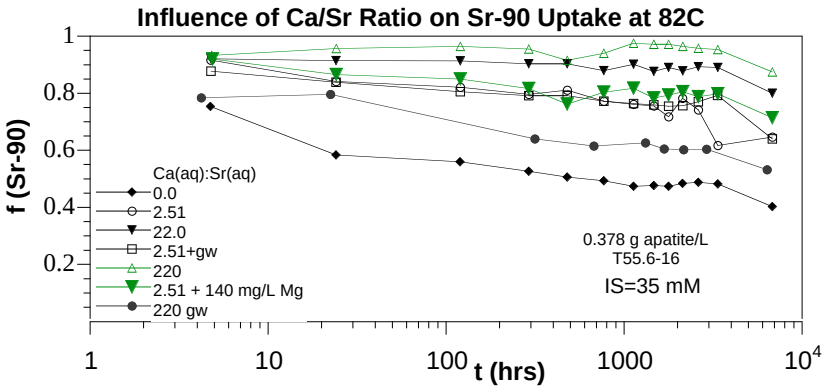
Influence of Ca/Sr Ratio on Sr-90 Uptake at 82C
f (Sr-90)
t (hrs)
Ca(aq):Sr(aq)
0.0
2.51
22.0
2.51+gw
220
2.51 + 140 mg/L Mg
220 gw
0.378 g apatite/L
T55.6-16
IS=35 mM

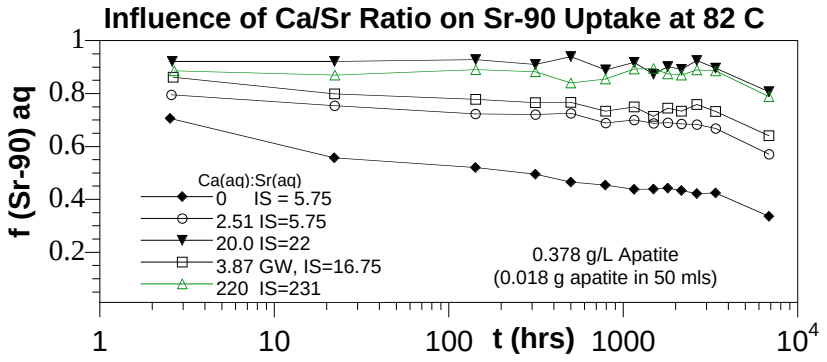
Influence of Ca/Sr Ratio on Sr-90 Uptake at 82 C
f (Sr-90) aq
t (hrs)
Ca(aq):Sr(aq)
0 IS = 5.75
2.51 IS=5.75
20.0 IS=22
3.87 GW, IS=16.75
220 IS=231
0.378 g/L Apatite
(0.018 g apatite in 50 mls)

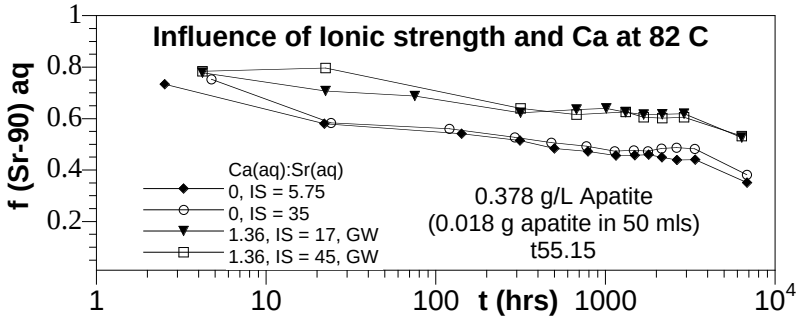
Influence of Ionic strength and Ca at 82 C
f (Sr-90) aq
t (hrs)
Ca(aq):Sr(aq)
0, IS = 5.75
0, IS = 35
1.36, IS = 17, GW
1.36, IS = 45, GW
0.378 g/L Apatite
(0.018 g apatite in 50 mls)
t55.15

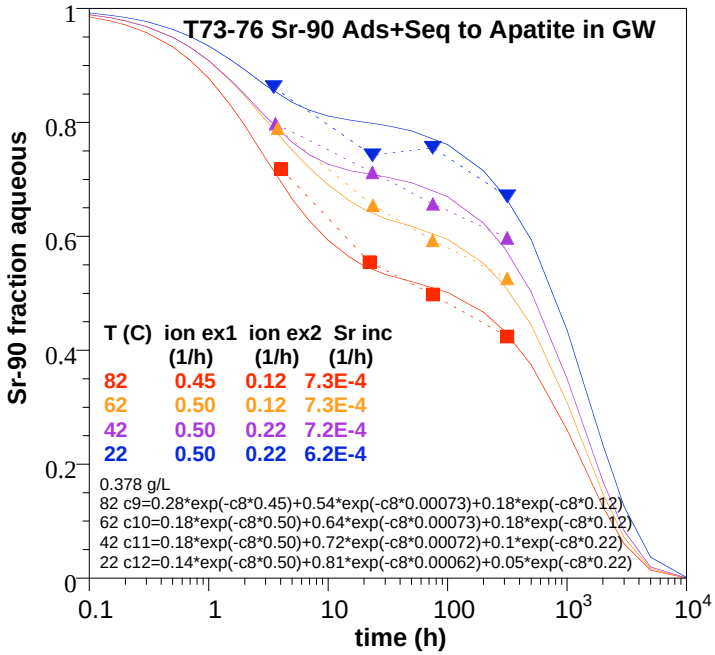
T73-76 Sr-90 Ads+Seq to Apatite in GW
Sr-90 fraction aqueous
time (h)
T (C) ion ex1 (1/h) ion ex2 (1/h) Sr inc (1/h)
82 0.45 0.12 7.3E-4
62 0.50 0.12 7.3E-4
42 0.50 0.22 7.2E-4
22 0.50 0.22 6.2E-4
0.378 g/L
82 c9=0.28*exp(-c8*0.45)+0.54*exp(-c8*0.00073)+0.18*exp(-c8*0.12)
62 c10=0.18*exp(-c8*0.50)+0.64*exp(-c8*0.00073)+0.18*exp(-c8*0.12)
42 c11=0.18*exp(-c8*0.50)+0.72*exp(-c8*0.00072)+0.1*exp(-c8*0.22)
22 c12=0.14*exp(-c8*0.50)+0.81*exp(-c8*0.00062)+0.05*exp(-c8*0.22)

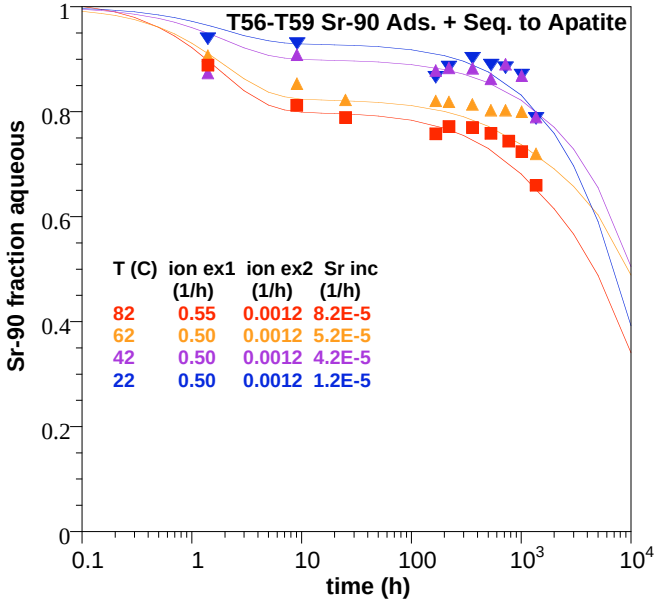
T56-T59 Sr-90 Ads. + Seq. to Apatite
Sr-90 fraction aqueous
time (h)
T (C) ion ex1 (1/h) ion ex2 (1/h) Sr inc (1/h)
82 0.55 0.0012 8.2E-5
62 0.50 0.0012 5.2E-5
42 0.50 0.0012 4.2E-5
22 0.50 0.0012 1.2E-5

A.5 Task 3 – Sr-90 Ion Exchange and Incorporation in Apatite

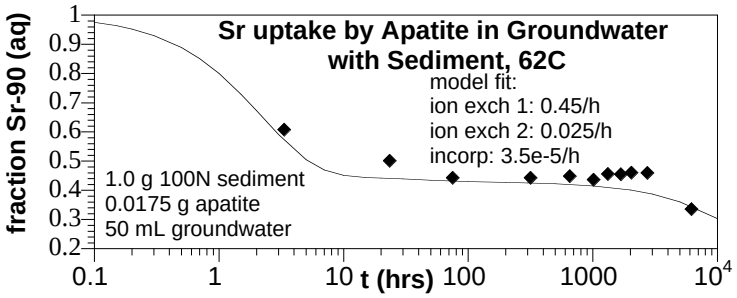

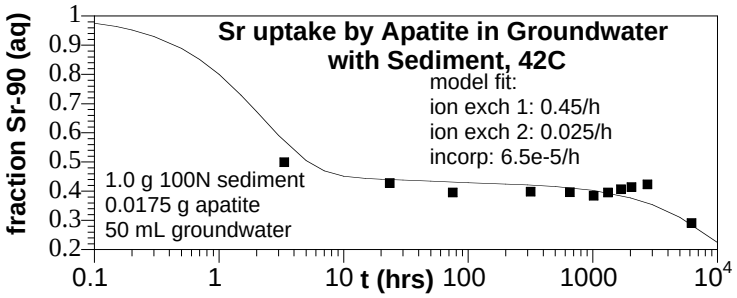

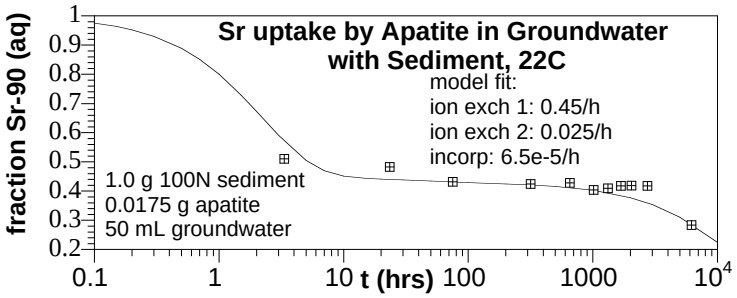

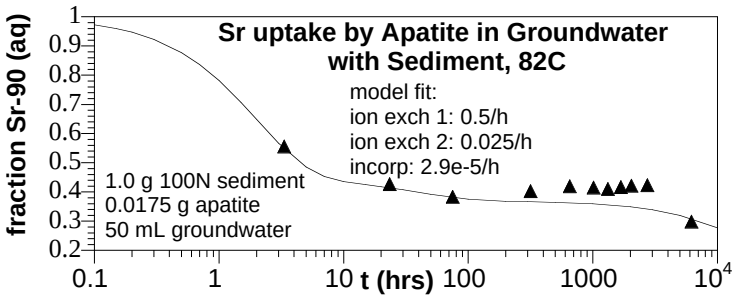

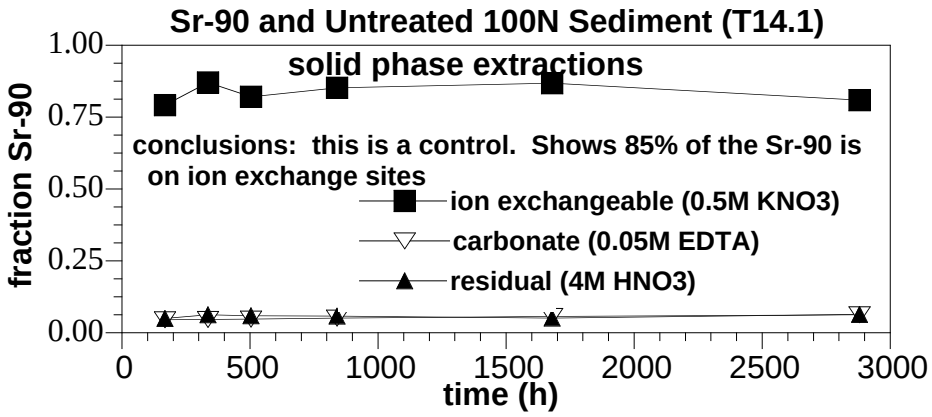
Sr-90 and Untreated 100N Sediment (T14.1)
solid phase extractions
conclusions: this is a control. Shows 85% of the Sr-90 is on ion exchange sites
ion exchangeable (0.5M KNO3)
carbonate (0.05M EDTA)
residual (4M HNO3)
fraction Sr-90
time (h)
1.00
0.75
0.50
0.25
0.00
0
500
1000
1500
2000
2500
3000

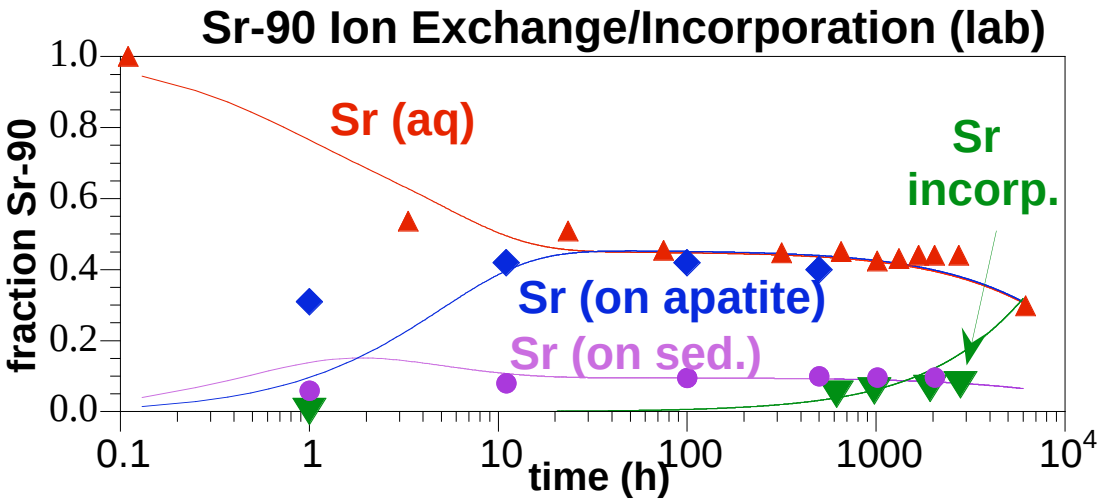
Sr-90 Ion Exchange/Incorporation (lab)
Sr (aq)
Sr incorp.
Sr (on apatite)
Sr (on sed.)
fraction Sr-90
time (h)
1.0
0.8
0.6
0.4
0.2
0.0
0.1
1
10
100
1000
10^4

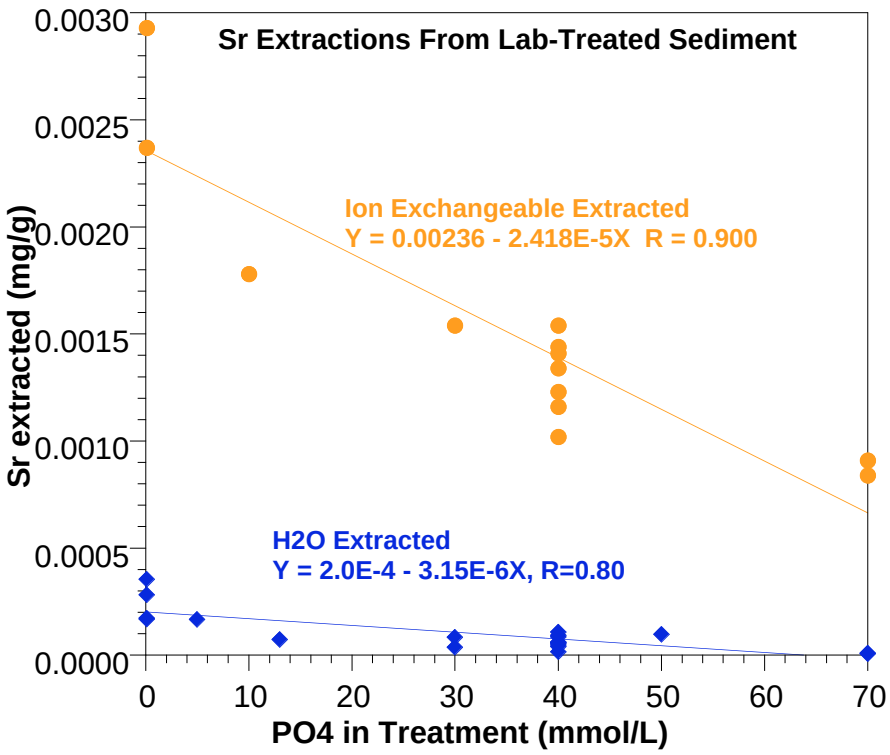
Sr Extractions From Lab-Treated Sediment
Ion Exchangeable Extracted
Y = 0.00236 - 2.418E-5X R = 0.900
H2O Extracted
Y = 2.0E-4 - 3.15E-6X, R=0.80
Sr extracted (mg/g)
PO4 in Treatment (mmol/L)
0.0030
0.0025
0.0020
0.0015
0.0010
0.0005
0.0000
0
10
20
30
40
50
60
70

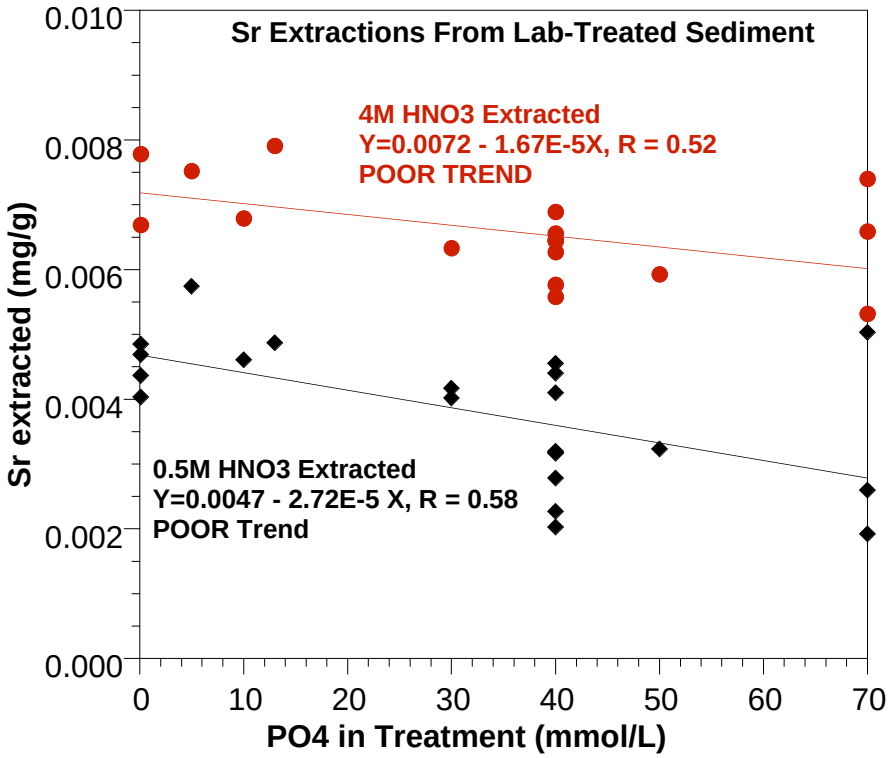
Sr Extractions From Lab-Treated Sediment
4M HNO3 Extracted
Y=0.0072 - 1.67E-5X, R = 0.52
POOR TREND
0.5M HNO3 Extracted
Y=0.0047 - 2.72E-5 X, R = 0.58
POOR Trend
Sr extracted (mg/g)
PO4 in Treatment (mmol/L)
0.010
0.008
0.006
0.004
0.002
0.000
0
10
20
30
40
50
60
70

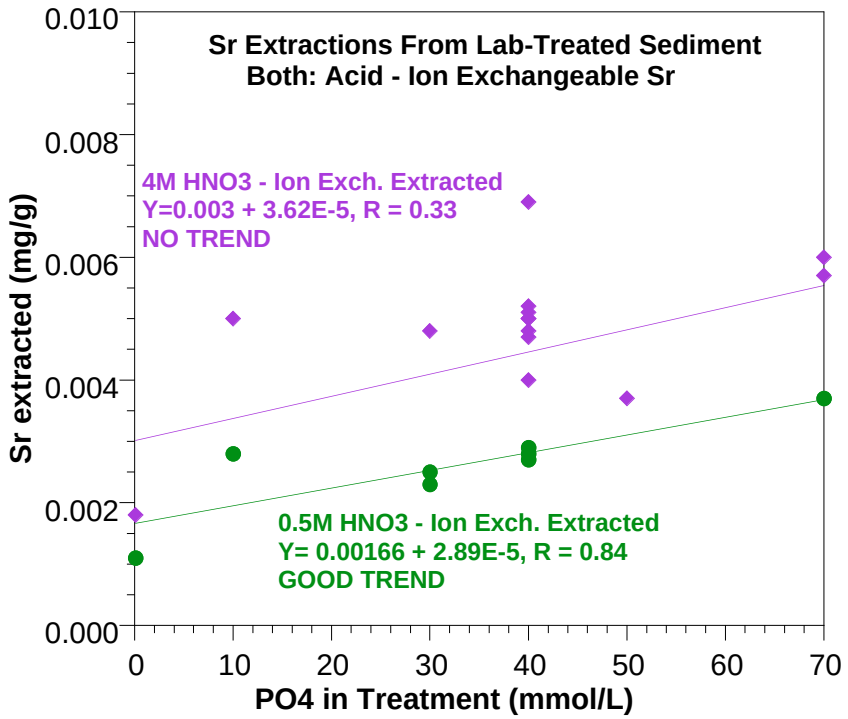
Sr Extractions From Lab-Treated Sediment
Both: Acid - Ion Exchangeable Sr
4M HNO3 - Ion Exch. Extracted
Y=0.003 + 3.62E-5, R = 0.33
NO TREND
0.5M HNO3 - Ion Exch. Extracted
Y= 0.00166 + 2.89E-5, R = 0.84
GOOD TREND
Sr extracted (mg/g)
0.010
0.008
0.006
0.004
0.002
0.000
0
10
20
30
40
50
60
70
PO4 in Treatment (mmol/L)

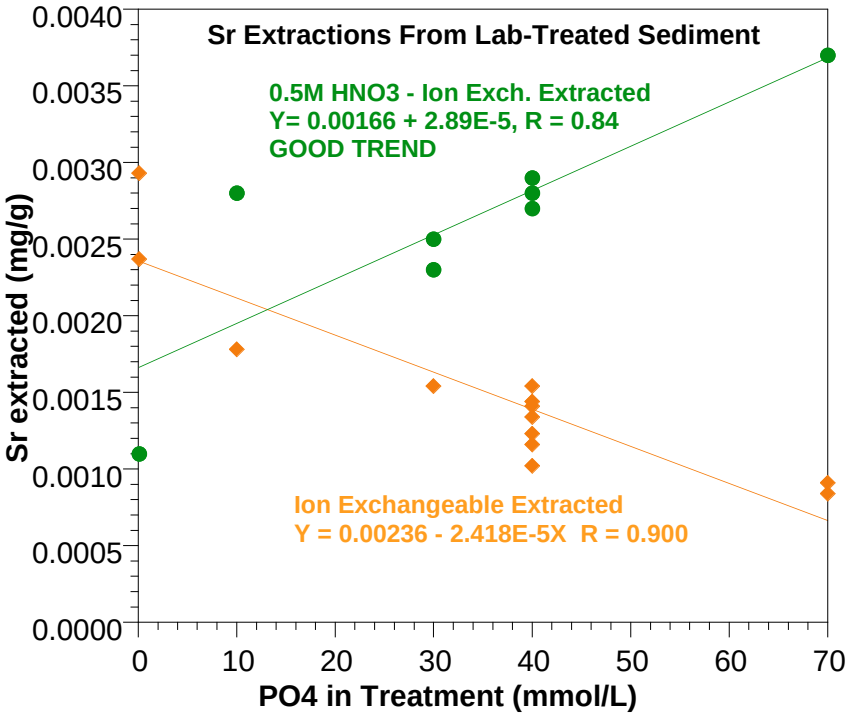
Sr Extractions From Lab-Treated Sediment
0.5M HNO3 - Ion Exch. Extracted
Y= 0.00166 + 2.89E-5, R = 0.84
GOOD TREND
Ion Exchangeable Extracted
Y = 0.00236 - 2.418E-5X R = 0.900
Sr extracted (mg/g)
0.0040
0.0035
0.0030
0.0025
0.0020
0.0015
0.0010
0.0005
0.0000
0
10
20
30
40
50
60
70
PO4 in Treatment (mmol/L)

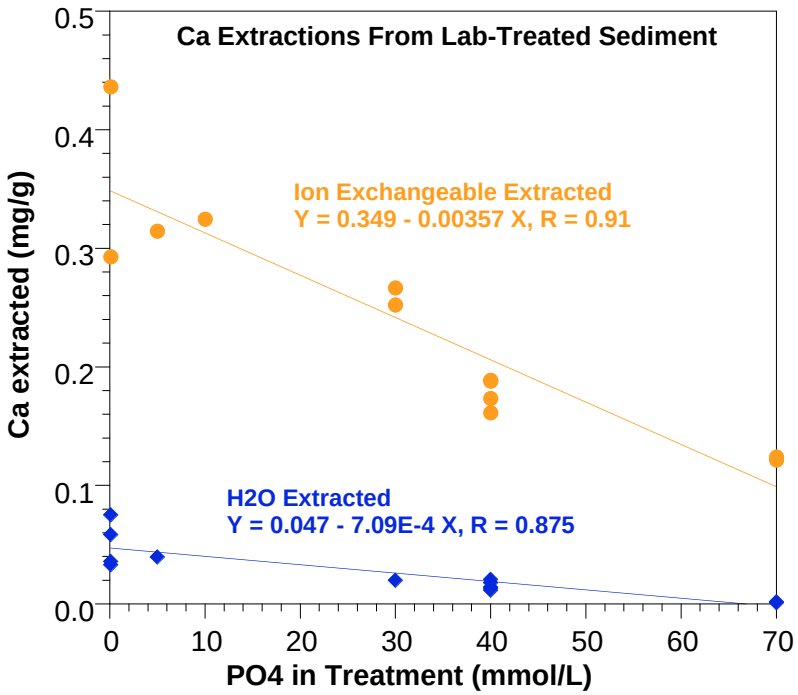
Ca Extractions From Lab-Treated Sediment
Ion Exchangeable Extracted
Y = 0.349 - 0.00357 X, R = 0.91
H2O Extracted
Y = 0.047 - 7.09E-4 X, R = 0.875
Ca extracted (mg/g)
PO4 in Treatment (mmol/L)
0.0
0.1
0.2
0.3
0.4
0.5
0
10
20
30
40
50
60
70

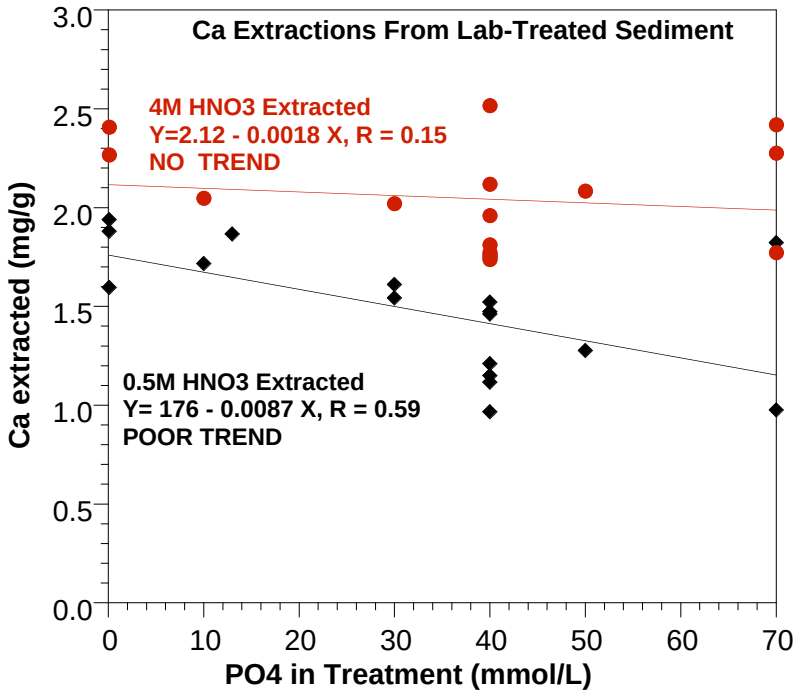
Ca Extractions From Lab-Treated Sediment
4M HNO3 Extracted
Y=2.12 - 0.0018 X, R = 0.15
NO TREND
0.5M HNO3 Extracted
Y= 176 - 0.0087 X, R = 0.59
POOR TREND
Ca extracted (mg/g)
PO4 in Treatment (mmol/L)
0.0
0.5
1.0
1.5
2.0
2.5
3.0
0
10
20
30
40
50
60
70

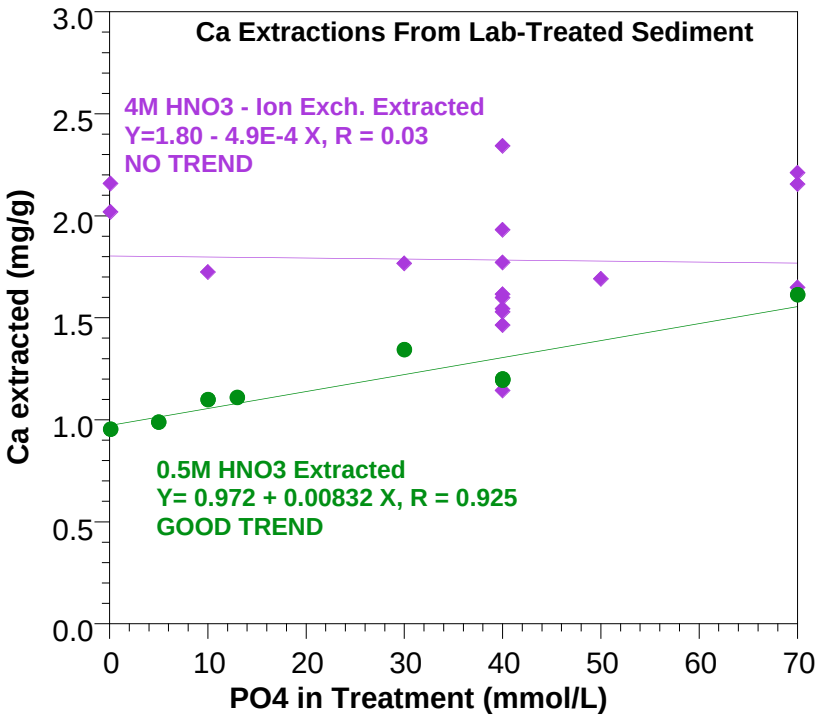
Ca Extractions From Lab-Treated Sediment
4M HNO3 - Ion Exch. Extracted
Y=1.80 - 4.9E-4 X, R = 0.03
NO TREND
0.5M HNO3 Extracted
Y= 0.972 + 0.00832 X, R = 0.925
GOOD TREND
Ca extracted (mg/g)
PO4 in Treatment (mmol/L)
0.0
0.5
1.0
1.5
2.0
2.5
3.0
0
10
20
30
40
50
60
70

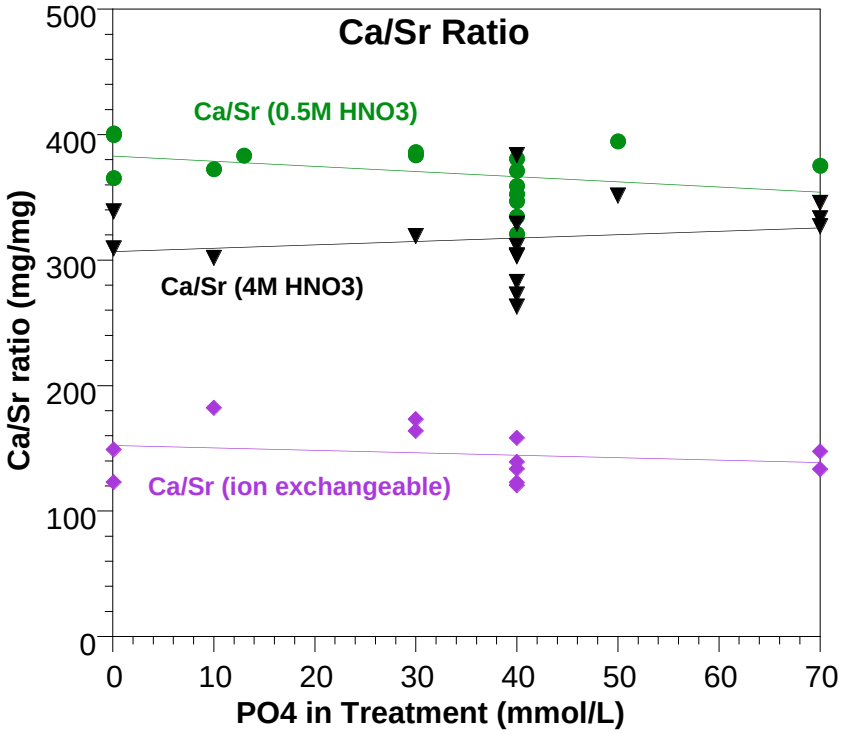
Ca/Sr Ratio
Ca/Sr (0.5M HNO3)
Ca/Sr (4M HNO3)
Ca/Sr (ion exchangeable)
Ca/Sr ratio (mg/mg)
PO4 in Treatment (mmol/L)
0
100
200
300
400
500
0
10
20
30
40
50
60
70

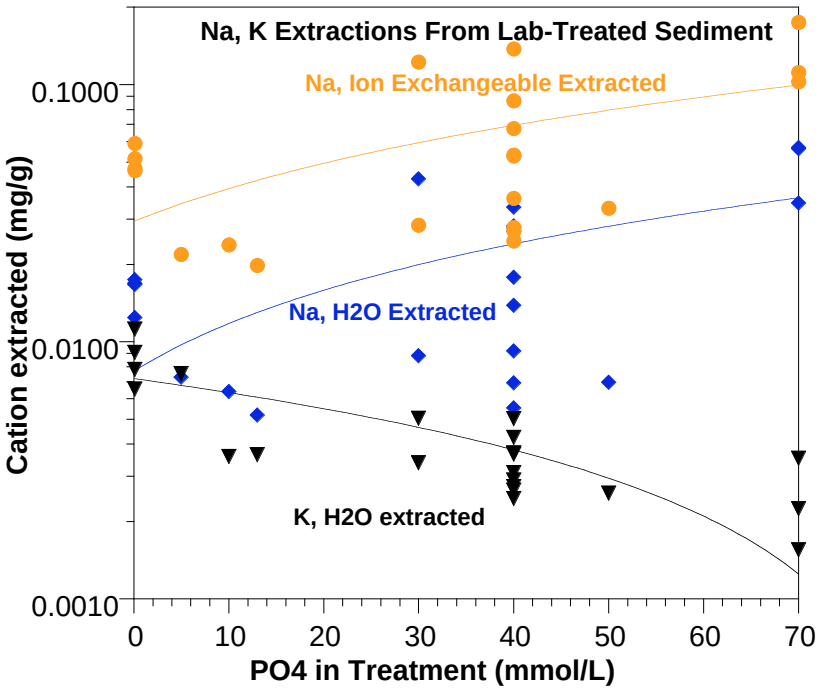
Na, K Extractions From Lab-Treated Sediment
Na, Ion Exchangeable Extracted
Na, H2O Extracted
K, H2O extracted
Cation extracted (mg/g)
0.1000
0.0100
0.0010
0
10
20
30
40
50
60
70
PO4 in Treatment (mmol/L)

A.6 Task 4 – Simulation of Sr Incorporation into Apatite

Calculation of Sr mass fraction on ion exchange sites of apatite and sediment at different sediment/apatite/water ratios.

							ion exchange equilibrium			
system	#	Kd, apa. (cm3/g)	Kd, sed. (cm3/g)	apatite mass (g)	sediment mass (g)	volume (mL)	fraction aqueous	fraction sorbed on apatite	fraction sorbed on sediment	fraction sorbed total
laboratory systems										
Sr/apatite only	1	1350		0.0038		50	0.9069	0.0931	0	0.0931
	2	1350		0.0038		1.0	0.1631	0.8369	0	0.8369
Sr/sediment only	3		25		0.0038	50	0.9981	0	0.0019	0.0019
	4		25		0.0038	1.0	0.9132	0	0.0868	0.0868
Sr/apatite/sed.	5	1350	25	0.0038	0.0038	50	0.9054	0.0929	0.0017	0.0946
	6	1350	25	0.0038	0.0038	1.0	0.1606	0.8241	0.0153	0.8394
	7	1350	25	0.0038	1.0	50	0.6240	0.0640	0.3120	0.3760
	8	1350	25	0	1.0	50	0.6667	0.0000	0.3333	0.3333
field systems										
Sr/sediment only	9	1350	25	0	1.0	0.2	0.0079	0.0000	0.9921	0.9921
Sr/sed./apatite	10	1350	25	0.00038	1.0	0.2	0.0078	0.0200	0.9723	0.9922
Sr/sed./apatite	11	1350	25	0.0038	1.0	0.2	0.0066	0.1691	0.8243	0.9934

Equilibrium cation exchange calculation using Gaines-Thomas activity convention with a single site (no K and no Mg).

from experimental/field data:

Species	aq conc (mg/L)	aq conc (mol/L)	aq conc (mmol/L)
Na	22	9.57E-04	0.957
K	0.82	2.10E-05	0.021
Ca	22	5.50E-04	0.550
Mg	4.3	1.77E-04	0.177
Sr	0.1	1.14E-06	0.001

(100N gw from T43,Y83-88)

CEC (meq/100 g) 4.00

Species	Charge	Aqueous conc [mmol/kg]
Na	1	1.00E+00
K	1	0.00E+00
Ca	2	5.50E-01
Mg	2	0.00E+00
Sr	2	1.14E-03

Selectivity coefs.	
K Na\K	0.20
K Na\Ca	0.40
K Na\Mg	0.50
K Na\Sr	0.40

Activity Final β	Adsorbed conc. qm (mmol/100 g)		Effective Kd	mass apatite (g)	mass sed (g)	sed. adsorbed mass (mmol)	apatite adsorbed mass (mmol)
4.13E-01	1.651431704	**Na**	1.6514	0.0175	1	0.016514	0.01549
0.00E+00	0	**K**	#DIV/0!	0.0175	1	0	0
5.86E-01	2.343710422	**Ca**	4.2613	0.0175	1	0.023437	0.021984
0.00E+00	0	**Mg**	#DIV/0!	0.0175	1	0	0
1.21E-03	0.004857873	**Sr**	4.2613	0.0175	1	4.86E-05	4.56E-05
1.000	4.000	**= sum**					

Equilibrium cation exchange calculation using Gaines-Thomas activity convention with a single site (no K and no Mg).

CEC (meq/100 g) 4

Species	Charge	Aqueous conc [mmol/kg]
Na	1	100.00
K	1	10.00
Ca	2	100.00
Mg	2	10.00
Sr	2	10.00

Selectivity coefs.	
K Na\K	0.2
K Na\Ca	0.4
K Na\Mg	0.5
K Na\Sr	0.4

Activity Final β	Adsorbed conc. qm (mol/100 g)		Effective Kd
6.46E-01	2.585606654	**Na**	0.0259
3.23E-01	1.292803327	**K**	0.1293
2.61E-02	0.104458778	**Ca**	0.0010
1.67E-03	0.006685362	**Mg**	0.0007
2.61E-03	0.010445878	**Sr**	0.0010

Geochemical Equilibrium Reaction Simulation (Geochemist Work Bench).
Ca-citrate equilibrium versus pH (deionized water, not groundwater).

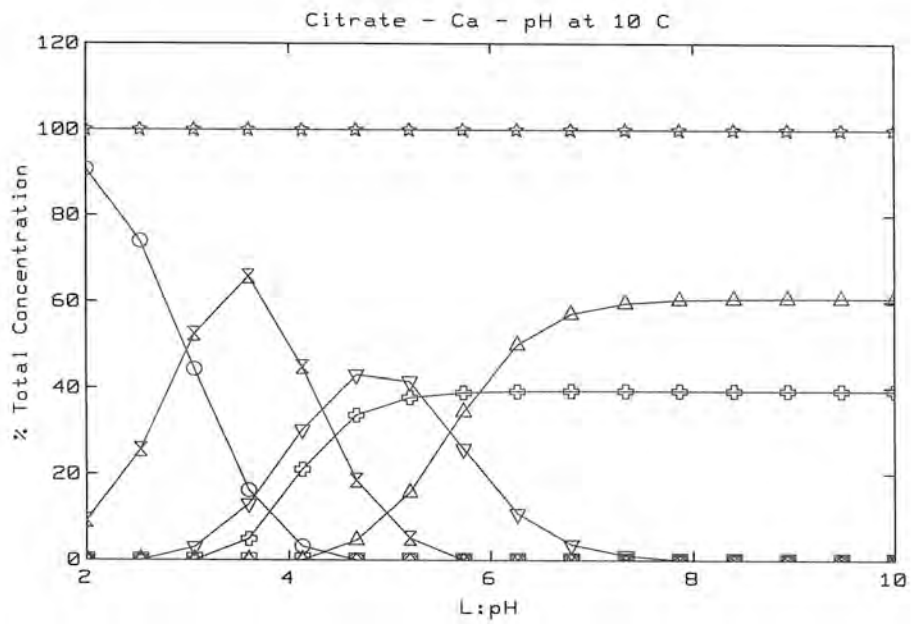

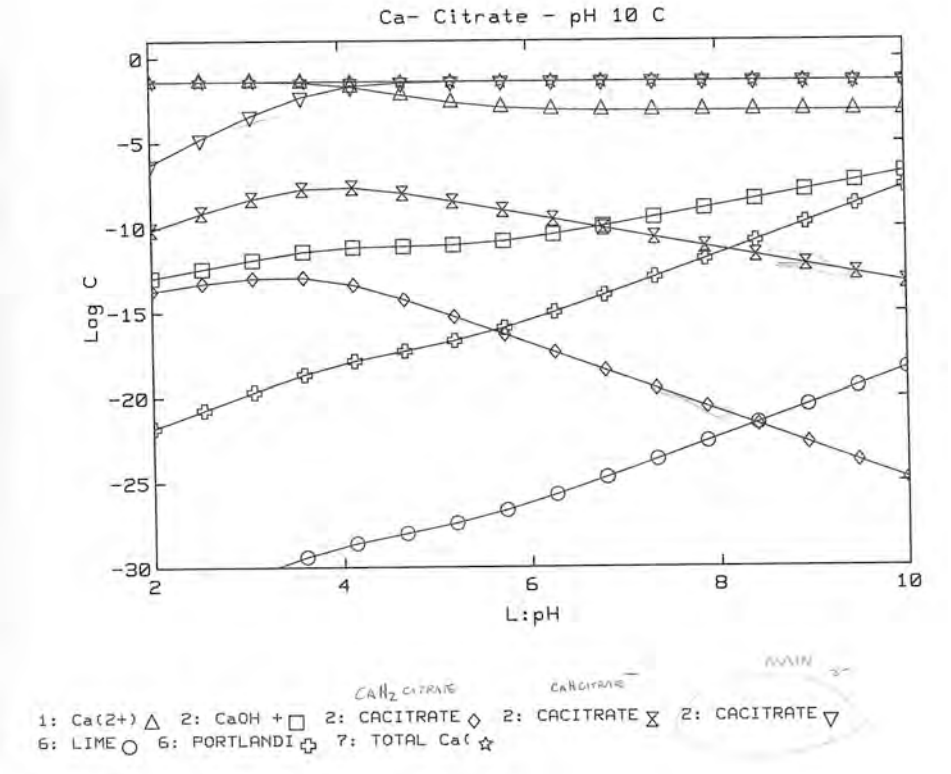

Geochemical Equilibrium Reaction Simulation (Geochemist Work Bench).
Simulation 2: 10 mM Na-citrate in oxic groundwater to determine citrate complexes.

Aqueous species	molality	mg/kg sol'n	act. coef.	log act.
Na+	0.02983	683.2	0.8261	-1.6084
Cl-	0.008568	302.7	0.8261	-2.1501
Ca-Citrate-	0.005089	1162.	0.8261	-2.3764
Citrate---	0.003532	665.5	0.1791	-3.1988
HCO3-	0.002622	159.4	0.8261	-2.6644
HPO4--	0.001888	180.6	0.4657	-3.0559
Na-Citrate--	0.0008160	172.4	0.4657	-3.4202
SO4--	0.0006385	61.11	0.4657	-3.5268
H4SiO4	0.0005401	51.72	1.0108	-3.2628
Mg-Citrate-	0.0005252	111.7	0.8261	-3.3627
NaHPO4-	0.0002779	32.94	0.8261	-3.6391
K+	0.0002044	7.963	0.8261	-3.7725
Ca++	0.0001822	7.275	0.4657	-4.0714
H2PO4-	0.0001714	16.56	0.8261	-3.8489
NaCl (aq)	9.135e-005	5.319	1.0108	-4.0346
H2CO3* (aq)	5.162e-005	3.190	1.0108	-4.2825
NaSO4-	4.840e-005	5.741	0.8261	-4.3982
H-Citrate--	3.306e-005	6.261	0.4657	-4.8127
CaHPO4 (aq)	3.105e-005	4.210	1.0108	-4.5032
NaHCO3 (aq)	2.888e-005	2.417	1.0108	-4.5347
F-	2.732e-005	0.5171	0.8261	-4.6465
Mg++	2.004e-005	0.4855	0.4657	-5.0300
CO3--	1.959e-005	1.171	0.4657	-5.0400
CaPO4-	9.059e-006	1.219	0.8261	-5.1259
NaH2PO4 (aq)	6.084e-006	0.7273	1.0108	-5.2111
H3SiO4-	5.998e-006	0.5684	0.8261	-5.3050
NaCO3-	5.826e-006	0.4818	0.8261	-5.3176
CaSO4 (aq)	5.444e-006	0.7384	1.0108	-5.2594
MgHPO4 (aq)	4.716e-006	0.5653	1.0108	-5.3217
Na2HPO4 (aq)	4.196e-006	0.5935	1.0108	-5.3725
K-Citrate--	2.783e-006	0.6327	0.4657	-5.8875
CaHCO3+	2.604e-006	0.2623	0.8261	-5.6673
Sr-Citrate-	2.296e-006	0.6329	0.8261	-5.7221
CaCl+	1.776e-006	0.1337	0.8261	-5.8335
KHPO4-	1.230e-006	0.1655	0.8261	-5.9932
CaH-Citrate (aq)	9.620e-007	0.2206	1.0108	-6.0122
OH-	8.295e-007	0.01406	0.8261	-6.1641

(minor species <10-7 mol/L not shown)

Simulation 3: 4 mM Ca, 10 mM citrate, and 2.4 mM PO_4 in oxic groundwater to determine citrate complexes (field injection mix #1).

Aqueous species	molality	mg/kg sol'n	act. coef.	log act.
Na+	0.02956	677.6	0.8202	-1.615
Citrate---	0.006643	1252.	0.1680	-2.9523
HCO3-	0.002625	159.7	0.8202	-2.6670
Na-Citrate--	0.001458	308.3	0.4526	-3.1806
Ca-Citrate-	0.001294	295.7	0.8202	-2.9741
Cl-	0.0006559	23.19	0.8202	-3.2692
SO4--	0.0006447	61.75	0.4526	-3.5349
H4SiO4	0.0005401	51.75	1.0120	-3.2624
Mg-Citrate-	0.0005387	114.6	0.8202	-3.3547
K+	0.0002040	7.954	0.8202	-3.7764
H-Citrate--	6.000e-005	11.37	0.4526	-4.5661
H2CO3* (aq)	5.125e-005	3.170	1.0120	-4.2851
NaSO4-	4.708e-005	5.588	0.8202	-4.4132
NaHCO3 (aq)	2.822e-005	2.364	1.0120	-4.5442
F-	2.736e-005	0.5183	0.8202	-4.6489
Ca++	2.682e-005	1.072	0.4526	-4.9157
CO3--	2.003e-005	1.198	0.4526	-5.0426
Mg++	1.190e-005	0.2886	0.4526	-5.2686
NaCl (aq)	6.826e-006	0.3978	1.0120	-5.1606
H3SiO4-	6.047e-006	0.5734	0.8202	-5.3045
NaCO3-	5.741e-006	0.4751	0.8202	-5.3271
K-Citrate--	5.006e-006	1.139	0.4526	-5.6448
Sr-Citrate-	2.415e-006	0.6663	0.8202	-5.7031
OH-	8.356e-007	0.01417	0.8202	-6.1641
CaSO4 (aq)	7.638e-007	0.1037	1.0120	-6.1118
NaF (aq)	5.185e-007	0.02170	1.0120	-6.2801
KSO4-	3.828e-007	0.05158	0.8202	-6.5031
CaHCO3+	3.732e-007	0.03762	0.8202	-6.5141
Ba-Citrate-	3.663e-007	0.1192	0.8202	-6.5223
MgSO4 (aq)	2.716e-007	0.03260	1.0120	-6.5608
CaH-Citrate (aq)	2.426e-007	0.05568	1.0120	-6.6099
MgHCO3+	1.602e-007	0.01363	0.8202	-6.8815
Sr++	1.457e-007	0.01273	0.4526	-7.1809
H4SiO4SO4--	1.002e-007	0.01921	0.4526	-7.3432
Fe-Citrate (aq)	5.358e-008	0.01308	1.0120	-7.2658
Fe(OH)2+	4.960e-008	0.004444	0.8202	-7.3906
MgH-Citrate (aq)	4.679e-008	0.01000	1.0120	-7.3247
KCl (aq)	4.583e-008	0.003407	1.0120	-7.3336
MgCO3 (aq)	4.266e-008	0.003587	1.0120	-7.3648

(minor species concentration not shown)

Simulation 4. This represents injection of 5 mM citrate and 2.5 mM acetate and 2.5 mM formate (i.e., half of the 10 mM citrate is degraded). The concentrations of acetate and formate are unrealistically high as there are further degradation products.

Aqueous species	molality	mg/kg sol'n	act. coef.	log act.
Na+	0.03049	698.8	0.8421	-1.5905
Cl-	0.008553	302.3	0.8421	-2.1425
Ca-Citrate-	0.004025	919.6	0.8421	-2.4699
HCO3-	0.002605	158.5	0.8421	-2.6588
Formate-	0.002465	110.6	0.8421	-2.6828
Acetate-	0.002441	143.7	0.8421	-2.6870
HPO4--	0.001694	162.1	0.5030	-3.0695
Ca++	0.0009658	38.59	0.5030	-3.3136
SO4--	0.0006071	58.14	0.5030	-3.5152
H4SiO4	0.0005403	51.77	1.0081	-3.2639
Citrate---	0.0004182	78.84	0.2130	-4.0502
Mg-Citrate-	0.0004084	86.89	0.8421	-3.4636
Al(OH)4-	0.0003897	36.92	0.8421	-3.4839
NaHPO4-	0.0002753	32.65	0.8421	-3.6348
K+	0.0002066	8.054	0.8421	-3.7595
CaHPO4 (aq)	0.0001728	23.44	1.0081	-3.7589
H2PO4-	0.0001630	15.76	0.8421	-3.8625
Na-Citrate--	0.0001109	23.44	0.5030	-4.2537
Mg++	0.0001045	2.532	0.5030	-4.2795
NaCl (aq)	9.713e-005	5.659	1.0081	-4.0091
H2CO3* (aq)	5.243e-005	3.242	1.0081	-4.2769
NaSO4-	5.080e-005	6.030	0.8421	-4.3687
CaPO4-	4.932e-005	6.641	0.8421	-4.3816
Na-Acetate (aq)	3.759e-005	3.074	1.0081	-4.4214
Fe(OH)2+	3.350e-005	3.002	0.8421	-4.5495
CaSO4 (aq)	3.210e-005	4.357	1.0081	-4.4900
Ca-Formate+	3.135e-005	2.660	0.8421	-4.5783
NaHCO3 (aq)	3.057e-005	2.560	1.0081	-4.5112
F-	2.706e-005	0.5126	0.8421	-4.6422
MgHPO4 (aq)	2.580e-005	3.094	1.0081	-4.5848
CO3--	1.837e-005	1.099	0.5030	-5.0343
Ca-Acetate+	1.746e-005	1.725	0.8421	-4.8326
CaHCO3+	1.482e-005	1.494	0.8421	-4.9038
Al-(Citrate)2---	1.393e-005	5.629	0.2130	-5.5275
CaCl+	1.015e-005	0.7645	0.8421	-5.0681
NaH2PO4 (aq)	6.161e-006	0.7370	1.0081	-5.2068
NaCO3-	6.033e-006	0.4993	0.8421	-5.2941
H3SiO4-	5.870e-006	0.5566	0.8421	-5.3060
Mn+++	5.461e-006	0.2991	0.2130	-5.9343
Na2HPO4 (aq)	4.428e-006	0.6267	1.0081	-5.3503
H-Citrate--	4.310e-006	0.8168	0.5030	-5.6640
Mg-Formate+	3.486e-006	0.2410	0.8421	-5.5323
Al(OH)3 (aq)	3.314e-006	0.2577	1.0081	-5.4762
Fe-Citrate (aq)	2.978e-006	0.7273	1.0081	-5.5226
MgSO4 (aq)	2.783e-006	0.3339	1.0081	-5.5520
Mg-Acetate+	2.334e-006	0.1940	0.8421	-5.7065
MgCl+	1.740e-006	0.1037	0.8421	-5.8340
Fe(OH)4-	1.676e-006	0.2070	0.8421	-5.8503
CaH2PO4+	1.632e-006	0.2230	0.8421	-5.8619
MgHCO3+	1.550e-006	0.1319	0.8421	-5.8842
Sr-Citrate-	1.402e-006	0.3868	0.8421	-5.9279
CaCO3 (aq)	1.239e-006	0.1236	1.0081	-5.9035
Fe(OH)3 (aq)	1.214e-006	0.1293	1.0081	-5.9123
KHPO4-	1.205e-006	0.1622	0.8421	-5.9938
H-Acetate (aq)	1.162e-006	0.06958	1.0081	-5.9313
Sr++	9.790e-007	0.08552	0.5030	-6.3077

Simulation 5. This represents all the citrate being degraded to 5 mM acetate and 5 mM formate. Again, this is rather unrealistic, but an endpoint.

Aqueous species	molality	mg/kg sol'n	act. coef.	log act.
Na+	0.03064	702.9	0.8355	-1.5917
Cl-	0.008518	301.3	0.8355	-2.1477
Acetate-	0.004768	280.9	0.8355	-2.3997
Formate-	0.004730	212.4	0.8355	-2.4032
Ca++	0.004046	161.8	0.4874	-2.7051
HCO3-	0.002555	155.5	0.8355	-2.6707
HPO4--	0.001304	124.9	0.4874	-3.1967
H4SiO4	0.0005402	51.80	1.0092	-3.2635
SO4--	0.0005304	50.84	0.4874	-3.5875
CaHPO4 (aq)	0.0005228	70.96	1.0092	-3.2777
Mg++	0.0004113	9.976	0.4874	-3.6980
Al(OH)4-	0.0002754	26.11	0.8355	-3.6381
Ca-Formate+	0.0002442	20.73	0.8355	-3.6903
K+	0.0002072	8.083	0.8355	-3.7617
NaHPO4-	0.0002065	24.50	0.8355	-3.7632
CaPO4-	0.0001505	20.28	0.8355	-3.9004
Ca-Acetate+	0.0001384	13.69	0.8355	-3.9368
H2PO4-	0.0001225	11.86	0.8355	-3.9897
Mn+++	0.0001183	6.485	0.1985	-4.6293
CaSO4 (aq)	0.0001102	14.97	1.0092	-3.9539
NaCl (aq)	9.563e-005	5.576	1.0092	-4.0155
MgHPO4 (aq)	7.336e-005	8.804	1.0092	-4.1306
Na-Acetate (aq)	7.258e-005	5.940	1.0092	-4.1352
CaHCO3+	5.898e-005	5.949	0.8355	-4.3073
H2CO3* (aq)	5.096e-005	3.153	1.0092	-4.2888
NaSO4-	4.323e-005	5.135	0.8355	-4.4422
CaCl+	4.104e-005	3.093	0.8355	-4.4648
NaHCO3 (aq)	2.963e-005	2.483	1.0092	-4.5243
F-	2.632e-005	0.4989	0.8355	-4.6577
Mg-Formate+	2.552e-005	1.765	0.8355	-4.6712
CO3--	1.844e-005	1.104	0.4874	-5.0463
Mg-Acetate+	1.739e-005	1.446	0.8355	-4.8377
Fe(OH)2+	1.319e-005	1.182	0.8355	-4.9579
MgSO4 (aq)	8.978e-006	1.078	1.0092	-5.0429
MgCl+	6.613e-006	0.3943	0.8355	-5.2576
H3SiO4-	5.922e-006	0.5619	0.8355	-5.3056
NaCO3-	5.900e-006	0.4885	0.8355	-5.3072
MgHCO3+	5.799e-006	0.4937	0.8355	-5.3147
CaH2PO4+	4.981e-006	0.6811	0.8355	-5.3808
CaCO3 (aq)	4.887e-006	0.4880	1.0092	-5.3070
NaH2PO4 (aq)	4.580e-006	0.5482	1.0092	-5.3352
Na2HPO4 (aq)	3.282e-006	0.4648	1.0092	-5.4799
Al(OH)3 (aq)	2.321e-006	0.1806	1.0092	-5.6303
H-Acetate (aq)	2.250e-006	0.1348	1.0092	-5.6439
Sr++	2.141e-006	0.1872	0.4874	-5.9815
MgCO3 (aq)	1.578e-006	0.1327	1.0092	-5.7980
KHPO4-	9.012e-007	0.1215	0.8355	-6.1232
OH-	8.201e-007	0.01391	0.8355	-6.1642

(minor species not shown)

Reaction Kinetics for Sr incorporation into Apatite

with ion exchange to sediment and apatite

```
Reactions (X = sediment ion exchange sites, Y = apatite ion exchange sites):
 1  nax + 0.5sr <=> na + 0.5srx with kf1,kb1 where nax = [cecs-0.5cax-0.5srx]
 2  nax + 0.5ca <=> na + 0.5cax with kf2,kb2
 3  nay + 0.5sr <=> na + 0.5sry with kf3,kb3 where nay = [ceca-0.5cay-0.5sry]
 4  nay + 0.5ca <=> na + 0.5cay with kf4,kb4
 5  0.5 sry <=> 0.5 srz  with kf5, kb5  Sr-Z = incorporated into apatite
    >>>eliminate nax and nay as components!

If an irreversible (forward or backward) reaction is desired,
 then make the other rate = 0.0
Note: Input parameters are all rates - if the Kd and one rate
 is known, calculate the other rate from the Law of Microscopic
 Reversibility (Kd = kf/kb).  Kd is calculated below for
 convenience, but is not used in calculations!
Consistent units must be used for solution and sorbed species (mmol)
All rate parameters are in the same units (1/hr for example),
 then time steps are in the same units (hours).
```

```
Components:
Sr = U0
Ca = U1
Na = U2
SrX = U3
CaX = U4
SrY = U5
CaY = U6
SrZ = U7
```

Parameters to modify:

time steps:

startt := 0.01

endt := 600.0

n := 5000

kf1 := 0.80 kb1 := 0.31

kf2 := 0.80 kb2 := 0.31

kf3 := 4.14 kb3 := 0.04

kf4 := 4.14 kb4 := 0.04

kf5 := 0.0000015 kb5 := 0.0000003

cecs := 0.011 ceca := 0.01

$kd1 := \frac{kf1}{kb1}$ $kd2 := \frac{kf2}{kb2}$ $kd3 := \frac{kf3}{kb3}$ $kd4 := \frac{kf4}{kb4}$ $kd5 := \frac{kf5}{kb5}$

kd1 = 2.581

kd2 = 2.581

kd3 = 103.5

kd4 = 103.5

kd5 = 5

Partial differential equations for each chemical component:

$$dsr(sr, ca, na, srx, cax, sry, cay, srz) := 0.5 \cdot kb1 \cdot na \cdot srx^{0.5} - kf1 \cdot (cecs - 0.5 \cdot cax - 0.5 \cdot srx) \cdot sr^{0.5} \cdot 0.5 + 0.5 \cdot kb3 \cdot na \cdot sry^{0.5} - kf3 \cdot (ceca - 0.5 \cdot cay - 0.5 \cdot sry) \cdot sr^{0.5} \cdot 0.5$$

$$dca(sr, ca, na, srx, cax, sry, cay, srz) := 0.5 \cdot kb2 \cdot na \cdot cax^{0.5} - 0.5 \cdot kf2 \cdot (cecs - 0.5 \cdot cax - 0.5 \cdot srx) \cdot ca^{0.5} + 0.5 \cdot kb4 \cdot na \cdot cay^{0.5} - 0.5 \cdot kf4 \cdot (ceca - 0.5 \cdot cay - 0.5 \cdot sry) \cdot ca^{0.5}$$

$$dna(sr, ca, na, srx, cax, sry, cay, srz) := kf1 \cdot (cecs - 0.5 \cdot cax - 0.5 \cdot srx) \cdot sr^{0.5} - kb1 \cdot na \cdot srx^{0.5} + kf2 \cdot (cecs - 0.5 \cdot cax - 0.5 \cdot srx) \cdot ca^{0.5} - kb2 \cdot na \cdot cax^{0.5} + kf3 \cdot (ceca - 0.5 \cdot cay - 0.5 \cdot sry) \cdot sr^{0.5} - kb3 \cdot na \cdot sry^{0.5} + kf4 \cdot (ceca - 0.5 \cdot cay - 0.5 \cdot sry) \cdot ca^{0.5} - kb4 \cdot na \cdot cay^{0.5}$$

$$dsrx(sr, ca, na, srx, cax, sry, cay, srz) := 0.5 \cdot kf1 \cdot (cecs - 0.5 \cdot cax - 0.5 \cdot srx) \cdot sr^{0.5} - 0.5 \cdot kb1 \cdot na \cdot srx^{0.5}$$

$$dcax(sr, ca, na, srx, cax, sry, cay, srz) := 0.5 \cdot kf2 \cdot (cecs - 0.5 \cdot cax - 0.5 \cdot srx) \cdot ca^{0.5} - 0.5 \cdot kb2 \cdot na \cdot cax^{0.5}$$

$$dsry(sr, ca, na, srx, cax, sry, cay, srz) := 0.5 \cdot kf3 \cdot (ceca - 0.5 \cdot cay - 0.5 \cdot sry) \cdot sr^{0.5} - 0.5 \cdot kb3 \cdot na \cdot sry^{0.5} + 0.5 \cdot kb5 \cdot srz^{0.5} - 0.5 \cdot kf5 \cdot sry^{0.5}$$

$$dcay(sr, ca, na, srx, cax, sry, cay, srz) := 0.5 \cdot kf4 \cdot (ceca - 0.5 \cdot cay - 0.5 \cdot sry) \cdot ca^{0.5} - 0.5 \cdot kb4 \cdot na \cdot cay^{0.5}$$

$$dsrz(sr, ca, na, srx, cax, sry, cay, srz) := 0.5 \cdot kf5 \cdot sry^{0.5} - 0.5 \cdot kb5 \cdot srz^{0.5}$$

Initial conditions:

$$u^{<0>} = \begin{bmatrix} 0.000057 \\ 0.019 \\ 0.05 \\ 0.0 \\ 0.0038 \\ 0.0 \\ 0.019 \\ 0.0 \end{bmatrix}$$

```
mass
units: mmol
Sr = U0
Ca = U1
Na = U2
SrX = U3
CaX = U4
SrY = U5
CaY = U6
SrZ = U7
```

Derivative vector:

$$F(t, u) := \begin{bmatrix} dsr(u_0, u_1, u_2, u_3, u_4, u_5, u_6, u_7) \\ dca(u_0, u_1, u_2, u_3, u_4, u_5, u_6, u_7) \\ dna(u_0, u_1, u_2, u_3, u_4, u_5, u_6, u_7) \\ dsrx(u_0, u_1, u_2, u_3, u_4, u_5, u_6, u_7) \\ dcax(u_0, u_1, u_2, u_3, u_4, u_5, u_6, u_7) \\ dsry(u_0, u_1, u_2, u_3, u_4, u_5, u_6, u_7) \\ dcay(u_0, u_1, u_2, u_3, u_4, u_5, u_6, u_7) \\ dsrz(u_0, u_1, u_2, u_3, u_4, u_5, u_6, u_7) \end{bmatrix}$$

Sr/Na exch. to sed. (2.58)

Ca/Na exch. to sed. (2.58)

Sr/Na exch. to ap. (138)

Ca/Na exch. to ap. (138)

Sr incorp to ap. (2)

$\frac{\langle u^{<j>}\rangle_0}{\langle u^{<0>}\rangle_0}$

$\frac{Fe_{mm}}{\langle u^{<0>}\rangle_0}$

kf1 = 0.8

kf2 = 0.8

kf3 = 4.14

kf4 = 4.14

$kf5 = 1.5 \cdot 10^{-6}$

kb1 = 0.31

kb2 = 0.31

kb3 = 0.04

kb4 = 0.04

$kb5 = 3 \cdot 10^{-7}$

kd1 = 2.581

kd2 = 2.581

kd3 = 103.5

kd4 = 103.5

kd5 = 5

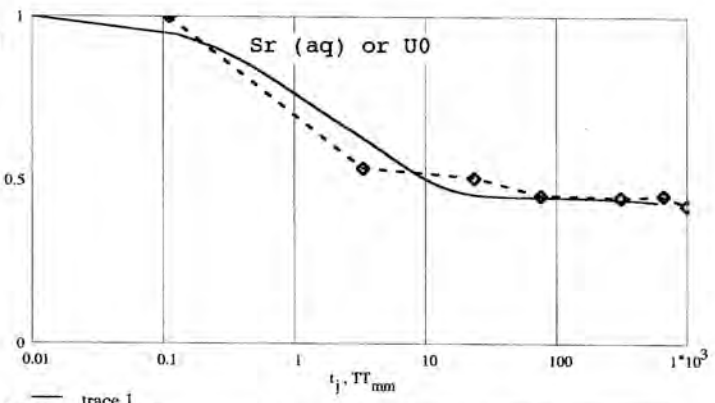

$\frac{\langle u^{<j>}\rangle_3}{\langle u^{<0>}\rangle_0}$

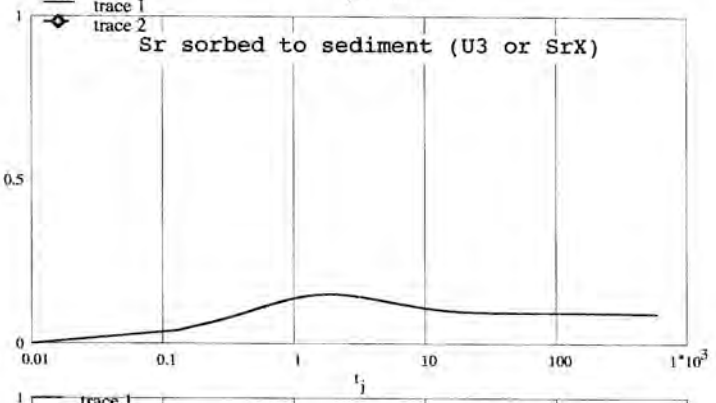

initial conditions (mol):

$$u^{<0>} = \begin{bmatrix} 5.7 \cdot 10^{-5} \\ 0.019 \\ 0.05 \\ 0 \\ 3.8 \cdot 10^{-3} \\ 0 \\ 0.019 \\ 0 \end{bmatrix}$$

Sr
Ca
Na
SrX
CaX
SrY
CaY
SrZ

$\frac{\langle u^{<j>}\rangle_5}{\langle u^{<0>}\rangle_0}$

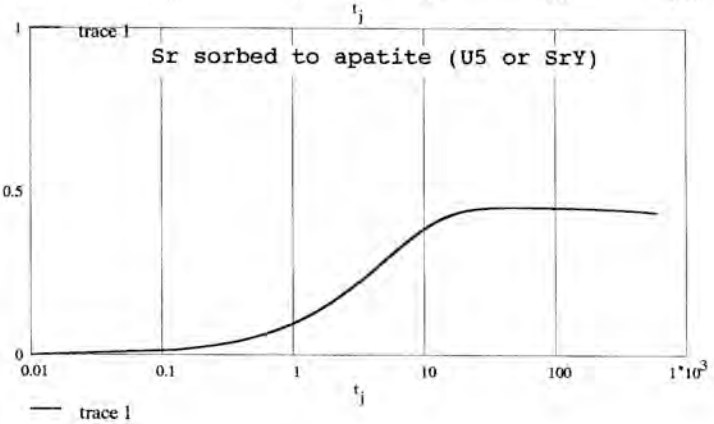

final conditions (mol):

$$u^{<n>} = \begin{bmatrix} 2.469 \cdot 10^{-5} \\ 0.019 \\ 0.05 \\ 5.237 \cdot 10^{-6} \\ 3.991 \cdot 10^{-3} \\ 2.491 \cdot 10^{-5} \\ 0.019 \\ 2.167 \cdot 10^{-6} \end{bmatrix}$$

$\frac{\langle u^{<j>}\rangle_7}{\langle u^{<0>}\rangle_0}$

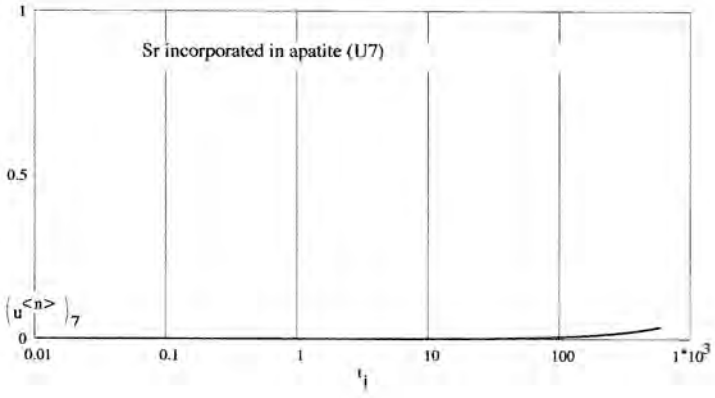

initial Sr

$Sri := \langle u^{<0>}\rangle_0$

$Sri = 5.7 \cdot 10^{-5}$

final Sr:

$Srf := \langle u^{<n>}\rangle_0 + \langle u^{<n>}\rangle_3 + \langle u^{<n>}\rangle_5 + \langle u^{<n>}\rangle_7$

$Srf = 5.7 \cdot 10^{-5}$

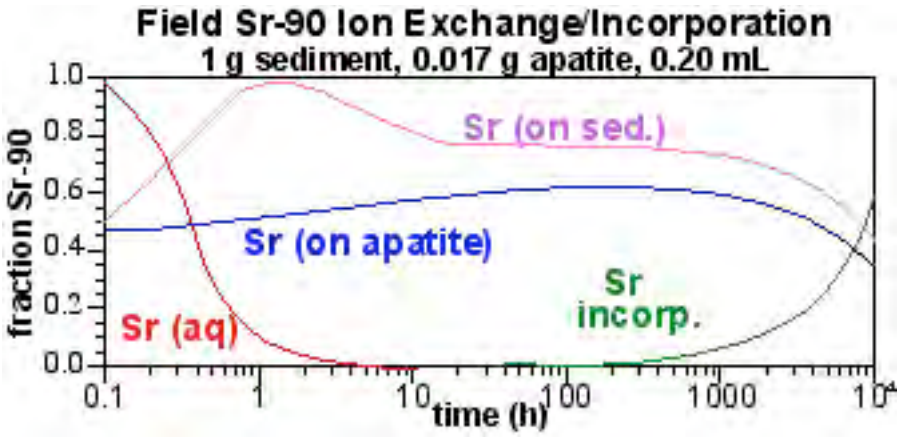

Field Sr-90 ion exchange/incorporation, 1 g sediment, 0.0034 g apatite (10 mM PO_4), 0.2 mL.

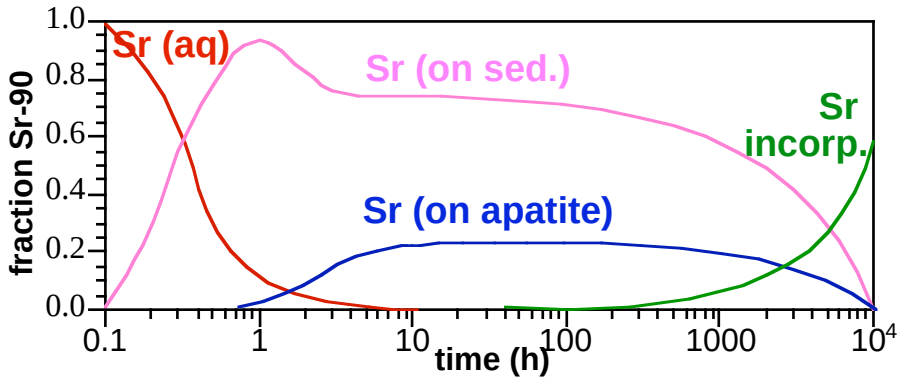

Lab Sr-90 ion exchange/incorporation, 1 g sediment, 0.0038 g apatite, 50 mL.

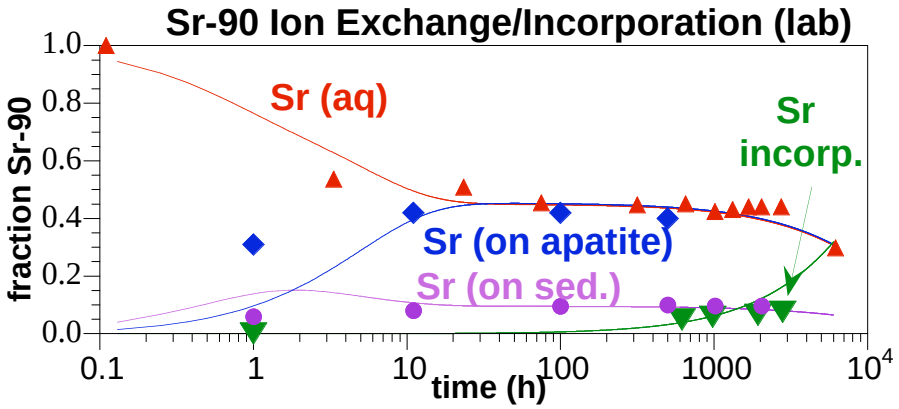

A.7 Task 4 – 1-D/2-D Simulation of Ca-Citrate-PO_4 Infiltration

STOMP Reactive Transport Simulations (batch,1-D, 2-D) of Ca-citrate-PO_4 injection, cation adsorption by ion exchange to sediment and apatite, citrate biodegradation, apatite precipitation, and Sr incorporation into apatite.

Aqueous Species (51)

```
CO3--
Ca++
Ca-citrate
CaCO3(aq)
CaCl+
CaH2PO4+
CaHCO3+
CaHPO4(aq)
CaNO3+
CaOH+
CaPO4-
Cl-
H+
H2CO3(aq)
H2PO4-
HCO3-
HPO4--
K+
KCl(aq)
KHPO4-
Mg++
MgCO3(aq)
MgHCO3+
MgHPO4(aq)
MgNO3+
MgOH+
MgPO4-
NH4+
NO3-
Na+,
NaCO3-
NaCl(aq)
NaHCO3(aq)
NaHPO4-
NaNO3(aq)
O2(aq)
OH-
Sr(c)++
Sr(c)CO3(aq)
Sr(c)Cl+
Sr(c)HCO3+
Sr(c)HPO4(aq)
Sr(c)NO3+
Sr(c)OH+
Sr(h)++
Sr(h)CO3(aq)
Sr(h)Cl+
Sr(h)HCO3+
Sr(h)HPO4(aq)
```

```
Solid Species (6)

C5H7O2N  (microbes)
Sr(h)CO3(s)
Sr(c)CO3(s) CaCO3(s)
Apatite
HPO4--(ads)
```

Exchanged Species (6)

```
Gaines-Thomas activity
convention
NaX,Na+
KX,K+
Sr(c)X2,Sr(c)++
Sr(h)X2,Sr(h)++
MgX2,Mg++
CaX2,Ca++
```

Sr(h)NO3+
Sr(h)OH+

STOMP Equilibrium Reactions (42)

Ca-citrate- = citrate--- + Ca++	-4.9198
Na-citrate-- = citrate--- + Na+	-1.3842
Mg-citrate- = citrate--- + Mg++	-4.8403
H-citrate-- = citrate--- + H+	-6.3755
K-citrate-- = citrate--- + K+	-1.0663
Sr-citrate- = citrate--- + Sr++	-4.4300
CaH-citrate(aq) = citrate--- + Ca++ + H+	-9.2598
CaCl+ = Ca++ + Cl-	-0.3757
NaCl(aq) = Na+ + Cl-	0.2503
H2CO3(aq) = 2H+ + CO3--	-16.8513
HCO3- = H+ + CO3--	-10.4212
HPO4-- = H+ + PO4---	-12.4675
NH3(aq) = NH4+ - H+	9.5703
NH4SO4- = NH4+ + SO4--	-1.03
NaSO4- = Na+ + SO4--	-0.7342
CaSO4(aq) = Ca++ + SO4--	-2.3157
NaNO3(aq) = Na+ + NO3-	0.55
NaHPO4- = Na+ + H+ + PO4---	-13.445
H2PO4- = 2H+ + PO4---	-19.6858
CaHPO4(aq) = Ca++ + H+ + PO4---	-15.0541
NaHCO3(aq) = Na+ + H+ + CO3--	-10.2045
NaCO3- = Na+ + CO3--	-1.3957
CaHCO3+ = Ca++ + H+ + CO3--	-11.4425
CaCO3(aq) = Ca++ + CO3--	-2.4118
OH- = - H+	14.00
MgHCO3+ = Mg++ + H+ + CO3--	-11.4605
MgSO4(aq) = Mg++ + SO4--	-2.2244
MgCl+ = Mg++ + Cl-	-0.5757
KCl(aq) = K+ + Cl-	0.2757
NaX + K+ = KX + Na+	1.322
2NaX + Mg++ = MgX2 + 2Na+	2.829
2NaX + Ca++ = CaX2 + 2Na+	3.147
2NaX + Sr++ = SrX2 + 2Na+	3.218
NaX + NH4+ = NH4X + Na+	1.322
Br- = Br-	0.0
HPO4-- = HPO4--(ads)	999
NH4+ = NH4+(ads)	999
Sr-apatite = apatite + 0.01Sr++ - 0.01Ca++	999
apatite = 5.00Ca++ + 3HPO4-- + H2O - 4H+	999
0.642C5H7O2N(s) = citrate--- + 0.0725H2O + 0.642NH4+ + 1.287O2(aq) + 2.358H+ - 2.788H2CO3(aq)	999

STOMP Kinetic Reactions

CaCO3(aq) = Ca++ + CO3--
apatite = 5.00Ca++ + 3HPO4-- + H2O - 4H+
SrCO3(aq) = Sr++ + CO3--
Citrate biodegradation using Monod kinetics
0.642C5H7O2N(s) = citrate--- + 0.0725H2O + 0.642NH4+ + 1.287O2(aq) + 2.358H+ - 2.788H2CO3(aq)
HPO4-- = HPO4--(ads)
Sr-apatite = apatite + 0.01Sr++ - 0.01Ca++

Simulation of 1-D Injection Experiment Y17 (PO_4 injection, no citrate).

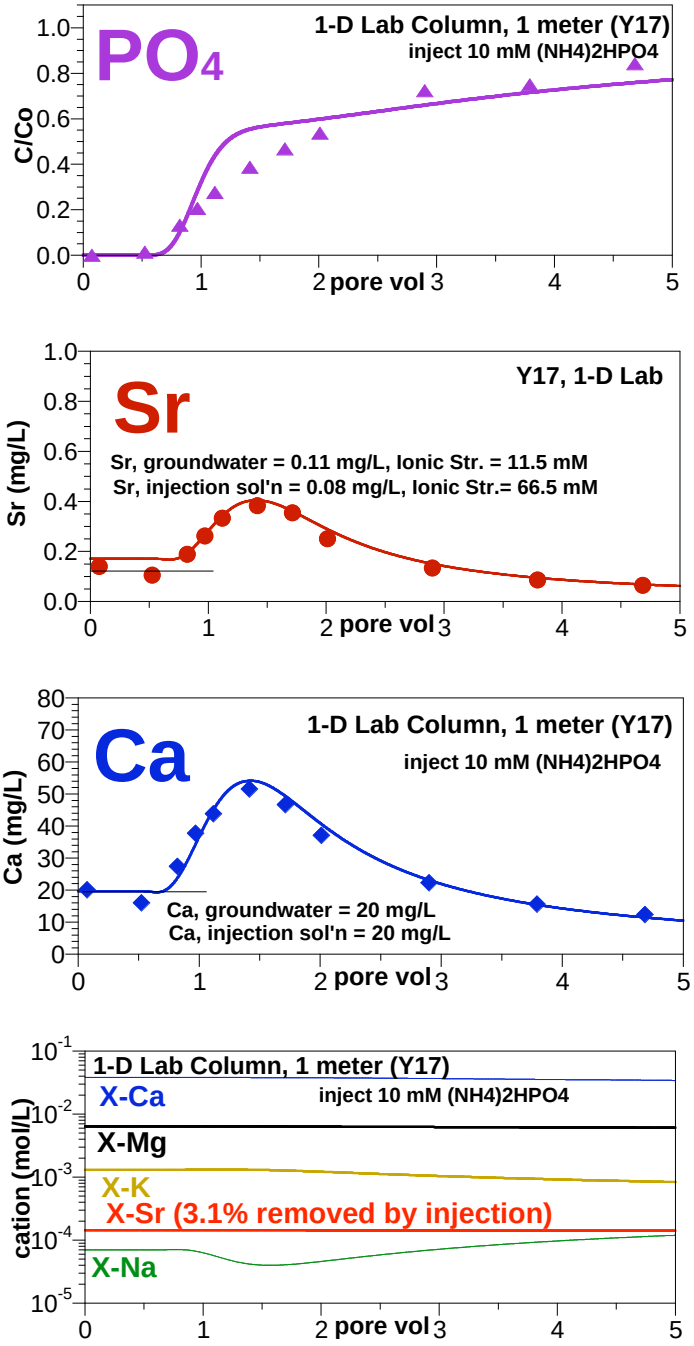

Simulation of 1-D Ca-Citrate-PO_4 Injection Experiment Y88.

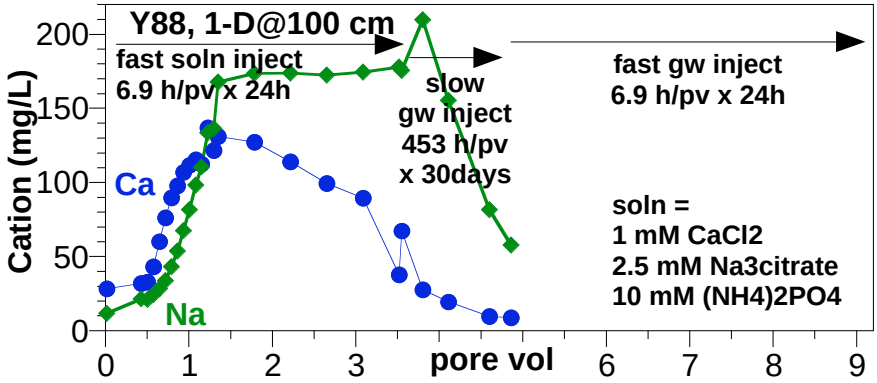

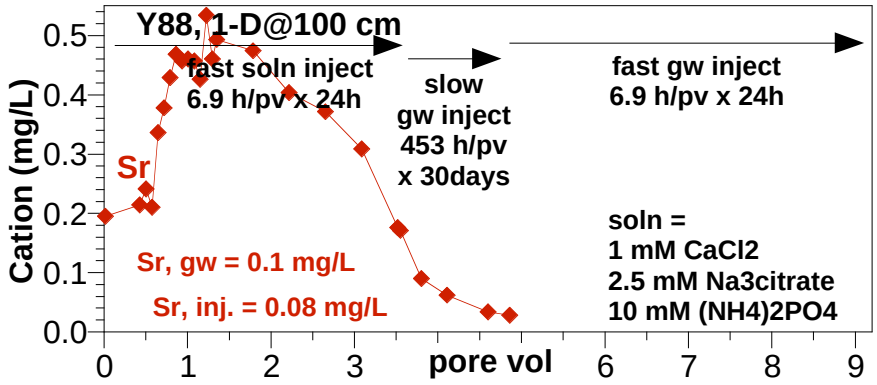

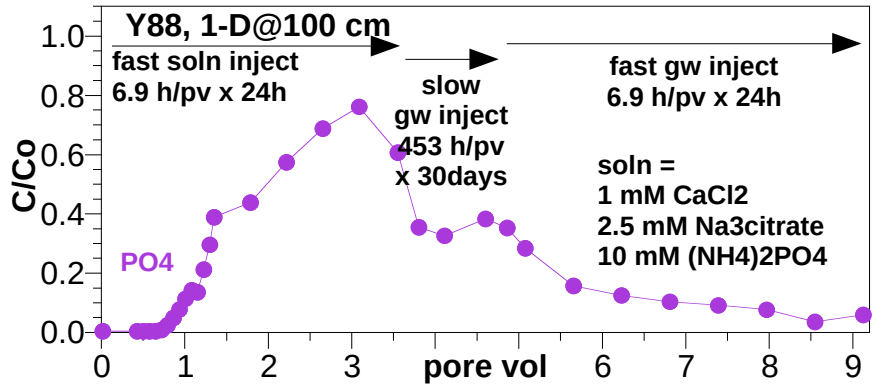

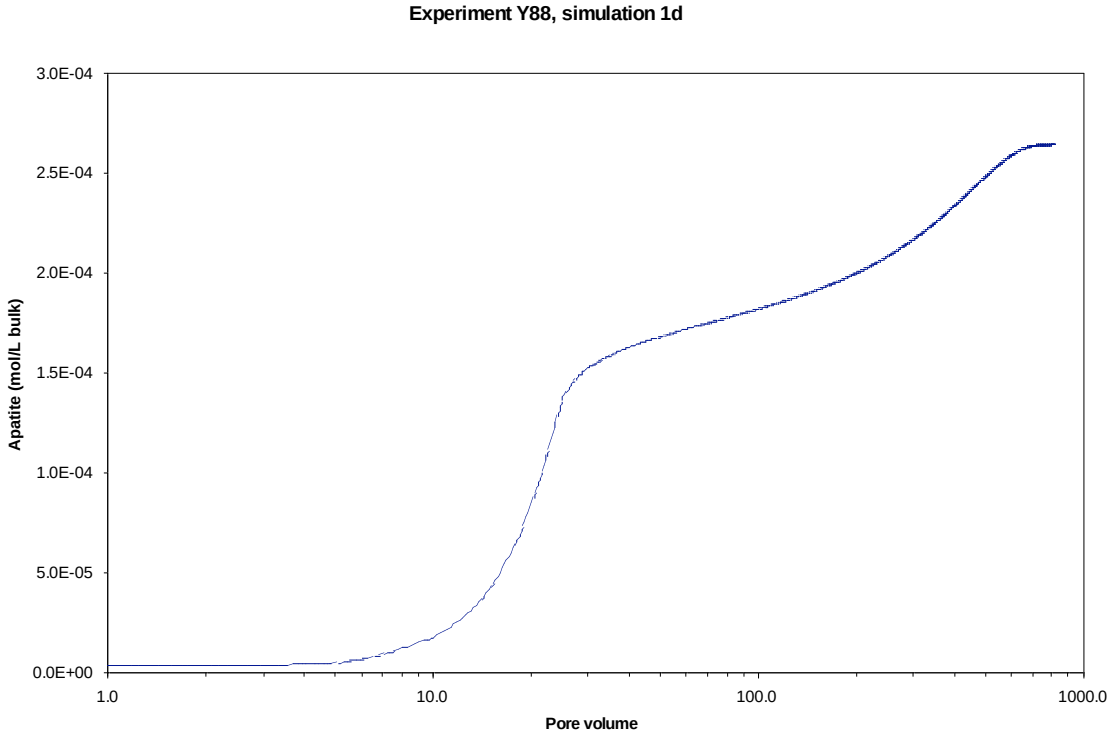
Experiment Y88, simulation 1d
3.0E-04
2.5E-04
2.0E-04
1.5E-04
1.0E-04
5.0E-05
0.0E+00
Apatite (mol/L bulk)
1.0
10.0
100.0
1000.0
Pore volume

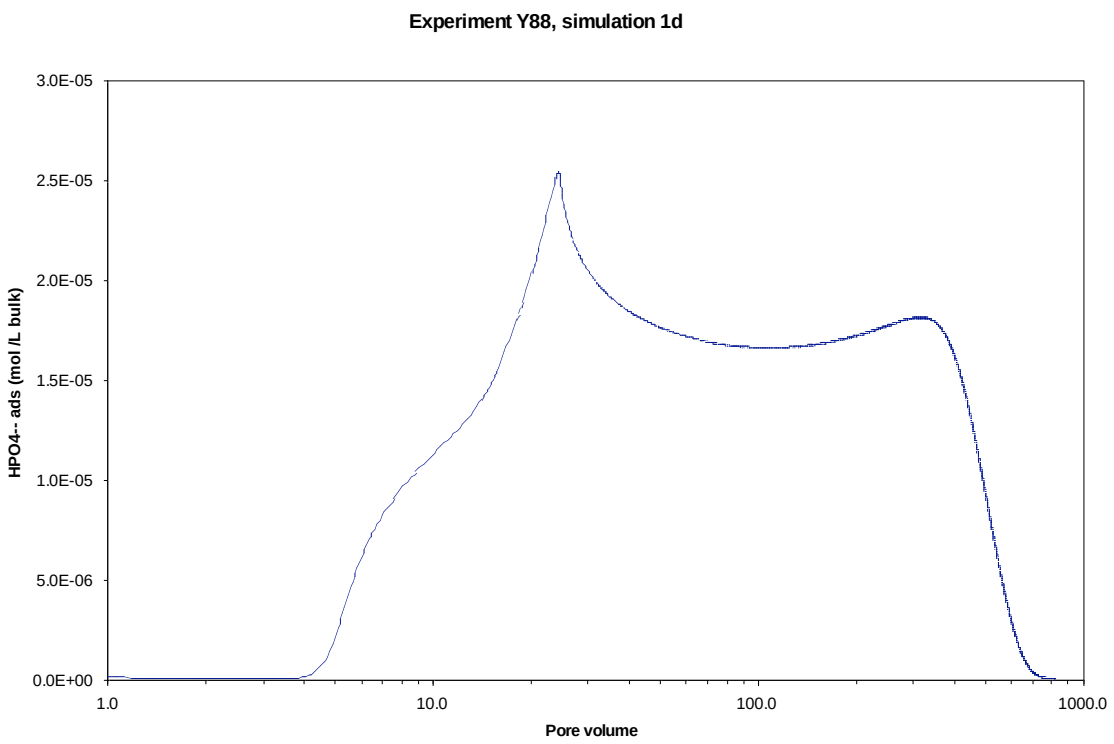
Experiment Y88, simulation 1d
3.0E-05
2.5E-05
2.0E-05
1.5E-05
1.0E-05
5.0E-06
0.0E+00
HPO4-- ads (mol /L bulk)
1.0
10.0
100.0
1000.0
Pore volume

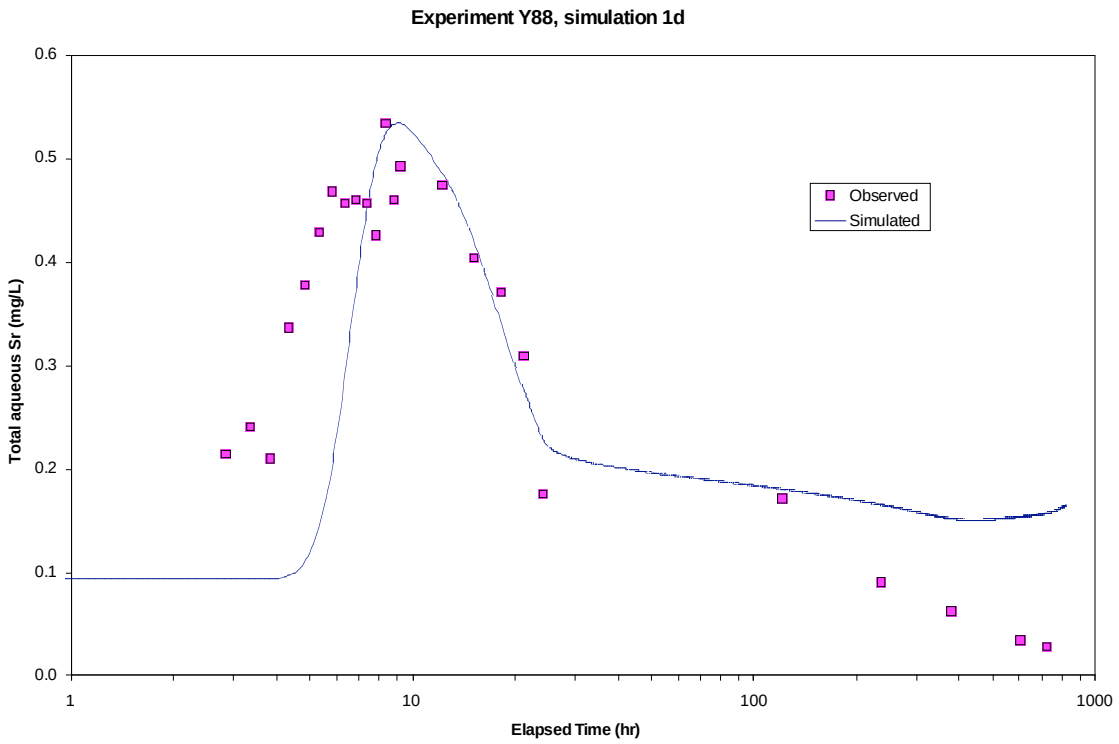
Experiment Y88, simulation 1d
Total aqueous Sr (mg/L)
Elapsed Time (hr)
Observed
Simulated
0.0
0.1
0.2
0.3
0.4
0.5
0.6
1
10
100
1000

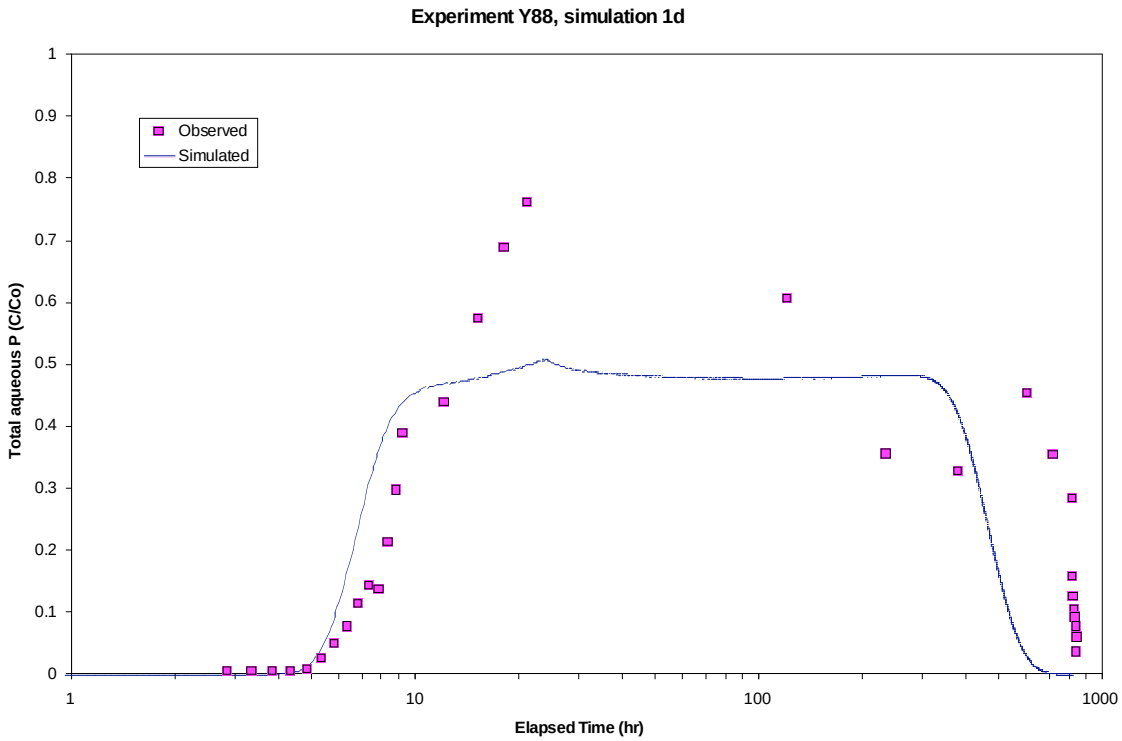
Experiment Y88, simulation 1d
Total aqueous P (C/Co)
Elapsed Time (hr)
Observed
Simulated
0
0.1
0.2
0.3
0.4
0.5
0.6
0.7
0.8
0.9
1
1
10
100
1000

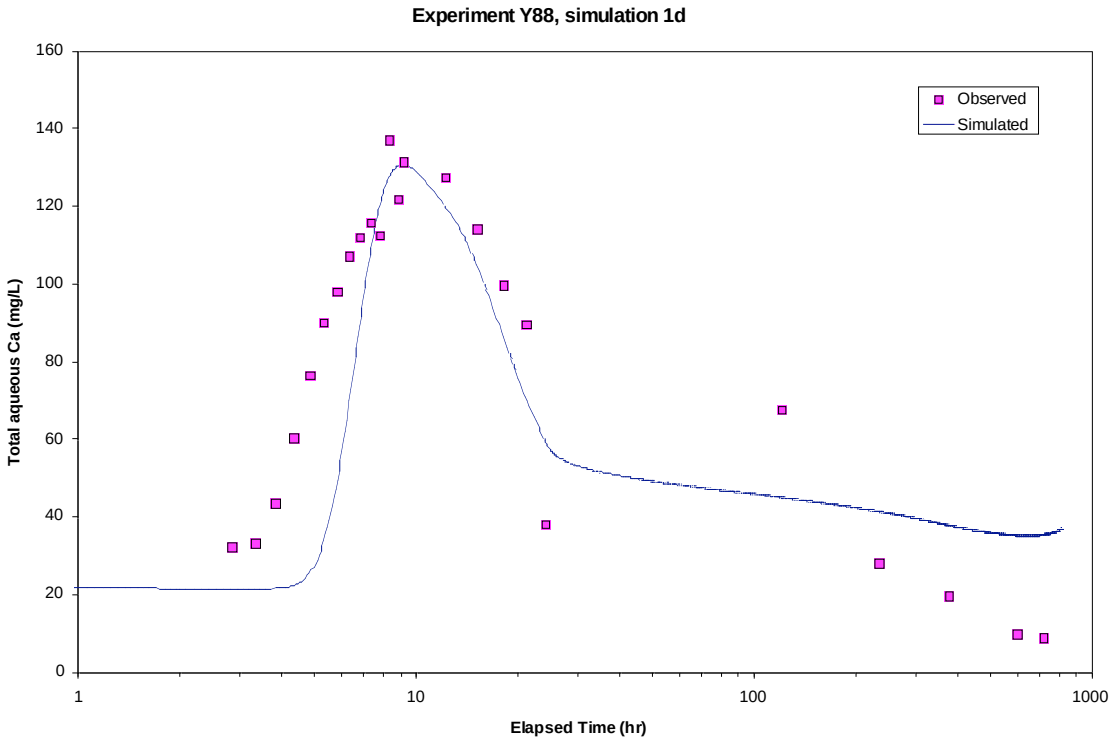
Experiment Y88, simulation 1d
Observed
Simulated
Total aqueous Ca (mg/L)
Elapsed Time (hr)
0
20
40
60
80
100
120
140
160
1
10
100
1000

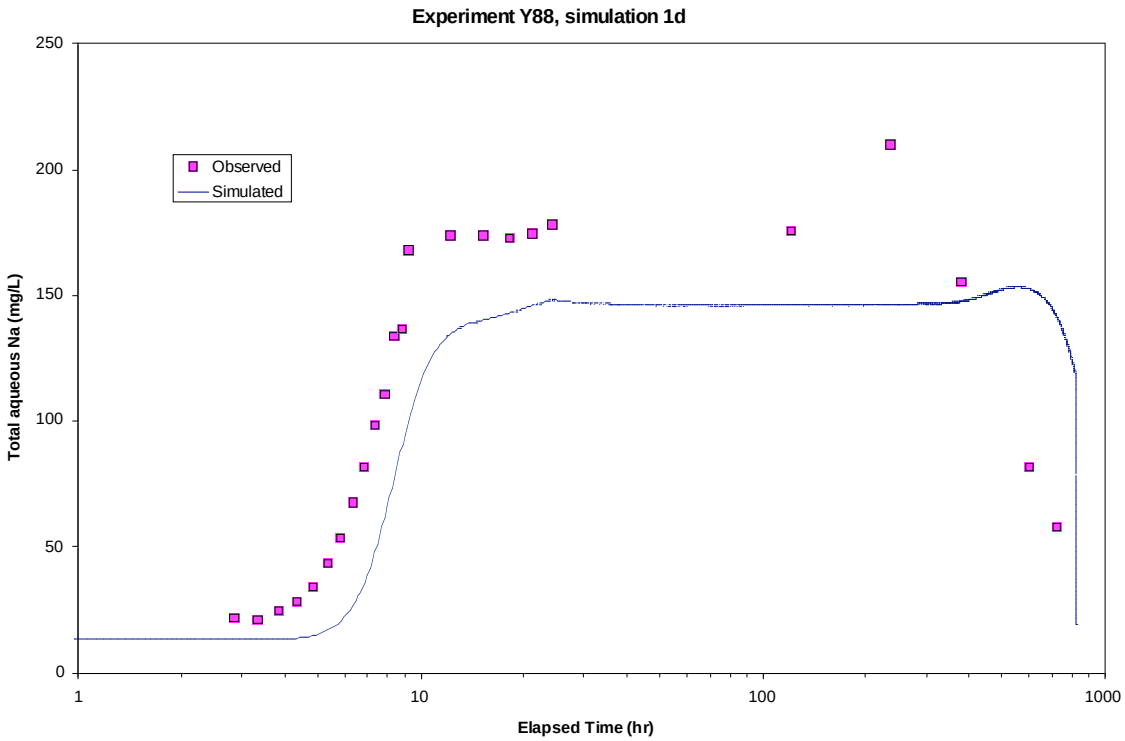
Experiment Y88, simulation 1d
Observed
Simulated
Total aqueous Na (mg/L)
Elapsed Time (hr)
0
50
100
150
200
250
1
10
100
1000

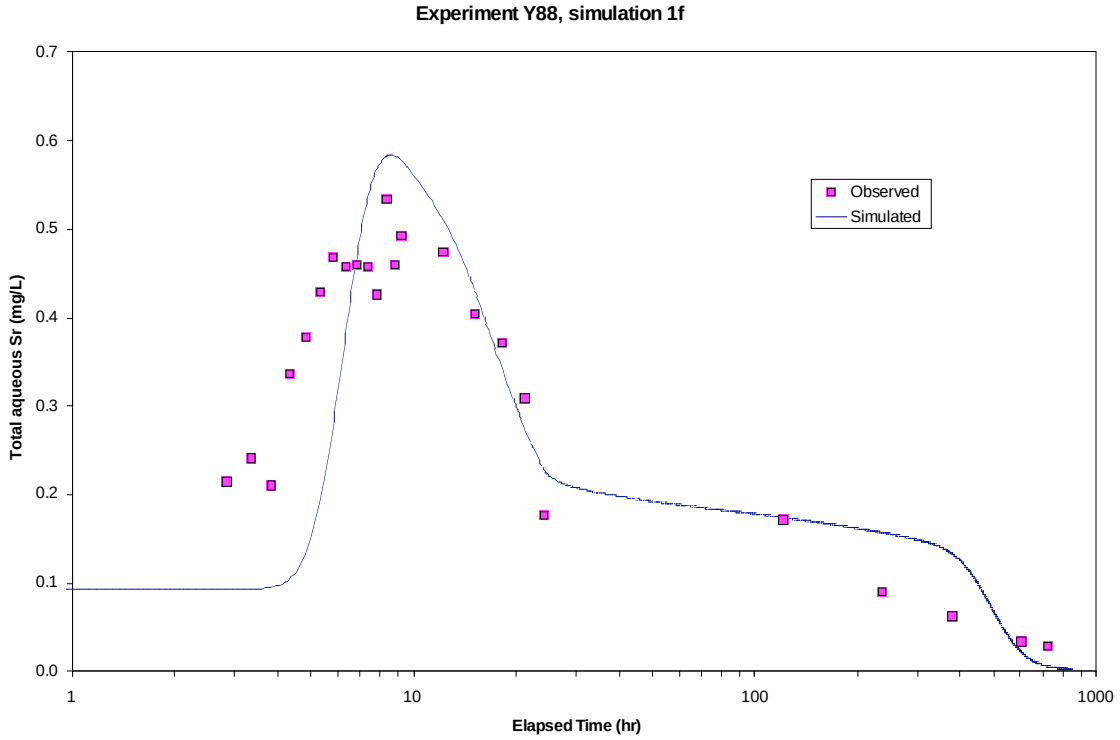
Experiment Y88, simulation 1f
Total aqueous Sr (mg/L)
Elapsed Time (hr)
Observed
Simulated
0.0
0.1
0.2
0.3
0.4
0.5
0.6
0.7
1
10
100
1000

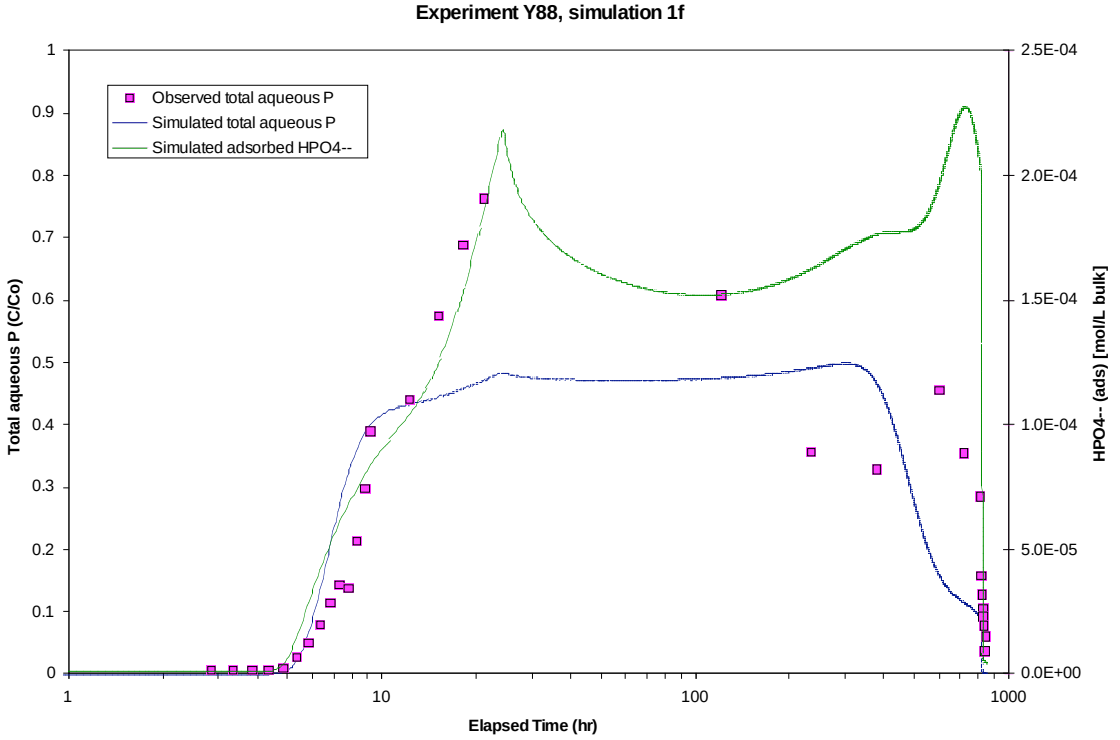
Experiment Y88, simulation 1f
Total aqueous P (C/Co)
HPO4-- (ads) [mol/L bulk]
Elapsed Time (hr)
Observed total aqueous P
Simulated total aqueous P
Simulated adsorbed HPO4--
0
0.1
0.2
0.3
0.4
0.5
0.6
0.7
0.8
0.9
1
0.0E+00
5.0E-05
1.0E-04
1.5E-04
2.0E-04
2.5E-04
1
10
100
1000

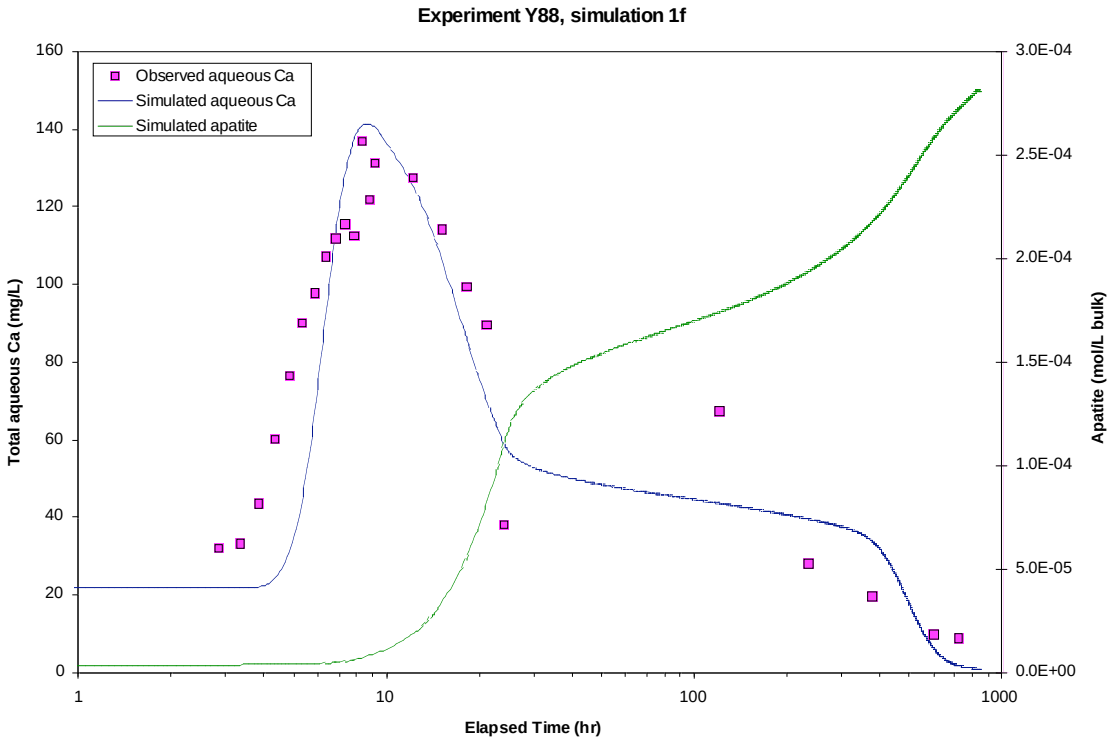
Experiment Y88, simulation 1f
Observed aqueous Ca
Simulated aqueous Ca
Simulated apatite
Total aqueous Ca (mg/L)
Apatite (mol/L bulk)
Elapsed Time (hr)
0
20
40
60
80
100
120
140
160
0.0E+00
5.0E-05
1.0E-04
1.5E-04
2.0E-04
2.5E-04
3.0E-04
1
10
100
1000

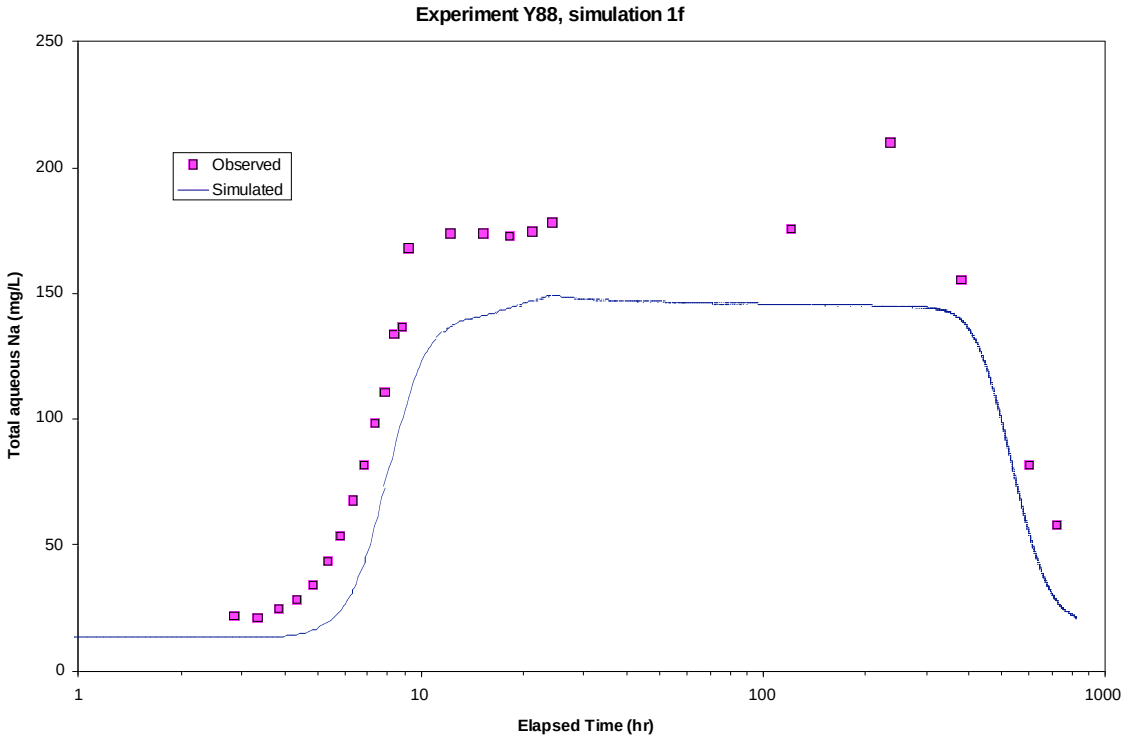
Experiment Y88, simulation 1f
Observed
Simulated
Total aqueous Na (mg/L)
Elapsed Time (hr)
0
50
100
150
200
250
1
10
100
1000

2-D Unsaturated Simulation of Ca-Citrate-PO_4 Infiltration – Laboratory Scale.
Fine-grained zone in coarse media (EMSL 2-D experiment).

Simulation 1: 0.4 cm/hour, steady-state aqueous saturation

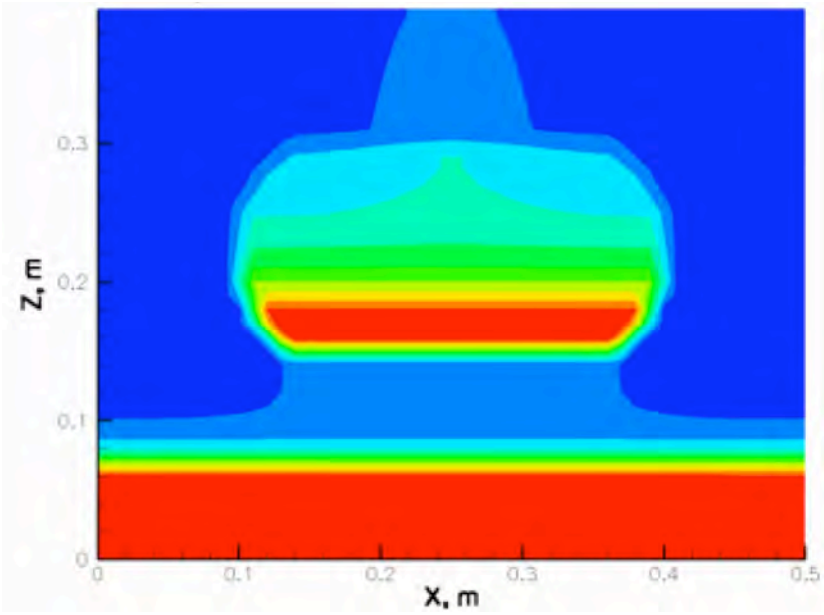

Simulation 2: 1.6 cm/hour, steady-state aqueous saturation

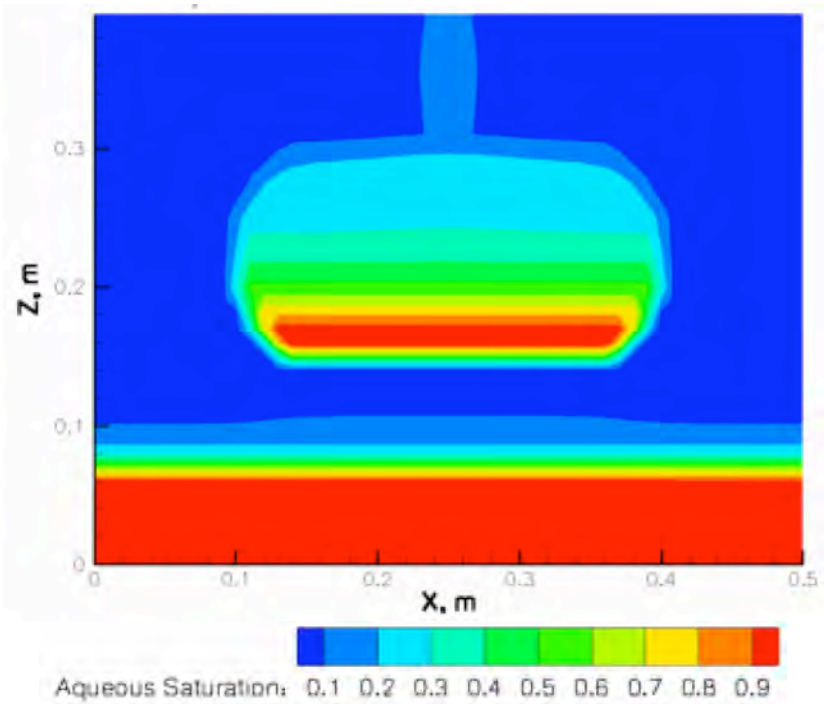

Simulation 1: 0.4 cm/hour, Ca-Citrate-PO_4 solution at 200 hours

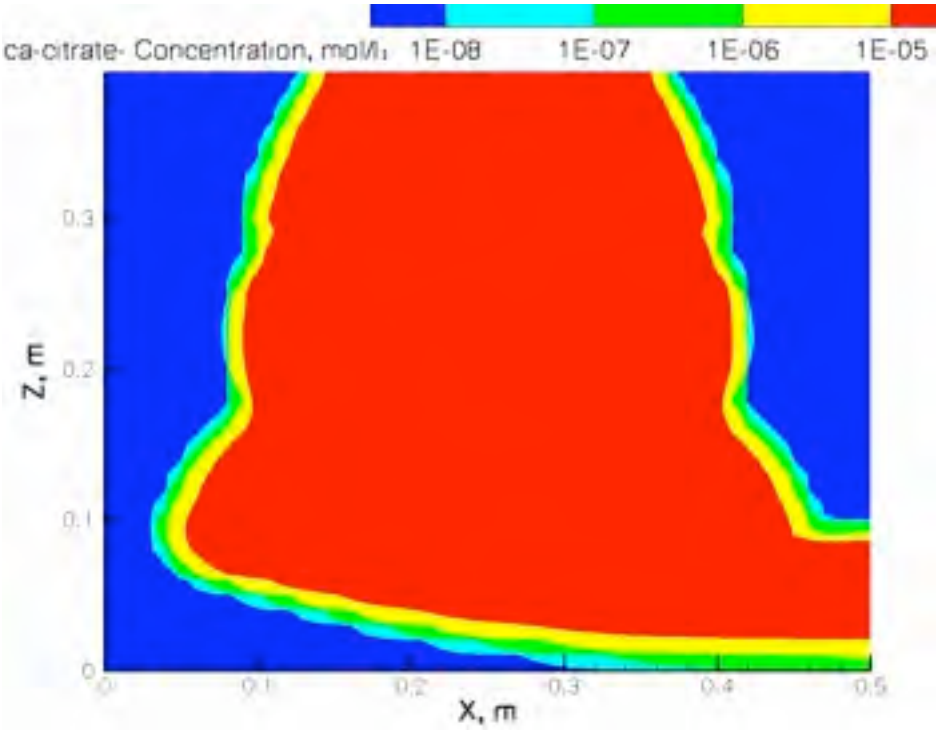

Simulation 1: 0.4 cm/hour, apatite concentration at 200 hours

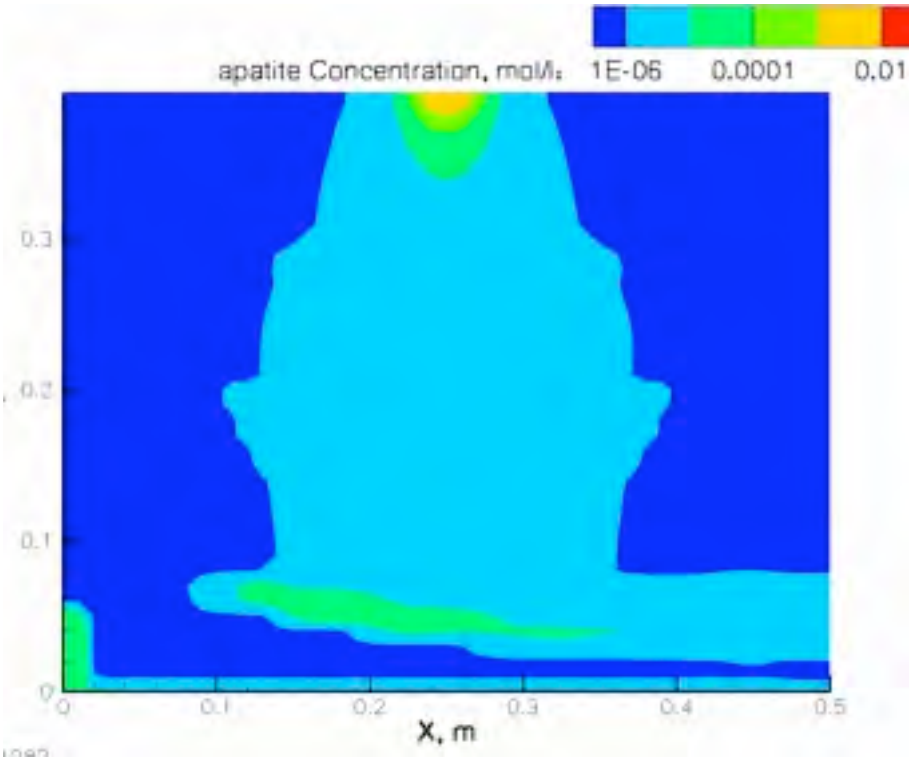

Simulation 2: 1.6 cm/hour, apatite concentration at 200 hours

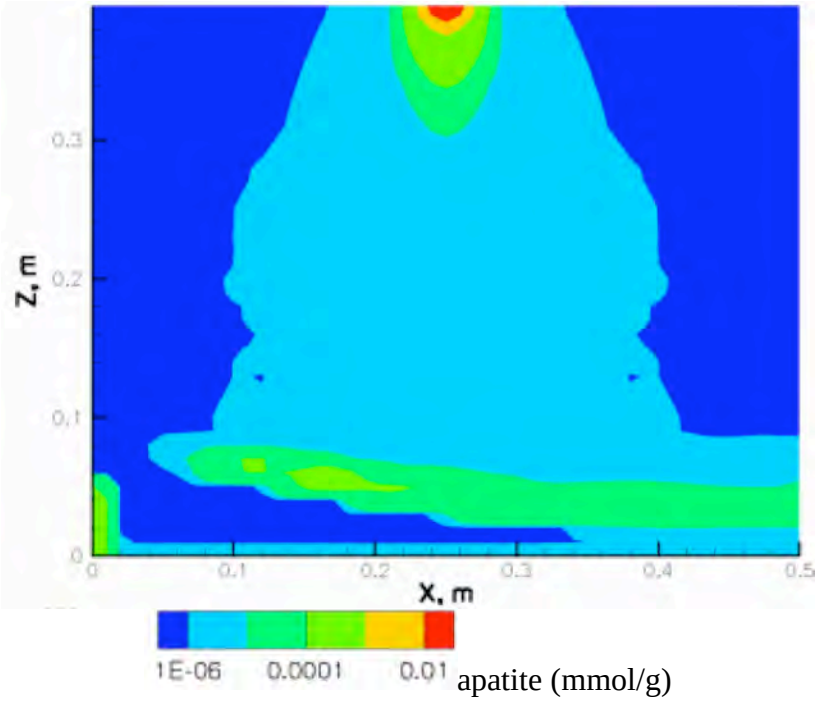

apatite (mmol/g)

Simulation 2: 1.6 cm/hour, microbial biomass at 200 hours

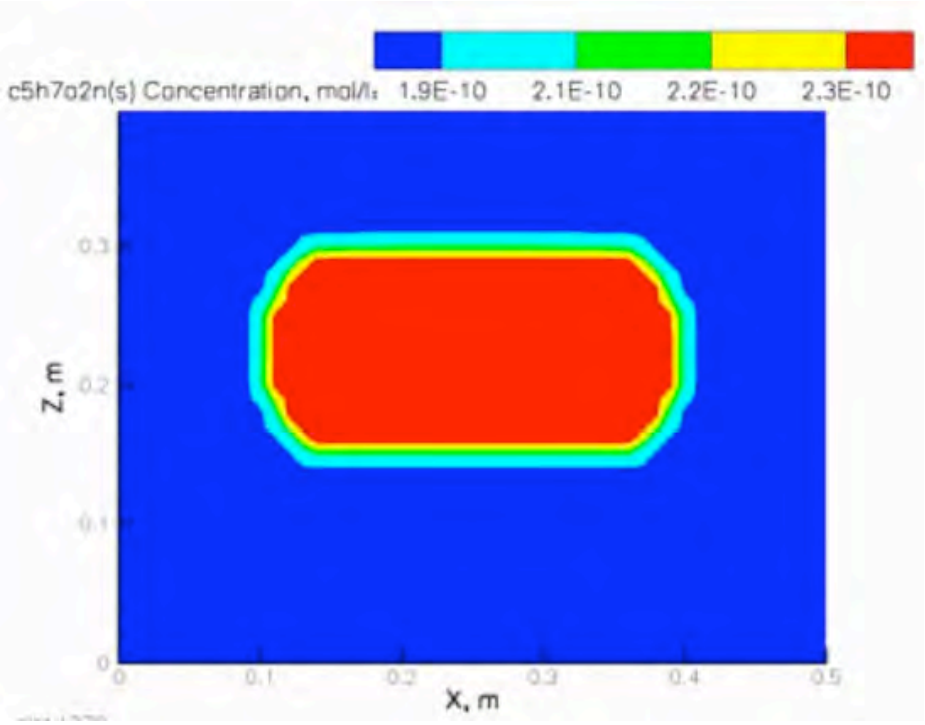

2-D Unsaturated Simulation of Ca-Citrate-PO_4 Infiltration – Laboratory Scale.
Coarse-grained zone in fine media.

Simulation 3: 0.4 cm/hour, steady-state aqueous saturation

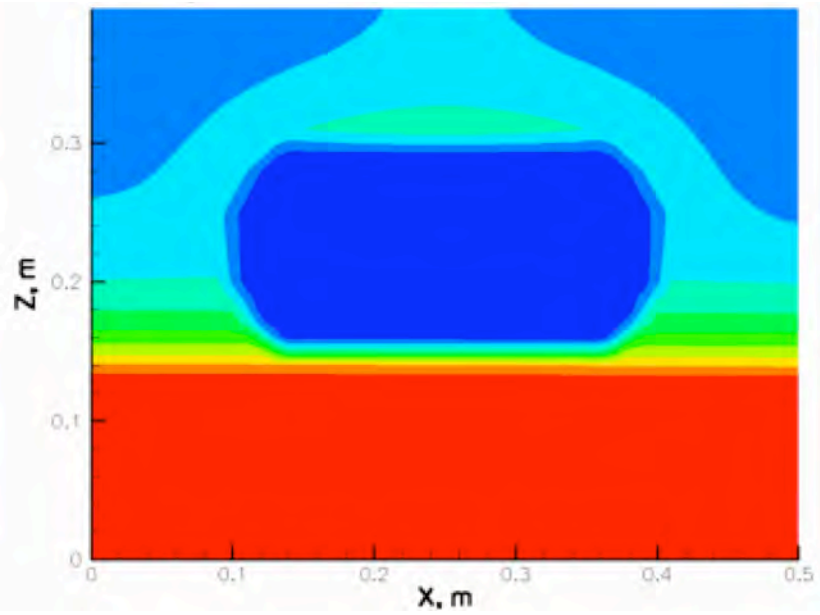

Simulation 4: 1.6 cm/hour, steady-state aqueous saturation

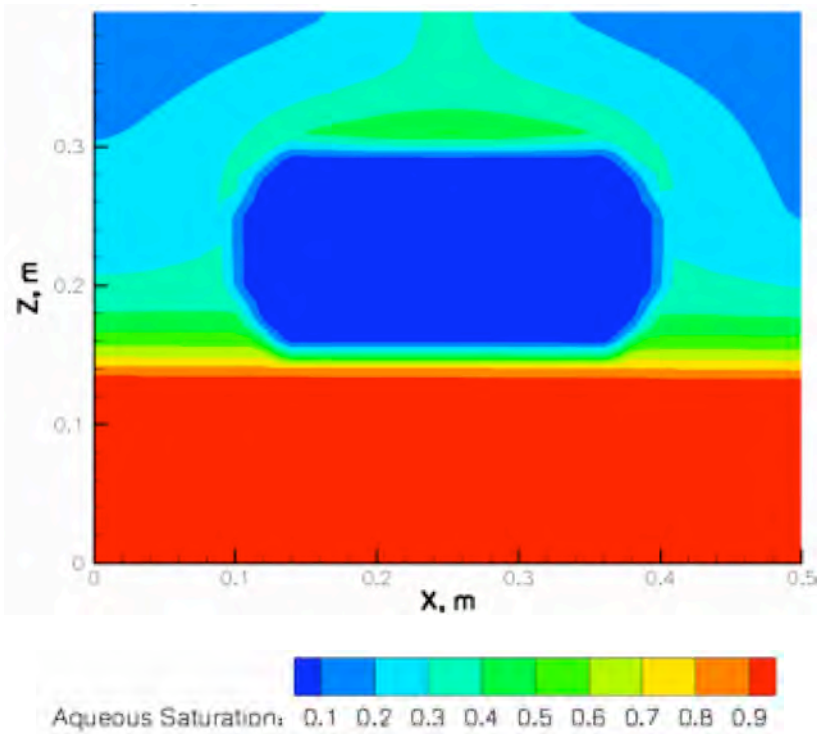

Simulation 3: 0.4 cm/hour, Ca-citrate-PO_4 solution concentration at 200 hours

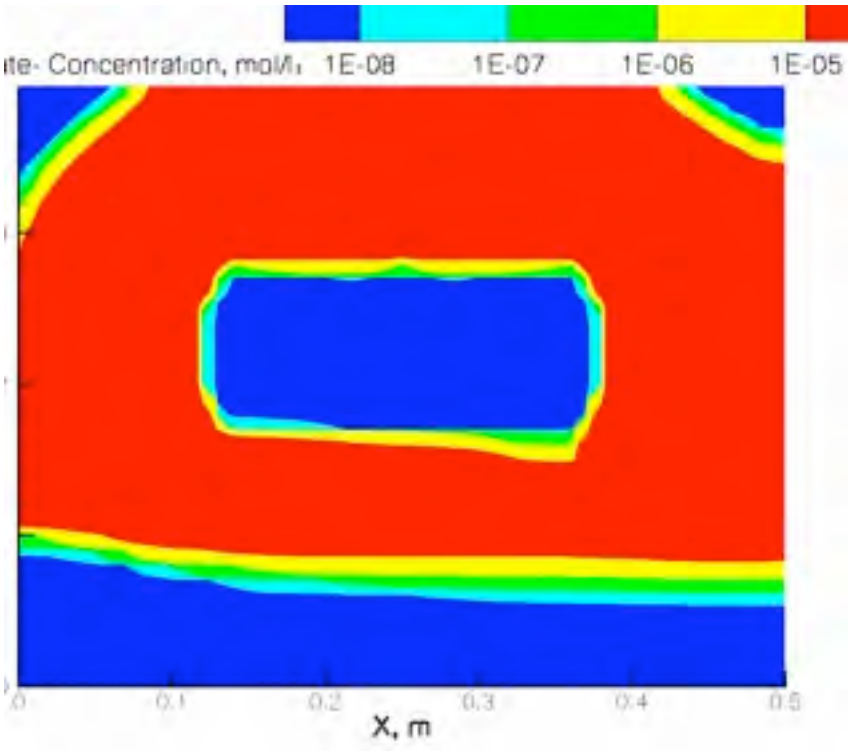

Simulation 3: 0.4 cm/hour, apatite concentration at 200 hours (mmol/g)

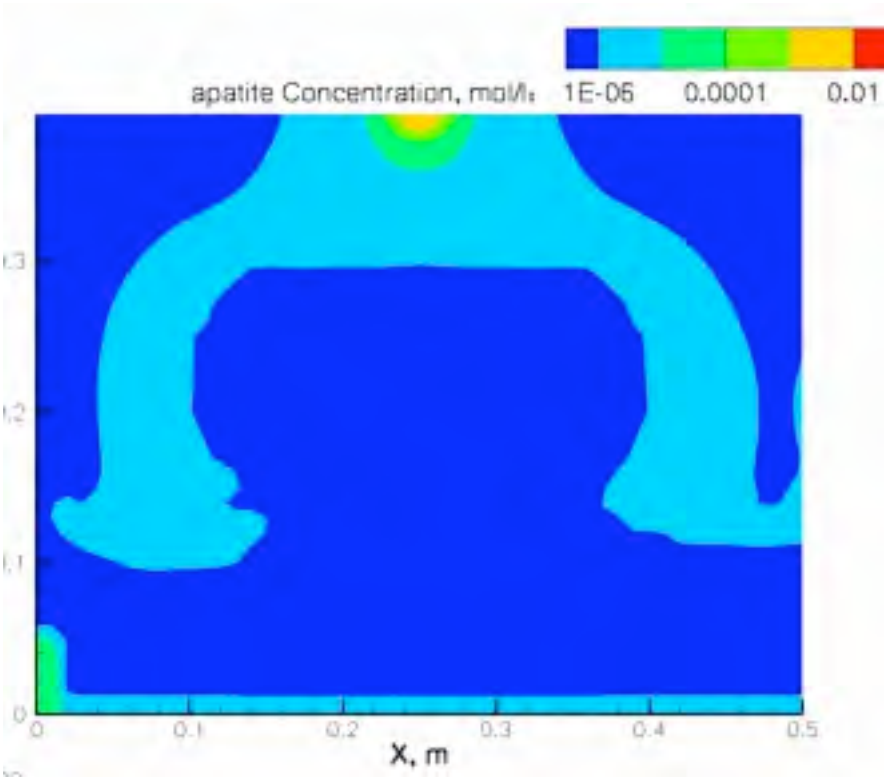

Simulation 4: 1.6 cm/hour, apatite concentration at 200 hours (mmol/g)

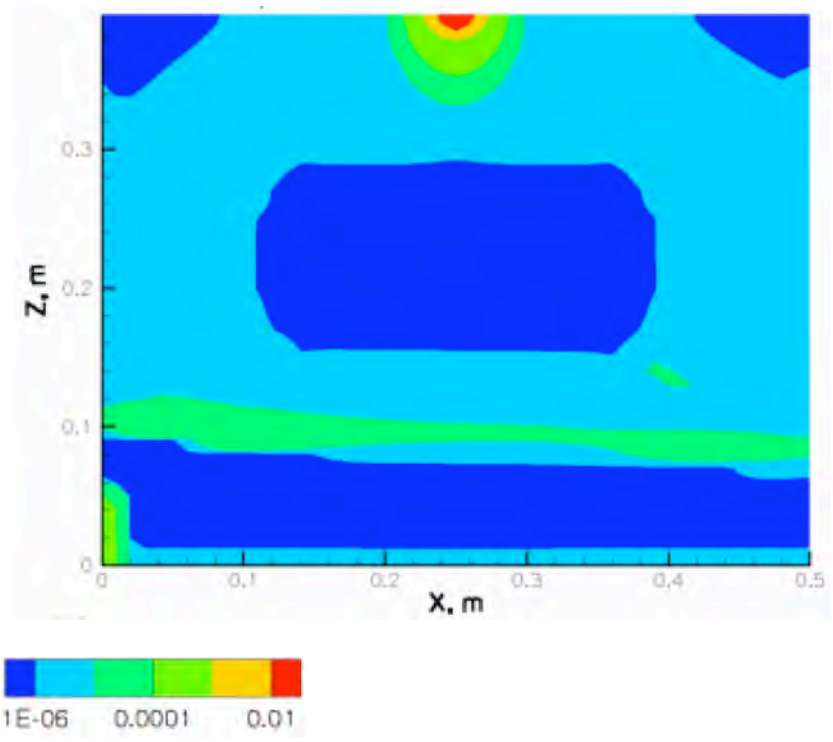

Simulation 4: 1.6 cm/hour, microbial biomass at 200 hours

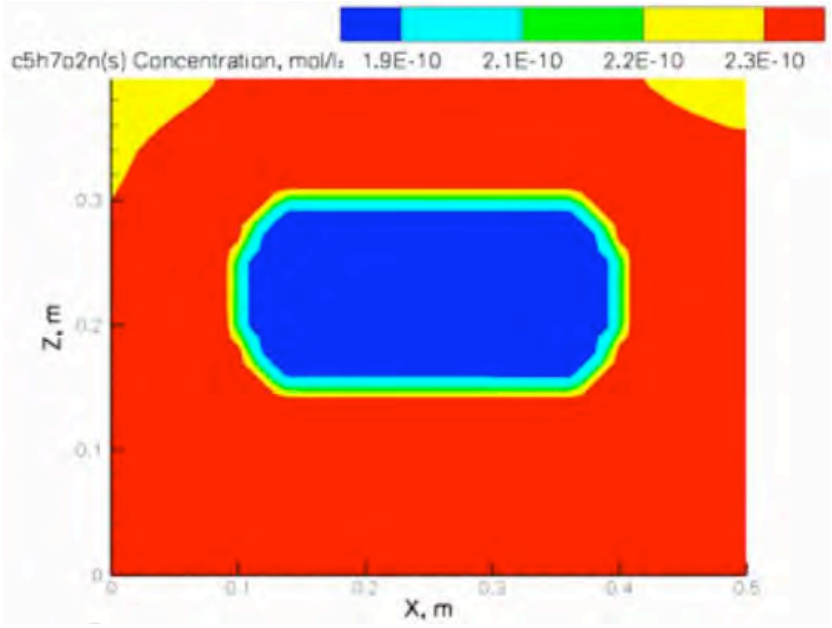

1-D Steady-state infiltration rate versus water saturation.
Green = 0.01 in./hour, red = 0.1 in./hour, blue = 1.0 in./hour

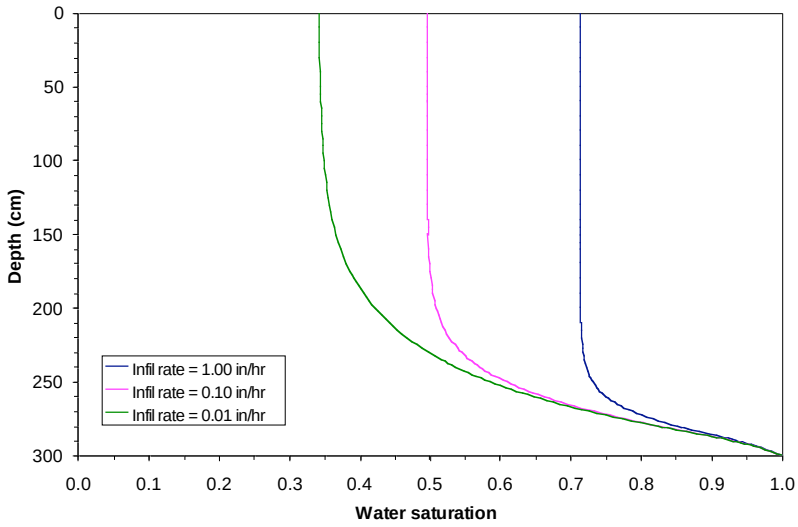

2-D Field Scale Simulation (2006) with only a few reactions:

1. citrate biodegradation
2. apatite precipitation
3. PO_4 sorption
4. cation ion exchange not included, K_d used.

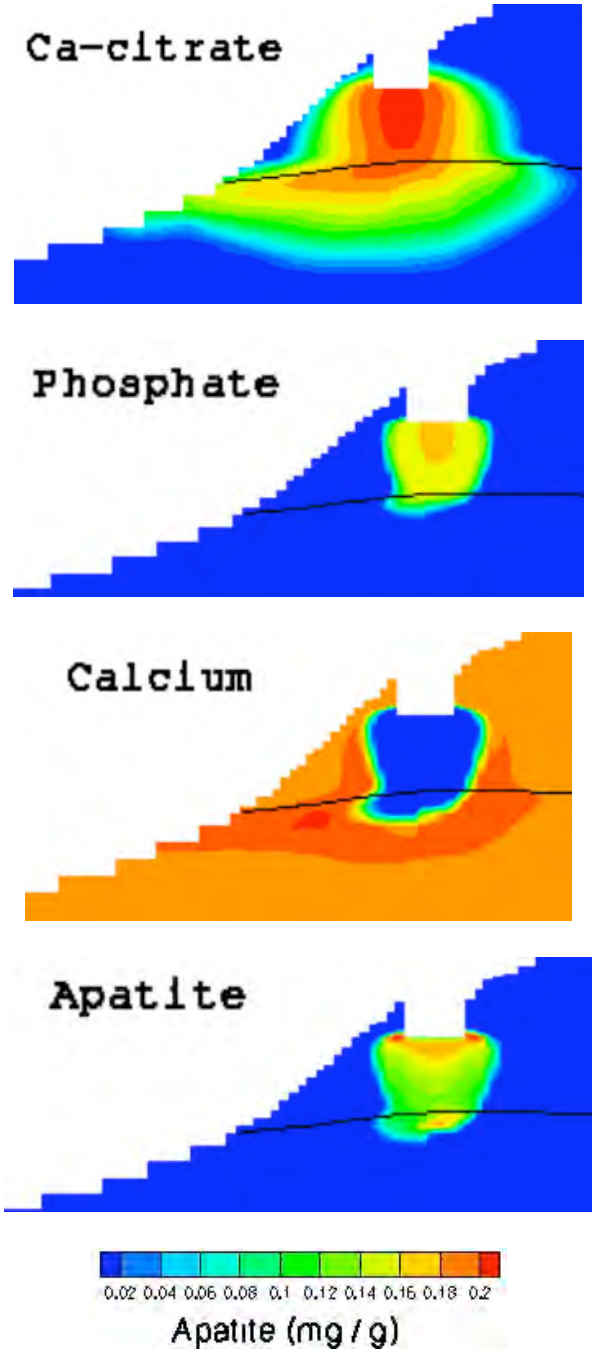

2-D Field Scale Simulation (2006) with only a few reactions: 0.1 cm/hour rate

2 days

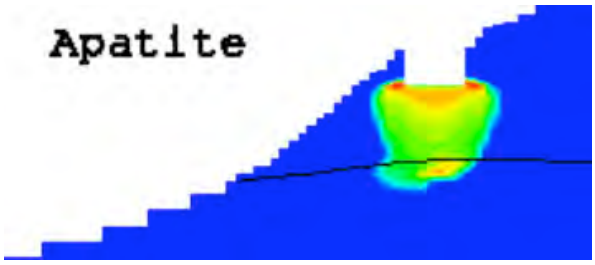

4 days

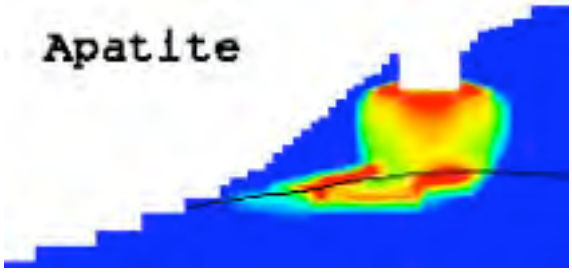

8 days

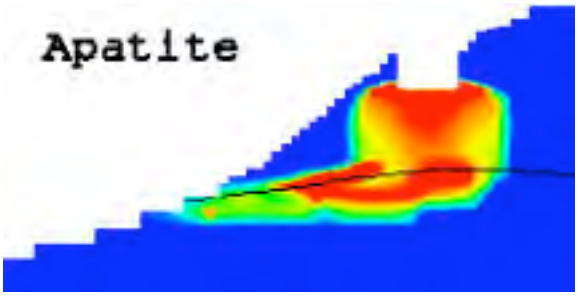

16 days

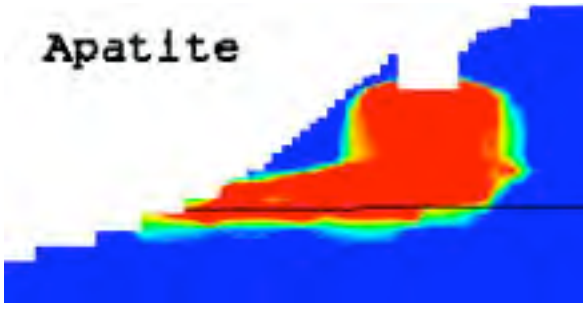

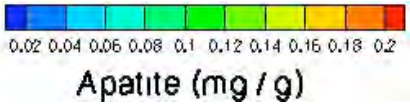

2-D Field Scale Simulation (2006) with only a few reactions: 1.0 cm/hour rate (ponded)

2 days

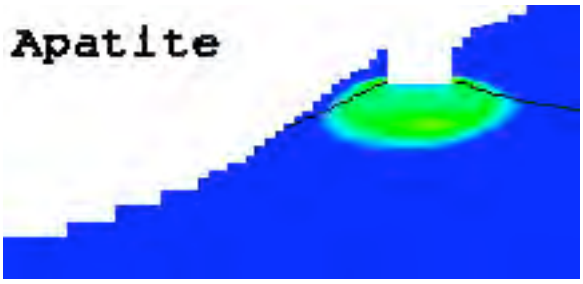

4 days

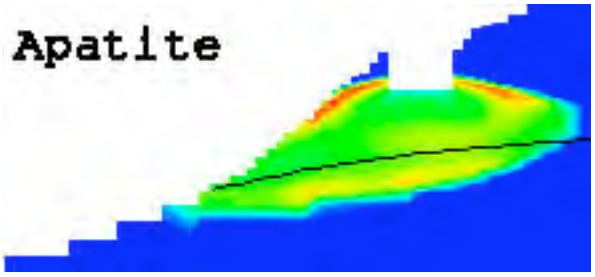

8 days

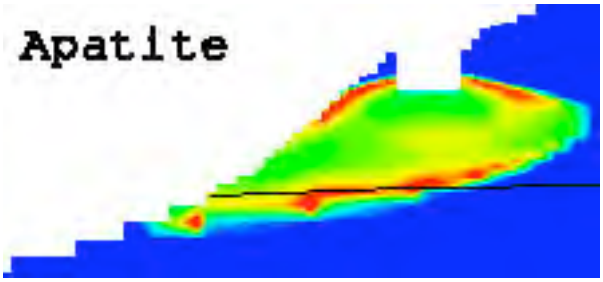

16 days

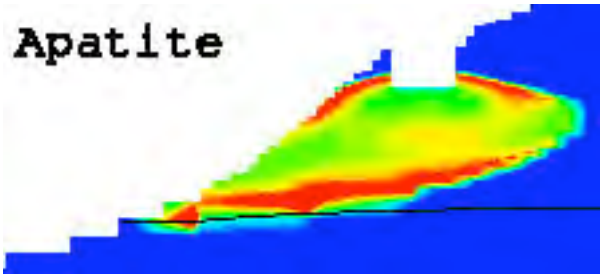

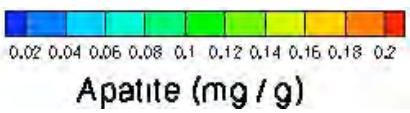

A.8 Task 5 – 2-D Infiltration Experiments of Ca-Citrate-PO4 Solution

Y125. 2-D Infiltration of 10 mM Ca-citrate-PO_4 solution, 8.33 mL/hour, 17.1 hours. Initial uniform water content, 0.036 g/g.

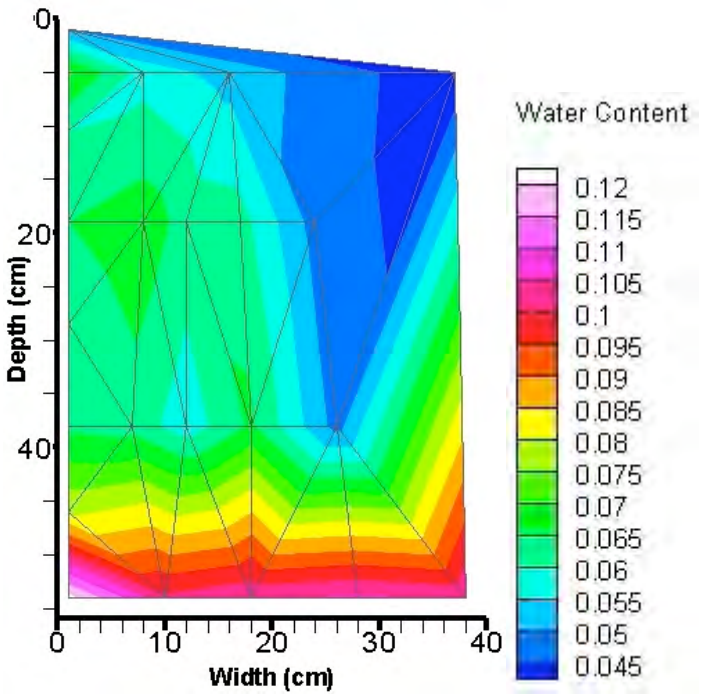

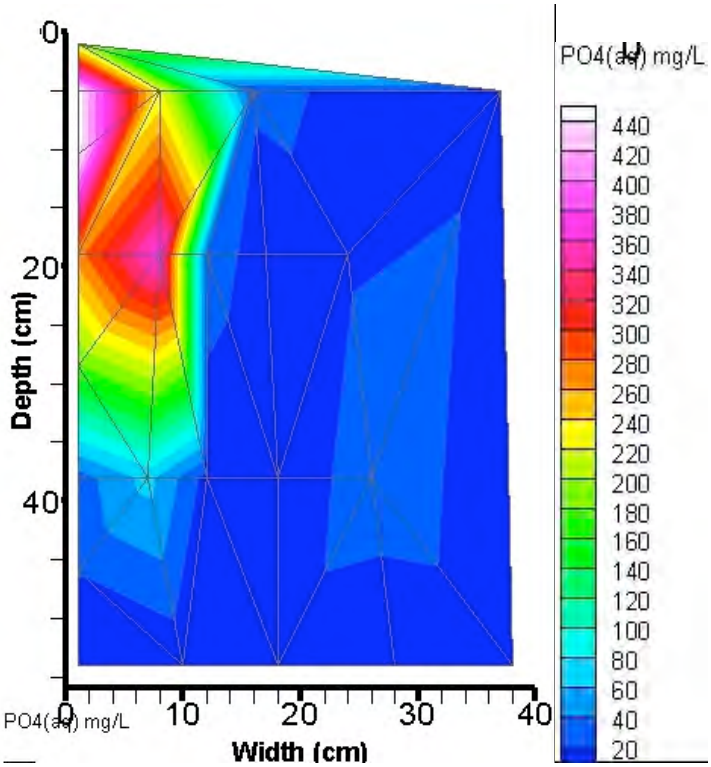

Y125.

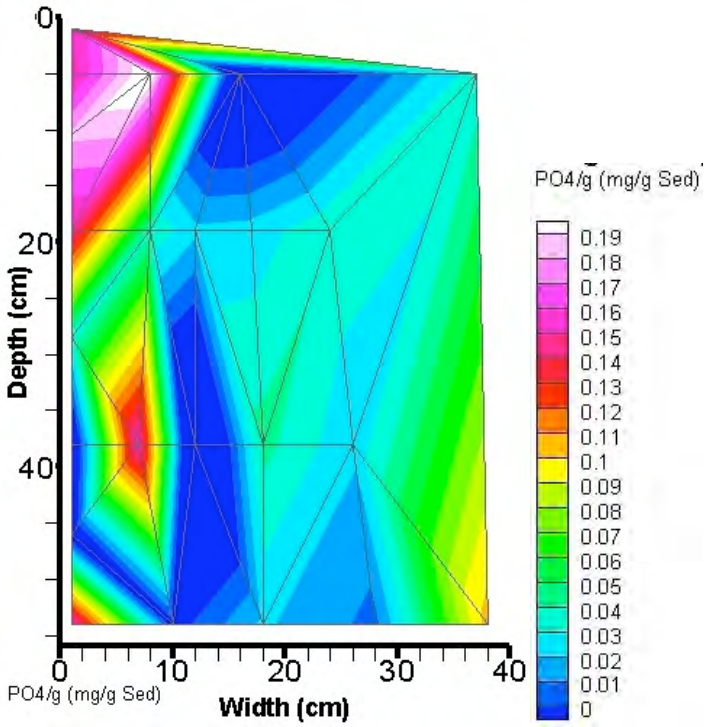
0
20
40
Depth (cm)
0
10
20
30
40
Width (cm)
PO4/g (mg/g Sed)
PO4/g (mg/g Sed)
0.19
0.18
0.17
0.16
0.15
0.14
0.13
0.12
0.11
0.1
0.09
0.08
0.07
0.06
0.05
0.04
0.03
0.02
0.01
0

Y126. 2-D Infiltration of 10 mM Ca-citrate-PO_4 solution, 3.32 mL/hour, 44 hours. Initial uniform water content, 0.015 g/g.

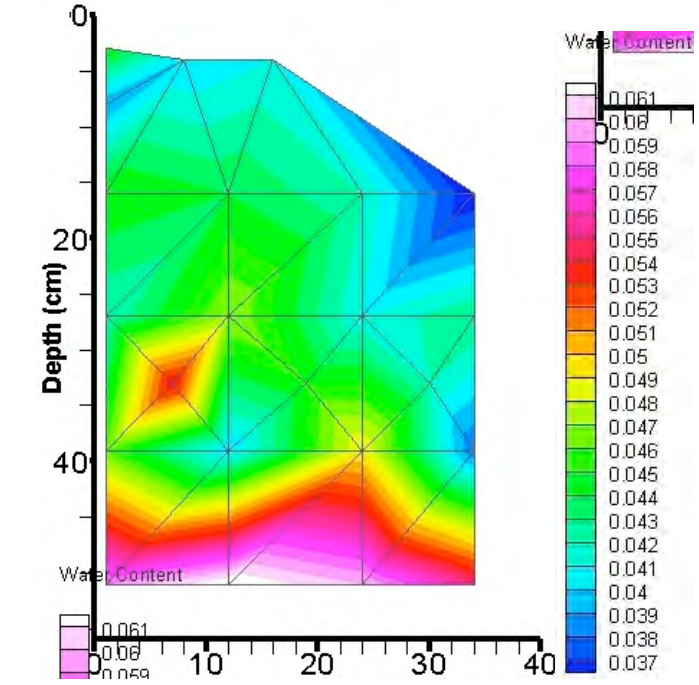

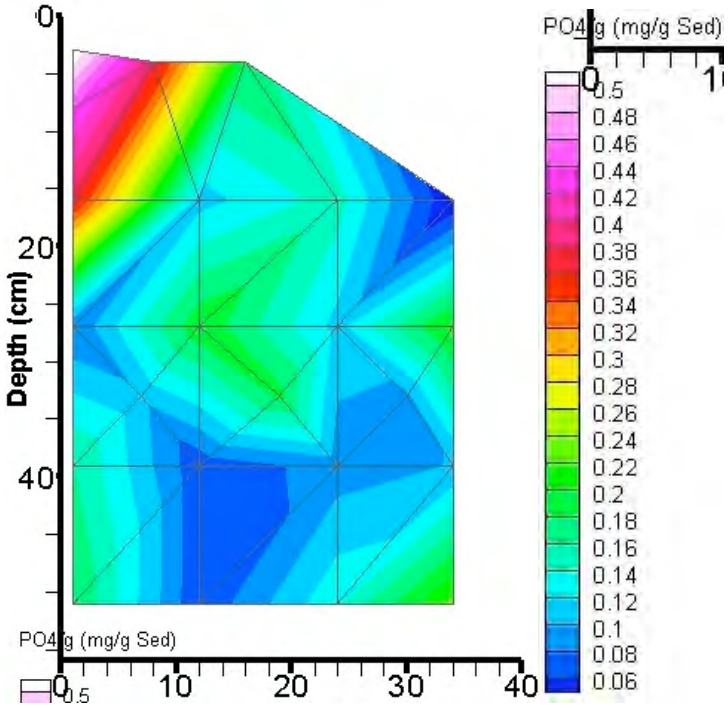

Y126.

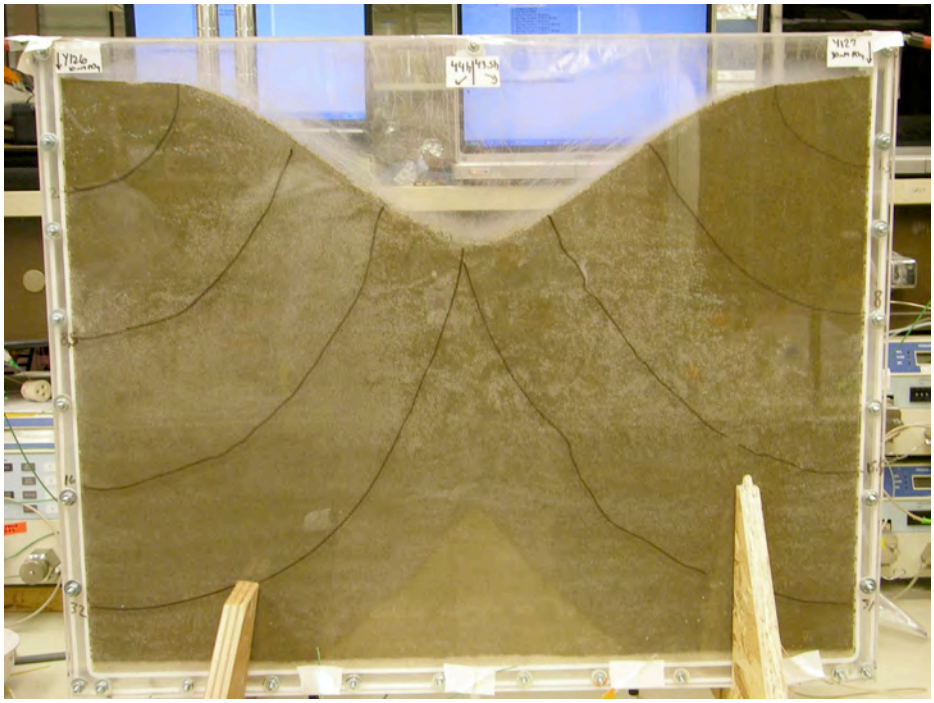

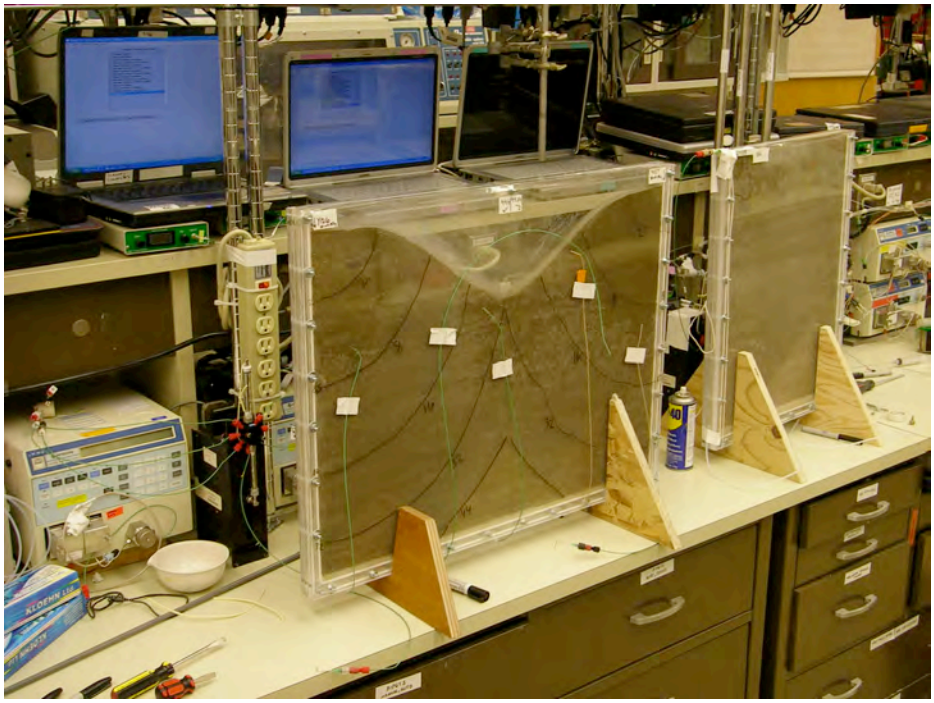

Y127. 2-D Infiltration of 30 mM Ca-citrate-PO_4 solution, 3.32 mL/hour, 44 hours. Initial uniform water content, 0.015 g/g.

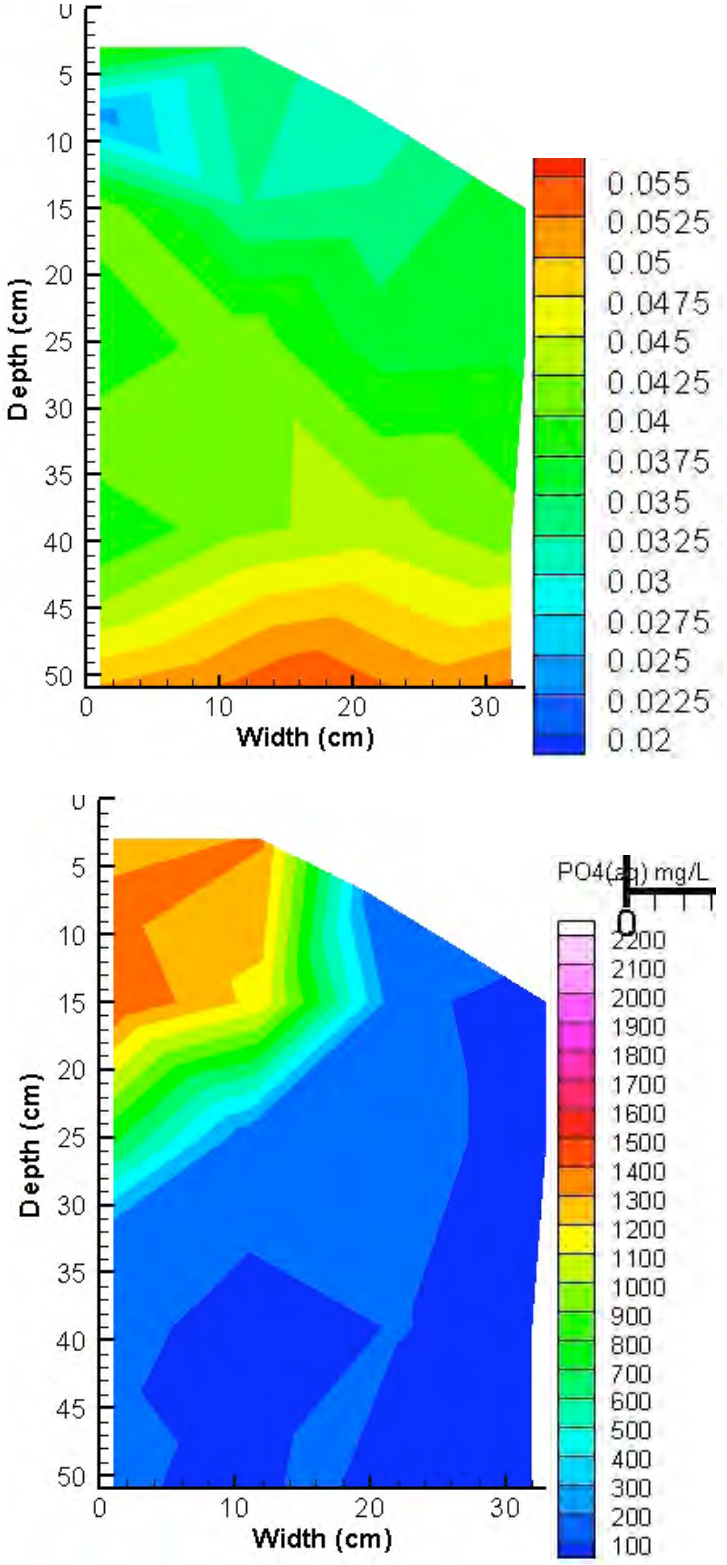

Y127.

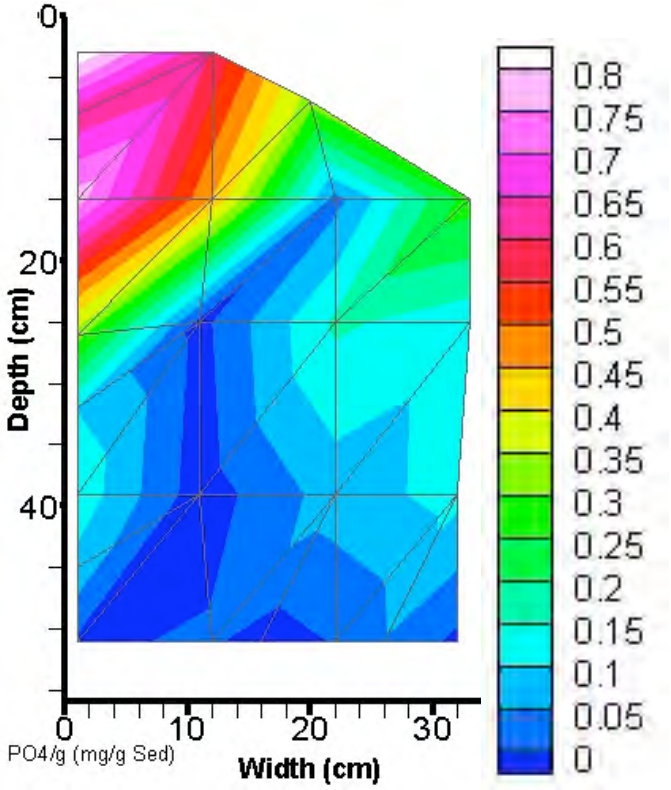
0
20
40
Depth (cm)
0
10
20
30
Width (cm)
PO4/g (mg/g Sed)
0.8
0.75
0.7
0.65
0.6
0.55
0.5
0.45
0.4
0.35
0.3
0.25
0.2
0.15
0.1
0.05
0

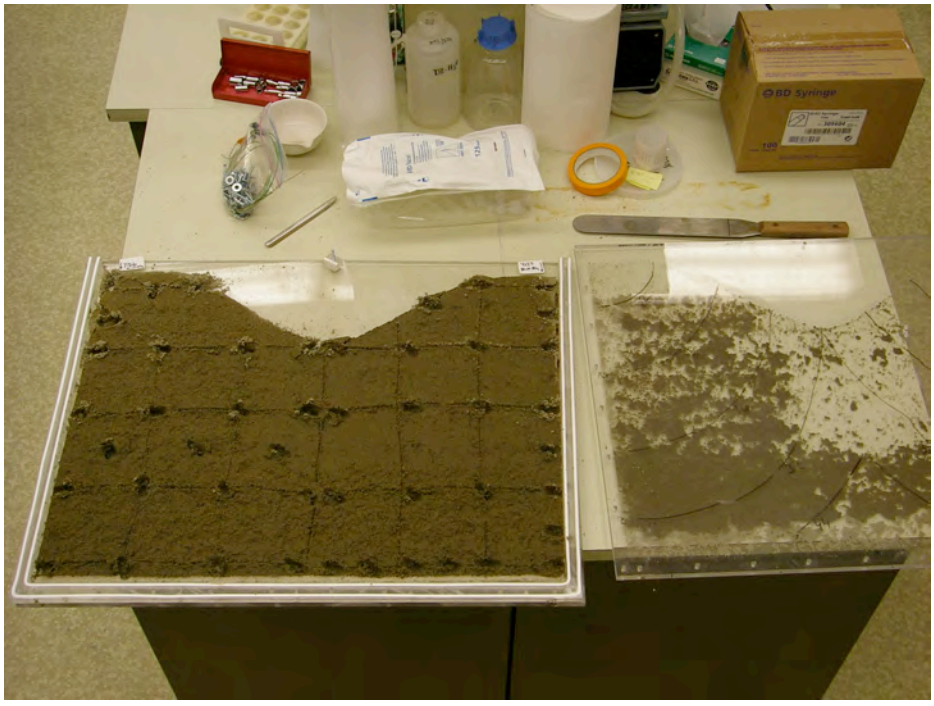

Y128. 2-D Infiltration of 7.4 mM Ca-citrate-PO_4 solution, 0.913 mL/hour, 113 hours. Initial uniform water content, 0.014 g/g.

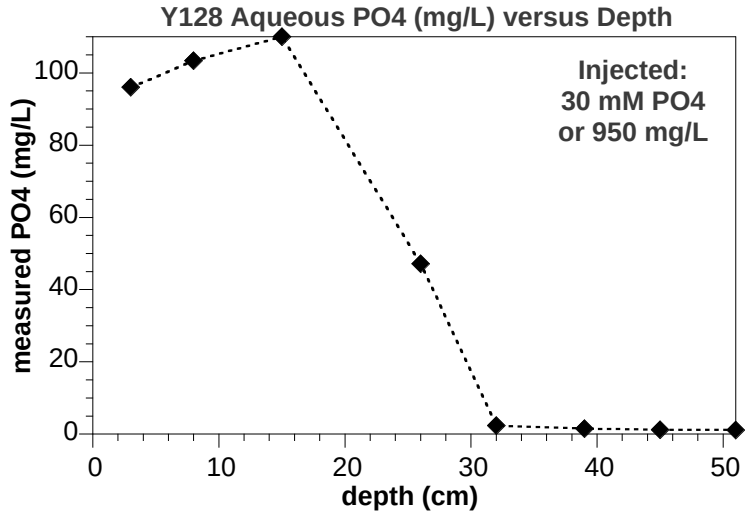

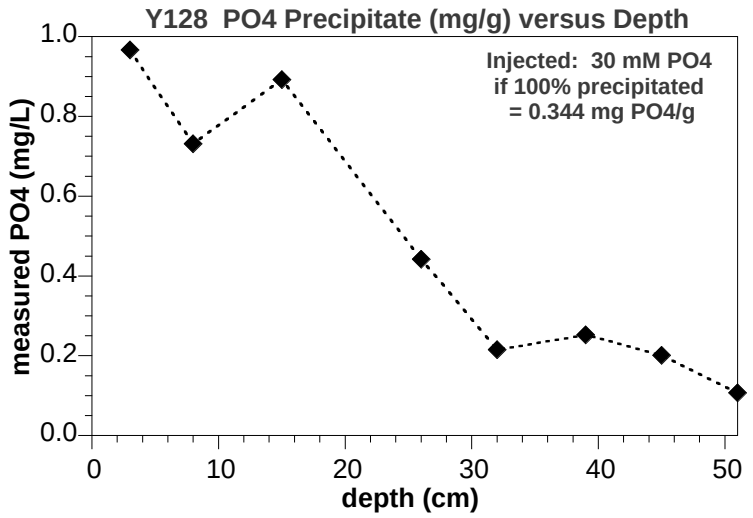

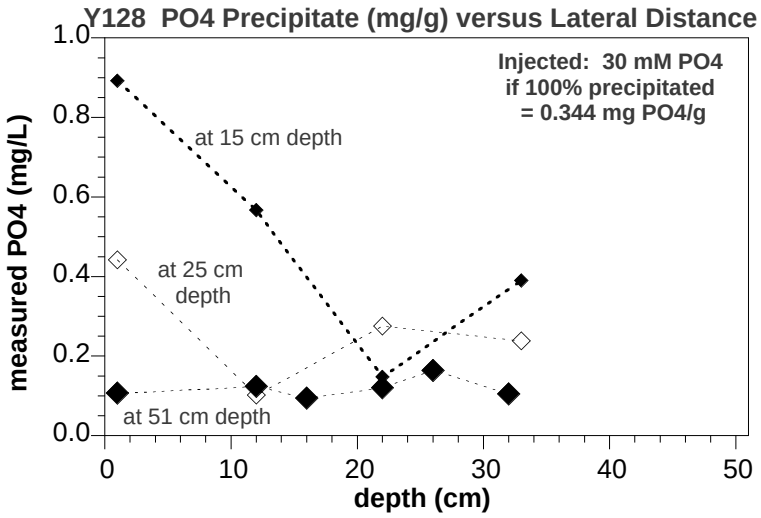

Y128.

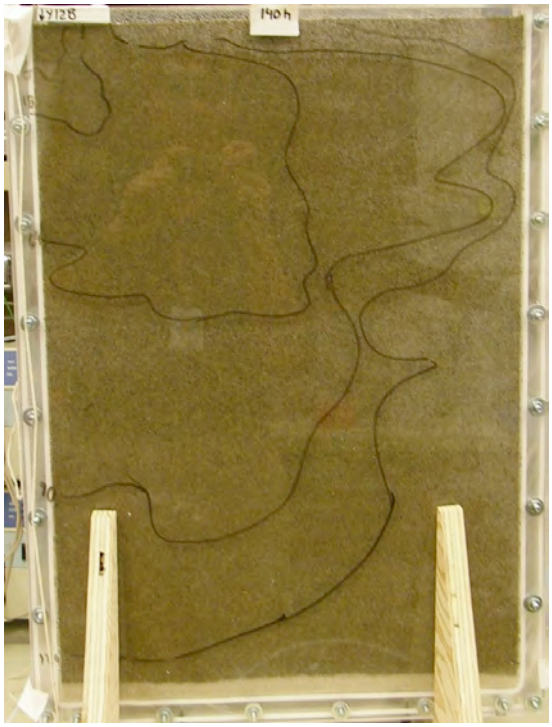

Y129. 2-D Infiltration of 30 mM Ca-citrate-PO_4 solution, 0.706 mL/hour, 281 hours. Initial uniform water content, 0.0148 g/g.

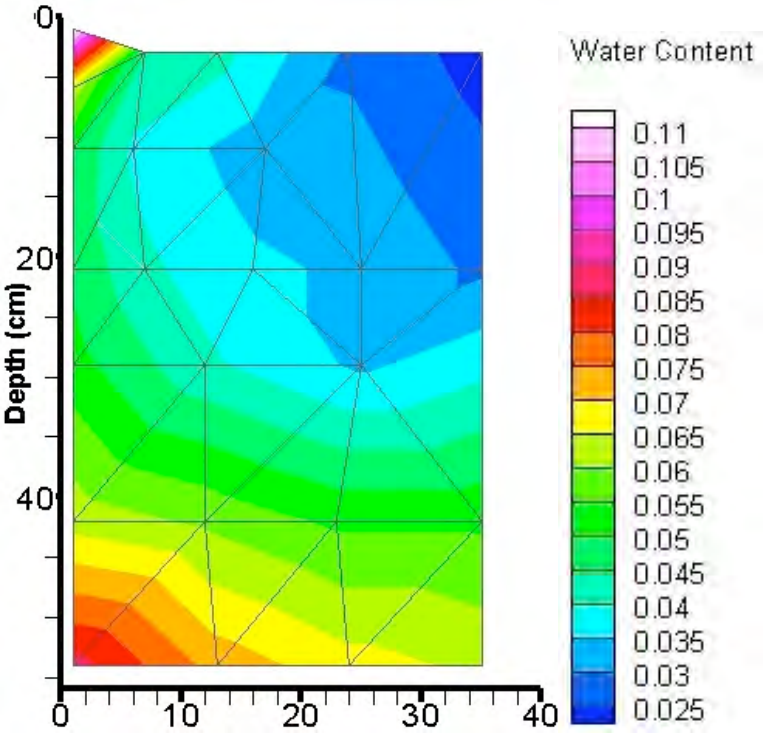

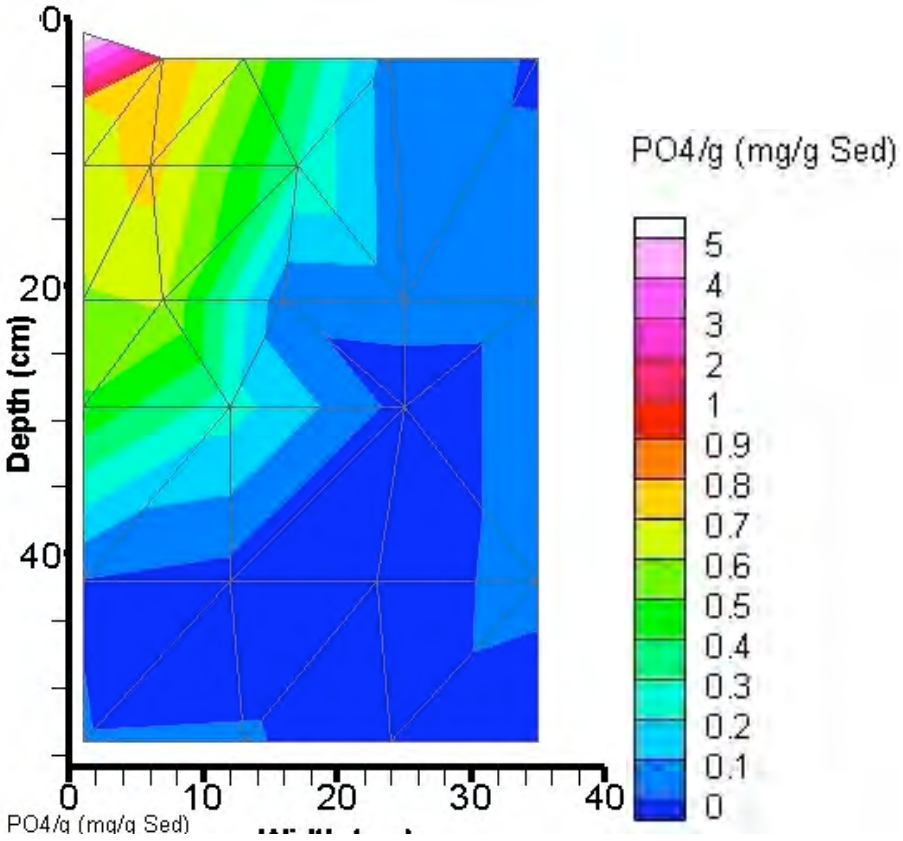

Y129.

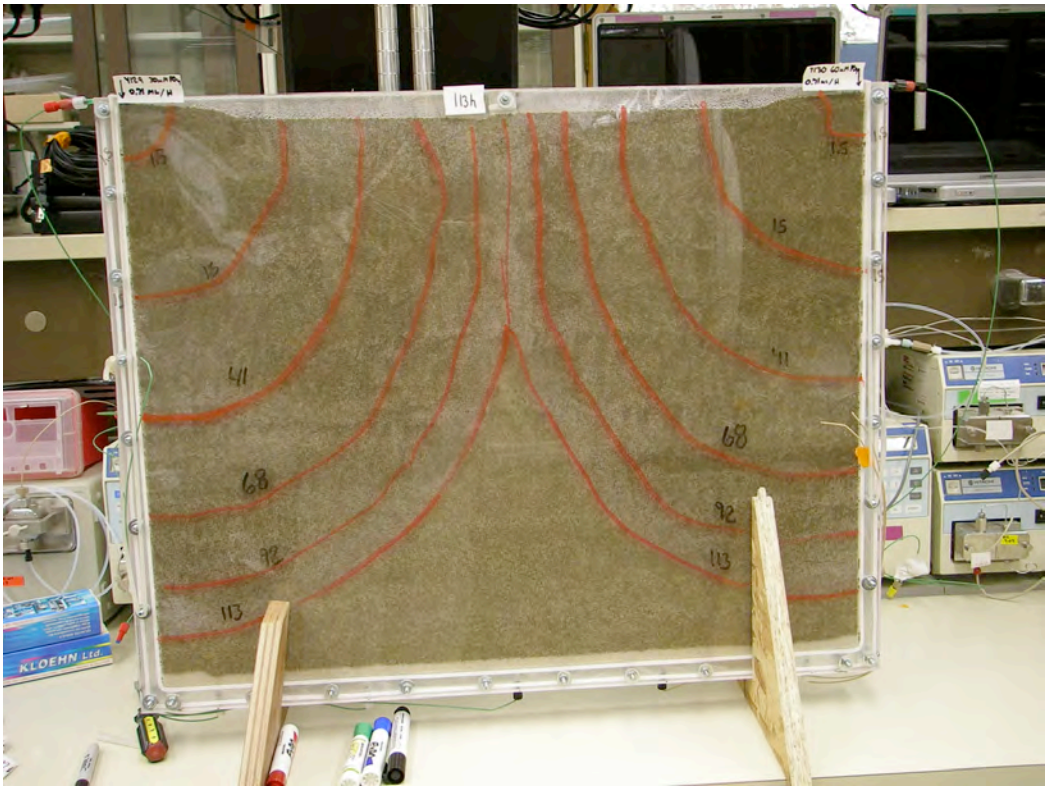

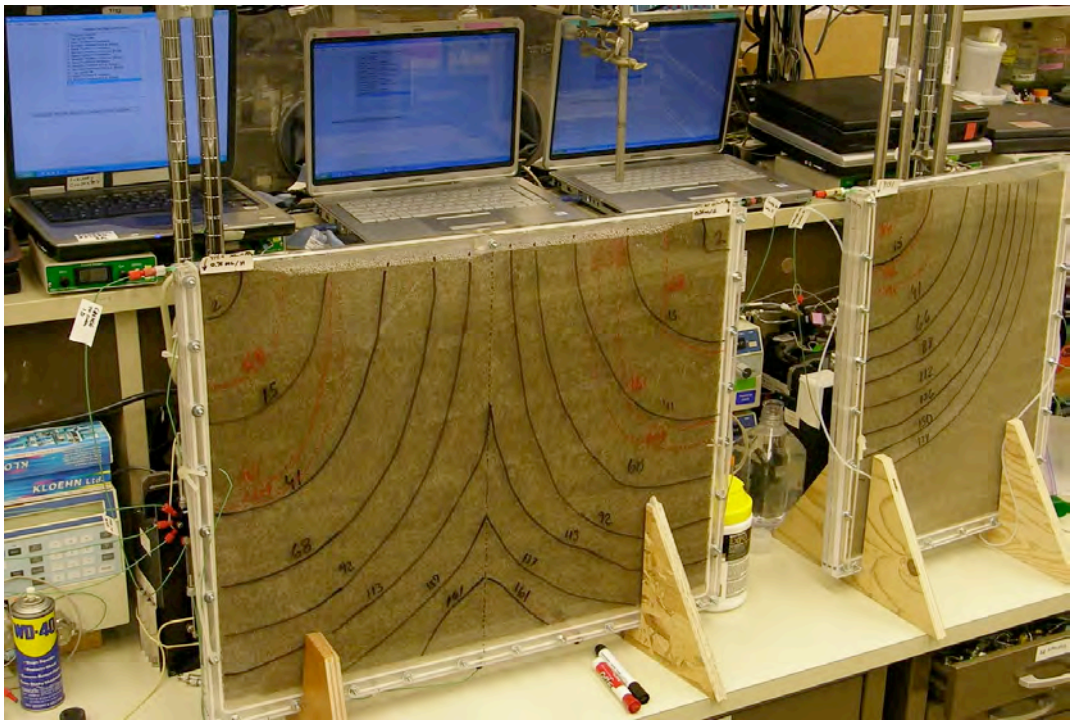

Y130. 2-D Infiltration of 60 mM Ca-citrate-PO_4 solution, 0.706 mL/hour, 281 hours. Initial uniform water content, 0.0148 g/g.

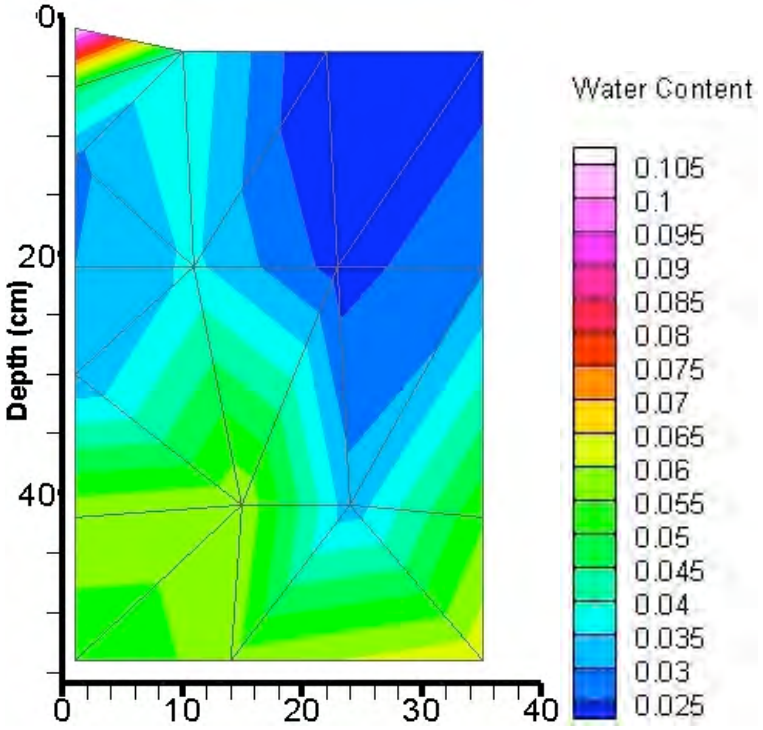

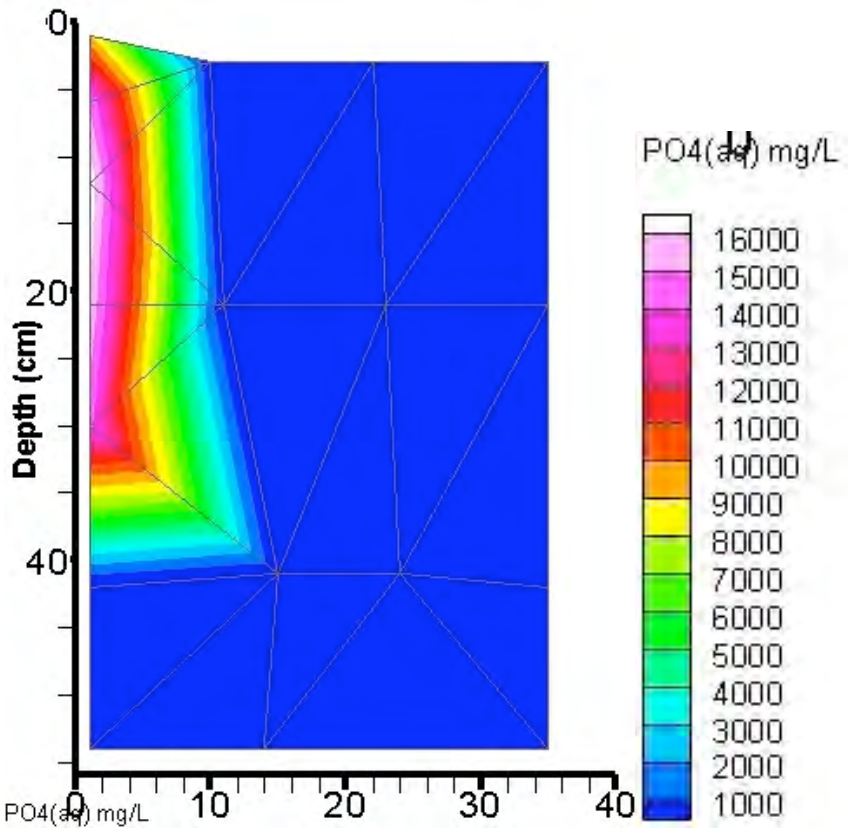

Y130.

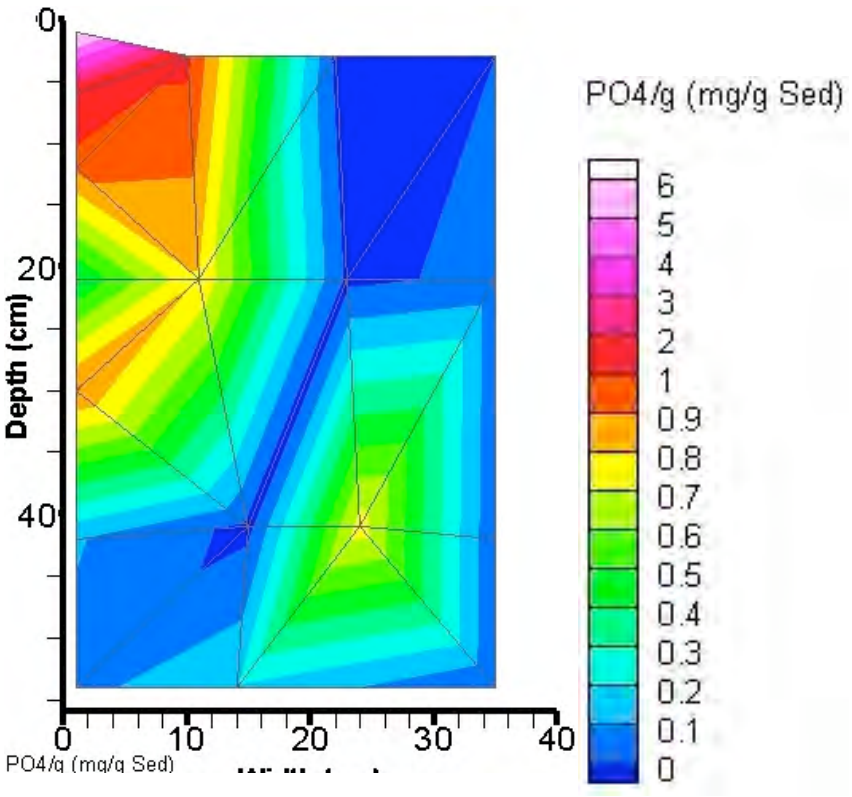
PO4/g (mg/g Sed)
6
5
4
3
2
1
0.9
0.8
0.7
0.6
0.5
0.4
0.3
0.2
0.1
0
Depth (cm)
0
20
40
0
10
20
30
40
PO4/g (mg/g Sed)

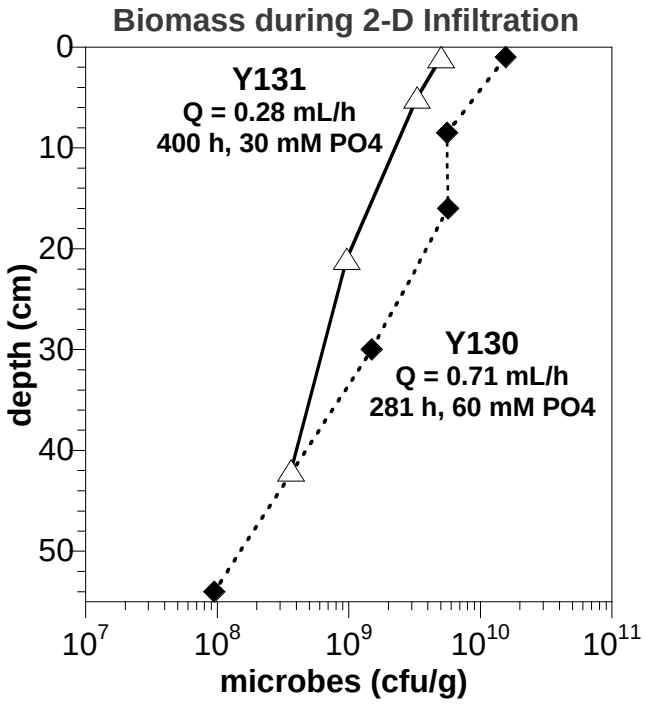
Biomass during 2-D Infiltration
Y131
Q = 0.28 mL/h
400 h, 30 mM PO4
Y130
Q = 0.71 mL/h
281 h, 60 mM PO4
depth (cm)
0
10
20
30
40
50
10^7
10^8
10^9
10^{10}
10^{11}
microbes (cfu/g)

Y131. 2-D Infiltration of 30 mM Ca-citrate-PO_4 solution, 0.28 mL/hour, 430 hours. Initial uniform water content, 0.0148 g/g.

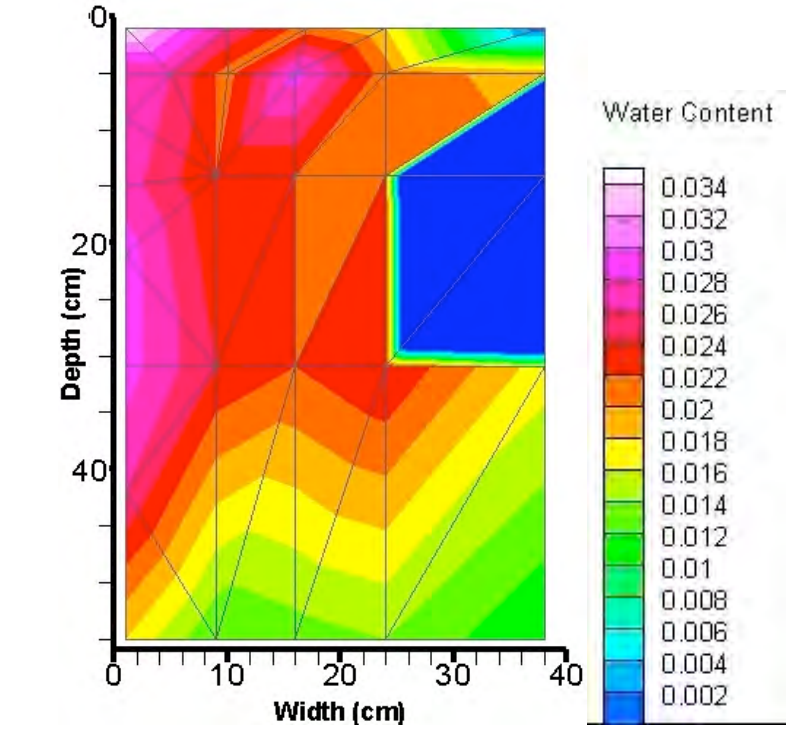

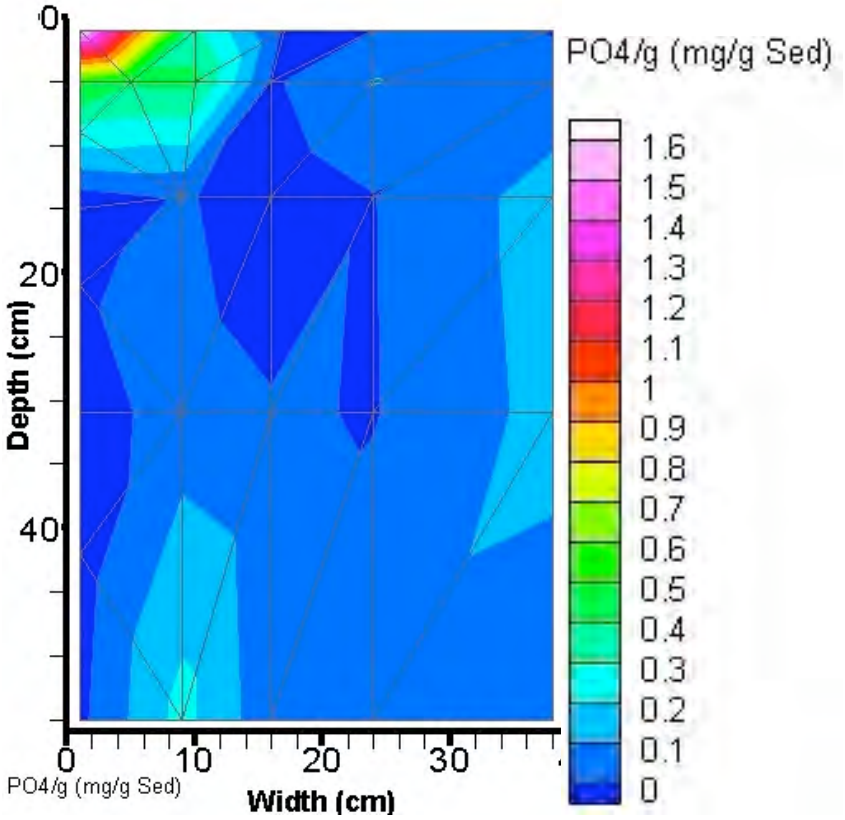

Y131.

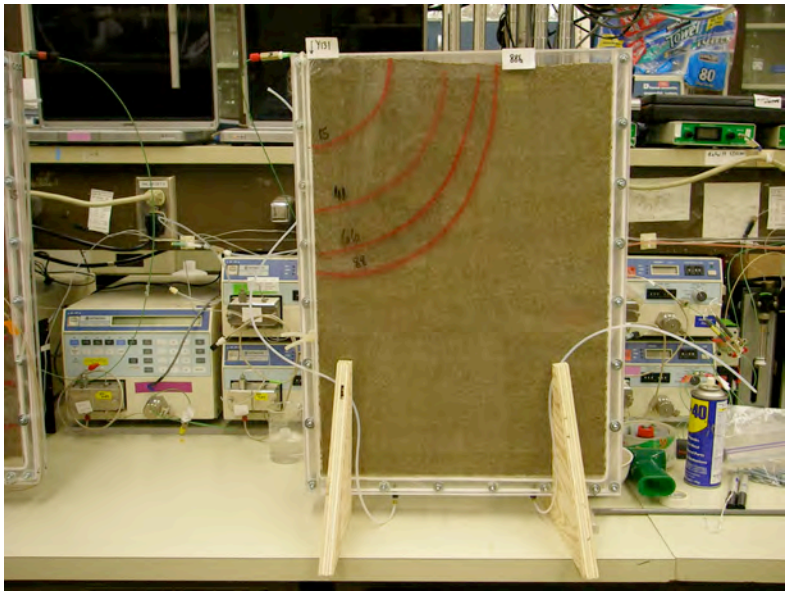

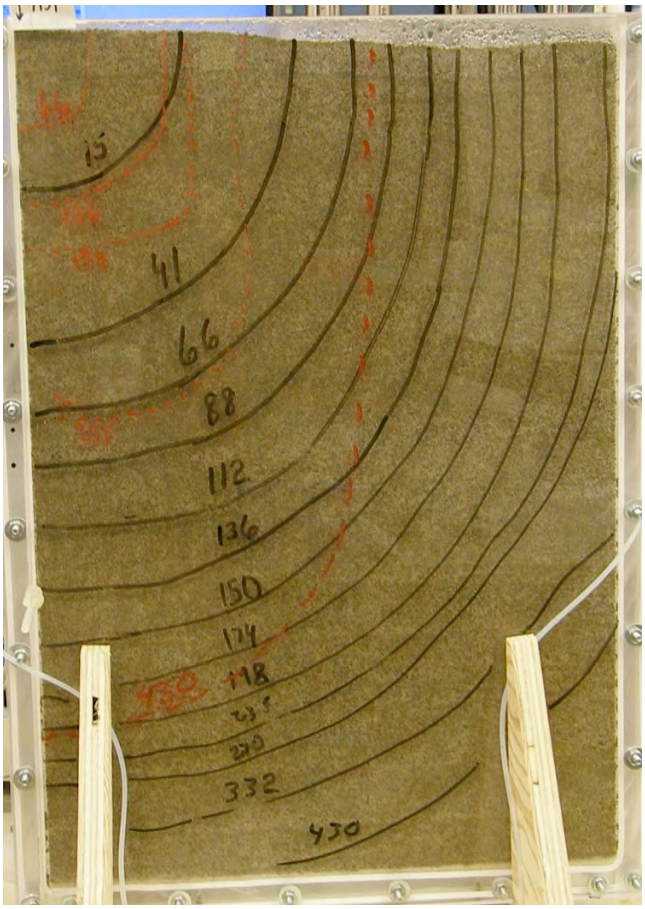

Y132. 2-D Infiltration of 30 mM Ca-citrate-PO_4 solution, 141.5 mL/hour, 70 minutes. Initial uniform water content, 0.0148 g/g.

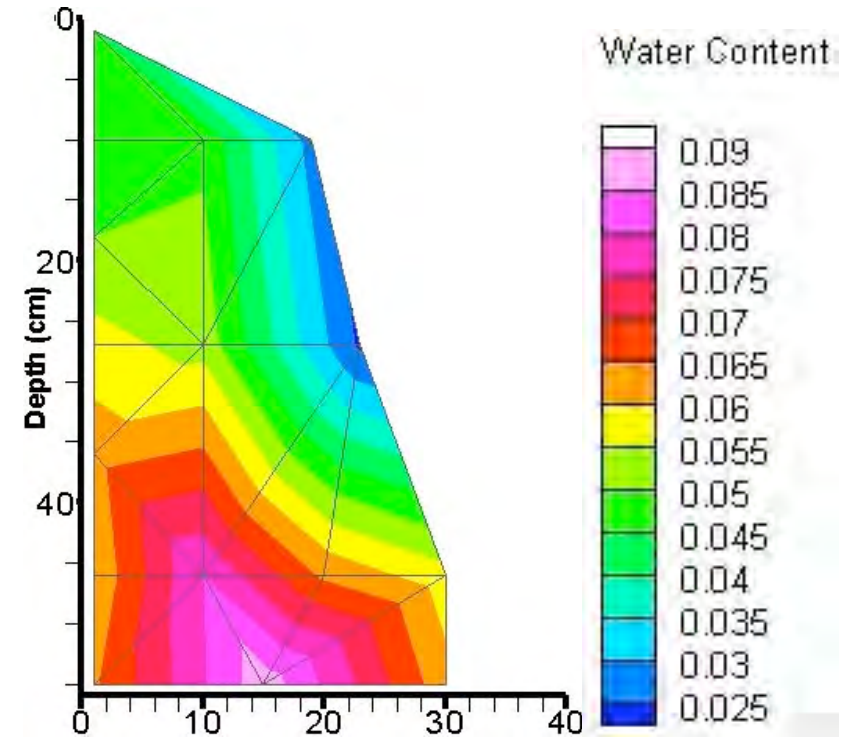

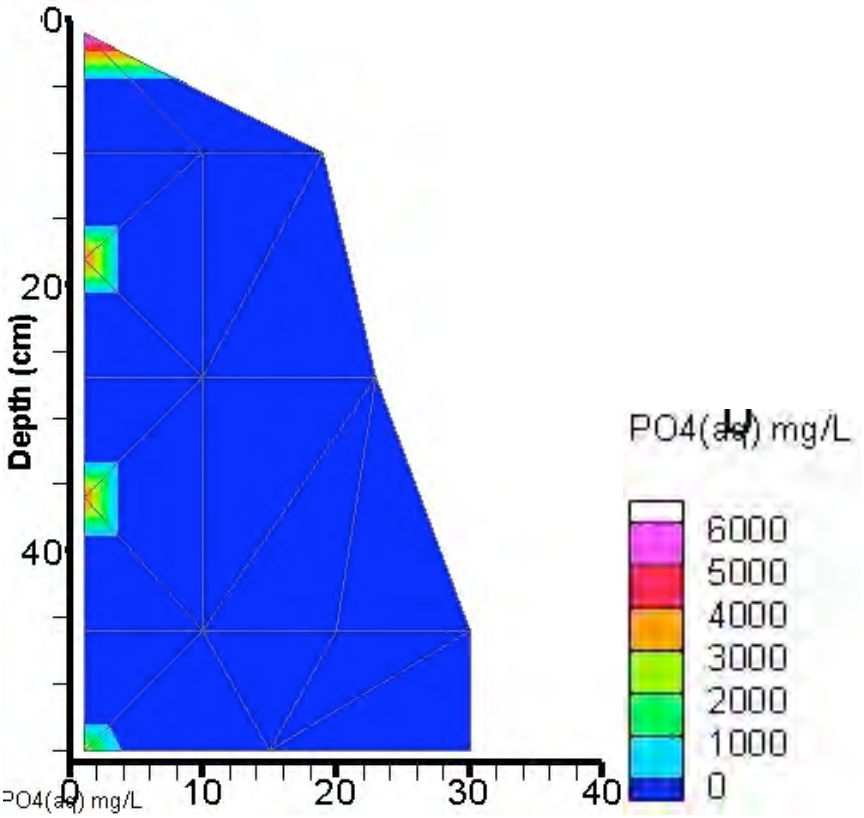

Y132.

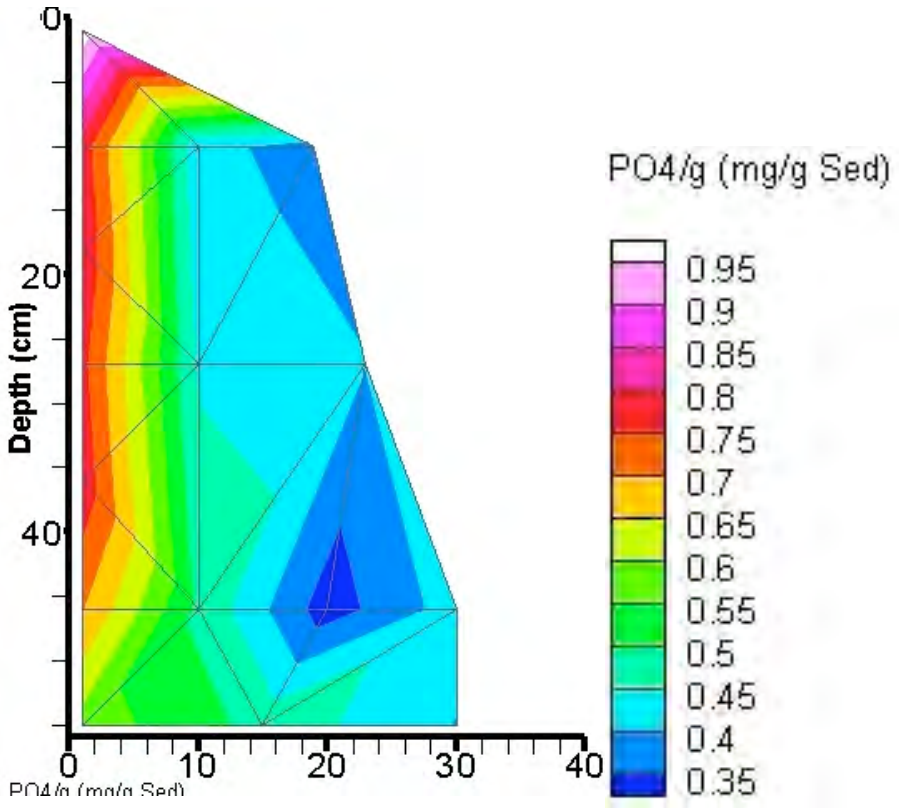
PO4/g (mg/g Sed)
0.95
0.9
0.85
0.8
0.75
0.7
0.65
0.6
0.55
0.5
0.45
0.4
0.35
Depth (cm)
0
20
40
0
10
20
30
40

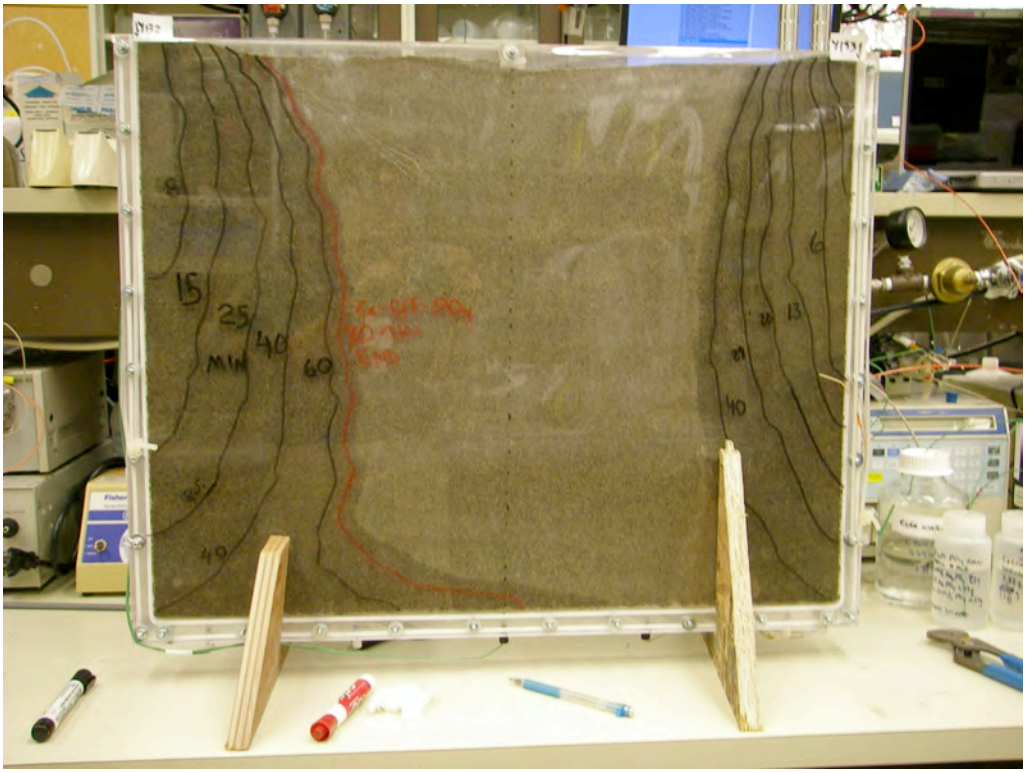

Y133. 2-D Infiltration of 30 mM Ca-citrate-PO_4 solution, 141.5 mL/hour, 70 minutes, then river water for 20 minutes. Initial uniform water content, 0.0148 g/g.

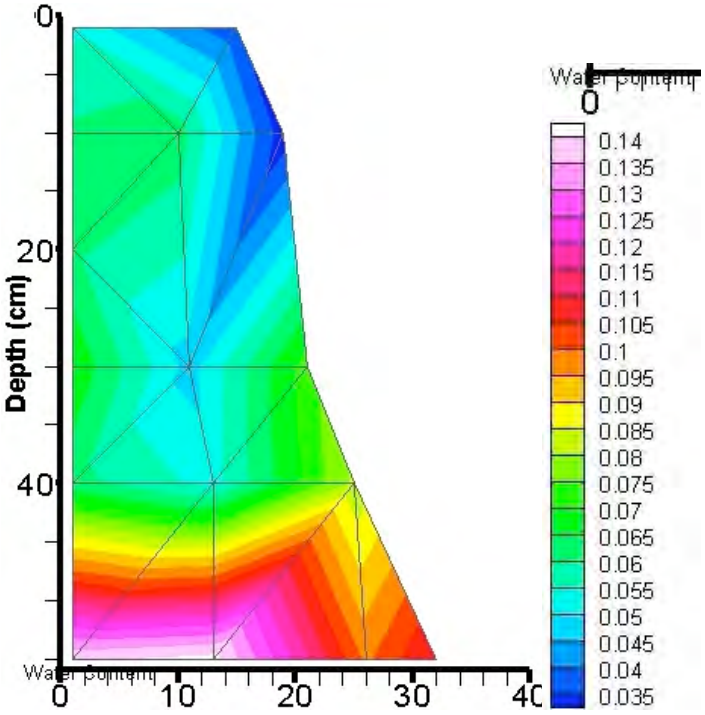

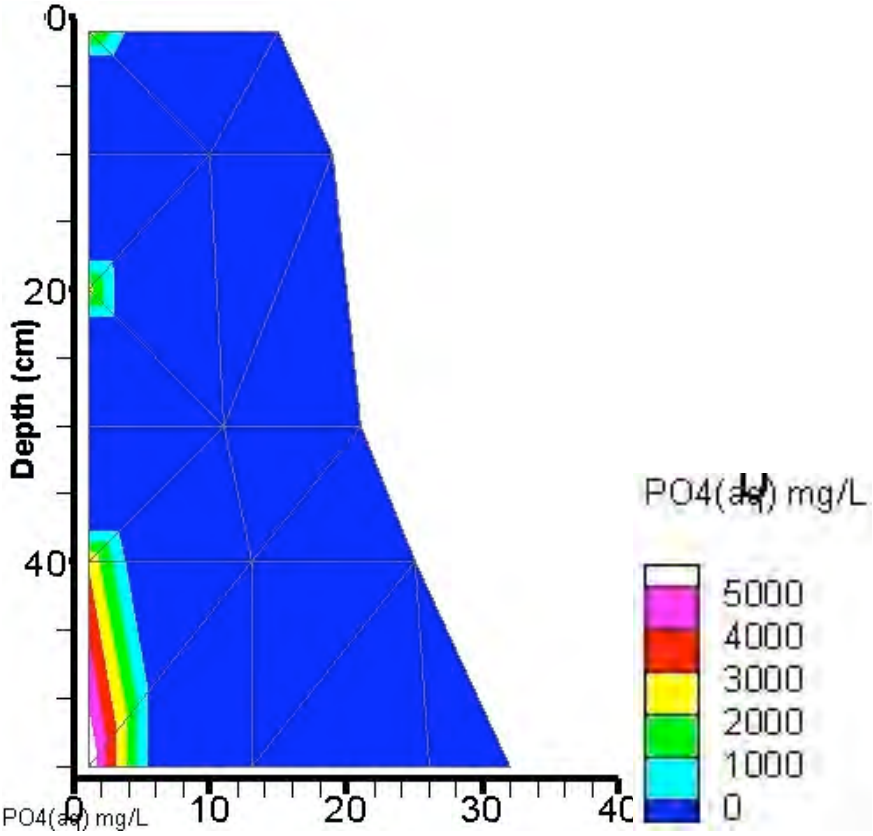

Y133.

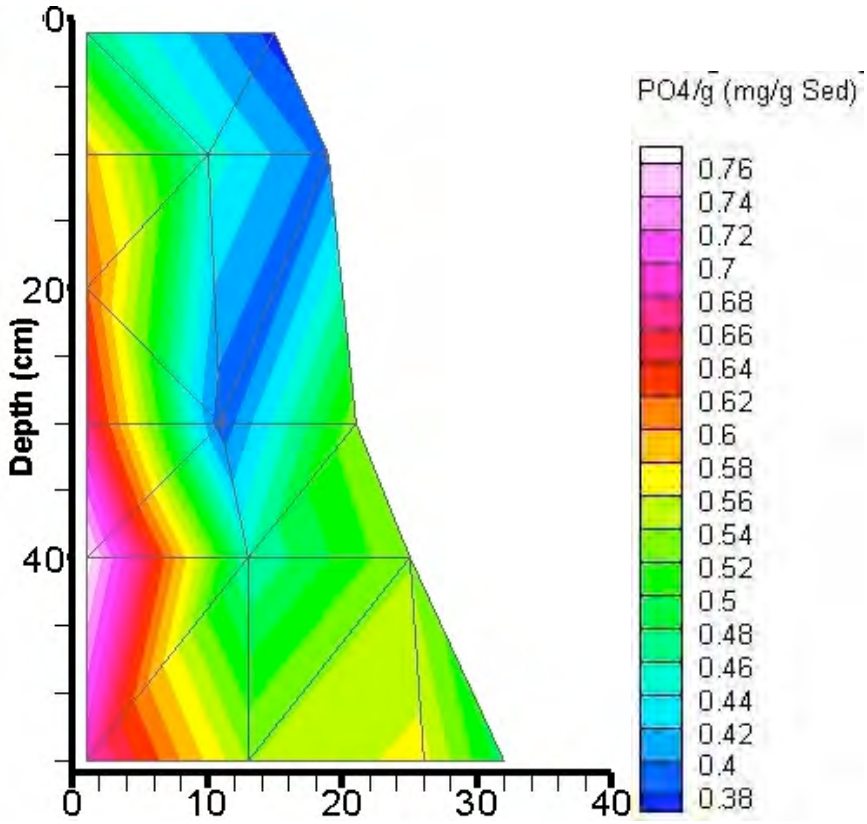
Depth (cm)
0
20
40
0
10
20
30
40
PO4/g (mg/g Sed)
0.76
0.74
0.72
0.7
0.68
0.66
0.64
0.62
0.6
0.58
0.56
0.54
0.52
0.5
0.48
0.46
0.44
0.42
0.4
0.38

Y125-Y133. Solution infiltration rate and resulting apatite precipitate shape.

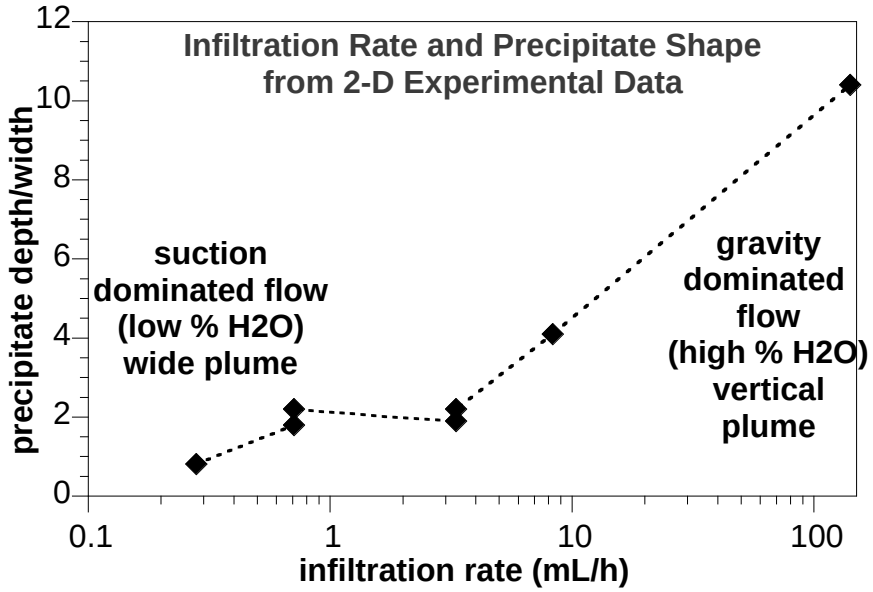

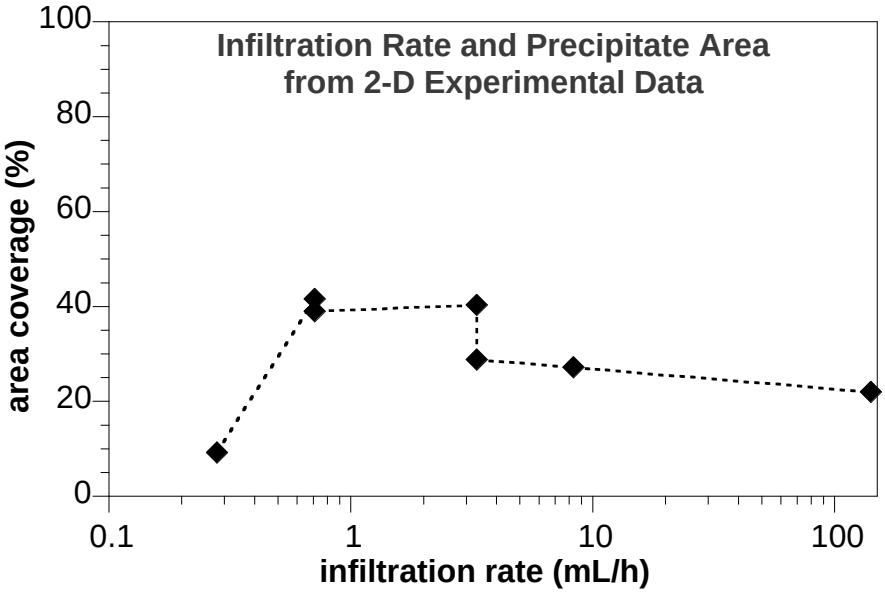

Y134. 2-D Infiltration of 60 mM Ca-citrate-PO_4 solution, 5.0 mL/hour, 40 hours, then river water for 24 hours. Initial uniform water content, 0.0148 g/g.

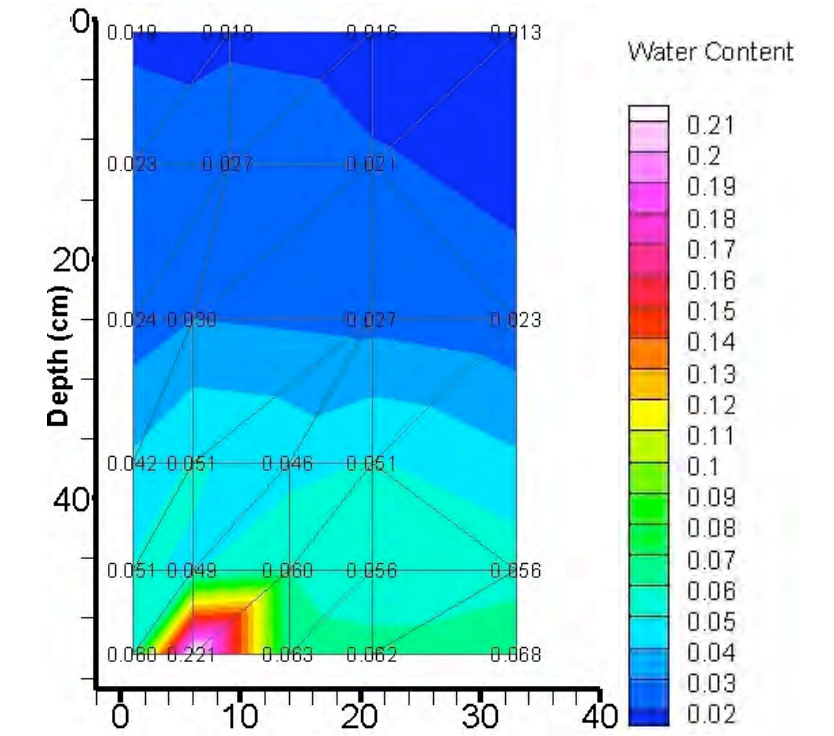

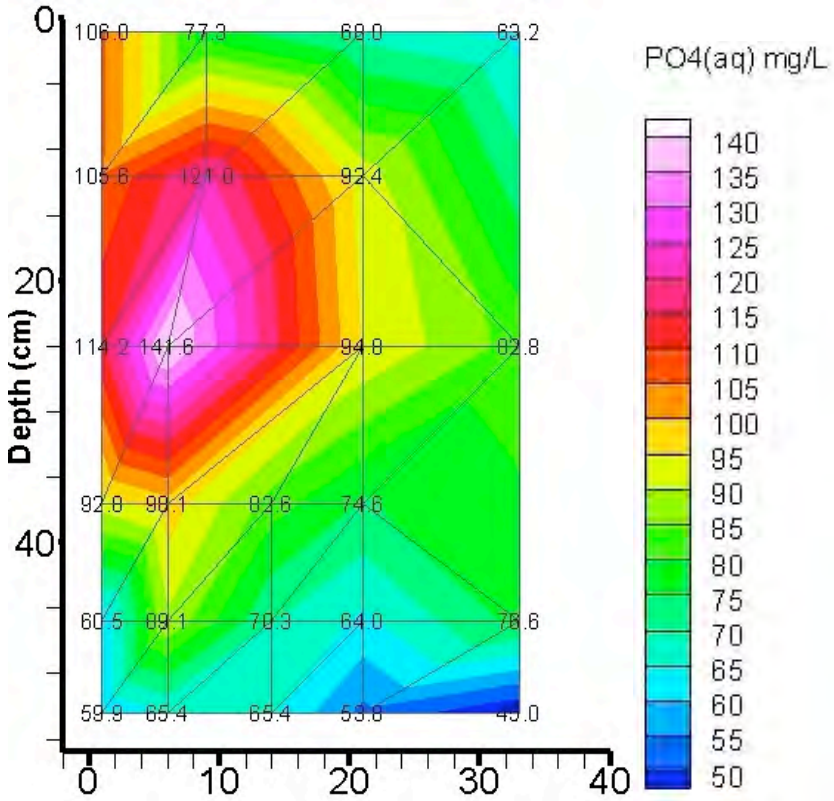

Y134.

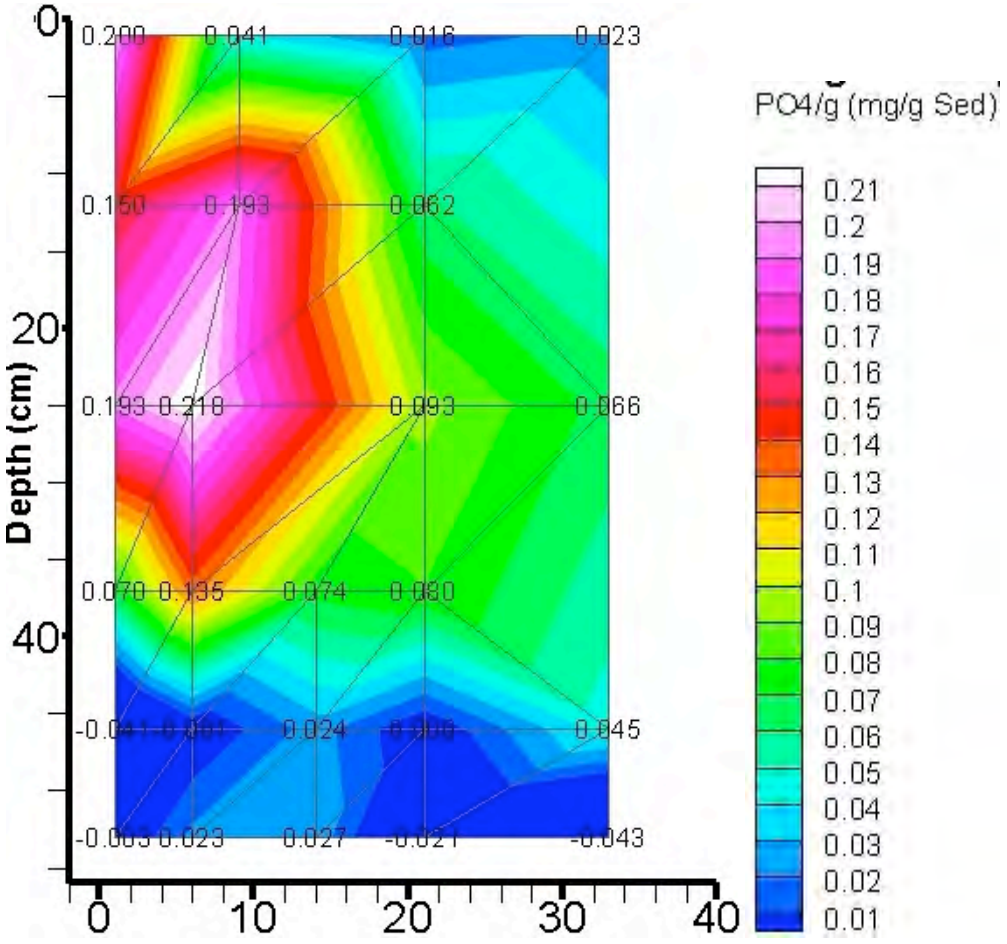
Depth (cm)
0
20
40
0
10
20
30
40
0.200
0.041
0.016
0.023
0.150
0.193
0.062
0.193
0.218
0.093
0.066
0.070
0.135
0.074
0.080
0.024
0.045
0.023
0.027
-0.021
-0.043
PO4/g (mg/g Sed)
0.21
0.2
0.19
0.18
0.17
0.16
0.15
0.14
0.13
0.12
0.11
0.1
0.09
0.08
0.07
0.06
0.05
0.04
0.03
0.02
0.01

Y135. 2-D Infiltration of 60 mM Ca-citrate-PO_4 + 2% isopropyl alcohol in river water solution, 5.0 mL/hour, 24 hours (same as Y134, but with bactericide).

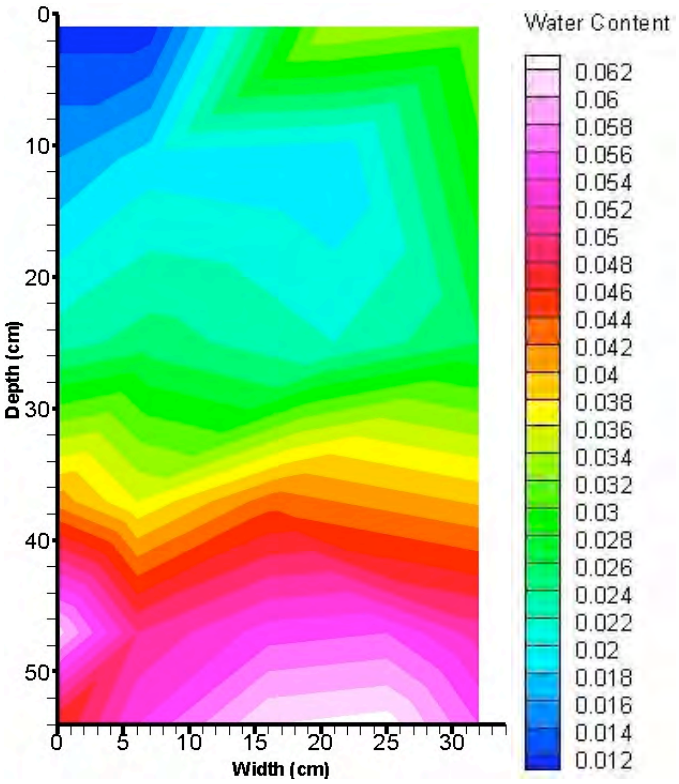

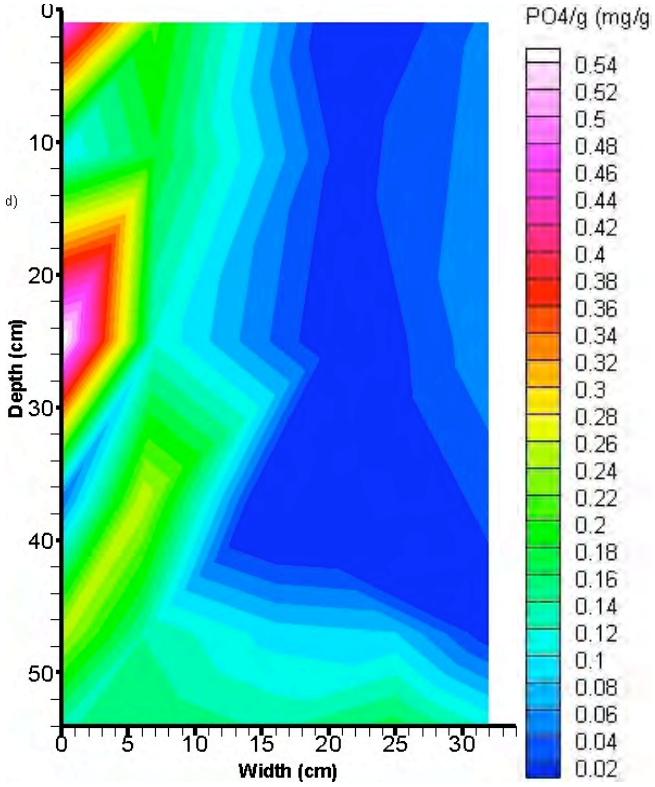

Y134, Y135.

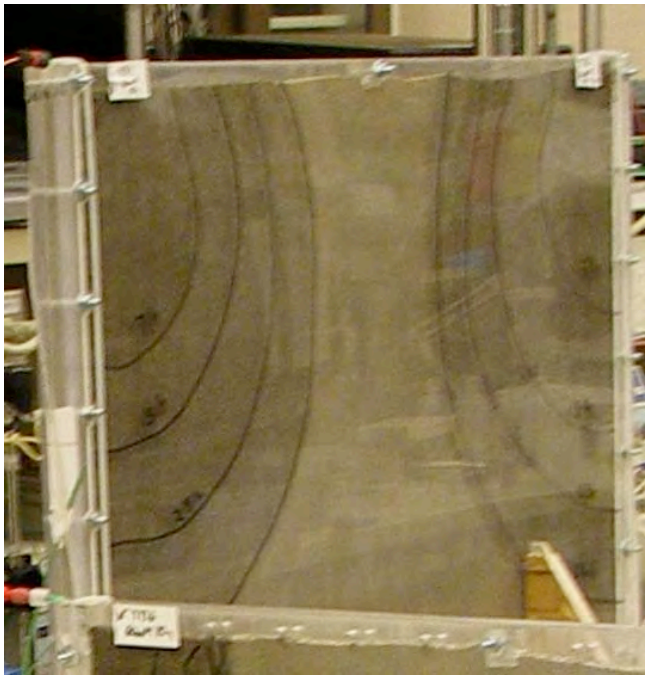

A.9 Task 5 – Solution Infiltration into 2-D Heterogeneous Systems

Y136. 2-D Infiltration of 60 mM Ca-citrate-PO_4 solution, 141.5 mL/hour (30 minutes), 5 mL/hour (10.1 hours), river water at 5.0 mL/hour (12 hours). Heterogeneous (high- and low-K lenses). Two upper boxes are low-K; larger lower box is a high-K zone.

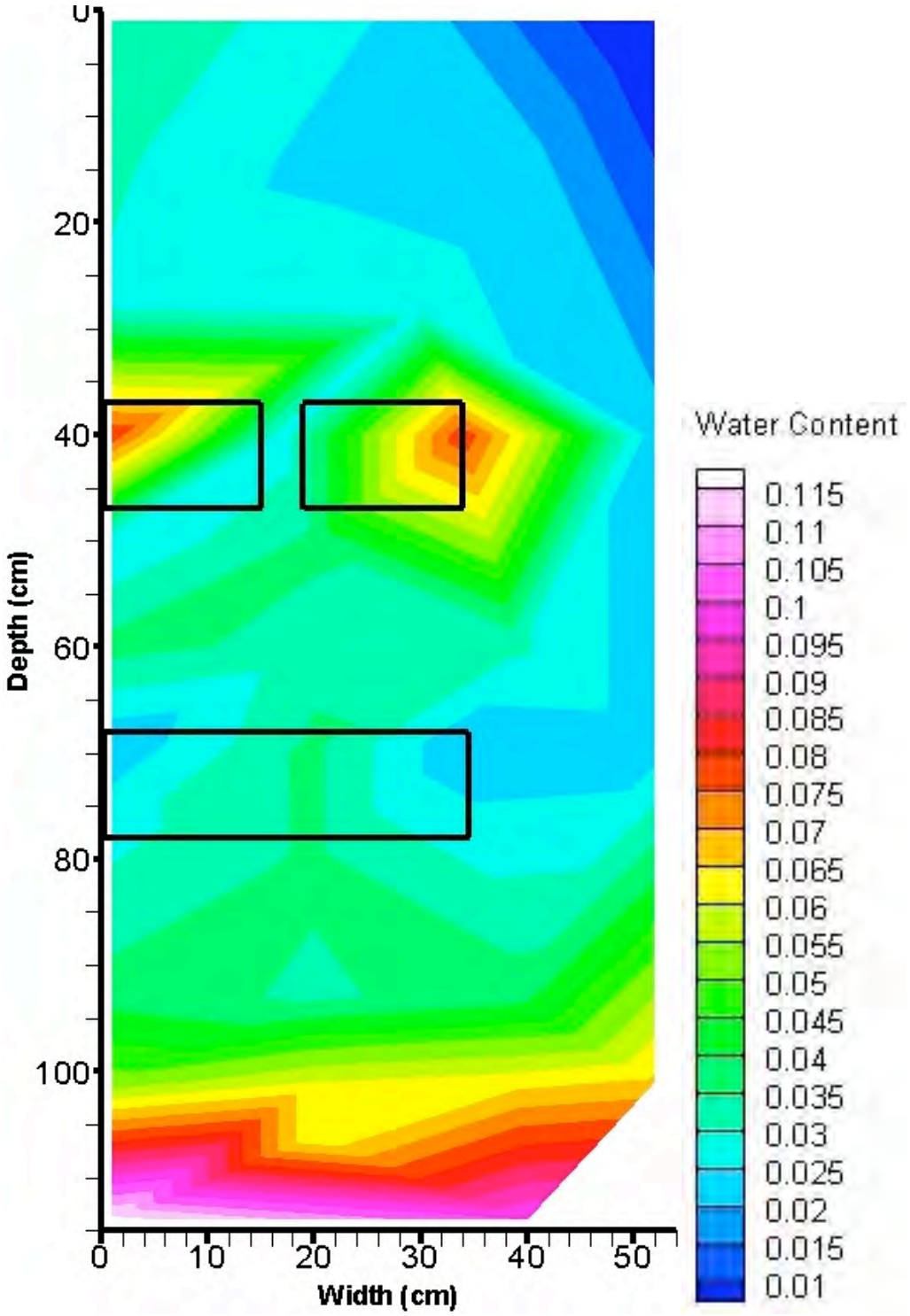

Y136. 2-D Infiltration of 60 mM Ca-citrate-PO_4 solution. Heterogeneous system.

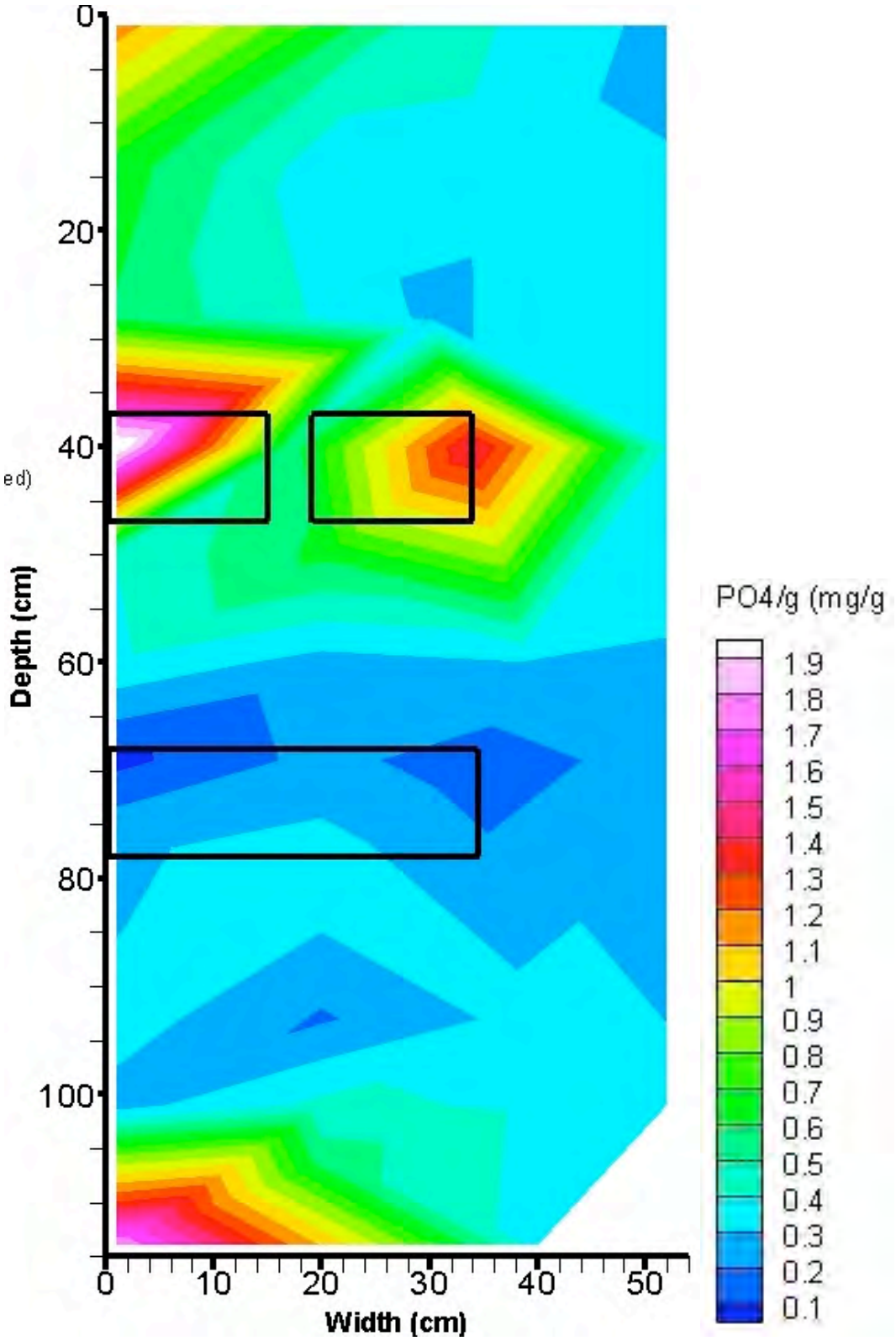

Y136. 2-D Infiltration of 60 mM Ca-citrate-PO_4 solution. Heterogeneous system. Pictures at 1 hour, 7 hours, and 11 hours.

Y137. 2-D Infiltration of 30 mM Ca-citrate-PO_4 solution, 141.5 mL/hour (0.73 hour), river water at 1.0 mL/hour (20.3 hours). Heterogeneous (low-K lens).

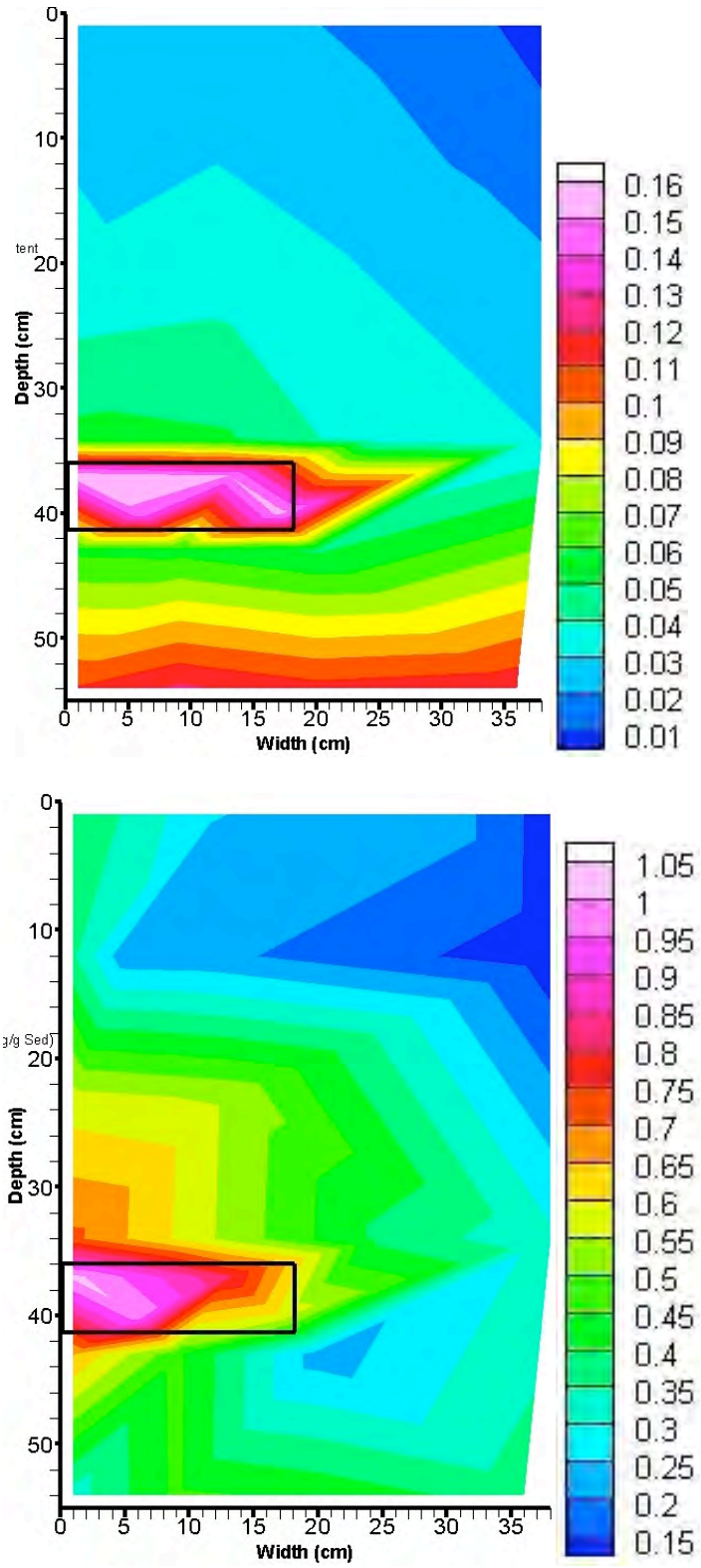

Y137.

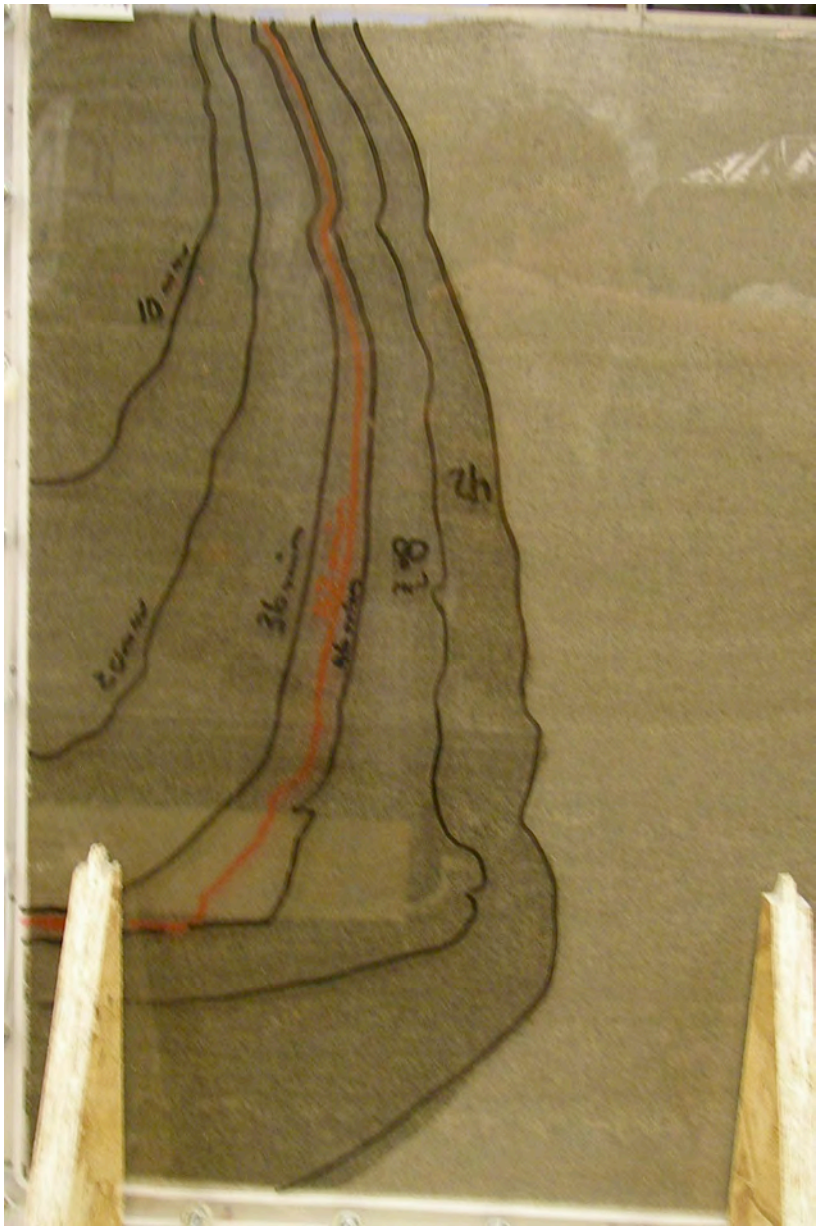

Y124. 2-D water infiltration demonstration.

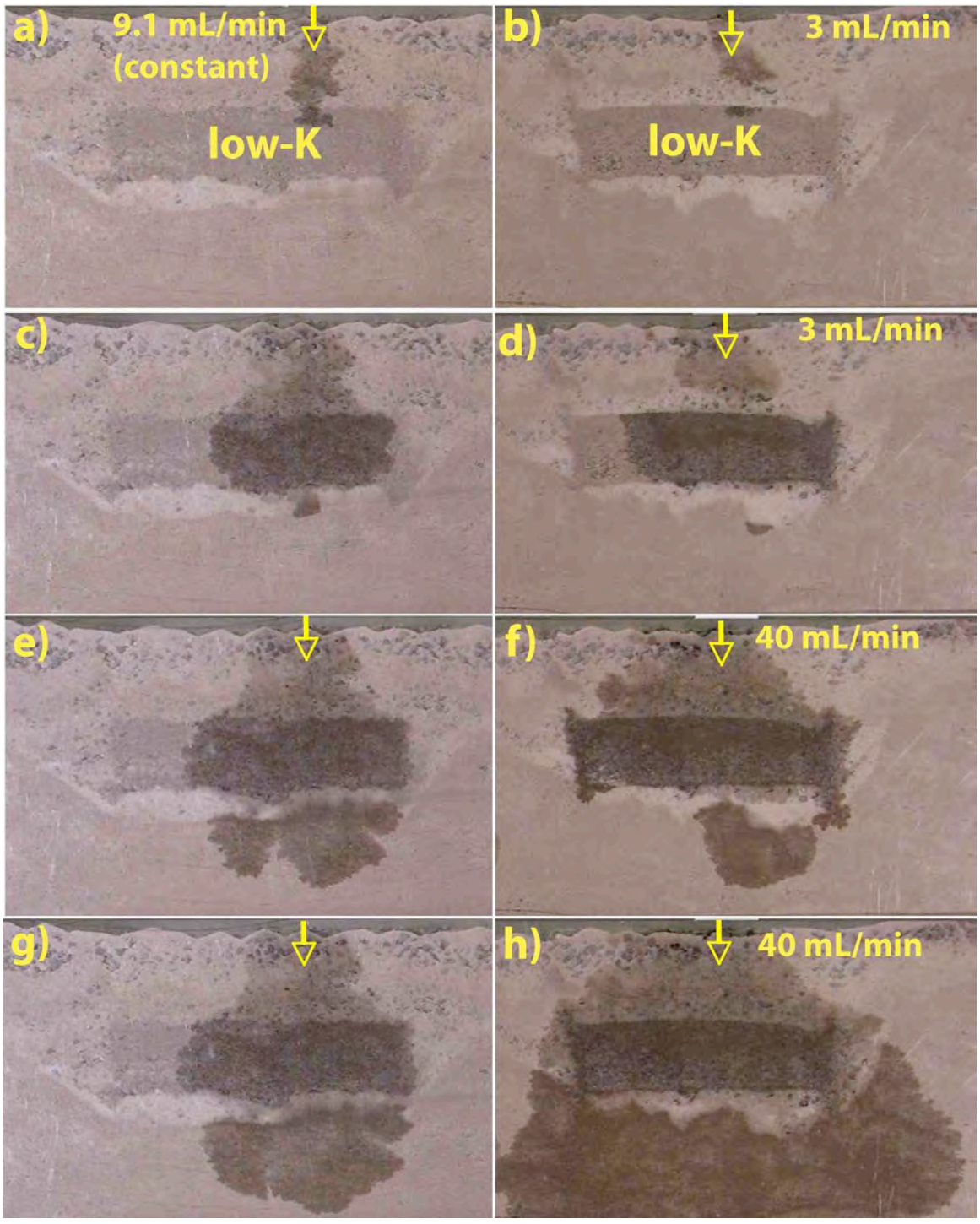

Y124. 2-D water infiltration demonstration.

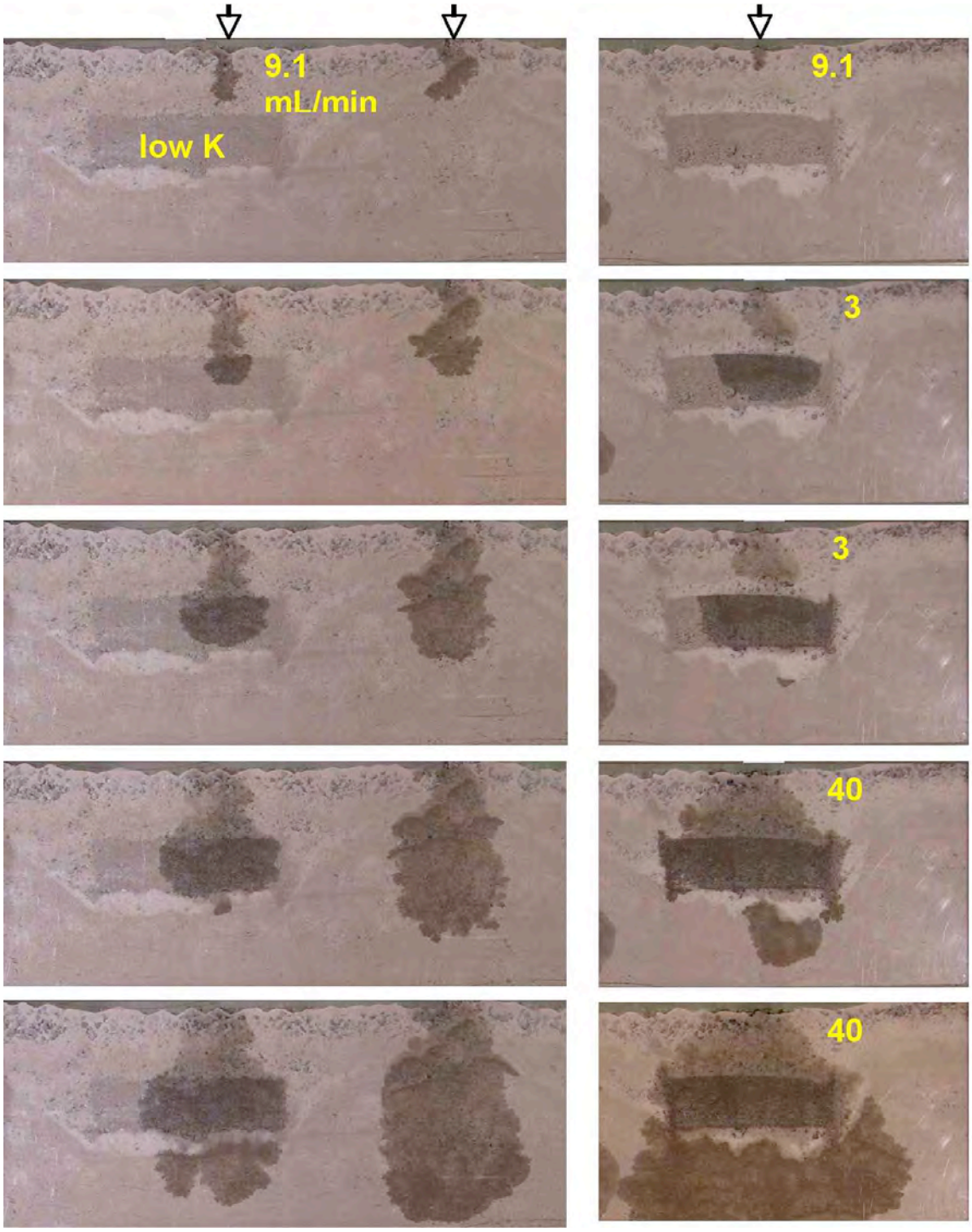

Y124. 2-D water infiltration demonstration.

EMSL-2 experiment. Ca-citrate-PO_4 (30 mM PO_4) solution infiltration into a 2-D system with low-K zone and lower water table (flowing).

Dye injection after Ca-citrate-PO_4 experiment.

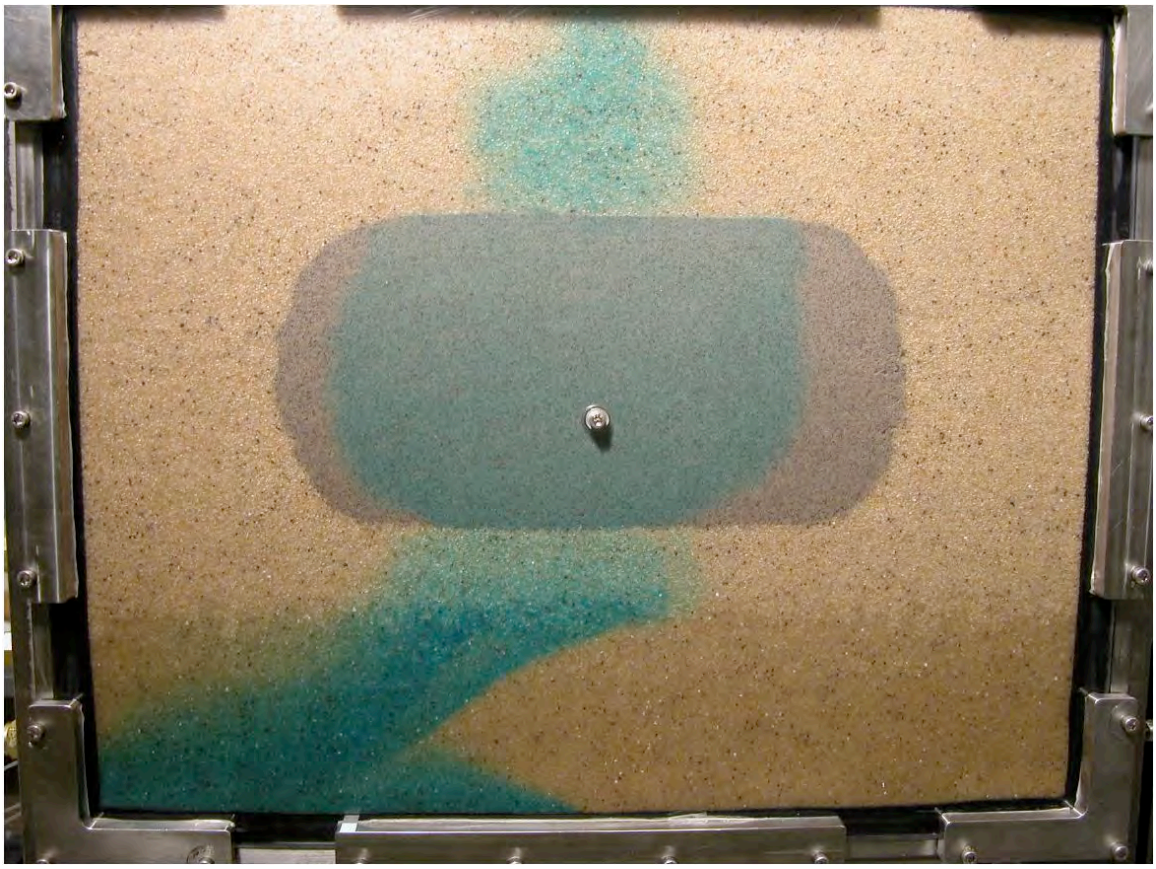

EMSL-2. Comparison of experimental and presimulation results.

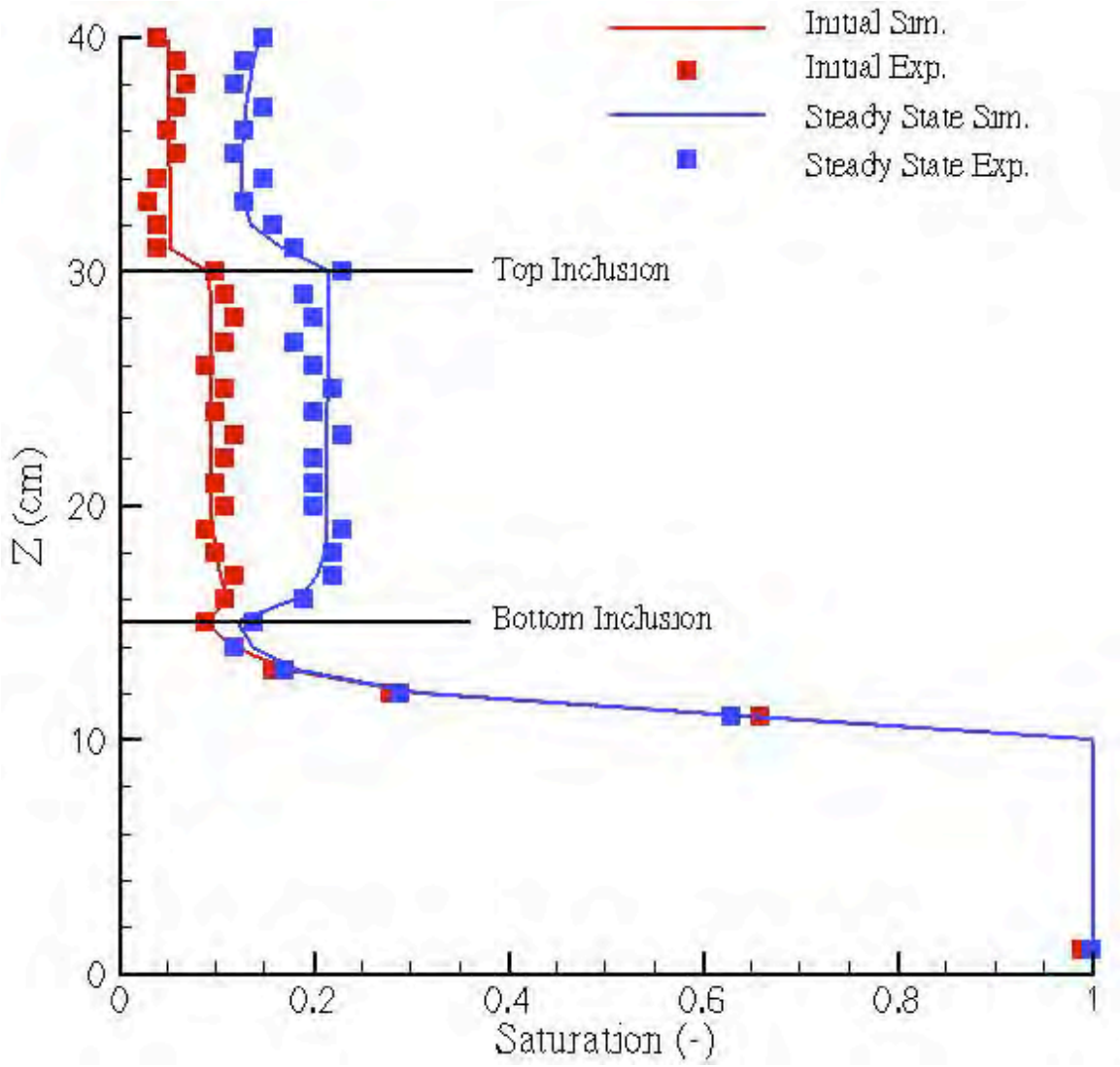

Simulation of Experiment EMSL-2.
Water Content - Initial Conditions

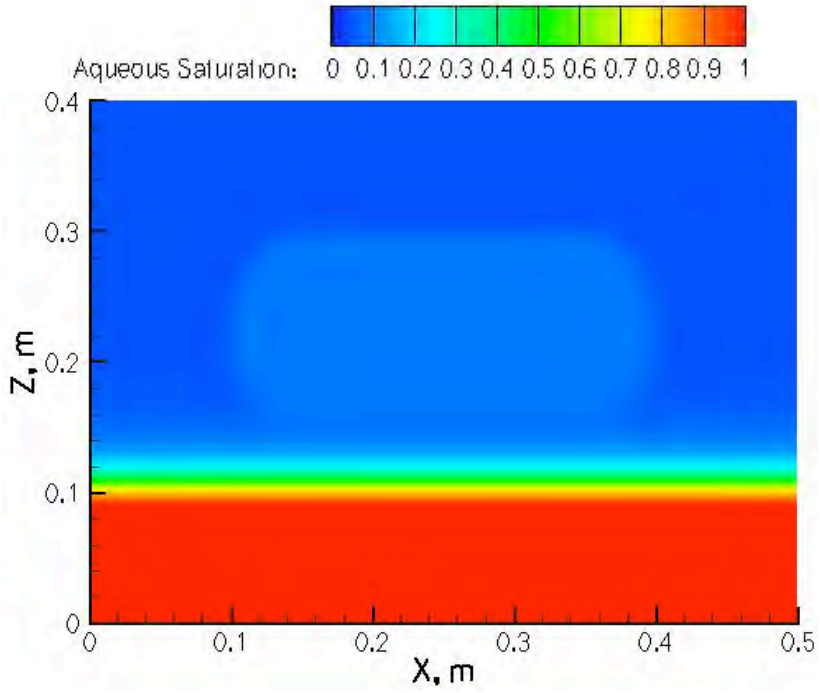

Water Content – Steady-State Infiltration at Large Time

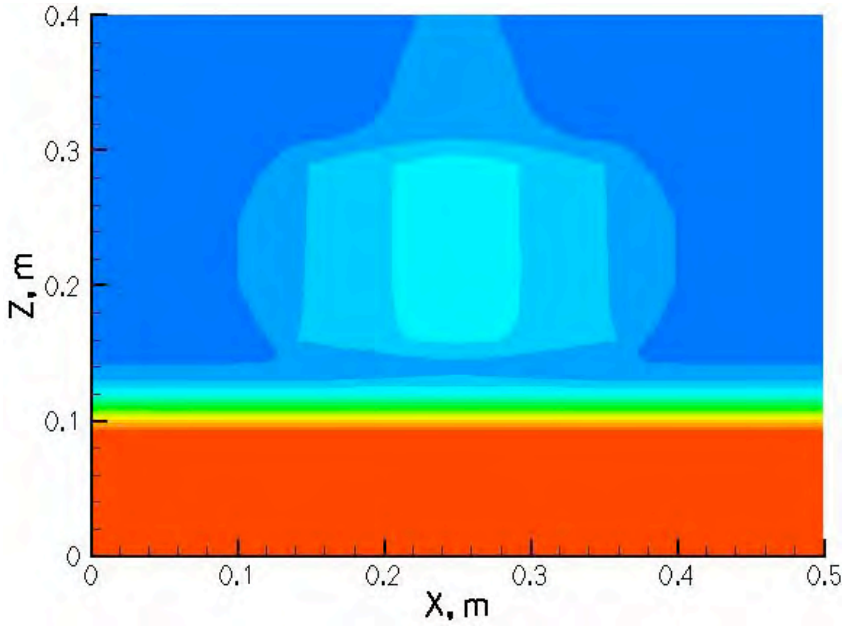

Y190. 2-D Infiltration of 60 mM Ca-citrate-PO_4 solution into a sediment system containing discontinuous low-K and high-K zones. Box is 2.44 m (8 ft) high by 1.22 m (4 ft) wide by 1.1 cm thick. Solution infiltration at 1260 mL/hour for 75 minutes followed by river water infiltration at 1260 mL/hour for 113 minutes.

Close up of a portion of Y190 experiment showing solution infiltration at interfaces of low-K and high-K layers.

Close up of a portion of Y190 experiment showing solution infiltration at interfaces of low-K and high-K layers.

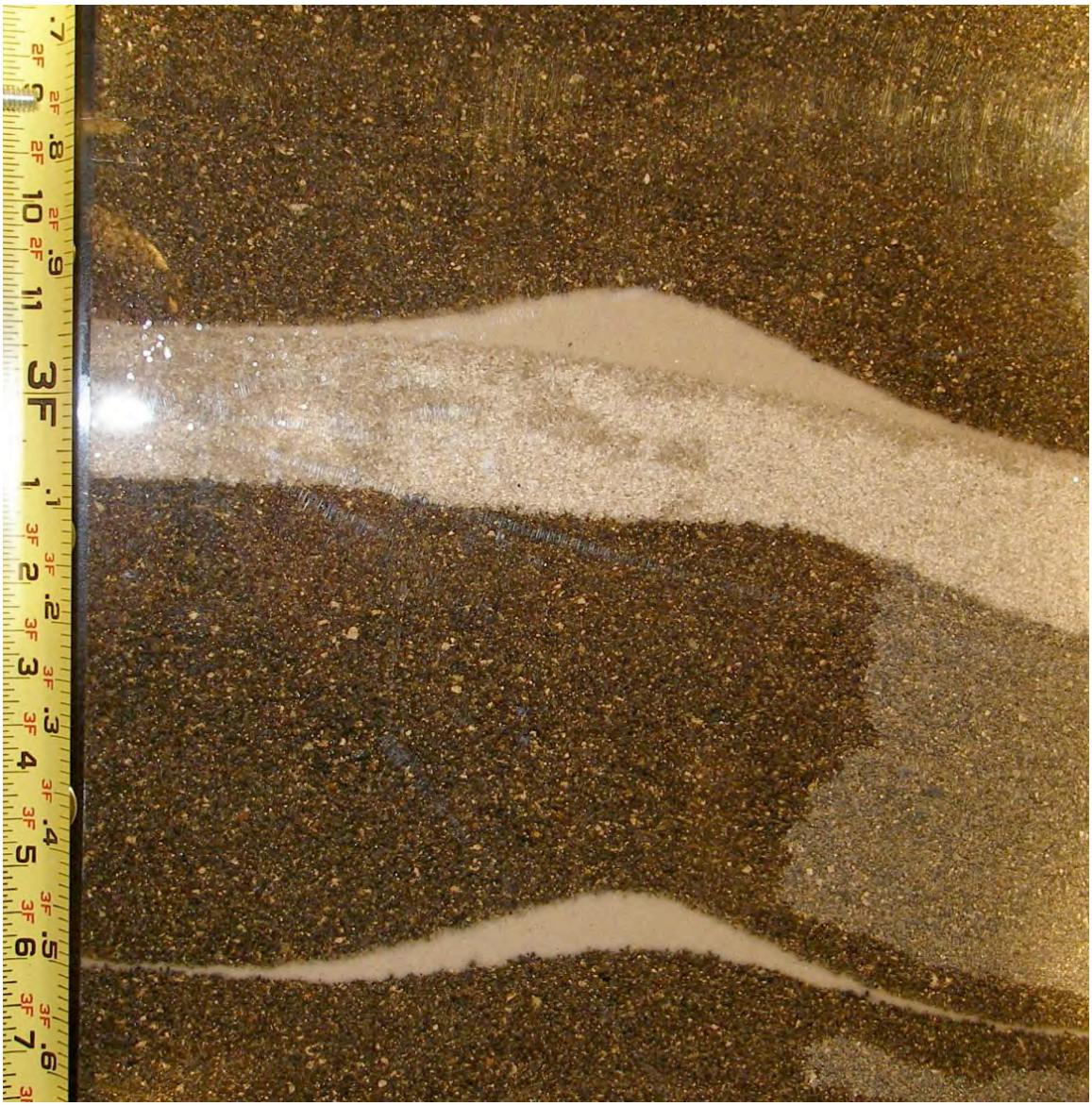

Y149. 2-D foam injection 20 mL/minute N2 for 22 hours, 1% surfactant (sodium lauryl ether sulfate, 3% water with 30 mM Ca-citrate-PO_4. Two low-K lenses.

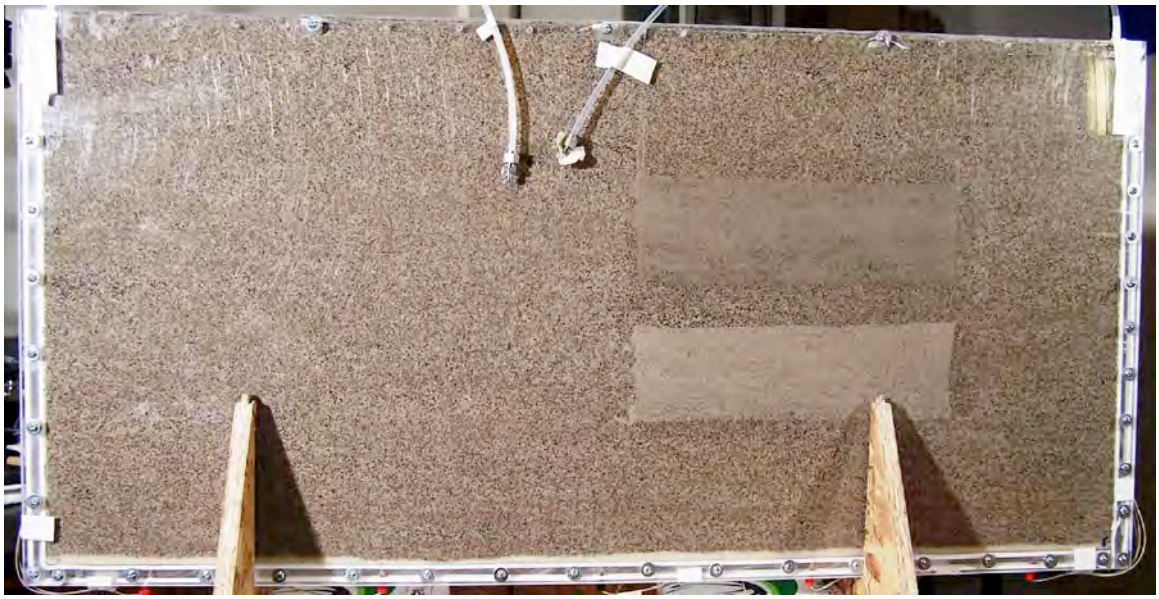

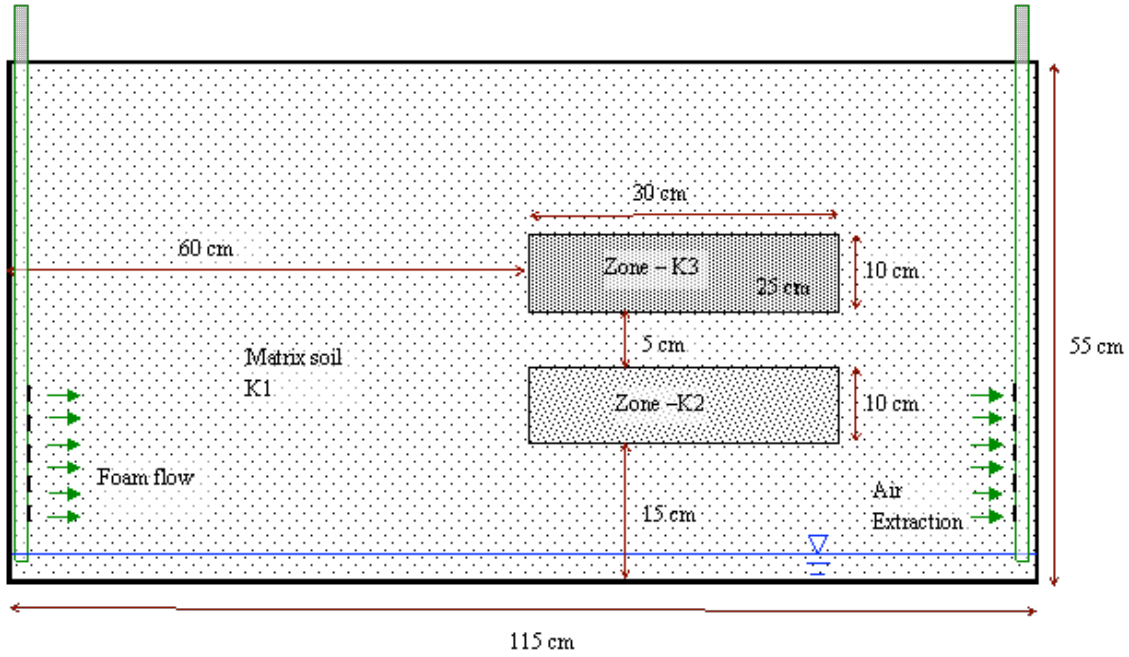

Y149.

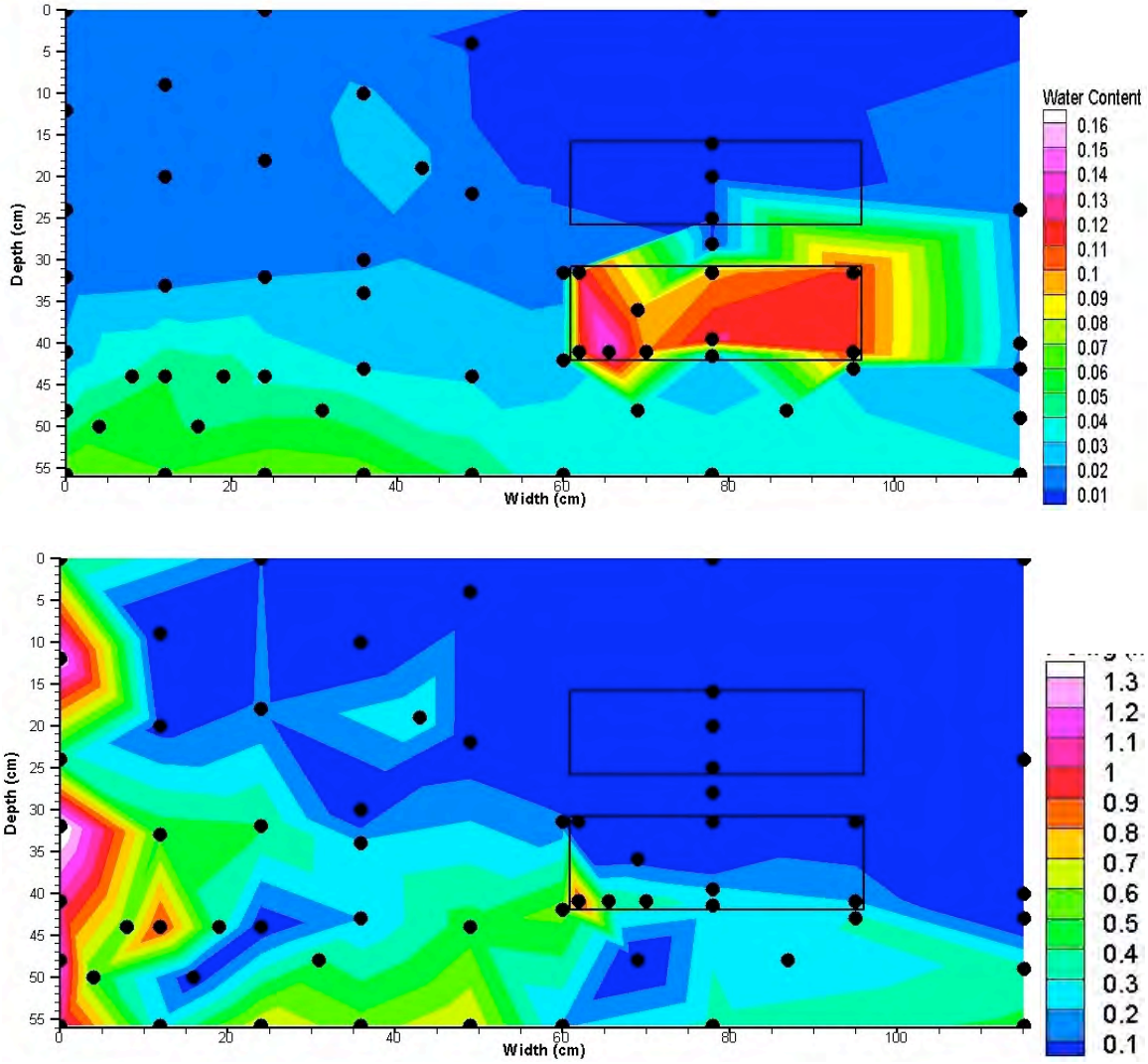
Water Content
0.16
0.15
0.14
0.13
0.12
0.11
0.1
0.09
0.08
0.07
0.06
0.05
0.04
0.03
0.02
0.01
Depth (cm)
Width (cm)
0
5
10
15
20
25
30
35
40
45
50
55
0
20
40
60
80
100
1.3
1.2
1.1
1
0.9
0.8
0.7
0.6
0.5
0.4
0.3
0.2
0.1

Y149.

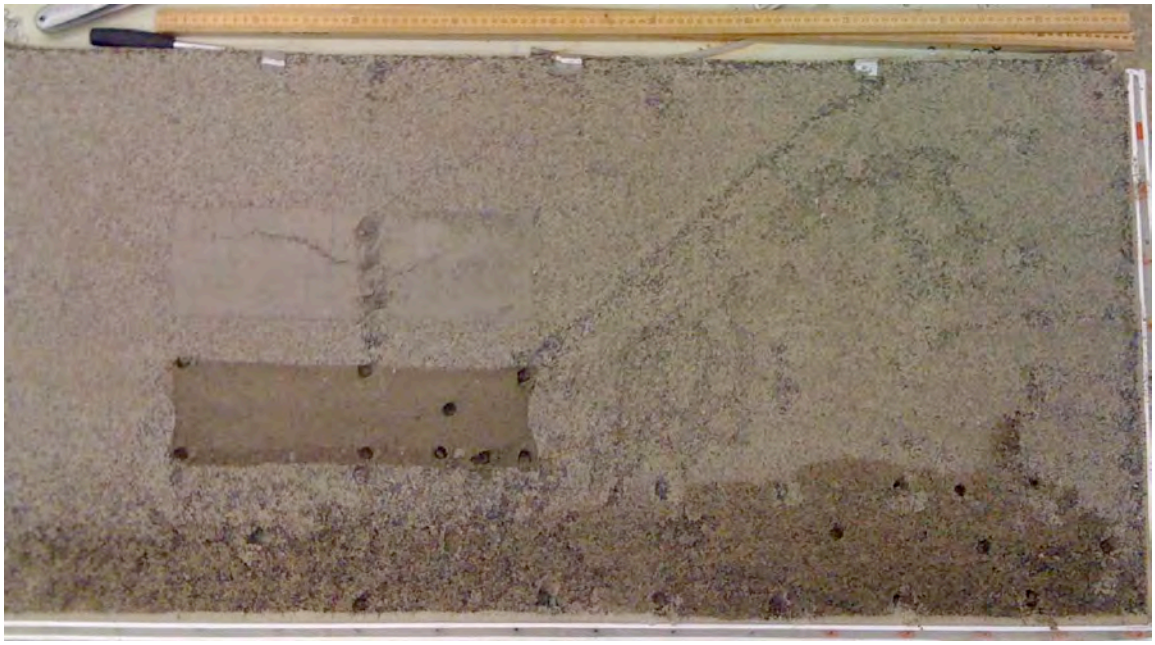

Y158. 2-D foam injection 60 mL/minute N2 for 22 hours, 1% surfactant (sodium lauryl ether sulfate, 1.88 mL/minute water with 30 mM Ca-citrate-PO_4. Two low-K lenses, one high-K.

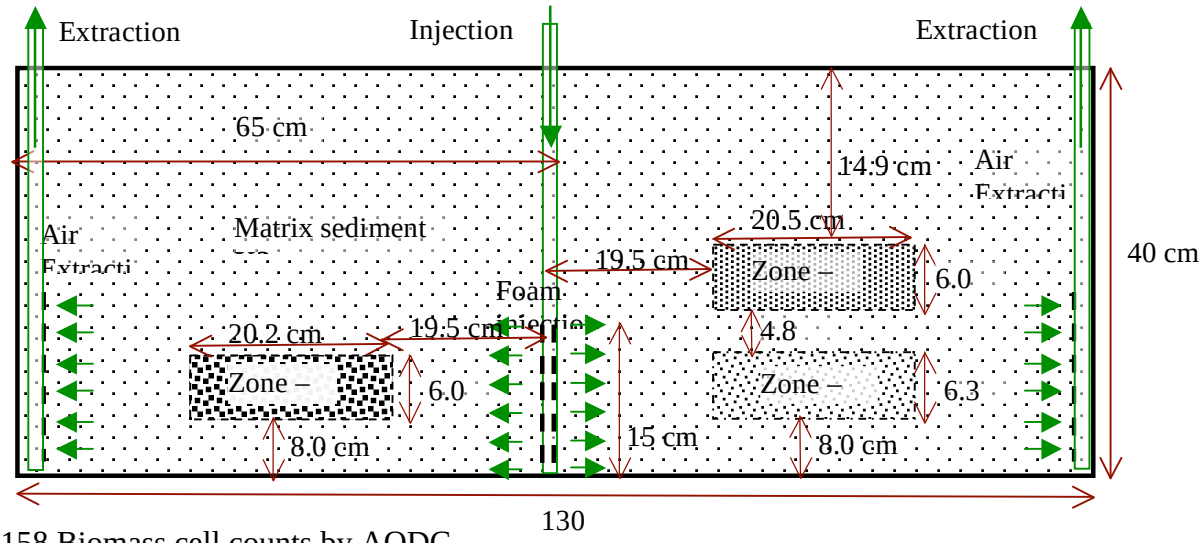

Y158 Biomass cell counts by AODC
Y158-HK1 4.13 E7 cells/mL (first effluent sample on high-K side)
Y158 HK6 8.97 E7 cells/mL (last effluent sample on high-K side)
Y158 B1 3.25E8 cells/mL (sediment sample at lower left corner [0,0])
Y158 B2 1.08E9 cells/mL (sediment sample at injection well [65,0])
Capillary rise of material (K1-K4) in Y158.

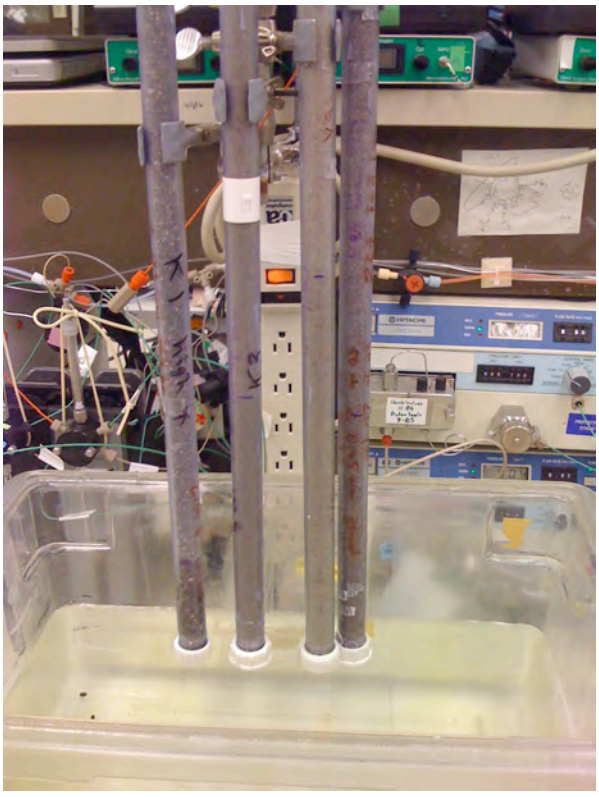

Y158. 2-D foam injection.

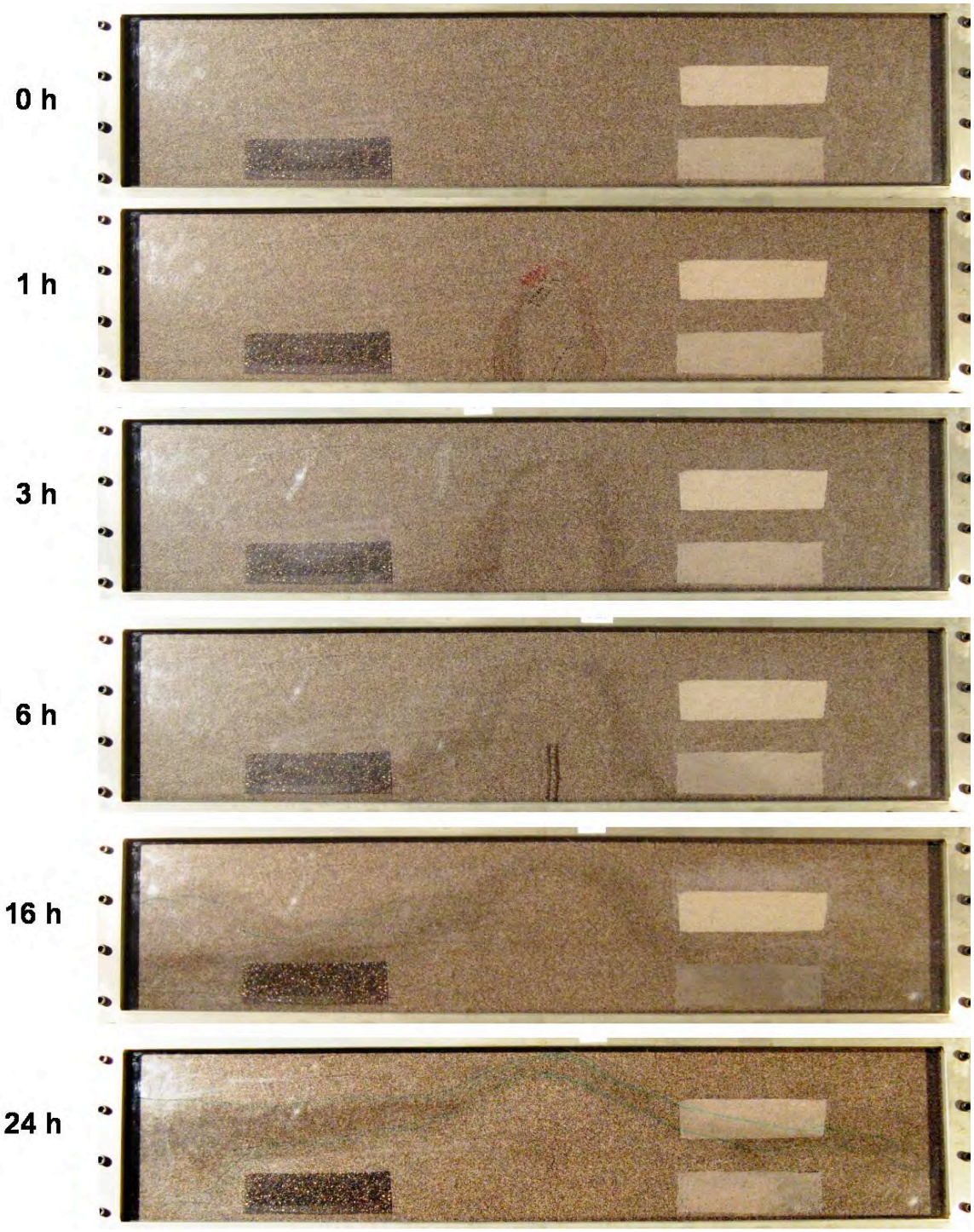

Y158. 2-D foam injection.

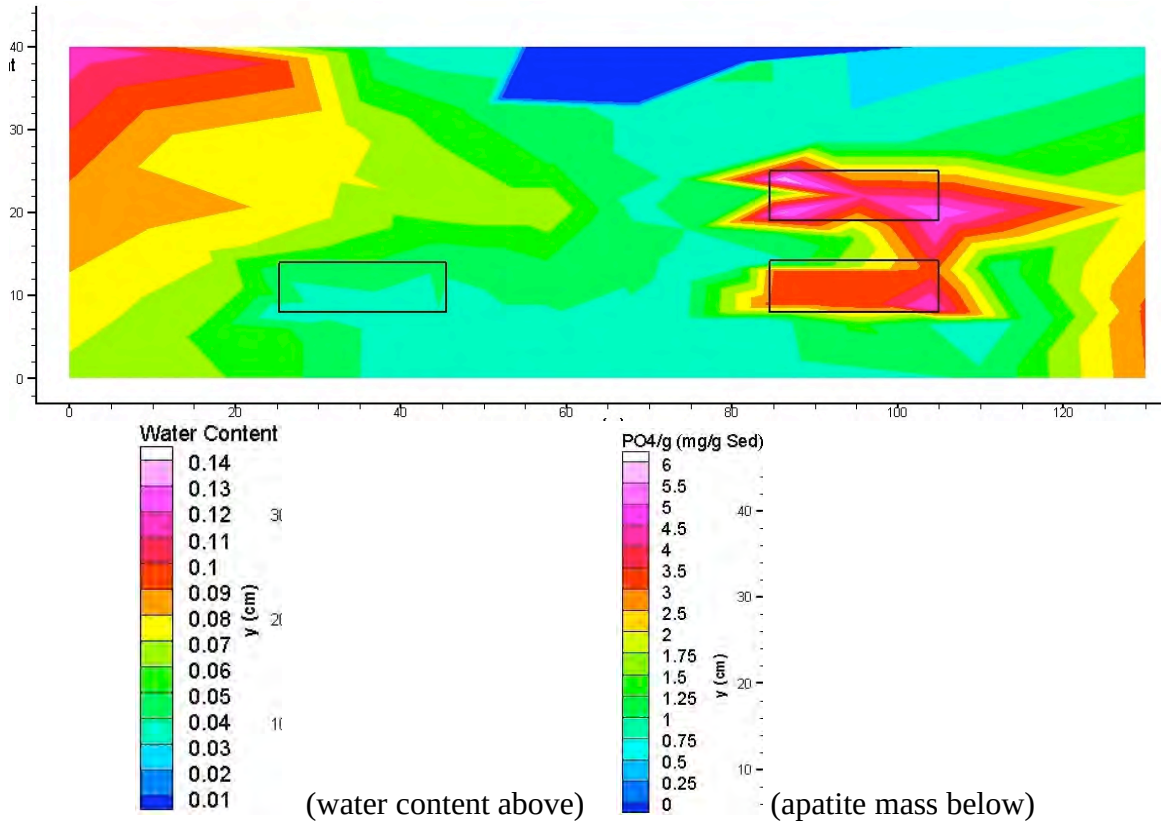

(water content above) (apatite mass below)

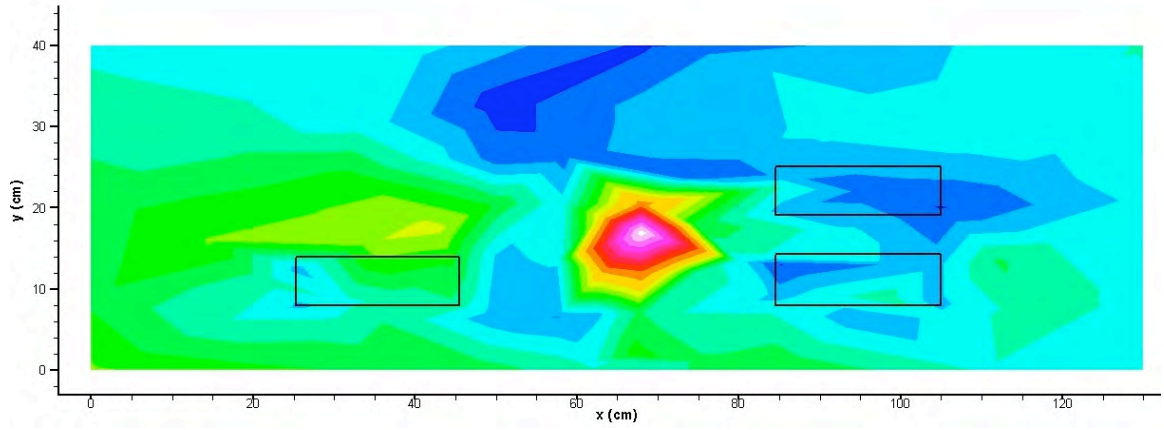

A.10 Task 5 – Sequential Solution/Water Infiltration into 2-D Systems

Y172. 2-D Infiltration of 40 mM Ca-citrate-PO_4 solution, 2.35 mL/minute x 55 minutes, then river water at 0.017 mL/minute x 23 hours (one injection).

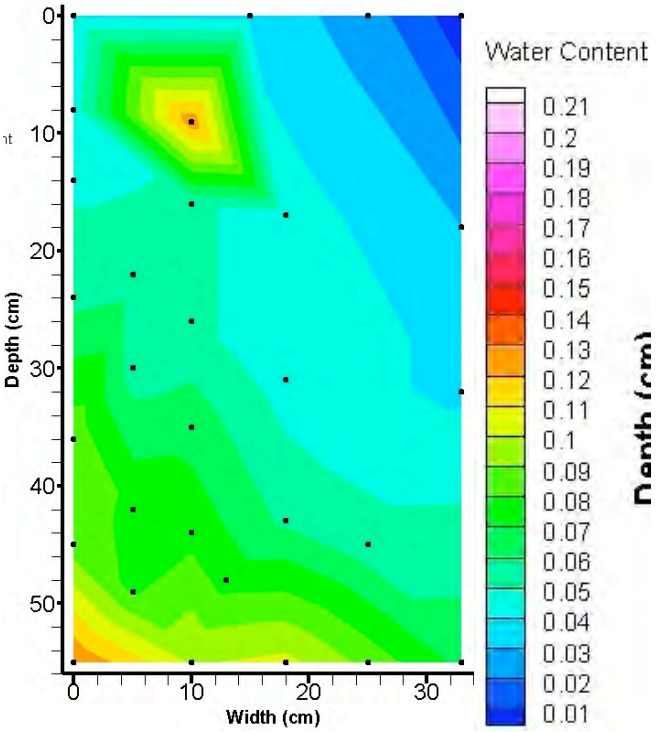

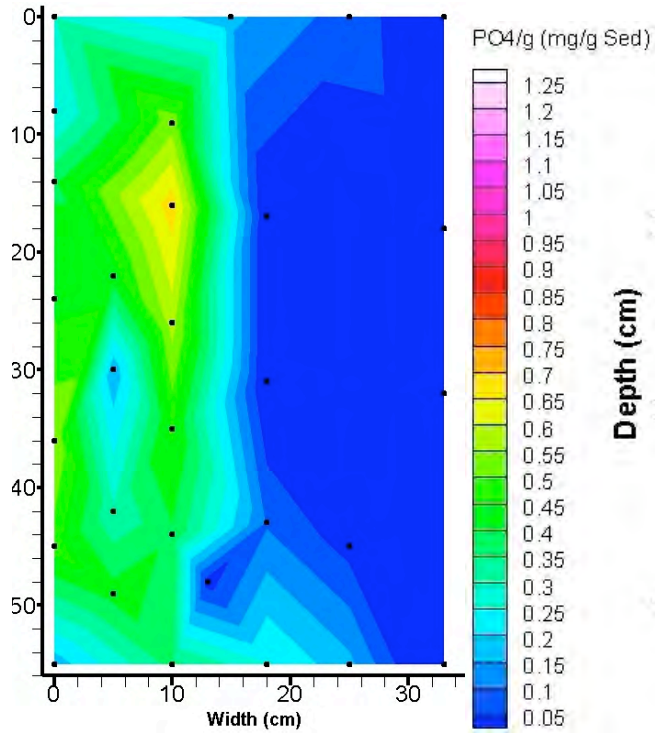

Y173. 2-D Infiltration of 40 mM Ca-citrate-PO_4 solution, 2.35mL/minute x 55 minutes, then river water at 0.017 mL/minute x 23 hours (two injections, 1 week apart).

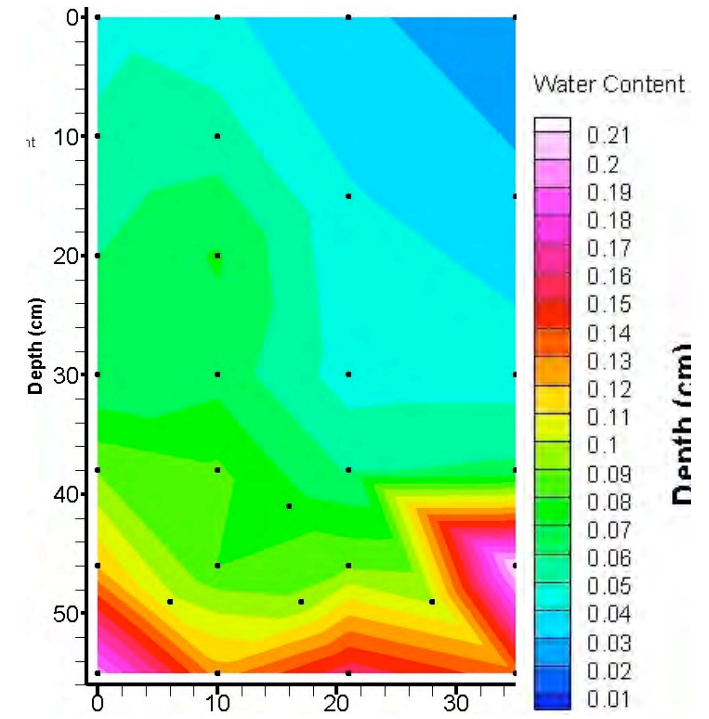

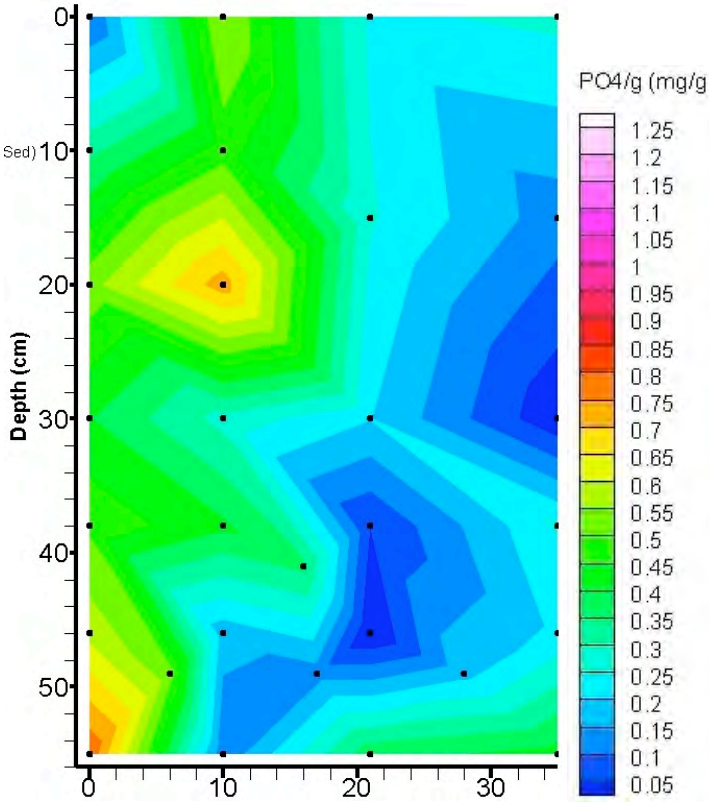

Y174. 2-D Infiltration of 40 mM Ca-citrate-PO_4 solution, 2.35mL/minute x 55 minutes, then river water at 0.017 mL/minute x 23 hours (three injections, 1 week apart).

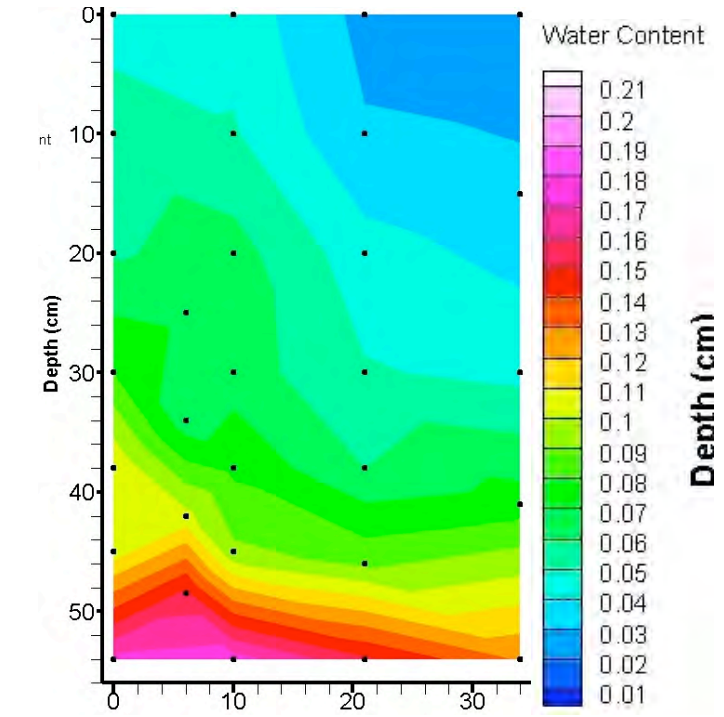

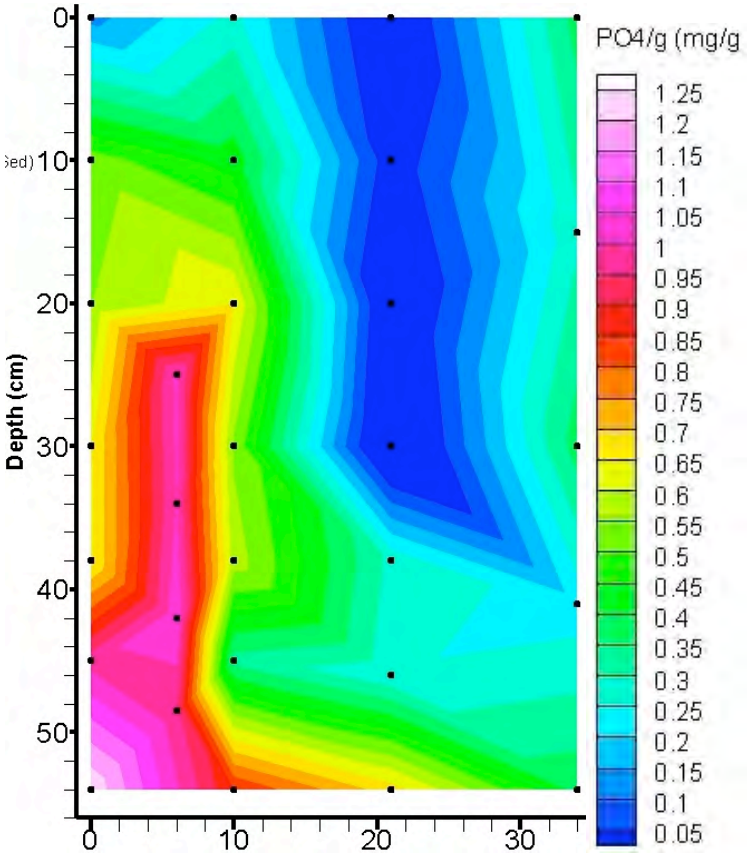

Y175. 2-D Infiltration of 40 mM Ca-citrate-PO_4 solution, 2.35 mL/minute x 55 minutes, then river water at 0.017 mL/minute x 23 hours (four injections, 1 week apart).

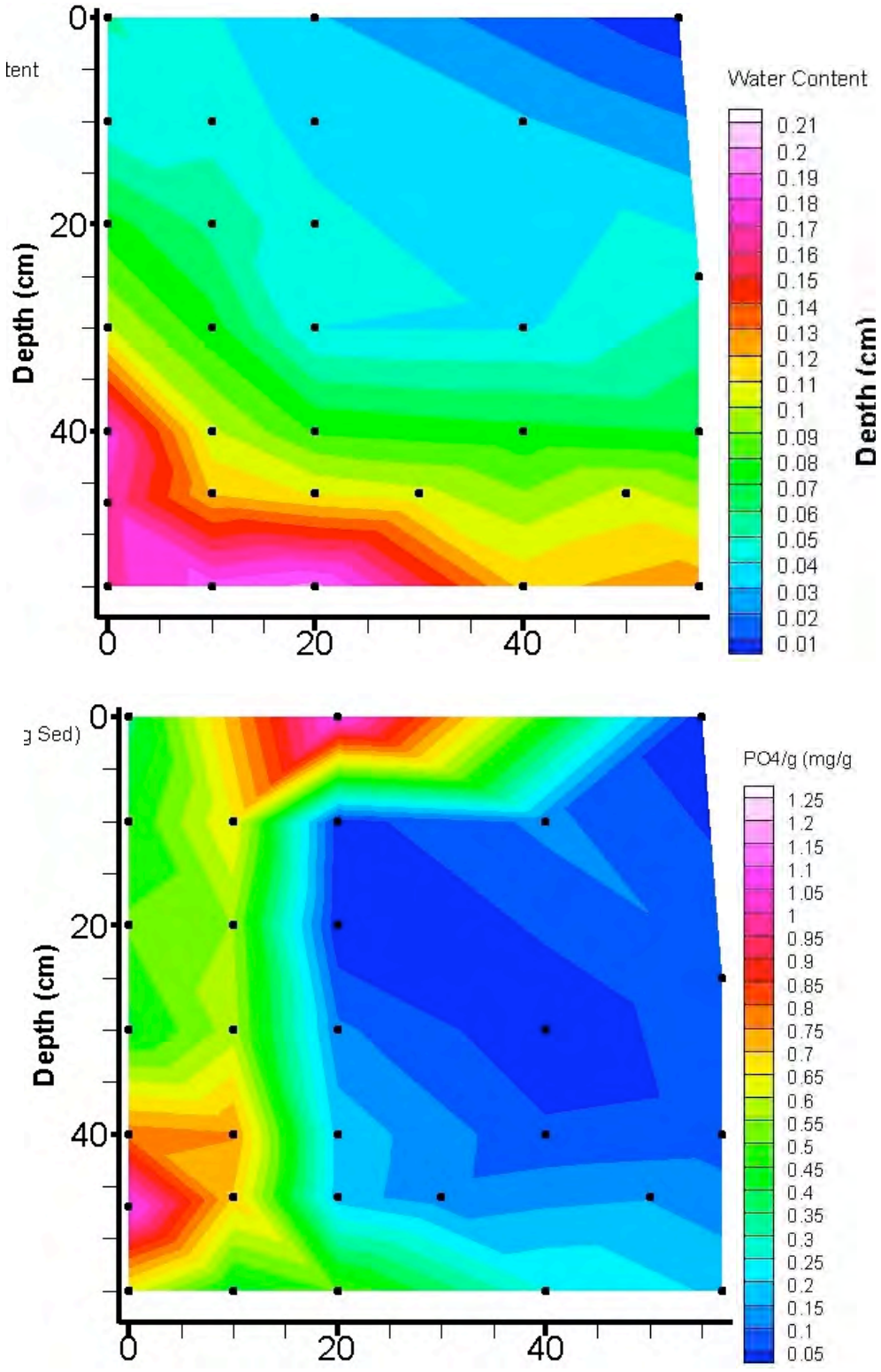

Y176. 2-D Infiltration of 40 mM Ca-citrate-PO_4 solution, 2.35 mL/minute x 55 minutes, then river water at 0.017 mL/minute x 23 hours (four injections, 1 week apart). Heterogeneous.

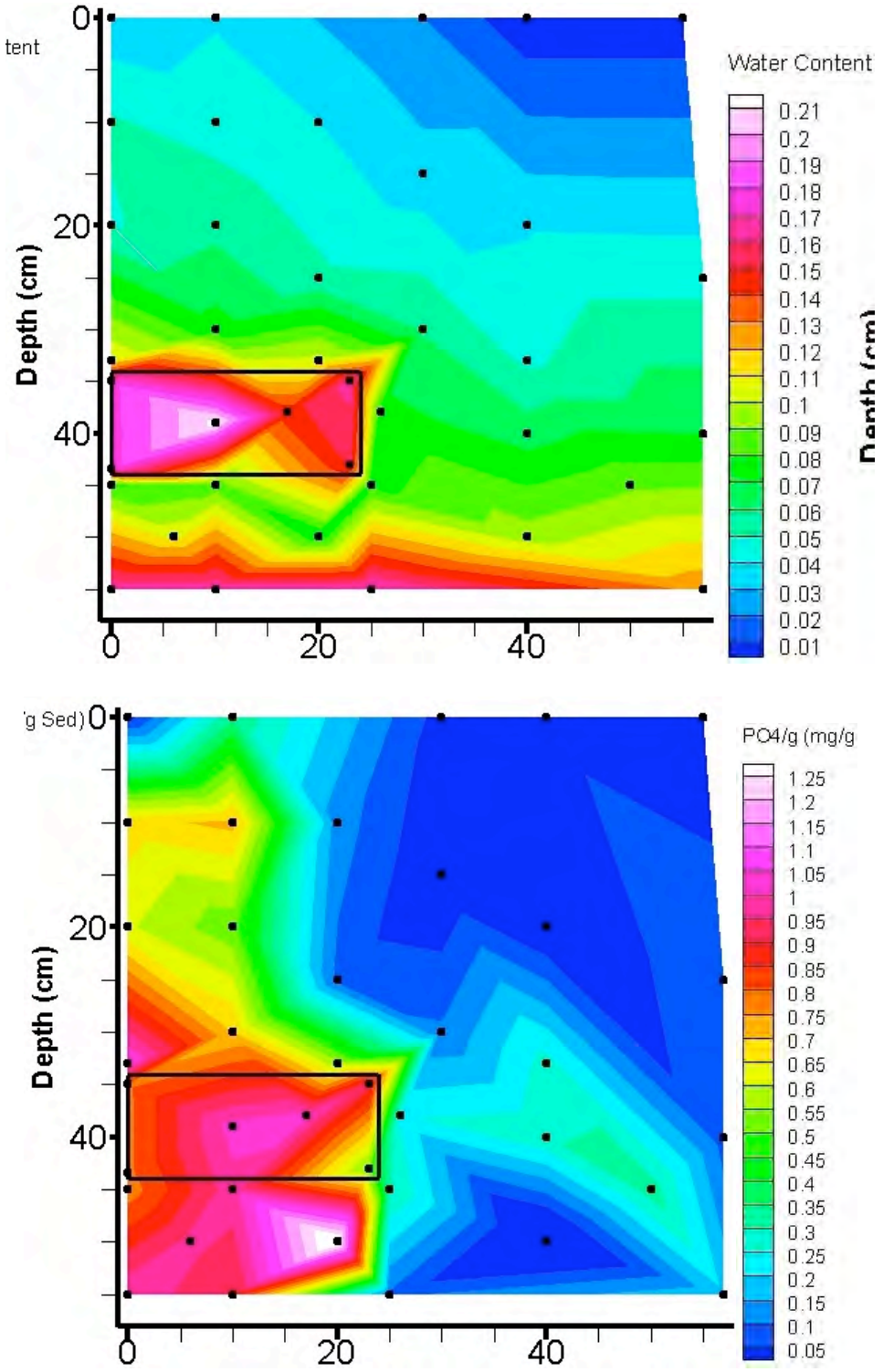

Y172-176.

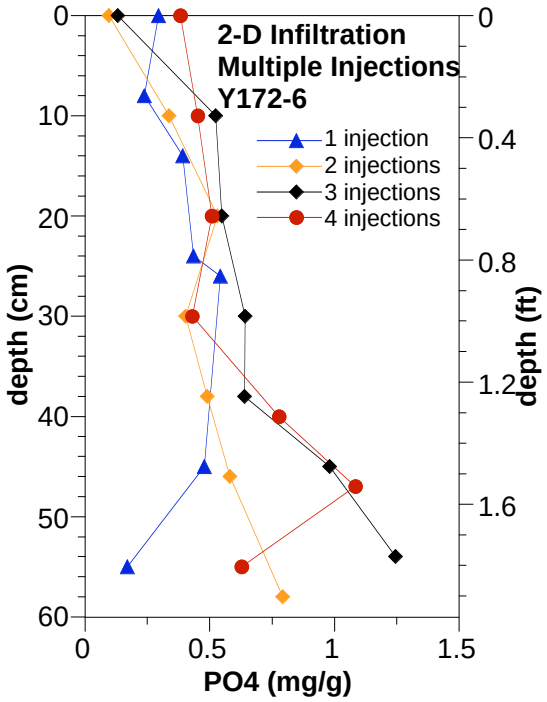
2-D Infiltration
Multiple Injections
Y172-6
1 injection
2 injections
3 injections
4 injections
depth (cm)
depth (ft)
PO4 (mg/g)
0
10
20
30
40
50
60
0.4
0.8
1.2
1.6
0.5
1
1.5

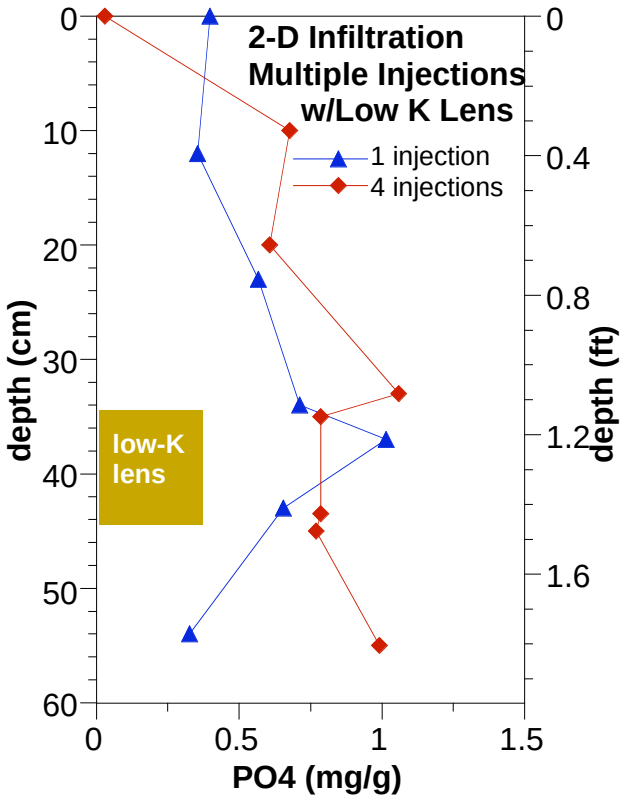
2-D Infiltration
Multiple Injections
w/Low K Lens
1 injection
4 injections
low-K
lens
depth (cm)
depth (ft)
PO4 (mg/g)
0
10
20
30
40
50
60
0.4
0.8
1.2
1.6
0.5
1
1.5

Y182A. Large 2-D Infiltration Experiment (8 ft x 4 ft x 0.5 in.)

Distribution

No. of Copies

Offsite

RC Moore
Sandia National Laboratories
P.O. Box 5800
Albuquerque, NM 87185-1136

RB Rowley
Office of Groundwater and Soil Remediation
EM-22/Cloverleaf Building
U.S. Department of Energy
1000 Independence Avenue, S.W.
Washington, DC 20585-2040

5 **Onsite**

U.S. Department of Energy, Richland Operations Office

JP Hanson	A5-11
JG Morse	A6-38
M Thompson (3)	A6-38

No. of Copies

CH2M HILL Plateau Remediation Company

WF Barrett	R3-60

14 **Pacific Northwest National Laboratory**

CA Burns	P7-25
RJ Fellows	K2-21
JS Fruchter (2)	K6-96
M Oostrom	K9-33
ML Rockhold	K9-36
JE Szecsody (5)	K3-61
VR Vermeul	K6-96
MD Williams	K6-96
L Zhong	K6-96

Pacific Northwest
NATIONAL LABORATORY

U.S. DEPARTMENT OF
ENERGY

902 Battelle Boulevard
P.O. Box 999
Richland, WA 99352
1-888-375-PNNL (7665)
www.pnl.gov